Reactor Science and Technology

JOURNAL OF NUCLEAR ENERGY PARTS A & B

EDITOR-IN-CHIEF
J. V. DUNWORTH

GENERAL EDITORS
J. GUÉRON G. RANDERS

EXECUTIVE EDITORS
G. W. K. FORD (U.K.) D. J. LITTLER (U.K.) W. K. ERGEN (U.S.A.)

EDITORIAL ADVISORY BOARD

T. E. ALLIBONE—Aldermaston
J. P. BAXTER—Sydney
H. J. BHABHA—Bombay
T. BJERGE—Röskilde
H. BRYNIELSSON—Stockholm
Sir JOHN COCKCROFT—Cambridge
Sir WILLIAM COOK—London
R. C. DALZELL—Washington
S. EKLUND—Stockholm
H. M. FINNISTON—Newcastle
J. GOENS—Mol-Donk
M. DE HEMPTINNE—Louvain
N. HILBERRY—Argonne
J. HOROWITZ—Saclay
F. IPPOLITO—Rome
G. C. LAURENCE—Chalk River
W. B. LEWIS—Chalk River
J. F. LOUTIT—Harwell
P. NOWACKI—Warsaw
J. M. OTERO—Madrid
Sir LEONARD OWEN—Risley
R. E. PEIERLS—Birmingham
F. PERRIN—Paris
L. ROTHERHAM—London
C. SALVETTI—Vienna
C. STARR—Canoga Park
J. F. ULRICH—Lisbon
ALVIN M. WEINBERG—Oak Ridge
J. J. WENT—Arnhem
K. WIRTZ—Karlsruhe
W. H. ZINN—Florida
W. J. ZUNTI—Zürich

VOL.
15
961

VOLUME 15
1961

PERGAMON PRESS
LONDON · OXFORD · NEW YORK · PARIS LOS ANGELES

REACTOR SCIENCE AND TECHNOLOGY
(Journal of Nuclear Energy Parts A & B)

EDITOR-IN-CHIEF
J. V. DUNWORTH: *Atomic Energy Establishment, Winfrith, Dorchester, Dorset*

GENERAL EDITORS
J. GUÉRON: *Brussels* G. RANDERS: *Lillestrøm*

EXECUTIVE EDITORS
G. W. K. FORD: (Engineering) *Atomic Energy Establishment, Winfrith, Dorchester, Dorset*
D. J. LITTLER: (Physics) *Central Electricity Generating Board, Friars House, Blackfriars Road, S.E.*1
W. K. ERGEN: *Oak Ridge National Laboratory, Oak Ridge, Tenn., U.S.A.*

Sub-Editor: P. C. GROOMS, Journals Dept., Pergamon Press Ltd., 4 Fitzroy Square, London W.1

NOTES FOR CONTRIBUTORS

I. General

1. Papers from authors in the United States should be submitted to the American Editor–Dr. W. K. ERGEN. Other papers, when concerned with *reactor science*, should be sent to Dr. D. J. LITTLER and when relative to *reactor technology*, manuscripts should be addressed to Mr. G. W. K. FORD. All papers should be concerned with original work in the field of nuclear energy. Progress reports and review articles will be accepted by the Editors from time to time.

2. Fifty free reprints of each paper are supplied. Additional copies can be supplied at a reasonable cost if ordered at the time when the first proofs are returned. A reprint order form will accompany proofs.

II. Script Requirements

1. Scripts should be typewritten, and double-spaced. It will be appreciated if authors will make clear any Greek characters which may be confused with ordinary letters or with other characters. Authors will receive proofs for correction when their contribution is first set, but there is rarely time for page proofs also to be sent for checking. This will be done, however, where the amount of alteration makes it advisable.

2. Illustrations should accompany the manuscript separately, and legends should also be typed on a separate sheet. It is requested that photographs should be kept to the minimum necessary. Line drawings that require to be redrawn should include all relevant details. If these are already well drawn it may be possible to reproduce them direct from the original, but in this case it is essential that the original drawings or good photo-prints should be provided. Any lettering on diagrams—other than Greek letters, symbols, etc.—should be stencilled and should be sufficiently large and bold to permit reproduction when the diagram has been reduced to a size suitable for appearance in the Journal. It is not possible to reproduce from 'dye-line' prints, or from prints with weak lines. Illustrations for reproduction should normally be about twice the final size required.

3. References to published literature should be quoted in the text as follows: SMITH (1950)—the date of publication, in parentheses, following the author's name. References should be listed together at the end of each paper and not given as footnotes. They should be arranged in alphabetical order (first author's surname) to appear as follows:

FERMI E. and MARSHALL L. (1947) *Phys. Rev.* **72,** 1139.

WARNER R. K. (1954) *Chem. Engng. Sci.* **3,** 77.

It is particularly requested that (*a*) author's initials and (*b*) the volume or part numbers and page numbers are given in every case.

4. The text of articles submitted should be concise and in a readily understandable style. The technical description of the methods used should only be given in detail when such methods are new. The essential contents of each paper should be briefly recapitulated in an abstract. French and German papers should be submitted with English abstracts and titles.

5. To conserve space, authors are requested to mark less important portions of the paper (such as description of methods, record of experimental results, etc.) for printing in smaller type.

Publishing Offices: 4 *Fitzroy Square, London W.*1 (*EUSton* 4455)
Annual subscription (A) *for libraries* £21 ($60) *including postage;* (B) *for private subscribers*
£10 10*s* ($29.40) *including postage*
Back numbers £8 ($24) *per volume*
Subscriptions should be sent to: Pergamon Press Ltd., Headington Hill Hall, Oxford
Pergamon Press, Inc., 122 *East* 55*th Street, New York* 22, *N.Y.*
Copyright © 1961 Pergamon Press, Ltd.

PERGAMON PRESS LTD.
4 FITZROY SQUARE, LONDON W.1 HEADINGTON HILL HALL, OXFORD
122 EAST 55TH STREET, NEW YORK 22, N.Y. 24 RUE DES ECOLES, PARIS V•

VOL
15
196

LIST OF CONTENTS

NUMBER 1

C. CARTER and G. ROWLANDS: Some topics in one-velocity neutron transport theory 1
E. J. AXTON and P. CROSS: The establishment of an absolutely calibrated neutron source 22
Letters to the Editors
S. W. STRAUSS: An empirical surface tension-temperature relation for liquid metals 28
B. P. RASTOGI and R. S. SINGH: Absorption in the 6·7 eV resonance of ^{235}U 29
L. S. KOTHARI and P. G. KHUBCHANDANI: Energy distribution of thermal neutrons in a finite beryllium oxide assembly 30
Book Reviews 32
Translations from *Atomnaya Energiya*
V. G. ZAGRAFOV: A method of estimating the critical parameters for arbitrarily shaped bodies of fissile material 36
P. L. KIRILLOV, F. A. KOZLOV, V. I. SUBBOTIN and N. M. TURCHIN: Removing oxides from liquid sodium and monitoring the oxide content 42
V. I. SPITSYN and M. M. GOLUTVINA: Isolation of carrier-free ^{233}Pa from irradiated thorium nitrate . . 47
P. I. KHRISTENKO: On the thermodynamic feasibility of driving turbines with organic liquids heated in nuclear reactors 50
G. M. NESMEYANOVA and G. M. ALKHAZASHVILI: Investigation of the role of oxidation-reduction processes when uranium oxides dissolve in acid media 54
Letters to the Editors
V. N. ANDREEV, O. D. KAZACHKOVSKII and N. V. KRASNOYAROV: The behaviour of a reactor with temperature self-regulation 59
B. G. DUBOVSKII: Sectionalized reactor systems 61
Z. I. SOLOV'EVA: Compound fission of uranium by 2·5 MeV neutrons 62
Books Received 64
Papers to be Published in Future Issues 65
Abstracts and Titles of Future Papers (*Atomnaya Energiya*) 66

VOL.
15
1961

NUMBERS 2/3

D. L. BOOTH: Steady states in reactors with positive reactivity coefficients 69
C. CARTER: Streaming due to holes in a reactor 76
F. T. ADLER: Reactor kinetics: integral equation formulation 81
P. N. COOPER, W. M. COOPER and K. FIRTH: The effect of cylindrical air voids in a highly enriched water-moderated core 86
R. K. THOMASSON: A general method of deriving responses and transfer functions in transient heat conduction phenomena 91
E. ERDIK: The experimental determination of fast fission factors in light water-moderated, slightly enriched uranium rod lattices 98
A. MOAT, D. S. MATHER and M. H. MCTAGGART: Some experimental determinations of the number of prompt neutrons from fission 102
C. CARTER and R. J. JARVIS: Influence of a cylindrical channel on a neutron flux which varies linearly in a direction perpendicular to the axis of the channel 113
A. GOODWIN JR. and C. L. SCHUSKE: Plexiglas- and graphite-moderated plutonium assemblies 120
D. C. C. GIBBS, M. GIBSON and W. A. COOPER: Long-term reactivity changes in irradiated thorium . . 130
L. R. BLAKE: Irradiation of uranium-metal and uranium-oxide fuel pins to high burn-up at high temperature 140
Abstracts and Titles of Future Papers (*Atomnaya Energiya*) 160

NUMBER 4

A. J. DERUYTTER: The fission cross section of ^{235}U from 0·01 eV to 0·1 eV and its absolute value at 0·0253 eV 165
W. J. MEGAW, R. C. CHADWICK, A. C. WELLS and J. E. BRIDGES: The oxidation and release of iodine-131 from uranium slugs oxidizing in air and carbon dioxide 176
M. C. WITTELS: Stored energy in the Oak Ridge Graphite Reactor—1960 185
H. TAKAHASHI: Generalization of the singular integral method for an anisotropic scattering medium . . 192
L. A. TAYLOR: The evaluation of worth of cylindrical control rods in reflected cylindrical cores with particular reference to the O.M.R. 196
D. C. STUPEGIA, R. R. HEINRICH and G. H. MCCLOUD: Neutron capture cross sections of ^{236}U . . . 200
J. CSIKAI, A. DARÓCZY and K. DEDE: Measurements of the diffusion length of thermal neutrons in water from 16 to 89°C and in diphyl (Dowtherm A) at 185°C 204
Book Review 209
Translations from *Atomnaya Energiya*
V. B. KLIMENTOV and V. M. GRIAZEV: Models for finding the control response and temperature coefficient of uranium-water reactors operating with intermediate energy neutrons 210

V. Bartošek: The burn-up of natural uranium in a homogeneous reactor 214
D. D. Kalafati: The effect of the temperature characteristics of a reactor on the choice of the optimum thermodynamic cycle for an atomic power station 220
Letters to the Editors
I. S. Dneprovskii: New isotopes of erbium and holmium 229
D. L. Broder, A. P. Kondrashov, A. A. Kutuzov and A. I. Lashuk: Effect of boron-containing layers on the yield of secondary gamma rays 229
Iu. K. Gus'kov, A. V. Zvonarev and V. P. Klichkova: An investigation of the e.m.f. developed when a system of semiconductors containing uranium is irradiated in a reactor 231
E. Aleksandrovich and M. Bartenbakh: Measurement of fast neutron flux distribution in the core of VVR-C reactor using electrical conductivity changes in germanium 233
Papers to be Published in Future Issues 235

AUTHOR INDEX TO VOLUME 15

Adler, F. T. p. 81
Aleksandrovich, E. p. 233
Alkhazashvili, G. M. p. 54
Andreev, V. N. p. 59
Axton, E. J. p. 22
Bartenbakh, M. p. 233
Bartošek, V. p. 214
Blake, L. R. p. 140
Booth, D. L. p. 69
Bresee, J. C. p. 32 (B.R.)
Bretscher, E. p. 33 (B.R.)
Bridges, J. E. p. 176
Broder, D. L. p. 229
Buddery, J. H. p. 34 (B.R.)
Carter, C. pp. 1, 76, 113
Chadwick, R. C. p. 176
Cooper, P. N. p. 86
Cooper, W. A. p. 130
Cooper, W. M. p. 86
Cross, P. p. 22
Csikai, J. p. 204
Daróczy, A. p. 204
Dede, K. p. 204
Deruytter, A. J. p. 165
Dneprovskii, I. S. p. 229
Dubovskii, B. G. p. 61
Erdik, E. p. 98
Firth, K. p. 86
Gibbs, D. C. C. p. 130
Gibson, M. p. 130
Golutvina, M. M. p. 47
Goodwin, A. Jr. p. 120
Griazev, V. M. p. 210
Gus'kov Iu. K. p. 231
Heinrich, R. R. p. 200
Jarvis, R. J. p. 113
Kalafati, D. D. p. 220
Kazachkovskii, O. D. p. 59
Khristenko, P. I. p. 50
Khubchandani, P. G. p. 30
Kinney, W. E. p. 34 (B.R.)
Kirillov, P. L. p. 42
Klichkova, V. P. p. 231
Klimentov, V. B. p. 210
Kondrashov, A. P. p. 229
Kothari, L. S. p. 30
Kozlov, F. A. p. 42
Krasnoyarov, N. V. p. 59
Kutuzov, A. A. p. 229
Lashuk, A. I. p. 229
Leslie, D. C. p. 209 (B.R.)
Marable, J. H. p. 35 (B.R.)
Mather, D. S. p. 102
McCloud, G. H. p. 200
McTaggart, M. H. p. 102
Megaw, W. J. p. 176
Moat, A. p. 102
Nesmeyanova, G. M. p. 54
Rastogi, B. P. p. 29
Rowlands, G. p. 1
Schuske, C. L. p. 120
Singh, R. S. p. 29
Solov'eva, Z. I. p. 62
Spitsyn, V. I. p. 47
Strauss, S. W. p. 28
Stupegia, D. C. p. 200
Subbotin, V. I. p. 42
Sykes, J. B. p. 34 (B.R.)
Takahashi, H. p. 192
Taylor, L. A. p. 196
Thomasson, R. K. p. 91
Turchin, N. M. p. 42
Wells, A. C. p. 176
Wittels, M. C. p. 185
Zagrafov, V. G. p. 36
Zvonarev, A. V. p. 231

Note: (B.R.) indicates Book Review.

VOL
15
196

Reactor Science and Technology (Journal of Nuclear Energy, Parts A/B), 1961, Vol. 15, pp. 1 to 21. Pergamon Press Ltd. Printed in Northern Ireland

SOME TOPICS IN ONE-VELOCITY NEUTRON TRANSPORT THEORY

C. CARTER and G. ROWLANDS
Atomic Energy Research Establishment, Harwell, Berks.

(*Received* 3 *June* 1960)

Abstract—Some recent developments in one-velocity neutron transport theory are reviewed. Emphasis is placed on the most appropriate mathematical methods to use when obtaining numerical solutions on large electronic digital computers and on the possibilities of introducing simple corrections to diffusion theory in the vicinity of sources, boundaries and strong absorbers.

VOL. 15 1961

1. INTRODUCTION

IN this article, we have tried to review recent progress in neutron transport theory. In general, we have confined ourselves to developments since the publication of DAVISON's treatise on *Neutron Transport Theory* (DAVISON, 1957). In order to produce a reasonably compact article, we have considered only a few selected topics in energy-independent transport theory. The review should be of wider significance, however, for the solution of the energy-independent transport equation is an essential part of the solution of energy-dependent problems when the multigroup method is used. In this method, a one-velocity equation must be solved for each energy group, with sources due to the transfer of neutrons from other groups.

The mathematical formulation of neutron transport theory is treated by DAVISON (1957). The theory may be formulated in two equivalent ways. We can consider the conservation of neutrons within a volume element dv within the solid angle element $d\Omega$ about the direction Ω. We then equate the loss of neutrons due to absorption, scattering, and leakage, to the gain of neutrons due to sources and scattering. This gives the Boltzmann integro-differential transport equation.

The second formulation of neutron transport considers the total number of neutrons at every point as the sum of all neutrons from other points which have travelled without collision from other points in the medium. This gives an integral equation for the neutron density.

1.1 *Notation*

$N(\mathbf{r}, \mathbf{\Omega})\, dv\, d\Omega$ = the number of neutrons in the volume element dv around the point $\mathbf{r}$, and travelling in a direction lying within a solid angle $d\Omega$ around the direction $\mathbf{\Omega}$

$S(\mathbf{r}, \mathbf{\Omega})\, dv\, d\mathbf{\Omega}$ = the number of neutrons lying within $dv\, d\mathbf{\Omega}$ emitted by the independent neutron sources

$f(\mathbf{\Omega}' \to \mathbf{\Omega})\, d\Omega$ = the probability that a neutron moving in direction $\mathbf{\Omega}'$ before a collision will be moving in a direction within the solid angle $d\Omega$ after a collision

c = the total number of secondary neutrons after a collision

l = the mean distance travelled by a neutron between collisions

$\Psi(\mathbf{r}, \mathbf{\Omega}) = vN(\mathbf{r}, \mathbf{\Omega})$, where v is the neutron velocity

$\rho(\mathbf{r}) = \int \Psi(\mathbf{r}\ \mathbf{\Omega})\, d\mathbf{\Omega}$; $S(\mathbf{r}) = \int S(\mathbf{r}, \mathbf{\Omega})\, d\mathbf{\Omega}$;

$$\tau(\mathbf{r},\mathbf{r}') = \int_0^{|\mathbf{r}-\mathbf{r}'|} \frac{dx}{l(\mathbf{r}+\mathbf{\Omega}x)} = \text{optical distance between } \mathbf{r} \text{ and } \mathbf{r}'.$$

1.2 *Basic theory*

The Boltzmann integro-differential equation is

$$\mathbf{\Omega} \cdot \operatorname{grad} \Psi(\mathbf{r},\mathbf{\Omega}) + \Psi(\mathbf{r},\mathbf{\Omega})/l(\mathbf{r}) = \\ = \frac{c}{l(\mathbf{r})} \int \Psi(\mathbf{r},\mathbf{\Omega}') f(\mathbf{\Omega}' \to \mathbf{\Omega})\, d\mathbf{\Omega}' + S(\mathbf{r},\mathbf{\Omega}). \quad (1.1)$$

The integral equation with isotropic scattering is

$$\rho(\mathbf{r}) = \int \frac{e^{-\tau(\mathbf{r},\mathbf{r}')}}{|\mathbf{r}-\mathbf{r}'|^2} \left\{ \frac{c(\mathbf{r}')}{4\pi l(\mathbf{r}')} \rho(\mathbf{r}') + S(\mathbf{r}') \right\} dv'. \quad (1.2)$$

When solving a problem, it is a matter of convenience whether to start with the Boltzmann equation or the integral equation and we shall use both in this article.

The explicit form for $\mathbf{\Omega} \cdot \operatorname{grad}$ in the Boltzmann equation depends on the co-ordinate system used. In one-dimensional slab geometry $\mathbf{\Omega} \cdot \operatorname{grad} = \mu \dfrac{\partial}{\partial z}$, where μ is the angle between the z axis and $\mathbf{\Omega}$.

In one-dimensional spherical geometry $\mathbf{\Omega} \cdot \operatorname{grad} = \mu \dfrac{\partial}{\partial r} + \left(\dfrac{1-\mu}{r}\right)^2 \dfrac{\partial}{\partial \mu}$, where μ is now the angle between $\mathbf{\Omega}$ and the radius vector.

In an infinite source-free medium, DAVISON shows

that the transport equation reduces to a differential equation

$$\nabla^2\rho(\mathbf{r}) = \rho(\mathbf{r})/L^2, \tag{1.3}$$

where

$$\frac{1}{c} = \frac{L}{2l}\log\left(\frac{L+l}{L-l}\right). \tag{1.4}$$

Equation (1.3) is the asymptotic diffusion equation and L is the asymptotic diffusion length. In a finite medium containing sources, the solution for $\rho(\mathbf{r})$ can be written

$$\rho(\mathbf{r}) = \rho_{as}(\mathbf{r}) + \rho_{tr}(\mathbf{r}), \tag{1.5}$$

where $\rho_{as}(\mathbf{r})$ is a solution of equation (1.3) and $\rho_{tr}(\mathbf{r})$ is a transport correction which is significant only within distances of the order of a mean free path from sources and boundaries.

An equation of the same form as (1.3) is obtained if we assume that

$$\Psi(\mathbf{r},\boldsymbol{\Omega}) = \frac{1}{4\pi}[\rho(\mathbf{r}) + \boldsymbol{\Omega}\,.\,\mathbf{J}(\mathbf{r})], \tag{1.6}$$

but now

$$l^2/L^2 = 3(1-c). \tag{1.7}$$

This is the so-called P_1 approximation and is equivalent to asymptotic diffusion theory for $(1-c) \ll 1$. The approximation breaks down near boundaries and sources, since the angular variation of $\Psi(\mathbf{r},\boldsymbol{\Omega})$ is then more complicated than indicated by equation (1.6). It is possible to use a more complicated expansion than (1.6) and this is the principle of various expansion methods which are reviewed in Section 2 of this article.

We have indicated that diffusion theory is generally adequate except near sources and boundaries, so that diffusion theory could be more widely used if a simple and accurate correction could be made near sources and boundaries. In Section 3 we review some interesting work originated by GROSJEAN. He considers the neutron flux due to an isotropic source in an infinite medium and shows that it can be represented very accurately by the sum of a flux due to neutrons travelling direct from the source and a scattered neutron flux which satisfies a diffusion-type equation. We indicate how a similar separation might be made in the vicinity of boundaries.

Diffusion theory also breaks down when c is small. Here it is appropriate to express the flux as an expansion in c. This is the principle of the multiple scattering techniques reviewed in Section 4 of this article.

An increasing amount of neutron transport calculations are being done on large electronic digital computers and we have mentioned in this review some of the more important programmes available for this purpose. We have not attempted, however, to produce a compendium of such programmes, but rather to discuss the basic principles on which they are based. NATHER and SANGREN (1959; 1960) have published a comprehensive list of Nuclear Reactor Codes available up to the end of 1959.

2. EXPANSION METHODS OF SOLVING THE TRANSPORT EQUATION

2.1 *Introduction*

A useful method of solving the transport equation is to expand the neutron flux $\Psi(\mathbf{r},\boldsymbol{\Omega})$ in terms of a series of known linearly independent functions of $\boldsymbol{\Omega}$, $\phi_n(\boldsymbol{\Omega})$:

$$\Psi(\mathbf{r},\boldsymbol{\Omega}) = \sum_{n=0}^{\infty}\psi_n(\mathbf{r})\phi_n(\boldsymbol{\Omega}). \tag{2.1}$$

On substituting this series into the transport equation and using the known properties of the $\phi_n(\boldsymbol{\Omega})$ one obtains an infinite set of coupled first-order linear differential equations. In practice, the infinite series is cut off at the Nth term and there remains a set of $(N+1)$ equations to determine the $(N+1)$ spatial functions $\psi_n(\mathbf{r})$. These equations can be solved formally in a homogeneous medium in terms of arbitrary coefficients which must be determined from boundary conditions at the boundary of the medium. The actual boundary condition is that $\Psi(\mathbf{r},\boldsymbol{\Omega})$ is continuous at an interface between two media and that $\Psi(\mathbf{r},\boldsymbol{\Omega})$, at a free boundary, is zero for $\boldsymbol{\Omega}$ directed into the medium. In a finite order approximation to $\Psi(\mathbf{r},\boldsymbol{\Omega})$ the condition at an interface requires the continuity of all $\Psi_n(\mathbf{r})$, but the condition at a free boundary can only be satisfied approximately.

The best known example of the expansion method is the spherical harmonics method, in which the $\phi_n(\boldsymbol{\Omega})$ are spherical harmonics. There is an extensive literature on this method, and there is a fairly comprehensive treatment of it in DAVISON (1957), so we shall not discuss it further in this paper, except to compare it with other methods. For a given order of approximation, the spherical harmonic expansion gives the best approximation to $\Psi(\mathbf{r},\boldsymbol{\Omega})$ in the least squares sense and it is natural to enquire whether some other type of expansion might be more useful in certain problems.

For problems with plane or spherical symmetry, $\boldsymbol{\Omega}$ can be expressed in terms of a single co-ordinate μ, and one can choose the Tchebysheff polynomials $T_n(\mu)$ as the $\phi_n(\boldsymbol{\Omega})$ in equation (2.1). (ASPELUND 1958, CONKIE 1959a). The Tchebysheff expansion has the property of giving the least maximum error in $\Psi(\mathbf{r},\boldsymbol{\Omega})$. On substituting the Tchebysheff expansion into the one-dimensional Boltzmann equation with isotropic

VOL 15 196

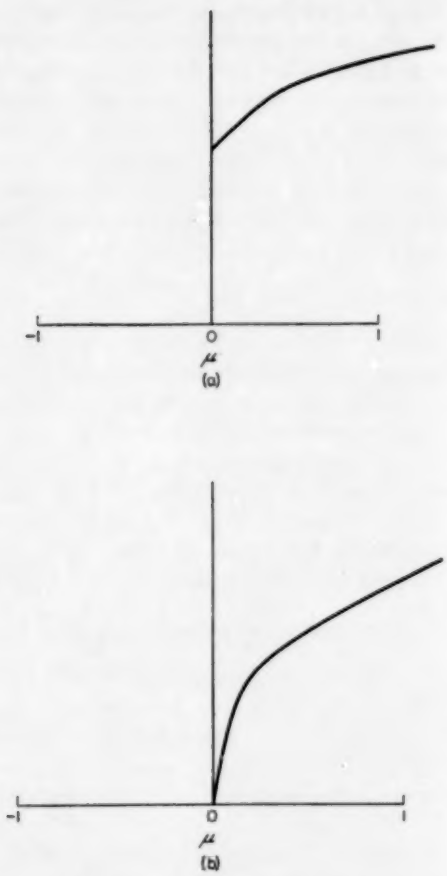

FIG. 1.

scattering, we obtain the system of equations:

$$\frac{d}{dz}\psi_1(z) + \frac{(1-c)}{l}\psi_0(z) + \frac{2c}{l}\sum_{n=1}\frac{\psi_{2n}(z)}{4n^2-1} = \int_{-1}^{+1}\frac{S(\mu,z)\,d\mu}{\sqrt{1-\mu^2}}, \tag{2.2}$$

$$\frac{d}{dz}\psi_{n+1}(z) + \frac{d}{dz}\psi_{n-1}(z) + \frac{2}{l}\psi_n(z) = \int_{-1}^{+1}\frac{S(\mu,z)T_n(\mu)\,d\mu}{\sqrt{1-\mu^2}}, \quad n>0.$$

The most general solution of a set of linear equations of the form (2.2) is

$$\psi_n(z) = \sum_i A_{n,i}\exp(\nu_i z/l), \tag{2.3}$$

where the $A_{n,i}$ are determined partly from the coupling between the equations and partly from the boundary conditions. The ν_i are the roots of a determinant of order $(N+1)$ in the Nth order approximation.

At a free boundary two types of boundary condition have been used. Mark sets Ψ zero at $\frac{N}{2}$ discrete inward directions, whilst Marshek sets to zero $\frac{N}{2}$ integrals over the incoming hemisphere. These boundary conditions are discussed at length by DAVISON (1957), with reference to the spherical harmonic expansion.

Both the spherical harmonics and Tchebysheff expansions use the same analytic approximation over the whole range of variation of Ω and we shall describe them as full range approximations. One might, however, divide the solid angle into a number of ranges and use a different analytic approximation in each range. Equation (2.1) then splits up into a number of equations, one for each range and with different $\Psi_n(\mathbf{r})$ and $\phi_n(\Omega)$ for each range. This method is adopted, for example, in CARLSON'S S_n method of solving the transport equation (CARLSON and BELL, 1958). In plane or spherical geometry, the range of μ from -1 to $+1$ is divided into N equal intervals and $\Psi(\mathbf{r},\mu)$ taken to vary linearly with μ in each interval. The CARLSON method was designed to be a stable procedure for finding numerical solutions of the transport equation but there is a more fundamental reason why a full range approximation may not be the most appropriate one to use and we now consider this in some detail.

As stated above, $\psi(\mathbf{r},\Omega)$ must vanish at a free boundary for all incoming directions of Ω, but is non-zero for outgoing directions. Let μ be the cosine of the angle between Ω and the outgoing normal. At the boundary it can be demonstrated that ψ is discontinuous at $\mu = 0$ if the boundary is plane and that $\frac{\partial\psi}{\partial\mu}$ is discontinuous at $\mu = 0$ if the boundary is convex. Thus the variation of $\Psi(\mathbf{r},\mu)$ at the boundary will have a form similar to that given in Figs. 1(a) or 1(b).

A little way in from the surface the discontinuity in Ψ will be absent and the flux variation will have a form similar to that given in Fig. 2.

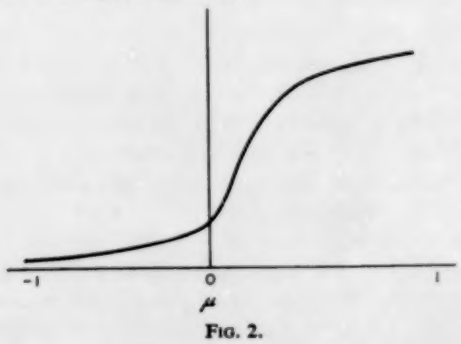

FIG. 2.

At distances within the order of one mean free path from a free surface, the flux variation near $\mu = 0$ is more rapid than that in the rest of the range and a full range approximation, which treats all parts of the range with comparable accuracy, will run into difficulties. Perhaps the best procedure would be to use a high-order expansion in a small range $|\mu| < \varepsilon$ near $\mu = 0$ and two low-order expansions for $-1 < \mu < -\varepsilon$ and $\varepsilon < \mu < 1$. So far as we know, this type of approximation has never been tried and it might involve considerable complexity.

A method for dealing with the anomalous flux variation near $\mu = 0$ in the boundary region which has been used with some success is the double-range approximation in which different expansions are used for $\mu <$ or > 0. No continuity condition is stipulated at $\mu = 0$, so that the method may give a discontinuity at $\mu = 0$, even away from a free surface. However, it is clear that the type of flux variation in Fig. 2 may be approximated better by two straight lines, one for $\mu < 0$ and another for $\mu > 0$, than by a single cubic curve.

The double-range spherical harmonic expansion in plane geometry has been considered recently by several authors (YVON, 1957; ZIERING and SCHIFF, 1958 and KOPPE and BLASSER, 1958). The appropriate expansions replacing equation (2.1) are

$$\Psi(x,\mu) = \sum_{n=0} (2n+1)\psi_n^{+} P_n(2\mu - 1), \quad \mu > 0,$$
$$= \sum_{n=0} (2n+1)\psi_n^{-} P_n(2\mu + 1), \quad \mu < 0, \quad (2.4)$$

and the system of equations obtained by substituting this expansion into the Boltzmann equation with isotropic scattering is

$$(n+1)\frac{d}{dx}\psi_{n+1}^{\pm}(x) + n\frac{d}{dx}\psi_{n-1}^{\pm}(x) + (2n+1) \times \left(\frac{2}{l} \pm \frac{d}{dx}\right)\psi_n^{\pm}(x) = \frac{c}{l}\{\psi_0^{+}(x) + \psi_0^{-}(x)\}\delta_{n,0} + 2(2n+1)\int^{\pm} S(\mu,x)P_n(2\mu \mp 1)\,d\mu. \quad (2.5)$$

The $P_n^{\pm}$ approximation is obtained by putting $\psi_{n+1}^{\pm} = 0$. The most general solution of (2.5) is again of the form (2.3). The ν_i are now the roots of a determinant of order $2(N+1)$. In fact, all expansion methods have a general solution similar to (2.3) and one way of assessing different methods is by comparing the values of ν_i which they yield.

One interesting property of the double range expansion is that it is now possible to satisfy the free boundary condition exactly by putting all $\psi_n^{-}(x)$ zero on the boundary.

The extension of the double-range expansion method to more complicated geometry raises certain problems. The transport equation now contains a derivative with respect to μ and some care is necessary in evaluating this near the discontinuity at $\mu = 0$ (DRAWBAUGH and NODERER, 1959). A further difficulty in cylindrical geometry is that the neutron flux now depends on a second angular co-ordinate, θ, the angle that the projection of $\boldsymbol{\Omega}$ on a tangential plane makes with the axis of the cylinder. There are $\frac{n+2}{2}$ or $\frac{n+3}{2}$ independent spherical harmonics of order n, so that the P_3 approximation, for example, involves 6 radial functions rather than the 4 in plane or spherical geometry, but in the $P_1^{\pm}$ approximation, which also requires 4 functions in plane geometry, there is no natural way of including dependence on θ and published work to date has omitted it. Presumably θ dependence would be included in the $P_2^{\pm}$ approximation when it can be included naturally. This procedure would mean that the $P_N^{\pm}$ approximation would include $\frac{N^2}{2}$ or $(N^2-1)/2$ harmonics with θ dependence compared with $N(N+1)$ in the P_{2N+1} approximation, whereas both approximations involve $2(N+1)$ harmonics without θ dependence. Thus the full range expansion method would treat the θ dependence relatively more accurately than the comparable double-range expansion. It may well be that the full-range expansion gives more consideration to the θ dependence than is really warranted for it is only near boundaries with a small radius of curvature that we would expect the θ dependence to be important.

The extension of the double-range P_N approximation to two-dimensional Cartesian geometry has been considered by SCHIFF and ZIERING (1960).

2.2 *Comparison of different expansion methods*

In Table 1 we give ν_0 as a function of c, obtained by several different methods. ν_0, being the lowest root in equation (2.3), is the term which governs the behaviour of the flux in the asymptotic region remote from sources and boundaries. The rigorous values of ν_0 in a source-free infinite medium is given in the last column and comparison with this value indicates how good the approximation is likely to be in the asymptotic region. For completeness we have given ν_0 over the range of c from 1·0 to 0, but it should be remembered that ν_0 has physical significance only when c is close to 1.

As we might have expected, we see that the P_{2N+1} approximation is superior to both the T_{2N+1} and the $P_n^{\pm}$ approximations, but all approximations converge

TABLE 1.—VALUE OF ν_0 IN VARIOUS APPROXIMATIONS

C	P_1	P_3	P_5	T_1	T_3	T_5	$P_0^{\pm}$	$P_1^{\pm}$	$P_3^{\pm}$	Exact
1·0	0	0	0	0	0	0	0	0	0	0
0·9	0·5477	0·5256	0·5254	0·4472	0·5228	0·5253	0·6324	0·5278	0·5255	0·5254
0·8	0·7746	0·7119	0·7105	0·6325	0·7028	0·7097	0·8944	0·7202	0·7113	0·7104
0·7	0·9487	0·8345	0·8291	0·7746	0·8165	0·8265	1·0954	0·8522	0·8322	0·8286
0·6	1·0954	0·9226	0·9096	0·8944	0·8944	0·9030	1·2649	0·9518	0·9173	0·9073
0·5	1·2247	0·9888	0·9647	1·0000	0·9502	0·9524	1·4142	0·0309	0·9793	0·9575
0·4	1·3416	1·0398	1·0026	1·0954	0·9914	0·9840	1·5492	1·0954	1·0255	0·9856
0·3	1·4491	1·0801	1·0291	1·1832	1·0227	1·0046	1·6733	1·1493	1·0607	0·9974
0·2	1·5492	1·1126	1·0480	1·2649	1·0471	1·0180	1·7889	1·1948	1·0880	0·9999
0·1	1·6432	1·1392	1·0619	1·3416	1·0666	1·0282	1·8974	1·2340	1·1096	1·0000
0·0	1·7321	1·1613	1·0724	1·4142	1·0824	1·0353	2·0000	1·2680	1·1254	1·0000

rapidly. Thus, while the $P_0^{\pm}$ method is considerably worse than the P_1 method, $P_1^{\pm}$ is only slightly worse than P_3 and is much better than P_1.

The second test of an approximation method is its treatment of the flux near a boundary. This is most easily done by applying the method to the Milne problem in which a purely scattering medium occupies the half-space, $x > 0$, and the half-space, $x < 0$ is vacuum. For $x \to \infty$, the neutron flux is taken to vary as $x + x_0$. An exact calculation gives $x_0 = 0{\cdot}7104l$. In Table 2 we give the values of x_0/l calculated using

TABLE 2.—ASYMPTOTIC EXTRAPOLATION LENGTH FOR THE MILNE PROBLEM IN VARIOUS APPROXIMATIONS

	P_{2N-1}		T_{2N-1}		$P_N^{\pm}$
N	Mark	Marshak	Mark	Marshak	
0	0·5774	0·6667	0·7071	0·7854	0·5000
1	0·6940	0·7051	0·6942	0·7129	0·7113
2	0·7039	0·7082	0·7021	—	0·7106

Exact value = 0·7104

various approximations. For the full range methods, the results are given using both Marshak and Mark boundary conditions.

In all except the lowest order, it is clear that the double range method is giving considerably better results than the full range methods. The Tchebysheff expansion seems to have few advantages, although CONKIE (1959a) has shown that it gives rather better results than the full-range spherical harmonic expansion for the Milne problem with capture.

We now reach some tentative conclusions about the merits of the various methods. The P_1 approximation (diffusion theory) is usually better than any other expansion of the same order. In many problems, diffusion theory is adequate but a better approximation may be desirable when considering small regions in which boundary effects persist right through the region or when a region has appreciable capture ($c \ll 1$). For small regions we would expect the half-range expansion to give better results than the full-range method, whilst when $c \ll 1$ in a region, the successive generation method discussed in Section 4 is appropriate. There are probably few problems in which the P_{2N+1} method ($N > 0$) will give appreciably better results than $P_N^{\pm}$, but many in which the converse is the case.

2.3 *Numerical treatment of expansion methods*

The analytic treatment of expansion methods, in which $\psi_n(\mathbf{r})$ is written in the form of equation (2.3), is algebraically tedious except for the lowest order approximations, and it is desirable to use numerical methods at an early stage in the analysis. A survey of calculation techniques has been given by BARREISS (1958). One is to transform the set of $\psi_n(\mathbf{r})$ into a set of discrete ordinates $\Psi(\mathbf{r},\boldsymbol{\Omega}_k)$ and then solve the equations for the $\Psi(\mathbf{r},\boldsymbol{\Omega}_k)$ numerically. This procedure is discussed in Section (2.4). In this section, we shall describe an iterative method for solving the P_N or $P_N^{\pm}$ equations, due to GELBARD, DAVIS and PEARSON (1959), in which, starting from the P_1 approximation, we solve for increasing values of N until the required accuracy is obtained. This is an attractive method since the P_1 approximation is often quite a reasonable approximation and the iterative scheme is likely to converge rapidly.

In the full range spherical harmonic expansion in plane geometry, we put

$$\phi_n(x) = \psi_{2n}(x), \quad J_n(x) = \psi_{2n-1}(x).$$

Then the set of equations for the Boltzmann equation

may be written

$$\left(\frac{2n+1}{4n+1}\right)J_n'(x) + \frac{2n}{4n+1}J_{n-1}'(x) + \Sigma_{2n}\,\phi_n(x) = S_{2n}(x),$$
$$\left(\frac{2n+2}{4n+3}\right)\phi_{n+1}'(x) + \left(\frac{2n+1}{4n+3}\right)\phi_n'(x) + \Sigma_{2n+1}J_n(x) = S_{2n+1}(x). \tag{2.6}$$

Define vectors $\mathbf{J}, \boldsymbol{\phi}, \mathbf{S}$ and $\mathbf{R}$, whose components are J_n, ϕ_n, $(4n+1)S_{2n}$ and $(4n+3)S_{2n+1}$ respectively. Also define diagonal matrices $\mathbf{D}$ and $\boldsymbol{\Sigma}$ with components $D_{nn} = 1/(4n+3)\Sigma_{2n+1}$ and $\Sigma_{nn} = (4n+1)\Sigma_{2n}$ respectively. Then (2.6) may be written

$$\mathbf{AJ}' + \boldsymbol{\Sigma}\boldsymbol{\phi} = \mathbf{S},$$
$$\mathbf{B}\boldsymbol{\phi}' + \mathbf{D}^{-1}\mathbf{J} = \mathbf{R}, \tag{2.7}$$

where the terms of the matrices $\mathbf{A}$ and $\mathbf{B}$ are obvious from inspection of equations (2.6).

Eliminating $\mathbf{J}$ from equations (2.7) we have

$$-\mathbf{ADB}\boldsymbol{\phi}'' + \boldsymbol{\Sigma}\boldsymbol{\phi} = \mathbf{S} - \mathbf{ADR}. \tag{2.8}$$

Now define $\mathbf{X} = \mathbf{B}\boldsymbol{\phi}$ (2.9)

and operate on (2.8) with $\mathbf{A}^{-1}$ to obtain

$$-\mathbf{DX}'' + \mathbf{A}^{-1}\boldsymbol{\Sigma}\mathbf{B}^{-1}\mathbf{X} = \mathbf{A}^{-1}\mathbf{S} - \mathbf{DR}. \tag{2.10}$$

Equation (2.10) has the same form as multigroup diffusion theory equations, and so may be solved using existing computer programmes. This possibility is discussed more fully below.

The P_{2N+1} approximation consists of neglecting in equations (2.7) all terms in $\mathbf{A}$ and $\mathbf{B}$ outside the first $(N+1)$ rows and columns. We denote these approximate matrices by $\mathbf{A}_N$ and $\mathbf{B}_N$, and note that from their definitions, $\mathbf{A}$ is a triangular matrix with zeros above the diagonal, and $\mathbf{B}$ is a triangular matrix with zeros below the diagonal. Because of these triangularity properties it is easily demonstrated that

$$(\mathbf{ADB})_N = \mathbf{A}_N\mathbf{D}_N\mathbf{B}_N,$$
$$(\mathbf{A}^{-1})_N = (\mathbf{A}_N)^{-1},$$
$$(\mathbf{B}^{-1})_N = (\mathbf{B}_N)^{-1}, \tag{2.11}$$
$$(\mathbf{A}^{-1}\boldsymbol{\Sigma}\mathbf{B}^{-1})_N = (\mathbf{A}_N)^{-1}\boldsymbol{\Sigma}_N(\mathbf{B}_N)^{-1},$$

but

$$(\mathbf{BA})_N \neq \mathbf{B}_N\mathbf{A}_N,$$
$$(\mathbf{B}^{-1}\mathbf{A}^{-1})_N \neq (\mathbf{B}_N)^{-1}(\mathbf{A}_N)^{-1}.$$

From equations (2.11), it follows that the P_{2N+1} approximation is obtained from (2.10) by neglecting all terms outside the first $(N+1)$ rows and columns in the matrices $\mathbf{A}^{-1}\boldsymbol{\Sigma}\mathbf{B}^{-1}$ and $\mathbf{A}^{-1}$. The obvious way of solving equations (2.10) is to take all $\mathbf{X}_N = 0$, except $\mathbf{X}_0$, solve for $\mathbf{X}_0$, (this is the P_1 appropriation) and then use this value of $\mathbf{X}_0$ to solve for $\mathbf{X}_1$ and so on.

The above procedure is not unique since the matrix $\mathbf{ADB}$ can be represented as the product of two triangular matrices in infinitely many ways, but it is obviously convenient to use the representation which occurs naturally. The transformation (2.9) also has the advantage that it gives $\mathbf{J} = \mathbf{D}(\mathbf{R} - \mathbf{X}')$.

The double-range spherical harmonic expansion equation in plane geometry can be reduced to a form similar to (2.10) but without its elegant properties. We put

$$\phi_n{}^D(x) = \psi_n{}^+(x) + \psi_n{}^-(x),$$
$$J_n{}^D(x) = \psi_n{}^+(x) - \psi_n{}^-(x), \quad \text{for } n \text{ even},$$

and (2.12)

$$\phi_n{}^D(x) = \psi_n{}^+(x) - \psi_n{}^-(x),$$
$$J_n{}^D(x) = \psi_n{}^+(x) + \psi_n{}^-(x), \quad \text{for } n \text{ odd}.$$

It is convenient to express the set of equations for the double-range expansions in terms of scattering cross sections and source functions expanded in full range expansions. In order to do this we express the full-range ϕ_n, J_n in terms of the double-range $\phi_n{}^D, J_n{}^D$ as

$$\boldsymbol{\phi} = \mathbf{F}\boldsymbol{\phi}^D,$$
$$\mathbf{J} = \mathbf{G}\mathbf{J}^D. \tag{2.13}$$

If we substitute these equations into (2.7) we obtain

$$\mathbf{M}\mathbf{J}^{D\prime} + \boldsymbol{\phi}^D = \mathbf{F}^{-1}\boldsymbol{\Sigma}^{-1}\mathbf{S},$$
$$\mathbf{N}\boldsymbol{\phi}^{D\prime} + \mathbf{J}^D = \mathbf{G}^{-1}\mathbf{DR}, \tag{2.14}$$

where

$$\mathbf{M} = \mathbf{F}^{-1}\boldsymbol{\Sigma}^{-1}\mathbf{AG},$$
$$\mathbf{N} = \mathbf{G}^{-1}\mathbf{DBF}, \tag{2.15}$$

and (2.10) becomes

$$-\mathbf{DX}'' + \mathbf{GM}^{-1}\mathbf{N}^{-1}\mathbf{G}^{-1}\mathbf{DX} = \mathbf{GM}^{-1}\mathbf{F}^{-1}\boldsymbol{\Sigma}^{-1}\mathbf{S} - \mathbf{DR}'. \tag{2.16}$$

In the $P_N{}^{\pm}$ approximation, only the first $(N+1)$ rows and columns of the matrices $\mathbf{F}$, $\mathbf{G}$, $\mathbf{M}$ and $\mathbf{N}$ are included. Equation (2.16) does not have the elegant properties of (2.10), because $(\mathbf{GM}^{-1})_N \neq \mathbf{G}_N(\mathbf{M}_N)^{-1}$, $(\mathbf{N}^{-1}\mathbf{G}^{-1})_N \neq (\mathbf{N}_N)^{-1}(\mathbf{G}_N)^{-1}$.

Any expansion method can be put into the form of (2.16), once the appropriate transformations (2.13) are known. This method is again not unique, but as given, it does link up closely with the full-range expansion method. It means, for example, that in the $P_N{}^{\pm}$ approximation for $N > 0$, the first iteration, in which

VOL 15 196

all $\mathbf{X}_N$ except $\mathbf{X}_0$ are neglected, gives the P_1 equations. and not the $P_0^{\pm}$ equations.

It can be seen that equations (2.10) and (2.16) have the same form as multigroup diffusion theory equations. This has made it possible to use existing multigroup computer programmes with no modifications, but a special IBM 704 programme, FLIP, has also been developed (ANDERSON *et al.*, 1959). The boundary conditions in (2.10) and (2.16) require the continuity of all components of $\mathbf{X}$ and $\mathbf{DX}'$ at interfaces, just as in multigroup theory. At a free boundary the boundary conditions take the form

$$\mathbf{X}' = \mathbf{TX}. \tag{2.17}$$

This type of condition can be used in the FLIP 2 programme, but not in a normal multigroup programme. In many problems, however, the exact free boundary conditions are not crucial and it is adequate to take $\mathbf{X} = 0$ at an extrapolated boundary.

The above formalism can be applied to problems in spherical or cylindrical geometry, but it is now found that the coupling terms in equations (2.10) or (2.16) contain spatial derivatives. This makes it impossible to use existing multigroup programmes without considerable modification, but the method is still an attractive one. Two IBM 704 programmes are available (DAVIS *et al.*, 1959). CLIP solves the one-dimensional P_3 equations in cylindrical geometry and TRIP solves the two-dimensional P_3 equations in Cartesian co-ordinates.

VOL. 15 1961

2.4 *Discrete ordinate forms of expansion methods*

The one-dimensional Boltzmann equation may be written

$$\mu \Psi'(r,\mu) + \Sigma_t \Psi + \frac{1}{r} f(\mu) \frac{\partial \Psi}{\partial \mu} = S(\mu,r) + \frac{1}{2} \int_{-1}^{+1} \Sigma_s(\mu') \Psi(\mu')\, d\mu' \tag{2.18}$$

where $f(\mu) = 0$ in plane geometry
and $f(\mu) = (1 - \mu^2)$ in spherical geometry.
The discrete ordinate approximation to this equation consists in considering Ψ at $(N + 1)$ discrete values of μ, denoted by μ_k, where $k = 0, 1, \ldots, N$. The derivative and integral with respect to μ in (2.18) are represented by summations over the Ψ_k. Thus in the vector notation used in the previous subsection, we have

$$\boldsymbol{\mu} \boldsymbol{\Psi} + \boldsymbol{\Sigma}_T \boldsymbol{\Psi} + \frac{1}{r} \boldsymbol{\beta} \boldsymbol{\Psi} = \mathbf{S} + \boldsymbol{\alpha} \boldsymbol{\Psi}. \tag{2.19}$$

On the other hand, an expansion method, of order N, is formulated in terms of $(N + 1)\psi_n$ and may be written

$$\mathbf{M}\boldsymbol{\psi}' + \boldsymbol{\Sigma}_T \boldsymbol{\psi} + \frac{1}{r} \mathbf{B} \boldsymbol{\psi} = \mathbf{Q} + \mathbf{A} \boldsymbol{\psi}. \tag{2.20}$$

Since both $\boldsymbol{\Psi}$ and $\boldsymbol{\psi}$ have $(N + 1)$ components we should expect to be able to transform (2.19) into the form of (2.20) and vice versa by a linear transformation (GOERTZEL, 1958).

$$\text{In (2.20) put } \boldsymbol{\psi} = \mathbf{F} \boldsymbol{\Psi}. \tag{2.21}$$

Then

$$\mathbf{F}^{-1}\mathbf{M}\mathbf{F}\boldsymbol{\Psi} + \boldsymbol{\Sigma}_T \boldsymbol{\Psi} + \frac{1}{r} \mathbf{F}^{-1}\mathbf{B}\mathbf{F}\boldsymbol{\Psi} = \mathbf{F}^{-1}\mathbf{Q} + \mathbf{F}^{-1}\mathbf{A}\mathbf{F}\boldsymbol{\Psi} \tag{2.22}$$

This will be of the form of (2.19), if $\mathbf{F}^{-1}\mathbf{MF}$ is the diagonal matrix $\boldsymbol{\mu}$. Thus the $\mathbf{F}$ to be used in (2.2) is the one that diagonalizes $\mathbf{M}$ by a similarity transformation, and the discrete ordinates μ_k are the eigenvalues of $\mathbf{M}$.

Every expansion method therefore has its corresponding discrete ordinate formulation. The full-range spherical harmonic method for example gives the familiar Gaussian discrete ordinate method of Chandrasekhar and Wick, (DAVISON, 1957) whilst the double range spherical harmonic expansion is equivalent to SYKES' double Gaussian discrete ordinate method (SYKES, 1951).

The discrete ordinate formulation provides a possible method of solving the transport equation numerically. The solution is started at an outer boundary with $\Psi_{-k} = 0$, where $-k$ indicates that $\mu_k < 0$. A step by step method can then be used to solve (2.19) as a set of coupled first-order linear equations in the Ψ_{-k}. Since there is no boundary condition at the outer boundary for the Ψ_{+k}, trial values must be assumed for these in the terms $\boldsymbol{\alpha}\boldsymbol{\Psi}$ and $\boldsymbol{\beta}\boldsymbol{\Psi}$. In plane geometry, $\boldsymbol{\beta} = 0$, so that trial values are required only in the scattering term $\boldsymbol{\alpha}\boldsymbol{\Psi}$.

The solution of (2.19) for Ψ_{-k} proceeds until the other boundary is reached, when the equations for Ψ_{+k} can be solved step by step in the opposite direction. The process is iterative.

The double Gaussian discrete ordinate method is used in the American programme RDR 5 for the Naval Ordnance Computer.

2.5 *Comparison of numerical methods*

In the last two sections, we have described two different methods of solving the Boltzmann equation. Both are iterative methods, one iterating upwards from the diffusion approximation, and the other iterating on the scattering term in the Boltzmann equation. Thus,

in general, we would expect the first method to converge most rapidly for weak absorption and the second for weak scattering. In practice, the first method has been found to converge more rapidly than the second for a wide range of problems (GELBARD *et al.*, 1959). CARLSON's S_n method is in many ways similar to the discrete ordinate method. It is probably the most widely used programme at the moment and considerable thought has been given to its rate of convergence (BLUE and FLATT, 1960). However, on theoretical grounds, we should expect the double Gaussian discrete ordinate method used in the RDR.5 code to be superior to the S_n method, since it represents the angular flux by an analytic function rather than by a piecemeal linear function.

If the Boltzmann equation is being solved as part of a multigroup theory calculation, then the source term in (2.19) represents neutrons being transferred from other groups. In this case iteration is required on both $\mathbf{S}$ and $\boldsymbol{\alpha\Psi}$. In a many group problem, $\mathbf{S}$ may be much larger than $\boldsymbol{\alpha\Psi}$, and the $\mathbf{S}$ iteration becomes more crucial than the iteration on $\boldsymbol{\alpha\Psi}$. In this case, there might be little to choose between the two methods of solving the one-velocity Boltzmann equation, the main problem now being how to speed up the convergence on the iterations between different groups.

3. SIMPLE ANALYTIC APPROXIMATIONS

3.1 *Introduction*

In the General Introduction it was pointed out that large errors in diffusion theory are to be expected near isolated sources and also near boundaries. This suggests that the first step in a programme to find an alternative to diffusion theory, which does not suffer from these difficulties, should be a consideration of the solution of the Boltzmann equation appropriate to an isolated source in an infinite homogeneous medium.

The exact solution of this problem is well known (see for example DAVISON, Chapter 5), but, of course, it is a simple approximate solution, with errors less than those in diffusion theory, which we require. Recently GROSJEAN (1956a) has obtained an approximate solution, which, for $c < 1$, gives values correct to a few per cent over a range of distances from the source where the solution decreases by a factor of 10^{-3}. For $c > 1$ this accuracy is not obtained. GROSJEAN expresses the solution of the Boltzmann equation as the sum of two terms: the first arises from those neutrons which have yet to have a collision, whilst the second term satisfies a diffusion type equation, but with coefficients different from those appearing in the usual form of diffusion theory. This form for the approximate solution is obtained after a rather lengthy and complicated discussion of the Boltzmann equation.

It is the purpose of this section to discuss in detail the basic idea behind the GROSJEAN approximation, that is the separation of the solution of the Boltzmann equation into two terms, to show how GROSJEAN's results may be obtained in a simple manner, and to extend the treatment to all values of c.

Other authors (see for example the review article by TRIPLETT (1958)) have proposed different methods of approximation, but these do not compare in accuracy with the GROSJEAN approximation and so they will not be considered in detail in this article.

The second step in a programme to find an alternative to diffusion theory is to consider a finite medium and so find the effect of boundaries. To this end we use a result obtained by various authors (see for example CASE, DE HOFFMANN and PLACZEK (1953) Chapter V) that any finite medium problem is equivalent to a number of infinite medium problems in which effective sources take the place of boundaries.

However it is still found necessary to introduce further methods of approximations, otherwise the final solutions are far too complicated. Some such methods are discussed below, but since there are very few cases where finite media problems have been solved exactly, it is difficult to test these methods to see which is the best, bearing in mind the need for a final method which is relatively simple but accurate. For this reason the treatment of finite media is not at present in such a complete state as it is for infinite ones. However the present status of the finite medium problem is considered below.

3.2 *Infinite media—General theory*

For simplicity we restrict ourselves to plane geometry, where the Boltzmann equation for the angular flux $\Psi(x,\mu)$ in an infinite medium is

$$\mu\Psi'(x,\mu) + \Psi/l = S(x,\mu) + \frac{c}{l}\sum_{n=0}\frac{(2n+1)}{4\pi} b_n \psi_n(x) P_n(\mu), \quad (3.1)$$

where

$$\Psi(x,\mu) = \sum \frac{(2n+1)}{4\pi} \psi_n(x) P_n(\mu), \quad (3.2)$$

with $P_n(\mu)$ the Legendre polynomial of order n. The coefficients b_n which give a measure of the anisotropic scattering are defined such that

$$b_n = \int f(\boldsymbol{\Omega}' \rightarrow \boldsymbol{\Omega})\, P_n(\boldsymbol{\Omega}' \,.\, \boldsymbol{\Omega})\, d(\boldsymbol{\Omega} \,.\, \boldsymbol{\Omega}'), \quad (3.3)$$

where $f(\boldsymbol{\Omega}' \rightarrow \boldsymbol{\Omega})$ is defined in the General Introduction and is so normalized that $b_0 = 1$. A more detailed

discussion of the above equations is given in DAVISON (Chapter 17).

A formal solution of (3.1) may be obtained in the following way. We subject it to a complex Fourier transform and find after slight rearrangement that

$$(\bar{\Psi},\mu) = \frac{\bar{S}(p,\mu)l}{1 - ip\mu l} + \frac{c}{4\pi}\sum_{n=0}\frac{(2n+1)b_n\,\bar{\psi}_n(p)\,P_n(\mu)}{1 - ip\mu l}, \tag{3.4}$$

where

$$\bar{\Psi}(p,\mu) = \int_{-\infty}^{+\infty}\Psi(x,\mu)e^{ipx}\,dx, \tag{3.5}$$

and a similar convention holds for the other transforms. If we multiply both sides by $P_n(\mu)$ and integrate over all μ we find

$$\psi_n(p) = \sum_{m=0}(2m+1)A_{n,m}\{l\bar{S}_m(p) + cb_m\bar{\psi}_m(p)\}, \tag{3.6}$$

where

$$A_{n,m}(p) = \frac{1}{2}\int_{-1}^{+1}\frac{P_n(w)P_m(w)\,dw}{1 - ipwl}. \tag{3.7}$$

In particular, for $n = m = 0$, $A_{0,0} = \tan^{-1}pl/pl$.

A formal solution may in principle be obtained by solving (3.6) for $\bar{\psi}_n(p)$ in terms of the A's and S's and then inverting the transform. However even where the number of b_n's is finite and relatively small this process is exceedingly complicated. In the following we shall consider some special cases.

3.3 *Isotropic scattering and isotropic source* ($b_n = 0$, $S_n = 0$, for $n > 0$)

In this case equation (3.6) may be rearranged into the form

$$\bar{\psi}_n(p) = \bar{S}_0(p)lA_{0,n}/(1 - cA_{0,0}), \tag{3.8}$$

and in particular

$$\bar{\psi}_0(p) = \bar{S}_0lA_{0,0}/(1 - cA_{0,0}). \tag{3.9}$$

Thus we may write

$$\psi_0(x) = \frac{l}{2\pi}\int_{-\infty}^{+\infty}\frac{\bar{S}_0(p)A_{0,0}}{1 - cA_{0,0}}\cdot e^{-ipx}\,dp. \tag{3.10}$$

For a delta function source at the origin, $\bar{S}_0(p)$ is a constant, equal to S_0 say, and the inversion of the above transform is discussed in detail by DAVISON (Chapter V), where it is shown that

$$\psi_0(x) = \frac{S_0l(L^2 - l^2)}{Lc(cL^2 + l^2 - L^2)}e^{-|x|/L} + X(x), \tag{3.11}$$

where L satisifies equation (1.4), and $X(x)$ is a complicated function of x/l and c.

3.4 *Methods of approximation*

It is found that $X(x)$ is of order $e^{-x/l}$ and hence for $c \sim 1$ ($L \geqslant l$) and for $x \geqslant 3l$ this term may be neglected in comparison with the first term in (3.11). This approximation forms the basis of asymptotic diffusion theory since it is readily seen that if we neglect the term $X(x)$ then $\psi_0(x)$ satisfies the diffusion equation

$$D\psi_0''(x) - \frac{(1-c)}{l}\psi_0(x) = -AS_0\,\delta(x), \tag{3.12}$$

with

$$D = (1-c)L^2/l, \tag{3.13}$$

and

$$A = \frac{2(L^2 - l^2)(1-c)}{c(cL^2 + l^2 - L^2)}.$$

For $c \sim 1$, $A \sim 1$ and $D \sim l/3$. It is expected that asymptotic diffusion theory will give reasonably accurate values of $\psi_0(x)$ for all x greater than a few mean free paths as long as the value of c is close to unity. Thus, if we are to obtain a better approximation to $\psi_0(x)$, it seems essential to concentrate on the region near the source and in particular on values of c not close to unity.

Near the source it is expected on physical grounds that the major contribution to the exact $\psi_0(x)$ will come from those neutrons that have yet to have a collision, that is those that come direct from the source. (This contribution may be obtained by solving (3.1), for the case of c being identically zero.) Further, for small c, the neutrons which have still to make a collision will make the major contribution to $\psi_0(x)$ for all x. Thus it seems very probable that if the uncollided neutrons were treated exactly then an approximate treatment of the remaining contribution to $\psi_0(x)$ on the lines of diffusion theory would give reasonable values for $\psi_0(x)$ for all c and all x. Expressed mathematically we write

$$\psi_0(x) = \psi_{0,s}(x) + \psi_{0,d}(x), \tag{3.14}$$

where $\psi_{0,s}(x)$ is the contribution due to those neutrons which have not had a collision. The transform of $\psi_{0,s}(x)$ is obtained from (3.9) by putting $c = 0$ and in this way we find

$$\bar{\psi}_{0,s}(p) = \bar{S}_0lA_{0,0}, \tag{3.15}$$

and

$$\bar{\psi}_{0,d}(p) = \bar{S}_0lcA_{0,0}^2/(1 - cA_{0,0}). \tag{3.16}$$

Using (3.15), or otherwise, it is readily shown for $\bar{S}_0(\rho) = S_0$, that

$$\psi_{0,s}(x) = \frac{S_0}{2}E_1(|x|/l) = \frac{S_0}{2}\int_1^{\infty}e^{-t|x|/l}\frac{dt}{t}. \tag{3.17}$$

The transform $\bar{\psi}_{0,d}$ may also be inverted and written in

the form of (3.11), with a different form for $X(x)$, which is still of order e^{-x}/l, however. Thus if we neglect this correction term, $\psi_{0,d}(x)$ satisfies equation (3.12). We now find that the above method of approximation leads to the result

$$\psi_0(x) = S_0[\tfrac{1}{2}E_1(|x|/l) + Be^{-|x|/L}] \qquad (3.18)$$

where

$$B = Al/2L(1 - c). \qquad (3.19)$$

Although we have neglected the term $X(x)$, we expect the above expression for $\psi_0(x)$ to give much more accurate values than those obtained simply from a solution of (3.12). Before discussing the accuracy of the above solutions we shall discuss some other methods of approximation.

In evaluating the transform given by (3.10) it may be noted that the largest contribution to the integral will arise from values of p about zero, since for large p, $A_{0,0} \approx 1/p$. This suggests that a reasonable approximation to (3.10) may be obtained by replacing $A_{0,0}$ by its expansion near $p = 0$. In this way we find

$$\psi_0(x) = \frac{S_0 l}{2\pi}\int_{-\infty}^{+\infty} \frac{e^{-ipx}\,dp}{(1 - c) + p^2l^2/3}, \qquad (3.20)$$

where we have neglected terms of order p^4. It is readily shown that the above form for ψ_0 satisfies equation (3.12) with

$$D = l/3, \qquad A = 1 \qquad (3.21)$$

so that from (3.13)

$$l^2/L^2 = 3(1 - c).$$

This is in fact the same result as obtained by the so-called P_1 approximation, that is ordinary diffusion theory. Alternatively we may consider the above procedure as a method of obtaining an approximation to $\psi_0(x)$ which has the correct zero and second-order moments.

A better approximation is expected if instead of applying the above method of approximation to $\psi_0(x)$ we apply it to $\psi_{0,d}(x)$ only. In this way we find that $\psi_{0,d}(x)$ again satisfies an equation of the form (3.12) but with

$$D = (2 - c)l/3, \qquad A = c, \qquad (3.22)$$

and $l^2/L^2 = 3(1 - c)/(2 - c)$.

This particular form for the equation defining $\psi_{0,d}(x)$ was first given by GROSJEAN (1956a). This form for $\psi_0(x)$ also has the correct zero order moment (it satisfies the neutron conservation condition), and the correct-second order moment.

It may be noted that the above approximation to $\bar{\psi}_0(p)$ is of order $3S_0/p^2l$ for $p \to \infty$ (cf. equation 3.20), whilst the correct asymptotic form is $S_0\pi/2p$. Whereas, the approximation for $\bar{\psi}_{0,d}$ has the asymptotic form $c3S_0/(2 - c)p^2l$ for $p \to \infty$, whilst the correct form is $cS_0\pi^2/4p^2l$. In the approximation for $\bar{\psi}_{0,d}$ we get the correct dependence on p for $p \to 0$ and $p \to \infty$, although for $p \to \infty$ the coefficients of p^2 are in the ratio of $(2 - c)/3$ to $4/\pi^2$, whilst for $\bar{\psi}_0$ the dependence on p for $p \to \infty$ is different. Thus we expect that the above method of approximation will give more accurate values of $\psi_{0,d}(x)$ than of $\psi_0(x)$. Furthermore for c satisfying the equation

$$\frac{(2 - c)}{3} = 4/\pi^2,$$

that is $c = 0{\cdot}784$, the errors in $\psi_{0,d}(x)$ are expected to be a minimum.

3.5 *Further extensions*

The methods of approximation considered above may be extended to obtain other approximate forms for $\psi_0(x)$. For example we could write

$$\bar{\psi}_0(p) = lS_0\{A_{0,0} + cA_{0,0}^2 + c^2A_{0,0}^3/(1 - cA_{0,0})\}, \qquad (3.23)$$

and treat the first two terms exactly and the third to the diffusion approximation. This however leads to rather a complicated form for $\psi_0(x)$ in that the second term is not easily evaluated. This method bears very close resemblance to the method of multiple scattering which is discussed elsewhere in this article, and the above suggests that the flux calculated using a multiple scattering formalism should be corrected by adding a diffusion-type term which represents an approximation to the higher-order terms usually neglected.

Another possible method of improving the approximation is to retain terms of order p^4 in the expansion for $A_{0,0}$. In fact an expansion of $A_{0,0}$ to order p^4 leads to an equation which is identical to that obtained to the P_3 approximation in the spherical harmonics method. However, as it is found that the approximations already obtained give values of $\psi_0(x)$ correct to within a few per cent it was not thought worthwhile to obtain more accurate but more complicated formula.

Other authors, TRIPLETT (1958) have replaced the kernel of the integral appearing in (3.10) by simple expansions in p^2 and have obtained other approximations for $\psi_0(x)$. In particular there is the approximate formula obtained by RICHARDS (1955). TRIPLETT shows that of all the formulas that he considers, RICHARDS's formula gives the best agreement for the case of a plane source in an infinite medium. However GROSJEAN compares the values of $\psi_0(x)$ obtained by using equation (3.18) with the exact values and also with values obtained by using RICHARDS's method of

approximation and finds that his method of approximation is far superior. In view of these results, the various formula considered in the review article by TRIPLETT will not be considered further in this report.

3.6 *Numerical results*

To compare the various approximations to $\psi_0(x)$ obtained above we have found it desirable to consider cases of $c < 1$ separately from those where $c > 1$.

For $c < 1$ we have considered the percentage difference in the various forms for $\psi_0(x)$ as a function of the distance x/l. The exact values of $\psi_0(x)$ are obtained from the results given by CASE, DE HOFFMANN and PLACZEK (1953). It may be noted that the form for $\psi_0(x)$ as given by (3.18) is exact for $c = 0$. In general the form for $\psi_0(x)$ is given by (3.18) with the value of L and B depending on the value of c and on the method of approximation. For example in the approximation proposed by GROSJEAN, the value of L is given by (3.22),

$$L^2 = \frac{(2-c)}{3(1-c)} l^2, \tag{3.24}$$

and the value of B is given in terms of L and c by (3.19).

The percentage errors in the various approximations to $\psi_0(x)$ have been evaluated for a range of values of c from 0 to 1, and for $c = 0{\cdot}3$ and $0{\cdot}9$ the results are shown in Figs. 3(a) and 3(b). We find that the method of approximation suggested by GROSJEAN gives values of $\psi_0(x)$ for all values of c between 0 and 1 with a maximum error of order 6 per cent. For particular values of c and ranges of x/l other approximations give more accurate results, for example, as $c \to 1$ the flux for $x/l \geqslant 1$ is best represented by equation (3.18) but with B and L calculated using asymptotic diffusion theory. However it is only the GROSJEAN approximation that may be applied universally for all $c < 1$. The results do suggest that even better agreement may be obtained by using a value of L slightly different from that given by (3.24), but in general the possible increase in accuracy does not outweigh the disadvantage of a more complicated form for L.

The accuracy of this simple extension to diffusion theory is somewhat surprising, even more so when it is remembered that an error of less than 6 per cent is found for a range of values of x/l in which the flux decreases by a factor of 10^{-3}.

For $c > 1$ it is most convenient to consider the actual value of the function $\psi_0(x)$. This function is now an oscillatory function of x/l and good agreement of any approximate form with the exact expression is only expected if the period of oscillation is the same. For this reason it is to be expected that the GROSJEAN approximation will not give such good agreement as for $c < 1$. In fact it is found that the GROSJEAN approximation is extremely poor except for $c \leqslant 1{\cdot}3$ and $x/l \leqslant 3$. Very much better agreement is obtained if values of B and L as calculated from asymptotic diffusion theory are used. The above two approximate forms for $\psi_0(x)$ are compared with the exact value for $c = 1{\cdot}1$ and $1{\cdot}5$ in Figs. 3(c) and 3(d) respectively.

Asymptotic diffusion theory gives good agreement with the exact value of $\psi_0(x)$ except for small x. In particular for $x \to 0$, this approximation to $\psi_0(x)$ tends to zero whilst the correct value has a logarithmic singularity at $x = 0$. The method of approximation discussed above shows the correct behaviour as x approaches zero.

It is concluded from the work discussed above that an approximation of the form given by equation (3.18) can be made to give good agreement with the exact value of $\psi_0(x)$ by suitable choice of the constants B and L. For $c < 1$, the values of B and L as given by the GROSJEAN approximation are the best for the range of x/l where $\psi_0(x)$ decreases by a factor of order 10^{-3} from its value at $x/l = 0{\cdot}1$. For $c > 0{\cdot}9$ the best values for B and L are those calculated using asymptotic diffusion theory. However it must be remembered that as $x/l \to \infty$ the exact value of $\psi_0(x)$ approaches the value given by asymptotic diffusion theory so that this form of approximation must be used in any discussion of asymptotic values, that is for large values of x/l.

3.7 *Higher-order components* ($b_n = 0$, $S_n = 0$, $n > 0$)

The transforms of the higher-order components of $\Psi(x,\mu)$ are given by equation (3.8) which may be written in the form

$$\bar{\psi}_n(p) = S_0 l A_{0,n} + S_0 l c\, A_{0,n} A_{0,0}/(1 - c\, A_{0,0}). \tag{3.25}$$

The transform of the first term is readily expressible in terms of the E_n functions. The second term may be treated in a manner similar to the way we obtained $\psi_{0,a}(x)$ in the above, namely expanding it about $p = 0$ and then carrying out the inverse transform. It is found that this term then satisfies an equation of the form (3.12) but with A and D different functions of c depending on the order n. The disadvantage of this method is that the $\psi_n(x)$'s will contain terms of the form $e^{-x/L}$ with L depending on the order n. Further, although the approximation to the second term is made to have the correct dependence on p for $p \to 0$, for $p \to \infty$ it behaves as p^{n-2} whilst the correct dependence is $1/p^2$, so that it is only for $n = 0$ that we have the correct dependence on p for both $p \to 0$ and $p \to \infty$.

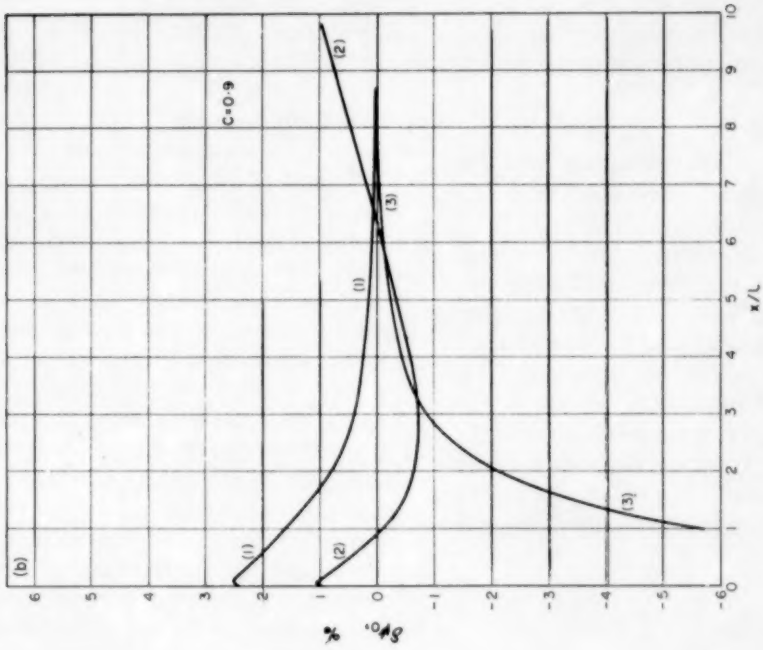

FIG. 3(b).—The percentage error in various approximations to $\psi_0(x)$ for $c = 0{\cdot}9$. The labelling of the graphs is the same as in Fig. 3(a).

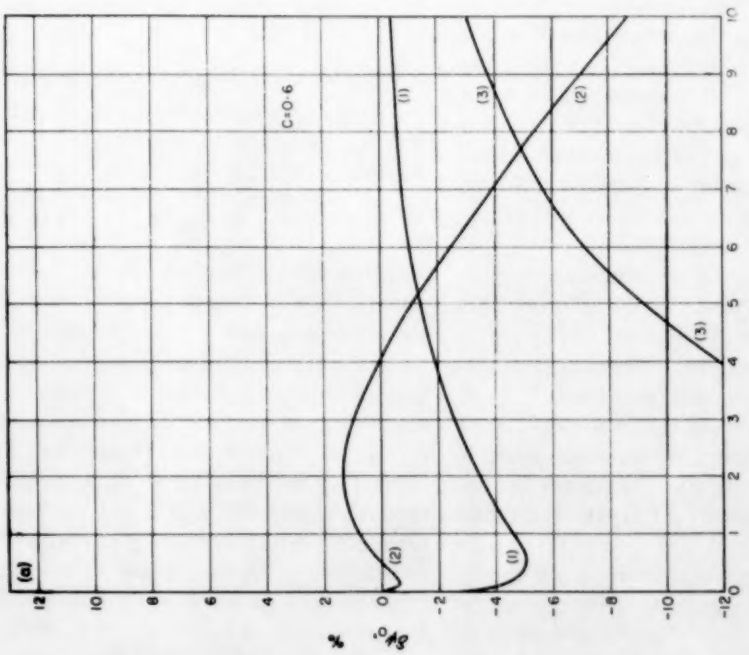

FIG. 3(a).—The percentage error, as a function of x/l, in various approximations to the neutron flux $\psi_0(x)$, for $c = 0{\cdot}6$. For graphs labelled (1) and (2), $\psi_0(x)$ is as given by (3.18) with the following values for B and L:
(1) L given by (1.4) and B by (3.19) with A given by (3.13).
(2) L given by (3.24) and B by (3.19) with $A = c$ (GROSJEAN approximation).
The graph labelled (3) corresponds to asymptotic diffusion theory.

VOL
15
196

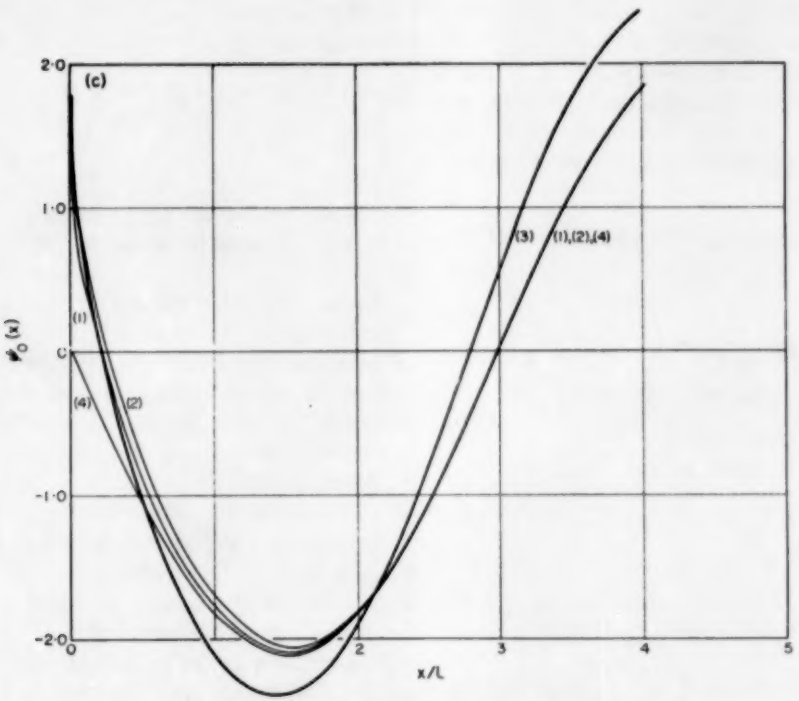

FIG. 3(c).—A plot of the total flux as a function of x/l for $c = 1{\cdot}3$. The exact value is labelled (1), whilst (2) and (3) denote approximations of the form given by (3.18). For (2) L is given by (1.4) and B by (3.19) with A given by (3.13) whilst for (3) (GROSJEAN approximation), L is given by (3.24), B by (3.19) with $A = c$. (4) Denotes the value calculated using asymptotic diffusion theory.

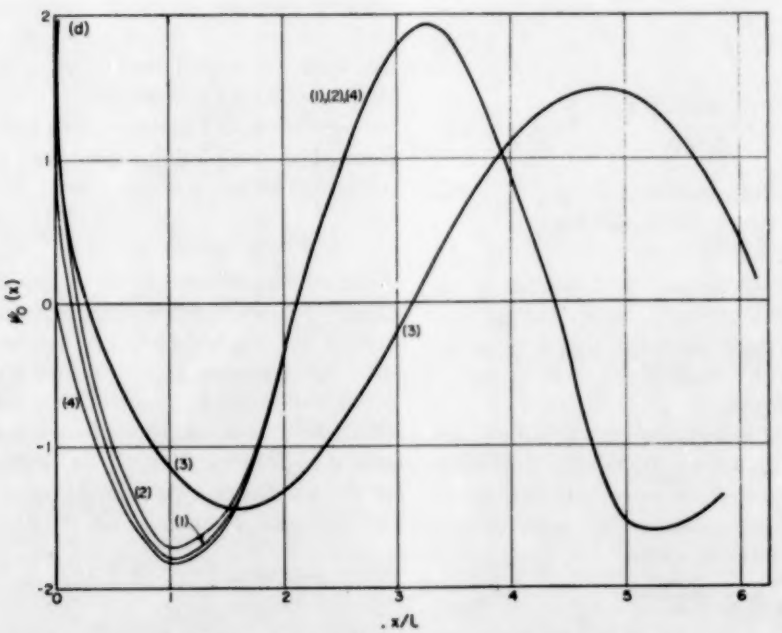

FIG. 3(d).—A plot of $\psi_0(x)$ for $c = 1{\cdot}5$. The labelling is the same as in Fig. 3(c).

A different method of obtaining these higher-order components will now be considered.

It will be noted that if in (3.1) we put $b_n = 0$ for all $n > 0$ and assume $\psi_0(x)$ known, then we have an ordinary first-order differential equation in x for $\Psi(x,\mu)$. In particular if we integrate this equation over all μ we get

$$\psi_1'(x) + \psi_0/l = S_0(x) + c\psi_0(x)/l. \tag{3.26}$$

The solution of this equation is

$$\psi_1(x) = \frac{(1-c)}{l}\int_x^\infty \psi_0(x')\,dx' - \int_x^\infty S_0(x')\,dx', \quad \text{for } \mu > 0,$$
$$= -\frac{(1-c)}{l}\int_{-\infty}^x \psi_0(x')\,dx' + \int_{-\infty}^x S_0(x')\,dx', \quad \text{for } \mu < 0, \tag{3.27}$$

where we have used the condition that $\psi_1 \to 0$ for $|x| \to \infty$. For $S_0(x) = S_0\delta(x)$, the flux $\psi_0(x)$ is a function of $|x|$ only and the above reduces to

$$\psi_1(x) = H(x)\frac{(1-c)}{l}\int_x^\infty \psi_0(x')\,dx', \tag{3.28}$$

for all $x \neq 0$ and where

$$H(x) = +1 \quad \text{for} \quad x > 0,$$
$$= -1 \quad \text{for} \quad x < 0.$$

Substitution of (3.18) into (3.28) gives

$$\psi_1(x) = H(x)(1-c)S_0\left\{\tfrac{1}{2}E_2(|x|/l) + \frac{BL}{l}\,e^{-|x|/L}\right\}. \tag{3.29}$$

This may also be written in the form

$$\psi_1(x) = (1-c)\psi_{1,s}(x) - D\psi_{0,d}'(x), \tag{3.30}$$

where $\psi_{1,s}$ is the uncollided contribution to $\psi_1(x)$. The second term is similar to the expression for the current in ordinary diffusion theory.

GROSJEAN (1956b) has obtained an expression for the current due to a point source in an infinite medium and when this expression is transformed to plane geometry we obtain a value of $\psi_1(x)$ in complete agreement with the above.

To obtain the higher components we multiply equation (3.1), with $b_n = 0$, for $n > 0$, by $P_n(\mu)$ and integrate over all μ. In this way we obtain the recurrence relationship which forms the basis of the spherical harmonics method, namely,

$$(n+1)\psi_{n+1}' + n\psi_{n-1}' + \frac{(2n+1)}{l}\,\psi_n = 0, \tag{3.31}$$

for all $n > 0$. Thus with the knowledge of the two lowest components, $\psi_0(x)$ and $\psi_1(x)$, it is possible to obtain all the higher components. In particular

$$\psi_2(x) = \tfrac{3}{4}(1-c)E_3(|x|/l) - \tfrac{1}{4}E_1(|x|/l) + \frac{B}{2}\left(\frac{3D}{l} - 1\right)e^{-|x|/L} \tag{3.32}$$

The advantage of the above method is that it gives relatively simple expressions for the components of $\Psi(x,\mu)$.

The accuracy of the above approximations for the components $\psi_n(x)$ is difficult to determine without a knowledge of the exact values of the quantities. The authors are unaware of any numerical values of these quantities except of course for $n = 0$. However we may make some estimate of the errors to be expected in the following manner.

If we consider the expression for $\psi_1(x)$ as given by (3.28) we see that the error in $\psi_1(x)$ can be related to the error in $\psi_0(x)$. The errors in the value of $\psi_0(x)$, as given by (3.18), have been discussed in (3.6). From this discussion we may conclude that the errors in the expression for $\psi_1(x)$ as given by (3.29) will, for $c < 1$ and $x/l \leqslant 4$, be less than the error in $\psi_0(x)$ since the errors in $\psi_0(x)$ change sign in the region of $0 < x/l < 4$. For $c < 1$ and $x/l > 4$ the errors will be greater than those in $\psi_0(x)$ if $\psi_0(x)$ is calculated using L given by (3.24). For $c \sim 1$ this error may be reduced by using the value of L calculated from asymptotic diffusion theory. For $c \geqslant 0{\cdot}9$ the largest errors are expected for small values of x/l since it is for such values of x/l that the largest errors appear in $\psi_0(x)$. We may use similar arguments to discuss the errors in the higher components. Thus we conclude that the errors in the components ψ_n calculated using (3.26) and (3.31) are expected to be of the same order as those in the expression for $\psi_0(x)$ as given by (3.18).

3.8 *Anisotropic scattering*

The above analysis may be extended in two distinct ways; (i) to include the effect of anisotropic sources, and (ii), to include the effect of anisotropic scattering. Since the case of an anisotropic source will be treated in the section on 'Finite media' we will not discuss it further here. The inclusion of anisotropic scattering is quite straightforward and if we demand that $\psi_{0,d}(x)$ satisfies a diffusion type of equation of the form given by (3.12) then A equals c and

$$D = \frac{[(2-c) + (1-c)^2 b_1]}{3(1-b_1 c)}\,l. \tag{3.33}$$

It will be noted that D does not depend on b_n for $n > 1$. This is a consequence of demanding that $\psi_{0,d}$ satisfies

VOL 15 196

a diffusion type of equation. Higher-order terms will only appear when higher-order terms of p are retained in the expansion for $\psi_{0,d}(p)$.

3.9 *Finite media—General method*

For the case of the finite media with plane symmetry, the Boltzmann equation is still of the form given by (3.1) but the quantities c, l and b_n are now functions of position. (In what follows we assume isotropic scattering, that is $b_n = 0$ for $n > 0$). In practice these quantities are constant over finite regions but vary discontinuously at the boundary between regions.

The result, which is fundamental to the method of treating finite media as discussed below, is that it is possible to reduce a finite medium problem to a number of infinite medium problems. A discussion of the method of reduction is given by CASE, DE HOFFMANN and PLACZEK (1953, Chapter, V). These authors show that any finite medium problem is equivalent to a number of infinite medium problems in which effective neutron sources take the place of boundary conditions. Thus it seems that the method of approximation discussed in the first part of this section may be used in conjunction with the above result to study finite medium problems. This possibility will be discussed below.

To illustrate the method we consider the problem of determining the flux in two adjacent half-spaces which contain homogeneous material with different values of c and l. That is, $c(x)$ equals c^+, a constant, for $x > 0$ and equals c^- for $x < 0$. A similar convention applies to $l(x)$. The correct flux in these two media we denote by Ψ^+ and Ψ^-. Now consider an infinite homogeneous medium with $c(x) = c^+$, $l(x) = l^+$, throughout, and with any sources in the region $x > 0$, still present but those for $x < 0$ removed. At the surface $x = 0$ introduce a fictitious source equal to $\mu\Psi(0,\mu)$ and let the solution of this infinite medium problem be $\Phi(x,\mu)$. If we impose the condition that $\Phi(x,\mu) \equiv 0$ for $x < 0$ then $\Phi(x,\mu) = \Psi^+$ for all μ and for $x > 0$. For with $\Phi(x,\mu) = 0$ for $x < 0$, the total inward flux ($\mu > 0$) at $x = 0$ must be $\Psi^+(0,\mu)$, that is the contribution from the fictitious source only, and since the value of $\Psi^+(0,\mu)$ for $\mu > 0$ is sufficient to determine uniquely the value of $\Psi(x,\mu)$ for $x > 0$ and all μ, then $\Phi(x,\mu)$, as defined above, must equal $\Psi^+(x,\mu)$ for all $x > 0$.

If the half-space $x < 0$ is a vacuum then $\Psi^+(0,\mu) = 0$ for $\mu < 0$ and this used in conjunction with the above is sufficient to determine $\Psi^+(x,\mu)$. However in general, the above method must be applied separately and successively to each region. A more detailed discussion of this method is given by CASE, DE HOFFMANN and PLACZEK (1953, Chapter V).

The main difficulty in applying the above method is at once apparent. The fictitious source which replaces the boundary condition depends on the solution of the problem, namely $\Psi^+(0,\mu)$, and the above method gives an integral equation for this quantity. If we use an approximate solution of the infinite medium problem then we obtain an integral equation for $\Psi^+(0,\mu)$ with an approximate kernel. Unfortunately this approximate equation is no more easily solved than the exact equation and the solutions when obtained are extremely complicated and not amenable to numerical evaluation. The solution of the Milne problem using the above method is discussed in detail by CASE, DE HOFFMANN and PLACZEK (1953, Chapter V).

Thus the direct application of the approximate solution of the infinite medium problem obtained in the first part of this section leads to a method of solving the finite medium problem which is as complicated as the exact method. Since we are primarily interested in an approximate method it is essential that some further method of approximation be introduced. Further this method must be reasonably simple to apply or else the advantage of having obtained a simple solution of the infinite medium problem is lost. One such method of approximation will be discussed with reference to the Milne problem.

3.10 *Approximate method*

We consider a homogeneous medium occupying the half-space $x > 0$, the half-space $x < 0$ being a vacuum. An isotropic source is present in the positive half-space. Using the result discussed above, we consider the infinite medium problem in which the material that was in the positive half-space extends over all the space and a surface source equal to $\mu\Psi^+(0,\mu)$ is present at $x = 0$. Then

$$\mu\Phi' + \Phi/l = \frac{c}{4\pi l}\,\Phi_0 + S(x) + \mu\Psi^+(0,\mu)\,\delta(x). \tag{3.34}$$

We write

$$\Phi(x,\mu) = R(x,\mu) + T(x,\mu), \tag{3.35}$$

where

$$\mu\,T' + T/l = \mu\Psi^+(0,\mu)\,\delta(x), \tag{3.36}$$

then $R(x,\mu)$ satisfies the equation

$$\mu R' + R/l = \frac{c}{4\pi l}\,R_0 + S(x) + \frac{c}{l}\,\frac{T_0(x)}{4\pi}. \tag{3.37}$$

This is an equation for an isotropic source in an infinite medium and the solution may be written in the form

$$R_0(x) = \int_{-\infty}^{+\infty}\left[\frac{c}{l}\,T_0(x') + S_0(x')\right]G(|x - x'|)\,dx', \tag{3.38}$$

where $G(x)$ is the infinite medium Green's function and is given to a good approximation by (3.18). (The above is exact and if we apply the condition that $\phi_0(x) = 0$ for all $x < 0$ then we obtain an integral equation for $T_0(x)$).

The first step in the approximate method is to write $\Psi^+(0,\mu)$ in parametric form. For example we may write

$$\Psi^+(0,\mu) = \frac{1}{4\pi} \sum_{n=0} A_n \mu^n, \tag{3.39}$$

for $\mu < 0$ and since in this particular example $\Psi^+(0,\mu) = 0$ for $\mu > 0$, the above determines $\Psi^+(0,\mu)$ for all μ. In general the value of $\Psi^+(0,\mu)$ would have to be expressed in parametric form for $\mu > 0$ as well. It is then readily shown that

$$T_0(x) = 0 \quad \text{for} \quad x > 0,$$

$$= -\tfrac{1}{2} \sum_{n=0} (-1)^n A_n E_{n+2}(|x|/l) \quad \text{for} \quad x < 0. \tag{3.40}$$

If this form for $T_0(x)$ is substituted into (3.38) and the approximate form for $G(x)$ as given by (3.18) then used for $x > 0$, then for $S_0(x) = S_0\,\delta(x - \bar{x})$,

$$\phi_0(x) = R_0(x) = S_0 G(|x - \bar{x}|) - \sum_{n=0} (-1)^n A_n M_{n+2}(x), \tag{3.41}$$

with

$$M_n(x) = \frac{c}{2}[\tfrac{1}{2} G_{1n}''(x/l) + B N_n(x/l) e^{-x/L}] \tag{3.42}$$

where

$$N_n(x) = \int_0^\infty E_n(t) e^{-xt}\, dt, \tag{3.43}$$

and

$$G_{1n}''(x) = \int_0^\infty E_1(x + t) E_n(t)\, dt. \tag{3.44}$$

This latter function is considered in detail by KOURGANOFF (1953, Appendix A.1). Somewhat similar expressions to that given above for $\phi_0(x)$ may be obtained for the higher components of $\Phi(x,\mu)$ by the method given in Section 3.7.

Before we can identify $\Phi(x,\mu)$ with $\Psi^+(x,\mu)$ it is necessary to impose the condition that $\Phi(x,\mu) = 0$ for all $x < 0$. However since we have used an approximation to $\Psi^+(0,\mu)$ this condition is too stringent. This suggests that we put $\phi_0(x) = 0$ at the same number of points as there are A_n's rather than for all $x < 0$. However if we take the above equation for $\phi_0(x)$ as an equation for $\psi_0^+(x)$ containing a number of unknown constants then there are a number of ways in which we may determine them. The actual manner will depend to some extent on the problem and on the degree of complexity that can be tolerated. The best procedure for the determination of these constants is, as yet, somewhat arbitrary and further work on this problem is required. Two possible ways of determining these constants are considered below.

3.11 *The Milne problem*

In this case we consider the limit as the real source S_0 tends to infinity, that is $\bar{x} \to \infty$. To determine the constants we demand that the above estimate for $\psi_0^+(x)$ satisfies the exact integral equation, namely

$$\psi_0^+(x) = \frac{c}{2} \int_0^\infty E_1(|x - x'|/l) \psi_0^+(x')\, dx'. \tag{3.45}$$

For simplicity we consider only one constant, A_0, and assume that the expression for $\phi_0(x)$ as given by (3.41) satisfies (3.45) at $x = 0$. Once this constant is determined we have, by identifying $\psi_0^+(x)$ with $\psi_0(x)$ for $x > 0$, a solution of (3.45) for all positive x. An expression for $\psi_1^+(x)$ is readily obtained by using the method given in the first part of this section, and in particular we may calculate $\psi_1^+(0)/\psi_0^+(0)$. Values of this quantity, together with the exact value obtained from CASE, DE HOFFMANN and PLACZEK, are given in Table 3(a).

Another quantity of interest is the extrapolation length x_0. To determine this it is necessary to know the flux in the range $\infty \gg x/l \gg 0$. It was shown in the first part of this section that the best values of B and L to be used in equation (3.18) for small values of x/l were those given by the GROSJEAN method, but for large values of x/l asymptotic diffusion theory gave the best values. Thus in calculating the values of A_0 from the boundary condition we use the GROSJEAN values of B and L, and use the values obtained from asymptotic diffusion in evaluating the flux in the region

$$\infty \gg \frac{x}{l} \gg 0.$$

Values of $x_0 c$ calculated in this manner are given in Table 3(b) together with the exact value obtained from CASE, DE HOFFMANN and PLACZEK.

An alternative condition that may be used to determine A_0 is obtained by demanding that the total inward current at the boundary is zero. This gives the Marshak boundary condition that

$$\int_{-1}^0 \mu \Psi^+(0,\mu)\, d\mu = 0, \tag{3.46}$$

and may readily be expressed as a condition on the components of $\Psi(x,\mu)$. These components may be obtained from the above expression for $\psi_0^+(x)$. The values of ψ_1^+/ψ_0^+ and $x_0 c$ obtained in this way using

VOL 15 196

TABLE 3(a).—VALUES OF $-\psi_1^+(0)/\psi_0^+(0)$ FOR THE MILNE PROBLEM

c	(1)	(2)	(3)	(4)	(5)
0·1	·949	·948	·961	·781	·737
0·3	·839	·836	·876	·719	·725
0·5	·739	·736	·797	·657	·703
0·7	·661	·657	·738	·594	·672
0·9	·602	·594	·690	·531	·648
1·0	·577	·571	·665	·500	·638

TABLE 3(b).—VALUES OF x_0c FOR THE MILNE PROBLEM

c	(1)	(2)	(3)	(4)	(5)
0·1	·854	·861	·729	—	—
0·3	·749	·763	·525	·870	1·095
0·5	·721	·732	·471	·633	·770
0·7	·713	·727	·458	·603	·697
0·9	·710	·730	·469	·625	·603
1·0	·710	·744	0·500	·667	·5

(1) Exact value.
(2) A_0 calculated using (3·45).
(3) A calculated using (3·45).
(4) A calculated using (3·46).
(5) A_0 calculated using (3·46).

VOL. 15 1961

equation (3.46) with terms up to and including $\psi_2^+(0)$ are given in Tables 3(a) and 3(b) respectively.

GROSJEAN (1958a) has suggested that in treating finite medium problems the direct contribution from the fictitious source $T_0(x)$ be neglected, in which case equation (3.41) for $\phi_0(x)$ reduces to

$$\phi_0(x) = S_0 G(|x - \tilde{x}|) - Ae^{-x/L}, \qquad (3.47)$$

where there is only one constant no matter how many constants are taken in the expression for $\mu\Psi^+(0,\mu)$. This constant has been determined using both conditions given above and the values of ψ_1^+/ψ_0^+ and x_0c are given in Tables 3(a) and 3(b) respectively.

CONKIE (1959b) has suggested that the constants in equation (3.41) should be determined using diffusion theory, in which case $A_n = 0$ for $n > 2$. This procedure leads to good values of x_0c for c about 1, but for other values of c is totally inadequate.

In conclusion we see that the method described above with one constant to be determined by an integral condition gives results appropriate to the Milne problem with sufficient accuracy for most purposes. It is expected that for problems where there are real sources near the boundary the errors involved in applying the above methods will be much less than those in the Milne problem since a large contribution to the flux will come from the real source. That this is so is seen from a discussion of the following problem.

3.12 *The albedo for a half-space*

In this case a real source is situated in the half-space $x < 0$ and emits neutrons which enter the media at $x = 0$. The albedo is the ratio of the neutron current returning across the plane $x = 0$ to that entering this plane. It is seen that the above method may be extended to deal with this case.

However, GROSJEAN (1958b) has discussed this problem and taken the flux to be given by equation (3.47), but with the first term now representing the contribution from the real source at the boundary. The constant A was determined using the condition given by (3.46). In this way GROSJEAN found that the value of the albedo is given correct to within 2 per cent for all values of c less than 1 if he includes the $\psi_2^+(0)$ term in satisfying equation (3.46). Neglect of this term introduces errors of order 10 per cent.

GROSJEAN also considered the transmission of neutrons through a plane homogeneous slab of finite thickness. In this case, fictitious boundary sources must be introduced at both boundaries but otherwise this problem is basically the same as the one above. A solution for all c is obtained but only in the case of $c = 1$ are the errors discussed. Good agreement is obtained except where the incident neutrons direction is nearly parallel to the face of the slab in which case errors of at most 10 per cent are found.

3.13 *Summary and conclusions*

Approximate methods for the solution of the Boltzmann equation in an infinite media have been discussed in the first part of this section. The results are summarized at the end of (3.6). In the second part of this section a method for the solution of the Boltzmann equation in finite media has been discussed. The method requires the introduction of a subsidiary condition on the solution of an infinite medium problem, and two distinct conditions have been considered in some detail.

These conditions are not the only ones and are not necessarily the best. In fact the question of which is the best type of condition to use remains to some extent unanswered. The best type of condition to use depends on the accuracy required and on the complexity that can be tolerated.

The above results do suggest that in problems where the real sources are at a large distance from the boundaries then it seems essential to include the direct contribution to the flux from the fictitious boundary sources.

Although the discussion throughout this section has been confined to simple problems in plane geometry,

the method should be applicable to more complicated problems and to other geometries.

4. MULTIPLE SCATTERING METHODS

4.1 *Introduction*

We have seen that the CARLSON and discrete ordinate methods for solving the transport equation involve an iteration on c, the ratio of scattering to total cross section, and thus multiple scattering processes are implicit in their use. Again the GROSJEAN method, described in Section 3, separates out the unscattered flux and approximates the scattered flux by diffusion theory. In this section, we discuss the formal process of expanding the flux in a series in c (STUART, 1958).

The one-velocity integral equation is

$$\rho(\mathbf{r}) = \int K(\mathbf{r}-\mathbf{r}')\left\{S(\mathbf{r}') + \frac{c}{4\pi l}\rho(\mathbf{r}')\right\} dV'. \quad (4.1)$$

This equation may be expanded into a Neumann-Liouville series by repeated iterations:

$$\rho(\mathbf{r}) = \sum_{n=0} c^n \rho_n(\mathbf{r}), \quad (4.2)$$

where

$$\rho_0(\mathbf{r}) = \int K(\mathbf{r}-\mathbf{r}')S(\mathbf{r}')\, dV', \quad (4.3)$$

and

$$\rho_n(\mathbf{r}) = \frac{1}{4\pi l}\int K(\mathbf{r}-\mathbf{r}')\,\rho_{n-1}(\mathbf{r}')\, dV' \text{ for } n > 0. \quad (4.4)$$

$c^n\rho_n(\mathbf{r})$ is the neutron flux for neutrons which have had n scattering collisions.

The main use of this type of solution is for treating small strongly absorbing bodies surrounded by large weakly absorbing media. Diffusion theory may be used in the medium provided the small absorbing body is replaced by an appropriate boundary condition given in equation (4.17) below. Alternatively, it is possible to define effective cross sections in the small absorber so that diffusion theory may be used inside the absorber as well as in the medium. This procedure is discussed in Subsection (4.3).

4.2 *Theory*

We first assume a plausible form for the angular distribution of neutrons incident on the body. An isotropic distribution is often used but other terms with (cosine)^m dependence may be added. STUART and WOODRUFF (1958) have suggested using the diffusion theory form for the incident flux at the surface of the body

$$\Psi(\mathbf{r}_s,\boldsymbol{\Omega}) = \frac{1}{4\pi}(\rho(\mathbf{r}_s) + 3D_0\boldsymbol{\Omega}\,.\,\nabla\rho(\mathbf{r}_s)), \quad (4.5)$$

where D_0 is the diffusion constant of the surrounding media, pointing out that this distribution is a good approximation for the extreme case of the exit neutron distribution from an infinite half-space. For many applications it is unnecessary to know the detailed variation of $\rho_n(\mathbf{r})$ with $\mathbf{r}$. Instead we define the collision probability, P_n as the probability that a neutron which has suffered n collisions in the body will suffer at least one more collision therein. This definition gives immediately that

$$P_0 = \frac{\frac{1}{l}\int_v \rho_0(\mathbf{r})\, dV}{\int_s\int^{+}\Psi(\mathbf{r}_s,\boldsymbol{\Omega})\, d\Omega\, ds,} \quad (4.6)$$

and

$$P_n = \int_v \rho_n(\mathbf{r})\, dV \Big/ \int_v \rho_{n-1}(\mathbf{r})\, dV, \quad n > 0 \quad (4.7)$$

where $\int^+$ denotes integration over neutrons moving into the body.

STUART and WOODRUFF have tabulated $\rho_n(\mathbf{r})$ and P_n for infinite cylindrical rods for a range of radii. They considered separately the flux and current components of the incident flux of equation (4.5) and thus tabulate $\rho_{n,m}(\mathbf{r})$ and $P_{n,m}$ where $m = 1$ refers to the isotropic flux component and $m = 2$ refers to the current component. We give their values of $P_{n,m}$ in Table 4(a). The last column in this table, P_c, is the probability that neutrons born uniformly in the rod will have a collision in the rod. It can be shown (CASE, DE HOFFMANN and PLACZEK 1953, Chapter 2) that P_c is simply related to $P_{0,1}$ by

$$P_{0,1} = \frac{2R}{l}(1 - P_c), \quad (4.8)$$

where R is the radius of the rod. From the definition of $P_{n,m}$, the probability that an incident neutron originating from a (cosine)^m source is absorbed in the rod is

$$\beta_m = (1-c)\sum_{n=0} c^n P_{n,m}\, P_{n-1,m} \ldots P_{0,m}. \quad (4.9)$$

If the incident current is evaluated by using (4.5), that is

$$J^{\text{in}} = \rho_s/4 + J_s/2, \quad (4.10)$$

where the suffix S denotes the value at the surface and $J_s = -D_0\,|\text{grad}\,\rho_s|$, then the total probability of absorption in the rod, the blackness β, is

$$\beta = (\beta_1\rho_s/4 + \beta_2 J_s/2)\Big/\left(\frac{\rho_s}{4} + \frac{J_s}{2}\right). \quad (4.11)$$

TABLE 4(a).—COLLISION PROBABILITIES IN INFINITE CYLINDERS, RADIUS R

R/l	$P_{0,1}$	$P_{0,2}$	$P_{1,1}$	$P_{1,2}$	$P_{2,1}$	$P_{2,2}$	$P_{3,1}$	$P_{4,1}$	$P_{5,1}$	P_e
0·5	·5960	·6075	·3977	·4060	·4111	·4140	·4154	·4169	·4175	·4040
0·6	·6574	·6709	·4432	·4531	·4598	·4633	·4653	·4674	·4682	·4522
0·7	·7081	·7231	·4823	·4935	·5020	·5062	·5088	·5115	·5126	·4943
0·8	·7502	·7663	·5158	·5284	·5387	·5435	·5469	·5503	·5517	·5313
0·9	·7853	·8021	·5499	·5587	·5708	·5762	·5804	·5845	·5863	·5639
1·0	·8146	·8318	·5700	·5849	·5989	·6049	·6100	·6148	·6170	·5928
1·1	·8393	·8566	·5919	·6077	·6236	·6302	·6361	·6417	·6443	·6187
1·2	·8601	·8774	·6109	·6276	·6453	·6524	·6592	·6657	·6687	·6418
1·3	·8777	·8948	·6275	·6450	·6645	·6721	·6798	·6870	·6906	·6626
1·4	·8927	·9094	·6421	·6801	·6814	·6895	·6981	·7062	·7103	·6814
1·5	·9055	·9218	·6548	·6735	·6964	·7049	·7144	·7233	·7279	·6984
1·6	·9164	·9323	·6660	·6851	·7097	·7186	·7289	·7386	·7438	·7139
1·7	·9258	·9412	·6759	·6953	·7215	·7307	·7419	·7524	·7581	·7280
1·8	·9338	·9487	·6845	·7049	·7320	·7415	·7535	·7648	·7711	·7409
1·9	·9408	·9552	·6922	·7117	·7414	·7511	·7639	·7760	·7828	·7527
2·0	·9468	·9608	·6991	·7197	·7497	·7597	·7732	·7860	·7933	·7636

TABLE 4(b).—COLLISION PROBABILITY FOR SLAB, THICKNESS t

t/l	P_e
0	0·0000
0·1	·1629
0·2	·2597
0·3	·3335
0·4	·3932
0·5	·4432
0·6	·4859
0·7	·5229
0·8	·5554
0·9	·5841
1·0	·6097
1·1	0·6326
1·2	0·6533
1·3	0·6720
1·4	0·6890
1·5	0·7045
1·6	0·7187
1·7	0·7317
1·8	0·7437
1·9	0·7548
2·0	0·7651

If we make the additional assumption that the rod exit neutron distribution also has the functional form of diffusion theory, then

$$J^{\text{out}} = \rho_s/4 - J_s/2. \tag{4.12}$$

Since

$$\beta = (J^{\text{in}} - J^{\text{out}})/J^{\text{in}}, \tag{4.13}$$

we have

$$J_s = \frac{\rho_s}{2} \cdot \frac{\beta}{2-\beta}, \tag{4.14}$$

and

$$\beta = \frac{\beta_1 + \dfrac{\beta}{2-\beta} \cdot \beta_2}{1 + \dfrac{\beta}{2-\beta}},$$

or

$$\beta = \frac{\beta_1}{1 + (\beta_1 - \beta_2)/2}. \tag{4.15}$$

It is clear from Table 4(b) that $P_{n,2}$ is never very different from $P_{n,1}$ and hence $(\beta_1 - \beta_2)$ is small and $\beta \approx \beta_1$. This explains why the assumption of isotropic incident flux may give a good approximation to β, even when the assumption is obviously invalid.

With the assumptions (4.10) and (4.12), we may express the disadvantage factor, F, of the rod, and the linear extrapolation length, λ, at the rod surface in terms of the blackness, β. We have

$$F = \frac{\rho_s}{\langle \rho \rangle} = \frac{\Sigma_a R \rho_s}{2J_s} = \Sigma_a R \left(\frac{2-\beta}{\beta} \right), \tag{4.16}$$

and

$$\lambda = \frac{\rho_s}{\rho_s'} = \frac{D_0 \rho_s}{J_s} = \frac{l_0}{3} \left(\frac{2-\beta}{\beta} \right). \tag{4.17}$$

Thus β, F and λ can be determined from β_1 and β_2, which are given by the infinite series (4.9). It is clear from Table 4(a) that $P_{n,m}$ rapidly approaches an asymptotic value as n increases. If we take $P_{n,m} = P_{\infty,m}$ for all $n > k$, then the infinite series for $n > k$ is a geometric series and can be summed.

Examination of Table 4(a) suggests that a good approximation to β should be obtained by assuming an isotropic incident flux ($P_{n,m} = P_{n,1}$) and taking

$P_n = P_e$ for all $n > 0$. This is equivalent to assuming that the scattered flux is uniform across the rod. We now obtain

$$\beta = \frac{(1-c)P_{0,1}}{1-cP_e}. \tag{4.18}$$

Since $P_{0,1}$ is related to P_e by equation (4.8), β is now expressed entirely in terms of P_e. STUART (1957) shows that equation (4.18) is in fact very accurate for $R < l$, or $c \ll 1$. These are of course just the conditions under which we should expect the multiple scattering technique to be useful. If $c \ll 1$, then the series (4.2) converges rapidly, whilst if the body is small, the probability of a collision occurring in it is small.

Equation (4.18) for the blackness is applicable to bodies of any shape. All that is required is a calculation of P_e. Then $P_{0,1}$ is related to P_e by

$$P_{0,1} = \frac{4V}{Sl}(1-P_e), \tag{4.19}$$

where V is the volume and S the total surface area $1 - P_e$ is also equal to the self-shielding factor, f, when the body is immersed in a uniform flux. Tables of P_e for slabs, spheres and cylinders are given by CASE, DE HOFFMANN and PLACZEK (1953), whilst DWORK *et al.*, (1955) and JEWITT and BARDEN (1958) have given curves of f for hollow cylinders. DRESNER (1959, 1960) has derived certain inequalities which permit the estimation of P_e for convex solids of irregular shape by comparison with regular solids for which P_e is known.

4.3 *Application to thin regions*

WACHSPRESS (1958) has used equation (4.18) to show that by a suitable modification of cross sections it is possible to apply diffusion theory to a thin slab. From (4.18), the escape probability E is given by

$$E = 1 - \beta = 1 - \frac{(1-c)P_{0,1}}{1-cP_e}. \tag{4.20}$$

P_e is given as a function of t/l, where t is the slab thickness, in Table 4(b). $P_{0,1}$ is related to P_e by equation (4.19) with $V/S = t/2$. The probability of escaping without a collision is $E_0 = 1 - P_0$. Since we are assuming isotropic scattering in the slab, the reflection probability is given by

$$R = \tfrac{1}{2}(E - E_0) = \frac{cP_0}{2}\left(\frac{1-P_e}{1-cP_e}\right), \tag{4.21}$$

and the transmission probability

$$T = E - R = (1-P_0) + \frac{cP_0}{2}\cdot\left(\frac{1-P_e}{1-cP_e}\right). \tag{4.22}$$

Denote the two surfaces of the slab by suffices 1 and 2. Then with a uniform source density S in the slab we have

$$\begin{aligned} J_2^{\text{out}} &= TJ_1^{\text{in}} + RJ_2^{\text{in}} + \frac{E}{2}St, \\ J_1^{\text{out}} &= TJ_2^{\text{in}} + RJ_1^{\text{in}} + \frac{E}{2}St, \end{aligned} \tag{4.23}$$

and the assumptions (4.10) and (4.12) then give

$$\begin{aligned} J_1 &= \gamma\rho_1 - \varepsilon\rho_2/4 - \alpha St/2, \\ J_2 &= -\gamma\rho_2 + \varepsilon\rho_1/4 + \alpha St/2, \end{aligned} \tag{4.24}$$

where

$$\begin{aligned} \gamma &= \tfrac{1}{2}\frac{(1+T^2-R^2)}{(1+R)^2-T^2}, \\ \varepsilon &= \frac{4T}{(1+R)^2-T^2}, \\ \alpha &= 2E/(1+E). \end{aligned} \tag{4.25}$$

Putting $J_n = -D\nabla\rho_n$ in (4.24) gives

$$-D(\nabla\rho_2 - \nabla\rho_1) + (2\gamma - \varepsilon/2)\left(\frac{\rho_1+\rho_2}{2}\right) = \alpha St. \tag{4.26}$$

Now the finite difference form of the diffusion equation with mesh length t is

$$-D(\nabla\rho_2 - \nabla\rho_1) + \Sigma_a\left(\frac{\rho_1+\rho_2}{2}\right)t = St. \tag{4.27}$$

Equation (4.26) has the form (4.27) if we define an effective source

$$S_{\text{eff}} = \alpha S, \tag{4.28}$$

and an effective cross section

$$\begin{aligned} \Sigma_{a,\text{eff}} &= \frac{1}{t}\left(2\gamma - \frac{\varepsilon}{2}\right), \\ &= \frac{\Sigma_a}{\dfrac{1-cP_e}{1-P_e} - \Sigma_a t}. \end{aligned} \tag{4.29}$$

WACHSPRESS actually compares his equations with a finite difference form of the diffusion length with mesh length $\frac{1}{2}t$. By taking the finite difference approximation to $\nabla\phi\rho$ at the centre of the slab to be $(\rho_2 - \rho_1)/t$, he deduces an effective diffusion coefficient to be used in the slab

$$D_{\text{eff}} = \frac{t\varepsilon}{4}. \tag{4.30}$$

The use of equations (4.28), (4.29) and (4.30) enables

diffusion theory to be used satisfactorily even for strongly absorbing slabs. For a black thin slab, WACHSPRESS shows that the equations are equivalent to using an extrapolation length at the slab surface of $2/3\ l$ in place of the exact value of $0{\cdot}71\ l$.

Acknowledgment—The authors would like to thank MR. J. CODD for his helpful suggestions during the writing of this article.

REFERENCES

ANDERSON B. L., DAVIS J. A., GELBARD E. M. and JARVIS P. H. (1959) WAPD–TM–134.

ASPELUND O. (1958) *Proceedings of the Second International Conference on the Peaceful Uses of Atomic Energy, Geneva*, P/573. United Nations, N.Y.

BARREISS E. H. (1958) *Proceedings of the Second International Conference on the Peaceful Uses of Atomic Energy, Geneva*, P/639. United Nations, N.Y.

BLUE E. and FLATT H. P. (1960) *Nucl. Sci. Engng.* **7**, 127.

CARLSON B. G. and BELL G. I. (1958) *Proceedings of the Second International Conference on the Peaceful Uses of Atomic Energy, Geneva*, P/2386. United Nations, N.Y.

CASE K. M., DE HOFFMANN F. and PLACZEK G. (1953) *Introduction to the Theory of Neutron Diffusion*—I. Los Alamos Scientific Laboratory.

CONKIE W. R. (1959a) *Nucl. Sci. Engng.* **6**, 260.

CONKIE W. R. (1959b) *Nucl. Sci. Engng.* **6**, 267.

DAVIS J., GELBARD E. and PEARSON J. (1959) *Nucl. Sci. Engng.* **6**, 251.

DAVISON B. (1957) *Neutron Transport Theory*, O.U.P.

DRAWBAUGH D. W. and NODERER L. C. (1959) *Nucl. Sci. Engng.* **6**, 79.

DRESNER L. (1959) *Nucl. Sci. Engng.* **6**, 63.

DRESNER L. (1960) *Nucl. Sci. Engng.* **7**, 260.

DWORK J., HOFMAN P. L., HURWITZ H. JR. and CLANCY E. F. (1955) KAPL-1262.

GELBARD E., DAVIS J. and PEARSON J. (1959) *Nucl. Sci. Engng.* **5**, 36.

GOERTZEL G. (1958) *Nucl. Sci. Engng.* **4**, 581.

GROSJEAN C. C. (1956a) *Nuovo Cimento* **3**, 1262.

GROSJEAN C. C. (1956b) *Nuovo Cimento* **4**, 582.

GROSJEAN C. C. (1958a) *Proceedings of the Second International Conference on the Peaceful Uses of Atomic Energy, Geneva*, P/1691. United Nations, N.Y.

GROSJEAN C. C. (1958b) *Proceedings of the Second International Conference on the Peaceful Uses of Atomic Energy, Geneva*, P/1692. United Nations, N.Y.

JEWITT P. A. and BARDEN S. E. (1958) *J. Nucl. Energy* **7**, 222.

KOPPE H. and BLASSER G. (1958) *Nukleonik* **1**, 64.

KOURGANOFF V. (1952) *Basic Methods in Transfer Problems*, O.U.P.

NATHER V. and SANGREN W. (1959) *Commun. Assoc. Comp. Mach.* **2**, 6; (1960) *ibid.* **3**, 1.

RICHARDS P. I. (1955) *Phys. Rev.* **100**, 517.

SCHIFF D. and ZIERING S. (1960) *Nucl. Sci. Engng.* **7**, 172.

STUART G. W. (1957) *Nucl. Sci. Engng.* **2**, 617.

STUART G. W. (1958) *Proceedings of the Second International Conference on the Peaceful Uses of Atomic Energy, Geneva*, P/624. United Nations, N.Y.

STUART G. W. and WOODRUFF R. W. (1958) *Nucl. Sci. Engng.* **3**, 399.

SYKES J. B. (1951) *Roy. astr. Soc.* (Monthly Not.) **111**, 377.

TRIPLETT J. R. (1958) *Proceedings of the Second International Conference on the Peaceful Uses of Atomic Energy, Geneva*, P/1869. United Nations, N.Y.

WACHSPRESS E. L. (1957) *Nucl. Sci. Engng.* **3**, 186.

YVON J. (1957) *J. Nucl. Energy* **4**, 305.

ZIERING S. and SCHIFF D. (1958) *Nucl. Sci. Engng.* **3**, 635.

VOL. 15 1961

Reactor Science and Technology (Journal of Nuclear Energy, Parts A/B), 1961, Vol. 15, pp. 22 to 27. Pergamon Press Ltd. Printed in Northern Ireland

THE ESTABLISHMENT OF AN ABSOLUTELY CALIBRATED NEUTRON SOURCE

E. J. AXTON and P. CROSS
Applied Physics Division, National Physical Laboratory, Teddington, Middx.

(*Received* 16 *September* 1960)

Abstract—A 400 mc Ra–Be photoneutron source has been adopted as the national standard source. It has been calibrated by the method of absolute determination of ^{56}Mn produced in the ^{55}Mn (n,γ) ^{56}Mn reaction. The calibration agrees within 1 per cent with an international average. The standard error is ± 1 per cent. The error is mainly due to the uncertainty in the knowledge of the manganese and hydrogen thermal neutron capture cross sections. In addition there may be a systematic error not exceeding 1·0 per cent associated with $4\pi\beta$ proportional counting.

1. INTRODUCTION

CURRENT methods of absolute calibration of neutron sources, and the present status of absolute comparisons, have been adequately described in recent literature (RICHMOND, 1958; LARSSON, 1958). To set up a reliable British standard a 400 mc Ra–Be (γ,n) source, nominal output $1{\cdot}7 \times 10^5$ n/sec has been adopted. Initially, the source is to be calibrated by two independent methods. (a) The helium generated in the source by the ^{9}Be (γ,n)2^{4}He reaction is extracted and measured, and gives directly the total number of neutrons emitted by the source during the period of the irradiation. The method was originally proposed by GLÜCKAUF and PANETH (1938) and has been described by MARTIN and MARTIN (1954) who initiated the present work and will be responsible for the helium determination. Six sources were prepared of which three are to be dissolved when a measurable quantity of helium has accumulated. (b) The ^{56}Mn produced by the ^{55}Mn (n,γ) ^{56}Mn reaction in the well-known manganese bath experiment is determined absolutely (O'NEAL and SCHARFF-GOLDHABER, 1946; ALDER and HUBER, 1949; DE JUREN and CHIN, 1955; GEIGER and WHYTE, 1959).

The present paper describes the calibration, by the latter method, of the N.P.L. sources and the 200 mc Ra–Be (α,n) source of the National Research Council of Canada.

2. DESCRIPTION OF SOURCES

The six photoneutron sources are designated 4*A*, 4*N*, 3*B*, 3*M*, 2*C*, 2*L*. The number refers to the particular 400 mc radium source and the letter to the beryllium capsule. The average dimensions of the nominally identical beryllium cylinders are: diameter 1·50 cm, height 2·45 cm, wall thickness and base and lid thickness 0·40 cm. *L*, *M*, *N* are to be dissolved for the helium measurement. The 200 mc Ra–Be (α,n) source of the N.R.C. Ottawa has been described by GEIGER (1959).

3. PRINCIPLE OF METHOD

The method is based on the thermalization and capture of neutrons in an aqueous solution of manganese sulphate and the subsequent determination (based on $4\pi\beta$ proportional counting) of the absolute disintegration rate of the resulting ^{56}Mn. In the ideal case, i.e. in an infinite volume of solution, irradiated by a point source of neutrons situated at the centre, in which all the capture cross sections vary inversely as the neutron velocity ($\propto 1/v$) and in the absence of fast neutron capture processes, the fraction, f, of neutrons captured by manganese would be given by

$$f = \frac{C_{Mn}\sigma_{Mn}}{C_{Mn}(\sigma_{Mn} + \sigma_S) + C_H\sigma_H} = \frac{1}{1 + \dfrac{\sigma_S}{\sigma_{Mn}} + \dfrac{C_H \cdot \sigma_H}{C_{Mn}\,\sigma_{Mn}}}$$

where C_{Mn} and C_H are the concentrations of manganese and hydrogen nuclei per unit volume of solution, and σ_{Mn}, σ_S and σ_H are the manganese, sulphur and hydrogen thermal neutron capture cross sections respectively. At equilibrium the ^{56}Mn disintegration rate becomes equal to the rate of neutron capture by ^{55}Mn, after which the solution is thoroughly stirred and a sample is removed for dip-counting. The neutron emission rate, Q, of the source is then given by

$$Q = \frac{N_{Mn}\,V \times 3{\cdot}7 \times 10^4}{f\varepsilon}$$

where N_{Mn} is the number of events per second recorded

by the counters, ε is the efficiency of the counters in counts/second per microcurie of ^{56}Mn activity per litre of solution and V is the total volume in litres of the solution irradiated. To obtain ε, a sample of ^{56}Mn in a solution of high specific activity is standardized by absolute β-particle counting with a 4π proportional counter. Concurrently an aliquot of the same solution is stirred into the inactive moderating solution, which is then dip-counted in the normal way.

In practice it is necessary to make corrections for the following effects: resonance capture of neutrons by manganese; self-absorption of β-particles by the sources used for 4π counting; neutron capture in the source and source mounting; escape of neutrons from the boundaries of the solution due to the finite size of the tank; fast neutron capture in oxygen and sulphur.

4. APPARATUS AND PROCEDURE

For the (γ,n) sources the solution was contained in a spherical glass vessel of internal diameter 49·85 cm. The volume, 64·86 litres, was obtained by reference to a calibrated 10 litre flask. The level of the solution was adjusted daily to a datum line which was itself adjusted to allow for the change in volume of the vessel due to fluctuations of ambient temperature. The volume of irradiated solution was thus maintained constant to within $\pm$0·05 per cent. For the α,n source a similar procedure was adopted using a spherical stainless steel vessel 97·94 cm in internal diameter, 491·91 litres in volume. Each source was mounted in a thin polystyrene cup at the centre of a thin, water-tight, spherical polystyrene container 8·9 cm in diameter. The container was held at the centre of the tank by means of a thin Terylene thread passing through a rubber bung at the base of the tank. Positioning was achieved to within $\pm$1 mm by means of a depth gauge. Each irradiation was continued for about 16 hr after which the solution was stirred thoroughly and a sample removed for dip-counting. The counting assembly, housed in a four inch thick lead castle, consisted of five thin-walled G.M. counters type B24 immersed in the solution. A paralysis time of 400 $\pm$15 μ sec was imposed. The rate of decay of the ^{56}Mn was in accordance with the published half-life of 2·586 $\pm$0·005 hours (BISHOP, WILSON and HALBAN, 1950). Corrections were applied for dead-time losses, for background effects, for radioactive decay and for the finite duration of the irradiation. Corrected count rates of about 50 c/s were obtained with the (γ,n) sources, and 130 c/s with the (α,n) source. The background counting rate, obtained with the counters immersed in inactive solution of the same strength, remained fairly constant at about 2 c/s.

A few percent of the neutrons emitted by each photoneutron source are produced by α-particle bombardment of the materials comprising the radium source itself. As these neutrons will not enter into the helium determination, their contribution must be separately measured and deducted in each case in order that the two measurements may be correlated.

The ratio C_H/C_{Mn} was obtained by heating to constant weight, at 300°C, a weighed quantity of the solution. This measurement was carried out regularly throughout the calibration, giving $C_H/C_{Mn} = 31{\cdot}07 \pm 0{\cdot}03$ for the solution in the large sphere, and $C_H/C_{Mn} = 30{\cdot}85 \pm 0{\cdot}03$ for the solution in the small sphere.

Published values were adopted for the thermal neutron capture cross sections:

σ_H	0·332 $\pm$ 0·002 barns,	HUGHES and SCHWARTZ (1957)
σ_S	0·49 $\pm$ 0·02 barns,	HUGHES and HARVEY (1955)
σ_{Mn}	13·25 $\pm$ 0·2 barns.	

The manganese cross section is a weighted mean of the values given by HUGHES and HARVEY (1955), DE JUREN and CHIN (1955), CUMMINS and SPURWAY (1957).

5. DETERMINATION OF ε

Pile irradiated $MnSO_4$ was obtained from AERE Harwell in the form of an aqueous solution containing 100 μg $MnSO_4$ per gramme of water. Six samples were prepared by evaporating between 30 and 100 mg of the solution on to VYNS film 10 μg per cm^2 in thickness rendered conducting with evaporated gold 10 μg per cm^2 in thickness. The 4π counter is similar in design to that of HAWKINGS *et al.* (1952) and has been described by PERRY (1957).

For each source the voltage plateau was found to be flat within the statistical accuracy of the counting ($\pm$0·2 per cent) over the range 1·7 to 2·0 kV.

A figure of 19·25 $\pm$ 0·05 μc/g was obtained for the specific activity of the solution at the start of the measurements. Concurrently, appropriate quantities of the solution were added to the solution in the two tanks which were then thoroughly stirred before samples were removed for dip-counting in the normal way. No significant difference was observed between the counter sensitivities as determined with the solution from the two tanks, and a weighted mean of all measurements gave a value of $(2{\cdot}595 \pm 0{\cdot}003) \times 10^4$ c/s per gramme of active solution added per litre of tank solution. Hence $\varepsilon = (1{\cdot}348 \pm 0{\cdot}004) \times 10^3$ c/s per μc/litre. Later, the standardization was repeated, giving $\varepsilon = (1{\cdot}346 \pm 0{\cdot}003) \times 10^3$ c/s per

μc/litre. As the value of N_{Mn} for any given source also remained constant within the statistical limits over the period of the work, the efficiency of the counters was assumed to remain constant at $(1{\cdot}347 \pm 0{\cdot}003) \times 10^3$ c/s per μc/litre.

6. CORRECTIONS NECESSARY TO DETERMINE THE ABSOLUTE NEUTRON YIELD

6.1. *Resonance neutron capture in manganese*

Due to resonances in the capture cross section versus energy curve, manganese captures slightly more neutrons than would an ideal absorber $\left(\sigma\alpha\frac{1}{v}\right)$ with the same capture cross section for thermal neutrons. With the method of DE JUREN and CHIN (1955) it can be shown that, for the chemical concentration used here, σ_{Mn} in equation (1) should be increased by 1·9 per cent with a standard error of $\pm 0{\cdot}5$.

6.2. *Systematic errors associated with 4π-counting*

As is well known, the major sources of systematic error associated with the 4π-counter are (1) the uncertainty of the source self-absorption of β-particles, (2) the uncertainty of the paralysis time (3) the limit of sensitivity of the counter.

6.2.1. *Self-absorption of sources prepared for 4π β-counting.* The mass of solid $MnSO_4$ comprising the sources was varied from about 3 μg to 10 μg in order to determine whether more self-absorption was apparent with the thicker sources. However, careful measurements of magnified optical projections of the sources revealed that the average thickness of the sources was substantially uniform at about $0{\cdot}75 \pm 0{\cdot}2$ mg/cm^2, on the assumption that the salt crystallized out as $MnSO_4{\cdot}4H_2O$. The problem of computing accurately the average thickness of crystal which the β-particles are required to penetrate, and the fraction of the β-particles which are stopped in that thickness of absorber, is necessarily complex. As the correction is in any case small it can be assumed with sufficient accuracy for the present purposes that the average thickness of absorber penetrated is half the total thickness, viz. 0·375 mg/cm^2; estimates of the absorption correction can then be obtained in a number of ways:

(a) The maximum energies, and the branching ratios of the ^{56}Mn decay scheme obtained by ELLIOT and DEUTSCH (1943) are: 2·86 MeV, 60 per cent; 1·05 MeV, 25 per cent; 0·73 MeV 15 per cent; and the spectra shapes correspond with the allowed shape predicted by the Fermi β-decay theory. This is substantiated theoretically by the evidence of the nuclear spin change: $\Delta J = 1$, no change of parity; (STROMINGER, HOLLANDER and SEABORG, 1958). The energy spectrum of the β-particles is now plotted assuming the allowed shape, and those particles whose range in $MnSO_4$ crystals is less than 0·375 mg/cm^2 are considered to be absorbed. Particles of energy up to 15 keV are stopped in 0·38 mg/aluminium (KATZ and PENFOLD, 1952) and the range depends little on the absorbing material except for hydrogen and the heavy elements. The correction comes out to 0·95 per cent on this basis. This increases to 1·25 per cent if one uses the branching ratios and maximum energies: 2·81 MeV 50 per cent; 1·04 MeV, 30 per cent; 0·65 MeV, 20 per cent (SIEGBAHN, 1946).

(b) On the assumption of an exponential absorption one may calculate the absorption coefficients for the individual elements and maximum β-particle energies using the range-energy relations of KATZ and PENFOLD (1952) and the atomic number-absorption coefficient relations of ABID HUSAIN and PUTMAN (1957). The total correction, 0·53 per cent, obtained with the first of the above decay schemes, is the sum of the corrections computed for the absorption in appropriate thicknesses of the individual elements. The result is correspondingly higher with the alternative decay scheme.

(c) A similar calculation using absorption coefficients based on the energy relationship of BARNARD *et al.* (1959) yields a correction of 0·38 per cent for the first decay scheme.

(d) MEISTER (1958) measured the self-absorption of ^{56}Mn β-particles in foils of metallic manganese. Foils of varying thickness (δ) were irradiated in a thermal neutron flux and the specific counting rate in 4π-geometry determined as a function of δ. By extrapolation to zero δ the self-absorption was determined for a number of values of δ. Interpolation on these data yields a correction of 0·5 per cent for self-absorption in a foil thickness of 0·75 mg/cm^2.

In the present work a correction of $+0{\cdot}7$ per cent has been added to the count rates obtained with the 4π-counter, since this procedure is unlikely to lead to a systematic error exceeding $+0{\cdot}7$ per cent to $-0{\cdot}5$ per cent.

6.2.2. The paralysis time of the counting circuit is $(5 \pm 0{\cdot}5)$ μsec. This uncertainty produces an error not exceeding 0·1 per cent in the corrected counting rate.

6.2.3. Considerations of the shape of the β-particle spectrum, the slope of the counting plateau, and the variation with voltage of the gas amplification of the counter, indicate that less than 0·15 per cent of the

particles will have insufficient energy to operate the counter.

It is concluded that the count rates obtained with the 4π-counter are subject to a systematic error not exceeding 1·0 per cent.

6.3. *Thermal neutron absorption in the neutron source and container*

RICHMOND and GARDNER (1957) showed that, by mounting the source at the centre of a four inch cavity, the thermal neutron flux in the source region was reduced sufficiently for the source self-absorption to be negligible. GEIGER and WHYTE (1959) computed a correction of (0·4 ± 0·2) per cent for the absorption of thermal neutrons in the N.R.C. source. It would be expected, therefore, that if the container used in the present experiment were to be flooded, the apparent output of the source after due correction for the change in fast neutron escape would be reduced by the amount of GEIGER's correction. However, this measurement resulted in no significant reduction in the measured output. The source was then re-measured in the absence of the source holder, the apparent absorption in which was 0·15 per cent with a standard error of ±0·15. In the case of the NPL sources, the loss of neutrons in the polystyrene was estimated by doubling and trebling the thickness. The correction obtained was 0·19 per cent with a standard error of ±0·15. It seems appropriate, in view of these results, to apply a correction of ÷0·15 per cent to the measurements made with both types of source.

6.4. *Neutron escape*

A shielded long counter (HANSON and MCKIBBEN, 1947) was used to determine the fraction of the neutrons emitted which escaped from the boundaries of the tanks. In the case of the (α,n) source the escape was measured from both tanks, with and without the polystyrene source holder; i.e. for four different values of r, the 'moderator path length.' The results are best fitted by the exponential $2{\cdot}14 \exp(-0{\cdot}116\, r)$.

The problem has been discussed by HANNA and RUNNALLS (1956). It appears that the number of neutrons which escape beyond a distance r from a Ra–Be (α,n) source in water (for $r >$ about 15 cm) is given approximately by the exponential $A \exp(-r/L_r)$: where A and L_r are constants; the number escaping from a bare sphere is greater by a boundary factor, B, and the corresponding expression for a Ra–Be (α,n) source in concentrated manganese sulphate solution is $B'A' \exp(-r/Lr')$. HANNA and RUNNALLS show that B is estimated at 1·4, B' at 1·3, $A \sim A'$, and the measurements of RUSH (1948) indicate that $A = 1{\cdot}9$ and $L_R = 9{\cdot}47_4$. L_R' is approximately equal to L_R since the increase in the slowing down length due to the reduced concentration of hydrogen nuclei is counteracted by the decrease due to inelastic scattering in the heavier elements in the solution.

The results obtained here indicate that $B'A' = 2{\cdot}14$ and $L_R' = 0{\cdot}91\, L_R$. Thus it appears that the heavier elements in the solution make a greater contribution to the slowing down of the neutrons than might be expected.

The leakage from the large sphere amounts to 1·2 per cent. This is in agreement with the figure obtained using the values $B'A' = 2{\cdot}47$, $L_R' = 0{\cdot}89\, L_R$ calculated by HANNA and RUNNALLS (1956) from experimental results by RUMSEY and WARD (1948).

Neutron escape from the small tank was 0·036 per cent for photoneutrons emitted by the beryllium nuclei, and 8·4 per cent for the neutrons emitted by the materials comprising the radium sources. (The latter figure may be compared with ~20 per cent for the escape of Ra–Be alpha-neutrons from the small sphere.)

6.5. *Fast neutron capture, in oxygen and sulphur*

The loss of fast neutrons from Ra–Be (α,n) sources in water due to threshold reactions in oxygen was measured by DE TROYER and TAVERNIER (1954) who compared the slowing down density of indium resonance neutrons in water and in paraffin oil. The interpretation of the results is that (2·2 ± 0·3) per cent of the neutrons emitted by the source are captured at high energies by the oxygen in the water. (See also GEIGER and WHYTE, 1959.) Due to the additional oxygen in manganese sulphate solution, the oxygen loss will be greater by a factor of approximately 1·26 viz. 2·8 per cent. To calculate the fraction of fast neutrons which produce reactions in sulphur it is necessary to compare the capture cross sections of oxygen and sulphur over the limited range for which they have been measured. GEIGER and WHYTE (1959) estimated that the average absorption cross section for sulphur is about twice that of oxygen over the range of energies from 2 MeV to 13 MeV. This leads to a total correction of (3·0 ± 0·5) per cent for the fast neutron capture in oxygen and sulphur for Ra–Be (α,n) sources in manganese sulphate solution of the concentration used. The maximum energy of the neutrons emitted by the Ra–Be (γ,n) sources is below the threshold for these reactions, and no correction is necessary with these sources.

VOL. 15 1961

Table 1.—Neutron emission rates of six Ra–Be (γ,n) sources

Source	Directly measured neutron emission from Be ($\times 10^{-5}$ n/sec)	Indirectly measured neutron emission from Be ($\times 10^{-5}$ n/sec)	M_{Ra} (g)	M_{Be} (g)	n/sec $\times 10^{-4}$ / $M_{Ra} \times M_{Be}$	Total neutron emission including α-neutrons ($\times 10^{-5}$ n/sec)
2*C*		1·621	0·3737	6·6572	6·52	1·664
3*B*	1·572		0·3769	6·3031	6·62	1·615
4*A*	1·671		0·3769	6·7456	6·57	1·714
2*L*		1·685	0·3737	6·8186	6·61	1·729
3*M*	1·699		0·3769	6·8179	6·61	1·743
4*N*		1·701	0·3769	6·8238	6·61	1·744

7. ABSOLUTE NEUTRON EMISSION RATES DETERMINED BY THE MANGANESE BATH TECHNIQUE

The corrected value for the output of the N.R.C. source is $3{\cdot}15 \times 10^6$ n/sec. The corresponding values for sources 3*B*, 3*M*, 4*A* are shown in column 2 of Table 1. Previous extensive comparisons (by manganese bath measurements and with BF_3 counters) between the six photoneutron sources, have established their relative neutron emission rates on an arbitrary scale with a standard error of $\pm 0{\cdot}15$ per cent. Column 3 shows the neutron ouput of the remaining three sources based on these comparisons.

Since the sources were constructed to be as similar as possible, it is of interest to compare their neutron outputs with the product $M_{Ra} \times M_{Be}$ where M_{Ra} is the effective content of the radium source, obtained from a γ-ray ionization comparison with the N.P.L. secondary radium standards, and M_{Be} is the mass of the beryllium cylinder. M_{Ra} and M_{Be} are shown in columns 4 and 5, both sets of figures being uncertain in the 4th decimal place. Column 6 shows that the neutron output is proportional to this product with the exception of source 2*C*. Beryllium cylinder *C* appears to be slightly corroded, so that some of the mass may be due to some element other than beryllium.

The total emission rates, including the neutrons emitted by the radium sources, are shown in the last column. Source 3*B* is now regarded as the primary standard and source 2*C* is a reference standard available for comparisons at other standardizing laboratories. The radium source 4 has developed a radon leak, and measurements with sources 4*A* and 4*N* have been discontinued.

8. ACCURACY

The random errors α associated with each stage of the calibration are shown, expressed as a percentage, in Table 2 together with the weight W with which the error influences the final value for the neutron emission rate. The sum $[\Sigma(\omega,\alpha)^2]^{1/2}$ of the random errors results in an uncertainty of ± 1 per cent for the output of the α,n source and rather less for the γ,n sources. In addition there may be a systematic error not exceeding 1·0 per cent associated with the efficiency of the 4π-counter.

9. DISCUSSION

The source 4*N* has been compared with the following standard sources (Richmond, 1958): N.B.S. Ra–Be (γ,n) source II; Oxford U.K. Rd–Th. D_2O (γ,n); Harwell U.K. Ra–Be (α,n); Basle Switzerland Ra–Be (α,n). The N.R.C. source has recently been calibrated by the following laboratories (Geiger, 1960): N.B.S., U.S.A.; A.B.A. Sweden; UMHK, Belgium; P.T.B., Germany; N.R.C. Canada. Through these two sets of comparisons it is possible to compare the N.P.L. calibrations indirectly with a large number of absolute calibrations carried out at other laboratories by widely differing methods. It turns out that the N.P.L. calibrations are within 1 per cent of the average for the rest of the world (Axton, 1961).

10. CONCLUSIONS

A British standard 400 mc Ra–Be photoneutron source has been established and calibrated absolutely with an uncertainty of less than ± 2 per cent. The

Table 2.—Random errors in absolute calibration of neutron sources by manganese bath technique

	% Standard error	Weight W
Dip counting rate	0·2	1
ε	0·2	1
C_H/C_{Mn}	0·1	0·4
Manganese resonance correction	0·5	0·45
Escape correction*	0·1	1
Fast neutron capture correction*	0·5	1
σ_H	0·6	0·45
σ_{Mn}	1·5	0·45
σ_S	4·1	0·02

* Not applicable to γ,n sources.

major errors remaining are: $\pm 0{\cdot}7$ per cent due to the uncertainty in the knowledge of the manganese and hydrogen thermal neutron capture cross sections; and $+0{\cdot}7$ per cent to $-0{\cdot}5$ per cent due to the uncertainty in the source self-absorption for the 4π-counter. In principle the first of these errors may be eliminated with the use of a heavy water manganese sulphate bath; however a correction must be made to allow for production of photoneutrons in the heavy water. The second of these errors may be reduced by the use of the $4\pi\beta$-γ coincidence counting technique. International comparisons so far carried out show that the absolute calibrations agree within 1 per cent with the average for the rest of the world.

Acknowledgments—We are indebted to Messrs. A. Williams, R. Sara, B. Owen, and J. Dale of the Radioactivity Standards Group for the standardization of the ^{56}Mn solution and to Mr. F. Howie, Dr. N. E. Topp and Dr. G. R. Davies, of the National Chemical Laboratory for their advice and assistance.

The work described has been carried out as part of the general research programme of the National Physical Laboratory and this paper is published with the permission of the Director.

REFERENCES

Abid Husain S. and Putman J. L. (1957) *Proc. phys. soc. Lond.* **70A,** 304.

Alder F. and Huber P. (1949) *Helv. phys. Acta.* **22,** 368.

Axton E. J. (1961) *Nucleonics* **19,** 90.

Barnard G. P., Axton E. J. and Marsh A. R. S. (1959) *Phys. med. Biol.* **3,** 366.

Bishop G. R., Wilson P. and Halban H. (1950) *Phys. Rev.* **77,** 416.

Cummins J. D. and Spurway A. H. (1957) AERE R/M 100.

Elliot L. G. and Deutsch M. (1943) *Phys. Rev.* **64,** 321.

Geiger K. W. and Whyte G. N. (1959) *Canad. J. Phys.* **37,** 256.

Geiger K. W. (1960) *Canad. J. Phys.* **38,** 569.

Glückauf E. and Paneth F. A. (1938) *Proc. roy. Soc.* **A165,** 229.

Hanna G. C. and Runnalls O. J. C. (1956) *Canad. J. Phys.* **34,** 959.

Hanson A. O. and McKibben J. L. (1947) *Phys. Rev.* **72,** 673.

Hawkings R. C., Merritt W. F. and Craven J. H. (1952) *Recent Developments and Techniques in the Maintenance of Standards.* HMSO, 35.

Hughes D. J. and Harvey J. A. (1955) BNL-325.

Hughes D. J. and Schwartz R. B. (1957) BNL-325. Supplement No. 1.

de Juren J. and Chin J. (1955) *J. Res. Nat. bur. Stand.* **55,** 311.

Katz L. and Penfold A. S. (1952) *Rev. mod. Phys.* **24,** 28.

Larsson K. E. (1958) *J. Nucl. Energy.* **6,** 322.

Martin E. B. M. and Martin G. R. (1954) *See* Littler D. J. (1957) AERE NP/R 1577.

Meister H. (1958) *Z. Naturf.* **13a,** 722.

O'Neal R. D. and Scharff-Goldhaber G. (1946) *Phys. Rev.* **69,** 368.

Perry W. E. (1957) *Strahlentherapie* **102,** 370.

Richmond R. and Gardner B. J. (1957) AERE R/R 2097.

Richmond R. (1958) *Progr. Nucl. Energy, Series* I, **2,** 165.

Rumsey V. H. and Ward A. G. (1948) Unpublished. *See* Hanna G. C. and Runnalls O. J. C. (1956).

Rush J. H. (1948) *Phys. Rev.* **73,** 271.

Siegbahn K. (1946) *Arkiv. Mat. astr. Fys.* **33A,** No. 10.

Strominger D., Hollander J. M. and Seaborg G. T. (1958) *Rev. mod. Phys.* **30,** 585.

de Troyer A. and Tavernier G. C. (1954) *Bull. Acad. roy. Belg.* **40,** 150.

VOL. 15 1961

Reactor Science and Technology (Journal of Nuclear Energy, Parts A/B), 1961, Vol. 15, pp. 28 to 31. Pergamon Press Ltd. Printed in Northern Ireland

LETTERS TO THE EDITORS

An empirical surface tension-temperature relation for liquid metals

(*First received* 23 *November* 1960 *and in revised form* 14 *December* 1960)

A KNOWLEDGE of the surface tensions of liquid metals employed as high-temperature coolants in the heat exchangers of nuclear reactors is of considerable importance because the surface tension affects wetting of the heat exchanger tubes by the liquid metal, and this in turn is a factor which affects the heat transfer characteristics of the system, and which may also play an important role in determining the rate and extent of liquid metal attack of the container wall (TAYLOR, 1954–55). In a previous investigation (STRAUSS, 1960) it was found that the surface tensions of liquid metals at their melting points, γ_m, could be correlated with their energies of vaporization per unit volume, S. A least-squares treatment of the data* yielded the following empirical relation:

$$\gamma_m = 0{\cdot}59S^{2/3}. \tag{1}$$

Since the use of this equation is restricted to the melting temperature, the present investigation was carried out to determine whether a satisfactory surface tension-temperature relation for liquid metals could be obtained by combining equation (1) with equations deduced from a consideration of the almost linear temperature dependence of surface tension and the vanishing of the surface tension at the critical temperature, and the results are given in the present paper.

* The data for magnesium, zinc, cadmium, and mercury, whose points on a log γ_m — log S plot showed the largest deviations (STRAUS 1960), were not included in the least-squares treatment; since the surface tension-temperature relation to be used in the present paper will contain the parameter S, the temperature dependence of the surface tensions of these elements will not be considered.

The equation

$$\gamma = A - BT, \tag{2}$$

where γ is the surface tension at the temperature T, and A and B are constants, is a satisfactory approximation of the surface tension-temperature relation because surface tensions of most liquids usually decrease nearly linearly with rise in temperature (PARTINGTON, 1955; BIKERMAN, 1958). Considering that at the melting point, T_m, the surface tension can be estimated from equation (1), and that the surface tension becomes zero at the critical temperature, T_c, we can write

$$0{\cdot}59S^{2/3} = A - BT_m \tag{3}$$

and

$$0 = A - BT_c. \tag{4}$$

A solution of the three simultaneous linear equations (2), (3), and (4) gives the following empirical surface tension-temperature relation for liquid metals:

$$\gamma = 0{\cdot}59S^{2/3}\left[\frac{T_c - T}{T_c - T_m}\right]^{\dagger}. \tag{5}$$

† It is interesting to note that equation (5) can be obtained by combining equation (1) with the empirical Eotvos equation (PARTINGTON, 1955) as follows: At temperatures T and T_m, the Eotvos equation can be written as $\gamma = \frac{k(T_c - T)}{(Mv)^{2/3}}$, and $\gamma_m = \frac{k(T_c - T_m)}{(Mv_m)^{2/3}}$, where M is the molecular weight of the liquid, v and v_m the specific volumes at T and T_m, and k the Eotvos constant which is found to nearly constant and equal to about 2·1 for certain organic liquids but which is not a constant for other substances including liquid metals (ADAM, 1952). If the first equation is divided by the second and if we assume as a first approximation that the ratio $\left(\frac{v_m}{v}\right)$ is unity since the specific volume of a liquid increases but slightly with increase in temperature except near the critical temperature (BIKERMAN, 1958) the resulting equation can then be combined with equation (1) to yield equation (5).

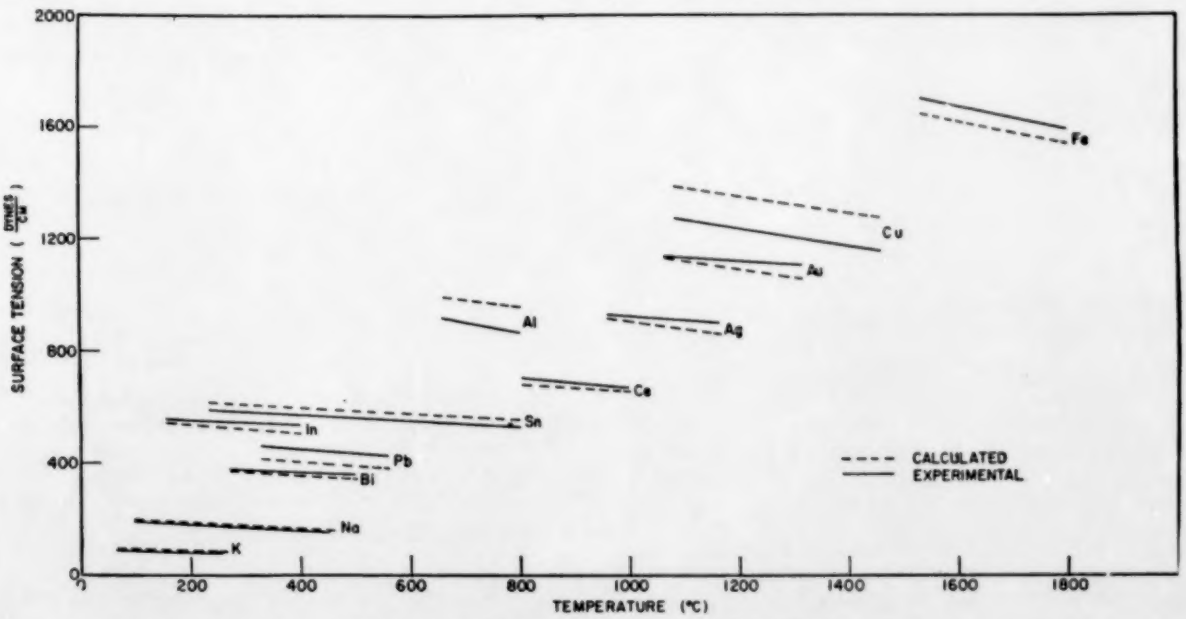

FIG. 1.—Surface tension-temperature plots for liquid metals.

VOL 15 196

TABLE 1.—SOURCES OF SURFACE TENSION DATA

Element	Reference*	Element	Reference	Element	Reference
Ag	KRAUSE (1929)	Ce	PULLIAM and FITZSIMMONS (1955)	K	*Liquid Metals Handbook* (1952)
Al	SMITHELLS (1955)	Cu	ALLEN and KINGERY (1959)	Na	TAYLOR (1954–55)
Au	KRAUSE (1929)	Fe	ALLEN and KINGERY (1959)	Pb	MELFORD and HOAR (1956–57); SMITHELLS (1955)
Bi	*Liquid Metals Handbook* (1952)	In	MELFORD and HOAR (1956–57)	Sn	MELFORD and HOAR (1956–57); PELZEL (1948)

* The methods of measurement were given in a previous paper (STRAUSS, 1960).

At this time only a limited test could be made of the applicability of equation (5) to liquid metals because of the scarcity of experimental $\gamma - T$ data.

Figure 1 shows a comparison of $\gamma - T$ plots obtained from experimentally reported data, the sources of which are referred to in Table 1, with plots obtained by use of equation (5). The melting and critical temperatures used were those reported by HANSEN (1958) and by GATES and THODOS (1960), respectively; the source for S data used was given in a previous paper (STRAUSS, 1960). It was found that for the temperature ranges plotted, the differences between the experimental and calculated surface tensions were less than eleven per cent.

Acknowledgment—This work is part of the liquid metal studies supported by the Bureau of Naval Weapons, Code RRMA-2.

Metallurgy Division S. W. STRAUSS
U.S. Naval Research Laboratory
Washington 25, D.C.

REFERENCES

ADAM N. K. (1952) *The Physics and Chemistry of Surfaces*, O.U.P., p. 158.
ALLEN B. C. and KINGERY W. D. (1959) *Trans. Amer. Inst. min. metall. petrol. Engrs.* **215**, 30.
BIKERMAN J. J. (1958) *Surface Chemistry*, Academic Press, New York, p. 52.
GATES D. S. and THODOS G. (1960) *Amer. Inst. Chem. Engrs. J.* **6**, 50.
HANSEN M. (1958) *Constitution of Binary Alloys*, McGraw-Hill, New York, p. 1262.
KRAUSE R. W. and SAUERWALD F. (1929) *Z. Anorg. Chem.* **181**, 353.
Liquid Metals Handbook (1952) U.S. Atomic Energy Commission and Department of the Navy, p. 40.
MELFORD D. A. and HOAR T. P. (1956–57) *J. Inst. Met.* **85**, 197.
PELZEL E. (1948) *Berg-Huttmannische Monatshefte* **93**, 248.
PULLIAM G. R. and FITZSIMMONS E. S. (1955) *Reactions of Cerium and Lanthanum with Ceramic Oxides*. Ames Lab. Report No. ISC-659.
SMITHELLS C. J. (1955) *Metals Reference Book*, Interscience, New York, p. 639.
STRAUSS S. W. (1960) *Nucl. Sci. Engng.* **8**, 362.
TAYLOR J. W. (1954–55) *J. Inst. Met.* **83**, 143.

Absorption in the 6·7 eV resonance of ^{238}U

(*Received* 17 *February* 1961)

RESONANCE absorption probabilities in homogeneous mixtures of U and H were calculated with two approximate methods—the narrow resonance (NR) and the narrow resonance with infinitely heavy absorber (NRIA) by SPINNEY (1956)) and these were compared with those obtained by the numerical solutions of the exact expression. Nine resonances in ^{238}U were calculated by the exact method and compared with the results of the two approximations. But for the lowest resonance of 6·7 eV the exact calculation was not done and hence the validity of the two approximations for this resonance had not been ascertained (SAMPSON and CHERNICK, 1957). The exact calculation for the 6·7 eV resonance is briefly reported here and is compared with the results obtained by NR and NRIA approximations.

Theory

Given a unit source of neutrons at energy E_0 in a homogeneous mixture of U and H, the fraction absorbed during slowing down to a given energy, E, is given by

$$1 - p(E) = \int_E^{E_0} F(E') \frac{\Sigma_a}{\Sigma_t} dE' \qquad (1)$$

where $F(E)$, the collision density at energy E, satisfies the equation

$$F(E) = \int_E^{E_0} \frac{F(E')\Sigma_H}{\Sigma_t E'} dE' + \int_E^{E/\alpha} \frac{F(E')\Sigma_{es}}{\Sigma_t E'(1-\alpha)} dE' + \frac{\Sigma_H}{E_0(\Sigma_H + \Sigma_a)} \qquad (2)$$

$\Sigma_t(E)$ is the macroscopic total cross section in the mixture, $\Sigma_a(E)$ is the absorption cross section, $\Sigma_{es}(E)$ is the scattering cross section of U and Σ_H is the scattering cross section of H assumed to be constant. Also, if $\Sigma_R(E)$ is the resonance cross section in U and Σ_p is the potential scattering cross section (also assumed to be constant), then $\Sigma_a(E) = \frac{\Gamma_\gamma}{\Gamma}\Sigma_R(E)$ and $\Sigma_{es}(E) = \frac{\Gamma_n}{\Gamma}\Sigma_R(E) + \Sigma_p$, where Γ_γ, Γ_n and Γ are the radiative capture, the neutron and the total widths respectively. The

practical width as defined by WIGNER *et al.*, (1955) is fixed for the 6·7 eV resonance with 1:1 ratio of H and U as 1·26 eV. The maximum possible energy loss in U($\approx(1-\alpha)E_R$) is found to be very small compared to the practical width fixed above. The exact evaluation of equation (2) is made numerically between the limiting values of the practical width. Twelve steps are needed to cover this region of practical width. Each step is further sub-divided into seven intervals for evaluating $F(E)$. Asymptotic value for the collision density $1/(\bar{\xi}E)$ is assumed beyond the limits of the practical width. The following values of the constants are used for the calculation: $\alpha = 0{\cdot}9833$; $\xi = 0{\cdot}6502$ (for 1:1 mixture of H and U); $\sigma_H = 20$ barns; $\sigma_p = 10{\cdot}9$ barns; $\Gamma_\gamma = 0{\cdot}025$ eV; $\Gamma_n = 0{\cdot}00145$ eV; $\Gamma = 0{\cdot}02645$.

Results and comparison

The value of $(1-p)$ thus obtained is 0·1206. We compare this value with those obtained by NR and NRIA approximations in Table 1 below.

TABLE 1

Resonance energy	Values of $(1-p)$		
	NR	NRIA	Exact
6·7 eV	0·1663 (0·1775)	0·1281 (0·1468)	0·1206

The values given in Table 1 do not take account of Doppler broadening. Values under NR and NRIA approximations obtained by SPINNEY (1957) are given in the brackets. The difference appears to be due to change in the constants.

We thus conclude that the NRIA approximation seems to be more valid for the 6·7 eV resonance in ^{238}U as suggested by SPINNEY.

Atomic Energy Establishment
Trombay, Bombay 1, *India*

B. P. RASTOGI
R. S. SINGH

REFERENCES

SAMPSON J. B. and CHERNICK J. (1957) KAPL-1754.
SPINNEY K. T. (1956) BNL-433.
SPINNEY K. T. (1957) *J. Nucl. Energy* **6**, 53.
WIGNER E. P. *et al.* (1955) *J. appl. Phys.* **26**, 260.

Energy distribution of thermal neutrons in a finite beryllium oxide assembly

(*Received* 13 *February* 1961)

THE problem of diffusion cooling of neutrons has been studied in considerable detail both theoretically (NELKIN, 1958; SINGWI and KOTHARI, 1958; SINGWI, 1960; JHA, 1960) and experimentally (ANTONOV *et al.*, 1955; BECKURTS, 1957; IYENGAR *et al.*, 1957; DE SAUSSURE and SILVER, 1959; KLOVERSTOM and KOMOTO, 1958; ANDREWS, 1960—for greater details and a critical review of the present experimental status, this thesis may be consulted). The agreement between the two sets of results is good only for the diffusion constant D_0, but is far from satisfactory for the diffusion cooling constant C. The experimental values of C are about 2 to 3 times higher than the theoretical values so far obtained.

In making the calculations, all authors except for JHA (1960), have assumed some convenient form for the energy distribution of neutrons inside the moderator assembly. It is also known (SINGWI and KOTHARI, 1958) that the value of C can depend sensitively on the energy variation of transport mean free path, λ_{tr}. One therefore expects the calculated value of C also to depend sensitively on the assumed neutron spectrum and the low theoretical value could be due to this assumption.

For beryllium, JHA (1960) had calculated the decay constant λ for some values of the buckling B^2, using an iteration procedure which also simultaneously gave him the form of the equilibrium neutron energy distribution. Thus, in his approach no assumption regarding the neutron energy spectrum was made to start with. If we plot his values of λ as a function of B^2 and fit a curve of the form

$$\lambda = \Sigma_a v + D_0 B^2 - CB^4,$$

(Σ_a is the macroscopic absorption cross section for neutrons of velocity v) we get a value of C nearly equal to 4×10^5 cm^4/s. This is higher than the experimental value of ANDREWS (1960) who gets $C = (3{\cdot}00 \pm 0{\cdot}30) \times 10^5$ cm^4/s. However it is not surprising that the two values do not agree. Firstly, the values of transport cross section, σ_{tr}, used by JHA are not exactly the same as for beryllium (KOTHARI and SINGWI, 1958) but have been slightly modified to suit his calculations. The scattering kernels used are based on the Debye model of the solid which may not be strictly correct, and further all integrations have been done on a desk calculator so that the integration mesh was not as fine as one would have wished. The important point to note is that the calculated value of C depends sensitively, not only on the variation of λ_{tr} with energy, but also on the form of neutron energy distribution that is assumed.

To test this conclusion further calculations similar to those of JHA (1960) were made for beryllium oxide and are briefly reported here. The values of the diffusion coefficient $D = \lambda_{tr}/3$ used in the calculations are given in Fig. 1 as curve D. The other curves give the equilibrium flux distributions of neutrons for different values of the buckling.

For the scattering kernel we have used the first term of the Placzek expansion. An energy interval of $0{\cdot}02\, k_0\Theta$ (k_0 is the Boltzmann constant and $\Theta = 1200^\circ$K is the Debye temperature of beryllium oxide) has been used for integration up to an energy $E_1 = 0{\cdot}1\, k_0\Theta$ and beyond this an energy interval of $0{\cdot}1\, k_0\Theta$ has been used.

In Table 1 we give the calculated values of the decay constant λ for different bucklings. The mean energy of the equilibrium neutron energy distribution is also given in the table. By plotting λ against B^2 we get $D_0 = 1{\cdot}16 \times 10^5$ cm^2/s and $C \approx 5 \times 10^5$ cm^4/s. Though the calculations have been made by slightly modifying the energy variation of λ_{tr} with energy from that for BeO (KOTHARI and SINGWI, 1958) one may compare these results with the experimental values of KLOVERSTROM and KOMOTO (1958) who obtain $D_0 = 1{\cdot}41 \pm 0{\cdot}05 \times 10^5$ cm^2/s and $C = 5{\cdot}4 \pm 1{\cdot}3 \times 10^5$ cm^4/s.

The value of C calculated here is larger by a factor 9 than the earlier value of SINGWI and KOTHARI (1958), and by a factor

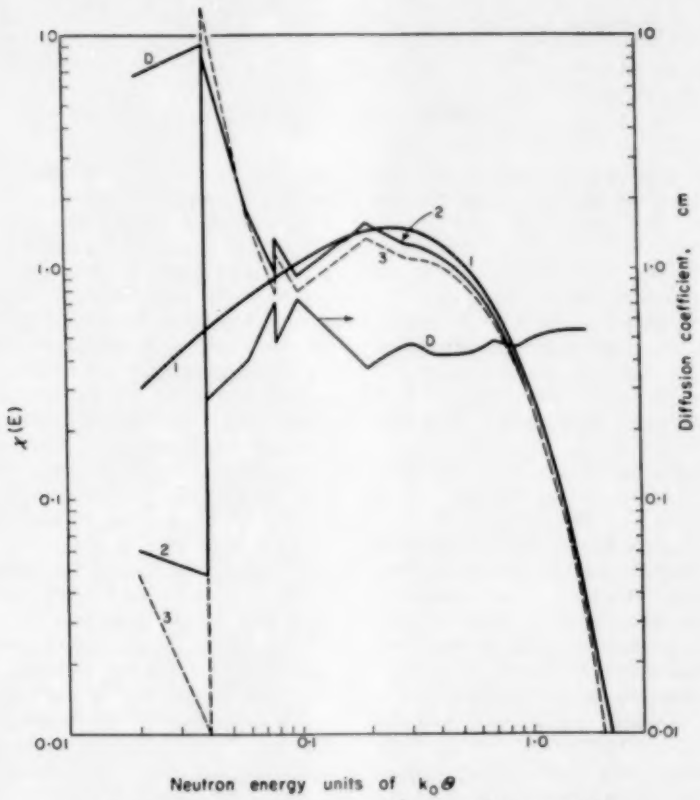

FIG. 1.—Curve D gives the values of the diffusion coefficient $D = \lambda_{tr}/3$ for beryllium oxide as a function of neutron energy that have been used in the calculations. Curve 1 is the Maxwellian flux distribution whereas curves 2 and 3 represent the equilibrium flux distributions, $\chi(E)$ for $B^2 = 3{\cdot}20 \times 10^{-2}$ and $4{\cdot}64 \times 10^{-2}$ cm^{-2}, respectively.

TABLE 1

$B^2 \times 10^3$ cm^{-2}	λ sec^{-1}	$\bar{E}$ in units of k_0
0	110	450°K
1·10	1385	425
2·07	2360	407
3·20	3185	—
4·64	3860	316

Density of BeO = 2·96 g/cm^3
$\Sigma_{a0} = 110$ sec^{-1}.

of 2·5 from the value of SINGWI (1960) which again shows that in calculating C, it is extremely important to take a correct neutron energy distribution.

L. S. KOTHARI*
P. G. KHUBCHANDANI

Atomic Energy Establishment
Trombay, Apollo Pier Road
Bombay 1, *India*

* Present address: Physics Department, Panjab University, Chandigarh, India.

REFERENCES

ANDREWS W. M. (1960) USAEC Report No. UCRL-6083.

ANTONOV A. V., ISAKOFF A. J., MURIN I. D., NEUPROCOYEV B. A., FRANK I. M., SHAPIRO F. L. and SHTRANISH I. V. (1955) *Proceedings of the First International Conference on the Peaceful Uses of Atomic Energy, Geneva*, Vol. 5, p. 3. United Nations, New York (1955).

BECKURTS K. H. (1957) *Nucl. Sci. Engng.* **2**, 516.

IYENGAR S. B. D., MANI G. S., RAMANNA R., UMAKANTH N. (1957) *Proc. Ind. Acad. Sci.* **45**, 215, 224.

JHA S. (1960) *J. Nucl. Energy* Part A: *Reactor Sci.* **12**, 89.

KLOVERSTROM F. A. and KOMOTO T. T. (1958) *Trans. Amer. Nucl. Soc.* Annual Meeting (June) p. 94.

KOTHARI L. S. and SINGWI K. S. (1958) *Proceedings of the Second International Conference on the Peaceful Uses of Atomic Energy*, Vol. 16, p. 325. United Nations, New York (1958).

NELKIN M. (1958) *J. Nucl. Energy* **8**, 48.

DE SAUSSURE G. and SILVER E. G. (1959) USAEC Report No. ORNL-2641.

SINGWI K. S. (1960) *Ark. Fys.* **16**, 385.

SINGWI K. S. and KOTHARI L. S. (1958) *Proceedings of the Second International Conference on the Peaceful Uses of Atomic Energy*, Vol. 16, p. 316. United Nations, New York (1958); (1958) *J. Nucl. Energy* **8**, 59.

VOL. 15 1961

Reactor Science and Technology (Journal of Nuclear Energy, Parts A/B), 1961, Vol. 15, pp. 32 to 35. Pergamon Press Ltd. Printed in Northern Ireland

BOOK REVIEWS

Gas-Cooled Reactors, The Franklin Institute and The American Nuclear Society. Published by Journal of the Franklin Institute, Philadelphia, Pa. 1960. 349 pp., $5.

THE technology of gas-cooled reactors is growing at a faster rate than that of any other reactor type. The two chief stimuli for this growth in the United States have been (a) the greatly improved performance of the newer British power reactors compared with the original Calder Hall reactors, and (b) the accumulation of performance data on high temperature ceramic-type fuels with heat transfer properties matching those of high pressure gas coolants.

The Franklin Institute and the Delaware Valley Section of the American Nuclear Society, in sponsoring the Gas-Cooled Reactor Symposium in Philadelphia, February 10 and 11, 1960, presented a balanced programme covering reactor systems, power plant components, loop installations, and fuel element development. The proceedings of the symposium, contained in Monograph No. 7 of the *Journal of the Franklin Institute*, is a valuable document with a particularly useful collection of tabular and graphical data and many illustrations.

Twenty-three papers are contained in the monograph. The first, a summary of gas-cooled central power reactor systems, by Charpie and Perry of ORNL, provides an excellent survey of the civilian gas-cooled power-reactor programme. The interrupted history of gas-cooled reactors in the United States is traced, beginning in 1942 and ending in 1947 when the so-called Daniels Pile programme was cancelled. American work began again in 1956 and has grown phenomenally along lines which deviate from the established British technology, being characterized by an attempt to increase the reactor power density and operating temperature at the expense of isotopic enrichment. The summary paper emphasizes the importance of high burn-up, temperature, and power density in the reduction of power costs and the need for the development of reactor systems using unclad elements in order to achieve significant cost reductions.

Even in new reactor types there is a great similarity between U.S. reactor designs and other advanced gas-cooled reactors abroad. The EGCR at Oak Ridge has its analogues in the AGR at Windscale, England and some proposals for the HTGC research programme of the Australian Atomic Energy Commission. The Pebble Bed Reactor design of Sanderson and Porter is quite similar to the BBC-Krupp Reactor at Mannheim, Germany. Finally, the HTGR designed by General Atomics is much like the Dragon Project reactor experiment of OEEC at Winfrith, England. Among the civilian non-mobile gas-cooled reactors described at the symposium, only the Turret experiment at Los Alamos is unique to the USAEC.

The High-temperature, Gas-cooled, Graphite-moderated Reactor (HTGR) is the subject of the second paper, which is the first of several papers describing high temperature unclad reactor systems. These reactors have certain common characteristics: the fuel is basically fuelled graphite and the coolant stream, at least part of which will probably become grossly contaminated, is provided with some type of coolant clean-up. The HTGR or its British counterpart are also discussed in the tenth, thirteenth, and sixteenth papers. The latter paper was an address at the symposium banquet by Sir William Cook of the UKAEA which describes the entire British gas-cooled reactor programme.

The third and fourth papers describe two mobile direct-cycle reactors with clad fuel elements. The first reactor is for power generation in remote locations (ML-1) and the second is for propulsion of a merchant ship (MGCR). The specifications for the Army Gas-cooled Reactor require that the components from which the system can be field-assembled weigh a maximum of 15 tons. By disconnecting the reactor from the turbine-compressor generator (by opening the primary coolant system), two portable packages may be produced at the expense of only limited shielding during reactor operation. The table of ML-1 performance characteristics illustrates this problem with a specified 5 mr/hr background at the control cab 500 ft from the reactor. After shutdown and 24 hours decay, the intensity 25 ft from the reactor centre will be 15 mr/hr.

With no containment shell nor coolant clean-up provided for field use of the ML-1, the requirement for fuel cladding integrity will be certainly as stringent as for any reactor yet designed. Fuel and coolant leaks during operation could make reactor maintenance or disassembly extremely hazardous.

The basis for design of the fuel elements for the Gas-cooled Reactor Experiment I, the first test facility for the army gas-cooled reactor programme, is described in the fourteenth paper, and the complete power conversion equipment for the ML-1 is the subject of the twenty-first paper. The former is of interest only as it illustrates a method of calculation, since the annular fuel design will not be repeated in the ML-1. The latter is a thorough discussion of the design features of the plant which will deliver 300 to 500 kW of power for remote use. As an interesting sidelight to the development of the ML-1 power plant components, the twenty-third paper was presented by members of the Franklin Institute on studies of the use of gas bearings for closed-cycle gas turbine rotors. The work was originated in 1955 to meet army requirements and is now sponsored by ONR.

The Maritime Gas-cooled Reactor, described in the fourth, thirteenth, and twentieth papers, has a much higher power rating than the ML-1 (22,000 shaft horsepower or approximately 16 MW compared to 300–500 kW). The design takes advantage of a unique feature of a direct cycle gas-cooled power plant. By varying the coolant inventory (readily accomplished by bleeding coolant from a high pressure compressor to an accumulator), the cycle efficiency can be held constant over a wide range of power requirements. The fourth paper points out the cost advantage of constant efficiency for a ship which must operate at less than normal power for extended periods due to weather or confined waters. The thirteenth paper, considerably shortened editorially, describes the fuel element development programme for the MGCR as well as the HTGR and again stresses the importance of fuel element integrity in a direct cycle reactor. The gas turbine for the Maritime Gas-cooled Reactor is the subject of the twentieth paper, which points out that due to the compact design a volume saving of 30 per cent is possible compared with a pressurized water reactor with the same output.

The reactor concept which is given the most extensive treatment in the monograph is the slightly enriched, UO_2-fuelled, stainless or beryllium-clad, indirect-cycle reactor exemplified by

the Experimental Gas-cooled Reactor now under construction near Oak Ridge National Laboratory in Tennessee. The fifth paper offers a summary of the important design features of the EGCR. The reactor has dual capability of power production (22 MW net) and experimental study of advanced fuels. The eight inpile loops may be operated at a maximum thermal power of 1·5 MW/loop with a variety of coolants, while twenty core positions cooled by the main helium coolant may be assigned for experimental use.

The EGCR fuel element design criteria and specifications are discussed in the eleventh paper. An analysis is presented which led to a decision to limit fuel-element thermal instability by mid-point spacers in the seven-rod cluster. Additional information on EGCR fuel development is contained in the twelfth paper which covers the development of improved pellet-fabrication methods, the results of inpile irradiation tests, and a review of cladding and manufacturing problems.

The Australian programme to develop a gas-cooled power reactor, covered in the sixth paper which was not scheduled but was presented informally at the symposium, is based on a thorium-uranium fuel cycle. In place of the slightly enriched EGCR fuel the AAEC is studying various chemical mixtures of thorium and ^{235}U which could be canned in beryllium. The HTGC reactor coolant will be CO_2, and beryllium and graphite are being considered for reflector and moderator. The British Advanced Gas-cooled Reactor (AGR) will be completed in April 1961 and will probably have achieved at least one year's operating experience before the EGCR goes critical. The similarity of the two designs, as indicated in the sixteenth paper, will make a comparison of the operating experiences very valuable.

Other design studies, contained in the nineteenth paper, are being carried out to prepare gas-cooled in-pile test facilities at ORNL. One loop described in the paper will be installed in the Oak Ridge Research Reactor, while the others will be incorporated in the EGCR. A typical experimental installation of a HTGR-type fuel element in the ORR is shown. Only a few design features for the EGCR loops are mentioned. It is interesting to compare the latter discussion with the description of a similar gas-cooled in-pile loop nearing completion in the Plutonium Recycle Test Reactor at Hanford, Washington. In the twenty-second paper, the PRTR loop is described in detail and solutions to many difficult design problems are presented. The difference in detail is the result of the difference between 5 and 18 months design effort.

The Pebble Bed Reactor is a high temperature system which anticipates one fundamental problem of reactors with high power density, the need for frequent refuelling. The design of Sanderson and Porter, described in the seventh paper, is based on spherical graphite fuel elements which flow by gravity through the active core of the reactor. The core is divided into two regions by a cylindrical graphite wall, and thermal breeding with very long doubling times may be achieved by the thorium-^{233}U cycle. The PBR fuel development programme is extensively reported in the fifteenth paper.

One of the basic differences between the PBR programme and the BBC-Krupp Pebble Bed Reactor is revealed in one of the objectives of the two fuel development efforts. By coating the fuel particles in a graphite matrix or by coating the entire ball, the PBR programme is aimed toward reducing the permeability of the graphite elements to a minimum. The paper on the BBC-Krupp reactor (the eighth paper) states that the graphite alone can provide optimum permeability; values less than 10^{-7} cm²/sec may lead to severe cracking of the balls due to internal gas pressure. The implication is that there is an optimum fission product leakage rate and that the coolant purification system must simply be sized for that rate.

The Turret experimental reactor at Los Alamos, discussed in the ninth paper, has a unique design to solve the same refuelling problem which influenced the PBR. Graphite fuel pins are to be periodically loaded into a rotating cylindrical core by an electric ram and spent elements will drop through the centre to a fuel discharge port. Helium at 1600°F will be fed to the 3 MW reactor and will exit at 2400°F!

The coolant temperature is much higher than is necessary for any conventional power installation. It represents a potential coupling of nuclear and fossil fuels by using nuclear heat to gasify coal. In the process, steam, coal, and high temperature (>1800°F) heat produce hydrogen and carbon monoxide. The product can be combined to produce liquid fuels and industrial chemicals. Nuclear reactors have the unique ability to produce heat at any temperature at which it can be removed, and chemical energy in the form of liquid fuels will always be necessary for uses like automobile engines.

The chemical part of the process has been simulated in high temperature out-of-pile loop experiments by the Bureau of Mines, reported in the seventeenth paper. The results indicate that operation with helium at temperatures of 2300° to 2500°F and 250 p.s.i.g. is probably feasible. However, problems were encountered such as severe high-temperature creep distortion of a compressor rotor which emphasizes the extreme difficulty of maintenance-free operation with nuclear heat and a high level of fission product activity.

The eighteenth paper graphically illustrates the major difference between the American and British technology for gas-cooled reactors. The development of blowers and power supplies for gas-cooled reactors in the U.K. is described. The presentation is quite mature and is clearly an attempt at design optimization. Additionally, a very useful hypothetical design is contained in the Appendix to the paper. In similar areas of gas-cooled reactor technology, the American design and development work can be described as feasibility studies. Comparing the beginning dates for the Calder Hall reactor and EGCR construction, 1953 and 1960, the reason for the difference is clear. The paper does show that many more years will probably pass before the word 'optimization' can properly be applied to the development of American gas-cooled reactors.

J. C. BRESEE

Nuclear Photo-Disintegration (Oxford Library of the Physical Sciences), J. S. LEVINGER, O.U.P., 1960. 144 pp., 15*s*.

PROFESSOR LEVINGER is an authority on the theory of nuclear photo-disintegration, having published many valuable contributions to this field since 1949. His monograph contains, as an introduction, the basic theory of the electronic photo-effect, followed by the modifications necessary to deal with the more complex situation found in nuclei. As a piece of scientific writing I find it very concentrated in its theoretical aspects. The starting point of a theoretical argument is generally a relation taken from some text book for the sake of saving space, such as that due to Mott and Sneddon or Heitler or a formula from a paper in a scientific journal. This may be unavoidable but soon leads to an array of heavy tomes around the reader.

VOL. 15 1961

The various derivations are very brief, encouraging the reader to arm himself with paper, pencil and time. The scope of the text comprises nuclear interactions of gamma rays of energies from about 2 to 150 MeV, confining the field to classical nuclear physics. Special care is devoted to sum rules and their relation to nuclear models. The first part of the monograph deals with the absorption of the quantum, and the last quarter is devoted to secondary processes leading to disintegrations, with the mission of protons, alphas, etc. Here the results of much experimental material are ably analysed in terms of models and types of process involved. It is evident that the experimental side is often shaky when accurate data are required for the assessment of theories. Better experiments are urgently needed; one can only hope that the production of monochromatic gamma rays of variable energy, which are soon to be available in some laboratories, will permit the nuclear physicist to overcome the intrinsic difficulties associated with the use of the bremsradiation as it is practised at present. With this prospect in view, it would be wise to keep Professor Levinger's monograph handy as a ready source of information.

E. BRETSCHER

Third Metallurgy Symposium on Corrosion (Saclay 1959), Commissariat a l'Energie Atomique, 1959. 240 pp., 70*s*.

THIS book is a record of the symposium on corrosion held at Saclay from 29 June to 1 July 1959, and contains the 20 papers presented, together with the relevant discussions on each paper. Only two of the papers are in English, the rest being in French, but each paper contains an abstract in English. Most of the papers are concerned with corrosion in the Atomic Energy field, as one would expect, but within this field there are papers on a diversity of topics, half the papers being on high temperature oxidation and half on aqueous corrosion.

The aqueous corrosion of stainless steels receives most attention, five papers being devoted to this topic. Other aqueous corrosion work described includes zirconium in high temperature water (one paper), inconel in high temperature water (one paper), the effect of sulphur compounds on aqueous corrosion of steel (two papers), the use of the potentiostat in aqueous corrosion (one paper) and sea-water corrosion (one paper.)

The papers on high temperature oxidation include three on the morphology of oxide films, one on general concepts of oxidation and one on diffusion mechanisms. Papers on the oxidation of specific materials comprise one on graphite, two on magnesium, one on uranium and one on high temperature iron-nickel-chromium alloys.

The book is well produced on high quality paper and the quality of many of the numerous micrographs reproduced is very good indeed. Two criticisms are that in a few cases important details of photographs are omitted (e.g. magnifications and in some cases even identifications) and that in several cases there is a remarkable waste of space in the presentation of figures; for example, on pages 16, 17 and 18 graphs showing very approximate relationships are printed on blocks 8 in. × 6 in. Only a few misprints were noticed.

In general, the book is authoritative and likely to be of use to a large number of workers in the corrosion field. In view of the high standard of the paper, the large number of photographs reproduced and the probably relatively limited circulation, the price seems very reasonable.

J. H. BUDDERY

Translation from Russian for Scientists, C. R. BUXTON and H. SHELDON JACKSON Blackie, London and Glasgow, 1960. 299 pp., 30*s*.

IT is being realized to an increasing extent that much important and interesting scientific work is published in Russian, and also that the cost of obtaining accurate translations is high. One product of this realization has been a desire on the part of many scientists to learn at least enough Russian to make out the general sense and possible implications of any particular paper. The consequent demand has led to the appearance of several books from which such a knowledge of Russian may be acquired, and one of the best of such books is that by Mr. Buxton and Mr. Jackson here reviewed.

After introducing the alphabet, with several pages of reading practice, the authors proceed to a concise outline of the grammar necessary for the purpose in view. There follow exercises consisting of single sentences, then 17 short passages with notes on the more difficult points, and finally 168 passages of varying length divided about equally between physical and chemical subjects (biology is poorly represented). There is a useful list of Russian abbreviations, and a vocabulary of the words used in the reading matter.

Among several praiseworthy features are the early introduction of the italic letters (although the student is given little opportunity to practise them) and extensive lists of conjunctions, prepositions, prefixes, suffixes and word families. Nor are there many serious errors in the book. There are, however, a number of minor inaccuracies which should be corrected in future editions. The vocabulary at the end of the book has several words out of order, two even on the wrong page. and many words are omitted. Some of these, according to the Preface, are 'words whose meanings should be obvious to any student of science'. This ought not to include, for example, *paragraf* (which does not mean 'paragraph') or *impul's* (which has more meanings than the obvious one). Other words are inadequately rendered. Proper names in the texts are printed in capitals, presumably to help the student, but the practice is very rare in Russian, and the initial capital should be sufficient guide. A few notes on chemical nomenclature would have been useful, and so would keys, at least to the alphabet-reading and English-Russian exercises. If these relatively unimportant defects are attended to, the authors will have given us an excellent and very useful textbook of scientific Russian.

J. B. SYKES

Review of Digital Computers and Nuclear Reactor Calculations, WARD C. SANGREN, Wiley, N.Y., 1960. 208 pp., $8.50.

THIS book's main feature is a good, compact survey and evaluation of the common techniques used in the numerical solution of the equations found in a wide class of physical problems. The prescriptions for numerically differentiating and integrating and the techniques for solving partial differential equations, are presented clearly though without derivation.

Most of the equations of reactor physics to which computers have been applied are considered to some extent. Quite properly, the Boltzmann equation receives the most attention. The diffusion approximation is treated in great detail with a complete derivation of the one-dimensional, multi-group equations and their reduction to a form suitable for machine computation.

VOL 15 196

One-velocity and few-group problems are considered and the two- and three-dimensional techniques are of particular interest.

The S_n and Monte Carlo methods, as the two most important methods of solving the Boltzmann equation, are discussed in some detail. The S_n equations are derived and the essentials of the method are given. The introduction to the Monte Carlo method is quite good, clearly presenting the salient features of the technique and discussing its limitations. The P_L approximation perhaps merits more than mention.

The introduction to computers themselves suffers from the inclusion of too much irrelevant data and a total lack of illustrations. A table of, at least, the major computers listing their speed, memory capacity, and cost would have been helpful. The discussion of programming acquaints the reader with some of the problems, tools, and language of the coder.

The book has generally met the need for a compilation of numerical reactor analysis techniques presented in clear and simple terms. The beginner will find it an adequate introduction to this field.

W. E. KINNEY

Elementary Introduction to Nuclear Reactor Physics, S. E. LIVERHANT, Wiley, N.Y., 1960. 447 pp., $9.75.

AMONG the books which had appeared prior to the publication of this present volume, none was particularly adapted as a text to the needs of an undergraduate course in reactor physics. The present volume was written to fulfill these needs.

The opening chapters review the fundamentals of elementary nuclear physics. The topics considered are the standard ones. There is a description of radioactivity and of the structure of the nucleus, a discussion of nuclear forces, the compound nucleus, nuclear reactions, and a presentation of the fission process. The treatment is brief but clear and direct. In this, the author has been able to avoid unnecessary complications without doing an injustice to the material.

The central and main portion of the book concerns nuclear reactors and their associated neutron populations. A system of classification of reactors is given, and there are tabulated brief data for a number of existing reactors, some of which are further described in the text along with the use of figures. Methods and formulae are given for the calculation of criticality conditions, and many numerical examples are performed. But, by the author's limitation on the level of the presentation, it is unlikely that the student will gain therefrom an adequate understanding of the methods of describing neutron populations in nuclear reactors. In particular, the concepts of the neutron flux and the neutron current density vector are discussed insufficiently to make their relation clear, and the diffusion approximation is given only in an appendix without the criteria necessary for determining its validity.

The final chapters discuss the various nuclear radiations and radiation protection. By using these final chapters in conjunction with the opening chapters on nuclear physics, this book may be made to serve also as a text for a short preparatory nuclear physics course for potential reactor engineers.

For pedagogic reasons the author has restricted his presentation to a level which, I feel, is too limited. Nevertheless, he has conducted an excellent review of pertinent nuclear physics and has been able to convey an overall descriptive conception of reactors and to impart some of the more important ideas associated with the calculational methods. Throughout the book illustrations, tables, and numerical examples are used profusely. Each chapter is concluded with a valuable set of problems and a bibliography. Answers to the problems are given at the back.

This book should meet with a favourable reception by those teaching reactor physics at the undergraduate level.

J. H. MARABLE

VOL.
15
1961

Reactor Science and Technology (Journal of Nuclear Energy, Parts A/B), 1961, Vol. 15, pp. 36 to 41. Pergamon Press Ltd. Printed in Northern Ireland

A METHOD OF ESTIMATING THE CRITICAL PARAMETERS FOR ARBITRARILY SHAPED BODIES OF FISSILE MATERIAL*

V. G. ZAGRAFOV

Abstract—This article describes an approximate method of determining the critical parameters for one or more bodies of arbitrary shape consisting of fissile material. In contrast to the variational method, the method proposed here is extremely simple and gives results which err on the safe side where the handling of fissile substances is concerned. For this reason the method may prove useful for engineering calculations.

The method is applicable to fast neutron systems if they can be described sufficiently accurately by the single velocity approximation.

THE DERIVATION OF THE BASIC RELATION

THE critical parameters for a body of material fissile under neutron bombardment are determined by Peierls' integral equation[1]

$$\phi(\mathbf{r}) = \frac{1}{\gamma}\int_V \alpha(\mathbf{r}')\phi(\mathbf{r}')K(\mathbf{r}, \mathbf{r}')\,dV', \qquad (1)$$

where $\phi(\mathbf{r})$ is the eigenfunction which coincides with the distribution function of the neutron density in the critical state; $\alpha(\mathbf{r})$ is the inverse mean free path of the neutrons and γ is the eigenvalue of the equation. The kernel $K(\mathbf{r}, \mathbf{r}')$ is determined by the expression

$$K(\mathbf{r}, \mathbf{r}') = \frac{\exp\left(-\int \alpha\, dl\right)}{4\pi l^2}, \qquad l = |\mathbf{r} - \mathbf{r}'|.$$

The integration is over the volume of the body.

Equation (1) is valid for a body consisting of a material which is homogeneous in composition, but it is not necessary to assume that the density of the material is constant throughout the volume V.

In the critical state the first eigenvalue γ coincides with one of the constants of the material, namely the inverse of the mean neutron multiplication coefficient for a single collision with a nucleus,

$$\gamma_m = \frac{\sigma_f + \sigma_s + \sigma_c}{\nu\sigma_f + \sigma_s},$$

where σ_f, σ_s and σ_c are the elementary cross sections per atom for fission, scattering and capture, and ν is the number of neutrons per fission. The difference between the eigenvalue and the material constant $\Delta\gamma = \gamma_m - \gamma$ characterizes the degree to which the system is removed from its critical state. An increase in the required value of γ implies that a fissile material is safer to handle, because this increase is associated with a decrease in the actual subcriticality $\Delta\gamma$ of the system.

An upper limit for the eigenvalue γ can easily be obtained from equation (1) if we know the position in space, $\mathbf{r}_0$, where the neutron density is greatest. In this case we can replace $\phi(\mathbf{r})$ by a constant and obtain as an upper limit for γ

$$\gamma = \int \alpha(\mathbf{r})K(\mathbf{r}_0, \mathbf{r})\,dV.$$

However, this method is inconvenient in practice, firstly because it gives a large error, and secondly, because the position of the maximum neutron density in a body of arbitrary form is not as a rule precisely known. One can state definitely only that this maximum must lie in a certain region.

To obtain a more useful method for estimating γ we single out a region, V_i, which includes the position of the neutron density maximum. For brevity we shall from now on call the volume V_i the *primary region* and the remaining volume of the body the *complementary region*, and we shall associate the suffixes i and e respectively with these two regions and with all quantities applying to them.

We assume that $\phi(\mathbf{r}) = \text{constant}$, and integrate equation (1) over the primary region:

$$\gamma = \frac{1}{V_i}\int_{V_i} dV \int_V \alpha(\mathbf{r}')K(\mathbf{r}_i, \mathbf{r}')\,dV'.$$

We transform the interior integral, using the fact that the integration may be extended over the whole of space, because outside the body $\alpha = 0$ (this is important in extending the result for a system of interacting bodies). We perform the integration in two steps. We integrate first in the direction $\boldsymbol{\Omega}$ along

* Translated by N. KEMMER from *Atomnaya Energiya* **8**, 23 (1960).

the ray emerging from the point $\mathbf{r}_i$, and then over the complete solid angle:

$$\int \alpha(\mathbf{r}')K(\mathbf{r}_i, \mathbf{r}')\,dV' = \int_{4\pi}\int_0^\infty \alpha(\mathbf{r}')\frac{\exp(-\int\alpha\,dl)}{4\pi l^2}\,l^2\,dl\,d\Omega$$

$$= \int_{4\pi}\frac{d\Omega}{4\pi}\int_0^{u_\infty} e^{-u}\,du,$$

where

$$u = \int_0^l \alpha\,dl; \quad u_\infty = \int_0^\infty \alpha\,dl;$$

u_∞ is the optical path length along the ray from the point $\mathbf{r}_i$ to infinity.*

Integrating along the ray we obtain

$$1 - \gamma = \frac{1}{V_i}\int_{V_i} dV \int e^{-u_\infty}\frac{d\Omega}{4\pi}.$$

We split the optical length of the ray u_∞ into two parts,

$$u_\infty = L + t,$$

where L is the optical distance along the ray from the point $\mathbf{r}_i$ to the surface of the region and t is the optical path length along the same ray from the surface of the primary region to infinity. Then we have, on changing the order of integration,

$$1 - \gamma = \frac{1}{V_i}\int\frac{d\Omega}{4\pi}\int_{V_i} e^{-L}e^{-t}\,dV. \qquad (2)$$

We now transform the interior integral, which is a function of the direction $\boldsymbol{\Omega}$. We consider the case when the density of the substance is constant through the primary region. Expressing all linear dimensions in the primary region in units of mean free path, we put $dV = dL\,dS$, where dS is the surface element normal to the direction $\boldsymbol{\Omega}$. We integrate along dL:

$$1 - \gamma = \frac{1}{V_i}\int\frac{d\Omega}{4\pi}\int(1 - e^{-L_0})e^{-t}\,dS,$$

where L_0 is the 'optical thickness' of the primary region along the ray passing through the elementary surface dS in the direction $\boldsymbol{\Omega}$. (Fig. 1). We replace the optical path length t by its average value across the section S, $\bar{t}(\boldsymbol{\Omega})$:

$$1 - \gamma = \frac{1}{V_i}\int e^{-\bar{t}(\boldsymbol{\Omega})}\frac{d\Omega}{4\pi}\int_S(1 - e^{-L_0})\,dS. \qquad (3)$$

The relation (3) becomes simpler if one chooses the primary region in the form of a sphere. In this case as a result of the symmetry of the sphere the integral over S in equation (3) does not depend on direction.

* For brevity we use the term *optical path length* to denote length expressed in units of the mean free path of the neutrons.

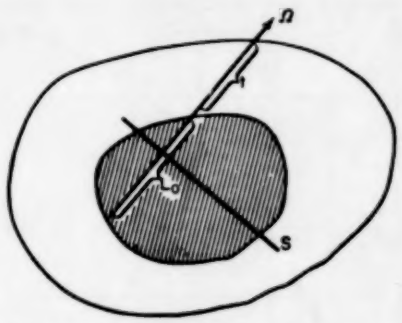

FIG. 1.—Scheme of integration. The primary region is shaded.

For a primary unit sphere the critical parameter γ_0 is determined in our approximation by the relation (3) with $t = 0$:

$$1 - \gamma_0 = \frac{1}{V_i}\int_S(1 - e^{-L_0})\,dS. \qquad (4)$$

Dividing each side of equation (3) by the corresponding side of equation (4) we obtain a relation between the required quantity γ and the value γ_0 for the unit primary sphere:

$$\frac{1 - \gamma}{1 - \gamma_0} = \int_{4\pi} e^{-\bar{t}(\boldsymbol{\Omega})}\frac{d\Omega}{4\pi}. \qquad (5)$$

If in the following we understand by γ_0 the eigenvalue of γ for the sphere, determined from the exact equations, we simultaneously satisfy the limiting case when the complementary region vanishes.

To simplify expression (5) we use the fact that the averaging over the quantity t is performed with the weight function $(1 - e^{-L_0})$, i.e. the greatest contribution to the average value $\bar{t}(\boldsymbol{\Omega})$ comes from the central region of the section S. We assume that $\bar{t}(\boldsymbol{\Omega})$ coincides with the value $t_0(\boldsymbol{\Omega})$ for the ray passing through the centre of the primary sphere. The error resulting from this approximation will in general have different signs for different directions of $\boldsymbol{\Omega}$, and will smooth out on integrating over the whole solid angle. It is shown below that this error does not change the sign of the total error.

The final relation has the following form

$$\frac{1 - \gamma}{1 - \gamma_0} = \int_{4\pi} e^{-t_0(\boldsymbol{\Omega})}\frac{d\Omega}{4\pi}. \qquad (6)$$

The dependence of γ_0 on the optical radius of the unit primary sphere is given in Fig. 2. The part of the curve for $\gamma_0(R)$ corresponding to a sphere whose dimensions are large and comparable with the mean free path of the neutrons was obtained by asymptotic diffusion methods, which give a high accuracy in this

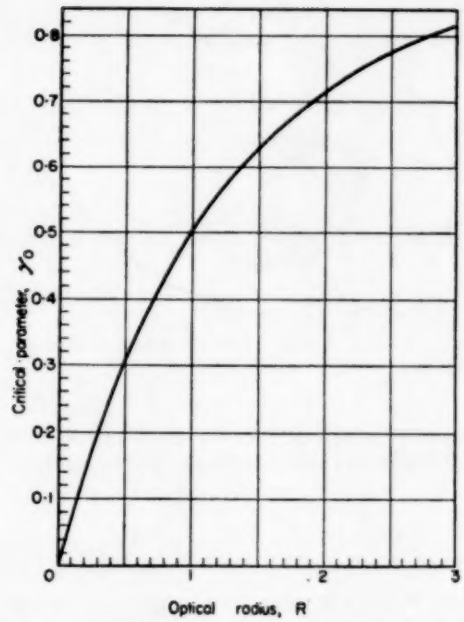

FIG. 2.—Dependence of the critical parameter γ_0 on the optical radius R for a unit sphere.

region.[2] For $R \ll 1$ the relation given by PEIERLS is valid[1]

$$\gamma_0 = R(0{\cdot}78 - 0{\cdot}39R).$$

As both parts of the curve go over very smoothly one into the other the interpolation between them in the small intermediate region gives very reliable results.

Relation (6) remains valid when the density of the substance in the primary sphere is an arbitrary function of the distance from the centre of the sphere. One can convince oneself of this by obtaining expression (6) directly from expression (2). This can prove useful if the density distribution of the substance in the primary sphere allows the determination of γ_0 by an exact method (for instance if there is a spherical cavity in the centre of the sphere).

It should be remembered that relation (6) is valid for any arbitrary distribution of the density in the complementary region. However, the relation can also be used for arbitrary density distributions in the whole of the body. For this purpose it is sufficient either to take as the value of γ_0 an enhanced value corresponding for instance to the maximum density of the substance in the primary region, or to confine the primary region to dimensions in which the density of the substance is practically constant. In doing this one must ensure that the point of maximum neutron density is contained in the primary region. In first approximation the position of the maximum neutron density corresponds to the minimum of the quantity

$$\int e^{-u_\infty} \frac{d\Omega}{4\pi}.$$

ERRORS INTRODUCED BY THE METHOD

The errors of the method are of two kinds. The basic error $\delta_1\gamma$, which arises from replacing the true neutron density distribution by a constant quantity, leads to an increase in γ. The second error, $\delta_2\gamma$, has the opposite sign and arises from the inaccurate averaging of the quantity t in relation (6). To determine the sign of the total error, we consider the behaviour of these two errors when the dimensions of the primary region are changed.

In the limiting case in which the primary region shrinks to a point in the vicinity of the neutron density maximum the error $\delta_2\gamma$ vanishes, because the region over which t is averaged (the cross section of the primary sphere) tends to zero, while $\delta_1\gamma$ takes on its maximum value. This is the case in which the errors introduced by the method are greatest. In the other limiting case in which $x = V_i/V = 1$ both errors tend to zero. Near this limit the error $\delta_2\gamma$ increases in importance because of the smallness of the first error. To show that the error $\delta_2\gamma$ is less than $\delta_1\gamma$ in absolute magnitude for $x \simeq 1$ we find the derivatives of these errors, $(\partial/\partial x)(\delta\gamma/\gamma)_{x=1}$, by comparing the approximate solution with the exact solution for the limiting case $(1 - x) = \Delta V/V \ll 1$, which we can obtain with the aid of perturbation theory.[3]*

According to perturbation theory we have

$$\frac{\Delta\gamma}{\gamma} = k\frac{\Delta V}{V},$$

where $\Delta\gamma = \gamma - \gamma_0$; $k = \dfrac{\overline{\phi_e^2}}{\overline{\phi^2}}$, $\overline{\phi^2} = \dfrac{1}{V}\int \phi^2\, dV$. (7)

We find $\delta_1\gamma$ from relation (3), which does not include the error $\delta_2\gamma$. After a transformation we obtain for the case of a small complementary region

$$\Delta_1\gamma = \gamma - \gamma_0 = \frac{\Delta V}{V}\int_{4\pi}(1 - e^{-L_0})\frac{d\Omega}{4\pi}, \quad (8)$$

where the integration is performed along rays emerging from the volume ΔV. For a spherical primary volume having radius R we put approximatelyt

$$2\int(1 - e^{-L_0})\frac{d\Omega}{4\pi} = \frac{1}{S}\int(1 - e^{-L_0})\, dS, \quad S = \pi R^2. \quad (9)$$

* The perturbation theory was independently developed by N. A. Dmitrev in 1948[4].

† For the accuracy of this approximation see the section on two spheres.

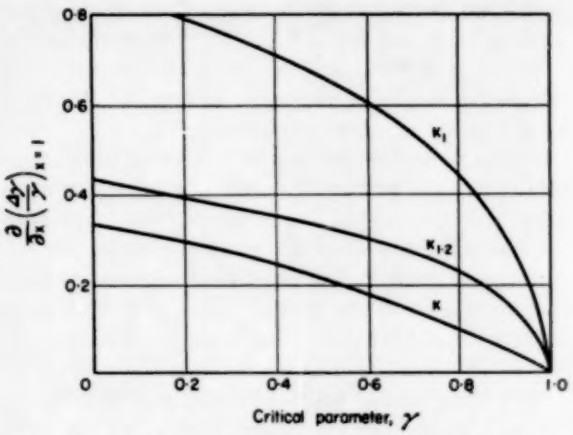

FIG. 3.—Dependence of the derivatives of the errors for $x = 1$ on the constant γ for the exact solution: curve k; for the approximate solution without the error $\delta_2\gamma$: curve k_1; and for the solution containing both errors: curve $k_{1,2}$.

Then relation (8), taking into account (4) and (9), assumes the following form:

$$\frac{\Delta_1\gamma}{\gamma} = k_1\frac{\Delta V}{V}, \qquad k_1 = \frac{2}{3}R\frac{1-\gamma}{\gamma}.$$

Similarly we obtain from relation (6), which includes both errors,

$$\frac{\Delta_{1,2}\gamma}{\gamma} = k_{1,2}\frac{\Delta V}{V}, \qquad k_{1,2} = \frac{1}{3}R\frac{1-\gamma}{\gamma}.$$

Figure 3 represents the dependence of the derivative $(\partial/\partial x)(\Delta\gamma/\gamma)_{x=1}$ on the constant γ for the exact solution, for the approximate solution without the error $\delta_2\gamma$, and for the solution containing both errors. In the limiting case $\gamma \ll 1$ the values of the derivatives were determined by the method described by PEIERLS[1]. In the range $0{\cdot}3 < \gamma < 1$ the asymptotic diffusion method[2] was used.

Comparing the derivatives of the expressions for the first and second errors when $x = 1$:

$$\frac{\partial}{\partial x}\left(\frac{\delta_1\gamma}{\gamma}\right) = k - k_1 \quad \text{and} \quad \frac{\partial}{\partial x}\left(\frac{\delta_2\gamma}{\gamma}\right) = k_1 - k_{1,2},$$

we see that the inequalities

$$\left|\frac{\partial}{\delta x}\left(\frac{\delta_1\gamma}{\gamma}\right)\right| > \frac{\partial x}{\partial}\left(\frac{\delta_2\gamma}{\gamma}\right) \quad \text{and} \quad \frac{\partial}{\partial x}\left(\frac{\delta_1\gamma}{\gamma} + \frac{\delta_2\gamma}{\gamma}\right) < 0,$$

are always valid, as we set out to prove.

If the dimensions of the primary volume are decreased the total error increases, reaching its greatest value when the primary region shrinks to a point. The error due to the averaging of the neutron density then reaches its maximum and the error of opposite sign connected with the averaging of the quantity t becomes zero. Therefore in solving specific problems it is appropriate to choose the primary volume in the form of a sphere of the greatest possible size, i.e. a sphere inscribed in the geometric form of the body. In doing this the basic requirement, that the maximum of neutron density lies within the volume of the primary sphere, is sure to be satisfied.

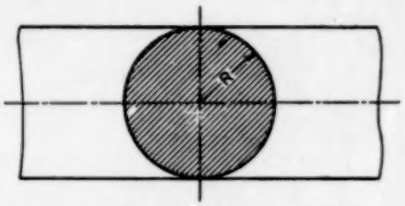

FIG. 4.—Position of the primary sphere in the slab.

COMPARISON OF CALCULATED AND EXPERIMENTAL DATA

We compare the results obtained by the method described with the experimental data for systems of different geometrical shapes made of Orelloy 93·5* published by GRAVES and PAXTON[5] The parameter γ_m for Oy(93·5) is 0·74, which agrees with the measured critical mass for a sphere of Oy(93·5), namely 51·3 kg.[5] The neutron mean free path is $\alpha^{-1} = 4$ cm.

Infinite slab

We inscribe the primary sphere in the slab, as shown in Fig. 4. Performing the integration on the right-hand side of relation (6) we obtain the critical equation for the slab

$$\frac{1-\gamma}{1-\gamma_0(R)} = 1 + Re^R Ei(-R). \qquad (10)$$

For the value $\gamma = \gamma_m = 0{\cdot}74$ we find from equation (10) that $R = 0{\cdot}77$, i.e. the critical thickness of the slab is $H = 2R\alpha^{-1} = 6{\cdot}16$ cm.

The critical slab thickness found by asymptotic diffusion methods, with material parameters consistent with the measured critical mass of an Oy(93·5) sphere, is 6·57 cm. The critical thickness of the slab obtained by extrapolation of experimental data is $H \simeq 6{\cdot}1$ cm.[5]

Infinite cylinder

For an infinite cylinder of Oy(93·5) we obtain from equations (6) $R = 1{\cdot}45$; $D = 2R\alpha^{-1} = 11{\cdot}6$ cm.

The measured critical diameter D for an infinite cylinder of Oy(93·5) is 12·4 cm.[5] The critical diameter of a cylinder calculated by the asymptotic diffusion method is also $D = 12{\cdot}4$ cm.

* Orelloy 93·5 or Oy(93·5) is metallic uranium containing 93·5 per cent of the isotope ^{235}U.

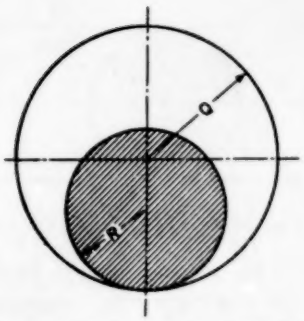

FIG. 5.—Sphere with eccentrically placed primary sphere.

A sphere

We estimate the critical radius a of a sphere of Oy(93·5) using equation (6). To do this we place the primary sphere of radius R eccentrically, as shown in Fig. 5. Performing the integrations in relation (6) over the complementary region we obtain:

for $R = 0{\cdot}75a$ $a = 1{\cdot}9$, $r = a\alpha^{-1} = 7{\cdot}6$ cm;
for $R = 0{\cdot}5a$ $a = 1{\cdot}95$, $r = 7{\cdot}8$ cm.

The measured critical radius r of an Oy(93·5) sphere with a density of 18·8 g/cm³ is 8·7 cm.[5]

As R decreases further the error decreases and for $R < 0{\cdot}37a$ it changes sign. This serves to illustrate the fact that the requirement that the maximum of neutron density should be within the primary zone is sufficient but not necessary to obtain a result which errs on the safe side.

Two spheres

For a system of two identical spheres, one of which is taken to be primary, relation (6) has the following form

$$\frac{1-\gamma}{1-\gamma_0} = 1 - \frac{\Omega}{4\pi}(1-g), \quad g = \frac{1}{\Omega}\int_{\Omega} e^{-t}\, d\Omega, \quad (11)$$

where $\Omega = \frac{1}{2}\left(1 - \sqrt{1 - \left(\frac{R}{b}\right)^2}\right)$ is the solid angle subtended by the second sphere at the centre of the first (b is the distance between the centres of the spheres). The function g characterizes the transparency of the sphere.

We can, with high accuracy, take g to be equal to the transparency coefficient g_0 of the sphere for a plane beam of neutrons:

$$g_0 = \frac{1}{S}\int_S e^{-t}\, dS = \frac{1 - e^{-2R}(1+2R)}{2R^2}, \; S = \pi R^2. \quad (12)$$

Comparison with the result of the exact integration in equation (11) shows that the replacement of g by g_0 leads to a negligibly small error. Even in the most unfavourable case $b = 2R$, the error does not exceed 1 per cent in the quantity $1 - g$.* This approach allows the results to be generalized to the case of a large number of interacting spheres.

Figure 6 curve A shows how, according to relations (11) and (12), the critical radius of Oy(93·5) spheres expressed in units of the neutron mean free path depends on the relative distance between the centres of the spheres, b/R. Curve B shows for comparison the dependence of the critical radius R on b/R when calculated according to the method described by STUART[6].

Relation (11) was verified experimentally by B. D. Stsiborsky and M. I. Kuvshinov for two Oy spheres placed in contact with each other. The results of the measurements coincided, within the limits of experimental error, with the results of the calculation from equation (11). The good agreement between calculation and experiment is explained by the fact that the mean values of the neutron density in the primary and complementary regions are in this case the same, because the spheres are identical.

Equation (11) is valid also for a system consisting of several spheres. In this case one chooses as the primary region one of the spheres near the centre of the system, where the neutron density is a maximum, and the solid angle Ω in expression (11) is summed over all the other spheres (if they do not screen one another).

System consisting of a large number of spheres

We apply relation (6) to a system consisting of a large number of spheres of radius R uniformly distributed over the volume of a sphere of radius a with a mean sphere-density of n per unit volume. We choose as the primary sphere one of the spheres at the centre of the system.

Each sphere of a system can be characterized by the effective cross section it presents for neutron interaction:

$$\sigma = (1 - g_0)S, \; S = \pi R^2, \quad (13)$$

where g_0 is determined from expression (12). The mean free path of the neutrons in the system is

$$\alpha^{-1} = [(1 - g_0)Sn]^{-1}. \quad (14)$$

Taking into account expressions (13) and (14) we obtain the critical relation for the system of spheres in the following form

$$\frac{1-\gamma}{1-\gamma_0} = e^{-(1-g_0)Sna},$$

* The sign of this error is favourable from the safety angle.

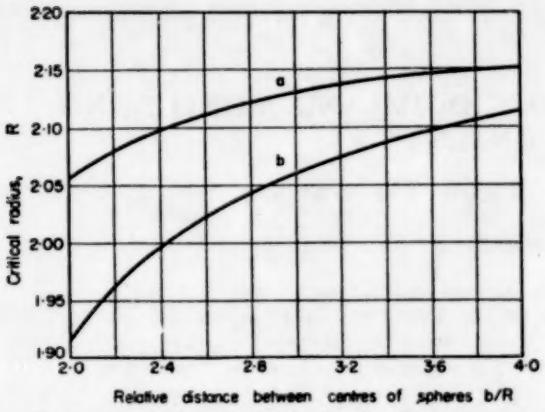

FIG. 6.—Dependence of the critical radius R on the relative distance b/R between the centres for system of two spheres: (a) according to equation (11); (b) according to the method of STUART.[6]

or, more conveniently,

$$\frac{3}{4}(1-g_0)N\left(\frac{R}{a}\right)^2 = \ln\frac{1-\gamma_0}{1-\gamma} \qquad (15)$$

where N is the total number of spheres in the system.

Since the primary sphere is at the maximum of the neutron density, equation (15) is biased in the direction of safety, i.e. it either underestimates the critical number of spheres in the system, or, if the number of spheres, N, is given, it overestimates the critical radius of the system.

To estimate the size of this safety factor we note that in the system the distribution of mean neutron density along a radius is the same in first approximation as the distribution of neutrons in a unit sphere of fissile material whose material constant $\gamma' = 1/Q$, where Q is the multiplication coefficient for neutrons incident on each sphere of our system.* Therefore having determined the critical radius R' of this sphere by the same method that we use to determine the critical radius a of a system of spheres we obtain the same error in the critical radius in these two cases.

We place the primary sphere centrally in a sphere of a substance with constant γ' and let the radius of the primary sphere tend to zero. We find from relation (6) a lower limit for the critical radius of the sphere R'

$$R' = |\ln(1-\gamma')|.$$

Comparing the quantity R' with the exact value of the critical radius of the sphere $R(\gamma')$ and introducing the same kind of relative correction into expression (15) we obtain a corrected critical relation for our system of spheres:

$$\frac{3}{4}(1-g_0)N\left(\frac{R}{a}\right)^2 = \frac{R(\gamma')}{|\ln(1-\gamma')|}\ln\frac{1-\gamma_0}{1-\gamma}, \qquad (16)$$

where $\gamma' = 1/Q$ and $R(\gamma')$ is determined for instance from Fig. 2.

We stress that owing to the absence of experimental data only relation (15) can serve as a working formula which certainly includes a safety factor. The size of this factor is estimated from expression (16).

CONCLUSIONS

The analysis of the errors performed above and the comparison with experimental data confirms that the sign of the error is constant irrespective of the particular problem. This is very important in dealing with problems concerned with the safe handling of fissile materials.

The proposed method is especially effective in calculating critical parameters for a group of bodies of fissile material, when other methods become particularly unwieldy. The method is applicable for arbitrary density distributions of the fissile material. Thus the present approximate method can be applied to all systems consisting of homogeneous (in composition) fissile material without moderators or reflecting envelopes.

REFERENCES

1. PEIERLS R. E., *Proc. Camb. phil. Soc.* **35**, 610 (1939).
2. CODD D., SHEPHEARD L. and TAIT D., *The Physics of Fast Neutron Reactors*, p. 300. Symposium on Advances in Nuclear Energy, Publishers of Foreign Literature (1958).
3. FUCHS K., *Proc. phys. Soc.* **62A**, 791 (1949).
4. USACHEV L. N., *Proceedings of the First International Conference on the Peaceful Uses of Atomic Energy, Geneva*, 1955, Vol. 5. United Nations N.Y.
5. GRAVES G. and PAXTON H., *Nucleonics* **15**, 90 (1957).
6. STUART G., *J. appl. Phys.* **27**, 1294 (1956).

* The method of determining the multiplication coefficient is explained by FUCHS.[3]

VOL. 15 1961

Reactor Science and Technology (Journal of Nuclear Energy, Parts A/B), 1961, Vol. 15, pp. 42 to 46. Pergamon Press Ltd. Printed in Northern Ireland

REMOVING OXIDES FROM LIQUID SODIUM AND MONITORING THE OXIDE CONTENT*

P. L. KIRILLOV, F. A. KOZLOV, V. I. SUBBOTIN and N. M. TURCHIN

(*Received* 20 *April* 1959)

Abstract—The presence of oxides in sodium used as a heat-exchange fluid accelerates corrosion of the pipelines, and may cause blockages in the cold parts of the loop. We report experiments with an apparatus for measuring the oxygen content of liquid sodium, and with cold traps for collecting the oxides. Our results will be useful in designing experimental or industrial plant based on a sodium or sodium-potassium alloy coolant.

1. INTRODUCTION

THE employment of sodium as a heat-exchange fluid has until now been made difficult by the fact that there are no methods for freeing the sodium from oxides, and for monitoring the oxygen content. The presence of oxides in liquid sodium accelerates the corrosion of structural materials[1] (e.g. of stainless steel, see Table 1); precipitation of oxides in the cold parts of the loop hinders the transfer of heat to the coolant[2], and may lead to blockages in the pipelines.

We have been testing instruments for measuring the oxide content of sodium, and traps for collecting the oxides, using a test loop (Fig. 1) with the following characteristics:

volume of metal in loop	0·100–0·450 m^3;
oxygen content	0·1–0·001 per cent;†
working temperatures	110–550°C;
pump pressure	6–10 kg cm^{-2};
total length of pipelines	~50 m;
diameter of pipes	25–48 mm.

All parts of the loop were provided with electric heaters for the preliminary heating of the metal. Under operating conditions the metal was heated by means of electric or gas ovens.

TABLE 1.—LEACHING OF THE COMPONENTS OF STAINLESS STEEL IN CONTACT WITH SODIUM AT 496°C

	Solution rate (mg cm^{-2} $month^{-1}$)	
	In sodium with 0·003% oxygen	In sodium with 0·01% oxygen
Iron	2·5	40
Cobalt	0·2	1
Tantalum	1·0	4
Manganese	7·2	26

* Translated by G. RYBACK from *Atomnaya Energiya* **8**, 30 (1960).
† Concentrations are given in per cent by weight throughout.

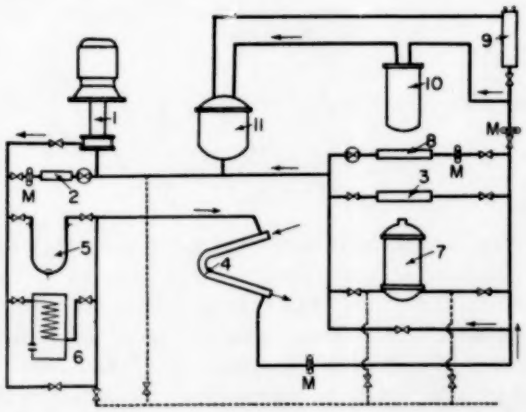

FIG. 1.—Diagram of the test loop: (1) pump; (2) and (8) plugging indicators; (3) sampling device; (4) heat-exchanger (sodium–sodium-potassium alloy); (5) electric oven; (6) gas heater; (7) heat-exchanger (sodium–water); (9) measuring tank; (10) cold trap; (11) pump tank; *M*, magnetic flowmeters.

2. AN INSTRUMENT FOR MEASURING THE OXYGEN CONTENT OF LIQUID SODIUM

There are several chemical methods for measuring the oxygen content of liquid sodium, such as the amalgam separation method,[3] the butyl bromide method,[4] the distillation method[5] and the vacuum fusion method.[6] These methods are somewhat involved and time-consuming, require special equipment, and are further complicated by the fact that radioactive sodium has to be treated. The most difficult operations are the sampling and the introduction of the sample into the measuring apparatus, without contamination with oxygen.

Our measurements of the oxygen content of sodium were made with a plugging indicator, the principle of which has been known for some years.[7,8] The method is based on the precipitation of oxides from a stream of liquid sodium flowing through small apertures. This occurs when the temperature falls

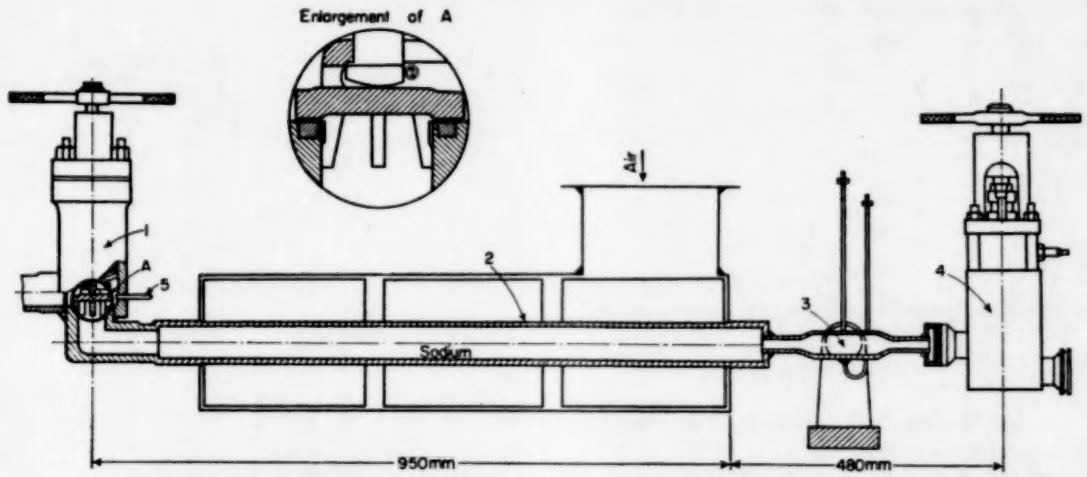

FIG. 2.—Design of the plugging indicator: (1) main valve with radial holes in the piston; (2) heat-exchanger (sodium–air); (3) flow-meter; (4) control valve; (5) thermocouple measuring temperature in the plugging zone.

below the saturation temperature for the oxide solution and leads to plugging of the apertures. Although the method does not call for precision apparatus it does ensure the required degree of accuracy over a wide range of oxide concentrations. The precipitation temperature having been determined, the concentration of oxygen in liquid sodium is given by the equation[9–14]

$$W = 2{\cdot}7 \times 10^{-4} \left(\frac{t}{100}\right)^{3{\cdot}6}, \qquad (1)$$

where W is the solubility of oxygen in sodium (per cent by weight) and t the temperature (°C).

In the plugging indicator shown in Fig. 2 the moment of precipitation was indicated by a fall in the flow rate registered by the flow-meter. In this apparatus the valve (1) which had several radial holes in the piston was placed to allow the oxides to be flushed out easily after each determination. The metal was cooled by air from a fan. A slightly modified recording electronic potentiometer EPP-09 with a time constant of 8 sec recorded the temperature and flow rate simultaneously (see Fig. 3). The characteristics of the three versions of the device which we have examined are given in Table 2.

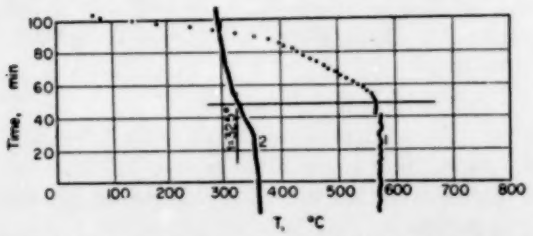

FIG. 3.—A specimen record produced by plugging indicator: (1) e.m.f. from magnetic flow-meter; (2) temperature at the plugged holes:

To select the best design we investigated the dependence of the instrument reading on the rate at which the metal flowed through the holes, the number and size of the holes, and the rate of cooling of the metal. In these experiments the oxygen content was 0·002–0·1 per cent, and the temperature 110–550°C. For each of the three versions (as a rule, two were compared in each experiment) we measured the variation of the reading with the rate of flow for two concentrations of oxygen. At flow speeds between 2·5 and 14 m sec^{-1} the plugging temperature remained constant (Fig. 4), but at lower speeds the temperature reading was low, for reasons which are at present unknown.

The temperature reading decreased by 2·5 per cent when the size of the holes was changed from 0·5 × 0·5 to 1 × 1 mm. The number of holes must be sufficiently large (10 to 15) to obtain accurate results when some are accidently blocked.

The temperature reading is independent of the rate of cooling providing the oxygen content is constant (0·008–0·02 per cent); the flow speed is 2·5–13 m sec^{-1}; and the rate of cooling at the apertures is 0·3–37 deg min^{-1}. A cooling rate greater than 10 deg

TABLE 2.—CHARACTERISTICS OF PLUGGING INDICATORS

	Model		
	A	*B*	*C*
Number of holes in valve	16	16	34
Size of holes (mm)	1 × 1	1 × 1	0·5 × 0·5
Diameter of heat-exchanger pipe (mm)	25	49	49
Total area of heat exchanger (m^2)	0·45	0·72	0·72

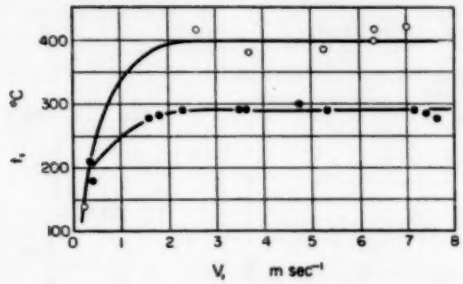

FIG. 4.—Relationship between plugging temperature and flow speed of metal through the holes:
○ 0·031 per cent oxygen;
● 0·013 per cent oxygen.

min^{-1} is undesirable since it can lead to erroneous plugging temperature readings.

The instrument readings were checked by chemical analysis of the metal accumulated in the trap after a certain period of operation. Table 3 compares the chemical data and the instrument readings; the agreement is seen to be satisfactory.

3. COLD TRAPS FOR REMOVING OXIDES

The principles underlying the working of cold traps are as follows.[7,8,15] The liquid metal flowing from hot parts of the loop is cooled and the precipitated oxides are subsequently filtered off. The efficiency of the purification process is enhanced by maintaining the trap at a low temperature, since the solubility of sodium oxides in sodium decreases with falling temperature.

The trap (Fig. 5) consists of a cylindrical tank (2) enclosing an inner cavity (8) and an outer cavity (9), both filled with stainless steel shavings or wire (3) [but see below]. The jacket (1) in which the tank is placed contains boiling toluene, which absorbs heat from the sodium, and the toluene vapour is condensed on a coil (5) carrying tap water. This complicated cooling system has been adopted as a safety precaution in the event of an escape of liquid sodium. The lower part of the trap forms a sump (6) in which the oxides accumulate. The cone (7) reduces the speed of metal flowing through the sump. The trap is heated before use by nichrome heaters placed in the central well (4).

TABLE 3.—OXIDE CONTENT IN TRAP, DETERMINED BY PLUGGING INDICATOR AND CHEMICAL ANALYSIS

Trap No.	Plugging indicator (g)	Gas analysis (g)
1	890 ± 100	1000 ± 500
10	4750 ± 700	6200 ± 900

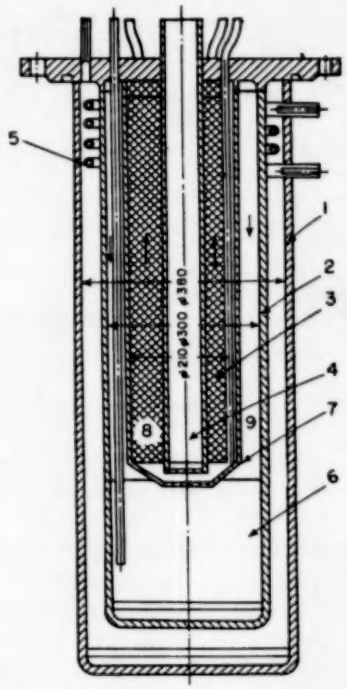

FIG. 5.—Design of a 32-litre cold trap.

The fall in the oxygen content of sodium which has passed through the trap is given by the material balance equation

$$\gamma V dc = \gamma Q(c - c')\, d\tau, \qquad (2)$$

where V is the volume of sodium in the loop (m^3); c is the concentration of oxygen in the sodium (%); c' is the solubility of oxygen in sodium at the minimum trap temperature t' (per cent); Q is the rate of flow of sodium through the trap ($m^3\ hr^{-1}$); γ is the density of the metal at the loop temperature ($kg\ m^{-3}$); and τ is the working time of the loop (hr).

Equation (2) implies the following assumptions: (a) the volume of the trap is smaller than the volume of the loop; (b) the quantity of metal flowing through the trap is small compared with that flowing through the loop; and (c) all the precipitated oxides remain in the trap, i.e. the oxygen concentration in the metal leaving the trap corresponds to the solubility at the minimum trap temperature. Integration of equation (2) gives

$$c = c' + (c_0 - c')e^{-n}. \qquad (3)$$

where c_0 is the concentration of oxygen in the sodium before purification and n is the number of times the total volume of sodium in the loop has passed through the trap in time τ.

In developing the trap, it was necessary to determine (a) the highest degree of purification achieved by

TABLE 4.—CHARACTERISTICS OF TWO TESTED COLD TRAPS

	Capacity of trap (*l* of sodium)		
	32*	47	
Duration of experiment (hr)	624	720	1900
Duration of circulation of metal (hr)	105	130	336
Flow rate ($m^3 hr^{-1}$)	0·117–0·100	0·336–0·250	0·500–0·160
Flow speed of metal (mm sec^{-1})			
in outer cavity	1·75–1·5	2·82–2·1	11–3·5
in inner cavity	1·95–1·6	2·74–2·0	2·9–0·6
Temperature of metal (°C)			
at trap inlet	310–420	450–270	370–284
inside trap	140–217	200–120	226–160
at trap outlet	148–280	300–180	180–125
Toluene vapour pressure (atm)			
working range	0·5–3	0·0–2	0·0–2
maximum	11	10	4·5
Oxygen content of sodium prior to operation of cold trap (%)			
working range	0·044–0·02	0·04–0·02	0·03–0·015
maximum	0·083	0·055	0·045
Quantity of oxides collected by trap (g)	3010	4750	4850
Quantity of oxides collected by trap (per cent of the metal inside trap)	10	14	10

* The sump was found to contain 13·2 per cent oxides (per cent of the metal inside trap); this quantity was determined from the density, the densities of sodium and its oxide differing by a factor of more than two.

VOL. 15 1961

means of the trap; (b) the maximum quantity of accumulated oxides; and (c) the suitability of the construction as a whole, and its thermal and mechanical characteristics. In the experiments the metal was made to circulate through the traps at a given rate for a certain period, and the oxygen concentration was measured before and after this process. This was repeated until the oxygen content decreased to the desired level and the results were compared with the calculated curve given by equation (3). Oxides were being carried out of the trap if the experimental curve was above the calculated curve. By decreasing the flow rate the experimental points were made to fall on or approach closely to, the calculated curve. The oxygen was introduced into the sodium either by mixing the metal with oxidized sodium, or by adding sodium peroxide.

Table 4 shows the experimental results for two versions of the cold trap. The following conclusions can be drawn.

(1) The cold trap is capable of lowering the oxygen concentration to 0·002 per cent.

(2) The required level of purity can readily be achieved under suitable working conditions.

(3) Oxides which have accumulated in the trap improve the filtering capacity of the trap. High rates of flow through the trap allow considerable escape of oxides from the trap.

(4) A low temperature at the inlet to the trap and a low mean temperature inside the trap increase the filtering capacity.

(5) The oxide capacity of the trap depends on its design, on the nature and density of the filling, and on the working conditions.

(6) At equal flow rates, a filling consisting of shavings is more efficient in retaining oxides than one of 0·5 mm diameter wire.

By filling only the inner cavity (8) with shavings (100 kg m^{-3}), by increasing the volume of the sump, and by increasing the time spent by the metal in the sump, the oxide capacity of the trap has been increased to 10 per cent.

If the oxygen concentration was $\geqslant$0·1 per cent, the trap soon blocked. In such cases the metal was first circulated through the trap without the toluene, using the trap merely as a mechanical filter, until the oxygen content fell to 0·06–0·05 per cent. Toluene was then added and the filtration continued. Typical working characteristics of the trap are illustrated in Fig. 6.

It should be noted that the oxide capacity of the trap is largely determined by the working conditions. For example, at a flow rate of 0·080–0·117 $m^3 hr^{-1}$ the capacity is only 4 per cent; at 0·270–0·500 $m^3 hr^{-1}$ the capacity reaches 10 per cent, owing to more uniform distribution of the oxides inside the trap at the higher speed.

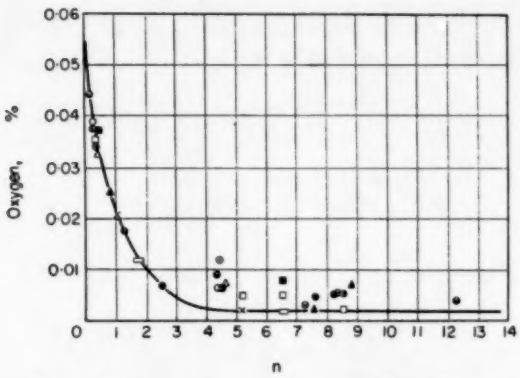

FIG. 6.—Decrease in oxygen concentration in sodium during operation of the cold trap. The thick line represents the theoretical curve (equation (3)); experimental points are for the following flow rates of sodium through the trap ($m^3\ hr^{-1}$):
● 0·168;
▲ and □ 0·250;
■, □, ×, ⊗, ⊕ and △ 0·285;
◒ and ⊙ 0·300;
○ and ◑ 0·335.

To find out where in the trap the oxides accumulate, the inner and outer cavities were blown through with gas after the experiments, and in some cases the sump contents were analysed. Experiments with various traps and analyses of the sump contents after the experiments lead to the following conclusion about the importance of the various components of the trap.

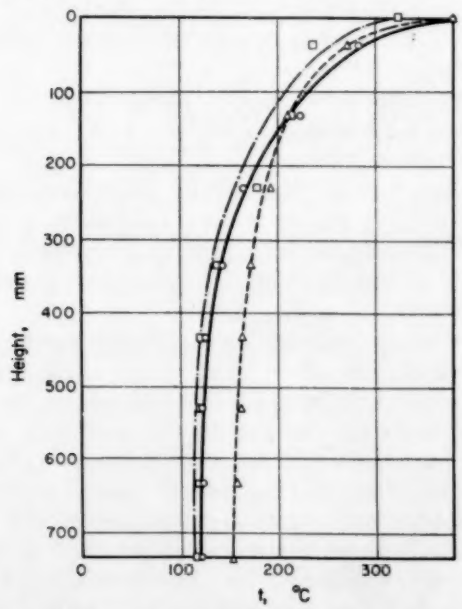

FIG. 7.—Vertical temperature distribution inside trap for different flow rates of sodium ($m^3\ hr^{-1}$):
□ 0·140;
○ 0·080;
△ 0·060.

Precipitation of oxides occurs in the outer cavity; measurements of the temperature distribution in the trap (Fig. 7) indicate that the oxides are almost entirely precipitated near the inlet into the trap, where the temperature of the metal falls from 300–450°C to 180–200°C in 14 cm. This explains the previously observed[13] increase in the hydraulic resistance of traps, which is due to plugging of the outer cavity. For this reason we omitted the filling from the outer cavity.

The cooled metal passes from the outer cavity to the upper part of the sump, which constitutes 10–14 per cent of the total volume of the trap. Our experimental results show that the quantity of oxide retained in the sump is negligible.

It should be noted that overflow and blind pipes which are relatively cold act as diffusion traps and, depending on the oxygen content of the metal and on the relative temperature of the blind pipe and the loop, are capable either of collecting oxides or of returning them to the loop.

REFERENCES

1. BAUS R. A. and BOGARD A. D., *Proceedings of the First International Conference on the Peaceful Uses of Atomic Energy, Geneva*, Vol. 9, p. 356. United Nations, N.Y. (1956).
2. KIRILLOV P. L., SUBBOTIN V. I., SUVOROV M. IA. and TROIANOV M. F., *Reactor Tech.* (*J. Nucl. Energy* Part B) **1**, 123 (1959).
3. PEPKOWITZ L. P. and JUDD W. C., *Analyt. Chem.* **22**, 1283 (1950).
4. WHITE J. C., ROSS W. J. and ROWAN R., *Analyt. Chem.* **26**, 210 (1954).
5. WHITE J. C., *Nucl. Sci. Abstracts* **11**, 8290 (1957).
6. KLIACHKO IU. A., *Analysis of Gases, Non-Metallic Inclusions and Carbides in Steel*, Metallurgizdat, Moscow (1953).
7. *Liquid Metals Handbook* (Sodium (NaK) Suppl.) JACKSON C. B. (Ed.) 3 edn. (1955).
8. BRUGGEMANN W. H., *J. Amer. Inst. Chem. Engng.*, **2**, 153 (1956).
9. SIEGEL S., CARTER R., BOWMAN F. and HAYWARD B., *Proceedings of the First International Conference on the Peaceful Uses of Atomic Energy, Geneva*, Vol. 9, p. 321. United Nations, N.Y. (1956).
10. GRAY I. L., NEAL R. L. and VOORHEES B. G., *Nucleonics* **14**, 10, 34 (1956).
11. *Reactor Engineering Lectures* (Presented by MCLAIN S.) ANL, (1955).
12. MCINTOSH A. B. and BAGLEY K. Q., *J. Brit. Nucl. Energy Conference* **3**, 15 (1958).
13. FARIS F. E. *et al.*, *Proceedings of the Second International Conference on the Peaceful Uses of Atomic Energy, Geneva*, P/452 United Nations, N.Y. (1958).
14. SALMON O. N. and CASHMAN T. J., *Solubility of Sodium Monoxide in Liquid Sodium*. Report KAPL-1653 (1956).
15. *Nuclear Reactors* Vol. 2, Chap. 17. U.S. Atomic Energy Commission (1955).

Reactor Science and Technology (Journal of Nuclear Energy, Parts A/B), 1961, Vol. 15, pp. 47 to 49. Pergamon Press Ltd. Printed in Northern Ireland

ISOLATION OF CARRIER-FREE ^{233}Pa FROM IRRADIATED THORIUM NITRATE*

V. I. SPITSYN and M. M. GOLUTVINA

(*Received* 13 *November* 1959)

Abstract—A method is given for the isolation of carrier-free ^{233}Pa from thorium nitrate irradiated with slow neutrons. It consists of isolating ^{233}Pa from the thorium nitrate solution by sorption on a MnO_2 precipitate; extracting the cupferron complex of protactinium with amyl acetate; re-extracting the protactinium into aqueous citric acid; and decomposing the citrate complex by oxidation with nitric acid. Good separation from α- and β-emitters was achieved. The isolated radioisotope was identified by its half-life period. The method will be found useful for obtaining carrier-free ^{233}Pa, which can be employed as a tracer in chemical studies on protactinium, and in investigations of the extraction of protactinium from natural raw materials and of the separation of ^{233}Pa from thorium during the preparation of ^{233}U.

1. INTRODUCTION

THE following process is used to obtain ^{233}Pa from thorium:

$$^{232}\text{Th}(n,\gamma)^{233}\text{Th} \xrightarrow[t_{1/2}=22\cdot1\ \text{min}]{\beta^-} {}^{233}\text{Pa} \xrightarrow[t_{1/2}=27\cdot0\ \text{days}]{\beta^-} {}^{233}\text{U} \xrightarrow{\alpha} \ldots$$

The neutron activation cross section of ^{232}Th is[1] $7\cdot33 \pm 0\cdot12$ barn. The ^{233}Pa so obtained[2] is usually contaminated with thorium and various radioisotopes derived from ^{233}U by neutron-induced fission. The literature contains several papers[3–5] dealing with the isolation of ^{233}Pa.

We have based our work on the papers of MADDOCK and MILES.[6,7] Before the method of these authors could be adopted, we had to carry out detailed investigations to determine suitable conditions for each stage of the purification process.

2. INVESTIGATION OF THE MANGANESE DIOXIDE PRECIPITATION

Protactinium was separated from thorium and zirconium by sorption on a precipitate of manganese dioxide, a phenomenon first described by GROSSE and AGRUSS.[8] Manganese dioxide was prepared in one of the following ways:

$$2KMnO_4 + 3MnSO_4 + 2H_2O = 5MnO_2 + K_2SO_4 + 2H_2SO_4$$

or

$$KClO_3 + 3MnSO_4 + 3H_2O = 3MnO_2 + KCl + 3H_2SO_4.$$

The sorption of protactinium on MnO_2 is efficient and almost independent of the conditions of precipitation; sorption is most complete and most selective when MnO_2 is precipitated from a strongly acid solution. Citric acid and fluorides interfere by forming stable, soluble complexes with the protactinium. To study the sorption of ^{233}Pa by precipitated MnO_2, we carried out the following experiments with freshly irradiated thorium nitrate, which was dissolved in 7-N nitric acid and diluted to a specific activity of $\sim 5 \times 10^{-4}$ counts min^{-1} ml^{-1}. An end-window counter was used having a mica window of 1·8 mg cm^{-2} thickness.

The solution (3 ml) and 5 per cent manganese sulphate solution (0·5 ml) were heated on a water-bath to 80°C. The addition of 0·5 per cent potassium permanganate solution (0·8 ml) precipitated MnO_2, which was coagulated by heating for 20 min. After the addition of more potassium permanganate solution (0·8 ml), the precipitate was separated by centrifuging and dissolved in 7-N nitric acid (1 ml) containing a small amount of sodium nitrite. The yield of MnO_2 was 1 mg per ml of solution. It was shown that 97 per cent of the initial activity was adsorbed by the precipitate.

In subsequent experiments the purification was improved by carrying out three precipitations of the MnO_2, the yield being increased to 4·4 mg per ml of solution. 98 per cent of the initial activity was adsorbed by the precipitate.

3. INVESTIGATION OF THE CUPFERRON EXTRACTION

Amyl acetate extraction of the cupferron complex of protactinium was employed to free ^{233}Pa from trace impurities sorbed by the MnO_2. The precipitated MnO_2, prepared as described above and dissolved in hot concentrated hydrochloric acid, was treated with an equal volume of a saturated aqueous solution of

* Translated by G. RYBACK from *Atomnaya Energiya* **8**, 117 (1960).

VOL. 15 1961

TABLE 1.—AMYL ACETATE EXTRACTION OF ^{233}Pa CUPFERRONATE FROM 6-N HYDROCHLORIC ACID

β-activity of amyl acetate phase (% of initial activity)	β-activity of aqueous phase (% of initial activity)
107	2
113	3
111	4
76	1
80	1
116	5
Average 100	Average 3

cupferron containing a small quantity of hydroquinone as stabilizer. The mixture was then shaken with an equal volume of amyl acetate, the volumes of the two phases being measured before and after shaking. The results given in Table 1 show that protactinium cupferronate is satisfactorily extracted by amyl acetate from 6-N hydrochloric acid.

To re-extract the protactinium into aqueous solution, the amyl acetate solution was shaken for 5 minutes with an equal volume of 1-M citric acid. On heating the mixture on the water-bath for 40 min the cupferronate decomposed and the protactinium passed into the aqueous phase, in which it formed a stable complex with citric acid. When cold the mixture was again shaken for 5 minutes, and the volumes and activities of the separated phases were then measured. It was shown that 85–90 per cent of the activity originally present in the amyl acetate solution passed into the citric acid solution. The latter was then repeatedly treated with hot concentrated nitric acid.

TABLE 2.—SEPARATION OF ^{233}Pa FROM α-EMITTERS DURING ISOLATION FROM IRRADIATED THORIUM NITRATE

MnO_2 precipitation	α-activity of precipitate (% of initial activity)	
	1	2
First precipitation	43	42
Second precipitation	14	10
Third precipitation	8	5

4. DISCUSSION

It was shown in the course of our work that most of the stages in the isolation of ^{233}Pa are successful only if the mineral acid concentration is high (≥6–7 N). When the acidity was lowered to 3–3·5 N, the results deteriorated considerably, adsorption on the walls of the vessel increased, and the experiments became poorly reproducible.

The degree to which the ^{233}Pa was purified of α-emitters (e.g. uranium and thorium) present in the original solution was determined, using a zinc sulphide crystal scintillation counter. The results (Table 2) show that the main separation from α-emitters occurs in the course of the three precipitations of the MnO_2, and is completed at the amyl acetate stage (the amyl acetate phase has zero activity).

On the basis of our experiments the following method has been developed for the isolation of carrier-free ^{233}Pa from irradiated thorium nitrate.

5. EXPERIMENTAL METHOD

A solution of freshly irradiated thorium nitrate in 7-N nitric acid was mixed with 10 per cent manganese sulphate solution (0·2 ml per 1 ml of the thorium solution) and heated to 80°C on the water-bath. 1 per cent potassium permanganate solution (0·5 ml per ml of the thorium solution) was stirred slowly in. The MnO_2 precipitate was coagulated by heating on the water-bath for 20 min, centrifuged off, and dissolved in hot concentrated nitric acid containing a small quantity of sodium nitrite. The solution so

TABLE 3.—ISOLATION OF ^{233}Pa FROM IRRADIATED THORIUM NITRATE
(Original solution in 7-N nitric acid; yield of MnO_2 precipitate 4·4 mg per 1 ml of solution)

Activity (% of initial activity)							
Three-fold MnO_2 precipitation		Extraction with amyl acetate from 6-N HCl			Re-extraction with M citric acid		
Sorbed by precipitate	Mother-liquors	Amyl acetate phase 1	Aqueous phase	Remaining on walls of vessel	Citric acid phase	Amyl acetate phase 2	Remaining on walls of vessel
99	1	95	2	3	112	0	0
99	2	91	3	6	81	0	19
98	1	92	2	6	83	0	17
93	—	93	—	—	89	—	—
103	—	90	—	—	86	—	—

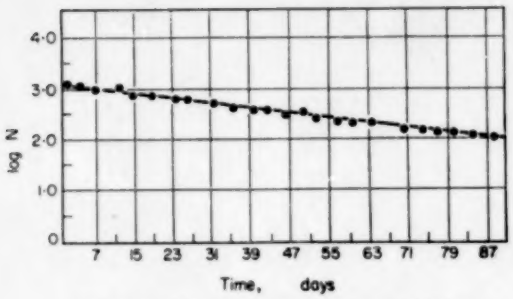

FIG. 1.—β-decay curve of the isolated ^{233}Pa.

obtained was diluted with an equal volume of water, and the precipitation of MnO_2 repeated twice. The final MnO_2 precipitate was dissolved in hot 6-N hydrochloric acid. To this solution was added an equal volume of cupferron solution (7 g cupferron and 0·2 g hydroquinone dissolved in and made up to 100 ml with 6-N hydrochloric acid, and filtered), and the liquids after being well mixed were transferred to a separating funnel. The vessel which originally contained the solutions was washed out with two portions of amyl acetate (total volume equal to the combined volumes of the acid and the cupferron solutions), which were then added to the separating funnel. After shaking for 5 minutes the phases were allowed to separate. The protactinium was re-extracted from the organic phase by an equal volume of 1-M citric acid solution, the mixed organic and aqueous phases being heated on the water-bath for 30 minutes with occasional shaking. The aqueous phase containing the ^{233}Pa was separated when the mixture had cooled.

6. RESULTS

Table 3 shows the results obtained by the above method. The relative mean square deviation of the activity measurements was ± 3 per cent. It was possible to extract up to 70 per cent of the ^{233}Pa activity from samples of freshly irradiated thorium nitrate. The β-decay of the isolated radioisotope (Fig. 1) confirms its identity; the observed half-life of 27 days agrees well with the value in the literature.

The extent to which the protactinium is freed from fission fragments has not been specially determined, but the measured half-life suggests that no significant amounts of these are carried through the purification process.

REFERENCES

1. *Neutron Cross Sections.* BNL–325, New York (1958).
2. STROMINGER D., HOLLANDER J. M. and SEABORG G. T., *Rev. mod. Phys.* **30,** 585 (1958).
3. FUDGE A. J. and WOODHEAD J. L., *Analyst* **81,** 417 (1956).
4. FUDGE A. J. and WOODHEAD J. L., *Chem. Industr.* **33,** 1122 (1957).
5. GOBLE A. G. and MADDOCK A. G., *Trans. Faraday Soc.* **55,** 591 (1959).
6. MADDOCK A. G. and MILES G. L., *J. chem. Soc.* (*Suppl.*) 248 (1949).
7. MADDOCK A. G. and MILES G. L., *J. chem. Soc.* (*Suppl.*) 253 (1949).
8. GROSSE A. and AGRUSS M. S., *J. amer. chem. Soc.* **57,** 438 (1935).

VOL. 15 1961

Reactor Science and Technology (Journal of Nuclear Energy, Parts A/B), 1961, Vol. 15, pp. 50 to 53. Pergamon Press Ltd. Printed in Northern Ireland

ON THE THERMODYNAMIC FEASIBILITY OF DRIVING TURBINES WITH ORGANIC LIQUIDS HEATED IN NUCLEAR REACTORS*

P. I. KHRISTENKO

(*Received* 11 *April* 1959)

Abstract—This article examines the feasibility of using heated organic liquids as the working substances of turbines. Diphenyl oxide, diphenyl, dowtherm etc., can be used as such liquids. The liquids are heated in power reactors, and can be evaporated in the nozzle of the turbine. In adiabatic expansion the vapour of such liquids is superheated, although its temperature drops. The parameters of the thermodynamic cycle of a power reactor in which dowtherm is used as the coolant are considered as an example.

CERTAIN organic coolants (e.g. diphenyl oxide) possess a property which makes it possible to drive a turbine directly with the organic liquid heated in the reactor, without producing water vapour.

It is known that, in the adiabatic expansion of the saturated vapour of any liquid, the state of the vapour during expansion depends on the physical properties of the liquid, i.e. on the relation between the heat capacity of the liquid and its latent heat of evaporation[1]. For example, if saturated water or mercury vapour is adiabatically expanded, it will become wet in proportion with the expansion. On the other hand, saturated diphenyl oxide vapour will be superheated during adiabatic expansion, although its temperature drops in the process.

Analytically this phenomenon is described thus:

$$S'' = S' + \frac{r}{T},$$

where S'' is the entropy of the dry saturated vapour, S' is the entropy of the liquid, r is the latent heat of evaporation and T is the absolute temperature of the saturated vapour. Differentiating this equation with respect to the temperature T, we find

$$\frac{dS''}{dT} = \frac{1}{T}\left(C_L + \frac{dr}{dT} - \frac{r}{T}\right)$$

(since $T\,dS' = C\,dT$).

If the heat capacity of the liquid C_L is less in absolute magnitude than the expression $\left(\frac{dr}{dT} - \frac{r}{T}\right)$, then the increase in the entropy of the saturated vapour with the rise in temperature will be negative, which

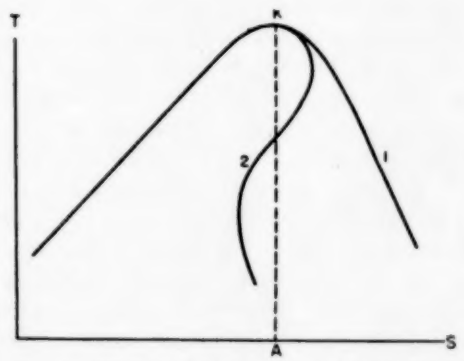

FIG. 1.—*TS* diagram for water and diphenyl oxide.

corresponds to curve 1 in Fig. 1. In this case the curve passes to the right of the ordinate KA drawn through the critical point. This type of curve corresponds to saturated water or mercury vapour, which becomes wet in adiabatic expansion. If the quantity C_L is greater than the absolute magnitude of the expression $\left(\frac{dr}{dT} - \frac{r}{T}\right)$, then the curve passes to the left of the ordinate KA (curve 2 in Fig. 1). The increase in the entropy of the saturated vapour will be positive; in adiabatic expansion such a vapour will be superheated.

The behaviour of saturated diphenyl oxide vapour gives a basis for assuming that heated diphenyl oxide can be used directly to drive a turbine. Figure 2 gives the *TS* diagram for diphenyl oxide. If diphenyl oxide, heated to a temperature T_1 is directed into a nozzle, where it will be adiabatically expanded to a temperature T_2, then from the nozzle (if it is long enough) will come a jet of superheated, saturated or slightly wet vapour, which can be directed immediately on to the turbine blades and then condensed in a condenser.

* Translated by D. R. H. PHILLIPS from *Atomnaya Energiya* **8**, 214 (1960).

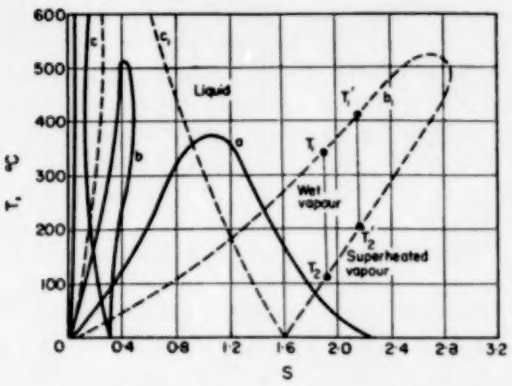

FIG. 2.—*TS* diagram for water, diphenyl oxide and mercury: (a) water; (b) diphenyl oxide; (c) mercury (relative to 1 kg of saturated vapour); (b_1) diphenyl oxide; (c_1) mercury (relative to 6 kg of saturated vapour).

It is clear that in the nozzle the heated liquid must start to boil and turn into superheated vapour.

The condition $C_L > \left|\frac{dr}{dT} - \frac{r}{T}\right|$, characterizing the capacity of certain liquids to evaporate as a whole in adiabatic expansion, is satisfied by a number of other liquids in addition to diphenyl oxide.

Figure 3 gives the *TS* diagrams[1] for diphenyl oxide, kerosene and ethyl ether. Apart from these liquids we can quote dowtherm (a eutectic mixture of diphenyl oxide and diphenyl), and obviously N-hexane, acetic acid and naphthalene.

The thermodynamic cycle of a heat engine, in which heated liquid is used directly, is shown in Fig. 4. The isobar *AB* (coinciding with the lower limiting

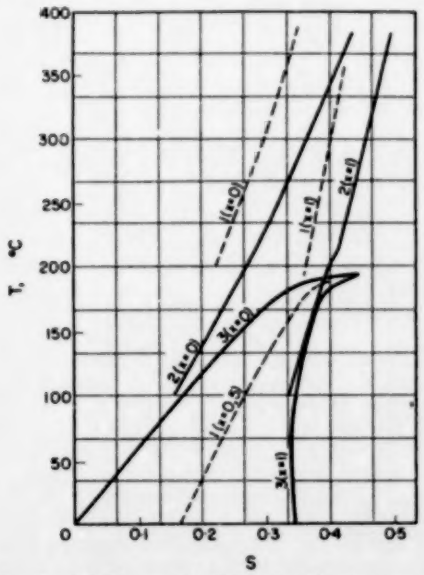

FIG. 3.—*TS* diagram for diphenyl oxide, kerosene and ethyl ether: (1) diphenyl oxide; (2) kerosene; (3) ethyl ether.

curve) characterizes the transfer of the heat to the liquid, the adiabatic curve *BC* represents the expansion of the liquid in the turbine nozzle, and the isotherm *CA* characterizes the condensation of the vapour.

If the working liquid satisfies the condition $C_L > \left|\frac{dr}{dT} - \frac{r}{T}\right|$, from an adequately long nozzle will come a vapour or a two-phase liquid. The cycle in question can be called a boiling liquid cycle.

The efficiency of such a cycle (if it is assumed that the heat capacity of the liquid is constant) is

$$\eta_t = 1 - \frac{T_2 \ln (T_1/T_2)}{T_1 - T_2} \qquad (1)$$

where T_1 is the upper temperature of the cycle and T_2

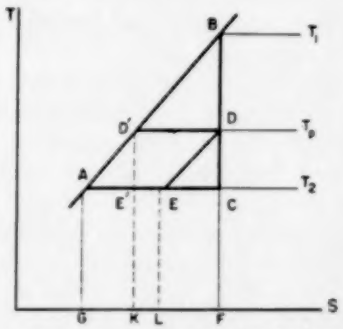

FIG. 4.—*TS* diagram of a boiling liquid cycle with regeneration.

is the lower temperature of the cycle (temperature in the condenser).

If we use the fact that in the *TS* diagram the lower limiting curve, coinciding with the isobar, within narrow temperature limits (e.g. for water up to 100°C) is approximately a straight line, it is possible to derive an approximate formula for the efficiency of the cycle:

$$\eta_t = \frac{T_1 - T_2}{T_1 + T_2}. \qquad (2)$$

If we compare the efficiency of the boiling liquid cycle with the efficiency of the Carnot cycle

$$\eta_t = \frac{T_1 - T_2}{T_1} \qquad (3)$$

with the same temperatures T_1 and T_2 in both cycles, it is clear that a machine operating on the Carnot cycle has an efficiency almost double that of a machine operating on the boiling liquid cycle. However the thermal efficiency of the boiling liquid cycle can be substantially increased (and even brought near to the Carnot cycle), if regeneration of the heat is used.

The theoretical regenerative boiling liquid cycle with an infinite number of stages (extractions) in the

VOL. 15 1961

TS diagram (Fig. 4) will be formed by the figure $ABDE$ or the figure $D'BCE'$.

The $ABDE$ cycle can be achieved both for boiling liquid droplets and for gas. It is a thermodynamic cycle similar to that which is achieved in a gas turbine in which the gas is heated at a constant pressure in a regenerative preheater and combustion chamber (lines AD' and $D'B$), expanded adiabatically in the turbine (line BD), cooled at a constant pressure in the regenerative preheater (line DE) and compressed isothermally in the compressor (line EA).

In running a heat engine on boiling liquid the lines AD' and $D'B$ correspond to heating the liquid in a multi-stage regenerative heater and heat generator, BD and DE to adiabatic expansion of the liquid at first without extraction and then with multi-stage extraction of the working substance, and the line EA to condensation of the vapour.

The $D'BCE'$ cycle is the cycle achieved in a gas turbine in which heating at constant pressure (line $D'E$) is followed by adiabatic expansion of the gas (line BC) and then isothermal and adiabatic compression (lines CE' and $E'D'$ respectively).

If we represent the regeneration temperature by T_p, then with the conditions adopted above, $C =$ constant and $C\,dT = T\,dS$, the efficiency of the cycle with regeneration is defined by the expression

$$\eta_t = 1 - \frac{T_2 \ln\left(\frac{T_1}{T_p}\right)}{T_1 - T_p}. \qquad (4)$$

The approximate value of this expression is

$$\eta_t = 1 - \frac{2T_2}{T_1 + T_p}.$$

We will examine the use of diphenyl oxide, heated in a reactor, as the working substance for a steam turbine. The critical temperature of diphenyl oxide is 530°C, the pressure in this case is 32·7 atm (absolute), at 350°C is 6 atm, at 450°C is 16·5 atm, at 150°C is 0·05 atm. Diphenyl oxide melts at a temperature of 28°C when pure but at much lower temperatures if it contains slight impurities. At high temperatures diphenyl oxide decomposes. Experiment has shown that when diphenyl oxide was maintained at 15 atm and 440°C for 700 hr, 1–2 per cent was decomposed.[2]

From the TS diagram of diphenyl oxide (see Fig. 2) it is possible to establish the limits of its application. The initial temperature of the liquid entering the machine is limited to 300–400°C (points T_1 and T_1'), the final temperature to 120–200°C (points T_2 and T_2'). These temperatures correspond to initial pressures of 2·0–16·5 atm and final ones of 0·015–0·15 atm. Since the final temperature of the diphenyl oxide vapour after passing through the turbine remains high (120–200°C), these machines should only be used for the first stage. The residual heat can either be used for district heating or for driving the second stage of a turbine using low-pressure water vapour.

In the latter case the reactor heat will be used in accordance with a binary thermodynamic cycle, the circuit and TS diagram of which are shown in Fig. 5. The first stage of this cycle is shown by the figure $D'BD$, bounded by the isobar $D'B$ on which heat is passed to the liquid diphenyl oxide in the reactor (1) (Fig. 5a), by the adiabatic curve BD' along which the heated diphenyl oxide expands during evaporation in the nozzle of the single (pressure) stage turbine (2) and by the isotherm DD' along which the diphenyl oxide vapour condenses in the condenser (3). This condenser serves at the same time as an evaporator for obtaining the saturated steam which is the working substance for the second stage of the binary cycle.

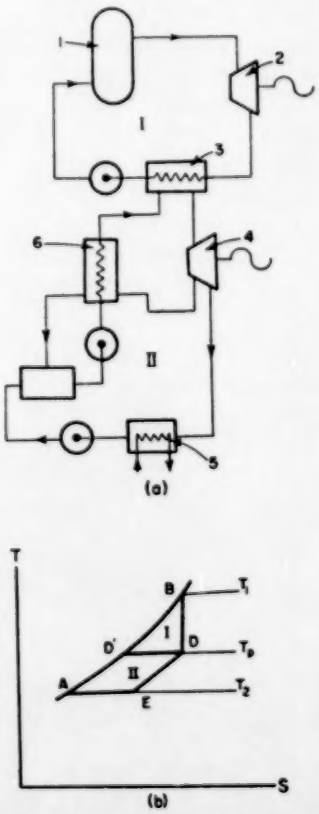

FIG. 5.—Circuit (a) and TS diagram (b) of the binary cycle. STAGE I: heated diphenyl oxide, stage II: saturated steam. (1) Reactor; (2, 4) turbines; (3, 5) condensers; (6) regenerative heater.

The second stage of the cycle is represented graphically by the figure $D'DEA$, bounded by the isotherm $D'D$ along which water in the condenser (3) evaporates to produce saturated steam, by the line DE, which represents the adiabatic expansion of the steam in the steam turbine (4) together with multi-stage extraction for regeneration, and by the isotherm EA and isobar AD', which correspond respectively to condensation of the steam in the condenser (5) and to heating of the water by the extracted steam in the regenerative heater (6).

The thermal efficiency of the binary cycle when using liquid diphenyl oxide (stage I) and water steam (stage II) (at temperatures $t_1 = 350°C$, $t_p = 200°C$ and cooler temperature $t_x = 35°C$) will be 0·43. If we assume an internal efficiency for the turbine $\eta_{i0} = 0{\cdot}75$, a mechanical efficiency $\eta_m = 0{\cdot}96$, an electrical efficiency $\eta_e = 0{\cdot}97$ and a utilization factor for the theoretical cycle of $\eta_i = 0{\cdot}9$, then such an installation can have an efficiency of up to 27 per cent. Bearing in mind that the pressure of the diphenyl oxide does not exceed 6 atm (absolute), and its temperature is only 350°C, this efficiency is very high.

In certain cases, for example in the planning of a nuclear engine for transport purposes, where the weight and dimensions of the installation are of great importance, one might limit oneself solely to the turbine operating on the vapour of the organic liquid. In this case the thermal efficiency of the thermodynamic cycle would be $\eta = 0{\cdot}2$–$0{\cdot}3$, and the total efficiency of the installation would be $\eta_s = 0{\cdot}13$–$0{\cdot}2$.

At the present time the most studied and the cheapest organic coolants are diphenyl, diphenyl oxide and their eutectic mixture dowtherm.

If we use dowtherm as the working substance, with an initial temperature and heat content of $t_f = 300°C$ and $i_f = 149{\cdot}5$ cal/kg (or alternatively $t_f = 400°C$ and $i_f = 219$ cal/kg) and allow for its expansion in the nozzle of the turbine to a state of saturated or slightly wet vapour, then from the turbine outlet will come in the first example vapour at a pressure of $P_v = 0{\cdot}017$ atm, with a specific volume of $V = 11{\cdot}5$ m³/kg and heat content of $i = 149{\cdot}5$ cal/kg, and in the second example vapour at a pressure of $P_v = 0{\cdot}25$ atm, with $V = 1{\cdot}0$ m³/kg and $i_v = 219$ cal/kg.

The heat drops Δi_1 and Δi_2 during adiabatic expansion of the liquid to a state of saturated vapour will be approximately 25 and 55 cal/kg respectively, and the rates of flow of the vapour from the turbine nozzle will be $c_1 \simeq 450$ and $c_2 \simeq 600$ m/sec. The magnitudes of these velocities, and the need for complete expansion of the boiling liquid to the saturated vapour state in the inlet nozzle of the turbine also determine its design. Apparently this will be an active turbine having a velocity stage with one or several (depending on its output) two-row or three-row disks.

If we consider the comparatively low vapour velocity at the exit from the nozzle of such a turbine and the low pressures and specific volumes of organic vapours, then the construction of turbines with outputs of several hundreds to several tens of thousands of kilowatts becomes possible. The cost of such turbines should not exceed the cost of ordinary turbines.

In addition one would, by using turbines operating with a liquid organic coolant heated in a reactor, eliminate the need for constructing steam generators with a first stage operating at a pressure of 30–40 atm.

The thermodynamic cycle of power extraction from nuclear reactors depends to a great extent on how the heat is withdrawn.

If the coolant does not change its aggregate state when heated in a reactor it is possible to obtain work from the energy of the coolant alone by cooling it in an engine from the high temperature imparted to it in the reactor down to the lower temperature corresponding to the cold source. The cycle examined should also serve as the theoretical thermodynamic cycle for such (non-boiling) reactors.

If the coolant does change its aggregate state in the reactor by boiling, work can be obtained from the latent heat of evaporation of the liquid, i.e. by expanding the vapour obtained from the reactor adiabatically in the engine. Part of the heat of this vapour is turned into work, and the vapour is then condensed. The theoretical thermodynamic cycle for such (boiling) reactors will be bounded by two isobars and two isotherms. The efficiency of such a cycle is equal to that of the Carnot cycle.

An intermediate position between boiling and non-boiling reactors is occupied by the uranium-graphite reactor being constructed in the U.S.S.R. which will have high-pressure water steam reheat. The regenerative thermodynamic cycle with steam reheat used in this reactor is normal for contemporary thermal power steam installations.

As we have shown, it is possible in principle to achieve an ideal theoretical cycle for coolants heated in a reactor, with the aid of liquids which are capable of evaporating as a whole in adiabatic expansion.

REFERENCES

1. SHYULE V., *Technical Thermodynamics*, Vol. I, Book 2, pp. 72 and 82. Gosenergizdat, Moscow-Leningrad (1934).
2. PRAETORIUS E., *V.D.I.* 7, No. 6 (1927).

VOL. 15 1961

Reactor Science and Technology (Journal of Nuclear Energy, Parts A/B), 1961, Vol. 15, pp. 54 to 58. Pergamon Press Ltd. Printed in Northern Ireland

INVESTIGATION OF THE ROLE OF OXIDATION-REDUCTION PROCESSES WHEN URANIUM OXIDES DISSOLVE IN ACID MEDIA*

G. M. NESMEYANOVA and G. M. ALKHAZASHVILI

(*Received* 11 *January* 1960)

Abstract—The acidity of the ore is of crucial importance in uranium extraction. As the passage of uranium into solution involves various chemical processes and is complicated by the presence of impurities in the ores, it is necessary to study the mechanism of uranium oxidation and the influence of various compounds which pass into solution during the leaching of the uranium ore.

In this paper are presented the results of an investigation into the oxidation and solution of uranium oxide in acid media and the influence on these processes of divalent iron compounds. For the first time the effects on uranium of various oxidizing agents are compared. It is shown that the oxidation of tetravalent uranium is not determined simply by the normal oxidation-reduction potential. The results obtained show that where considerable quantities of iron ions are present incomplete uranium extraction by a mixture of nitric and sulphuric acids in low concentrations is associated with the formation of complexes between Fe^{2-}, SO_4^{2-} and NO_3^- ions.

IT is well-known that unoxidized uranium minerals do not dissolve well in weak solutions of mineral acids and alkali carbonates. For this reason various oxidizing agents must be used to dissolve the maximum amount of uranium.

The solution of uranium involves various chemical processes and is complicated by the presence of numerous impurities in the ores. It is therefore necessary to study not only the mechanisms of uranium oxidation but also the influence on this process of various compounds which pass into solution during the acid leaching of uranium ores.

By studying these problems it is possible not only to establish theoretically the processes occurring when uranium is extracted from ores, but also to predetermine methods for intensifying these processes.

In recent years many papers have appeared which deal with the influence of various factors on the solubility of uranium. Reference [1] gives, in addition to data on uranium extraction as a function of the duration of the experiment, the temperature, the concentration of the acid and the size of the particles, data showing that when leaching with an acid medium the use of oxidizing agents improves the extraction of uranium into the solution. It has been shown[2] that changing the total concentration of a mixture of nitric (25 per cent) and sulphuric (75 per cent) acids from 13·5 to 107·6 g/l increases the extraction of uranium into solution from 61 to 80 and from 82 to 97 per cent, the initial values depending on the particle size and the agitation time. At a sulphuric acid concentration of 16·5 g/l the introduction of potassium chlorate, potassium permanganate, sodium bichromate and other oxidizing agents into the reaction mixture increases the extraction of uranium into solution. At the same time it is noted that in the presence of ferric ions the uranium dissolves well without the addition of an oxidizing agent. In the references already quoted, and also in [3,4] the influence of various factors on the extraction of uranium from ore material is described. As the ores contain a whole complex of minerals, data on the extraction of uranium into solution reflect the influence not only of the leaching factors (concentration, temperature etc.) but also of the various impurities contained in the ores.

We have performed a series of experiments with the oxides of uranium in order to study the influence of reagent concentration, temperature and processing time on the rate at which uranium dissolves. Sulphuric acid was used as the solvent, nitric acid, potassium chlorate, manganese dioxide, potassium permanganate and ferric salts as the oxidizing agents. The experiments were performed with controlled air temperatures. The batch of uranium oxide was 2 g in weight and 0·15 mm in size and the reagent expenditures were stoichiometric. The various combinations of uranium oxides, sulphuric acid solutions of several concentrations and oxidizing agents were placed in glass test tubes which were mounted on a rotatable disk. While the reactions proceeded the disk rotated at 200 r.p.m. The amounts

* Translated by R. D. M. HEGARTY from *Atomnaya Energiya* **8**, 330 (1960).

of tetravalent and hexavalent uranium were determined by the methods described in [5,6].

Figure 1 presents the results of the experiments in which uranium oxides were dissolved in sulphuric acid of various concentrations. In three hours almost no uranium dioxide dissolved in a solution of sulphuric acid at a concentration of 150 g/l and a temperature $t = 90°C$. This may be explained by the fact that the heat of formation of uranium dioxide is

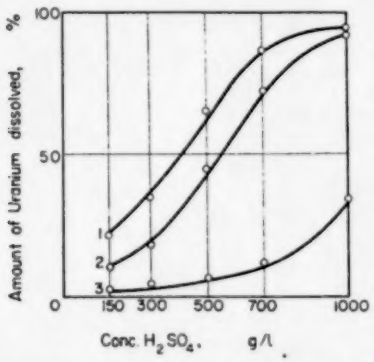

FIG. 1.—Influence of sulphuric acid concentration on the solution (1) of hexavalent uranium from the mixed oxide; (2) of tetravalent uranium from the mixed oxide; (3) of tetravalent uranium from the dioxide.

extremely high (270 kcal/mole). Under the same conditions relatively more uranium from the mixed oxide passed into solution.

In [2] a ratio of 25 per cent nitric acid to 75 per cent sulphuric acid is considered the optimum mixture for dissolving the mixed oxide of uranium. According to the reaction equations

$$3U_3O_8 + 2HNO_3 + 9H_2SO_4 = \\ = 9UO_2SO_4 + 2NO + 10H_2O$$

and

$$3UO_2 + 2HNO_3 + 3H_2SO = \\ = UO_2SO_4 + 2NO + 4H_2O$$

to dissolve the uranium completely the nitric and sulphuric acids must be mixed in the proportions 12·5 per cent HNO_3 and 87·5 per cent H_2SO_4 for the mixed oxide and for the dioxide 30 per cent HNO_3 and 70 per cent H_2SO_4. By altering the ratio of nitric and sulphuric acids over wide limits (Fig. 2) we have shown that maximum oxidation of the uranium in the mixed oxide is observed when the $HNO_3 : H_2SO_4$ ratio is 12·5 : 87·5; a further increase in the nitric acid content does not influence the uranium oxidation, which at $t = 90°C$ is 100 per cent. For uranium dioxide complete oxidation and solution occurs for a ratio $HNO_3 : H_2SO_4 = 30 : 70$, which is just as it should be from stoichiometry. At $t = 20°C$ a similar picture is observed for the mixed oxide, but uranium dioxide behaves differently. This is explained not only by the fact that uranium in the dioxide is more difficult to oxidize, but also by the weak oxidizing properties of nitric acid at low temperatures. Under similar conditions (constant temperature and reaction time) the effect of the initial sulphuric acid concentration varies with different oxidizing agents (Fig. 3). At $t = 20°C$ increasing the sulphuric acid concentration

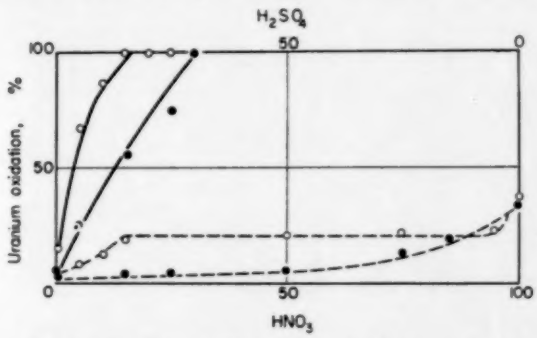

FIG. 2.—Dependence of uranium oxidation on the quantity of nitric acid in a mixture of nitric and sulphuric acids at a total concentration of 100 g/l and reaction time 3 hr. ○: mixed oxide of uranium; ●: uranium dioxide; ———: $t = 90°C$; – – – –: $t = 20°C$.

from 5 to 100 g/l has little effect on the oxidation of mixed uranium oxide by permanganate, potassium chlorate and nitric acid, but at $t = 90°C$ the sulphuric acid concentration plays a decisive part in oxidation with nitric acid. The mixed oxide of uranium dissolves completely at a sulphuric acid concentration of 100 g/l in the presence of oxidizing agents such as nitric acid and a ferric salt. In the presence of manganese dioxide on the other hand oxidation of the uranium is scarcely affected by changing the sulphuric acid concentration over a range of 50–150 g/l.

At a sulphuric acid concentration of 100 g/l uranium is completely oxidized and dissolved only when ferric iron compounds and nitric acid are used as oxidizing agents. We therefore studied the speed with which the mixed oxide dissolved (Fig. 4). At $t = 20°C$ not one of the oxidizing agents used oxidizes and dissolves the uranium completely even after 38 hr. At $t = 90°C$ the worst results were obtained with manganese dioxide. Complete solution of the mixed oxide of uranium is slower with potassium chlorate than with nitric acid and the iron salt.

Figure 5 presents typical curves showing how the temperature affects the rate at which uranium oxidizes and dissolves. For nitric acid at temperatures from 20° to 40°C especially rapid oxidation of the uranium is observed. In sulphuric acid with added nitric acid or

VOL. 15 1961

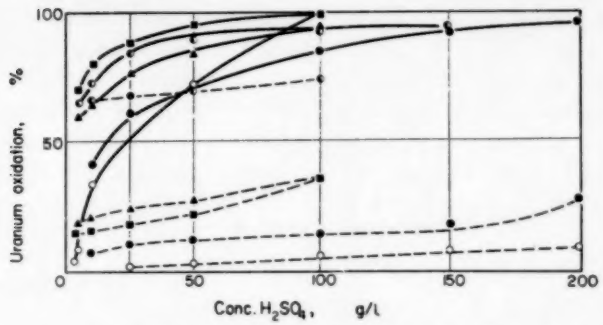

FIG. 3.—The degree of oxidation of uranium for various initial concentrations of sulphuric acid with oxidizing agents. ○: nitric acid; ●: potassium chlorate; ◐: potassium permanganate; ▲: manganese dioxide; ■: ferric sulphate; ———: $t = 90°C$; - - - -: $t = 20°C$; reaction time = 3 hr.

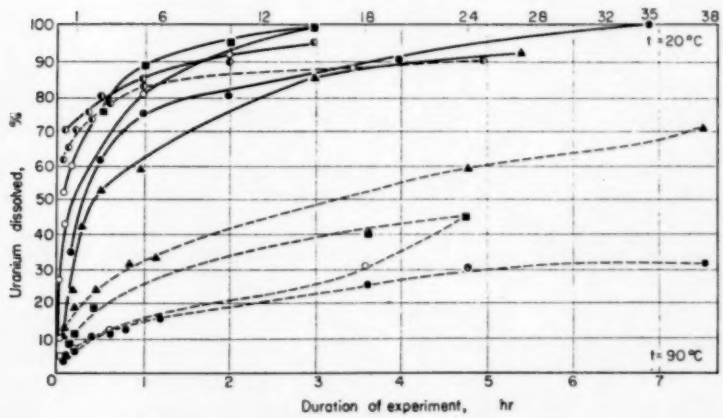

FIG. 4.—Influence of reaction time on the amount of uranium dissolved when the mixed oxide is treated with sulphuric acid and the oxidizing agents. ○: nitric acid; ●: potassium chlorate; ◐: potassium permanganate; ▲: manganese dioxide; ■: ferric sulphate; ———: $t = 90°C$; - - - -: $t = 20°C$.

potassium chlorate the amount of uranium dissolved varies almost linearly with temperature. For mixtures of sulphuric acid with ferric sulphate, manganese dioxide and potassium permanganate the amount of mixed oxide dissolved varies more rapidly when $t = 20 \div 60°C$ than when $t = 60 \div 90°C$. A comparison of the curves of Fig. 5 shows clearly that the influence of temperature on the amount of uranium dissolved is comparatively small only when potassium permanganate is used. This is explained by the fact that in this case the reaction occurs in the diffusion region. The results obtained show that in the presence of oxidizing agents the extent to which the mixed oxide of uranium dissolves is largely determined by the mechanism of the process and by purely kinetic factors.

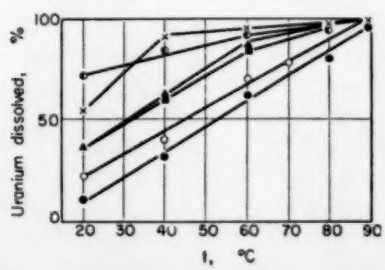

FIG. 5.—Influence of temperature on the amount of uranium dissolved during treatment of the mixed oxide with nitric acid (×) and sulphuric acid together with the oxidizing agents. ○: nitric acid; ●: potassium chlorate; ◐: potassium permanganate; ▲: manganese dioxide; ■: ferric sulphate. Concentration of acids 100 g/l; reaction time = 3 hr.

If one compares the degree to which uranium is oxidized by various oxidizing agents at a sulphuric acid concentration of 25 g/l, it can be seen that the most effective oxidizing agent for uranium is potassium permanganate. A mixture of nitric and sulphuric acids with potassium chlorate gives the worst results. In the presence of divalent iron the picture changes

abruptly. If oxidation and solution of the mixed oxide of uranium proceed according to one of the following reactions:

$$3U_3O_8 - 3FeSO_4 - 24HNO_3 = 9UO_2(NO_3)_2 - Fe(NO_3)_3 - Fe_2(SO_4)_3 - 3NO - 12H_2O;$$

$$2U_3O_8 - KClO_3 - 2FeSO_4 - 7H_2SO_4 = 6UO_2SO_4 + Fe_2(SO_4)_3 - KCl - 3H_2O;$$

$$2U_3O_8 - 3MnO_2 + 2FeSO_4 - 10H_2SO_4 = 6UO_2SO_4 - Fe_2(SO_4)_3 - 3MnSO_4 - 10H_2O;$$

$$2U_3O_8 - 2HNO_3 - 2FeSO_4 - 7H_2SO_4 = 6UO_2SO_4 + Fe_2(SO_4)_3 - 2NO - 8H_2O,$$

then for oxidizing agents such as potassium chlorate, manganese dioxide and nitric acid, in the absence of sulphuric acid, an increase is observed in the degree of uranium oxidation (Fig. 6). On the other hand, for a mixture of sulphuric and nitric acids the presence of divalent iron is characterized by a sharp reduction in the rate of oxidation of the uranium. In the first case iron plays the part of a catalyst, accelerating the process, and in the second case it retards it.

Reference [2] describes a similar situation. When ore was treated with a mixture of nitric and sulphuric acids of total concentration 108·5 g/l the best extraction of uranium into solution was obtained from the ore which had been more coarsely crushed. The longer the ore was crushed in a ball mill, the less the extraction of uranium into solution (95–72 per cent), while when finely ground ore was treated a considerable amount of iron passed into solution. However it is considered[2] that the reduced uranium extraction can hardly be explained by the presence of iron, as nitric

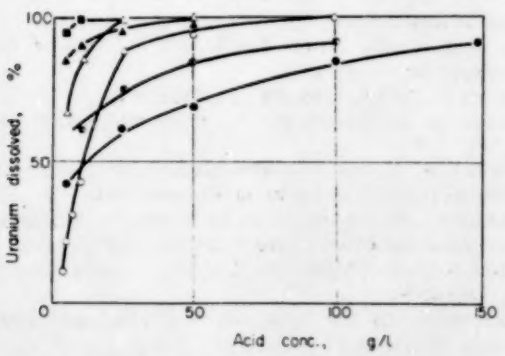

FIG. 6.—Influence of compounds of divalent iron on the amount of uranium dissolved by nitric acid (○, △) and sulphuric acid together with the oxidizing agents (potassium chlorate (●, ▲) and manganese dioxide (◐, ■)) at $t = 90°C$, dependence on initial acid concentration: ○, ●, ◐: without Fe^{2+}, reaction time 3 hr; △, ▲, ■: with Fe^{2+}; reaction time 1 hr.

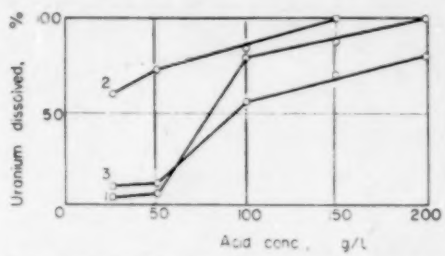

FIG. 7.—Influence of divalent iron compounds on the amount of uranium dissolved by a mixture of nitric and sulphuric acids as a function of the total acid concentration (1) in the presence of Fe^{2+}; (2) in the absence of Fe^{2+}, $t = 90°C$, reaction time 3 hr; (3) oxidation of Fe^{2+}.

acid was used in excess, in relation to the amount of iron present.

Figure 7 shows how compounds of divalent iron affect the oxidation of uranium by a mixture of nitric and sulphuric acids for various initial concentrations of these acids. At concentrations of 25–150 g/l the amount of uranium dissolved suddenly decreases, and this is connected with the formation of complexes in the system Fe^{2+}, SO_4^{2-}, NO_3^-.

Oxidation processes occurring in the presence of nitric acid are autocatalytic: in them the oxides of nitrogen play the part of catalysts. Therefore if the decomposition products from nitric acid are bound into complexes of the type $[Fe(NO)]SO_4$, $NO^-[Fe(NO_3)_3]^-$ or $Fe_2(SO_4)_3NO_3$, which tinge the solutions dark brown, the oxidizing power of the nitric acid is reduced.

According to the results quoted in [7] the acidity of the solution has a pronounced influence on the absorption of oxides of nitrogen. In [8] it is shown that the solubility of nitric oxide in solutions of divalent iron salts varies with temperature according to the Clausius-Clapeyron equation, but the variation deviates from Henry's law. As the nitric acid concentration increases, absorption of oxides of nitrogen by iron salts decreases.[9] Figure 8 shows that when the total concentration of a mixture of nitric and sulphuric acids is brought to 200 g/l the inhibiting influence of divalent iron ceases and the mixed oxide dissolves completely.

Although the value of the normal oxidation-reduction potential of the system Fe^{2+}/Fe^{3+} is 0·77 V, the smallest value for any of the oxidizing agents studied, compounds of ferric iron at $t = 90°C$ are better oxidizing agents than potassium chlorate or manganese dioxide (Fig. 8). It follows from this that in a sulphuric acid medium containing the two oxidizing agents—nitric acid and a ferric salt—compounds of trivalent iron serve as the oxidizing agent for the uranium. Nitric acid, within the limits of total concentration represented by mixtures of nitric and

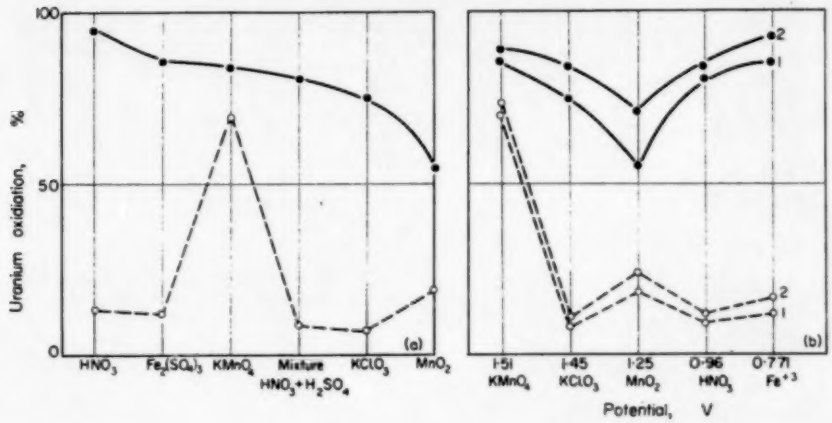

(a) (b)

FIG. 8.—Comparative characteristics of oxidizing agents: (a) in order of decreasing oxidizing power in relation to uranium; (b) in order of decreasing oxidation-reduction potentials. Duration of experiment: (1) 1 hr; (2) 2 hr; ——— : $t = 90°C$; – – – – : $t = 20°C$.

sulphuric acids of 25–150 g/l, is bound into a complex by the ferrous ions liberated, and does not take part in the uranium oxidation process. Retardation of the uranium oxidation by added ferric ions begins to appear at an equimolar ratio of nitric acid to ferric sulphate. A gradual increase in the amount of ferric salt present increases the extent to which the mixed oxide of uranium dissolves. Here the ferrous ion content is related to the quantity of uranium oxidized according to the reaction

$$U_3O_8 + Fe_2(SO_4)_3 + 2H_2SO_4 = \\ = 3UO_2SO_4 + 2FeSO_4 + 2H_2O,$$

i.e. the uranium oxidizes as if the nitric acid was not present in the reaction mixture.

The following conclusions may be drawn from the foregoing.

1. We have studied the influence of reagent concentration, reaction time and temperature on the extent to which uranium oxides oxidize and dissolve in an acid medium.

2. The influence of reagent concentration and temperature on the oxidation process is smallest with potassium permanganate. In spite of the relatively low oxidation-reduction potential of Fe^{2+}/Fe^{3+} in relation to U^{4+}/UO_2^{2+}, iron salts at $t = 90°C$ are in an acid medium the most effective oxidizing agents for uranium.

3. It has been established that if iron compounds are not present in the solution the least effective oxidizing agents for uranium are potassium chlorate and manganese dioxide. When ferrous ions are introduced into the reaction mixture, these oxidizing agents completely oxidize uranium even in comparatively dilute solutions of the acids. In the presence of ionized iron salts high concentrations of a mixture of nitric and sulphuric acids are required to oxidize uranium and iron.

4. It has been established that in the presence of considerable quantities of ionized iron salts the oxidation of uranium by a mixture of nitric and sulphuric acids is retarded as a result of complex-formation processes.

REFERENCES

1. MERVIN G. *et al.*, *Chemistry of Nuclear Fuel* p. 91, Goskhimizdat, Moscow (1956).
2. GUNN B., CAVERS S., and VAN CLEAVE A., *Canad. J. Res. (Technol.)* **34**, 379 (1956).
3. ARDEN T., *Industr. Chem. Mfr.* **32**, 202 (1956).
4. GANDIN A. and SCHUHMANN R., *J. Metals, N.Y.* **8**, 1065 (1956).
5. RODDEN K. I., *The Analytical Chemistry of Uranium and Thorium*, p. 66 Izd-vo inostr. lit. Moscow (1956).
6. ALIMARIN I. P., *Zavodsk. laboratoriya* Nos. 5–6, 545 (1940).
7. ADDISON C. and LEWIS J., *Quart. Rev.* **9**, 115 (1955).
8. GANZ S. N. and MAMON L. I., *Zh. prikl. khim., Leningr.* **26**, 1005 (1953).
9. SIROTKIN G. D. and STAROSTIN V. V., *Zh. prikl. khim., Leningr.* **27**, 1141 (1954).

Reactor Science and Technology (Journal of Nuclear Energy, Parts A/B), 1961, Vol. 15, pp. 59 to 63. Pergamon Press Ltd. Printed in Northern Ireland

LETTERS TO THE EDITORS

The behaviour of a reactor with temperature self-regulation*

(*Received* 8 *January* 1959)

A STUDY of the physics of fast neutron reactors[1,2] shows that two different types of reactivity change take place when the reactor power is increased: (a) comparatively fast changes which are associated mainly with the mechanical deformation of the fuel elements and with coolant expansion and (b) slow changes associated with the expansion of the reactor structural components. For a number of processes the reactivity power factor may be regarded as a combination of an instantaneous power factor p and a delayed power factor k associated with an average time delay τ. The factors p and k may be either positive or negative. This separation of the power factor into two parts applies also to intermediate and thermal reactors.

Several authors[3–6] have studied the influence of temperature effects on reactor behaviour. In the work reported here we studied the general behaviour of a reactor in which the only control was that introduced by the temperature effects mentioned above. The neutrons were divided into two groups: instantaneous (zero lifetime) and delayed (lifetime τ_0). It was assumed that when the reactor is shut down the delayed power contribution falls off exponentially with time. With these assumptions the reactor kinetic equations have the form†

$$W(t) = \frac{\beta}{\tau_0[\beta - \rho(t)]}\int_{-\infty}^{t} W(t')\exp\left(-\frac{t-t'}{\tau_0}\right)dt', \qquad [\rho(t) < \beta]; \tag{1}$$

$$\rho(t) = \rho_0 + pW(t) + \frac{k}{\tau}\int_{-\infty}^{t} W(t')\exp\left(-\frac{t-t'}{\tau}\right)dt', \tag{2}$$

where $W(t)$ is the reactor power, $\rho(t)$ is the reactivity, β is the effective fraction of delayed neutrons, and ρ_0 is the reactivity of the cold reactor (with $W(t) = 0$).

This set of equations reduces to a linear differential equation for $W(t)$ (or for $\rho(t)$) which, with the substitutions $W(t) = x$, $\tau W'(t) = y$, leads to the form

$$\frac{dy}{dx} = \frac{A_1y^3 + A_2y^2x + A_3yx^2 + A_4x^3 + A_5y^2 + A_6yx + A_7x^2}{A_8yx^2 + A_9yx}, \tag{3}$$

where A_1–A_9 are constant coefficients which are functions of k, p, τ, τ_0, β, ρ_0. Since the behaviour of the integral curves in the XY-plane is very strongly influenced by their behaviour in the neighbourhood of the singular points, we investigated all six singular points in equation (3).‡

The most interesting singular points occur at $x = 0$, $y = 0$ and at $x = -\frac{\rho_0}{k+p}$; $y = 0$. The behaviour in the neighbourhood of the first singular point determines the characteristic variation of the reactor power as it rises from zero, while the behaviour near the second singular point determines how the reactor behaves in power regions close to the stationary power level, in the time during which the reactivity ρ_0 introduced by the controlling devices is being compensated by temperature effects. The conditions for the existence of such a point is $k - p < 0$ (with $\rho_0 > 0$). An examination of the solutions of equation (3) in the neighbourhood of the singular point at zero showed that in all cases where $0 < \rho_0 < \beta$, the reactor power increases from zero according to the law

$$W(t) = W_0\exp\left(\frac{\rho_0 t}{(\beta - \rho_0)\tau_0}\right).$$

In the neighbourhood of the stationary point, the solutions of equation (3) are more varied; they are aperiodically stable (*AS*) and aperiodically unstable (*AU*) solutions (singular point a node), oscillatory stable (*OS*) and oscillatory unstable (*OU*) solutions (singular point a focus) and unstable solutions of a special type which we shall call type *U* solutions. These differ from the others by virtue of the fact that only two curves pass through the singular point (i.e. the singular point is a saddle). This is in contrast to the other solutions in which an infinite number of curves pass through the singular point. Figure 1 shows the general form of the domains of existence of these solutions in terms of the co-ordinates ρ_0/β and $p/(k-p)$. Curves I–IV satisfy the equations:

$$\left(\frac{\rho_0}{\beta}\right)_{I,II} = \frac{-1 - ac + 2a \pm \sqrt{(1 + ac - 2a)^2 - (1 - ac)^2}}{(1 - ac)^2};$$

$$\left(\frac{\rho_0}{\beta}\right)_{III} = -\frac{1}{c}; \qquad \left(\frac{\rho_0}{\beta}\right)_{IV} = -\frac{1}{1 + ac},$$

where $a = \tau/\tau_0$ and $c = p/(k + p)$. When $\tau < \tau_0$, the regions *OS*, *OU* and *AU* vanish.

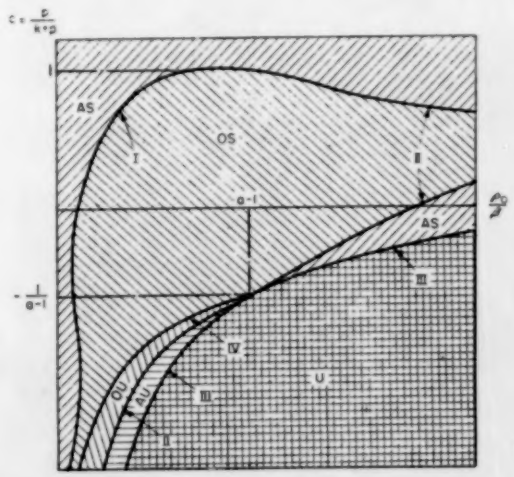

FIG. 1.—Domains of existence of the different solutions of equation (3) in the neighbourhoods of the stationary point.

* Translated by D. L. ALLAN from *Atomnaya Energiya* **7**, 363 (1959).

† See, for example, Reference[3].

‡ See, for example, Reference[7].

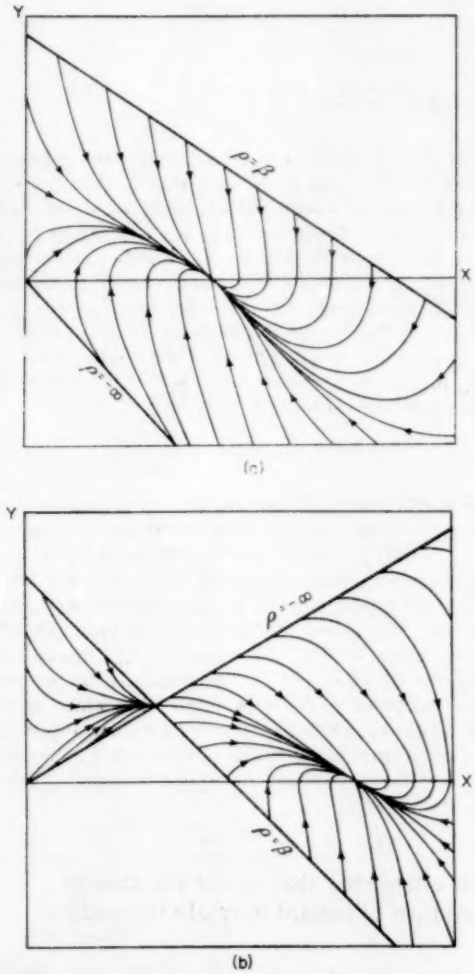

FIG. 2.—Aperiodically stable solutions of equation (3) ending at a stationary point.
(a) solutions in a type (i) region; (b) solutions in a type (iii) region.

In the case of the oscillatory solutions, the small power oscillations are sinusoidal. They have a period

$$T = \frac{4\pi\tau(\beta + c\rho_0)}{\sqrt{4\rho a(\beta + c\rho_0) - (\beta + \rho_0 - ac\rho_0)^2}}$$

and a logarithmic decrement

$$\delta = -\frac{\beta - \rho_0 - ac\rho_0}{2(\beta - c\rho_0)} T.$$

From a study of the particular properties of equations (1) and (2) and of the remaining singular points it is possible to follow the behaviour of the integral curves completely. We restricted our study to that part of the phase plane XY for which a physical meaning could be attached to the solutions of equation (1). These regions were bounded by the straight lines

$$y = (1 - a)x \quad \text{and} \quad y = \frac{x}{c} - \frac{(1 - a)\beta - \rho_0}{p},$$

for which $\rho(t) = -\infty$ and $\rho(t) = \beta$.

According to the values of the constant coefficients in equations (1) and (2), one obtains four different kinds of region.

(i) A singly-connected region enclosing the neighbourhoods of the zero and stationary points.

(ii) Two regions which meet each other at a single point, with the neighbourhoods of the zero and stationary singular points located in one of the regions.

(iii) Two regions, similar to (ii), but with the neighbourhoods of the zero and stationary singular points located in different regions.

(iv) Two detached singly-connected regions with the neighbourhoods of the zero and stationary singular points located in different regions.

In type (i) regions the stationary point is always stable and a transition from the zero power zone to the stationary power zone always takes place. In the case of type (ii) regions, a transition from the zero power to the stationary power zone is also possible and occurs when the solutions at the stationary point are stable (*AS* or *OS*). In the case of type (iii) regions, the integral curves pass out of the zero power zone into the stationary point zone under the same conditions which apply in the case of type (ii) regions. In the converse case, the integral curves pass out of the zero power zone and go to infinity without entering the region containing the stationary point. Naturally, in the case of type (iv) regions, it is not possible to go from zero to stationary power if only the temperature self-regulation of the reactor is available to keep $\rho(t) < \beta$.

When $p < 0$ all the integral curves end at a stationary point and when $p > 0$ only those integral curves from a specific region of the phase space (including the zero power zone) enter a stable stationary point. Outside this region all the integral curves (with, occasionally, a single exception) avoid the stationary point region and go off to infinity. In particular, the boundary of these regions is formed by the segments of the straight line

$$x = \frac{\beta - a\beta - \rho_0}{2p - pa + k}.$$

If the stationary point is unstable, all the integral curves go to infinity.

Figures 2–4 present some typical examples of the behaviour of the integral curves. Figure 2 shows solutions of the *AS* type which

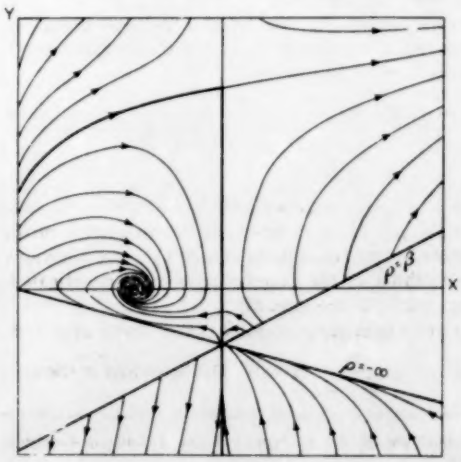

FIG. 3.—Oscillatory stable solutions of equation (3) at a stationary point for a type (ii) region.

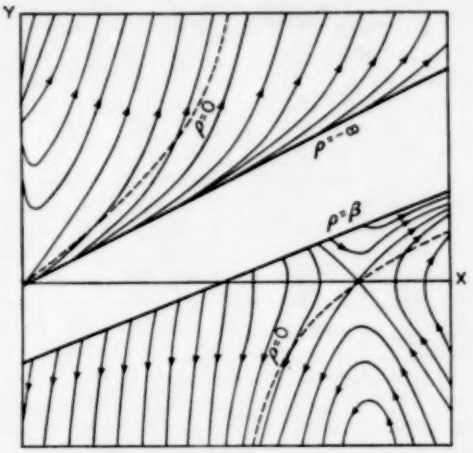

FIG. 4.—Unstable solutions of equation (3) for a type (iv) region.

end at a stationary point for type (i) and (iii) regions, while Fig. 3 gives solutions of the *OS* type at a stationary point for a type (ii) region (the boundaries which separate solutions converging towards the stationary point are separate from the rest of the solutions). An example of an unstable type *U* solution for a type (iv) region is shown in Fig. 4. The broken lines represent the condition $\rho(t) = 0$. From Fig. 4 (top right-hand corner) it can be seen that the reactor power progressively increases (tending to some limit), while $\rho(t)$ is negative. This regime of operation is dependent upon a positive temperature coefficient and arises sometimes when $p > 0$.

If we confine ourselves to the examination of a single neutron group with an average lifetime (valid for slow processes), then the solutions are found in the region represented by the half-plane *XY*. The number of singular points is reduced to two; the zero and stationary singular points. In the stationary point domain the following types of solution remain: *AS*, *OS*, *OU* and *AU* as the power rises for $p > 0$, and *AS*, *OS* and *AS* for $p < 0$.

Acknowledgment—The authors thank A. I. LEIPUNSKII for his interest in this work.

V. N. ANDREEV
O. D. KAZACHKOVSKII
N. V. KRASNOYAROV

REFERENCES

1. LEIPUNSKII A. I. *et al.*, *Proceedings of the Second International Conference on the Peaceful Uses of Atomic Energy, Geneva*, Vol. 9, p. 348. United Nations, New York (1959).
2. THALGOTT F., *Proceedings of the Second International Conference on the Peaceful Uses of Atomic Energy, Geneva*, Vol. 12, p. 242. United Nations, New York, (1959).
3. WELTON T. A., *Proceedings of the First International Conference on the Peaceful Uses of Atomic Energy, Geneva*, Vol. 5, p. 377. United Nations, New York (1956).
4. ACKROYD R., KINCHIN G., MANN J. and MCCULLEN J., *Proceedings of the Second International Conference on the Peaceful Uses of Atomic Energy, Geneva*, Vol. 12, p. 230. United Nations, New York (1959).
5. SCHUL'TZ M., *Control of Nuclear Reactors and Power Plants*, McGraw-Hill, New York (1955).
6. ERGEN W. and WEINBERG A., *Physica, s'Grav.* **20**, 413 (1954).
7. NEMITSKII V. V. and STEPANOV V. V., *Qualitative Theory of Differential Equations*, Gostekhizdat Moscow-Leningrad, (1947).

Sectionalized reactor systems*†

(*Received* 6 *January* 1959)

A SECTIONALIZED reactor system is one in which a high-energy-density critical reactor (acting as a neutron 'trigger') is followed by a succession of sub-critical sections which operate as neutron multipliers. Neutron valves, which pass neutrons in one direction only, are placed at the boundary between the critical reactor and the first sub-critical section, and also between the individual sub-critical sections. These valves consist of a layer of ^{235}U, which is 'black' to thermal neutrons, a layer of cadmium (or, better still, a layer of thorium or highly depleted uranium), and a layer of moderating material. The uranium layer is on the side facing the critical reactor or the preceding sub-critical section and the neutrons can pass only in the direction uranium to moderator. The multiplication factor of each sub-critical section is determined by its nearness to criticality.

Of the neutrons which leak out of a sub-critical section the overwhelming majority are unable to pass back, since if they start to traverse the neutron valve in the reverse direction they are slowed down in the moderator and are captured by the absorbing layer.

BORST[1] has independently described‡ a neutron valve for isolating the sub-critical sections in convergatron systems, in which it is essential in the event of an emergency to guard against an uncontrollable release of reactor power. The efficiency of the neutron valve can be increased by placing a thin layer of water or some other hydrogenous material close to the cadmium layer. The hydrogen scattering cross section for the fast fission neutrons is significantly less than that for slow neutrons and consequently the hydrogen layer lets the fast neutrons through the neutron valve in the forward direction but impedes the flow of slow and thermal neutrons into the absorbing layer. Thus the water layer behaves as a valve when irradiated on one side by fast neutrons and substantially reduces the number of neutrons absorbed in the absorbing layer. Calculations made by V. V. Orlov show that with a water layer ~2 cm thick the neutron transmission through the valve may reach 0·9. It should be mentioned that a neutron valve can be used to protect any type of reactor, including fast and intermediate reactors. The energy production of the sub-critical sections is such that a substantial increase in the burn-up of fissile isotopes can be achieved. As an illustration, we give the essential parameters of a sectionalized reactor system having the same lattice arrangement as the reactor of the First Atomic Power Station[3].

Lattice multiplication factor	1·38
Total neutron leakage (per cent)	28

---

* Translated by D. L. ALLAN from *Atomnaya Energiya* **7**, 456 (1959).

† Paper presented to the Physics Section of the Scientific Council of the Board of Atomic Energy Utilization Physics Institute in the presence of the Council of Ministers of the U.S.S.R. (1957).

‡ A neutron valve has also been described by DUBOVSKII *et al.*[2]

Geometrical leakage of neutrons through the side face (per cent)	12
Fraction of neutrons from the critical reactor which pass through the valve and undergo multiplication in the sub-critical section (per cent)	10
The effective multiplication factor k_{eff} of a sub-critical section which operates at the same power as the critical reactor	0·90

An effective multiplication factor of 0·90 can be obtained in a sub-critical section either at the expense of a reduction in the loading, making allowance for the shape of the sub-critical assembly (ring section), or by loading depleted fuel elements into the lattice. At the same time the burn-up of the fuel can be increased two or three times, since the reserve reactivity at burn-up during a run of the atomic power station reactor is 0·03. The fact that power can be produced by a sub-critical reactor for which $k_{eff} < 1$ means that a sectionalized reactor system can be used to provide extremely high fluxes of thermal neutrons. In fact, in a sub-critical reactor having the same neutron multiplication and leakage parameters as a critical reactor, the thermal neutron utilization coefficient can be reduced in conformity with the value of k_{eff}, at the expense of an increase in the quantity of constructional materials. Thus for the same thermal load it is possible to increase the thermal neutron flux. For the lattice used in the atomic power station reactor it is possible to increase the thermal neutron flux by nearly a factor of three by reducing k_{eff} from 1 to 0·7.

To obtain the highest neutron fluxes it is advantageous to employ a 'convergent' sectionalized reactor system in which an outer ring-shaped critical reactor is the trigger which irradiates an adjacent inner sub-critical section with neutrons. This inner section in turn irradiates the adjacent central section. In such a 'convergent' system the neutron valve passes neutrons from the circumference towards the centre. An interesting application of sectionalized reactor systems is their use as pulsed neutron sources to provide intense pulsed neutron fluxes.

Acknowledgments—The author thanks A. K. KRASIN, I. I. BONDARENKO and L. A. GERASEVA for their interest in this work and for valuable advice.

B. G. DUBOVSKII

REFERENCES

1. BORST L., *Phys. Rev.* **107**, 905 (1957).
2. DUBOVSKII B. G., KAMAEV A. V. and MAKAROV E. F., *J. Nucl. Energy* **6**, 172 (1958).
3. KRASIN A. K., DUBOVSKII B. G., DOIL'NITSIN E. IA., MATALIN L. A., INIUTIN E. I., KAMAEV A. V. and LANTSOV M. N., *J. Nucl. Energy* **3**, 227 (1956).

Compound fission of uranium by 2·5 MeV neutrons*

(*Received* 20 *June* 1959)

COMPOUND fission of heavy nuclei by thermal and epithermal neutrons in which a long-range alpha particle is emitted has been studied extensively. It appears, however, that compound fission by high-energy neutrons received comparatively little attention. The negative result published in[1] was accepted as proof that compound fission is characteristic of ^{235}U and is related to the lower excitation levels of fissile nuclei. Subsequent findings[2,3] however have shown that 2·5 and 14 MeV neutrons can induce compound fission in uranium.

This note is concerned with investigations into the compound fission of uranium by 2·5 MeV neutrons.

Type P–9 photo-emulsions were loaded with a 4 per cent aqueous solution of $UO_2\,Na(C_2H_3O_2)_3$ of natural isotopic composition. These emulsions are adequate to discriminate between particles of different charges. To reduce the soft neutron background the plates were placed in cadmium cylinders filled with boron and the irradiation time was chosen so that the background of secondary particles did not interfere unduly with observations.

During scanning both the compound fission and the total number of binary fission events were registered. Altogether 50 ternary fissions were found in about 30,000 fission events, i.e. one fission in 600 is a ternary event involving the formation of an alpha-particle. Corresponding probabilities for ternary fission

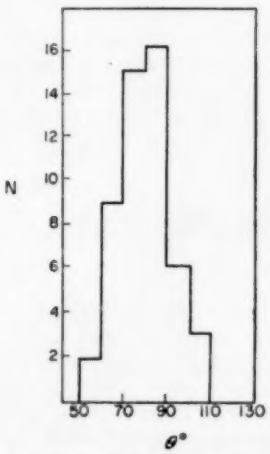

FIG. 1.—Angular distribution of α-particles about the direction of the light fission fragment.

are about 1 in 350 for thermal neutrons and about 1 in 1,100 for 14 MeV neutrons[3] and it may therefore be concluded that the probability of this rare event decreases with the increasing excitation energy. It must be remembered, however, that thermal neutrons cause fission in ^{235}U, while in experiments involving fast neutrons fission occurs in ^{238}U.

To establish whether the probability of ternary fission depends on the isotopic composition of uranium, a control experiment was performed. In this the emulsion was charged with a uranium salt containing approximately one-fifth as much ^{235}U as natural uranium. The emulsion was irradiated with 2·5 MeV neutrons and the probability for ternary fission was found to be independent of the ^{235}U content. It can be concluded therefore that the observed ternary fissions occurred in ^{238}U.

Compound fission by 2·5 MeV neutrons is similar to compound fission by neutrons of other energies, thus:

(a) fission is asymmetric and the average ranges of the light and heavy fragments are in the ratio $R_L/R_H = 1{\cdot}3$;

(b) in the angular distribution of α-particles the slight shift from 90° to the direction of motion of the light fragment was found, (Fig. 1);

* Translated by J. ADAM from *Atomnaya Energiya* **8**, 137 (1960).

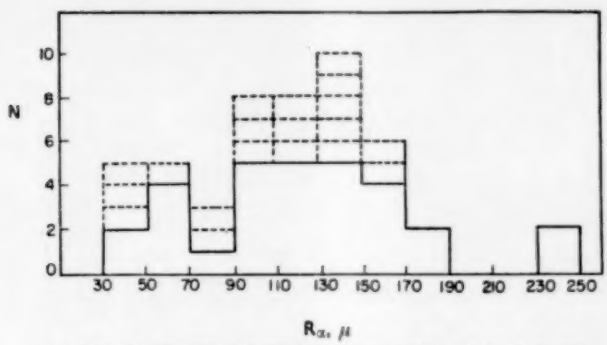

FIG. 2.—Range distribution of α-particles formed in the fission of uranium by 2·5 MeV neutrons.
— — — — —: Tracks leaving the emulsion.

(c) the distribution of α-particle ranges in the emulsion shows a broad maximum at $R_\alpha = 130\ \mu$ (Fig. 2) which corresponds to an energy of 16 MeV.

Acknowledgment—The author wishes to thank N. A. PERFILOV for help in this work.

Z. I. SOLOV'EVA

REFERENCES

1. TSIEN SAN-TSIANG, CHASTEL R., HO ZAH-WEI and VIGNERON L., *J. Phys. Radium* **8**, 165,200 (1947).
2. TITTERTON E. W., *Phys. Rev.* **83**, 673 (1951).
3. PERFILOV H. A. and SOLOV'EVA Z. I., *Atomnaya Energiya* **5**, 175 (1958).

VOL.
15
1961

Reactor Science and Technology (Journal of Nuclear Energy Parts A/B) 1961, Vol. 15, p. 64. Pergamon Press Ltd. Printed in Northern Ireland

BOOKS RECEIVED

BONDI H., BONNER W. B., LYTTLETON R. A. and WHITROW G. J. *Rival Theories of Cosmology*, A Symposium and Discussion of Modern Theories of the Structure of the Universe. Oxford University Press, London, 1960. 64 pp., 9*s* 6*d*.

DE VRIES L. *The Book of the Atom*, Macmillan, New York, 1960. 267 pp., $3.95.

AUGENSTINE L. G. *Radiation Research*—Supplement 2: *Bioenergetics*, Academic Press, New York, 1960. 685 pp., $10.

ScB-Bulletins (*Physica*) Bookimpex, Nederland, March 1961. 76 pp., Annually $5.50 or 38*s*.

LOUTIT J. F. and SCOTT RUSSELL R. *Progress in Nuclear Energy* Series VI—*Biological Sciences*. Volume 3 *The Entry of Fission Products into Food Chains*, Pergamon Press, London, 1961. 154 pp., 45*s*.

ABRAGAM A. *The Principles of Nuclear Magnetism*. Clarendon Press, Oxford, 1961. 599 pp., 84*s*.

Reactors of the World, Second Series (Published in Association with *Nuclear Engineering*). Temple Press, London, April 1961, 17*s* 6*d*.

The Physical Review Volume 121, No. 6, Second Series. American Physical Society, March 1961. $3.

The Physical Review, Volume 122, No. 1, Second Series. American Physical Society, April 1961. $3.

ZUCKER A., HALBERT E. C. and HOWARD F. T. *Proceedings of the Second Conference on Reactions between Complex Nuclei*. John Wiley, New York. 319 pp., 56*s*.

GLINER B. M. *Determination of the Mechanical and Technological Properties of Metals*. Pergamon Press, London, 1960. 160 pp., 50*s*.

SANDERS J. H. *The Fundamental Atomic Constants*, Oxford University Press, 1961. 88 pp., 10*s*.

The Physical Review, Volume 121, No. 1, Second Series. American Physical Society, January 1961.

BLANC D. and AMBROSINO G. *Eléments de Physique Nucléaire*. Masson & Cie, Paris. 238 pp., 30 NF.

DOWSETT H. M. *The Structure of the Atom*. Stephen Austin Ltd., Hertford, England, 30*s*.

Ionizing Radiation in Space. (A wall chart prepared and distributed by Contract Sales Dept., Tracerlab. Inc., Waltham, Mass. and Richmond Calif. U.S.A.) 1961.

VOL
15
196

Reactor Science and Technology (Journal of Nuclear Energy Parts A/B) 1961, Vol. 15, p. 65. Pergamon Press Ltd. Printed in Northern Ireland

PAPERS TO BE PUBLISHED IN FUTURE ISSUES

E. ERDIK: **The experimental determination of fast fission factors in light water-moderated, slightly enriched uranium rod lattices.**

C. CARTER: **Streaming due to holes in a reactor.**

R. K. THOMASSON: **A general method of deriving responses and transfer functions in transient heat conduction phenomena.**

P. N. COOPER, W. M. COOPER and K. FIRTH: **The effect of cylindrical air voids in a highly enriched water-moderated core.**

F. T. ADLER and Y. D. NALIBOFF: **Reactor kinetics: integral equation formulation.**

W. J. MEGAW, R. C. CHADWICK, A. C. WELLS and J. E BRIDGES: **The oxidation and release of iodine-131 from uranium slugs oxidizing in air and carbon dioxide.**

M. C. WITTELS: **Stored energy in the Oak Ridge graphite reactor—1960.**

H. TAKAHASHI: **Generalization of the singular integral method for an anisotropic scattering medium.**

A. J. DERUYTTER: **The fission cross section of ^{233}U from 0·01 eV to 0·1 eV and its absolute value at 0·0253 eV.**

J. CSIKAI, A. DAROCZY and K. DEDE: **Measurements of the diffusion length of thermal neutrons in water from 16 to 89°C and in diphyl (Dowtherm A) at 185°C.**

VOL.
15
1961

Reactor Science and Technology (Journal of Nuclear Energy, Parts A/B) 1961, Vol. 15, pp. 66 to 68. Pergamon Press Ltd. Printed in Northern Ireland

ABSTRACTS AND TITLES OF FUTURE PAPERS

Atomnaya Energiya

Vol. 10, No. 2

Use of the moment method for calculating the spatial and energy distributions of the neutron fluxes produced by point and two-dimensional sources in an unbounded medium: A. R. PTITSYN.

A method is given for calculating the spatial and energy distributions of the neutron fluxes produced in an unbounded medium by plane and point sources. The density $\psi(x, E)$ is sought in the form $\psi(x, E) = \sum_{i=1}^{N} d_i(E)K[b_i(E)x]$. The form of the function $K(x)$ is unimportant and may be selected on the basis of physical considerations. The $2N$ parameters a_i, b_i are found from $2N$ spatial moments of $\psi(x, E)$. Distributions are given for hydrogen and water; those for water are compared with experimental results. Comparison with Wick's exact solution for hydrogen shows that it is sufficient to use four moments to find the spatial distribution with adequate accuracy up to distances of 20 mean free paths.

Production of an azimuthally varying magnetic field: R. A. MESHCHEROV and E. S. MIRONOV.

A method is presented for calculating the surfaces of poles designed to produce a magnetic field which has an azimuthal variation of specified extent and whose mean value follows a specified law along a radius. A description is given of experiments with an analogue for the field of a 1½-metre cyclotron having an azimuthally varying field.

Thermal stresses in the walls of a reactor having fluctuating internal heat sources: B. I. MAKSIMENKO, K. N. NIKITIN and L. I. BASHKIROV.

The thermal stresses set up during transient states covering a wide range in heat loading may exceed the stresses set up in steady states. The rate of change of loading must be restricted in order to ensure that the components will work reliably. The geometrical forms of components can be referred to the two commonest types, namely flat walls and cylindrical walls. A solution to the equations for transient heat flow in such walls is used to compare the stresses arising in the two types during transient modes of operation.

Reaction between solid UO_2 and solid MnO_2 in solutions of sulphuric acid: E. A. KANEVSKII and V. A. PCHELKIN.

A study is reported of the reactions of UO_2 with MnO_2 in sulphuric acid (in relation to the use of pyrolusite in acid leaching of uranium ores); various possible mechanisms are discussed. The experimental results show that the reactions occur at the meeting points of the hydrated surface layers of UO_2 and MnO_2; the rate of the process is restricted by steric hindrance. The same basis is used to discuss the role of iron in the reactions between pyrolusite and primary uranium minerals during acid leaching.

A study of the behaviour of UF_6 in organic solvents: N. P. GALKIN, B. N. SUDARIKOV, V. A. ZAITSEV, D. A. VLASOV and V. G. KOSAREV.

Published material is used for a brief review of the various methods of making UF_4 from UF_6; those suitable for use in reductive melting are stressed. Free-energy data are given for some of the reactions, and the effects of some factors on the purity and apparent density of the UF_4 are discussed. The advantages and disadvantages of the various methods are considered.

Methods of reducing UF_6: N. P. GALKIN, B. N. SUDARIKOV and V. A. ZAITSEV.

Solubility and rate of solution are reported for UF_6 in carbon tetrachloride, chloroform, dichloromethane unsymmetrical dichloroethane, s-tetrachloroethane, pentachloroethane, trifluorotrichloroethane, trichloroethane, and tetrachloropropane. It is found that solutions of UF_6 in carbon tetrachloride, tetrachloroethane, pentachloroethane and trifluorotrichloroethane are stable for two weeks at 20°C, whereas those in chloroform, dichloromethane, and dichloroethane are unstable. It is found that UF_6 reacts with these organic solvents in the following way at 60–100°C. UF_6 is first formed and is afterwards reduced to indefinite fluorides containing much U^{IV} and then to UF_4 itself.

Letters to the Editor

The mechanisms whereby fast nucleons interact with nuclei: V. S. BARASHENKOV, V. M. MAL'TSEV and E. K. MIKHUL.

Measurement of the radiative capture cross section of ^{127}I for fast neutrons: YU. YA. STAVISSKII, V. A. TOLSTIKOV and V. N. KONONOV.

A beta ray source based on ^{198}Au for use in studies of the physical properties of materials under irradiation: M. A. MOKUL'SKII and YU. S. LAZURKIN.

A generator producing a strong flux of neutrons having energies of 14 or 2·5 MeV: V. I. PETROV.

The effects of radiation of the electrochemical behaviour of 1Kh18N9T steel: V. V. GERASIMOV and V. N. ALEKSANDROVA.

A method of studying slowing-down processes for fission fragments in metals: N. A. PROTOPOPOV, YU. B. SHISHKIN, V. M. KUL'GAVCHUK and V. I. SOBOLEV.

Melting points and other parameters of the lower oxides of niobium: O. P. KOLCHIN and N. V. SUMAROKOVA.

High-temperature hardness of some alloys based on niobium: I. I. KORNILOV and R. S. POLYAKOVA.

The characteristics of irradiated glasses: ZDENEK SPURNY.

Build-up factors for heterogeneous shields: L. R. KIMEL.

Solution to the kinetic equation for a medium having a point source emitting in a single direction: E. B. BRESHENKOVA and V. V. ORLOV.

Effects of inelastic scattering in uranium on the moderation length for neutrons in water: B. A. LEVIN, E. V. MARCHENKO and D. V. TIMOSHUK.

News of Science and Technology

Bibliography

Vol. 10, No. 3

The 230cm adjustable-energy cyclotron at Livermore: H. ERNANDEZ, J. PETERSON, B. SMITH and S. TAYLOR.

A description is given of a cyclotron in which protons can be accelerated to energies ranging from 2·6 to 15 MeV; deuterons, from 5·2 to 12·5 MeV; and α-particles, from 10·4 to 25 MeV. The magnet is 230 cm in diameter and produces a leakage field of special form, which is such as to reduce the divergence of the external beam. The resonant circuit to one dee is supplied by a generator consisting of a quartz-crystal oscillator feeding a power amplifier; the frequency is adjustable from 4·0 to 9·5 Mc/s by steps of 55 kc/s. The current in the external beam is restricted to 200 μA in order to avoid damaging the deflecting electrode; 15–25 per cent of the beam can be extracted. The total energy spread in the external beam is 2 per cent, the duration of one phase bunch being about 2 per cent of the period of oscillation. Most of the extracted beam is contained within an elliptic cone having angles of 0·6° and 0·3°.

Selection of the best parameters for a nuclear power station: A. YA. KRAMEROV.

A system of equations is derived to define the best parameters for a nuclear power station (the parameters that provide electric power at the least cost). It is assumed that the type of system, the principal components, and the materials have already been selected; the problem is that of selecting the best numerical values for the parameters. Fairly general approximate relations are used for the dependence of cost on the parameters. The coupling between the parameters is taken account via equations describing the processes in the system and the restrictions that are imposed on safety grounds.

The system of equations can be used to check the parameters of any proposed two-circuit system which includes a non-boiling reactor and has a defined maximum temperature for the fuel elements. Examples are given of expressions for the best parameters in terms of other parameters; these have been derived from the system of equations.

Resistance of steels and alloys of zirconium to corrosion in solutions of boric acid at various temperatures: M. A. TOLSTAYA, S. V. BOGATYREVA and G. N. GRADUSOV.

Results are given from corrosion tests performed in solutions of boric acid at high temperatures and pressures on 1Kh18N9T steel, Zr alloys containing 1 and 2 per cent Nb, and on carbon steel type 20. The materials were tested under static conditions in autoclaves; the boric acid concentration was varied from 0·23 to 1·13 g/l in tests at 335°C and 140 atm lasting 1000 and 2000 hr, and was 5·65 g/l in tests at 310°C and 100 atm lasting 150 hr. It is demonstrated that boric acid can be used in the fine-control system of a nuclear power station.

Results are also given for solutions of boric acid used at 40°C with free access of oxygen, the materials being in this case steel 20, alloy steel Kh5M2, stainless steel OKh13, and 1Kh18N9T steel. These results show that OKh13 steel can be used for storage tanks.

Nature of the residual defects in single crystals after neutron irradiation and deformation: E. V. KOLONTSOVA.

X-ray diffraction and etching methods have been used to study the defects produced by radiation in LiF and α-quartz and by deformation in LiF, aluminium, etc. Some common features are detected.

The use of ammonium carbonate for purifying uranium: N. P. GALKIN, A. A. MAIOROV, G. A. POLONNIKOVA, V. G. SHCHERBAKOVA and L. V. UTKINA.

Pure $(NH_4)_2U_2O_7$ (solid) has been used in conjunction with solutions of $(NH_4)_2CO_3$ and NH_4HCO_3, salting-out tests have been made with $(NH_4)_2CO_3$ [solid deposited $(NH_4)_4UO_2(CO_3)_3$], and studies have been made of the behaviour of some impurities during crystallizations. It has proved possible to select conditions for obtaining the largest crystals of $(NH_4)_4UO_2(CO_3)_3$; it has been found that certain impurities (Cu, Na, P, V) are removed very effectively in crystallization, as well as the others (Fe and Al) already known to be removable in this way.

Radioactivity and the physicochemical properties of a material: L. M. KOPYTIN and YU. V. GAGARINSKII.

Some special properties of radioactive substances are discussed, and it is concluded that these features arise from self-irradiation. Any system containing radioelements is not at equilibrium; the proportion of particles (molecules, atoms, ions) having high energies is larger than the equilibrium value. Any region which is involved in stopping α-rays, β-rays, or recoil atoms has excess free energy and an increased concentration of defects. These two features must affect the vapour pressure, solubility, dissociation pressure, equilibrium constants of reactions, specific heat, density, electrical conductivity, thermal conductivity, and other properties, as well as the type of phase transition to be expected. Some properties reported in the literature for various radioactive substances are considered from this point of view.

Uses of the stable isotopes of boron: S. P. POTAPOV.

A brief review is given of the main trends in the use of the stable isotopes of boron as enriched materials, which are required on account of the nuclear parameters of the isotopes. For example, a neutron flux can be transformed to a flux of heavily ionizing particles by means of the reaction $^{10}B(n, \alpha)^7Li$, which has a high cross section for thermal neutrons; in consequence the reaction has use in medicine, in nuclear research, and in radiation chemistry. The difference between the neutron-capture cross sections of ^{10}B and ^{11}B may be of value in the design of reactors; e.g. ^{10}B may be used in control rods and shields.

Radioactive contamination of the air and of the River Neva in the region used for the fitting out trials of the *Lenin* icebreaker: YU. V. SIVINTSEV, V. A. KNIZHNIKOV, E. L. TELUSHKINA and A. D. TURKIN.

Studies are reported of the amounts of radioactive material found in the air of the main fitting berth, in the engine room, in the surrounding atmosphere, in the river water, and in the flora and fauna of nearby regions. The results show that the nuclear power plant of the *Lenin* icebreaker presents a very high standard of nuclear safety; the vessel presents no hazard to the crew, to the ports, to the ship's base station, or to the convoy of ships it is escorting.

Letters to the Editor

Production of monoenergetic beams of accelerated particles: F. R. ARUTYUNYAN and I. P. KARABEKOV.

Cross sections for (d, p) reactions: M. Z. MAKSIMOV.

Theory of the effective cross sections of heavy nuclei in the region of partial overlap between neutron resonances: A. A. LUK'YANOV and V. V. ORLOV.

Capture cross sections of Nb, Ni, and Fe for fast neutrons: YU. YA. STAVISSKII and A. V. SHAPAR.

Some comments on the measurement of photoneutron yields for thick specimens: V. I. GOMONAI, D. I. SIKORA and V. A. SHKODA-UL'YANOV.

Corrections for mutual screening in a solid lattice: N. I. LALETIN.

The effectiveness of a set of control rods arranged symmetrically in a ring within the core of a reactor provided with a reflector: V. I. NOSOV.

Approximate solution of the transport equation by means of the method of moments: I. S. NIKOLAISHVILI.

The growth of a bubble of vapour moving in a liquid heated throughout its volume: V. K. ZAVOISKII.

Haziguti's theory of the swelling of α-uranium under irradiation: YU. N. SOKURSKII.

Phase compositions of nickel-rich alloys in the Ni-Mo-B system: P. T. KOLOMYSTSEV and N. V. MOSKALEVA.

Separation of uranium from impurities by means of ammonium sulphite: N. P. GALKIN and G. A. POLONNIKOVA.

Quantitative spectroscopic method of determining the isotopic composition of boron: B. V. L'VOV and E. M. MOSICHEV.

News of Science and Technology

Bibliography

VOL
15
196

Reactor Science and Technology (Journal of Nuclear Energy, Parts A/B), 1961, Vol. 15, pp. 69 to 75. Pergamon Press Ltd. Printed in Northern Ireland

STEADY STATES IN REACTORS WITH POSITIVE REACTIVITY COEFFICIENTS

D. L. BOOTH
Atomic Power Division, English Electric Co. Ltd., Whetstone, Leicester

(*Received* 21 *October* 1960)

Abstract—The phenomena associated with the existence of two steady states with equilibrium xenon poisoning for the same distribution of fuel and absorbers are described. A general method for determining the conditions for spatial flux instability from an analysis of steady state flux distributions is presented as a related phenomenon.

1. INTRODUCTION

THE neutron flux distribution in low power reactors is determined mainly by the disposition of the fuel and absorbers. In power reactors there are additional effects due to the fission product ^{135}Xe and the temperature effects upon reactivity. These temperature effects have been discussed by SYRETT (1959), with special emphasis on graphite moderated reactors. The large positive feedback caused by positive moderator temperature reactivity coefficients in reactors with solid moderators leads to some interesting effects in reactor statics and reactor dynamics.

Possible steady states can be attained and maintained in actual reactors by suitable movements of control rods, or by other methods. In a reactor with a given distribution of fuel and a fixed coolant flow it is possible to obtain steady states at different power levels by altering the steady state value of some parameter such as the position of the control rods. This is because the net change in reactivity due to the combination of the control rod movement and the alteration in power level can be balanced against the difference in steady state neutron leakage. For reactors with net positive reactivity coefficients there are two exceptions to this rule. The first is that there is no steady state, with a fixed distribution of absorber, at any power level if the intrinsic reactivity before the inclusion of temperature and xenon effects is too high, or in other words, if too much neutron absorbing material is removed from a given reactor. The second is that there is an upper limit to the steady state power which can be obtained by adding absorber, at a limited number of positions, to a reactor with a fixed coolant flow.

The reasons for these effects, which are described in more detail below, are quite simple. An increase in the power level of a reactor with a net positive temperature coefficient of reactivity increases the steady state material buckling in the absence of xenon poisoning. As the change in neutron leakage with flux level is relatively small at low powers, an increase in the steady state power level requires a greater loading of neutron absorbers. Hence, in the absence of xenon poisoning there is no steady state if the absorber loading is less than that corresponding to the steady state at zero power.

The steady state poisoning due to ^{135}Xe increases with flux level, but the effect tends to a finite limiting value at high fluxes. If the moderator temperature reactivity coefficient is in a certain range, which depends on the reactor being considered, there are two possible steady states with equilibrium xenon poisoning and the same distribution of fuel and absorbers. In one of these there is a low power level and low xenon poisoning; in the other, the extra xenon poisoning is compensated by the reactivity released at the higher temperatures produced by the higher flux level. As absorbers are removed from a given reactor, the difference between the two steady state power levels decreases, and there is no steady state with equilibrium xenon poisoning if too much absorber is removed. This is illustrated by the calculation reported in Section 2, and by Fig. 1.

The existence of a maximum steady state power for a given reactor and coolant flow and various local absorber loadings is due to the change in flux distribution. A local increase in control rod strength causes a local depression in the steady state neutron flux, with a corresponding increase elsewhere, and a net change in the average flux level. The flux distortion is increased by further local increments in control rod strength. These distortions release reactivity elsewhere in the reactor, but have a diminishing effect upon the total reactivity, owing to the reduced importance of that region. Thus, if the flux distribution has been suitably distorted, a steady state with increased

control rod strength has a lower steady state power level, despite the presence of a positive temperature coefficient of reactivity. This occurs with or without equilibrium xenon poisoning. It is shown in Section 3 that the phenomenon is closely linked mathematically to that of spatial flux instability in the absence of xenon poisoning, and that it is possible to compute the conditions for flux instability without having to solve the time-dependent equations for the system. This leads to a great saving in computational effort. The method is illustrated by an example.

2. STEADY STATES WITH EQUILIBRIUM XENON POISONING

The existence of two steady states for the same distribution of fuel and absorbers may be illustrated by considering a single channel in the flattened region of a hypothetical gas-cooled uranium metal fuelled graphite moderated power reactor.

The details of the model, the equations, and the method of solution are summarized in Appendix 1. The moderator temperature coefficient of reactivity, β, and the criticality constant, k_0, of the unpoisoned reactor at gas inlet temperature were regarded as arbitrary parameters. As the coolant flow was the same in all cases, and the reactor uniform, the coolant temperature gives a measure of the total power produced in the channel.

The values of k_0 required for various channel heat ratings for values of β between -10 and $+25$ mn/°C* are plotted in Fig. 1. The main features of the graph have been discussed in Section 1. The graph also shows that small changes in k_0 near the maximum value for which there is a steady state correspond to large changes in the steady state power level with equilibrium xenon poisoning. In this example a moderator temperature coefficient of 1 mn/°C corresponds for constant inlet temperature roughly to 0·6 mn/°C on the coolant outlet temperature, and to 0·45 mn/kW on the channel heat rating.

The changes in the flux distribution, and hence in the temperature distributions, were studied by analysing the flux, ϕ, in the form

$$\phi(\theta) = \Phi(\sin\theta + A_2 \sin 2\theta) \qquad (1)$$

where the direction of increasing θ is that of increasing coolant temperature, and Φ is a constant. The value of A_2 was computed from the fluxes at the third and eighth of the ten axial mesh points in the core of the reactor. Figure 2 shows that A_2 is a linear function of the power level in the reactor. The results for this particular reactor may be represented by the empirical formula

$$A_2 = (0{\cdot}68 - 0{\cdot}36\beta)10^{-4}P$$

* 1 mn/°C = 1 milli-nile per degree centigrade = 1×10^{-5}/°C in reactivity.

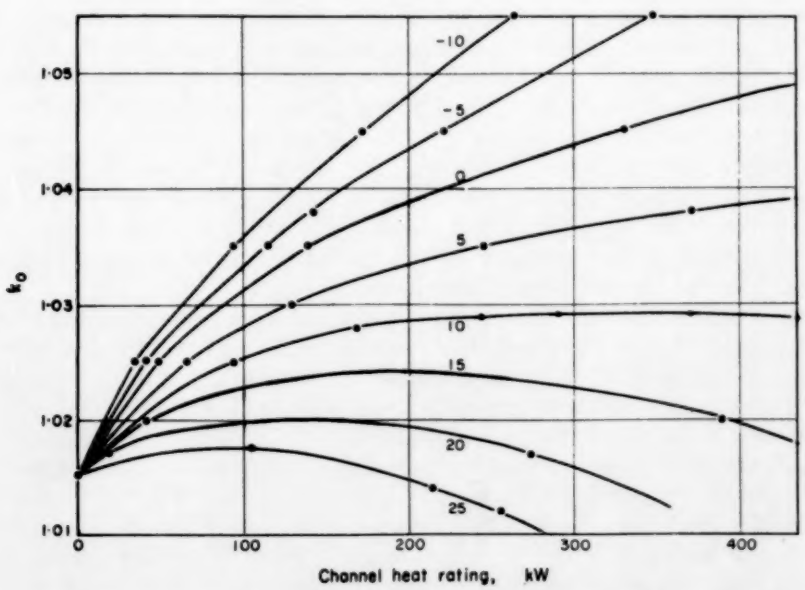

FIG. 1.—Steady state power for constant coolant flow, equilibrium xenon poisoning, and moderator temperature coefficients of reactivity between $\beta = -10$ and $\beta = +25$ mn/°C.

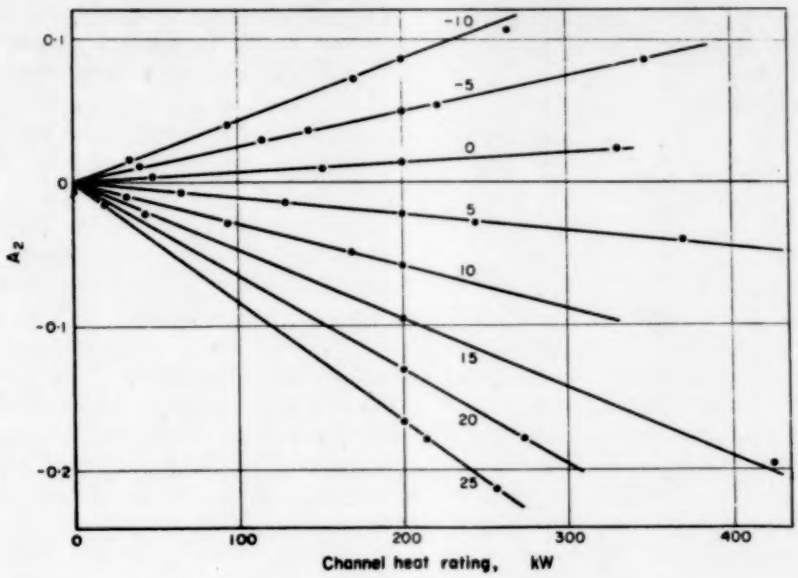

FIG. 2.—Steady state flux asymmetries for the cases presented in Fig. 1.

where β is the moderator temperature coefficient of reactivity in mn/°C and P is the channel heat rating in kilowatts. Thus increases in β or in the power level displace the position of maximum flux towards the hotter end of the reactor if β is greater than about 2 mn/°C. The states with maximum k_0 correspond to values of A_2 around −0·10 for this particular reactor. Similar results can be obtained for the more realistic case of a non-uniform reactor in which steady states are specified by the control rod position. Work on uniform reactors shows that the effects are principally determined by the moderator temperature reactivity coefficient.

The coolant flow and heat transfer data used in Fig. 1 were independent of the power level. It is usual in practice to reduce the coolant flow when decreasing load, so as to maintain steady temperatures in the system. If the load is not changed by more than, say, 30 per cent, the ratio of the actual power level to that corresponding to the maximum k_0 does not appreciably alter. If the uniform reactor of Fig. 1 were operated at $\beta = 10$ mn/°C and channel heat ratings around 300 kW, the required value of k_0 would be close to the maximum over a range of power levels. This would mean that in the steady state with equilibrium xenon poisoning the control rod position would be virtually independent of reactor power for any given coolant flow. This is unlikely to be of practical importance owing to the long time taken for the xenon poisoning to approach its equilibrium value.

3. STEADY STATES AND SPATIAL FLUX INSTABILITY

(a) *Theory*

It is convenient to start the discussion of the existence of a maximum steady state power level under certain conditions by considering the classic model analysis of spatial instability (WARD, 1956; HITCHCOCK, 1960). In this treatment the conditions for instability are found by considering the stability of small disturbances having an assumed spatial dependence. A solution of the form

$$\phi(\mathbf{r},t) = \phi_0(\mathbf{r}) + \sum_{n=0}^{\infty} a_n \phi_n(\mathbf{r})\, e^{\omega_n t}$$
$$T(\mathbf{r},t) = T_0(\mathbf{r}) + \sum_{n=0}^{\infty} b_n T_n(\mathbf{r})\, e^{\omega_n t} \qquad (2)$$
etc.

is sought for all the variables ϕ, T, etc. in the time-dependent equations, including the equation for the control rod position. Here $\phi_0(\mathbf{r})$ and $T_0(\mathbf{r})$ are the steady state values of the variables ϕ and T at the position $\mathbf{r}$; $\phi_n(\mathbf{r})$, $T_n(\mathbf{r})$ are suitable functions of position, and a_n, b_n amplitudes which may be complex. Substituting the solution (2) into the time-dependent equations, and subtracting the steady state equations, gives a set of equations involving the $e^{\omega_n t}$ and cross products. For small disturbances it is permissible to neglect the products of two small amplitudes, and so eliminate all terms other than the coefficients of the $e^{\omega_n t}$. These may be separately equated to zero, giving

sets of equations for the individual ω_n. As the stability of the modes depends upon the associated neutron leakage, the higher modes will be stable, and if the fundamental and the first $N-1$ modes are stabilized by the control system, it is only necessary to determine the conditions under which the Nth mode is stable. These are the conditions that the real part of ω_N shall be negative.

The most important case is that in which the instability is principally due to the xenon poisoning, and the time dependence of the equations for the flux and temperatures can be neglected relative to the slow variation in the xenon population. The threshold of instability is usually defined as the value which the moderator temperature coefficient of reactivity would have to exceed if the reactor were to be unstable. At the threshold for xenon instability, disturbances oscillate with constant amplitude and a period of about 30 hours (HITCHCOCK, 1960). Spatial instabilities which are primarily due to a positive temperature coefficient of reactivity occur with periods short compared with the half-life of ^{135}I. In this case it is permissible to neglect the variation in the xenon population, and to consider ω_N to be real. The threshold of instability is then at $\omega_N = 0$.

Under these conditions, as all the other modes are damped, after a suitable time the solution (2) for $\omega_N = 0$ becomes

$$\phi(\mathbf{r},t) = \phi_0(\mathbf{r}) + a_N\phi_N(\mathbf{r}) \qquad (3)$$
$$T(\mathbf{r},t) = T_0(\mathbf{r}) + b_N T_N(\mathbf{r})$$
$$\text{etc.}$$

The time does not appear on the right-hand side of solution (3), so that this is also a solution of the steady state equations for any non-zero values of $a_N, b_N, \ldots$. which are sufficiently small for the solution (2) to be a valid solution of the kinetic equations. Thus at the threshold for instability, there is an infinity of possible steady states. It is therefore possible to find the threshold for instability without having to solve the time-dependent equations.

It should be noted that the arguments given above are very general. The equations to be solved have not been written down, no set of spatial co-ordinates has been assumed, and the equations might equally well apply to systems other than nuclear reactors. The only assumptions are that a solution of the form (2) with non-zero $a_n, b_n, \ldots$ can be found for the time-dependent equations, and that the solution at the threshold reduces to (3) a suitable time after the initial disturbance. This corresponds to the conditions that all the ω_n have negative real parts, except ω_N, which is zero.

The validity of these assumptions can be tested by inspecting the time-dependent equations to see whether they can be linearized, and whether there is any mechanism for producing an oscillatory response. Complex values of ω_N are unlikely to be of physical importance if the times considered are short compared with the half-life of ^{135}I, but the assumption might be invalidated by non-linearities in the control system.

The steady state method of analysis is of interest because in reactions with solid moderators the difference between the physically significant threshold with xenon poisoning and the threshold at $\omega_N = 0$ is small compared with the influence on the threshold of such matters as the presence of harmonics in the steady state flux distribution. The object of stability analysis is to ensure that the reactor control system will easily be able to suppress spatial disturbances under any likely operating conditions; hence a small uncertainty in the difference between the two types of threshold is preferable to the large uncertainties introduced by the use of an inadequate mathematical model for the reactor. The difference between the two types of threshold can be estimated with sufficient accuracy from a simple model. The advantage of the steady state method for finding the threshold of instability is that it is much easier to solve steady state equations than to solve time-dependent ones. A further advantage is that it is possible to use existing computer programmes, and dispense with the need to write complicated programmes to solve the equations for the kinetics of reactor models which include the detailed non-uniformities of the reactor and the equations for all relevant temperatures.

The problem of finding the conditions for stability has therefore been reduced to that of finding the conditions under which there is a range of steady state solutions of the form (3). Thus the stability of a particular reactor design may be investigated by considering a family of reactors which differ from it only by the value of some parameter, such as the moderator temperature reactivity coefficient. One of the reactor equations is then made redundant by fixing one of the variables, for example the control rod position. The solution of the remaining equations is then computed for each member of the family of reactors, using values of the specified variable which differ slightly from the solutions of the complete set of equations. The threshold of instability is at that member of the family of reactors for which the solution of the incomplete set of equations with the perturbed value of the chosen variable is also a solution of the redundant equation. Thus the threshold can be evaluated in terms of the value which the chosen

parameter would have to have if the original reactor were to be marginally stable.

In the example described in the next section, the complete set of equations was the time-dependent set corresponding to the steady state equations which were solved, plus an equation for the control rod position required to maintain constant coolant outlet temperature. The threshold for spatial instability was found by computing the change in coolant outlet temperature which was produced by a small change in the steady state control rod position. At the threshold there was no change in the outlet temperature when the control rod position was slightly altered.

As the stability of a reactor decreases with power level, the arguments given above show that if the power level which is a solution of the steady state equations for a particular reactor is plotted as a function of one of the variables, the curve will have a maximum at the threshold of spatial instability at $\omega_N = 0$. The existence of this maximum power level was described in Section 1. This is the reverse of the situation shown in Fig. 1, when the value of k_0 which was required for a given steady state power level had a maximum value.

(b) *Application of axial instability*

The method described in the previous section may be illustrated by referring to computed axial flux and temperature distributions. The mathematical model used, and the method of solving the equations were the same as those used in Section 2 and are described in Appendix 1.

Most of the parameters used were appropriate to a hypothetical uniform reactor with a channel rating of 175 kW, and a fixed coolant flow. There was no xenon poisoning. The moderator temperature coefficient of reactivity was treated as a variable parameter, which was given artificially high values.

Moderator temperature coefficients of reactivity $\beta = +30, +40, \ldots, +80$mm/°C were chosen, and non-uniform flattening applied so that the unperturbed flux distributions were approximately sinusoidal, so as to make possible a comparison with other theories. The steady state in the absence of xenon poisoning was then computed for each value of β. The value of the criticality constant k_0 at gas inlet temperature at the eighth axial mesh point was increased by Δk_e, corresponding to movement of a control rod, and the perturbed steady state computed for each value of β. The increase of $+\Delta T_e$ in the coolant outlet temperature is proportional to the change in power level. Figure 3 is a plot of $\beta\Delta T_e$ against β for $\Delta k_e = 200$ mn and $\Delta k_e = 500$ mn. The graph shows that the results can be

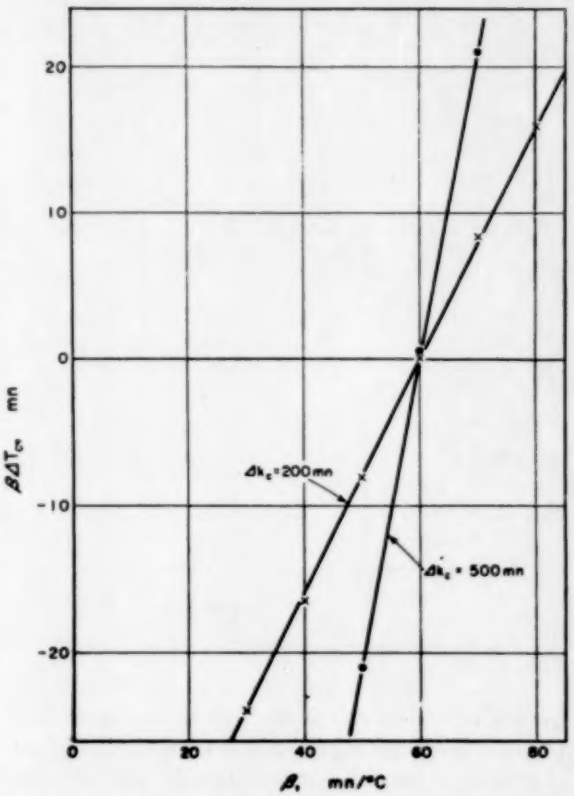

FIG. 3.—The change in steady state power level multiplied by the reactivity coefficient β, for fixed coolant flow and disturbances, $\Delta k_e = 200$ and 500 mn.

represented to a high degree of approximation by two straight lines which pass through zero at $\beta \approx 60$ mn/°C. The slope of the line for $\Delta k_e = 500$ mn is closely $2\frac{1}{2}$ times that of the line for $\Delta k_e = 200$ mn, showing that the perturbation is small enough for the effects to be linear.

The flux distribution was analysed in terms of equation (1); the results are plotted in Fig. 4 for $\Delta k_e = 200$ mn. This shows that the small local increase in k_0 which corresponds to a small withdrawal of control rods in the hotter portion of the reactor, displaced the maximum of the steady state flux distribution towards the hot end of the core for all values of β.

The two figures show that for a particular value of β close to 60 mn/°C it is possible to obtain steady states having the same power level but different control rod positions and flux distributions. This is the situation described in the previous section, where expressions (3) were solutions of the time-dependent reactor equations for a range of non-zero values of the coefficients a_N, b_N, etc. Thus the threshold at $\omega_N = 0$ can be found by

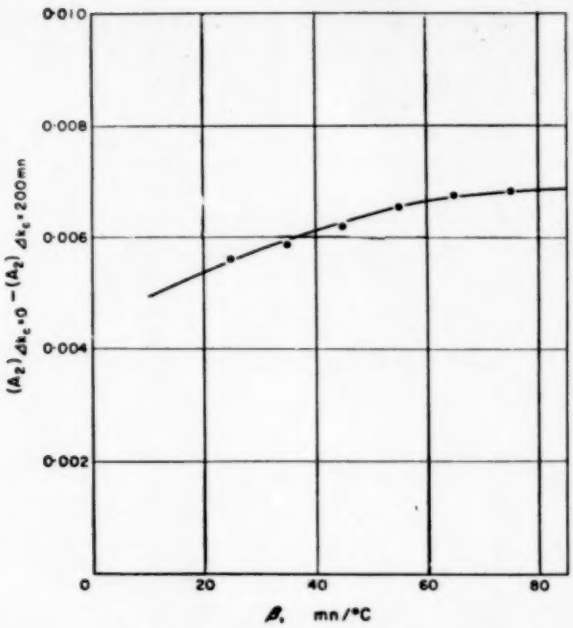

FIG. 4.—The change in asymmetry for $\Delta k_e = -200$ mn.

computing the steady states for various conditions. Figure 3 shows that the increase in local reactivity leads to a steady state with a smaller total power for values of β less than ~60 mn/°C. This is the normal behaviour for reactors with positive power coefficients of reactivity, as has been explained in Section 1. For values of β above 60 mn/°C, the withdrawal of control rods corresponds to an increase in the steady state power. This is because the increased neutron leakage due to the change in steady state flux distribution absorbs more reactivity than is released by the assumed control rod movement. In this situation the flux distribution is unstable, despite a control system which stabilizes the total power level.

The effects can be analysed in terms of the change induced in the steady state flux distribution by a given control rod movement. This is done in Appendix 2, where first-order perturbation theory is used to derive the conditon that the change $\Delta\Phi$ in power level shall be zero, if $A_2 = 0$ in the unperturbed flux distribution.

For the case described above, expression (A.5) gave an instability threshold of 66·5 mn/°C. The simple formula given by HITCHCOCK and ROBERTS (1960) led to 69·1 mn/°C. The differences between the results of the various methods are due to their differing choice of eigenfunctions, different heat equations, and the use of $A_2 = 0$ in the simple theories instead of the value $A_2 = 0{\cdot}092$ which was used in the numerical work.

At $\beta = 66{\cdot}5$ mn/°C, equation (A.4) gives a value $\Delta A_2 = -0{\cdot}0063$, which is in reasonable agreement with the $\Delta A_2 = -0{\cdot}0067$ given in Fig. 4. Equations (A.3) and (A.4) give an expression of the form

$$\Delta\Phi = \frac{P + Q\beta}{\beta^2 + R\beta + S}$$

for any given Δk_0. The dominant term in the denominator is $R\beta$, which explains why $\beta\Delta\Phi$, and hence $\beta\Delta T_c$, are, to a very good approximation, linear functions of β, as is shown in Fig. 3. This fact makes it easy to obtain a good estimate of the threshold by computing only a few steady states.

This example shows that the steady state method for finding the threshold of instability is simple to use, and gives results for a simple case which agree with those obtained by the usual methods. The great advantage of the steady state method is the ease with which the detailed non-uniformities of the reactor can be included in the calculations.

Acknowledgments—The author would like to thank MISS G. A. STAPLETON for her invaluable assistance with the numerical work, and to thank DR. T. O. JEFFRIES for stimulating discussions on the phenomena. He would also like to thank the English Electric Company Ltd. for permission to publish this paper.

REFERENCES

BALFOUR J. G., BOOTH D. L., BULLOCH R. S. and STANNERS W. F. (1959) *J. Brit. Nucl. Energy Conf.* **4**, 189.

HITCHCOCK A. (1960) *Nuclear Reactor Stability*, Temple Press.

HITCHCOCK A. and ROBERTS B. E. (1960) *Axial Stability of the Neutron Flux Distribution*. D.E.G. Report 128 (R).

SYRETT J. J. (1959) *Nucl. Power* **4**, (1), 95.

WARD A. G. (1956) *The Problem of Flux Instability in Large Power Reactors*. CRRP 657 (AECL 345).

APPENDIX 1

The model used in the numerical work

A single channel in the flattened region of a gas-cooled graphite moderated power reactor was considered. The equations were written in finite difference form; temperatures and neutron fluxes were computed at ten levels axially along the channel. One-group neutron diffusion theory was used, with linear reactivity feedbacks from the fuel surface temperature (−1·8 mn/°C) and from two positions in the moderator. The steady state xenon poisoning was computed at each mesh point for the work described in Section 2. The flux was assumed to be zero at two extrapolated end points.

The radial flow of heat at each of the ten axial mesh points was computed at six stations in the fuel, two in the magnox can, one in the coolant, and at four stations in the moderator. An axial equation was used for the coolant temperatures. The system was assumed to have radial symmetry; net radial leakage of heat, and axial heat conduction in the solids were neglected. The fuel element was assumed to be a continuous rod, with appropriately adjusted heat transfer coefficients. The Laplacian operators in the heat diffusion equations and the neutron diffusion equation were replaced by the equivalent first-order finite difference forms. The errors introduced by using finite differences

amount to a few degrees in centre fuel temperature, and are unimportant in the present work.

The equations were solved as an initial condition problem by a programme written for an English Electric 'DEUCE' computer. The set of equations and the programme for solving them have been described in more detail by BALFOUR, BOOTH, BULLOCH and STANNERS (1959).

APPENDIX 2

An analytic approximation for finding the threshold for axial instability

Let the unperturbed flux distribution in a uniform one-dimensional reactor be

$$\phi(\theta) = \Phi \sin \theta$$

where θ is a co-ordinate of position which is zero at the cool end of the reactor and Φ is a constant. The boundary conditions are that the flux is zero at $\theta = 0$ and at $\theta = \pi$.

A small local disturbance in reactivity, which is Δk_c between θ_1 and θ_2 and is zero elsewhere, alters the steady state flux distribution to the form

$$\phi'(\theta) = \Phi \sin \theta + \Delta\Phi \sin \theta + \Phi\Delta\Lambda \sin 2\theta. \qquad \text{(A.1)}$$

The resultant local changes in steady state reactivity may be written

$$\Delta k(\theta) = \Delta k_c(\theta) + (\alpha A + \beta B)\{\Delta\Phi \sin \theta + \Phi\Delta\Lambda \sin 2\theta\}$$
$$+ (\alpha + \beta)C\{(1 - \cos \theta)\Delta\Phi + \Phi\Delta\Lambda \sin 2\theta\} \qquad \text{(A.2)}$$

where α and β are the coefficients of reactivity associated with the fuel and moderator temperatures, A and B the steady state differences per unit flux between these temperatures and the coolant temperature and C the axial rate of change of coolant temperature per unit flux.

Application of first-order perturbation theory (BALFOUR *et al.*, 1959) gives two conditions that (A.1) shall be the steady state flux distribution corresponding to the reactivity changes (A.2):

$$0 = \frac{-\int \Delta k \sin^2 \theta \, d\theta / M_z^2}{\int \sin^2 \theta \, d\theta}$$

and

$$\Delta\Lambda = \left(1 + \frac{\Delta\Phi}{\Phi}\right) \frac{\int \sin \theta \sin 2\theta \, \Delta k \, d\theta / M_z^2}{3\pi^2/L^2 \int \sin^2 2\theta \, d\theta}$$

where M_z^2 is the axial migration area and L the extrapolated length of the reactor. The integrals may be taken over the range $0 < \theta < \pi$ without introducing appreciable errors.

Integrating, the equations become

$$0 = \frac{-1}{M_z^2}\{((\theta_2 - \theta_1) - \tfrac{1}{2}(\sin 2\theta_2 - \sin 2\theta_1))\frac{\Delta k_c}{\pi}$$
$$+ \frac{8}{3\pi}(\alpha A + \beta B)\Delta\Phi$$
$$+ (\alpha + \beta)C(\Delta\Phi + \tfrac{4}{3}\Phi\Delta\Lambda)\} \qquad \text{(A.3)}$$

$$\Delta\Lambda = \frac{1 + \Delta\Phi/\Phi}{3\pi^2 M_z^2/L^2}\left\{\frac{4}{3\pi}(\sin^3 \theta_2 - \sin^3 \theta_1)\Delta k_c\right.$$
$$\left. - \tfrac{1}{2}(\alpha + \beta)C\Delta\Phi + \frac{32}{15\pi}(\alpha A + \beta B)\Phi\Delta\Lambda\right\}. \qquad \text{(A.4)}$$

As Δk_c is known, these two equations determine the unknowns $\Delta\Phi$ and $\Delta\Lambda$ for any given β.

At the threshold of instability, $\Delta\Phi$ is zero, and for any Δk_c and $\Delta\Lambda$,

$$\left\{\frac{3\pi^2 M_z^2}{L_2} - \frac{32}{15\pi}(\alpha A + \beta B)\Phi\right\}$$
$$\times ((\theta_2 - \theta_1) - \tfrac{1}{2}(\sin 2\theta_2 - \sin 2\theta_1))$$
$$+ \{\sin^3 \theta_2 - \sin^3 \theta_1\}(\alpha + \beta)C\Phi = 0 \qquad \text{(A.5)}$$

Equation (A.5) may be used to determine the critical value of the temperature coefficient β.

VOL. 15 1961

Reactor Science and Technology (Journal of Nuclear Energy, Parts A/B), 1961, Vol. 15. pp. 76 to 80. Pergamon Press Ltd. Printed in Northern Ireland

STREAMING DUE TO HOLES IN A REACTOR

C. CARTER
Atomic Energy Research Establishment, Harwell, Berks.

(*Received* 5 *January* 1961)

Abstract—The effect of holes on a reactor is considered by using appropriate boundary conditions on the asymptotic neutron flux at the surface of the holes. For a flux variation along the hole, this method gives the same streaming correction as BEHRENS, but for a flux variation across the hole, the streaming correction is smaller than that given by BEHRENS' formula. Values of the radial streaming correction factor are compared with experimental and Monte Carlo results and also with values obtained from the iterative method of BENOIST.

1. INTRODUCTION

THE presence of holes in a nuclear reactor always causes a loss of reactivity due to the greater facility with which neutrons move from regions of high flux to regions of low flux. This phenomenon is commonly known as streaming and various attempts have been made to provide a theory of the effect (BEHRENS, 1954; BENOIST, 1959; GRANT, 1958). The problem has also been investigated by the Monte Carlo method and experimentally (SHAEFER and PARKYN, 1958). Streaming is usually included in diffusion theory reactor calculations as a correction to the migration area. In obtaining this correction, BEHRENS assumed that the migration area varies directly as the neutron mean square free path in a particular direction. LALETIN (1958) has shown that this assumption is true for neutron transport parallel to a hole but not perpendicular to it. GRANT (1958) has also questioned this assumption and has demonstrated that BEHRENS' transverse streaming correction is incorrect in slab geometry. A general treatment of neutron transport in a heterogeneous medium has been given by BENOIST (1959). He develops an iterative solution of the integral transport equation. When treating the streaming problem in a lattice of empty holes, his zero-order solution is equivalent to BEHRENS' theory. BENOIST's approach is very instructive but it is not clear whether his iterative scheme converges sufficiently rapidly to be convenient. The convergence is certainly slow in slab geometry, and some Monte Carlo results reproduced in Section 4 of this paper indicate that the convergence may also be slow in cylindrical geometry.

In the present report we shall obtain streaming corrections to the migration area by using boundary conditions at the surface of a hole. We consider a bare reactor with a lattice of parallel cylindrical holes going right through the reactor. Flux variation parallel to the holes gives rise to axial streaming whilst flux variation across the hole causes radial streaming. For the axial streaming, we use a boundary condition given by DAVISON (1951). The boundary condition for the radial streaming is given by CARTER and JARVIS (1960). The methods used in this report are applicable to the case where the holes contain fuel rods but new boundary conditions would have to be worked out.

2. AXIAL STREAMING

We consider an infinite lattice of holes with an axial flux variation of the form $\cos \alpha z$ in the direction parallel to the axis of the holes. We define an extrapolation length, λ = (mean flux over surface of hole)/(mean normal derivative over surface of hole). λ will be a function of α and of the size and shape of the hole and its evaluation will in general be a rather complicated problem in neutron transport theory. We shall later use the expression for λ obtained by DAVISON for a hole of circular cross section.

Let B^2 be the buckling in the reacting medium. Then the asymptotic flux $\phi(\mathbf{r})$ satisfies the equation

$$(\nabla^2 + B^2)\phi(\mathbf{r}) = 0 \qquad (2.1)$$

in the reacting medium, and $\nabla\phi(\mathbf{r}) = 0$ over a cell boundary. Now consider a homogeneous reactor with the same axial flux dependence. Let it have flux distribution $\phi_m(\mathbf{r})$ and buckling B_m^2 so that

$$(\nabla^2 + B_m^2)\phi_m(\mathbf{r}) = 0. \qquad (2.2)$$

Since the reactor is infinite radially, $\phi_m(\mathbf{r})$ has no radial dependence and $B_m^2 = \alpha^2$.

Multiply (2.1) by $\phi_m(\mathbf{r})$, (2.2) by $\phi(\mathbf{r})$, subtract and integrate over the lattice cell area.

Then,
$$B^2 - B_m^2 = \frac{\int_{Vm} (\phi \nabla^2 \phi_m - \phi_m \nabla^2 \phi)\, dV}{\int_{Vm} \phi \phi_m\, dV} = \frac{\int_s \nabla\phi \,.\, d\mathbf{S}}{\int_{Vm} \phi dV} \qquad (2.3)$$

where the surface integral is over the surface of the hole. If we take $\phi = \phi_m$ in the volume integral, then

$$\frac{B^2}{B_m^2} = 1 + \frac{2\pi a}{\lambda \alpha^2 V_m} = 1 + \frac{2W}{\lambda a \alpha^2} \qquad (2.4)$$

where
$$w = \frac{\pi a^2}{V_m} = \frac{\text{volume of holes}}{\text{volume of material}}. \qquad (2.5)$$

The critical equation for the reactor is

$$k - 1 = B^2 M^2. \qquad (2.6)$$

Alternatively, we can write the critical equation in terms of the buckling, B_m^2 of the homogenized reactor as

$$k - 1 = B_m^2 M_m^2, \qquad (2.7)$$

where, using (2.5),

$$S_z = \frac{M_m^2}{M^2} = \frac{B^2}{B_m^2} = 1 + \frac{2w}{\lambda a \alpha^2}. \qquad (2.8)$$

For $(\alpha a) \ll 1$, DAVISON's formula gives

$$\lambda = \frac{l}{\alpha^2 a(a + l)} \qquad (2.9)$$

where l is the mean free path in the reacting medium. Then (2.9) becomes

$$S_z = \frac{M_m^2}{M^2} = 1 + 2w\left(1 + \frac{a}{l}\right). \qquad (2.10)$$

3. RADIAL STREAMING

We wish to consider the effect of a lattice of holes in a reacting medium which is infinite in the direction of the holes. Thus all variations of neutron density are in a plane perpendicular to the axis of the holes.

We first consider a single cylindrical hole, radius a, in an infinite non-absorbing medium with mean free path l, in which the neutron flux varies linearly in a direction perpendicular to the axis of the hole. Thus the unperturbed flux is

$$\phi(\mathbf{r}) = \phi_0 + \mathbf{r} \,.\, \nabla\phi_0, \qquad (3.1)$$

where $\mathbf{r}$ is a two-dimensional vector in the plane perpendicular to the axis of the hole, and ϕ_0, $\nabla\phi_0$ are constant. The presence of the hole will perturb the flux in the region around it, and we find that the asymptotic flux becomes

$$\phi_{as}(\mathbf{r}) = \phi_0 + \mathbf{r} \,.\, \nabla\phi_0 \left[1 - b\frac{a^2}{r^2}\right] \qquad (3.2)$$

The coefficient b is a function of $\frac{a}{l}$ and can be determined by solving the transport equation for the system. This has been done by CARTER and JARVIS (1960; 1961). They find that b is approximated fairly well by

$$b = 1 - \frac{l}{2(a + l)} = \frac{1}{2}\left[1 + \frac{a}{a + l}\right]. \qquad (3.3)$$

The hole is in fact behaving as a dipole with strength proportional to the flux gradient across the hole. The coefficient b in equations (3.2) and (3.3) may be considered as the polarizability of the hole in an infinite medium. Before we can use this value of b in the streaming problem, we must consider what changes are introduced when we have a regular lattice of holes instead of a single hole in an infinite medium. We consider a cylindrical cell of radius R about a hole, such that the lattice cell area is $V_c = \pi R^2$. Then, from (3.2), the asymptotic flux at the cell boundary is

$$\phi_{as}(R) = \phi_0 + \mathbf{R} \,.\, \nabla\phi_0 \left[1 - b\frac{\pi a^2}{V_c}\right] \qquad (3.4)$$

and the mean flux gradient in the lattice is

$$\left(1 - b\frac{\pi a^2}{V_c}\right) \nabla\phi_0.$$

Thus the polarizability of a hole per unit mean flux gradient in the lattice is

$$b_l = \frac{b}{1 - b\frac{\pi a^2}{V_c}}. \qquad (3.5)$$

We shall now consider the behaviour of the asymptotic flux in a reactor containing a lattice of holes. The actual flux near a hole differs from the asymptotic flux by a transport correction term, but provided the holes are separated by more than a few mean free paths, the transport correction terms from different holes will not overlap significantly, and the overall reactivity will be given correctly by considering only the asymptotic flux. Physically, the approximation made is that a neutron has a negligible chance of passing through more than one hole between successive collisions. If this condition is not satisfied, there will be an interaction correction to our theory.

We consider a bare reactor with a lattice of N holes.

VOL. 15 1961

Let B^2 be the buckling in the reacting medium. Then the asymptotic flux $\phi(\mathbf{r})$ satisfies the equation

$$(\nabla^2 + B^2)\phi(\mathbf{r}) = 0 \tag{3.6}$$

in the reacting medium, V, i.e. the total volume V_0 of the reactor less the volume of the holes. Now consider a homogeneous reactor with the same volume V_0. Let it have flux distribution $\phi_m(\mathbf{r})$ and buckling B_m^2 so that

$$(\nabla^2 + B_m^2)\phi_m(\mathbf{r}) = 0 \tag{3.7}$$

over the whole volume V_0. $\phi(\mathbf{r})$ and $\phi_m(\mathbf{r}) = 0$ over surface of V_0. From (3.6) and 3.7) we obtain

$$B^2 - B_m^2 = \frac{\int_V (\phi\nabla^2\phi_m - \phi_m\nabla^2\phi)\,dV}{\int_v \phi\phi_m dV} = \sum_k \frac{\int_{S_k} (\phi_m\nabla\phi - \phi\nabla\phi_m)\,.\,d\mathbf{S}}{\int_v \phi\phi_m dV} \tag{3.8}$$

where the surface integral is over the surface of the kth hole and the summation is over all the holes.

Let r_k be the position of the centre of the kth hole, and $\mathbf{a}$ the vector from the centre of the hole to a point on its surface. We now expand ϕ_m, ϕ, ϕ_m and $\nabla\phi$ in Taylor series about r_k, retaining sufficient terms to give the surface integral correct to order $(Ba)^2$. Thus

$$\left.\begin{aligned} \phi_m(r_k + \mathbf{a}) &= \phi_m(r_k) + \mathbf{a}\,.\,\nabla\phi_m(r_k) + \ldots \\ \mathbf{a}\,.\,\nabla\phi_m(r_k + \mathbf{a}) &= \mathbf{a}\,.\,\nabla\phi_m(r_k) \\ &\quad + (\mathbf{a}\,.\,\nabla)^2\phi_m(r_k) + \ldots, \end{aligned}\right\} \tag{3.9}$$

and using equation (3.2),

$$\left.\begin{aligned} \phi(r_k + \mathbf{a}) &= \phi_m(r_k) \\ &\quad + (1 - b_l)\mathbf{a}\,.\,\nabla\phi_m(r_k) + \ldots \\ \mathbf{a}\,.\,\nabla\phi(r_k + a) &= (1 + b_l)\mathbf{a}\,.\,\nabla\phi_m(r_k) + \ldots \end{aligned}\right\} \tag{3.10}$$

Note that there is no need to include a term of order a^2 in $\mathbf{a}\,.\,\nabla\phi$ since $\mathbf{a}\,.\,\nabla\phi$ cannot have an angular independent component as there is no net current into the hole. Using equations (3.9) and (3.10), with θ as the angular co-ordinate of $\mathbf{a}$, we obtain, to order a^2,

$$\begin{aligned} &\int_{S_k} (\phi_m\nabla\phi - \phi\nabla\phi_m)\,.\,d\mathbf{S} \\ &= 2b_l\int_0^{2\pi} [\mathbf{a}\,.\,\nabla\phi_m\ (r_k)]^2 d \\ &\quad - \int_0^{2\pi} \phi_m(r_k)(\mathbf{a}\,.\,\nabla)^2\phi_m(r_k)\,d\theta \\ &= \pi a^2\{2b_l[\nabla\phi_m(r_k)]^2 + B_m^2\phi_m^2(r_k)\}. \end{aligned} \tag{3.11}$$

In equation (3.8) we now replace the summation over k by an integration and take

$$\int_v \phi\phi_m dV \simeq \frac{V}{V_0}\int \phi_m^2(\mathbf{r})\,dV. \tag{3.12}$$

Then

$$B^2 - B_m^2 = \frac{N\pi a^2}{V_0}\int \{B_m^2\phi_m^2(\mathbf{r}) + 2b_l\nabla\phi_m(\mathbf{r})]^2\}\,dV / \frac{V}{V_0} \times \int_{V_0} \phi_m^2(\mathbf{r})\,dV = \frac{V_0 - V}{V} B_m^2(1 + 2b_l). \tag{3.13}$$

With $w = \dfrac{V_0 - V}{V} = \dfrac{\text{volume of holes,}}{\text{volume of material}}$ we have

$$S_r = \frac{M_m^2}{M^2} = \frac{B^2}{B_m^2} = 1 + w(1 + 2b_l). \tag{3.14}$$

Using equations (3.3) and (3.5) for b_l, we obtain

$$S_r = 1 + w\left[2 + \frac{a + w\,(2a + l/2)}{a + l + wl/2}\right]. \tag{3.15}$$

An equation equivalent to (3.15) has been obtained by LESLIE (1960) by letting B^2 tend to zero in a Feinberg-Galanin individual source treatment of the problem.

4. DISCUSSION

Equation (2.10) for S_z is identical to the formulae obtained by BEHRENS and GRANT, thus confirming LALETIN's conclusion that BEHRENS' assumptions are valid for axial neutron transport. BEHRENS' formula for S_r is

$$S_r = 1 + w\left(2 + \frac{a}{l}\right) \tag{4.1}$$

which may be compared with our equation (3.15). In Table 1 we compare our equation (3.15) with the formulae of BEHRENS and BENOIST and with some Monte Carlo results given by SCHAEFER and PARKYN. The interaction correction is negligible in all cases except the 6 in. lattice pitch, where BENOIST has estimated that his second-order value of 2·80 should be increased to about 2·85.

The results in Table 1 do indicate that the BENOIST iteration series may be rather slowly convergent for small mean free paths and small lattice pitches. In all cases, except perhaps the 6 in. lattice pitch where interaction is significant, the trend of the successive BENOIST approximations is such that the limiting value might be expected to lie somewhere near our value. However, there is a marked discrepancy between our values and SCHAEFER's Monte Carlo results, particularly when the mean free path is small.*

*SCHAEFER G. W. (1960) (Private communication) has now amended his value of S_r for the 0·5 in. mean free path case to 2·1 ± 0·2.

In view of this discrepancy, Dr. J. Ashford of A.E.E. Winfrith has treated the case with 0·5 in. mean free path and 8 in. lattice pitch using the MCTU–1 programme on the Ferranti MERCURY computer. This is a Monte Carlo programme which tracks neutrons in three dimensions in a hexagonal lattice cell. Each neutron is tracked until it is absorbed. The programme is really designed for lattices containing fuel rods, and the statistics are rather poor in this case where the only absorption occurs in the moderator. Since we are interested in the limiting case of zero absorption, the programme was run for $\Sigma_a/\Sigma_t =$ ·20, ·04 and ·01. The programme produces a quantity T proportional to the sum of squares of the elementary path lengths. This should be compared with BEHREN's result. It also gives a quantity C representing correlation between successive neutron paths, which is to be compared with BENOIST's first-order correction. Finally it gives a quantity S proportional to the mean square distance travelled between birth and death. This represents the limit of the BENOIST series and may be compared directly with our formula (3.15). The complete results are given in Table 2.

In spite of the large uncertainties in the Monte Carlo values, there does seem to be good agreement with our formula (3.15) and a significant discrepancy between the MCTU–1 results and SCHAEFER's results given in Table 1.

In Table 3, we compare the theoretical formulae with some experimental results. The experiments of Mummery and Richey are quoted by SCHAEFER and PARKYN (1958). It can be seen that our values of S_r and S_z/S_r are in much better agreement with experiment than are BEHRENS' values.

TABLE 1.—RADIAL STREAMING CORRECTION FACTOR S_r (a = 2 IN.)

Mean free path (in.)	1·5	1·0	1·0	1·0	0·5
Lattice pitch (in.)	8	10	8	6	8
BEHRENS (BENOIST-zero-order)	1·81	1·57	1·98	3·14	2·47
BENOIST (first-order)	1·75	1·51	1·87	2·92	2·25
BENOIST (second-order)	1·72	1·48	1·82	2·80	2·13
Present work	1·70	1·41	1·73	2·79	1·78
Ashford (Monte Carlo)	—	—	1·86 ± ·03		1·70 ± ·10
SCHAEFER (Monte Carlo)	1·73 ± ·04	1·51 ± ·04	1·84 ± ·04	2·92 ± ·06	2·22 ± ·04

TABLE 2.—RADIAL STREAMING CORRECTION FACTOR, S_r, FOR LATTICE PITCH (8 IN.) OF EMPTY CHANNELS (RADIUS 2 IN.) WITH MEAN FREE PATH (0·5 IN.)

	Monte Carlo MCTU–1 programme			Theoretical values from Table 1
	$\frac{\Sigma_a}{\Sigma_t} = 0{\cdot}20$	$\frac{\Sigma_a}{\Sigma_t} = 0{\cdot}04$	$\frac{\Sigma_a}{\Sigma_t} = 0{\cdot}01$	$\frac{\Sigma_a}{\Sigma_t} = 0$
Based on T (BEHRENS)	2·25 ± ·02	2·35 ± ·21	2·29 ± ·09	2·47
Based on $T + 2C$ (first-order BENOIST)	2·12 ± ·05	2·13 ± ·17	2·07 ± ·08	2·25
Based on S (present work)	1·92 ± ·03	1·80 ± ·14	1·70 ± ·10	1·78

TABLE 3.—COMPARISON WITH EXPERIMENT

Experiment	Pitch (in.)	Channel dia. (in.)	S_z		S_r			S_z/S_r		
			Expt.	Theory	Expt.	BEHRENS	Present work	Expt.	BEHRENS	Present work
Mummery	8·25	3·77	2·13 ±·06	2·07	1·61 ±·05	1·73	1·56	1·32 ±·05	1·20	1·33
Richey	14	3·5 × 3·5	1·45 ±·04	1·37	1·22 ±·04	1·25	1·18	1·19 ±·04	1·10	1·17

VOL. 15 1961

5. CONCLUSIONS

The theoretical treatment of streaming in empty channels developed in this paper appears promising. The theory is in reasonably good agreement with other published results with the exception of SCHAEFER's Monte Carlo work. It would seem profitable to try to extend the theory to channels containing fuel rods. This requires the solution of rather complicated problems in neutron transport theory in order to find the appropriate boundary conditions to use at the channel boundaries. A knowledge of these boundary conditions would not only allow streaming correction factors to be calculated as in this paper, but, as pointed out by LESLIE (1960) it would make it possible to include streaming in a logical way in the Feinberg-Galamin individual rod theory for heterogeneous reactors.

Acknowledgments—The author would like to thank DR. D. C. LESLIE, DR. G. ROWLANDS and MR. J. CODD for their interest in this work and DR. J. ASHFORD for providing the Monte Carlo results from the MCTU-1 programme.

REFERENCES

BEHRENS D. J. (1954) *The Effect of Holes in a Reacting Material on the Passage of Neutrons, with Special Reference to the Critical Dimensions of a Reactor*. A.E.R.E. T/R 103.

BENOIST P. (1959) *A General Formulation of the Diffusion Coefficient in a Heterogeneous Medium Which May Contain Cavities*. S.P.M. 522 (Translated by I. S. GRANT as AERE-Trans. 842).

CARTER C. and JARVIS R. J. (1960) A.E.R.E. R 3366; (1961) *Reactor Sci. Technol. (J. Nucl. Energy* Parts A/B). This issue p. 113.

DAVISON B. (1951). *Influence of a Cylindrical Channel on a Periodic Neutron Density Distribution*. A.E.R.E. T/R 738.

GRANT I. S. (1958). *Neutron Streaming in Gas-Cooled Reactors*. A.E.R.E. R/R2568.

LALETIN N. I. (1958) *Proceedings of the Second International Conference on the Peaceful Uses of Atomic Energy, Geneva*, P/2189. United Nations, N.Y.

LESLIE D. C. (1960) Unpublished note.

SCHAEFER G. W. and PARKYN D. M. (1958). *Proceedings of the Second International Conference on the Peaceful Uses of Atomic Energy, Geneva*, P/310. United Nations, N.Y.

SCHAEFER G. W. (1960) Private Communication.

VOL
15
196

Reactor Science and Technology (Journal of Nuclear Energy, Parts A/B), 1961, Vol 15, pp. 81 to 85. Pergamon Press Ltd. Printed in Northern Ireland

REACTOR KINETICS: INTEGRAL EQUATION FORMULATION*

F. T. ADLER
Department of Physics, University of Illinois, Urbana, U.S.A.

(*First received* 23 *November* 1960 *and in revised form* 9 *January* 1961)

Abstract—The non-linear reactor kinetics equations are reduced to an integral equation for the neutron density which appears particularly suitable for computer applications. The computer programme described consists primarily of summing operations and appears to lead to better stability for equivalent time steps than other existing approaches. Any number of delayed neutron groups can be handled easily.

VOL. 15 1961

1. INTRODUCTION

THE purpose of this note is to cast the non-linear reactor kinetics equations in an integral form, which is particularly suitable for digital computer applications. The multiplication constant, k, may depend on time, neutron density, $n(t)$, void fraction and temperature. Void fraction and temperature may in turn depend on their appropriate relaxation constants as well as the flux history.

In the space-independent case, the integral equations can readily be solved numerically; a computer programme description for this case is given in Section 5 below. The functional form of k is arbitrary with regard to time and neutron density and can be specified in the programme by a subroutine. Thus a programme based on the integral equation formulation can readily be applied to a variety of situations and their effect on reactor performance, and be of particular usefulness in hazards analysis studies.

It is also possible to include the effects of spatial variations of the neutron density, $n(t)$. As indicated in WEINBERG and WIGNER (1958), the neutron flux, $\phi(x,t)$, and the densities of delayed emitters, $c_i(t)$, can be expanded in spatial eigenfunctions $\Psi(x)$ of the Helmholtz equation. Simple equations are obtained for the expansion coefficients when the temperature dependence of the cross sections is neglected. This case is of particular interest for the study of pulsed subcritical assemblies. The approach given here applies directly to the study of such spatially dependent problems, as will be indicated in Section 4.

If the assumption of temperature independent cross sections is not valid, a perturbation theory treatment is indicated, which is not considered here.

* Work performed in part under the auspices of the U.S. Atomic Energy Commission.

2. INTEGRAL EQUATION FORMULATION OF THE REACTOR KINETICS EQUATION

The space-averaged reactor kinetics equations may be written as

$$\frac{dn}{dt} = \{k[t,n(t)](1-\beta)-1\}n(t)/l + \sum_i \lambda_i C_i(t) + S_0(t) \tag{1}$$

$$\frac{dC_i}{dt} = -\lambda_i C_i(t) + \beta_i k[t,n(t)]n(t)/l \tag{2}$$

where S_0 represents an external source, l is the neutron life-time, $\beta = \Sigma\beta_i$ is the delayed neutron fraction, and the index i refers to the ith delayed neutron group.

Integration of equation (2) then gives

$$C_i(t) = C_i(0)\,e^{-\lambda_i t} + e^{-\lambda_i t}\int_0^t dt'\, e^{\lambda_i t'}\beta_i k[t',n(t')]n(t')/l \tag{3}$$

where $C_i(0)$ is the initial value of $C_i(t)$.

Substituting (3) into (1) leads immediately to

$$\frac{dn}{dt} = \{k[t,n(t)](1-\beta)-1\}n(t)/l + S_0(t) + \sum\lambda_i C_i(0)\,e^{-\lambda_i t} + \sum_i \lambda_i\, e^{-\lambda_i t}\int_0^t dt'\, e^{\lambda_i t'}\beta_i k[t',n(t')]n(t')/l. \tag{4}$$

Equation (4) may be written in the form

$$\frac{dn}{dt} = -n(t)/l + S(t) \tag{5}$$

which can also be integrated immediately:

$$n(t) = n(0)\,e^{-t/l} + e^{-t/l}\int_0^t dt'\, e^{t'/l}S(t'). \tag{6}$$

Or, explicitly, in the notation of equation (4):

$$n(t) = n(0)\,e^{-t/l} + e^{-t/l}[(1-\beta)/l] \times \int_0^t dt'\, e^{t'/l} k[t',n(t')]n(t') + \sum_i \lambda_i C_i(0)\, e^{-t/l} \int_0^t dt'\, [e^{-\lambda_i t'}\, e^{t'/l}] + e^{-t/l} \int_0^t dt'\, e^{t'/l} S_0(t') + \sum_i [\beta_i \lambda_i / l]\, e^{-t/l} \int_0^t dt'\, e^{-\lambda_i t'}\, e^{t'/l} \times \int_0^{t'} dt''\, e^{\lambda_i t''}\, k[t'',n(t'')]n(t''). \quad (7)$$

The third term in (7) is directly integrable, while the last can be reduced to single integrals by integrations by parts.

These simple transformations lead to the desired integral equation of Volterra type:

$$n(t) = F(t) + \int_0^t dt'\, G(t,t')k[t',n(t')]n(t') \quad (8)$$

where $F(t)$ is a known function depending on the initial conditions, $n(0)$ and $C_i(0)$, and on the external source $S_0(t)$:

$$F(t) = n(0)\, e^{-t/l} + \sum_i C_i(0)\, \frac{\lambda_i l}{1-\lambda_i l} \times [e^{-\lambda_i t} - e^{-t/l}] + e^{-t/l} \int_0^t dt' S_0(t')\, e^{t'/l} \quad (9)$$

From equation (7) it follows that the kernel of the integral equation, $G(t,t')$, can be expressed in the form:

$$G(t,t') = G(t-t') = (1/l)\left\{(1-\beta)\, e^{-(t-t')/l} + \sum_i \frac{\beta_i l \lambda_i}{1-l\lambda_i} [e^{-\lambda_i (t-t')} - e^{-(t-t')/l}]\right\} \quad (10)$$

We also note that

$$G(t,t) = G(0) = \frac{1}{l}(1-\beta) \quad (11)$$

and that for small Δt,

$$G(\Delta t) \simeq (1/l)\{(1-\beta) - (\Delta t/l)[(1-\beta) - \sum_i \beta_i \lambda_i l]\} \quad (11')$$

3. SOLUTION OF THE INTEGRAL EQUATION

Equation (8) is still completely general and cannot be solved analytically except by imposing simplifying assumptions on $k(t,n(t))$. On the other hand, equation (8) provides a suitable starting point for a numerical solution. A simple numerical procedure for evaluating the integral in equation (8) is here obtained by first expressing $n(t)$ algebraically in terms of already known quantities. For this purpose we assume that $n(t')$ is known for $t' \le t - \Delta t$. Then, from equation (8):

$$n(t) = F(t) + \int_0^{t-\Delta t} G(t-t')k[t',n(t')]n(t')\, dt' + \int_{t-\Delta t}^t G(t-t')\, k[t',n(t')]n(t')\, dt'. \quad (8')$$

The first two terms on the right-hand side do not involve the unknown value of $n(t)$*, and can be considered as given functions of t. To evaluate the last term, we choose a Δt small enough that the variation of $k[t',n(t')]n(t')$ in the integrand is correspondingly small, so that we may replace this factor by its average value:

$$\int_{t-\Delta t}^t G(t-t')k[t',n(t')]n(t')\, dt' = \tfrac{1}{2}\{k[t,n(t)]n(t) + k[t-\Delta t, n(t-\Delta t)]n(t-\Delta t)\} \int_{t-\Delta t}^t G(t-t')\, dt'. \quad (12)$$

The integration over the more rapidly varying function $G(t-t')\, dt'$ may be performed exactly. From equation (10) we have then:

$$\int_{t-\Delta t}^t G(t-t')\, dt' = \left\{(1-\beta) - \sum_i \frac{\beta_i \lambda_i l}{1-\lambda_i l}\right\} \times [1 - e^{-\Delta t/l}] + \sum_i \frac{\beta_i}{1-\lambda_i l} [1 - e^{-\lambda_i \Delta t}] \equiv B(\Delta t). \quad (13)$$

From equations (8'), (12), and (13) we then obtain:

$$n(t) = F(t) + \int_0^{t-\Delta t} G(t-t')k[t',n(t')]n(t')\, dt' + \tfrac{1}{2}\{k[t,n(t)]n(t) + k[t-\Delta t, n(t-\Delta t)] \times n(t-\Delta t)\}B(\Delta t). \quad (14)$$

Therefore, we obtain:

$$n(t) = \frac{F(t) + \int_0^{t-\Delta t} G(t-t')k[t',n(t')]n(t')\, dt' + \tfrac{1}{2}k[t-\Delta t, n(t-\Delta t)]n(t-\Delta t)B(\Delta t)}{1 - (\tfrac{1}{2})k[t,n(t)]B(\Delta t)} \quad (15)$$

* Although the integrand is a function of the upper limit, it is not necessary to recalculate the entire integral each time the upper limit is changed, since $G(t-t')$ consists of exponentials in $t-t'$, as shown in equation (10). The parts depending on t may be taken outside the integral, permitting a simple addition to be made to the integral at each time step.

In the simplest situation, k depends only on t in some prescribed manner, and not on $n(t)$:

$$k = k(t). \tag{A}$$

In this case, equation (15) gives an explicit prescription for a point-by-point evaluation of $n(t)$. In general, k depends on both t and $n(t)$:

$$k = k(t, n(t)). \tag{B}$$

In most cases of interest k is a smoothly varying function of $n(t)$, and normally varies less as a function of $n(t)$ than through its explicit dependency on t.

In the general case (B), we have equation (15) where the denominator contains $k(t,n(t))$. We solve this implicit equation by successive approximations: in the first step, $k(t,n(t-\Delta t))$ is used to calculate a first approximation $n_1(t)$ from equation (15). Further approximations $n_i(t)$ are obtained by calculating an $n_i(t)$ using $k(t,n_{i-1}(t))$ in the denominator. Because of the smooth variation of k with n, this iterative method will converge rapidly.

4. APPLICATION TO TYPICAL PROBLEMS

The integral equation approach is sufficiently flexible so that more complex problems can be treated readily by simple extensions of the formalism presented here. Two illustrations will be considered.

A. *Temperature and void coefficients*

The present approach applies also to problems in which k depends on the temperature T and the void fraction V:

$$k = k(t,T,V). \tag{C}$$

We consider the equations for T_1 and V, given by HETRICK and GAMBLE (1958):

$$\frac{dT_1}{dt} = \xi n(t) - \gamma_1 T_1(t) \tag{16}$$

$$\frac{dV}{dt} = an(t)E - \gamma_2 V(t) \tag{17}$$

$$E = \int_0^t dt' n(t') \tag{18}$$

where T_1 is the temperature rise above the initial temperature. E is the total energy release in an excursion. γ_1 and γ_2 are appropriate relaxation constants for T_1 and V. a is an adjustable parameter related to bubble growth and ξ relates the heat release by fission to the temperature increase.

In analogy with the procedure of Section 2, one can immediately obtain integral equations for T_1 and V in the form:

$$T_1(t) = \xi\, e^{-\gamma_1 t} \int_0^t dt'\, e^{\gamma_1 t'} n(t') \tag{19}$$

$$V(t) = V_0 e^{-\gamma_2 t} - a\, e^{-\gamma_2 t} \int_0^t dt'\, e^{\gamma_2 t'} n(t') \int_0^{t'} dt'' n(t'') \tag{20}$$

We note that the equations (19) and (20) are in a sense subsidiary equations since $n(t)$ depends on T_1 and V only through the effects of temperature and void fraction on k. To solve for $n(t)$, we now have to consider the set of coupled integral equations (8), (19) and (20). Equation (15) still holds in this general case, and is now an implicit equation, where the k in the denominator is a function of $n(t)$, $T_1(t)$, and $V(t)$. An iteration procedure, similar to that discussed under case (B) is again possible, k being a smoothly varying function of T_1, V, and $n(t)$.

In the first step of the iteration, $n(t)$ is calculated using

$$k = k\{t, T_1[t, n(t-\Delta t)], V[t, n(t-\Delta t)]\}$$

in the denominator. Successive approximations n_i to to $n(t)$ are then made by using the preceding approximation n_{i-1} for the calculation of $n(t)$. Convergence should be rapid, since the explicit dependency of k on t is taken into account exactly, as indicated in case (A).

B. *Spatial dependency*

The integral equation approach can also be applied to space-dependent problems. Heterogeneous systems will be considered in a subsequent paper. Here we consider only homogeneous pulsed assemblies and bare reactors. In this situation, the equations of case (A) apply immediately for each spatial mode, and the equations for the individual modes are uncoupled. Under less restrictive assumptions the equations for the separate modes are coupled, and a perturbation treatment is indicated.

Following WEINBERG and WIGNER (1958), we write the reactor equation in the form

$$\frac{1}{v}\frac{\partial \Phi}{\partial t} = D\nabla^2\Phi(x,t) - \Sigma_a\Phi(x,t) + (1-\beta)\int dx' H_p(x,x')\Sigma_f(x)\Phi(x,t) + \sum_i \lambda_i \int dx' H_d^{(i)}(x,x') C_i(x',t) + S_0(x,t) \tag{21}$$

$$\frac{\partial C_i}{\partial t} = \beta_i \nu \Sigma_f \Phi(x,t) - \lambda_i C_i(x,t) \tag{22}$$

where Φ is the suitably averaged thermal flux, Σ_a and Σ_f the thermal absorption and fission cross sections, H_p is the slowing down kernel for prompt neutrons, and $H_d^{(i)}$ is the slowing down kernel for the ith group of delayed neutrons.*

The flux, source and precursor densities may be expanded in a suitable set of orthonormal eigenfunctions. Using the well-known properties of displacement kernels, one can then obtain the following

* The influence of the fast effect and of resonance capture may be represented by multiplying H_p and $H_d^{(i)}$ by suitable constants.

set of equations for the Fourier amplitudes $\varphi_n(t)$, $S_n(t)$ and $C_n^{(i)}(t)$ of these quantities:

$$\frac{dC_j^{(i)}(t)}{dt} = \beta_i v\Sigma_f \varphi_j(t) - \lambda_i C_j^{(i)}(t) \qquad (23)$$

$$\frac{1}{v}\frac{d\varphi_j(t)}{dt} = [(1-\beta)v\Sigma_f H_p(B_j) - (DB_j^2 + \Sigma_a)] \times \varphi_j(t) + \sum_i \lambda_i H_d^{(i)}(B_j) C_j^{(i)}(t) \qquad (24)$$

Here B_j^2 is the buckling of the jth mode, and H_p and $H_d^{(i)}$ are the appropriate Fourier transforms of the slowing down kernels for prompt and delayed neutrons.

Equations (23) and (24) are identical in structure to equations (1) and (2). The complete programme described below can therefore be used to evaluate the expansion coefficients $\Phi_j(t)$ and $C_j^i(t)$ for bare reactors or assemblies. In particular, excepting normalization constants, $n_0(t) = \frac{1}{v}\varphi_0(t)$ and $C_0^{(i)}(t)$ represent the neutron and precursor populations in the system.

For brevity, we introduce the following notations:

(1) $l \equiv l_0 = 1/v(DB_0^2 + \Sigma_a)$ — the neutron lifetime in the zero-th mode;

(2) $\gamma_i \equiv H_d^{(i)}(B_0)$ — the probability for non-leakage and non-absorption during moderation for neutrons produced by the precursor group i;

(3) $k\gamma = v[\Sigma_f/(DB_0^2 + \Sigma_a)]H_p(B_0) \equiv k\gamma_t H_p(B_0)$ — the finite medium multiplication constant.

With this notation one obtains:

$$\frac{dn_0}{dt} = [(1-\beta)k(t)\gamma - 1]n_0(t)/l + \sum_i \lambda_i \gamma_i C_0^{(i)}(t) + S_0(t) \qquad (25)$$

$$\frac{dC_0^{(i)}}{dt} = -\lambda_i C_0^{(i)}(t) + \beta_i \gamma_t k(t) n(t)/l. \qquad (26)$$

The factors γ, γ_t and γ_i represent the effects of the finite size of the assembly considered. From equations (25) and (26) one can easily get an integral equation formally identical to equation (8). The form of the kernel $G(t-t')$ and of the function $F(t)$ is, however, different from the expressions given in equations (9) and (10). In the space-dependent problem one obtains for these functions:

$$F(t) = n(0)\,e^{-t/l} + \sum_i C_i(0)\frac{\lambda_i l\gamma_i}{1-l\lambda_i} \times [e^{-\lambda_i t} - e^{-t/l}] + e^{-t/l}\int_0^t dt' S_0(t')\,e^{t'/l} \qquad (9')$$

$$G(t-t') = \frac{1}{l}\left\{(1-\beta)\gamma\, e^{-(t-t')/l} + \gamma_t \sum_i \frac{\beta_i \lambda_i l \gamma_i}{1-l\lambda_i}[e^{-\lambda_i(t-t')} - e^{-(t-t')/l}]\right\} \qquad (10')$$

The integration procedure used in Section 3 applies here, too. Corresponding to equation (13), we introduce the abbreviation

$$B(\Delta t) = \left\{(1-\beta)\gamma - l\gamma_t \sum_i \frac{\beta_i \lambda_i \gamma_i}{1-l\lambda_i}\right\} \times [1 - e^{-\Delta t/l}] + \gamma_t \sum_i \frac{\beta_i \gamma_i}{1-l\lambda_i}(1 - e^{-\lambda_i \Delta t}) \qquad (13')$$

and find for $n(t)$ the solution:

$$n(t) = \left\{n_0\,e^{-t/l} + \sum_i C_i(0)\frac{\lambda_i l\gamma_i}{1-l\lambda_i}[e^{-\lambda_i t} - e^{-t/l}] + e^{-t/l}\int_0^t dt' S_0(t')\,e^{t'/l} + e^{-t/l}\left[(1-\beta)\gamma/l - \sum_i \frac{\beta_i \lambda_i \gamma_i \gamma_t}{1-l\lambda_i}\right]\int_0^{t-\Delta t} dt' k(t') n(t')\,e^{t'/l} + \sum_i \frac{\beta_i \lambda_i \gamma_i \gamma_t}{1-l\lambda_i}\,e^{-\lambda_i t}\int_0^{t-\Delta t} dt' k(t') n(t')\,e^{\lambda_i t'} + \tfrac{1}{2}k(t-\Delta t)n(t-\Delta t)B(\Delta t)\right\} \Big/ [1 - \tfrac{1}{2}k(t)B(\Delta t)] \qquad (15')$$

5. COMPUTER SOLUTIONS OF KINETICS PROBLEMS

Solutions to integral equations of the form of equation (8) can readily be obtained with a digital computer. In comparison with the usual direct numerical integration of equations (1) and (2), the computer solution of the integral equation appears to have several advantages:

First, and probably most important, the analytical approach leads to a calculation consisting of summing operations, unlike the usual schemes in which differences of the function and its derivatives are used. This should lead to better stability for equivalent time steps, or less computing time for the same stability.

Second, the number of groups of delayed neutrons is arbitrary. The amount of calculation needed for an increased number of groups is much less than that

needed for the usual numerical integration, where the complexity of the code increases with the number of groups, and difficulties in convergence arise for practical step sizes.

Third, no separate scheme is needed to start the calculation or to treat intervals where $n(t)$ or $k(t)$ vary rapidly. In the customary differential equation approach, a choice must be made between relatively inefficient methods of the Runga-Kutta type which can be used throughout the calculation, and other more complex methods which require separate start-up schemes. In the method given here, small time steps are taken for an initial period, of the order of the neutron generation time, to avoid introducing large relative errors into the integrals which describe the past history of the system. During this initial period, however, exactly the same method is used as in the rest of the programme. Thus it is possible to revert to small intervals when either $k(t)$ or $n(t)$ change by more than a prescribed amount in any given interval.

To illustrate the numerical stability of the programme, we consider the errors in $n(t)$ for different step sizes. In a representative case, the error in $n(t)$ was about 0·07 per cent for an initial step size equal to 1/10 of a generation time, and no detectable errors were found for step sizes of 1/100 or 1/1000 of a generation time.

A digital computer programme using the integral equation method allows, furthermore, for relatively large steps in time in intervals in which the functions $n(t)$ and $k(t)$ vary smoothly. The function $k[t,n(t)]$ may of course depend on the previous reactor history as well as on time.

REFERENCES

HETRICK D. L. and GAMBLE D. P. (1958) ANS, December; *see also* DURENFELD M. S. and GAMBLE D. G. (1959) ANS, November.

WEINBERG A. and WIGNER E. P. (1958) *The Physical Theory of Neutron Chain Reactors*, University of Chicago Press.

VOL.
15
1961

Reactor Science and Technology (Journal of Nuclear Energy, Parts A/B) 1961, Vol. 15, pp. 86 to 90. Pergamon Press Ltd. Printed in Northern Ireland

THE EFFECT OF CYLINDRICAL AIR VOIDS IN A HIGHLY ENRICHED WATER-MODERATED CORE

P. N. COOPER, W. M. COOPER and K. FIRTH
Associated Electrical Industries Ltd., Aldermaston, Berks.

(*Received* 2 *December* 1960)

Abstract—Measurements have been made in a light water-moderated, highly-enriched, uranium-fuelled, sub-critical facility of the variation in critical mass with diameter of a central air void. These measurements indicated that there would be no transient increase in reactivity if a central void were to collapse radially. Other measurements on the slow flooding of a 3 in. diameter central air void showed that there was a slight addition of reactivity in the early stages, reaching a maximum of about 0·1 per cent, but that a completely flooded void was much less reactive than the empty void. Two-group diffusion theory calculations for the initial and final states indicate that the results of the measurements are not affected by small changes in the enrichment of the uranium.

1. INTRODUCTION

THE highest thermal, epithermal and fast neutron fluxes in a reactor are usually at the centre of the core. In order to make full use of these fluxes it is necessary to remove a central fuel element and replace it with a void containing the experiment. Before loading such an arrangement into a core it is desirable to study fault conditions such as collapse and flooding of the void. Theoretical predictions of this information are complicated and laborious, therefore the necessary data are obtained more rapidly and reliably by experiment, e.g. with a sub-critical facility (BURDEN, 1958). The work reported below was undertaken in order to provide information for safety assessments concerning experiments in the core of MERLIN.

2. MEASUREMENTS IN THE SUB-CRITICAL FACILITY

It was necessary for these measurements to use fuel elements containing uranium enriched to different degrees in ^{235}U. Each complete fuel element contains a nominal 140 g of ^{235}U (FIRTH, 1958). Seventeen complete fuel elements are enriched to 80 per cent in ^{235}U. These were used in the more reactive positions in the core. The remainder are enriched to 93 per cent in ^{235}U. The method of measuring critical masses has been described in detail elsewhere (CHICK, 1958).

2.1 *Critical masses with a 3 in. diameter void*

A cylindrical void made of aluminium 3 in. diameter and 1/16 in. wall thickness replaced a central fuel element for the measurements. This extended from 2·8 cm below the bottom of the active core and through the top water reflector, which was 15 cm thick. The void was suitably weighted to prevent floating.

Critical mass measurements were made for the following cores:

1. core with 3 in. diameter central axial void
2. compact core (no void)
3. core with central 3 in. square water-filled hole.

The final core configurations for cores 1 and 3 are given in Figs. 1(a), and 1(b) respectively.

2.2 *Radial collapse of a central air void*

Measurements have been made, in the SPERT I reactor (BRIGHT, 1957), of the change in reactivity with the size of a non-central air void inserted in a fuel element position. It was found that although the reactivity change from the position completely filled with air to completely filled with water was small, there was a substantial increase in reactivity at intermediate positions. This reached a maximum of 0·35 per cent when the water annulus around the air void occupied about 30 per cent of the total void volume. Consequently measurements were made to determine if such an effect existed for a central air void in MERLIN. This could affect the transient behaviour of the reactor if the air void were to collapse suddenly under hydrostatic pressure.

Critical masses were measured for a series of diameters of aluminium voids all with 1/16 in. wall thickness. Cores 1 and 3 provided the end points for the measurements and the intermediate cores were:

4. core with 2·3/4 in. diameter central axial air void
5. core with 2·1/2 in. diameter central axial air void
6. core with 2·1/4 in. diameter central axial air void
7. core with 1·3/4 in. diameter central axial air void
8. core with 1·1/4 in. diameter central axial air void.

The final core arrangements for these are intermediate between those given in Figs. 1(a) and 1(b).

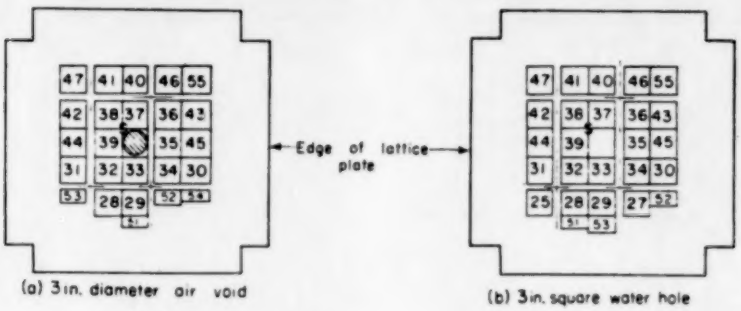

(a) 3 in. diameter air void (b) 3 in. square water hole

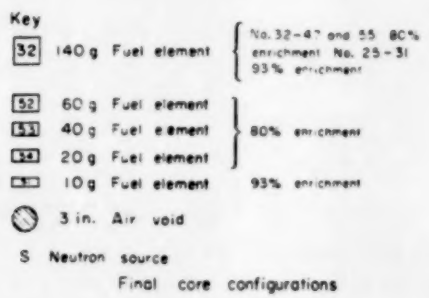
Key
32 140 g Fuel element
No. 32–47 and 55 80% enrichment No. 25–31 93% enrichment
52 60 g Fuel element
53 40 g Fuel element
54 20 g Fuel element
80% enrichment
51 10 g Fuel element 93% enrichment
3 in. Air void
S Neutron source

Final core configurations

FIG. 1.

TABLE 1.—EFFECT OF 3 IN. DIAMETER VOID

Core	Critical mass ^{235}U (g)	Change in critical mass ^{235}U (g)
1. 3 in. diameter axial air void	3121·0 ± 1·4	Reference core
2. Compact (no void)	2747·9 ± 1·7	−373·1 ± 2·2
3. 3 in. square water filled hole	3375·8 ± 0·9	−254·8 ± 1·7

The amounts of aluminium vary for each of the cores measured; however, since the maximum volume of aluminium present is only 6·5 per cent of the volume of the hole in the core, all the systems measured are a close approximation to air voids contained by infinitely thin walls.

2.3 *Slow flooding of a central air void*

The most likely fault which could develop in an air void immersed in water is a slow leak. An increase of reactivity may occur during the flooding of such a void placed centrally in a core. The effect of the 3 in. diameter void during flooding has been investigated by measuring the critical masses for a series of water heights in the void. These cores were:

9. water height 3 cm above bottom of active core
10. water height 9 cm above bottom of active core
11. water height 15 cm above bottom of active core
12. water height 30 cm above bottom of active core
13. water height 45 cm above bottom of active core.

Core 1, with the empty void, corresponds to a water height 2·8 cm below the bottom of the active core, and core 3 to a water height 75 cm above the bottom of the active core. The final core arrangements are intermediate between those given in Figs. 1(a) and 1(b).

3. RESULTS

3.1 *Critical masses with a 3 in. diameter void*

Table 1 summarizes the critical mass measurements listed in Section 2.1. Replacing a central fuel element with a 3 in. diameter air void increases the critical mass by 373 g ^{235}U, and if the air void is removed, leaving a water filled hole 3 in. square, the critical mass is increased by a further 255 g of ^{235}U.

3.2 *Effect of diameter of air void on critical mass*

Table 2 summarizes the measurements and Fig. 2 gives critical mass as a function of void volume, taking the 3 in. diameter void as 100 per cent. It is seen that the departure from a linear relationship is large, but that the lowest critical mass occurs for the largest void.

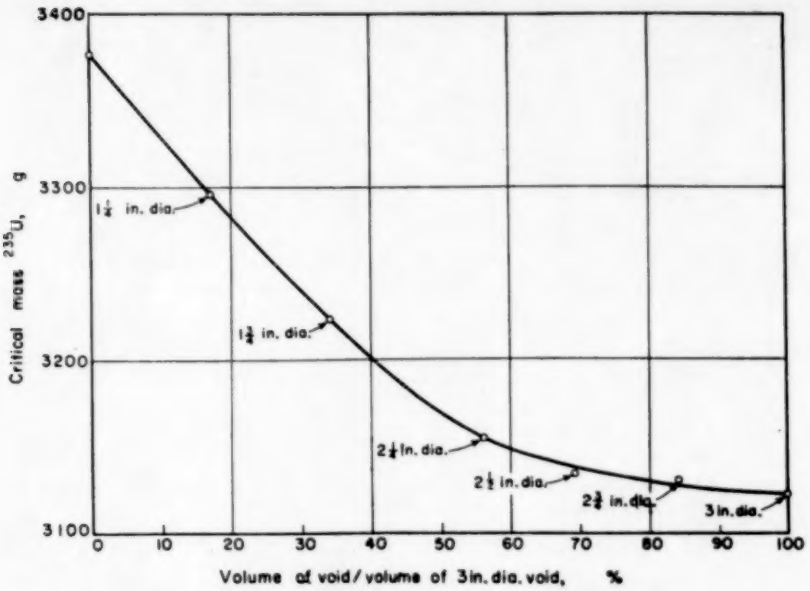

Fig. 2.—Variation of critical mass with void size.

Table 2.—Effect of diameter of air void

Core	Critical mass ^{235}U (g)	Change in critical mass ^{235}U (g)
1. 3 in. diameter axial air void	3121·0 ± 1·4	Reference core
4. 2·3/4 in. diameter axial air void	3128·6 ± 1·7	+7·6 ± 2·2
5. 2·1/2 in. diameter axial air void	3133·2 ± 1·3	+12·2 ± 1·9
6. 2·1/4 in. diameter axial air void	3154·1 ± 0·8	+33·1 ± 1·6
7. 1·3/4 in. diameter axial air void	3223·3 ± 2·1	+102·3 ± 2·6
8. 1·1/4 in. diameter axial air void	3294·8 ± 0·8	+173·8 ± 1·6
3. 3 in. square water-filled hole	3375·8 ± 0·9	+254·8 ± 1·7

3.3 *Slow flooding of 3 in. diameter void*

Table 3 summarizes the measurements and Fig. 3 gives critical mass as a function of water height in the void. In this case a slight decrease in critical mass is observed, reaching a maximum decrease of 14 g ^{235}U at a water depth of about 8 cm above the bottom of the active core.

4. CRITICAL MASS CALCULATIONS

4.1 *Fuel enrichment*

If cores containing central voids are loaded into the MERLIN reactor, they will initially contain uranium of 93 per cent enrichment only. Measurements on compact cores containing (a) only 93 per cent enrichment uranium and (b) mostly 80 per cent enrichment uranium have shown that the decrease in enrichment increases the critical mass by 70·1 ± 4·2 g ^{235}U. Two-group diffusion theory calculations predicted an increase of 53 g ^{235}U. If the only effect of reducing the enrichment is a small increase in critical mass, as would be expected, then the trends shown by these measurements can confidently be applied to cores of 93 per cent enrichment.

4.2 *Calculations for voided cores*

One-dimensional, two-group diffusion calculations were made for cylindrical cores containing cylindrical air voids equivalent in area to 3 in. square voids. This was the nearest approximation to a 3 in. diameter air void in a 3 in. square water hole which could reasonably be tackled in a hand calculation. Since Fig. 2 indicates that the critical mass does not vary much with void diameter for the larger voids, it was felt that this approximation was justified. Calculations were also made for cores containing a central water void. The size of this void was increased beyond 3 in. square for calculation purposes so that it touched the edge of the active fuel in adjacent elements. (The active area, in

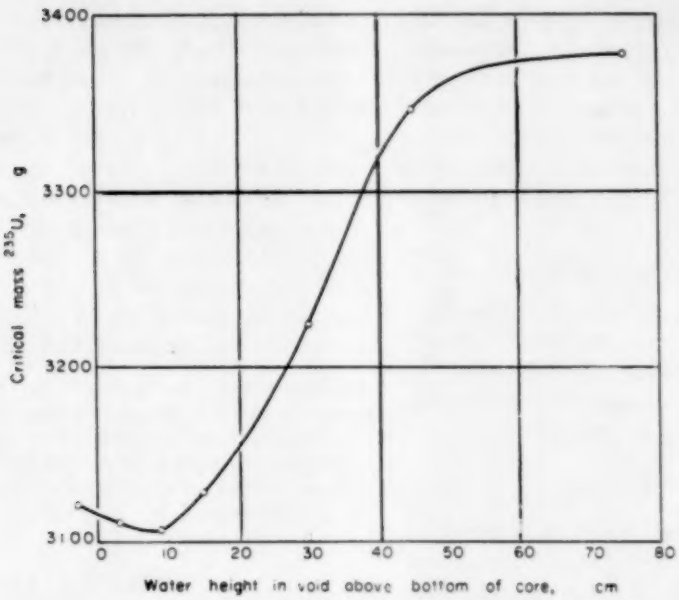

FIG. 3.—Variation of critical mass with water height in void.

TABLE 3.—FLOODING OF 3 IN. DIAMETER AIR VOID

Core	Critical mass ^{233}U (g)	Change in critical mass ^{233}U (g)
1. Water 2·8 cm below bottom of core (empty void)	3121·0 ± 1·4	Reference core
9. Water 3·0 cm above bottom of core	3111·1 ± 1·2	−9·9 ± 1·9
10. Water 9·0 cm above bottom of core	3107·1 ± 1·7	−13·9 ± 2·2
11. Water 15·0 cm above bottom of core	3128·0 ± 1·4	−7·0 ± 2·0
12. Water 30·0 cm above bottom of core	3222·3 ± 2·5	+101·3 ± 2·9
13. Water 45·0 cm above bottom of core	3344·4 ± 0·3	−223·4 ± 1·5
3. Water 75·0 cm above bottom of core (no void)	3375·8 ± 0·9	+254·8 ± 1·7

TABLE 4.—CALCULATED AND MEASURED CRITICAL MASSES

Core	Enrichment	Critical mass ^{233}U (g)	
		Calculated	Measured
Compact core	93%	2655	2663
Compact core	81·4%	2708	2733
3 in. square central air void	93%	3085	3052
3 in. square central air void	83·4%	3128	3121*
3 in. square central water void	93%	3291	3313
3 in. square central water void	83·4%	3335	3376

* 3 in. diameter central air void.

plan, of a 3 in. square element is only 2·36 in. × 2·50 in.) This correction was necessary to avoid overestimating the effect on the uranium of flux peaking close to the void since a homogenized core was assumed for the calculations. The calculations are, therefore, for the two extreme cases which have been investigated experimentally.

Each calculation was made for enrichments of 93 per cent and 83·4 per cent, the average enrichment of the voided cores. Table 4 summarizes the results of these calculations, and critical mass measurements for 93 per cent enriched cores are included (KERRIDGE, 1960).

4.3 *Discussion*

The calculations for the compact core did not predict completely the measured increase in critical

mass with decreasing enrichment. This is not fully understood and cannot be attributed to the presence of 1·6 per cent ^{236}U which replaces some of the ^{238}U, since these two uranium isotopes have almost identical resonance integrals. All the calculations indicate, however, an approximately constant increase in critical mass of about 45 g ^{235}U when mixed enrichment cores are used.

5. CONCLUSIONS

All the results are quoted in terms of critical mass. Change in critical mass for this particular core size and composition may be approximately related to reactivity by the following expression which was calculated by means of two-group diffusion theory:

$$\delta k_e/k_e = (1/5{\cdot}2)\ \delta m/m.$$

The measurements show that no serious addition of reactivity is likely to occur due to the collapse or slow flooding of a central air void. If a 3 in. diameter void were suddenly to collapse, Fig. 2. indicates that at all stages the critical mass would be increasing, and that no addition of reactivity would occur. For the case of flooding of the void there is a slight addition of reactivity in the early stages, reaching a maximum of about 0·1 per cent. Addition of this amount of reactivity would produce a stable doubling time of about 50 seconds.

Two-group critical mass calculations for the end points of these measurements show that a decrease in enrichment results in an approximately constant increase in critical mass. It is, therefore, to be expected that this will be true for the intermediate cases, and that a core of 93 per cent enrichment will have the same behaviour.

In SPERT I a non-central water void is more reactive than an air void in the same position. Our calculations for central air and water voids in a SPERT I core also show this trend. The difference between MERLIN and SPERT I arises because the SPERT I core is *undermoderated* compared with the MERLIN core.

Acknowledgments—The authors wish to thank Miss M. Cresswell for doing the computational work for the theoretical calculations and the experiments, Mr. R. S. Curtis for help in carrying out the experiments and Mr. M. Kerridge and Dr. A. J. Salmon for valuable discussions. They are also indebted to Dr. T. E. Allibone, C.B.E., F.R.S., Director of the Laboratory, for permission to publish this paper.

REFERENCES

Bright G. O. and Toole C. R. Jr. (1957) *Notes on the Effect on Reactivity of Water Annuli in Large Void Spaces in the SPERT I Reactor Core*. U.S.A.E.C. Report IDO–16382.

Burden D. F., Caesar E. A. Y. and Kerridge M. (1958) *Nucl. Engng*. **3**, No. 26, 198.

Chick D. R., Firth K., Kerridge M. and Salmon A. J. (1958) *Nature, Lond.* **181**, 1171.

Firth K. *et al.* (1958) *Proceedings of the Second International Conference on the Peaceful Uses of Atomic Energy, Geneva*, Paper A Conf. 15 P 1461. United Nations, N.Y.

Kerridge M. (1960) Private communication.

Reactor Science and Technology (Journal of Nuclear Energy, Parts A/B) 1961, Vol. 15, pp. 91 to 97. Pergamon Press Ltd. Printed in Northern Ireland

A GENERAL METHOD OF DERIVING RESPONSES AND TRANSFER FUNCTIONS IN TRANSIENT HEAT CONDUCTION PHENOMENA

R. K. THOMASSON
Dounreay Experimental Reactor Establishment, Dounreay, Thurso, Caithness

(*First received* 8 *March* 1960 *and in final form* 6 *December* 1960)

Abstract—A method of solving unsteady heat conduction problems is described. The solution is obtained by first finding the eigenvalues and eigenfunctions of an integral equation. Once these have been obtained it is possible to obtain ordinary differential equations or transfer functions describing the response to various disturbances in heat production and extraction.

The method is easy to apply to cases where the heat flow can be treated as one-dimensional and can be extended to cover two-dimensional cases.

As an example of the use of the method, the temperature responses of a fast reactor fuel pin to power changes and coolant temperature changes are derived.

VOL. 15 1961

1. INTRODUCTION

TRANSIENT heat conduction problems are often encountered in reactor technology. Changes of temperature in reactor fuel or moderator usually result in changes of reactivity which influence the reactor power, which in turn affects the temperature. The stability of this closed loop system affects very considerably the controllability and safety of the reactor. One part of this problem, i.e. finding the response of fuel or coolant temperature to power changes, is to a large extent a transient heat conduction problem. Because the heat conduction problem is only part of the reactor stability problem, the answer is often required in general terms, e.g. as a series of ordinary differential equations which might be used in an analogue computing study or as a transfer function to be used in a frequency response analysis. Similar results may be required in the study of some automatic temperature control systems.

For problems which can be specified in terms of one space variable (one-dimensional problems and cases of axial and spherical symmetry) the equation of transient heat conduction is

$$C(z)\frac{\partial T}{\partial t} = \frac{\partial}{\partial z}\left[B(z)\cdot\frac{\partial T}{\partial z}\right] \tag{1.1}$$

where $T(z,t)$ is the temperature, t the time and z the space co-ordinate. The density of thermal capacity $C(z)$ is $\sigma(z)2\pi z$ for cylindrical geometry and $\sigma(z)4\pi z^2$ for spherical geometry, where $\sigma(z)$, the thermal capacity per unit volume, is $\rho(z)\,C(z)$. The heat flow $B(z)$ due to unit temperature gradient across the z-co-ordinate surface, is $k(z)2\pi z$ for cylindrical geometry and $k(z)4\pi z^2$ for spherical geometry, where $k(z)$ is the thermal conductivity.

This equation is solved analytically in the standard heat transfer literature for some cases where $C(z)$ and $B(z)$ are simple functions. The problem usually treated is the perturbation of temperature from a steady state condition. Solutions of the type $T(z,t) = G(z)\,.\,H(t)$ are sought and substitution into (1.1) yields,

$$C(z)\,.\,G(z)\,.\,\frac{dH}{dt} = H(t)\,.\,\frac{d}{dz}\left[B(z)\,.\,\frac{dG}{dz}\right] \tag{1.2}$$

i.e.
$$\frac{dH/dt}{H(t)} = \frac{\dfrac{d}{dz}\left[B(z)\,.\,dG/dz\right]}{C(z)\,.\,G(z)} = -\lambda \text{ (say)}$$

and separating the variables we obtain

$$\frac{dH}{dt} + \lambda H(t) = 0 \tag{1.3}$$

$$\frac{d}{dz}\left[B(z)\frac{dG}{dz}\right] + \lambda C(z)\,.\,G(z) = 0\,. \tag{1.4}$$

The boundary conditions for this equation are usually of the following alternative forms:

$$\left.\begin{aligned}
&\text{(a)} \quad G(z) = 0 \text{ (zero perturbation of temperature at the boundary)}\\
&\text{(b)} \quad \frac{dG}{dz} = 0 \text{ (no heat flow at the boundary)}\\
&\text{(c)} \quad B(z)\frac{dG}{dz} = h_1 G(z) \text{ (lower boundary condition)}\\
&\text{or } -B(z)\frac{dG}{dz} = h_2 G(z) \text{ (upper boundary condition)}
\end{aligned}\right\} \tag{1.5}$$

Conditions (1.5 (c)) are the usual forced-convection boundary conditions.

Because of these boundary conditions, equation (1.4) has non-zero solutions only for certain values of λ. These values are known as the eigenvalues and the corresponding solutions for $G(z)$ are known as the eigenfunctions. The general solution of equation (1.1) is therefore of the form

$$T(z,t) = \sum_n A_n \,.\, G_n(z)\, e^{-\lambda_n t} \qquad (1.6)$$

where $G_n(z)$ is the eigenfunction corresponding to the eigenvalue λ_n, and the constants A_n depend on the initial conditions. The λ_n and $G_n(z)$ are conveniently called the 'decay constants' and 'decay modes' of the system.

Equation (1.4) is of the Sturm-Liouville form, which occurs in many physical problems and was originally derived for the classical problem of the non-homogeneous vibrating string. This problem is treated fully by COURANT and HILBERT (1953) who show that, when $B(z)$ and $C(z)$ are positive throughout the range and boundary conditions (1.5) apply, the eigenvalues are all real and positive. Thus the solution (1.6) approaches zero asymptotically as must be expected from the physical meaning of the problem.

When $C(z)$ and $B(z)$ take certain simple forms, the $G_n(z)$ can be expressed in terms of sine, cosine or Bessel functions, but very often the $G_n(z)$ cannot be expressed in terms of well-known functions and a numerical solution is necessary. Rather than solve equation (1.4) directly, it is more convenient to solve the integral equation equivalent to equation (1.4) and its boundary conditions.

2. DETERMINATION OF THERMAL DECAY CONSTANTS AND DECAY MODES

The integral equation equivalent to equation (1.4) and its boundary conditions is

$$G(z) = \lambda \int C(\zeta) \,.\, \phi(z,\zeta)\, G(\zeta) d\zeta \qquad (2.1)$$

where ζ is an auxiliary variable and where $\phi(z,\zeta)$ is the Green's function (or influence function) for the differential expression $d/dz[B(z) \,.\, dG/dz]$ satisfying prescribed conditions at the boundaries, the range of integration being defined by these boundaries. It can be regarded as the temperature distribution arising from a steady unit heat source placed at $z = \zeta$.

Green's function is easily obtained numerically in one-dimensional problems, but in two-dimensional problems it is difficult to calculate except in simple cases where the use of the integral equation method offers no advantage.

The differential expression $d/dz[B(z) \,.\, dG/dz]$ is self-adjoint and the Green's function $\phi(z \,.\, \zeta)$ is therefore symmetric (COURANT and HILBERT, 1953). The kernel $K(z,\zeta) = C(\zeta)\phi(z,\zeta)$ is said to be of polar form.

This type of integral equation and kernel occurs in problems connected with vibration of structures, and eigenfunctions and eigenvalues are often found by iterative procedures, although the problem is generally reduced to finding the latent roots and vectors of a matrix (DUNCAN and COLLAR, 1934) and this procedure is suggested here.

To facilitate numerical analysis, either the thermal capacity distribution may be made discrete instead of continuous (this cannot be done when the method is extended to two or three dimensions since, in these cases, point sources produce infinite temperatures) or a numerical integration formula may be used to replace the R.H.S. of equation (2.1). The integration then changes to a weighted summation of the values of $C(\zeta) \,.\, \phi(z,\zeta)\, G(z)$ for certain values of ζ and is evaluated only for the same values of z.

When this is done, the single integral equation (2.1) which must be satisfied for all z, is replaced by a number of simultaneous linear equations which may be expressed in the following matrix form

$$\tau\{g\} = [A]\{g\}, \qquad (2.2)$$

where $\tau = \dfrac{1}{\lambda}$ and $\{g\}$ is a column vector whose elements are the values of $G(z)$ at the chosen values of z, and the problem reduces to finding the latent roots τ_n and latent vectors $\{g\}_n$ of the $[A]$ matrix. The development of this matrix is treated more thoroughly in Section 5 of this article. The latent roots τ_n have the dimensions of time and are conveniently called the decay time constants.

If τ_n replaces $\dfrac{1}{\lambda_n}$ in equation (1.6) we have

$$T(z,t) = \sum_n A_n \,.\, e^{-(t/\tau_n)} G_n(z). \qquad (2.3)$$

The solutions of the matrix equation (2.2) are not exact solutions of equation (2.1) as only a finite number of eigenvalues are obtained, whereas equation (2.1) has an infinity of eigenvalues. The differences between the approximate and exact solutions for the eigenvalues τ_n and between the corresponding eigenfunctions are small, when n is small relative to the order of the matrix (in the author's experience reasonable accuracy is achieved when the order of the matrix is about three times the value of n). It will be seen later that it is generally necessary only to determine the larger values of τ_n and their associated eigenfunctions, so the error of the matrix equation approximation is not serious.

3. DETERMINATION OF ARBITRARY CONSTANTS A_n

Suppose the perturbed temperature distribution at $t = 0$ is $T_0(z)$. Then from equation (2.3)

$$T_0(z) = \sum_n A_n G_n(z). \tag{3.1}$$

Now because $\phi(z,\zeta)$ is symmetric the $G_n(z)$ have the property of *weighted* orthogonality with respect to the weighting function or thermal capacity function $C(z)$, i.e.

$$\int C(z) \,.\, G_n(z) \,.\, G_m(z) = 0 \text{ where } m \neq n \tag{3.2}$$

where the field of integration covers the whole body. (This can be proved by a simple extension of the proof of orthogonality of eigenfunctions of a real *symmetric* kernel given in MARGENAU and MURPHY (1955).

Multiply equation (3.1) by $C(z)\, G_m(z)$

$$C(z) \,.\, T_0(z) \,.\, G_m(z) = \sum_n A_n C(z) \,.\, G_m(z) \,.\, G_n(z) \tag{3.3}$$

Integrate over the whole body

$$\begin{aligned}\int C(z) \,.\, T_0(z) \,.\, G_m(z)\, dz &= \sum_{n=0}^{m-1} A_n \int C(z) \,.\, G_m(z) \,.\, G_n(z) \,.\, dz \\ &\quad + A_m \int C(z) \,.\, G_m^2(z) \,.\, dz \\ &\quad + \sum_{n=m+1}^{n=\infty} A_n \int C(z) \,.\, G_m(z) \,.\, G_n(z) \,.\, dz \\ &= A_m \int C(z) \,.\, G_m^2(z) \,.\, dz \end{aligned} \tag{3.4}$$

the other terms being zero because of the weighted orthogonality of the eigenfunctions

$$\therefore \qquad A_m = \frac{\int C(z) \,.\, T_0(z) \,.\, G_m(z)\, dz}{\int C(z) \,.\, G_m^2(z)\, dz}. \tag{3.5}$$

4. RESPONSES TO DISTURBANCES IN HEAT PRODUCTION AND EXTRACTION

The equation (2.3) merely describes how perturbations from a steady state decay to zero. The response to general disturbances in heat production and extraction is now required.

As an intermediate stage in determining the response to a general disturbance, it is convenient to first determine the response to a step disturbance. There are two reasons for this. First, the response is easy to obtain since after the step the temperature difference from the *new* steady state simply decays according to equation (2.3). Secondly, the type of response which occurs is easily recognizable as being associated with a particular transfer function and set of ordinary differential equations. Thus the response to a general disturbance can be derived.

Suppose θ represents one of the input variables e.g. in a fuel element θ could be coolant temperature or power density (θ must then represent a power distribution of a prescribed spacewise form). Let $T_s(z)$ be the steady state resulting from a unit change of θ. Then the temperature disturbance following a unit step of θ will be

$$T(z,t) = T_s(z) - \Sigma A_n\, e^{-(t/\tau_n)} G_n(z)$$

where
$$A_n = \frac{\int C(z) \,.\, T_s(z) \,.\, G_n(z) \,.\, dz}{\int C(z) \,.\, G_n^2(z)\, dz} \tag{4.1}$$

which may be rewritten

$$T(z,t) = \sum_n [A_n G_n(z) \,.\, (1 - e^{-(t/\tau_n)})]. \tag{4.2}$$

This response is easily recognizable as a sum of simple time constant responses and, therefore, if θ varies in any prescribed manner with time, the response $T(z,t)$ (of which the response (4.1) is a particular case) will be

$$T(z,t) = \Sigma A_n \,.\, G_n(z) \,.\, F_n(t) \tag{4.3}$$

where the $F_n(t)$ are given by the n ordinary differential equations

$$F_n(t) + \tau_n \frac{dF_n}{dt} = \theta(t). \tag{4.4}$$

The corresponding transfer function is

$$\frac{\bar{T}(z,p)}{\bar{\theta}(p)} = \Sigma \frac{A_n \,.\, G_n(z)}{1 + \tau_n p} \tag{4.5}$$

where p is the Laplace transform variable and $\bar{T}(z,p)$, $\bar{\theta}(p)$ are respectively the Laplace transforms of $T(z,t)$, $\theta(t)$.

A useful approximation to the response can be obtained by omitting the $\tau_n \,.\, \dfrac{dF_n}{dt}$ term in equation (4.4) for small values of τ_n, i.e. by assuming infinitely fast response in the fast modes. The transfer function (4.5) then takes the form

$$\frac{\bar{T}(z,p)}{\bar{\theta}(p)} = \sum_{n=1}^{m} \frac{A_n \,.\, G_n(z)}{1 - \tau_n \,.\, p} + \left\{T_s(z) - \sum_{n=1}^{m} A_n G_n(z)\right\} \tag{4.6}$$

where the τ_n are arranged in descending order of magnitude. In practice a sufficiently good answer may be obtained by using only a few decay modes. In the following example only three are used.

5. EXAMPLE: RESPONSE OF TYPICAL FAST REACTOR FUEL PIN TO CHANGES IN POWER AND COOLANT TEMPERATURE

If lengthwise conduction of heat is neglected, the radial temperature distribution at any lengthwise co-ordinate depends only on the power density and coolant temperature at that point. In the following example the disturbances in temperature due to

(i) a step in local power density,

(ii) a step change in coolant temperature, are found.

Numerical data

Details of fuel pin. Uranium fuel of constant enrichment, zirconium clad by co-extrusion. Fuel radius 0·462 cm, can radius 0·512 cm.

Physical constants:

		Uranium	*Zirconium*
Density (g/cm³)	ρ	18·7	6·55
Specific heat (cal g^{-1} °C^{-1})	c	0·036	0·083
Thermal density (ρc)	σ	0·670	0·550
Thermal conductivity (cal cm^{-1} sec^{-1} °C^{-1})	k_1	0·07	k_2 0·035

Heat transfer coefficient h (can to sodium coolant) = 1·42 cal cm^{-2} sec^{-1} °C^{-1} at 50 cm/sec flow velocity.

Temperature influence function

The temperature influence function $\phi(r,\xi)$, relative to a zero at the temperature of the sodium, is given by

$$\left.\begin{aligned}\phi(r,\xi) &= \frac{1}{2\pi}\left[\frac{1}{hb}+\frac{1}{k_2}\log\frac{b}{a}+\frac{1}{k_1}\log\frac{a}{r}\right] \\ &\qquad \text{for } r>\xi \text{ and } <a \\ \phi(r,\xi) &= \frac{1}{2\pi}\left[\frac{1}{hb}+\frac{1}{k_2}\log\frac{b}{r}\right] \\ &\qquad \text{for } r>\xi \text{ and } >a\end{aligned}\right\} \quad (5.1)$$

where $\phi(r,\xi)$ is the temperature at radius r due to a ring source of unit strength per unit length of pin at radius ξ. a, b are outside radii of fuel and can respectively. For $r<\xi$, ξ is substituted for r in the above formula. This function is drawn in Fig. 1 for the numerical values given above.

Thermal capacity function

The thermal capacity function allowing for the cylindrical geometry is

$$C(r) = 2\pi r\sigma$$

and is drawn in Fig. 2.

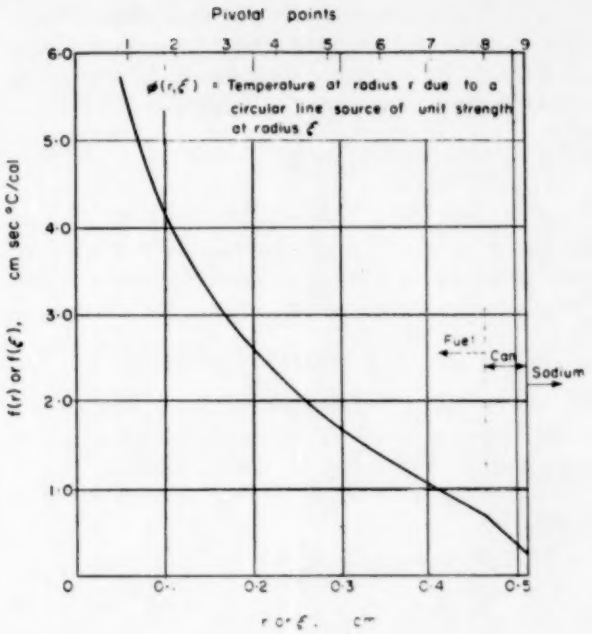

Notes: $\phi(r,\xi) = f(r)$ for $r>\xi$
$\phi(r,\xi) = f(\xi)$ for $\xi>r$

FIG. 1.—Temperature influence function $\phi(r,\xi)$.

Solution of the integral equation

Multiplication of the thermal capacity function $C(\xi)$ and the temperature influence function $\phi(r,\xi)$ gives the kernel function $K(r,\xi)$ (see Fig. 3) of the integral equation

$$\tau G(r) = \int_0^b G(\xi)\,K(r,\xi)\,d\xi \qquad (5.2)$$

the eigenvalues τ_n and the eigenfunctions G_n of which give the thermal decay time constants and thermal decay modes of the system.

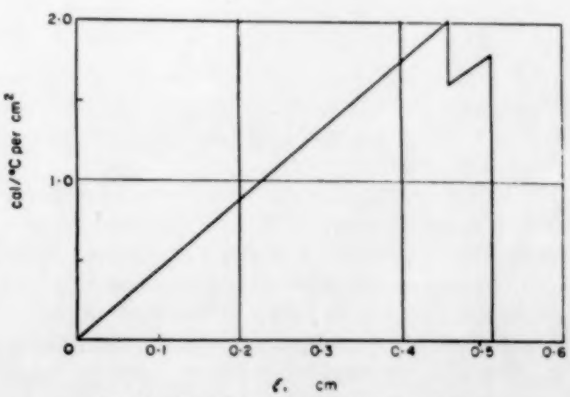

FIG. 2.—Thermal capacity distribution $C(\xi)$.

Using the trapezoidal rule* for numerical integration, the integration of this equation may be replaced by a weighted summation of the values of the integrand at the pivotal points ($\xi = r_1$, $\xi = r_2$ etc.) shown in Fig. 1. g_m, the value of $G(r)$ at $r = r_m$, the mth pivotal point is given by

$$\tau g_m = \sum_{n=1}^{9} a_n \cdot K_{mn} \cdot g_n \qquad (5.3)$$

where $K_{mn} = K(r = r_m, \xi = r_n)$ and the weights a_n are constants. (The value of the kernel at $\xi = 0$ is zero, so there is no g_0 term.)

There are nine equations of this type to be satisfied as opposed to the single equation (5.2) which would have to be satisfied for all r.

These equations may be written in the following matrix form:

$$\tau\{g\} = [K]\,[a]\,\{g\} \qquad (5.4)$$

where $[a]$ is a diagonal matrix, where the nth element of the mth row of K is K_{mn}, and $\{g\}$ is a column vector whose elements are the values of $G(r)$ at the specified r. Since

$$K(r,\xi) = \phi(r,\xi) \times C(\xi)$$

$$[K] = [\phi]\,[C]$$

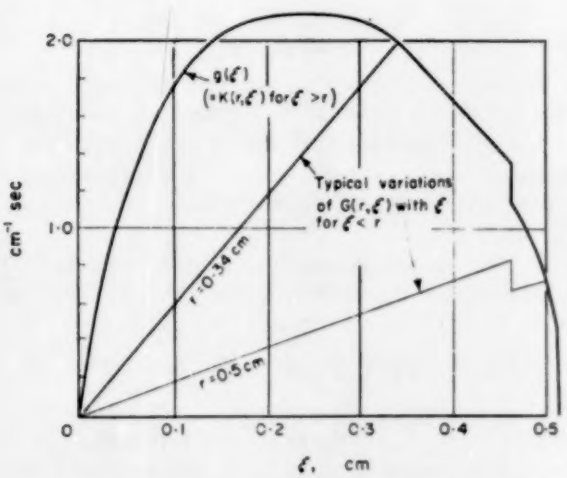

Notes: For $\xi > r$

$K(r,\xi) = g(\xi)$

For $\xi < r$

$K(r,\xi) = g(r) \times \dfrac{C(\xi)}{C(r)}$

FIG. 3.—Kernel function $K(r,\xi)$.

* The use of the trapezoidal rule is convenient because it gives a symmetric × diagonal form of matrix in equation (5.4) and thus ensures the orthogonality of its latent vectors. At the same time, the discontinuities in $\partial K/\partial\xi$ are taken account of. The integration is performed in two parts—fuel region and can region, because of the discontinuity in K at $r = a$.

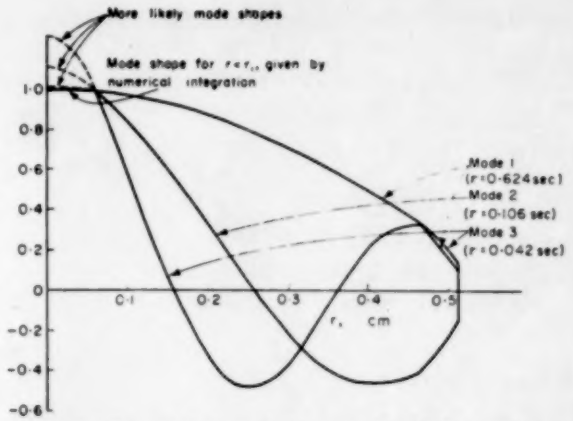

FIG. 4.—Computed thermal decay modes of fast reactor fuel pin.

where $[\phi]$ is a symmetric matrix and $[C]$ is a diagonal matrix with positive elements. Therefore,

$$[K]\,[a] = [\phi]\,[C.a] \qquad (5.5)$$

where $[C.a]$ is a diagonal matrix with $a_n \times C(r_n)$ as the nth element of the diagonal, these elements also being positive.

The latent roots of the product matrix are therefore real, and the latent vectors form an orthogonal set. The roots must also be positive since the temperature always tends to the steady state value in the absence of disturbances, a necessary and sufficient condition for this being that $[\phi]$ is positive definite.

The three largest latent roots and the corresponding vectors (plotted in Fig. 4) were found by the method of DUNCAN and COLLAR (1934) using a desk machine. (Digital computer programmes exist and generally it would be better to buy a small amount of time on a machine.)

When the matrix method is used and the variables for this example are substituted, equation (4.5) for the transfer function becomes

$$\frac{\bar{T}(r,p)}{\bar{\theta}(p)} = \sum_{n=1}^{9} \frac{A_n G_n(r)}{1 + \tau_n p} \qquad (5.6)$$

where

$$A_n = \frac{\sum_{m=1}^{9} C_m a_m T_{s_m} \cdot (g_m)_n}{\sum_{m=1}^{9} C_m a_m \cdot (g_m)_n^2} \qquad (5.7)$$

where $(g_m)_n$ = mth element of nth latent vector,

T_{s_m} = value of T_s at mth pivotal point.

Equation (5.5) has been approximated by

$$\frac{\bar{T}(r,p)}{\bar{\theta}(p)} = \sum_{n=1}^{3} \frac{A_n \cdot G_n(r)}{1 + \tau_n p} + \left\{ T_s(r) - \sum_{n=1}^{3} A_n G_n(r) \right\} \qquad (5.8)$$

since only the first 3 latent roots and vectors were found.

The incremental steady states $T_s(r)$ for unit increases in power and coolant temperature are the 'final steady state' lines of Figs. 5 and 6 respectively and, using the above method, the following approximate transfer functions were calculated.

Response to power disturbances:

$$\frac{\bar{T}(r,p)}{\overline{\Delta P}} = \frac{1{\cdot}272\,G_1(r)}{1+0{\cdot}624p} - \frac{0{\cdot}075\,G_2(r)}{1+0{\cdot}106p} + [T_s(r) - 1{\cdot}272\,G_1(r) + 0{\cdot}075\,G_2(r)] \quad (5.9)$$

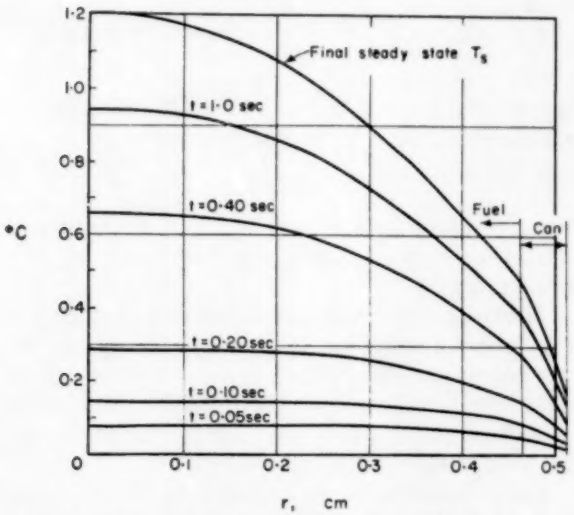

FIG. 5.—Response to step in power of 1 cal/sec per cm³ of fuel.

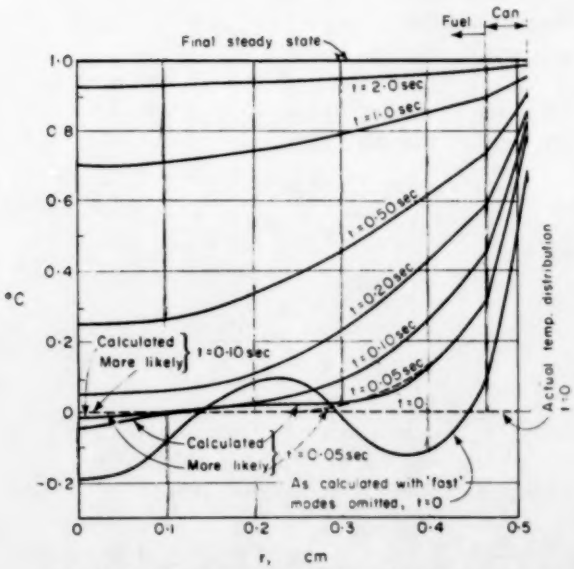
Fuel
Can
Final steady state
t = 2·0 sec
t = 1·0 sec
t = 0·50 sec
t = 0·20 sec
t = 0·10 sec
t = 0·05 sec
t = 0
Calculated More likely t = 0·10 sec
Calculated More likely t = 0·05 sec
As calculated with 'fast' modes omitted, t = 0
Actual temp. distribution t = 0
°C
r, cm

FIG. 6.—Response to step of 1°C in coolant temperature.

(the amount of the third mode in this response being insignificant), where T_s = incremental steady state due to local change of power density of 1 cal/sec per cm³ and $\Delta P(t)$ = local change of power density.

Response to change of coolant temperature:

$$\frac{\bar{T}(r,p)}{\bar{T}_c} = \frac{1{\cdot}450\,G_1(r)}{1+0{\cdot}624p} - \frac{0{\cdot}696\,G_2(r)}{1+0{\cdot}106p} + \frac{0{\cdot}412\,G_3(r)}{1+0{\cdot}042p} + [T_s(r) - 1{\cdot}450\,G_1(r) + 0{\cdot}0696\,G_2(r) - 0{\cdot}412\,G_3(r)] \quad (5.10)$$

The responses of incremental temperature distribution to unit steps of T_c and ΔP have been evaluated and are plotted in Figs. 5 and 6.

The effect of omitting the 'fast' modes is clearly shown in Fig. 6, but it is easy to interpolate between the true $t = 0$ values and the values for $t > 0{\cdot}2$ sec, where the effect of omitting the fast roots will be negligible.

Putting $p = i\omega$ in equations (5.8) and (5.9) gives the frequency responses of temperature to disturbances in T_c and ΔP. These frequency responses will be reasonably accurate in the range 0–3 c/s, but would be in error outside this range, because the assumption of infinitely fast response in the fast modes would no longer be a good approximation.

6. EXTENSION TO TWO-DIMENSIONAL PROBLEMS

So far, the discussion has been restricted to problems where the heat flow can be expressed in terms of a single space variable (i.e. infinite slab geometry and cases of axial or spherical symmetry). It is theoretically possible to extend the method to two or three-dimensional cases.

In the two-dimensional case, it is necessary to determine the eigenvalues λ_n and the eigenfunctions $G_n(x,y)$ of the integral equation:

$$G(x,y) = \lambda \iint C(\xi,\eta)\,.\,\phi(x,y;\ \xi,\eta)\,.\,G(\xi,\eta)\,d\xi,\,d\eta \quad (6.1)$$

where $\phi(x,y;\ \xi,\eta)$ is the temperature at (x,y) due to a unit heat source at point (ξ,η) and satisfying prescribed conditions at the boundary, and $C(x,y)$ is the areal density of thermal capacity.

Two difficulties in the two-dimensional problems are the determination of the 'temperature influence function' $\phi(x,y;\ \xi,\eta)$ and the large number of 'pivotal points' necessary for a sufficiently accurate representation of the problem. $\phi(x,y;\ \xi,\eta)$ can only be obtained theoretically in simple cases and, in some of these cases, the eigenfunctions can be expressed in terms of trigonometric, Bessel or similar functions without recourse to numerical methods.

Determination of $\phi(x,y;\ \xi,\eta)$ is possible with electrolytic tank methods—using varying depth to simulate varying conductivity. In the analogous problem of vibration of structures, two-dimensional influence coefficients of deflection are often obtained either by tests on full-size structures or on models, particularly in aircraft work where tests of this sort are fairly common. The author has not seen any transient heat conduction problems where the effort of an electrolytic tank determination of the Green's function would be justified, but such problems may exist.

Another difficulty arises due to the function $\phi(x,y;\ \xi,\eta)$ being infinite for $x = \xi$, $y = \eta$. This complicates the reduction of equation (6.1) to a matrix problem, but this reduction is possible if suitable assumptions for the variation of temperature between pivotal points are made.

Acknowledgment—The dimensions of the fuel pin in the example are in fact those of the fuel pin in the American EBRI Mk. III reactor, although the American reactor uses NaK coolant, whereas sodium coolant has been assumed in the example. The author is indebted to the U.S.A.E.C. for their permission to publish details of the pin.

REFERENCES

COURANT R. and HILBERT D. (1953) *Methods of Mathematical Physics*. Vol. 1, pp. 291–294, 354, Interscience, N.Y.

DUNCAN W. J. and COLLAR A. R. (1934) *Phil. Mag*. Ser. 7, **17**, 865.

MARGENAU H. and MURPHY G. M. (1955) *The Mathematics of Physics and Chemistry*, p. 528, Van Nostrand.

VOL.
15
1961

Reactor Science and Technology (Journal of Nuclear Energy, Parts A/B) 1961, Vol. 15. pp. 98 to 101. Pergamon Press Ltd. Printed in Northern Ireland

THE EXPERIMENTAL DETERMINATION OF FAST FISSION FACTORS IN LIGHT WATER-MODERATED, SLIGHTLY ENRICHED URANIUM ROD LATTICES*

E. ERDIK†
Brookhaven National Laboratory, Upton L.I., New York, U.S.A.

(*First received* 21 *April* 1960 *and in final form* 29 *December* 1960)

Abstract—The ratio, δ_{28}, of the fission rate in ^{238}U to that in ^{235}U was determined for various slightly enriched hexagonal miniature uranium rod lattices in light water. The experimental values of δ_{28} and ε are given for 1·0 per cent, 1·15 per cent and 1·3 per cent fuel enrichments, 1, 1·5, 2, 3 and 4 water-to-uranium volume ratios and 0·250 in., 0·387 in. and 0·600 in. rod diameters. The data presented are in some instances new; the remainder represent appreciable improvement over older values in that certain systematic and random errors have now been reduced.

INTRODUCTION

THE effect of direct fission of ^{238}U in a nuclear reactor is usually taken into account through use of the fast fission factor ε. This quantity is defined to be the number of neutrons slowing down past the ^{238}U fission threshold, per neutron from thermal fission.

In recent years a large amount of work has been done to provide information on the size of the fast fission factor in different circumstances (KOUTS and PRICE, 1953; KOUTS *et al.*, 1955, 1958; KOUTS and SHER, 1957; KLEIN *et al.*, 1958; FUTCH, 1959; PRICE, 1956; HILL, 1944). The importance of this parameter in helping to extend reactor core life has prompted this study, which is aimed simultaneously at enlarging the body of data available and improving the accuracy of some which has previously been reported. The improvements are partly made through a reduction of statistical error. In addition, certain systematic errors which have been present in the past have been reduced.

The fast fission factor is given in terms of measured quantities by the approximate formula (KOUTS and PRICE, 1953; KOUTS *et al.*, 1955, 1958; KOUTS and SHER, 1957):

$$\varepsilon - 1 = \left(\frac{\nu_{28}}{\nu_{25}} - \frac{1 + \alpha_{28}}{\nu_{25}}\right)\delta_{28} \qquad (1)$$

where the subscripts and most symbols have their usual meaning, and δ_{28} is the ratio of the fission rate in ^{238}U to that in ^{235}U. The experiments performed lead to values of δ_{28}.

MEASUREMENT OF FISSION PRODUCT ACTIVITIES

The method used is basically that first used by HILL (1944) as refined later (KOUTS and PRICE, 1953; KOUTS *et al.*, 1955, 1958; KOUTS and SHER, 1957; KLEIN *et al.*, 1958; FUTCH, 1959; PRICE, 1956). It makes use of the catcher technique to determine the relative fission product activities from ^{238}U and ^{235}U fissions, and employs a calibration measurement to relate this ratio to that of fission rates. The techniques and analysis have been fully described elsewhere (KOUTS and PRICE, 1953; PRICE, 1956), and we extract here only that portion which is needed to clarify aspects of the present work.

In the measurement of δ_{28}, two sets of catcher foils receive fission products respectively from a fuel rod and from a foil of depleted ^{238}U sandwiched between two sections of a fuel rod. The observed count rates of the catcher foils are called R_1 and R_2 respectively; each is a function of both the exposure time T and the interval t between the end of exposure and the time of counting. The observed experimental parameter is

$$B(t,T) = \frac{R_2(t,T)}{R_1(t,T)}. \qquad (2)$$

Briefly, $B(t,T)$ is the activity of the catcher foil near depleted uranium to the activity of the foil near the fuel rod. From this it follows that

$$\delta_{28} = K(t,T)\frac{B(t,T) - n_{25}/N_{25}}{n_{28}/N_{28} - B(t,T)} \qquad (3a)$$

where the symbols n and N are atom densities in the depleted foil and in the uranium rod, respectively (PRICE, 1956). The difference in fission products from

* Research performed under the auspices of the U.S. Atomic Energy Commission.

† Visiting scientist under auspices of the International Co-operation Administration. Permanent address: Faculty of Science, Ankara, Turkey.

the two isotopes of uranium causes $B(t,T)$ to differ from a constant value, and the factor $K(t,T)$ must be used to correct for the variation. A calibration experiment which evaluates the dependence of K on its parameters is essential.

CALIBRATION EXPERIMENT

The technique used to find $K(t,T)$ has also been fully reported elsewhere (KOUTS *et al.*, 1955 and 1958; PRICE, 1956). It makes use of a double fission chamber to measure the relative fission rates in ^{238}U and ^{235}U in a spectrally adjusted neutron flux; simultaneously in the same flux catcher foils are activated by depleted uranium and by uranium at natural or near natural isotopic content. The exposure time for the calibration experiment is chosen to be the same as the exposure time T used in fast fission factor measurements. Since we kept T constant at about ten minutes in the experiments and the calibration, only the variation of K with t was of importance. Three separate calibrations were done, with the results shown in Fig. 1. The error indications are the standard deviations of the three measurements.

The principle change introduced here is one of magnitude of K. Older measurements (KOUTS and PRICE, 1953; PRICE, 1956) of this function under the circumstances used in these measurements would lead to values about 7 per cent higher over the time interval of interest. The effect is that now δ_{28} must be reduced by essentially the ratio of the new to the old average values.

ANALYSIS

It was decided that the measurement was most simply done by choosing a range of values of t which leads to $K(t)$ having an average value of unity. This was easily arranged; in the interval 60 minutes $< t <$ 196 minutes $K(t)$ has a mean value of $1{\cdot}00 \pm 0{\cdot}03$. This time interval was chosen as well-suited to the foil counting arrangement. With this choice made, the analysis could be carried out with a simplified version of equation (3a):

$$\delta_{28} = \frac{\bar{B} - n_{25}/N_{25}}{n_{28}/N_{28} - \bar{B}} \tag{3b}$$

where $\bar{B}$ is the average value of B over the time interval. The error introduced is negligible, because by equation (3a) the time dependence of K and B nearly cancel. A number of tests on the data from individual measurements showed no significant difference between results found using both the exact expression (3a) and its approximate form (3b).

The conversion from δ_{28} to ε made use of recent values of the parameters (SHER and LEROY, 1960):

$$\nu_{28}/\nu_{25} = 1{\cdot}160$$
$$\nu_{25} = 2{\cdot}45$$
$$\nu_{28} = 2{\cdot}84.$$

Integration of recent cross-section results leads to $\alpha_{28} = 0{\cdot}107$. Use of these quantities in equation (1) leads to the result

$$\varepsilon - 1 = 0{\cdot}708\ \delta_{28}. \tag{4}$$

The coefficient is appreciably greater than the older value 0·557 (KOUTS and PRICE, 1953). The values reported here are therefore larger than previous ones, a trend partly compensated by the improvement in the calibration experiment.

RESULTS

Measurements of B were made in 26 lattices of slightly enriched uranium rods in ordinary water. The lattices differed in rod diameter, enrichment, and in water-to-fuel-volume ratio. All rods were contained in 0·028 inch thick aluminium tubes, with a radial air gap of 0·005 inches. The results, converted to δ_{28} and

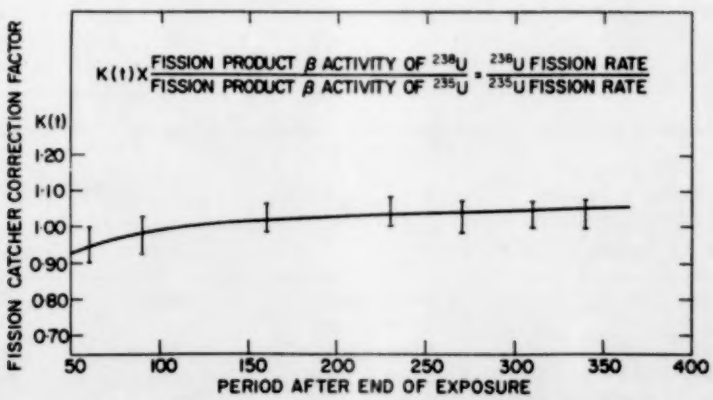

FIG. 1.—Correction factor $K(t)$ for fast fission factor measurement.

to ε, are listed in the Tables. δ_{28} is plotted in Fig. 2. Each point is the result of several measurements, the standard statistical error in $\bar{B}$ being between 0·0046 and 0·0063.

In all instances the fuel enrichment is nominal, the precise values being 1·299 per cent, 1·143 per cent and 1·027 per cent weight percent of ^{235}U. The water-to-fuel ratios are the actual ones, the aluminium and air being neglected. The transition from larger to small rods introduces progressively greater volume fractions of aluminium and air into the lattices, and this point certainly accounts for most of the observed reduction of δ_{28} as the rod size is diminished.

The fuel enrichment is seen to have little or no influence on the observed value of δ_{28}. This point is of importance in assessing the effect of fast neutron leakage on the results. The conclusion here is that the accuracy of the measurement does not lead to a clear evaluation of this small effect.

For convenience, the Tables list values of ε calculated with the old and the new versions of equation (4).

The effect of using the most recent nuclear parameters is seen to be very large.

Acknowledgments—I am particularly indebted to MR. H. WINDSOR for his many days of aid with the fission counting and many enlightening and helpful discussions.

I wish to express my appreciation to MR. A. TIERNEY for his

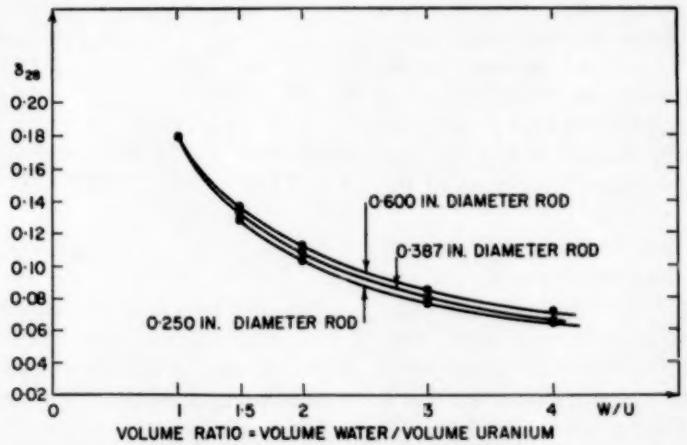

FIG. 2.—δ_{28}, as a function of W/U volume ratio.

TABLE 1.—EXPERIMENTAL VALUES OF THE FAST EFFECT AND FAST FISSION FACTOR FOR 0·250 IN. DIAMETER RODS

Volume ratio:	Enrichment (% ^{235}U by weight)			Average (δ_{28})	Fast fission factor	
W/U	1·0	1·15	1·3		$\varepsilon = 1 + 0{\cdot}557\,\delta_{28}$	$\varepsilon = 1 + 0{\cdot}708\,\delta_{28}$
1	—	—	—	—	—	—
1·5	0·129	0·126	—	0·128 ± 0·003	1·071	1·091
2	0·102	0·103	—	0·103 ± 0·003	1·057	1·073
3	0·077	0·077	—	0·077 ± 0·002	1·043	1·055
4	0·066	0·061	—	0·064 ± 0·002	1·036	1·045

TABLE 2.—EXPERIMENTAL VALUES OF THE FAST EFFECT AND FAST FISSION FACTOR FOR 0·387 IN. DIAMETER RODS

Volume ratio:	Enrichment (% ^{235}U by weight)			Average (δ_{28})	Fast fission factor	
W/U	1·0	1·15	1·3		$\varepsilon = 1 + 0{\cdot}557\,\delta_{28}$	$\varepsilon = 1 + 0{\cdot}708\,\delta_{28}$
1	0·187	0·177	0·176	0·180 ± 0·003	1·100	1·127
1·5	0·136	0·138	0·127	0·134 ± 0·002	1·075	1·095
2	0·109	0·106	0·108	0·108 ± 0·004	1·060	1·076
3	0·081	0·081	0·077	0·080 ± 0·003	1·045	1·057
4	0·068	0·064	0·066	0·066 ± 0·002	1·037	1·047

TABLE 3.—EXPERIMENTAL VALUES OF THE FAST EFFECT AND FAST FISSION FACTOR FOR 0·600 IN. DIAMETER RODS

Volume ratio:	Enrichment (% ^{235}U by weight)			Average (δ_{28})	Fast fission factor	
W/U	1·0	1·15	1·3		$\varepsilon = 1 + 0{\cdot}557\,\delta_{28}$	$\varepsilon = 1 + 0{\cdot}708\,\delta_{28}$
1	0·180	0·179	0·177	0·179 ± 0·002	1·100	1·127
1·5	0·144	0·142	0·126	0·137 ± 0·003	1·076	1·097
2	0·116	0·113	0·106	0·112 ± 0·004	1·062	1·079
3	0·081	0·086	0·084	0·084 ± 0·002	1·047	1·059
4	0·072	0·070	0·071	0·071 ± 0·002	1·040	1·050

very considerable assistance in the preparation of the experiments.

In particular, I would like to thank DR. H. KOUTS for his kind hospitality during my stay at Brookhaven National Laboratory.

REFERENCES

FUTCH A. H. (1959) *Nucl. Sci. Engng.* **5**, 61.

HILL D. L. (1944) *Fast Effect in Three Lattices.* Chicago Metallurgical Laboratory Report CF-1548.

KLEIN D., KRANZ A. Z., SMITH G. C., BEER S. and DE JUREN J. (1958) *Nucl. Sci. Engng.* **3**, 403.

KOUTS H. and PRICE G. (1953) *ε-Measurements.* BNL-1575.

KOUTS H., PRICE G., DOWNES K., SHER R. and WALSH V. (1955) *Proceedings of the First International Conference on the Peaceful Uses of Atomic Energy, Geneva,* P/600, Vol. 5, p. 183. United Nations, New York; (1958) *Proceedings of the Second International Conference on the Peaceful Uses of Atomic Energy, Geneva,* P/596, Vol. 12, p. 466. United Nations, New York.

KOUTS H. and SHER R. (1957) *Experimental Studies of Slightly-Enriched Uranium, Water-Moderated Lattices—I. 0·600 in. Diameter Rods.* Report BNL-486.

PRICE G. (1956) *Fast Effect Measurements.* BNL-1690.

SHER R. and LEROY J. (1960) *Reactor Sci.* (*J. Nucl. Energy* Part A) **12**, 101.

VOL.
15
1961

Reactor Science and Technology (Journal of Nuclear Energy Parts A/B) 1961, Vol. 15. pp. 102 to 112. Pergamon Press Ltd. Printed in Northern Ireland

SOME EXPERIMENTAL DETERMINATIONS OF THE NUMBER OF PROMPT NEUTRONS FROM FISSION

A. MOAT, D. S. MATHER and M. H. MCTAGGART
Atomic Weapons Research Establishment, Aldermaston, Berks.

(*Received* 19 *September* 1960)

Abstract—The average number of neutrons per fission, $\bar{\nu}$, has been measured for the spontaneous fission of ^{252}Cf. A large liquid scintillation counter was then used to compare some other $\bar{\nu}$ values with that of ^{252}Cf. The following results were obtained for prompt $\bar{\nu}$ values.

$\bar{\nu}$ ^{235}U 75 keV neutron induced fission	2·39 ± 0·05
$\bar{\nu}$ ^{235}U 2·5 MeV neutron induced fission	2·60 ± 0·08
$\bar{\nu}$ ^{235}U 14·2 MeV neutron induced fission	4·28 ± 0·08
$\bar{\nu}$ ^{238}U 14·2 MeV neutron induced fission	4·44 ± 0·12
$\bar{\nu}$ ^{240}Pu spontaneous fission	2·13 ± 0·05
$\bar{\nu}$ ^{252}Cf spontaneous fission	3·69 ± 0·07

These results are based on the assumption that ^{240}Pu and ^{252}Cf fission neutron spectra are identical; their dependence on these spectra is discussed.

1. INTRODUCTION

MEASUREMENTS of $\bar{\nu}$, the average number of neutrons emitted per fission, have been reported from several laboratories. Relatively few of these measurements are absolute (KALASHNIKOVA *et al.*, 1955; SANDERS, 1956; KENWARD *et al.*, 1959) the remainder generally being referred to $\bar{\nu}$ for thermal fission of ^{235}U. A summary table is given in a paper by LEACHMAN (1958), and it is noticeable that the accuracy of the $\bar{\nu}$ values is rather poor except for thermal and spontaneous fission.

The growing importance of fast reactors has emphasized the need to know accurately how the parameter $\bar{\nu}$ varies over a wide range of incident neutron energies. This paper reports some measurements for neutron energies of 75 keV, 2·5 MeV and 14·2 MeV, and also for spontaneous fission. Further work has been planned to determine the detailed variation of $\bar{\nu}$ with energy from thermal to about 20 MeV.

A loaded liquid scintillation counter (REINES *et al.*, 1954) was used as the neutron detector. This type of detector, with a fission chamber at its centre, gives one pulse coincident with a fission chamber pulse, followed by one delayed pulse for each fission neutron captured within the scintillator after being slowed down by the moderating material present. Efficiencies of about 80 per cent for detection of these capture pulses from fission neutrons are obtainable with large counters. The efficiency of the present counter was calibrated by reference to the Harwell ^{240}Pu standard neutron source (RICHMOND and GARDNER, 1957; RICHMOND, 1958). However, this source is not suitable for direct calibration of the scintillation counter since no fiducial pulse (as from a fission chamber, for example) is provided by the source, and also because the gamma-ray emission from the source would produce an intolerably large background rate. An indirect calibration was therefore necessary, and was performed in the following way. A determination of $\bar{\nu}$ for spontaneous fission of ^{252}Cf was carried out by measuring the fission rate of a ^{252}Cf sample and comparing its neutron output with that from the Harwell ^{240}Pu source. This comparison was made using detectors consisting of several BF_3 counters embedded in paraffin wax (such detectors commonly have efficiencies of about 1 per cent). A smaller sample of ^{252}Cf in a fission chamber was then placed at the centre of the scintillation counter, and the mean number of neutron capture pulses per fission was measured. The ratio of this number to $\bar{\nu}$ for ^{252}Cf gave the efficiency of the counter.

Loaded liquid scintillation counters have been used previously for comparison of $\bar{\nu}$ values for fission induced by low-energy neutrons and for spontaneous fission (DIVEN *et al.*, 1956; HICKS *et al.*, 1956). The extension of the method to higher energies necessitated the development of an efficient neutron shielding and collimating system. Neutrons were obtained from nuclear reactions induced by particle beams from a 3 MV Van de Graaff.

This paper supersedes a preliminary note (MOAT *et al.*, 1959) the final values given here being slightly higher than those previously quoted.

2. MEASUREMENT OF ^{252}Cf $\bar{\nu}$ FOR SPONTANEOUS FISSION

2.1 ^{252}Cf *neutron output determination*

A sample of ^{252}Cf deposited over a 3 cm diameter region on a thin (0·002 in.) Pt disk was supplied by Dr. J. Milsted of A.E.R.E. Harwell. The fission rate was approximately 650 fissions per second. The Harwell spontaneous fission source (RICHMOND and GARDNER, 1957) consists of 91·5 per cent ^{239}Pu and 8·5 per cent ^{240}Pu, and is contained in a 1 in. diameter spherical capsule. The neutron output of this source was taken as $(2{\cdot}036 \pm 0{\cdot}030) \times 10^4$ n/sec which is the value finally recommended by RICHMOND (1958), after calibration against source standards from a number of laboratories. The excellent agreement obtained by RICHMOND in these comparisons is taken as evidence for the reliability of the Harwell standard.

Two 'castle' detectors were used, each consisting of a cylinder of paraffin wax through which runs an axial hole. Several BF_3 counters were embedded in the wax with their axes parallel to that of the cylinder. The dimensions and other physical data are compared in Table 1, and the energy response curves of the two castles are shown in Fig. 1.

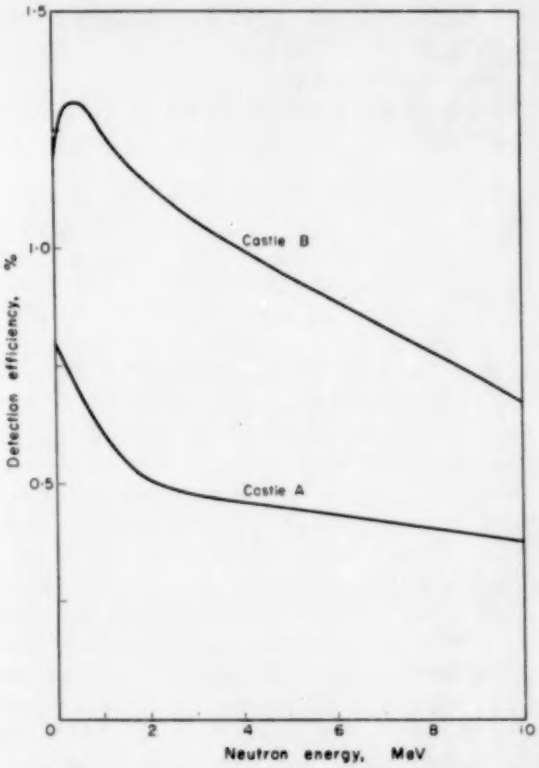

FIG. 1.—Assumed response curves of the 'wax castle' counters.

TABLE 1.—PHYSICAL DETAILS OF THE NEUTRON COUNTERS

Castle	External diameter (in.)	Internal diameter (in.)	Height (in.)	No. of BF_3 counters	Position of cadmium
A	42	18	19	3	No cadmium
B	16	5	19	6	Axial hole lined with Cd 0·010″ thick

A comparison between the Harwell spontaneous fission source and the ^{252}Cf sample was made by counting each source placed in turn at the centre of the castle. The sources were arranged so that their centres occupied the same position in the castle. Corrections were applied for scaler dead-time, for a small increase in the output of the Harwell source when inserted into the castle (Section 2.2(c)), and for 'softening' of the ^{240}Pu neutron spectrum (Section 2.2(b)). Table 2 shows the observed counting rates,

TABLE 2.—MEASUREMENTS MADE IN NEUTRON CASTLES

Date	Source	Castle	Count	Time (sec)	Rate counts/sec	Corrected for dead-time	Correction for reflected neutron multiplication (see Section 2.2(c))	Correction for softening of Pu spectrum (see Section 2.2(b))	Ratio $\frac{^{252}Cf}{^{240}Pu}$	Output of ^{252}Cf sample	^{252}Cf output corrected to 6.12.58*
3.12.58	^{252}Cf ^{240}Pu	*A*	34,153 111,341	2600 1000	13·136 111·34	13·178 111·72	−0·1%	−1·4%	0·1198	$2{\cdot}439 \times 10^3$	$(2{\cdot}431 \pm 0{\cdot}017) \times 10^3$
4.12.58	^{252}Cf ^{240}Pu	*A*	39,569 200,645	3000 1800	13·190 111·47	13·232 111·85	−0·1%	−1·4%	0·1201	$2{\cdot}445 \times 10^3$	$(2{\cdot}440 \pm 0{\cdot}017) \times 10^3$
5.12.58	^{252}Cf ^{240}Pu	*B*	39,767 275,642	1440 1200	27·616 229·70	27·795 233·64	−0·15%	−0·6%	0·1199	$2{\cdot}441 \times 10^3$	$(2{\cdot}438 \pm 0{\cdot}016) \times 10^3$

* This correction is for decay of the Cf sample. The error term does not include the error quoted for the Harwell source.

the corrected rates, and the ratios obtained with the two castles. The last column shows the data corrected for α-decay of the Cf sample.

The value finally taken for the output of the ^{252}Cf sample was $(2{\cdot}437 \pm 0{\cdot}040) \times 10^3$ n/sec.

2.2 *Possible sources of error in the neutron output measurement*

Three possible sources of error in the measurement described in Section 2.1 were considered. They were:

(a) The geometry of the standard source was different from that of the Cf sample and an error in the ratio of source strengths would occur if the efficiency of a castle was critically dependent on the position of the source of neutrons. Measurements made with a small test source showed that the maximum decrease in efficiency for a 1 in. displacement from the centre was 0·2 per cent for castle *A* and 0·5 per cent for *B*.

(b) KENWARD *et al.* (1959), have pointed out that the neutron energy spectrum from the ^{240}Pu source will be slightly different from the ^{240}Pu fission spectrum because some 6 per cent of emerging neutrons have been 'softened' by inelastic collisions through the plutonium metal. Furthermore, the neutron energy spectra from ^{240}Pu and ^{252}Cf fission may not be the same. Consequently source strength comparisons should ideally be made with a detector of flat response. The efficiencies of the two castles were measured at 24 keV, 197 keV and 827 keV using Sb–Be, Rd Th–D_2O and Rd Th–Be neutron sources. At higher energies only sources which emit a wide range of neutron energies were conveniently available, and the castle efficiencies were measured with 'mock-fission' and Ra–Be sources, with mean energies of 2·2 and 5·0 MeV respectively. The energy response curves (Fig. 1) were so drawn as to pass through the mono-energetic points, and to yield the measured efficiencies for mock-fission and Ra–Be when combined with the known spectra of these sources. The softened neutron spectrum emerging from a 1 in. diameter Pu sphere was computed on the AWRE IBM 709 by the Carlson method and taking for the input fission spectrum that measured by CRANBERG *et al.* (1956) for thermal fission of ^{235}U. The corrections for the softening effect are shown in column 9 of Table 2. In calculating the standard errors of the results given in column 12 it is assumed that these corrections are known to ± 25 per cent. TERRELL (1959), has reviewed experimental measurements of fission neutron spectra. For a particular fissioning nuclide he predicts an increase in fission spectrum mean energy, $\bar{E}$, with excitation of that nuclide and consequently with $\bar{\nu}$. He shows that the measured $\bar{E}$ values for *any* nuclide fall close to the predicted $\bar{E}$ versus $\bar{\nu}$ curve for ^{235}U. Using this evidence one might expect $\bar{E}$ for ^{252}Cf to be 2·12 MeV and that for ^{240}Pu to be 1·88 MeV. However, no measurement of the ^{240}Pu fission spectrum has been reported, and a preliminary measurement made here by T. S. Green indicates that the ^{252}Cf spectrum is perhaps softer than that reported by SMITH *et al.* (1957). A correction due to 250 keV difference in $\bar{E}$, assuming Maxwellian distributions, would increase the ^{252}Cf output as measured in castle *A* by 2·3 per cent and as measured in castle *B*, by 1·6 per cent. Such a correction is not made here since insufficient data are available on the fission spectra concerned.*

(c) The standard source consists of over 90 per cent ^{239}Pu which is thermally fissile, so that when the source is inside a wax castle multiplication of reflected neutrons must be considered. There are several pieces of evidence which indicate that this effect is small.

(i) There was no observable difference in the counting rates of castle *A* with and without a 0·015 in. thick cadmium box surrounding the ^{240}Pu source.

(ii) The emission of a 6 kg sphere of ^{239}Pu was found to increase by 3·5 per cent when inserted into castle *A*. The diameter of this sphere was 4 in., while that of the standard source is 1 in: the surface areas are therefore in the ratio 16 : 1. The surface multiplication† of the small source is calculated to be about 1·2 whereas that of the 6 kg sphere is greater than twice this value. The increase in emission for the source must therefore be less than 0·11 per cent.

(iii) RICHMOND and GARDNER (1957) showed during their work on source comparisons that the additional multiplication of this same source was $(-0{\cdot}1 \pm 0{\cdot}4)$ per cent in a 4 in. diameter cylindrical cavity in a wax castle.

(iv) The effect of multiplication, in castle *B*, of a 1 in. diameter sphere of ^{239}Pu has been studied by the Carlson method using 8 energy groups. For the purpose of this calculation the source was imagined

* The sensitivities of practical neutron detectors vary with neutron energy. Consequently there is a need for more accurate and extensive data on spontaneous and induced fission neutron spectra, which are required in the evaluation of correction factors. The need for these data will be more acutely felt as the accuracy of neutron experiments improves.

Note added in proof: A recent paper by BONNER (*Nucl. Phys.* (1961) **23**, 116) gives experimental results for several fission neutron spectra including ^{240}Pu and ^{252}Cf (mean energies 1·78 MeV and 2·05 MeV respectively). Using these spectra we find that the ^{252}Cf output as measured in castle *A* should be increased by 2·5 per cent, and as measured in castle *B*, by 1·7 per cent. Such a correction would increase all our $\bar{\nu}$ values by $(2{\cdot}1 \pm 0{\cdot}7)$ per cent.

† The surface multiplication of a mass of fissile material may be defined as the mean number of neutrons emitted due to one neutron entering the mass across its surface.

to be at the centre of a 5 in. diameter spherical cavity in a wax sphere of outer diameter 18 in; the result, 0·2 per cent increase in emission, is therefore an upper limit to the effect, the magnitude of which for cylindrical geometry, was estimated to be 0·15 per cent.

2.3 *The* ^{252}Cf *fission-rate determination*

For this measurement the ^{252}Cf sample was mounted on one plate of a parallel plate fission chamber. This chamber had a plate separation of 1 cm and was used with a continuous flow of 90 per cent argon, 10 per cent methane, at atmospheric pressure. The bias curve obtained, (Fig. 2), had a slope of 0·18 per cent per volt. The fission rate, 657 fissions/sec, was determined by extrapolation to zero bias. A correction of 2 counts/sec due to scaler dead-time was applied, and an error of ± 2 counts/sec assigned, giving 659 ± 2 fissions/sec.

The sample was inverted and a count made of pulses from the reverse side of the foil, to confirm that no fissile material had been deposited on that side of the platinum. No pulses were observed above the minimum discriminator bias of 5V.

2.4 *Result for* ^{252}Cf $\bar{\nu}$

Combining the figures obtained in Sections 2.1 and 2.3 above we find $\bar{\nu}$ ^{252}Cf $= 3{\cdot}70 \pm 0{\cdot}07$. Correction for the delayed neutron contribution (Cox *et al.*, 1958), gives a prompt $\bar{\nu}$ for ^{252}Cf spontaneous fission of $3{\cdot}69 \pm 0{\cdot}07$.

3. COMPARATIVE $\bar{\nu}$ MEASUREMENTS

3.1 *Method*

The comparative measurements were made using a 100 litre cadmium-loaded liquid scintillation counter. The principle of this type of detector is that the large volume of hydrogenous liquid slows down the neutrons; recoiling protons provide a prompt pulse coincident with the injection of a neutron. A loading element, usually cadmium, captures neutrons very efficiently as they approach thermal energy. Gamma-rays from these (n,γ) processes produce scintillations in the liquid mainly by the Compton effect. A single neutron would thus produce a pair of pulses, the mean delay of the capture pulse commonly being about 6 μsec. For the present type of experiment a fission chamber is contained within the scintillation counter. Capture pulses are then counted for a fixed time following each fission pulse from the fission chamber. The mean number of capture pulses per fission, together with the scintillation counter efficiency, yields a measure of $\bar{\nu}$ for the fissioning nuclide. The present scintillation counter was a pilot model having an efficiency of about 65 per cent. It was cylindrical, 27 in. long $\times$ 18 in. diameter, with a 2·5 in. diameter axial tube in the centre of which could be placed a small continuous-flow fission chamber. The liquid (Nuclear Enterprises NE312, 6 per cent Cd loaded) was viewed by eight 5 in. E.M.I. photo-multiplier tubes, type 6099, which were connected in two banks so that noise pulses could be rejected by a coincidence circuit. Figure 3 shows this counter positioned in its shielding system which was situated 25 feet from the analysing magnet of a 3 MV Van de Graaff accelerator.

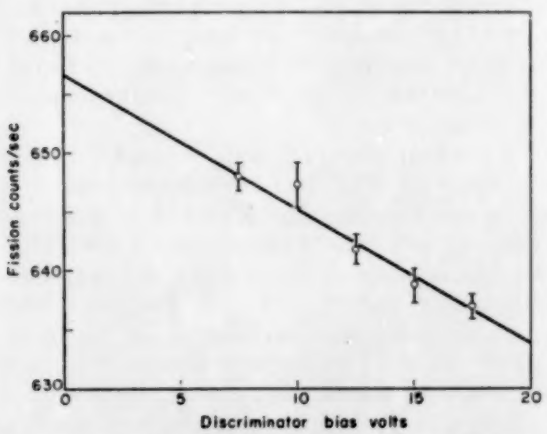

FIG. 2.—Bias curve for ^{252}Cf fission rate determination.

A block diagram of the electronic system is shown in Fig. 4. A fission chamber pulse arriving in coincidence with the prompt pulse from the scintillator liquid (due to fission gamma rays and knocked-on protons) was made to open a 'gate' for a fixed interval of 23 μsec. For the duration of this gate, scintillator pulses were passed to a multiple event analyser (GORE, 1960) of dead-time 0·22 μsec, which was arranged to give an output pulse with amplitude proportional to the number of input pulses. This output pulse was fed to a 100 channel pulse-height analyser.

A 'double-fission' circuit was provided so that a second fission pulse occurring during the gate vetoed the output. This ensured that neutron pulses from two fissions could not be added together, and would also be good protection against interference pulses, since these are usually of an oscillatory nature.

The efficiency of the scintillation counter was calibrated by placing a ^{252}Cf continuous flow fission chamber (about 30 fissions per second) in the centre of the axial tube through the scintillation counter, and measuring the number of neutron capture pulses per fission. The $\bar{\nu}$ measurements were carried out with a similar chamber containing 5 mg ^{240}Pu, and multi-plate chambers containing 130 mg natural uranium,

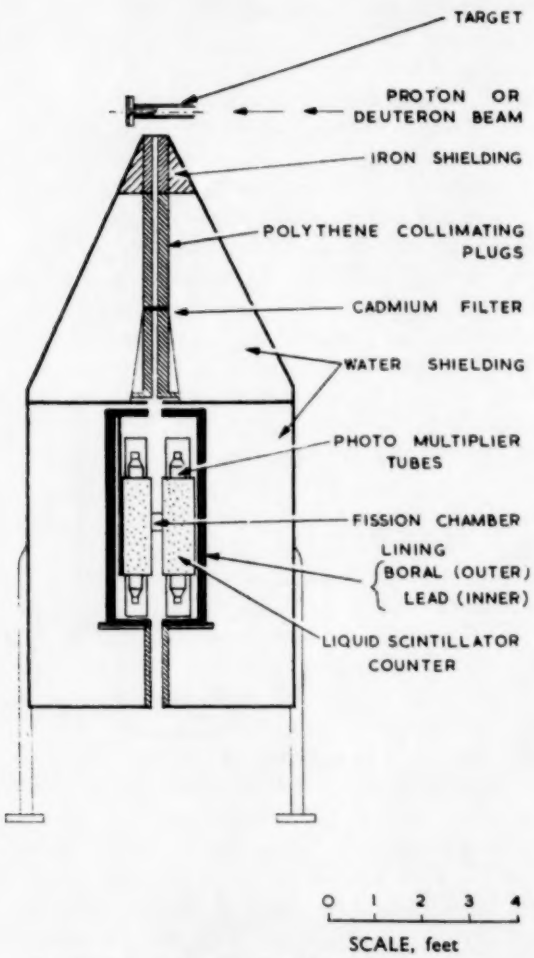

FIG. 3.—Schematic arrangement of scintillation counter, shielding system and collimator.

and 170 mg ^{235}U (nominal masses). For neutron-induced fission the neutrons were produced by the following reactions, the neutron laboratory angle being 90°.

75 keV neutrons: 1·30 MeV protons on tritium-zirconium target,
2·5 MeV neutrons: 1·0 MeV deuterons on deuterium-zirconium target,
14·2 MeV neutrons: 1·0 MeV deuterons on tritium-zirconium target.

3.2 *Neutron shielding system*

The neutron shield shown in Fig. 3 was designed to be effective up to 14 MeV neutron energy. The system was built on the 'shadow cone' principle, the angle of the cone being reduced as far as possible so that the minimum number of 14 MeV neutrons would be intercepted by it. The top 20 in. of the cone was made of iron so that the neutrons lose energy primarily by inelastic collisions; during this process many neutrons will also be scattered out of the sides of the iron cone. A 4 ft depth of water beyond the iron thermalizes the neutrons emerging towards the scintillation counter. Neutrons approaching the side walls of the shield are room-scattered neutrons and only a very small proportion are expected to have energies near to the primary neutron energy, so that 2 ft of water shielding was considered adequate.

Thermal neutrons passing out of the water towards the scintillation counter were stopped by a lining of boron carbide clad in aluminium ('Boral'). A sheet of $\frac{3}{8}$ in. lead inside this provided some absorption of the soft gamma rays from neutron capture in the boron. No special provision was made to remove the 2·2 MeV gamma rays from neutron captures in the hydrogen of the water, since the shielding system was already adequate. This contribution to the background could probably have been reduced significantly by loading the water with boric acid.

The neutron collimator was formed of cylindrical blocks 4 in. long, the five blocks nearest the target were made of iron and the rest were of Polythene. The first, third, fifth, etc. plugs counting from the target end of the collimator, were bored out with holes of progressively increased diameter, and were designed to produce a neutron beam 3 cm in diameter at the centre of the scintillation counter. The alternate blocks, i.e. second, fourth, etc. were provided with holes of 4 cm diameter as it was thought that some reduction of streaming of scattered neutrons into the beam would result from this construction. Cadmium filters were placed in the collimator to remove thermal neutrons from the beam.

Some rough tests of the efficiency of the water shielding were made by draining water from the tanks whilst 14 MeV neutrons were being produced at the target. An increase in background rate by approximately a factor of 3 was observed when the cone was emptied, and it was noticed that there was very little increase in background rate until the depth of water fell below about 15 in. Similarly a further factor of 3 increase was observed as each of the annular tanks was drained. (A cylindrical partition, not shown in Fig. 3, divided the annular water shield into two concentric compartments each 1 ft thick.) The iron cone presumably had a very large effect since the transmission was about 10^{-4} and the arrangement approached 'good geometry.' Unfortunately it was not practicable to repeat the experiment with the iron removed.

VOL 15 196

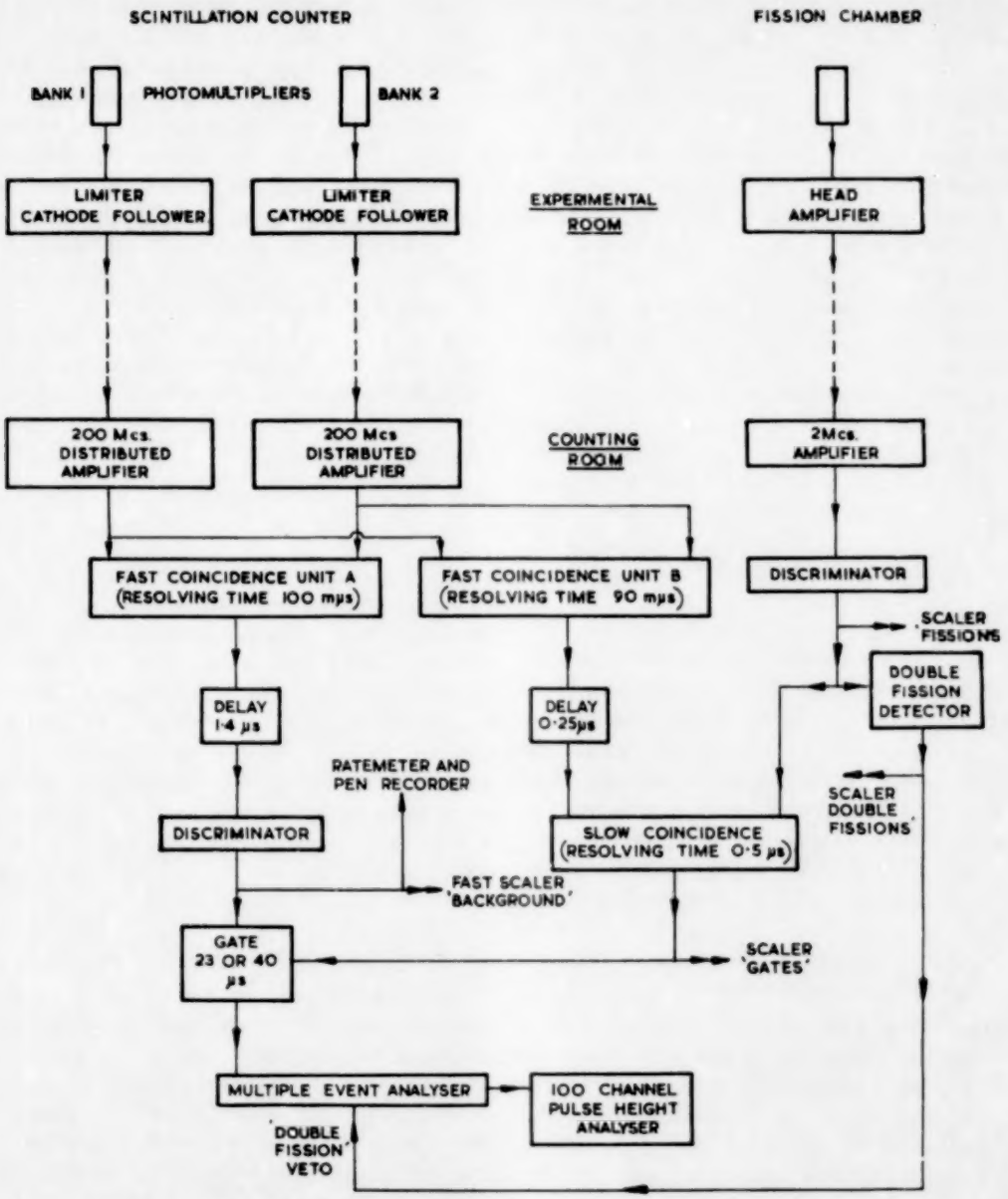

FIG. 4.—Block diagram of electronics for scintillation counter.

Typical counting rates of the scintillation counter were as follows:

(a) unshielded, no neutron source
$1{\cdot}0 \times 10^3$ counts/sec,

(b) fully shielded, no neutron source
$0{\cdot}4 \times 10^3$ counts/sec,

(c) fully shielded with 3×10^8 14 MeV neutron/sec emitted from the target
$7{\cdot}5 \times 10^3$ counts/sec.

3.3 *Experimental procedure*

The total counting time on each sample was accumulated from a series of short runs: this method had the advantages of reducing the effect of long-term changes in the background counting rate, and minimizing the loss of data which could occur in the event of equipment or accelerator failure. For calibrations the length of a run was 15 minutes and for the other runs the time was normally about two hours. Two or three separate

calibration runs were performed before and after a $\bar{\nu}$ determination and at intervals throughout the determination.

Background counts arose from scintillation counter pulses which were unrelated to a fission, but which occurred during the time the gate was open and hence were counted as neutron pulses. To make a correction for this it was necessary to know the average rate at which scintillation pulses from fast coincidence A unit (see Fig. 4) were being presented at the gate. A fast scaler (dead-time 0·25 μsec) counted these pulses. The background rate was usually about 0·3 counts per gate, and during a run was kept within about 10 per cent of the mean value by controlling the accelerator output current. The 'background' scaler records the fission neutron capture events in addition to true background, but the former is a negligible fraction of the total count except for the case of spontaneous fission, where a small correction was necessary. The true background for the spontaneous fission experiments amounted to about 0·02 counts per gate.

The pulse-height analyser display, the 'background' scaler count and the duration of the run provided sufficient data for the calculation of $\bar{\nu}$ values. However, in order to check that the equipment was functioning correctly, additional scalers counted the number of fission events, gating events and 'double fissions.' The gating rate varied from experiment to experiment, the approximate number of gates per hour for ^{235}U was 400 at 14 MeV, 100 at 2·5 MeV and 200 at 75 keV. For ^{240}Pu the rate was 1500 gates per hour and for ^{252}Cf 60,000 per hour.

3.4 *Treatment of scintillation counter data*

The data observed in an experimental run comprise the true fission neutron emission probabilities modified by three factors; counter efficiency, background counts, and dead-time of the recording instrument. After correction for the last two factors the resulting average count per gate will be equal to $\bar{\nu}$ multiplied by the counter efficiency: for comparative measurements in which a ratio of two $\bar{\nu}$ values is determined, the efficiency cancels out. It appears to be impracticable to correct for background and dead-time by exact analytical methods. In the past, approximate methods have been used (DIVEN *et al.*, 1956; HICKS *et al.*, 1956) the validity of which holds for a small loading of the capturing element, low background and short dead-time. These conditions are not adequately satisfied in the present case. We have recently devised a simulation method which is more generally applicable, the sole assumption being that the pulse width is small compared with the recording instrument dead-time. The Aldermaston IBM 704 computer was programmed to produce, by a sampling process, the probabilities $k_r(N,B)$ of observing r pulses when N neutron pulses were generated during the gating interval with the correct capture-time-spectrum of the scintillation counter, and B background pulses were generated with uniform probability throughout the gating interval.

The set of probabilities $k_r(N,B)$ was then used with the AWRE computer 'DEUCE' in a programme which synthesized the experimentally observed quantities P_0, P_1, etc. (where P_i is the fraction of gates containing i pulses), in the following way. If A_n is the probability that n fission neutron capture pulses occur per gate, and x is the mean background count per gate, then:

$$P_m = A_0 \sum_{j=m}^{J} b_j k_m(0,j) + A_1 \sum_{j=m-1}^{J} b_j k_m(1,j) + \ldots$$

where $b_j = \dfrac{x^j e^{-x}}{j!}$, and is the probability that j background pulses occur in the gate. The value of J taken for each summation is such that $b_{(J-1)}$ is negligible. The range of m in the present experiment was 0 to 9.

The set of simultaneous equations obtained was solved for A_0, A_1, etc. The sum ΣnA_n is the mean number of fission neutron pulses per gate, and the ratio of this to the corresponding sum for ^{252}Cf, multiplied by $\bar{\nu}$ for ^{252}Cf, yielded $\bar{\nu}$ for the nuclide investigated. For example:

$$\bar{\nu}(^{235}\text{U, 75 keV}) = \frac{\Sigma nA_n(^{235}\text{U, 75 keV})}{\Sigma nA_n(^{252}\text{Cf, spont.})} \cdot \bar{\nu}(^{252}\text{Cf, spont.}).$$

3.5 *Results of comparative measurements*

Table 3 contains the results of all the comparative measurements. The individual experimental runs were analysed separately and as an example Table 4 gives the details of the experiment for 75 keV neutrons on ^{235}U. A weighted mean of the ΣnA_n ratios from the last column of this table is entered in Table 3. The final column of Table 3 gives the $\bar{\nu}$ values obtained by taking $\bar{\nu}(^{252}\text{Cf, spont.}) = 3{\cdot}69 \pm 0{\cdot}07$.

3.6 *Assessment of errors*

The errors assigned to the ΣnA_n terms were based on the square root of the total number of neutron capture pulses observed in the run. It can be shown that this simplified procedure overestimates the errors slightly.

The coefficients $k_r(N,B)$ mentioned in Section 3.4 were themselves subject to random errors since they were produced by a sampling method, and it was necessary to know how these errors might affect the results obtained. The result of an experiment on ^{252}Cf was first processed using the original $k_r(N,B)$

TABLE 3.—SUMMARY OF COMPARATIVE MEASUREMENTS

Nuclide	Means of fissioning	Number of experimental runs	$\frac{\Sigma\, nA_n(\text{nuclide})}{\Sigma\, nA_n(^{252}\text{Cf spont.})}$	$\bar{\nu}$
^{235}U	75 keV neutron induced	12	0·647 ± 0·008	2·39 ± 0·05
^{235}U	2·5 MeV neutron induced	5	0·706 ± 0·016	2·60 ± 0·08
^{235}U	14·2 MeV neutron induced	13	1·159 ± 0·006	4·28 ± 0·08
^{238}U	14·2 MeV neutron induced	17	1·203 ± 0·023	4·44 ± 0·12
^{240}Pu	Spontaneous fission	3	0·576 ± 0·006	2·13 ± 0·05

coefficients, and then using the coefficients plus or minus one standard deviation, the positive or negative sign being chosen at random. The results of three runs were as follows:

original coefficients : $\Sigma nA_n = 2{\cdot}3022$
modified coefficients run 1: $\Sigma nA_n = 2{\cdot}3066$
modified coefficients run 2: $\Sigma nA_n = 2{\cdot}3006$.

This test was taken as evidence that no significant error was introduced by inaccuracies of these coefficients.

Errors quoted in column 5 of Table 3 are compounded from the errors in column 4 and the error on $\bar{\nu}$ ^{252}Cf.

3.7 *Effect of differences in fission neutron spectra*

It is generally assumed in this type of measurement that for all practical purposes fission neutron spectra are identical. If fission neutron spectra are in fact related to $\bar{\nu}$ values in the way suggested by TERRELL (1959), see Section 2.2(b), some error may be introduced when using liquid scintillation counters for $\bar{\nu}$ comparisons. This type of counter has an efficiency which falls with increasing neutron energy. A typical Monte-Carlo calculation for a 30 in. diameter spherical scintillation counter gave the following efficiencies: 0·93 at 0·1 MeV, 0·91 at 0·5 MeV, 0·92 at 1·5 MeV, 0·85 at 3 MeV, 0·55 at 14 MeV. This response would introduce an error of less than 1 per cent in a $\bar{\nu}$ ratio for which the two fission neutron spectra differ in mean energy, $\bar{E}$, by 0·25 MeV. The response of our scintillation counter was not measured. Monte-Carlo calculations predict a steeper efficiency fall-off with energy for this smaller counter, but this effect could conceivably have been cancelled by the poorer light collection from liquid near to the centre.

If one measured a $\bar{\nu}$ ratio, e.g. $\frac{\bar{\nu}\ ^{240}\text{Pu}}{\bar{\nu}\ ^{252}\text{Cf}}$, in each of two detectors known to have different response curves, the two measurements would be expected to disagree if the fission neutron spectra differ. This ratio has been measured by DIVEN *et al.* (1956) and by HICKS *et al.* (1956), both using cylindrical counters 30 in. diameter by 30 in. long; they obtained respectively 0·583 ± 0·007 and 0·591 ± 0·014 compared with our result, 0·576 ± 0·006. We conclude from the agreement of these results either that the response of our small counter is very similar to that of the 30 in. models, or that the fission neutron spectra are not very different. In either case it appears that the error made in this ratio determination will be small.

For fission at high energies the relationship between $\bar{E}$ and $\bar{\nu}$ is almost certainly different from that predicted by TERRELL since his analysis does not consider neutron evaporation prior to fission. For ^{235}U at 14 MeV, for example, the excitation is sufficient for the evaporation of two neutrons of mean energy 1 MeV followed by fission of ^{234}U. The mean energy of emitted neutrons may thus even be lower than that for thermal fission.

It may be concluded from the arguments presented above that only small errors due to spectral differences can have arisen in our comparisons of $\bar{\nu}$ values.

TABLE 4.—INDIVIDUAL RUNS FOR ^{235}U AT 75 keV

Date	Run no.	No. of ^{235}U fissions analysed	$\frac{\Sigma nA_n\ (^{235}\text{U, 75 keV})}{\Sigma nA_n\ (^{252}\text{Cf, spont.})}$
4.2.59	16	380	0·683
4.2.59	17	328	0·698
5.2.59	1	325	0·645
5.2.59	2	431	0·639
5.2.59	3	389	0·671
5.2.59	4	393	0·637
5.2.59	5	351	0·644
6.2.59	2	386	0·674
6.2.59	3	372	0·605
6.2.59	4	582	0·641
6.2.59	5	458	0·623
9.2.59	2	408	0·621

4. DISCUSSION

The average number of neutrons from the thermal fission of ^{235}U has been widely used as a standard for other $\bar{\nu}$ measurements. Assuming $\bar{\nu} = \bar{\nu}_{\text{thermal}} + 0{\cdot}135 \times$ energy in MeV, we have deduced from our

measurements at 75 keV a thermal $\bar{\nu}$ for ^{235}U; including delayed neutrons and reducing to three significant figures yields $\bar{\nu} = 2{\cdot}39 \pm 0{\cdot}05$, the same as the prompt value at 75 keV. It is of interest to compare this value with other direct measurements of this parameter. The first section of Table 5 lists the $\bar{\nu}(^{235}U$, thermal) values now available, whilst the remainder of that table compares our other $\bar{\nu}$ measurements with existing data. The 1960 edition of BNL-325 (HUGHES *et al.*, 1960) gives $\bar{\nu}(^{235}U$, thermal) $= 2{\cdot}43 \pm 0{\cdot}02$.

A comparison which can also be made is between our ratio of

$$\frac{\bar{\nu}(^{235}U,\ 75\ keV)}{\bar{\nu}(^{252}Cf,\ spont.)}$$

and the ratio of

$$\frac{\bar{\nu}(^{235}U,\ 80\ keV)}{\bar{\nu}(^{252}Cf,\ spont.)}$$

measured by DIVEN *et al.* (1956) using the same type of counter. The respective values of the ratio are $0{\cdot}647 \pm 0{\cdot}008$ and $0{\cdot}638 \pm 0{\cdot}010$.

Critical size experiments and calculations provide a means of testing $\bar{\nu}$ values, particularly in the energy range up to 3 MeV. Taking $\bar{\nu}$ for $^{235}U = 2{\cdot}46 + 0{\cdot}144\delta$, where δ is the incident neutron energy in MeV, and acceptable values for other ^{235}U nuclear data, it has been found here by J. B. Parker, E. D. Pendlebury and Underhill that the critical radius of a bare ^{235}U sphere as calculated by Carlson and Monte-Carlo methods is 10 per cent lower than the experimental value. A discrepancy in the same direction has been found by LOEWENSTEIN and OKRENT (1958).

The results of a number of trial calculations in which various parameters were adjusted showed that the critical mass was most sensitive to $\bar{\nu}$. It was also shown that if $\bar{\nu}$ alone is altered, good agreement between theory and experiment could be obtained by reducing its value by about 8 per cent over the entire energy range. A reduction of this magnitude is not supported

TABLE 5.—COMPARISON OF $\bar{\nu}$ VALUES WITH EXISTING DATA

Nuclide	Means of fissioning	Reference	$\bar{\nu}$	Standard
^{235}U	Thermal neutron induced	KALASHNIKOVA *et al.* (1955)	$2{\cdot}54 \pm 0{\cdot}10$*	Ra–Be source
	Thermal neutron induced	SANDERS (1956)	$2{\cdot}45 \pm 0{\cdot}15$*	Harwell Ra–Be source Old value $(9{\cdot}66 \pm 0{\cdot}4) \times 10^6$ n/sec
		Value above corrected to recently measured output of standard	$2{\cdot}32 \pm 0{\cdot}09$*	New value $(9{\cdot}09 \pm 0{\cdot}14) \times 10^6$ n/sec
	Thermal neutron induced	KENWARD *et al.* (1959)	$2{\cdot}420 \pm 0{\cdot}037$*	Harwell ^{240}Pu spontaneous fission source
	75 keV neutron induced but corrected to thermal and adjusted to include delayed contribution	Present paper	$2{\cdot}39 \pm 0{\cdot}05$*	$^{252}Cf\ \bar{\nu} = 3{\cdot}69 \pm 0{\cdot}07$
^{235}U	2·5 MeV neutron induced	JOHNSTONE (1955)	$2{\cdot}64 \pm 0{\cdot}19$	Harwell Ra–Be (Old value)
	2·5 MeV neutron induced	Present paper	$2{\cdot}60 \pm 0{\cdot}08$	$^{252}Cf\ \bar{\nu} = 3{\cdot}69 \pm 0{\cdot}07$
^{233}U	$15 \pm 0{\cdot}5$ MeV neutron induced	SMIRENKIN *et al.* (1958)	$4{\cdot}51 \pm 0{\cdot}19$	$\bar{\nu}(^{233}U$, thermal) $= 2{\cdot}47 \pm 0{\cdot}05$
	14·8 MeV neutron induced	PROTOPOPOV and BLINOV (1958)	$4{\cdot}7 \pm 0{\cdot}5$	$\bar{\nu}(^{233}U$, thermal) $= 2{\cdot}47 \pm 0{\cdot}05$
	14·1 MeV neutron induced	JOHNSTONE (1955)	$4{\cdot}52 \pm 0{\cdot}32$	Harwell Ra–Be (Old strength value)
	14 MeV neutron induced	GRAVES (1954)	$4{\cdot}1 \pm 0{\cdot}15$	
	14·1 MeV neutron induced	FLEROV and TALYZIN (1958)	$4{\cdot}12 \pm 0{\cdot}24$*	Values for non-elastic and fission cross sections
	14·2 MeV neutron induced	Present paper	$4{\cdot}28 \pm 0{\cdot}08$	$^{252}Cf\ \bar{\nu} = 3{\cdot}69 \pm 0{\cdot}07$

TABLE 5. (*Contd*).

Nuclide	Means of fissioning	Reference	$\bar{\nu}$	Standard
^{238}U	14 MeV neutron induced	GRAVES (1954)	3·5 ± 0·15	
	14·1 MeV neutron induced	JOHNSTONE (1955)	4·13 ± 0·25	Harwell Ra–Be (Old value)
	14·1 MeV neutron induced	FLEROV and TALYZIN (1958)	4·50 ± 0·32*	Values for non-elastic and fission cross-sections
	14·1 MeV neutron induced	FLEROV and TAMANOV (1958)	4·45 ± 0·35	Values for non-elastic, (n,2n) and fission cross sections
	14·2 MeV neutron induced	GAUDIN and LEROY (1958)	4·55 ± 0·15	$\bar{\nu}$(^{235}U, thermal) = 2·47 ± 0·03
	14·2 MeV neutron induced	Present paper	4·44 ± 0·12	^{252}Cf $\bar{\nu}$ = 3·69 ± 0·07
^{240}Pu	Spontaneous	BARCLAY *et al.* (1951)	2·84 ± 0·26	Harwell Ra–Be (Old value)
	Spontaneous	CRANE *et al.* (1956)	2·02 ± 0·11	^{252}Cf $\bar{\nu}$ = 3·52 ± 0·16
	Spontaneous	KALASHNIKOVA *et al.* (1955)	2·22 ± 0·11	Ra–Be source
	Spontaneous	DIVEN *et al.* (1956)	2·257 ± 0·045	$\bar{\nu}$(^{235}U, thermal) = 2·46 ± 0·03
	Spontaneous	JOHNSTONE (1955)	2·21 ± 0·13	Harwell Ra–Be (Old value)
	Spontaneous	Present paper	2·13 ± 0·05	^{252}Cf $\bar{\nu}$ = 3·69 ± 0·07
^{252}Cf	Spontaneous	CRANE *et al.* (1955)	3·53 ± 0·15*†	National Bureau of Standards Ra–Be
	Spontaneous	DIVEN *et al.* (1956)	3·869 ± 0·078	$\bar{\nu}$(^{235}U, thermal) = 2·46 ± 0·03
	Spontaneous	Present paper	3·69 ± 0·07	Harwell ^{240}Pu spontaneous fission source

* Includes delayed neutron contribution.
† But see also BOWMAN and THOMPSON (1959) where the value is given as 3·8 ± 0·16.

by the present experimental results. It should be noted, however, that better agreement can be achieved if $\bar{\nu}$ does not vary linearly with incident neutron energy. The accuracy of the 2·5 MeV value reported here was not sufficient to decide between linear and non-linear variation. Further measurements in the energy ranges thermal to 8 MeV and 12 to 23 MeV are now planned in an attempt to resolve this point. For these measurements a 30 in. diameter spherical counter will be used in a rotatable shielding system.

Acknowledgments—The authors wish to express their thanks to J. H. BIRD, A. MERCER, J. B. PARKER and E. D. PENDLEBURY of the Mathematical Physics Division for the Carlson and Monte-Carlo computations and many helpful discussions on critical sizes and dead-time problems; to W. G. GORE for the design of the special electronic equipment used; and to D. P. HAMMOND and the 3 MV Van de Graaff team. The experimental assistance of Mrs. M. A. DUNCAN, D. R. AKERS and E. R. CULLIFORD is gratefully acknowledged as also is the work of P. FIELDHOUSE in the later parts of the experiment. Helpful criticism by R. BATCHELOR has been valuable in the preparation of this report, and Dr. K. W. ALLEN has given enthusiastic support and encouragement throughout.

REFERENCES

ASHBY V. J., CATRON H. C., NEWKIRK L. L. and TAYLOR C. J. (1958) *Phys. Rev.* **111,** 616.
BARCLAY F. R., GALBRAITH W. and WHITEHOUSE W. J. (1951) *The Average Number of Neutrons Emitted in the Spontaneous Fission of ^{240}Pu.* A.E.R.E. Report N R 831.
BOWMAN H. R. and THOMPSON S. G. (1959) *The Prompt Radiations in the Spontaneous Fission of ^{252}Cf.* U.R.C.L. 5038 (Rev.).
COX S., FIELDS P., FRIEDMAN A., SJOBLOM R. and SMITH A. (1958) *Phys. Rev.* **112,** 960.
CRANBERG L., FRYE G., NERESON N. and ROSEN L. (1956) *Phys. Rev.* **103,** 662.
CRANE W. W. T., HIGGINS G. H. and THOMPSON S. G. (1955) *Phys. Rev.* **97,** 242.
CRANE W. W. T., HIGGINS G. H. and BOWMAN H. R. (1956) *Phys. Rev.* **101,** 1804.
DIVEN B. C., MARTIN H. C., TASCHEK R. F. and TERRELL J. (1956) *Phys. Rev.* **101,** 1012.

VOL. 15 1961

FLEROV N. N. and TALYZIN V. M. (1958) *Atomnaya Energiya* **5,** 653; (1960) *J. Nucl. Energy* **11,** 169. In English.

FLEROV N. N. and TAMANOV E. A. (1958) *Atomnaya Energiya* **5,** 654; (1960) *J. Nucl. Energy* **11,** 171. In English.

GAUDIN M. and LEROY J. L. (1958) *Proceedings of the Second International Conference on the Peaceful Uses of Atomic Energy, Geneva*, A. Conf. 15/P/1186, Part 2. United Nations, N.Y.

GORE W. G. (1960) *Nucl. instrum. Meth.* **7,** 320.

GRAVES E. R. (1954) Quoted by LEACHMAN R. B. *Proceedings of the Second International Conference on the Peaceful Uses of Atomic Energy, Geneva*, A. Conf. 15/P/2467. United Nations, N.Y.

HICKS D. A., ISE J. and PYLE R. V. (1955) *Phys. Rev.* **97,** 564; *Phys. Rev.* **101,** 1016.

HUGHES D. J., MAGURNO B. A. and BRUSSEL M. K. (1960) *Neutron Cross-Sections*, BNL-325, 2nd Edition, Supplement 1.

JOHNSTONE I. (1955) *A Measurement of the Average Number of Prompt Neutrons Emitted in Fission at High Energy*. A.E.R.E. Report NP R 1912.

KALASHNIKOVA V. I., LEBEDEV V. I., SPIVAK P. E. and ZAKHAROVA B. P. (1955) *Proceedings of the Conference of the Academy of Sciences, U.S.S.R: on the Peaceful Uses of Atomic Energy, Physics and Mathematics Section*. p. 156.

KENWARD C. J., RICHMOND R. and SANDERS J. E. (1959) *A Measurement of the Neutron Yield in Thermal Fission of* ^{233}U. A.E.R.E. Report R R2212 (Revised).

LEACHMAN R. B. (1958) *Proceedings of the Second International Conference on the Peaceful Uses of Atomic Energy, Geneva*. A. Conf. 15/P/2467. United Nations, N.Y.

LOEWENSTEIN W. B. and OKRENT D. (1958) *Proceedings of the Second International Conference on the Peaceful Uses of Atomic Energy, Geneva*, A. Conf. 15/P/637. United Nations, N.Y.

MOAT A., MCTAGGART M. H. and MATHER D. S. (1959) Unpublished information.

PROTOPOPOV A. N. and BLINOV M. V. (1958) *Atomnaya Energiya* **4,** 374; (1959) *J. Nucl. Energy* **9,** 207. In English.

REINES F., COWAN C. L., HARRISON F. B. and CARTER D. S. (1954) *Rev. sci. Instrum.* **25,** 1061.

RICHMOND R. and GARDNER B. J. (1957) *Calibration of Spontaneous Fission Neutron Sources*. A.E.R.E. Report R/R 2097.

RICHMOND R. (1958) *Progr. Nucl. Energy, Series* I, **2,** 165.

SANDERS J. E. (1956) *Comparison of the Average Number of Prompt Neutrons Emitted in Fission of Some Uranium and Plutonium Isotopes*. A.E.R.E. Report RP/R 1627; (1956) *J. Nucl. Energy* **2,** 247.

SMIRENKIN G. N., BONDARENKO I. I., KUTZAEVA A. S., MISHCHENKO KH. D., PROKHOROVA L. L. and SHEMATENKO B. P. (1958) *Atomnaya Energiya* **4,** 188; (1959) *J. Nucl. Energy* **9,** 155. In English.

SMITH A. B., FIELDS P. R. and ROBERTS J. H. (1957) *Phys. Rev* **108,** 411.

TERRELL J. (1959) *Phys. Rev.* **113,** 527.

VOL
15
196

Reactor Science and Technology (Journal of Nuclear Energy, Parts A/B), 1961, Vol. 15, pp. 113 to 119. Pergamon Press Ltd. Printed in Northern Ireland

INFLUENCE OF A CYLINDRICAL CHANNEL ON A NEUTRON FLUX WHICH VARIES LINEARLY IN A DIRECTION PERPENDICULAR TO THE AXIS OF THE CHANNEL

C. CARTER and R. J. JARVIS*
Atomic Energy Research Establishment, Harwell, Berks.

(*Received* 5 *January* 1961)

Abstract—The perturbation of the neutron flux in an infinite medium caused by a cylindrical channel is investigated when the unperturbed flux varies linearly in a direction perpendicular to the axis of the channel. The channel in fact behaves as a dipole and the dipole strength is calculated as a function of the channel radius. The results have important applications in the theory of transverse streaming.

1. INTRODUCTION

WHEN there is a flux gradient across a hole in a reactor, the transverse streaming of neutrons across the hole causes a loss of reactivity. In this report we consider the way in which the presence of the hole perturbs the neutron flux in the neighbourhood of the hole. The results obtained have been used by one of us in another paper (CARTER, 1961) to determine the reactivity loss due to transverse streaming.

We consider a cylindrical hole, radius a, in an infinite non-absorbing medium in which the asymptotic neutron flux varies linearly in a direction perpendicular to the axis of the hole. For convenience we shall take the mean free path in the medium as unit of length. In Section 2, we obtain an approximate solution, valid for $a \ll 1$, of the transport integral equation. In Section 3 we obtain an approximate solution valid for $a \gg 1$. In Section 4, we solve the Boltzmann integro-differential equation by the P_1 and P_3 spherical harmonics method. By interpolating between these approximations, we obtain an approximation which should be fairly accurate for all a.

2. SOLUTION OF THE INTEGRAL EQUATION FOR A SMALL HOLE

Following DAVISON (1951) the integral equation for the neutron flux may be reduced to two-dimensional form, in the plane perpendicular to the axis of the hole:

$$\phi(\mathbf{r}) = \frac{1}{2\pi}\int\int_{r'>a} \phi(\mathbf{r}')\,\frac{K_i(p'')}{p'}\,d^2\mathbf{r}' \qquad (2.1)$$

$$= \frac{1}{2\pi}\int_0^{2\pi} d\theta \int_0^{\infty} \phi(\mathbf{r}')K_i(p'')\,dp'', \qquad (2.2)$$

where

$$K_i(x) = \int_x^{\infty} K_0(t)\,dt, \qquad (2.3)$$

and $\mathbf{p}' = -\mathbf{r} + \mathbf{r}'$, the geometric distance between $\mathbf{r}$ and $\mathbf{r}'$, and $\mathbf{p}''$ is the optical distance between $\mathbf{r}$ and $\mathbf{r}'$, i.e. the part of the path length $\mathbf{p}'$ which lies in the medium. θ is the angle between $\mathbf{p}'$ and $\mathbf{r}$.

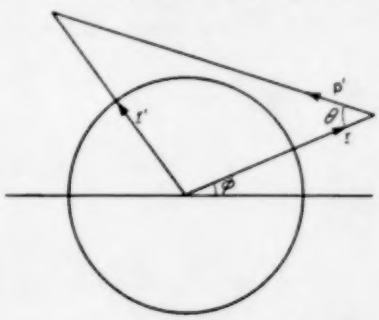

FIG. 1.

We now try to solve (2.2) for $a \ll 1$ by successive approximations.

Define

$$\mathbf{r}'' = \mathbf{r} + \mathbf{p}'' \qquad (2.4)$$

and put

$$\phi(\mathbf{r}) = \sum_{k=0}^{\infty} \phi_k(\mathbf{r}), \qquad (2.5)$$

where

$$\phi_k(\mathbf{r}) = \frac{1}{2\pi}\int_0^{2\pi} d\theta \int_0^{\infty} \phi_k(r'')K_i(p'')\,dp'' + f_k(\mathbf{r}), \qquad (2.6)$$

with $f_0(\mathbf{r}) = 0$

and $f_k(\mathbf{r}) = \frac{1}{2\pi}\int_0^{2\pi} d\theta \int_0^{\infty} \{\phi_{k-1}(\mathbf{r}') - \phi_{k-1}(\mathbf{r}'')\}K_i(p'')\,dp''$, for $k > 1$. (2.7)

(2.6) may be written

$$\phi_k(\mathbf{r}) = \frac{1}{2\pi}\int\int_{\text{all space}} \frac{K_i(|\mathbf{r}-\mathbf{r}''|)}{(|\mathbf{r}-\mathbf{r}''|)}\,\phi_k(\mathbf{r}'')\,d^2\mathbf{r}'' + f_k(\mathbf{r}) \qquad (2.8)$$

* Present address: Emmanuel College, Cambridge.

$\phi_0(\mathbf{r})$ is the flux in a source-free infinite medium and is therefore a solution of $\nabla^2\phi_0(\mathbf{r}) = 0$. For our problem, we take ϕ_0 to be the asymptotic flux

$$\phi_0(\mathbf{r}) = \text{constant} - r\cos\phi. \tag{2.9}$$

(a) $r > a$,

$$\mathbf{r}'' = \mathbf{r}' \qquad \text{when} \qquad \theta > \sin^{-1}a/r$$

or $$p'' \leqslant u = r\cos\theta - \sqrt{a^2 - r^2\sin^2\theta}.$$

When $$\theta < \sin^{-1}a/r \quad \text{and} \quad p'' > u.$$

$$|\mathbf{r}' - \mathbf{r}''| = \mu = 2\sqrt{a^2 - r^2\sin^2\theta}. \tag{2.10}$$

Expanding $\phi_{k-1}(\mathbf{r}')$ in a Taylor series about $\mathbf{r}''$, we have

$$\phi_{k-1}(\mathbf{r}') - \phi_{k-1}(\mathbf{r}'') = \sum_{n=1}^{\infty} \frac{\mu^n}{n!}\frac{\partial^n}{\partial p''^n}\phi_{k-1}(\mathbf{r}'') \tag{2.11}$$

Put $\sin\chi = \dfrac{r}{a}\sin\theta$, then

$$u = \sqrt{r^2 - a^2\sin^2\chi} - a\cos\chi \tag{2.12}$$

and (2.7) becomes

$$f_k(\mathbf{r}) = \sum_{n=1}^{\infty} \frac{2^n a^{n-1}}{n!2\pi r}\int_{-\pi/2}^{\pi/2} \frac{\cos^{n-1}\chi\, d\chi}{\sqrt{1 - \dfrac{a^2}{r^2}\sin^2\chi}} \times \int_u^{\infty} \left|\frac{\partial^n}{\partial p''^n}\phi_{k-1}(\mathbf{r}'')\right| K_i(p'')\, dp''. \tag{2.13}$$

For small a, using (2.13)

$$\phi_k(\mathbf{r}) \sim f_k(\mathbf{r}) \sim a^2\phi_{k-1}(\mathbf{r}) \sim a^{2k} \tag{2.14}$$

and we can evaluate $\phi(\mathbf{r})$ correct to order a^3 by calculating only

$$f_1(\mathbf{r}) \quad \text{and} \quad \phi_1(\mathbf{r}).$$

From (2.13),

since $\phi_0(r'') = \text{constant} - x - p''\cos(\theta - \phi)$

$$f_1(\mathbf{r}) = -\frac{2a^2\cos\phi}{\pi r}\int_0^{\pi/2}\cos^2\chi\, d\chi \times \int_u^{\infty} K_i(p'')\, dp'', \quad r > a. \tag{2.15}$$

(b) $r < a$,

$$p' - p'' = r\cos\theta - \sqrt{a^2 - r^2\sin^2\theta} \tag{2.16}$$

and $$f_k(\mathbf{r}) = \sum_{n=1}^{\infty}\frac{1}{n!2\pi}\int_0^{\pi/2}\left|r\cos\theta - \sqrt{a^2 - r^2\sin^2\theta}\right|^n d\theta \int_0^{\infty}\left|\frac{\partial^n}{\partial p''^n}\phi_{k-1}(\mathbf{r}'')\right| \times K_i(p'')\, dp''. \tag{2.17}$$

Again, for small a, $\phi_k(\mathbf{r}) \sim a^{2k}$. From (2.17),

$$f_1(\mathbf{r}) = -\frac{1}{2\pi}\int_0^{2\pi}\left|r\cos\theta - \sqrt{a^2 - r^2\sin^2\theta}\right| \times \cos(\theta - \phi)\, d\theta \int_0^{\infty}[K_i(p'')\, dp'' = -\frac{r}{2}\cos\phi, \qquad \text{for } r < a. \tag{2.18}$$

It is shown in Appendix 1 that the asymptotic solution of (2.8), where

$$f_k(\mathbf{r}) = g_k(r)\cos\phi, \qquad \text{is}$$

$$\phi_{\text{as}}(\mathbf{r}) = \frac{3\cos\phi}{2r}\int_0^{\infty} r^2 g_k(r)\, dr. \tag{2.19}$$

Now $$\int_0^{\infty} r^2 g_1(r)\, dr = -\frac{a^4}{8} - \frac{2a^2}{\pi}\int_0^{\pi/2}\cos^2\chi\, d\chi \times \int_a^{\infty} r\, dr\int_u^{\infty} K_i(p)\, dp. \tag{2.20}$$

Change integration variable from r to u, with

$$r\, dr = (u - a\cos\chi)\, du. \tag{2.21}$$

Using $$\int_u^{\infty} du\int_u^{\infty} K_i(p)\, dp = \frac{\pi}{4}$$

and $$\int_0^{\infty} u\, du\int_u^{\infty} K_i(p)\, dp = 2/3, \tag{2.22}$$

we have

$$\int_0^{\infty} r^2 g_1(r)\, dr = -\frac{a^4}{8} - \frac{a^2(1-a)}{3}. \tag{2.23}$$

Therefore to order a^3,

$$\phi_{\text{as}}(\mathbf{r}) = \text{constant} - r\cos\phi - \frac{a^2(1-a)}{2r}\cos\phi \tag{2.24}$$

3. SOLUTION OF THE INTEGRAL EQUATION FOR A LARGE HOLE

For $a \gg 1$, we put

$$r = a - x, \tag{3.1}$$

$$\phi(\mathbf{r}) = \phi(x)\cos\phi. \tag{3.2}$$

$$r\, dr = a\, dx. \tag{3.3}$$

Then, the integral equation (2.1) becomes

$$\phi(x) = \frac{a}{2\pi}\int_0^\infty \int_0^{2\pi} \phi(x')\,\frac{K_i(p''!)}{p'}\cos\theta'\,d\theta'\,dx' \quad (3.4)$$

Divide the range of integration in (3.4) into two parts corresponding to:

(i) neutrons reaching x from x' without passing through the hole, so that $p'' = p'$,

(ii) neutrons which pass through the hole.

In evaluating the contribution from (i), put $y' = a\sin\theta'$. Then the contribution is

$$\phi_1(x) = \frac{1}{2\pi}\int_0^\infty \int_{-\infty}^{+\infty} \phi(x')\,\frac{K_i(p')}{p'}\,dy'\,dx'. \quad (3.5)$$

Using the identity (Appendix 2)

$$E_1(x) = \frac{2}{\pi}\int_0^{\pi/2} K_i(x\sec\theta)\sec\theta\,d\theta, \quad (3.6)$$

with $y' = |x - x'|\tan\theta$, $p' = |x - x'|\sec\theta$, (3.7)

(3.5) becomes

$$\phi_1(x) = \tfrac{1}{2}\int_0^\infty E_1(|x - x'|)\,\phi(x')\,dx'. \quad (3.8)$$

This is the same integral as occurs in the Milne problem.

The contribution form (ii) occurs when

$$\theta' > \theta_0 = \sqrt{2\frac{x}{a}} + \sqrt{2\frac{x'}{a}}. \quad (3.9)$$

Then,
$$p' = 2a\sin\frac{\theta'}{2} \quad (3.10)$$

and
$$p'' = \frac{x + x'}{\sin\dfrac{\theta'}{2}}, \quad \text{if} \quad \theta \gg \theta_0.$$

This expression for p'' is correct only if $\theta \gg \theta_0$, but it is of the right order of magnitude even for $\theta \sim \theta_0$, and in the limit, $a \to \infty$, no error is introduced by using this approximation over the whole range of integration. Thus,

$$\phi_2(x) = \frac{1}{4\pi}\int_0^\infty \int_{\theta_0}^{2\pi-\theta_0} \frac{K_i(p'')\cos\theta'}{\sin\dfrac{\theta'}{2}}\,\phi(x')\,d\theta'\,dx',$$

and when $a \to \infty$,

$$\phi_2(x) = \frac{1}{4\pi}\int_0^\infty \int_0^{2\pi} \frac{\cos\theta'}{\sin\dfrac{\theta'}{2}}\,K_i\left(\frac{x - x'}{\sin\dfrac{\theta'}{2}}\right)\phi(x')\,d\theta'\,dx'$$

$$= \tfrac{1}{2}\int_0^\infty \left\{\frac{2}{\pi}\int_0^{\pi/2} K_i[(x + x')\sec\theta] \times (\sec\theta - 2\cos\theta)\,d\theta\right\}\phi(x')\,dx'. \quad (3.11)$$

In Appendix 2 we show that the kernel in equation (3.11) is

$$\frac{2}{\pi}\int_0^{\pi/2} K_i[(x + x')\sec\theta](\sec\theta - 2\cos\theta)\,d\theta = E_1(x + x') - 2E_2(x - x'). \quad (3.12)$$

Combining equations (3.8) and (3.11), the integral equation for $\phi(x)$, when $a \to \infty$, becomes

$$\phi(x) = \tfrac{1}{2}\int_0^\infty \{E_1(|x - x'|) + E_1(x + x') - 2E_2(x + x')\}\,\phi(x')\,dx'. \quad (3.13)$$

This is the equation for a Milne type problem with a kernel modified by the contribution from neutrons which pass through the hole. Equation (3.13) will have an asymptotic solution

$$\phi(x) \sim x + x_0. \quad (3.14)$$

Comparing this with the asymptotic solution for $\phi(\mathbf{r})$,

$$\phi(\mathbf{r}) \sim r\cos\theta - \frac{Ba^2}{r}\cos\theta, \quad (3.15)$$

we see that

$$B \sim \frac{a - x_0}{a + x_0} \sim 1 - 2\frac{x_0}{a}. \quad (3.16)$$

We have solved equation (3.13) approximately by a variational method (LeCaine, 1947) taking a trial function

$$q(x) = \phi(x) - x = x_0(1 - Ae^{-kx}). \quad (3.17)$$

The functional

$$F(q) = \frac{\displaystyle\int_0^\infty q^2(x)\,dx - \int_0^\infty \int_0^\infty \{\tfrac{1}{2}E_1(|x - x'|) + \tfrac{1}{2}E_1(x + x') - E_2(x + x')\}\,q(x)\,q(x')\,dx\,dx'}{\left[\displaystyle\int_0^\infty q(x)\{E_3(x) - E_4(x)\}\,dx\right]^2} \quad (3.18)$$

is minimized with respect to A and k. It can then be shown (Appendix 3) that

$$x_0 \geq \frac{3}{20} - \frac{3}{F(q)}. \tag{3.19}$$

We find that $F_{\min} = 47{\cdot}07$, for $k = 2$, giving $x_0 \geq 0{\cdot}21373$. In the Milne problem, we know that the trial function (3.17) gives x_0 correct to 0·00004, so that in our problem, we can be fairly confident that $x_0 = 0{\cdot}214$ is correct to 3 decimals. Thus, in equation (3.16), we have

$$B \sim 1 - \frac{0{\cdot}428}{a}. \tag{3.20}$$

4. P_3 SPHERICAL HARMONICS APPROXIMATION

In the previous sections we have obtained solutions of the problem for $a \ll 1$ and $a \gg 1$. For the general problem with any value of a, we shall now obtain an approximate solution using the P_3 spherical harmonics method. The details of the method are discussed by DAVISON (1958).

We take the axis of the hole as z-axis and denote spatial position, $\mathbf{r}$, by polar co-ordinates (r, θ) in the $x - y$ plane. The neutron direction Ω is given by angular co-ordinates (ξ, ϕ), where ξ is the angle Ω makes with the z-axis and ϕ is the angle that the projection of Ω on the $x - y$ plane makes with x-axis. Put $\omega = \theta - \phi$.

In the P_3 approximation, the neutron angular distribution is written as

$$\Psi(\mathbf{r},\boldsymbol{\Omega}) = \sum_{n=0}^{3} \frac{(2n-1)}{4\pi} \psi_n(\mathbf{r},\boldsymbol{\Omega}). \tag{4.1}$$

In a problem with no z-dependence, the ψ_n may be written

$$\left.\begin{aligned}
\psi_0(\mathbf{r},\boldsymbol{\Omega}) &= \phi_1(\mathbf{r}) - \phi_2(\mathbf{r}) \\
\psi_1(\mathbf{r},\boldsymbol{\Omega}) &= [\Omega_x X_x(\mathbf{r}) - \Omega_y X_y(\mathbf{r})] \\
&\quad - \tfrac{1}{3}\boldsymbol{\Omega} \cdot \nabla\phi_1(\mathbf{r}) \\
\psi_2(\mathbf{r},\boldsymbol{\Omega}) &= [(3\Omega_z^2 - \Omega^2)\,\Theta_1(\mathbf{r}) \\
&\quad + (\Omega_x^2 - \Omega_y^2)\,\Theta_2(\mathbf{r}) \\
&\quad - 2\Omega_x\Omega_y\Theta_3(\mathbf{r})] \\
&\quad - \tfrac{9}{7}(\boldsymbol{\Omega} \cdot \nabla)(\Omega_x X_x - \Omega_y X_y) \\
&\quad - \tfrac{1}{2}[3(\boldsymbol{\Omega} \cdot \nabla)^2 - \nabla^2] \\
&\quad \times (\tfrac{2}{15}\phi_1 - \tfrac{9}{70}\phi_2) \\
\psi_3(\mathbf{r},\boldsymbol{\Omega}) &= \tfrac{4}{7}\boldsymbol{\Omega} \cdot \nabla(5\psi_2 - \psi_0) - \tfrac{9}{7}\psi_1,
\end{aligned}\right\} \tag{4.2}$$

where $\phi_1(\mathbf{r})$, $\phi_2(\mathbf{r})$, the two components of $X(\mathbf{r})$, and the three components of $\Theta(\mathbf{r})$ satisfy certain differential equations and subsidiary conditions given by DAVISON. In particular, $\phi_1(\mathbf{r})$ is a solution of $\nabla^2\phi_1(\mathbf{r}) = 0$ and is in fact the asymptotic flux satisfying the diffusion equation in a non-absorbing medium.

Allowing for all the symmetry in our problem we find that we can write

$$\left.\begin{aligned}
\phi_1(\mathbf{r}) &= \text{constant} - \left(\frac{r}{a}\right)\cos\theta - B\left(\frac{a}{r}\right)\cos\theta \\
\phi_2(\mathbf{r}) &= CK_1(\nu_1 r)\cos\theta
\end{aligned}\right\} \tag{4.3}$$

$$\left.\begin{aligned}
X_x(\mathbf{r}) &= D\{K_0(\nu_2 r) - K_2(\nu_2 r \cos 2\theta\} \\
X_y(\mathbf{r}) &= -DK_2(\nu_2 r)\sin 2\theta
\end{aligned}\right\} \tag{4.4}$$

$$\left.\begin{aligned}
\Theta_1(\mathbf{r}) &= 2EK_1(\nu_3 r)\cos\theta \\
\Theta_2(\mathbf{r}) &= E\{K_1(\nu_3 r)\cos\theta + K_3(\nu_3 r)\cos 3\theta\} \\
\Theta_3(\mathbf{r}) &= E\{K_1(\nu_3 r)\sin\theta + K_3(\nu_3 r)\sin 3\theta\}
\end{aligned}\right\} \tag{4.5}$$

where

$$\nu_1^2 = 35/9, \quad \nu_2^2 = 7/3, \quad \nu_3^2 = 7, \tag{4.6}$$

and the four coefficients B, C, D and E are to be determined from the boundary conditions at the surface of the hole. The rigorous boundary condition is that the $\Psi(\mathbf{a},\boldsymbol{\Omega})$ is the same at the two points where a neutron path $\boldsymbol{\Omega}$ enters and leaves the hole i.e.

$$\chi(a, \theta, \xi, \omega) = \Psi(a, \theta, \xi, \omega) - \Psi(a, \pi - \theta - 2\omega;\ \xi, \pi - \omega) = 0. \tag{4.7}$$

In a finite order spherical harmonic approximation, it is not possible to satisfy this condition for all directions of $\boldsymbol{\Omega}$, and, following DAVISON's recommendations, we apply the following four integral Marshak boundary conditions.

$$\left.\begin{aligned}
&\int_0^{\pi} d\xi \int_{-\pi/2}^{\pi/2} d\omega\ \chi(a, \theta;\ \xi, \omega)\sin^2\xi\cos\omega = 0 \\
&\int_0^{\pi} d\xi \int_{-\pi/2}^{\pi/2} d\omega\ \chi(a, \theta;\ \xi, \omega)\sin^2\xi\sin\omega = 0 \\
&\int_0^{\pi} d\xi \int_{-\pi/2}^{\pi/2} d\omega\ \chi(a, \theta;\ \xi, \omega)\sin^4\xi\cos^3\omega = 0 \\
&\int_0^{\pi} d\xi \int_{-\pi/2}^{\pi/2} d\omega\ \chi(a, \theta;\ \xi, \omega) \\
&\qquad \times \sin^4\xi\cos^2\omega\sin\omega = 0
\end{aligned}\right\} \tag{4.8}$$

On applying these boundary conditions we obtain four rather complicated simultaneous linear equations for B, C, D and E. These equations were solved numerically for several values of a. The results are given in Table 1.

B is plotted against a in Fig. 2, together with the value $B = 2a/(2a + 1)$ obtained from P_1 approximation. It is clear that the spherical harmonic approximation is converging well for large a but not for small a. In Fig. 1, we also plot $1 - \dfrac{1}{2(1-a)}$ against a.

TABLE 1

a	B	C	D	E
0·2	·6979	−·05773	−·02558	−·02692
0·4	·7205	−·14318	−·05608	−·08356
0·6	·7429	−·2690	−·09417	−·19842
0·8	·7640	−·4443	−·14317	−·4195
1·0	·7835	−·6937	−·2067	−·8400
1·5	·8230	−2·0565	−·4697	−4·3315
2·0	·8539	−4·887	−·9847	−18·776
2·5	·8780	−14·601	−2·027	−88·83
3·0	·8967	−89·41	−4·176	−607·05

We suggest that this is probably quite a good estimate to B for all values of a. It has the correct behaviour for small a, and for large a, corresponds to replacing the 0·428 in equation (3.20) by $\frac{1}{2}$.

5. CONCLUSIONS

When a cylindrical hole of radius a is made in an infinite medium in which the unperturbed flux is $\phi_0(\mathbf{r}) = \text{constant} + r\cos\phi$, the asymptotic flux outside the hole is given approximately by

$$\phi_{as}(\mathbf{r}) = \text{constant} + r\cos\phi - \frac{a^2}{r} \times \left[1 - \frac{1}{2(1+a)}\right]\cos\phi.$$

The extra term added into the unperturbed flux is the flux arising from a dipole neutron source at the centre of the hole and of strength $a^2\left[1 - \frac{1}{2(1+a)}\right]$. The hole is in fact behaving as a polarized medium, the polarization being proportional to the gradient of the unperturbed flux.

REFERENCES

CARTER C. (1961) *Reactor Sci. Technol. (J. Nucl. Energy* Parts A/B). This issue, p. 76.

DAVISON B. (1951) *Influence of a Cylindrical Channel on a Periodic Neutron Density Distribution.* A.E.R.E. T/R 738.

DAVISON B. (1958) *Neutron Transport Theory*, Chapter 12, O.U.P.

LECAINE J. (1947) *Phys. Rev.* **72**, 564.

APPENDIX 1

We wish to find the asymptotic solution of

$$\rho(\mathbf{r}) = \frac{c}{2\pi}\int\int \rho(\mathbf{r}')\frac{K_1(|\mathbf{r}-\mathbf{r}'|)}{|\mathbf{r}-\mathbf{r}'|}\,d^2r' + f(\mathbf{r}). \qquad (A.1)$$

Taking two-dimensional Fourier transforms, we obtain a solution

$$\rho(\mathbf{r}) = \frac{1}{4\pi^2}\int\int \frac{\tilde{f}(\boldsymbol{\omega})\,e^{-i\boldsymbol{\omega}\cdot\mathbf{r}}\,d^2\omega}{1 - \frac{c}{\omega}\tan^{-1}\omega}. \qquad (A.2)$$

Consider case when $f(\mathbf{r}) = g(r)\cos\phi$ (A.3)

then
$$\tilde{f}(\omega) = \int_0^\infty rg(r)\,dr\int_0^{2\pi} e^{i\omega r\cos(\phi-\Omega)}\cos\phi\,d\phi = \cos\Omega\,\tilde{g}(\omega) \qquad (A.4)$$

where
$$\tilde{g}(\omega) = \int_0^\infty rg(r)\,dr\int_0^{2\pi} e^{i\omega r\cos\phi}\cos\phi\,d\phi = 2\pi i\int_0^\infty rg(r)J_1(\omega r)\,dr. \qquad (A.5)$$

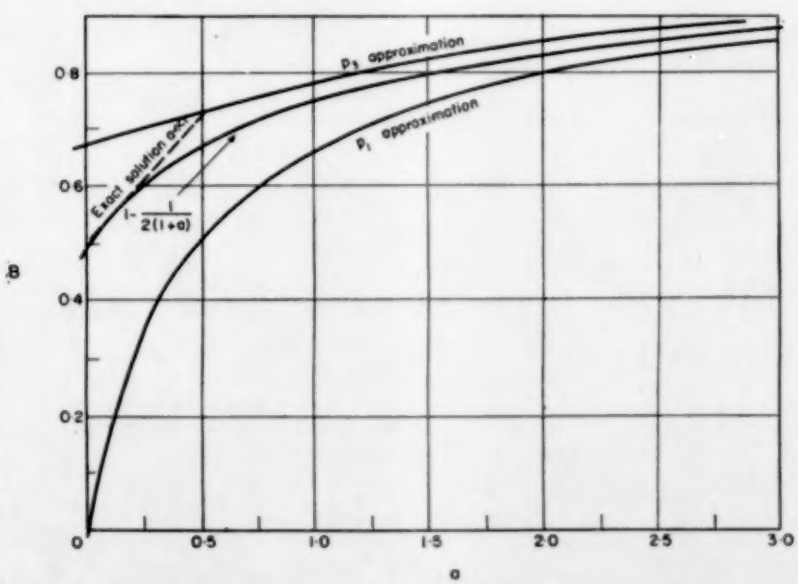

FIG. 2.—Value of the dipole term, B, in the asymptotic flux as a function of the hole radius a. The centre curve of $[1 - 1/2(1+a)]$ is a suggested interpolation between the various approximate calculations.

Therefore

$$\rho(\mathbf{r}) = \frac{1}{4\pi^2}\int_0^{\infty} \frac{\tilde{g}(\omega)\,\omega\,d\omega}{1-\frac{c}{\omega}\tan^{-1}\omega}\int_0^{2\pi} e^{i\omega r\cos(\phi-\Omega)}\cos\Omega\,d\Omega$$

$$= \frac{i\cos\phi}{2\pi}\int_0^{\infty}\frac{\tilde{g}(\omega)\omega J_1(\omega r)\,d\omega}{1-\frac{c}{\omega}\tan^{-1}\omega} \qquad (A.6)$$

$$= \frac{i\cos\phi}{4\pi}\int_0^{\infty}\{H_1^{(1)}(\omega r)+H_1^{(2)}(\omega r)\}$$

$$\times\frac{\omega\tilde{g}(\omega)\,d\omega}{1-\frac{c}{\omega}\tan^{-1}\omega}. \qquad (A.7)$$

Now $H_1^{(2)}(\omega r) = H_1^{(1)}(-\omega r)$, so that provided $\tilde{g}(\omega)$ is an odd function,

$$\rho(\mathbf{r}) = \frac{i\cos\phi}{4\pi}\int_{-\infty}^{\infty}\frac{\omega\tilde{g}(\omega)H_1^{(1)}(\omega r)\,d\omega}{1-\frac{c}{\omega}\tan^{-1}\omega}. \qquad (A.8)$$

Evaluate this integral by contour integration along the path shown. The contribution from the cuts from $-i$ to $+i\infty$ is of order

$$H_1^{(1)}(ir) = -\frac{2}{\pi}K_1(r). \qquad (A.9)$$

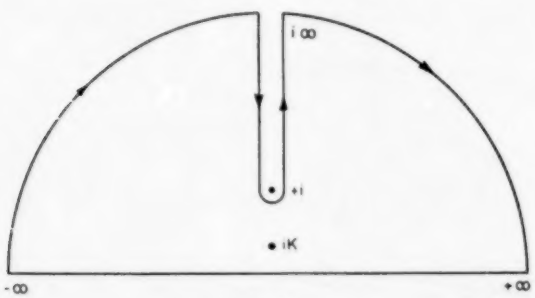

FIG. 3.

$\rho_{\mathrm{bs}}(\mathbf{r})$ is given by the contribution from the pole at $\omega = +i\kappa$, where

$$1 = \frac{c}{i\kappa}\tan^{-1}(i\kappa). \qquad (A.10)$$

Therefore

$$\rho_{\mathrm{bs}}(\mathbf{r}) = \frac{i\cos\phi\,2\pi i}{4\pi}\,\frac{i\kappa\,\tilde{g}(i\kappa)}{\frac{ic}{\kappa}\left[\frac{1}{1-\kappa^2}-\frac{1}{c}\right]}\,\frac{2}{\pi}K_1(\kappa r) \qquad (A.11)$$

For $c \to 1$, $\kappa^2 \to 3(1-c) \to 0$, $K_1(\kappa r) \to 1/\kappa r$

and
$$\tilde{g}(i\kappa) \to -\pi\kappa\int_0^{\infty} r^2 g(r)\,dr, \qquad (A.12)$$

so that

$$\rho_{\mathrm{bs}}(\mathbf{r}) \to \frac{3\cos\phi}{2r}\int_0^{\infty} r^2 g(r)\,dr. \qquad (A.13)$$

APPENDIX 2

To evaluate the integral $I_n = \frac{2}{\pi}\int_0^{\pi/2} K_i(x\sec\theta)\sec^{1-2n}\theta\,d\theta$ for $n = 0$ and 1. Put $y = x\tan\theta$ and use the identity

$$\frac{K_i(p)}{p} = \int_0^{\infty}\frac{e^{-\sqrt{z^2+p^2}}}{z^2+p^2}\,dz. \qquad (A.14)$$

Then,

$$I_n = \frac{2x^{2n}}{\pi}\int_0^{\infty}\int_0^{\infty}\frac{e^{-\sqrt{x^2+y^2+z^2}}\,dy\,dz}{(x^2-y^2-z^2)(x^2-y^2)^n}. \qquad (A.15)$$

Now convert to polar co-ordinates, $y = r\sin\phi$, $z = r\cos\phi$, and then put $r^2 = x^2(u^2-1)$. We obtain

$$I_n = \frac{2}{\pi}\int_1^{\infty}\int_0^{\pi/2}\frac{e^{-xu}\,d\phi\,du}{u(\cos^2\phi - u^2\sin^2\phi)^n}. \qquad (A.16)$$

Thus

$$\left.\begin{aligned} I_0 &= \int_0^{\infty}\frac{e^{-xu}\,du}{u} = E_1(x)\\ I_1 &= \int_0^{\infty}\frac{e^{-xu}\,du}{u^2} = E_2(x)\end{aligned}\right\} \qquad (A.17)$$

APPENDIX 3

Consider the integral equation

$$\phi(x) = \int_0^{\infty} K(x,x')\,\phi(x')\,dx', \qquad (A.18)$$

where $K(x,x') = K(x',x)$ is a symmetric kernel,

and
$$\int_0^{\infty} K(x,x')\,x'\,dx' - x = S(x) \qquad (A.19)$$

is bounded at infinity.

Put
$$\phi(x) = x + q(x). \qquad (A.20)$$

Then
$$q(x) = \int_0^{\infty} K(x',x')\,q(x')\,dx' + S(x). \qquad (A.21)$$

The variational method (LECAINE, 1947) applied to the integral equation (A.21) with a trial function $\tilde{q}(x)$ gives

$$F(\tilde{q}) = \frac{\int_0^{\infty}\tilde{q}^2(x)\,dx - \int_0^{\infty}\int_0^{\infty}\tilde{q}(x)\,K(x,x')\,\tilde{q}(x')\,dx'dx}{\left[\int_0^{\infty}\tilde{q}(x)\,S(x)\,dx\right]^2}$$

$$> \frac{1}{\int_0^{\infty} q(x)\,S(x)\,dx} \qquad (A.22)$$

the equality sign holding only when $\tilde{q} = q$.

Let $G(x_1,x)$ be the Green's function of the integral operator in equation (A.21), i.e.

$$G(x_1,x) = \int_0^{\infty} K(x,x')\,G(x_1,x')\,dx' + \delta(x-x_1). \qquad (A.23)$$

Then the solution of (A.21) may be written

$$q(x) = \int_0^{\infty} S(x_1)\,G(x_1,x)\,dx_1. \qquad (A.24)$$

Since K is symmetric, G is also symmetric by the optical reciprocity theorem. Thus, interchanging x_1 and x and letting $x_1 \to \infty$, we have

$$x_0 = q(\infty) = \int_0^\infty S(x) \overset{\mathscr{L}t}{x_1 \to \infty} G(x_1,x)\, dx. \qquad \text{(A.25)}$$

But $\overset{\mathscr{L}t}{x_1 \to \infty} G(x_1,x)$ is the solution of (A.18) normalized to unit current, i.e.

$$\overset{\mathscr{L}t}{x_1 \to \infty} G(x_1,x) = 3[x + q(x)] \qquad \text{(A.26)}$$

so that

$$x_0 = 3\int_0^\infty [x + q(x)]\, S(x)\, dx. \qquad \text{(A.27)}$$

Then, using equation (A.22), we have

$$x_0 \geqslant 3\int_0^\infty x\, S(x)\, dx + \frac{3}{F(\dot{q})}. \qquad \text{(A.28)}$$

In the integral equation (3.13) we have

$$K(x,x') = \tfrac{1}{2} E_1(|x - x'|) + \tfrac{1}{2} E_1(x + x') - E_2(x + x'), \qquad \text{(A.29)}$$

so that (A.19) gives

$$S(x) = E_2(x) - E_4(x), \qquad \text{(A.30)}$$

and (A.28) becomes (3.19) of the text.

VOL.
15
1961

Reactor Science and Technology (Journal of Nuclear Energy, Parts A/B), 1961, Vol. 15, pp. 120 to 129. Pergamon Press Ltd. Printed in Northern Ireland

PLEXIGLAS- AND GRAPHITE-MODERATED PLUTONIUM ASSEMBLIES*

A. GOODWIN JR. and C. L. SCHUSKE
Dow Chemical Co., Rocky Flats Plant, Denver, Colorado, U.S.A.

(*First received* 15 *October* 1960 *and in revised form* 20 *February* 1961)

Abstract—The critical masses of mixtures of plutonium and Plexiglas, and of plutonium and graphite have been determined.

The experimental data were derived from sub-critical neutron multiplication measurements on cylindrical assemblies containing these mixtures. The atomic ratios of moderator-to-fuel ranged from H:Pu = 0 to H:Pu ~ 100 and C:Pu = 0 to C:Pu ~ 10.

Theoretical values of critical masses were derived for water- and graphite-moderated systems of plutonium using 16-group transport and diffusion calculations. The atomic ratios of moderator-to-fuel ranged from H:Pu = 0 to H:Pu ~ 1000 and C:Pu = 0 to C:Pu ~ 35,000.

The authors' experience indicates that the result of this work is an inexpensive and reasonably accurate method for making nuclear safety calculations upon these systems.

1. INTRODUCTION

SUB-CRITICAL neutron multiplication measurements were made on cylindrical assemblies containing plutonium metal moderated with Plexiglas and graphite. These assemblies were constructed of alternate layers of moderator and metal disks. Methods of converting from finite cylinders to spheres are discussed. Extrapolations of the heterogeneous experimental data to homogeneous critical masses are also discussed.

Multigroup diffusion and transport calculations using sixteen energy groups were employed to compliment the experimental data.

The transport calculations were made using SNG and DSN codes for the IBM-704 computer (CARLSON, 1958; and CARLSON *et al.*, 1959).

The nuclear cross-section specifications were developed by HANSEN and ROACH (1960).

2. EXPERIMENTAL

2.1 *Experimental method*

The experiments were performed in a glove box to preclude the spread of contamination. No additional neutron source, other than that provided by the spontaneous fissioning of the fuel (primarily ^{240}Pu in the fuel) was used. This technique may have led to a consistent under-estimation of the critical mass in some cases, because these measurements were not taken closer than 70–85 per cent of the critical mass as determined by the $1/M$ extrapolations. Neutron source is added with the fuel and since this source alone would increase the counting rate, it will contribute to the measured multiplication, i.e. increase the measured multiplication. This effect will be masked, as one approaches critical, by the true multiplication and also because additions of fuel are usually made to regions of low importance.

The multiplication measurements were made using scaling equipment coupled to ^{10}B-lined counters moderated with polystyrene. A LiI(Eu) scintillator was also employed for these measurements.

The counters were located on the concrete floor approximately 90 cm directly below the assemblies.

The reciprocal multiplication curves were drawn in the following manner: An amount of fuel and moderator known to be considerably less than the critical amount was placed into position to be counted. The neutron flux measured by the counters was recorded as background for each of the four counters used in these measurements. Next a small increment of mass was added to this assembly. A 2-minute count was taken by each counter. Then a ratio of the background count to the count after the first addition provides a relative value of reciprocal multiplication $1/M$. This ratio is plotted on the ordinate and the corresponding total mass of the assembly is plotted on the abscissa. This process is repeated until the critical state is approached. A sample curve of this type is given in Fig. 1. In this case the $1/M$ values for the four counters were averaged to provide a single curve.

Four counters were used rather than a smaller number merely to provide an extra measure of safety during the build-up of these assemblies.

2.2 *Experimental materials*

2.2.1 *Plexiglas-plutonium assemblies*

A. Moderator and reflector density ~1·20 g/cm^3 (Rohm and Haas Plexiglas Type *R*).

* U.S. Atomic Energy Commission Contract AT (29–1)–1106.

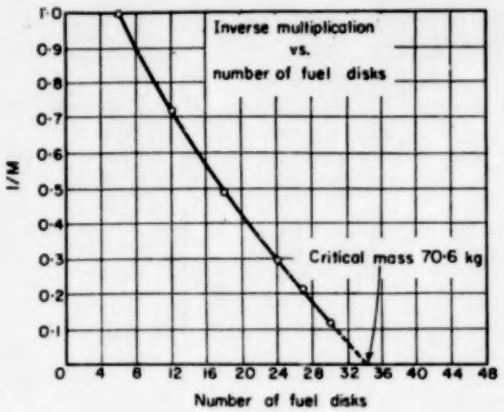

FIG. 1.

B. Fuel dimensions and moderator dimensions (see Tables 1, 2 and 3).
C. Fuel density ~15·8 g/cm³.

2.2.2 *Graphite-plutonium assemblies*

A. Moderator and reflector density 1·76 g/cm³ (National Carbon Grade CS-312).
B. Moderator and reflector dimensions: Disks 35·56 cm diameter and 1·27 cm thick.
C. Fuel density —15·8 g/cm³.
D. Fuel dimensions:
   1. 34·3 cm dia. × 0·142 cm
   2. 33·7 cm dia. × 0·137 cm
   3. 33·7 cm dia. × 0·142 cm.

2.3 *Results—plutonium-Plexiglas assemblies*

Neutron multiplication measurements were made on heterogeneous sub-critical cylindrical assemblies of Plexiglas and plutonium metal to ascertain the critical masses of several systems. Figure 2 provides a schematic of these assemblies. The experimental data (SCHUSKE, BIDINGER *et al.*, 1960; and BIDINGER *et al.*, 1960) thus obtained are exhibited in Tables 1, 2 and 3. It is to be noted in Tables 1, 2 and 3 that the H:Pu atomic ratios were arrived at from the average thickness values of both the plutonium fuel and Plexiglas moderator disks. A knowledge of the dimensional tolerance of the fuel and moderator disks indicate that an air void of approximately 1 per cent in volume is expected in each assembly. (No provisions to accurately measure the experimental heights were made.)

The equation for the density of fuel in an assembly is $\rho_{Pu} = \dfrac{22{\cdot}75}{\text{H:Pu} + 1{\cdot}44}$. This yields the density of the fuel in the assembly when values of H:Pu ratios are calculated from the above data.

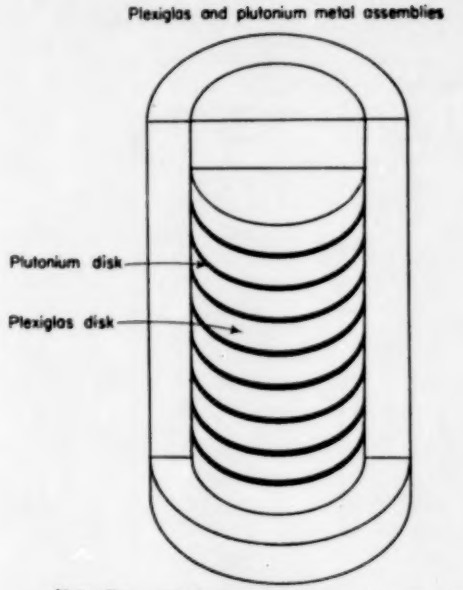
Plexiglas and plutonium metal assemblies
Plutonium disk
Plexiglas disk
Note: Top and bottom reflectors 10·2 cm thick
Lateral reflector 7·62 cm thick

FIG. 2.

For the benefit of the reader, actual masses used in the experiments are included in Tables 1, 2 and 3 so that the length of an extrapolation to the critical state is evident. No comment on accuracy of these critical extrapolations is attempted in this report.

The homogeneous cylindrical critical masses were obtained from the heterogeneous assemblies by plotting several metal disk thicknesses for a given H:Pu ratio as a function of the corresponding critical masses, and then extrapolating this relation to zero metal disk thickness. The technique is illustrated in Fig. 3.

The homogeneous cylindrical masses for both the bare and reflected cases obtained in this manner are given in Figs. 4 and 5. The reader can note the discontinuity of the 31·75 cm diameter cylinder in Figs. 4 and 5. This discontinuity is due in large part to the difference in the ^{240}Pu content of these two sets of data. (The actual ^{240}Pu contents are not available.)

The bare cylindrical homogeneous masses were then converted to spherical masses by the application of a method due to POND (1956). This method consists of letting $k = 1$ in the equation $k = \eta f u_f u_t$ and solving for ηf for each homogeneous case. Note u_f and u_t are the non-escape probabilities for fast and thermal neutrons. The escape probabilities are calculated from:

$$U_f = \frac{1}{(1 + B_f^2)(1 + 4{\cdot}2B_f^2)(1 + 20{\cdot}16B_f^2)}$$

TABLE 1.—EXPERIMENTAL DATA. BARE CYLINDER, 31·75 CM IN DIAMETER
(Heterogeneous Fuel Dispersion)

H:Pu atomic ratio	Mass of fuel in the experiment (kg)	Extrapolated critical mass (kg)	Density of fuel in the core (g/cm³)	Fuel thickness (cm)	Plexiglas disk thickness (cm)
1·6	40·42	56·5	7·48	0·293	0·292
5·5	35·17	39·9	3·27	0·160	0·617
5·9	29·40	38·4	3·10	0·293	1·20
6·1	29·40	38·1	3·02	0·146	0·617
11·4	20·21	26·6	1·77	0·146	1·20
11·6	22·05	30·1	1·74	0·439	3·69
11·7	22·05	27·6	1·73	0·293	2·46
16·8	16·54	20·4	1·25	0·146	1·82
20·3	16·05	22·2	1·05	0·040	0·617
35·6	10·67	12·6	0·614	0·093	2·46
39·8	14·48	18·4	0·552	0·161	4·93
45·7	9·63	11·9	0·483	0·080	2·98
47·6	8·56	10·3	0·464	0·040	1·49
72·3	12·92	16·4	0·309	0·093	4·93
90·7	6·65	8·5	0·247	0·048	3·63
92·9	4·99	5·9	0·241	0·024	1·82
94·2	5·35	7·4	0·238	0·040	3·02

TABLE 2.—EXPERIMENTAL DATA. BARE CYLINDERS, 45·72 CM IN DIAMETER
(Heterogeneous Fuel Dispersion)

H:Pu atomic ratio	Mass of fuel in the experiment (kg)	Extrapolated critical mass (kg)	Density of fuel in the core (g/cm³)	Fuel thickness (cm)	Plexiglas disk thickness (cm)
18·1	25·95	32·8	1·16	0·120	1·75
18·7	25·95	32·0	1·13	0·080	1·17
19·4	24·88	32·0	1·09	0·040	0·583
45·6	13·84	15·8	0·484	0·064	2·39
46·4	12·96	15·7	0·475	0·048	1·76
48·5	12·31	15·1	0·456	0·024	0·880
87·0	9·72	13·0	0·257	0·072	5·33
88·6	7·78	9·6	0·253	0·048	3·55
94·1	6·48	8·0	0·238	0·024	1·78

where

$$B_t^2 = \left(\frac{2{\cdot}4048}{R - 2{\cdot}5}\right)^2 + \left(\frac{3{\cdot}1416}{H + 5{\cdot}0}\right)^2$$

and

$$U_t = \frac{1}{1 - L^2 B_t^2}$$

where

$$B_t^2 = \left(\frac{2{\cdot}4048}{R - 0{\cdot}36}\right)^2 + \left(\frac{3{\cdot}1416}{H - 0{\cdot}72}\right)^2$$

where

L^2 = thermal diffusion length
R = cylinder radius in centimetres
H = cylinder height in centimetres.

The factor f is the thermal utilization and η the neutrons per absorption in the fuel. These values of ηf for the various experimental cases are then used to calculate critical sphere masses. These are given in Fig. 6. Infinite cylinder and slab parameters can also be derived by this method.

Reflected homogeneous spherical masses were derived by making use of the shape conversion factors arrived at from critical UO_2F_2 reflected cylindrical and spherical systems (BECK *et al.*, 1949). This method is not as reliable as that used for the bare cases. Figure 7 provides a plot of these data.

A series of sub-critical measurements made on plutonium metal assemblies tamped with Plexiglas have been empirically correlated (SCHUSKE, SMITH *et al.*, 1960). A total of seven experimental values were found to fit (within the experimental error) an empirical equation of the form:

$$(\sqrt{A} - 4{\cdot}45 \text{ cm})\,(h - 0{\cdot}635 \text{ cm}) = 27{\cdot}74 \text{ cm}^2$$

A = area of the base
h = critical height.

TABLE 3.—EXPERIMENTAL DATA. REFLECTED CYLINDERS, 31·75 CM IN DIAMETER
(Heterogeneous Fuel Dispersion)

H:Pu atomic ratio	Mass of fuel in the experiment (kg)	Extrapolated critical mass (kg)	Density of fuel in the core (g/cm³)	Fuel thickness (cm)	Plexiglas disk thickness (cm)
0·5	17·21	22·6	11·7	0·889	0·617
1·0	18·18	22·1	9·32	0·869	1·20
2·4	16·55	21·2	5·92	0·161	0·292
4·9	14·48	17·7	3·59	0·161	0·617
9·1	10·34	13·6	2·16	0·161	1·20
16·1	8·30	9·7	1·30	0·093	1·20
18·5	8·56	9·8	1·14	0·080	1·23
19·6	7·49	9·8	1·08	0·040	0·617
30·8	5·93	6·5	0·706	0·093	2·46
42·0	4·34	5·6	0·524	0·064	2·40
43·3	4·65	5·5	0·509	0·048	1·82
46·2	4·32	5·3	0·478	0·024	0·909
82·2	3·32	4·0	0·272	0·048	3·63
87·3	2·66	3·3	0·256	0·024	1·82
92·2	2·67	3·6	0·243	0·040	3·01

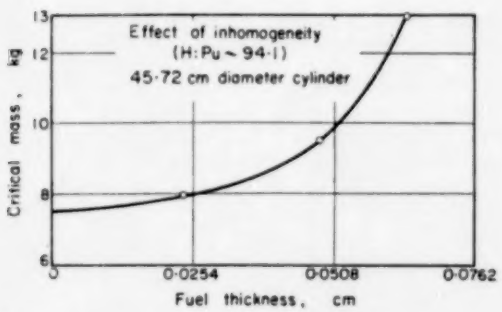

FIG. 3.

The constants in the equation are: $\sqrt{A_0} = 4{\cdot}45$ cm, the length of a side of an infinite cylinder of square cross section; $h_0 = 0{\cdot}635$ cm, the infinite slab thickness; and $C = 27{\cdot}74$ cm², an empirical constant. This type of equation was previously found to fit data for a variety of cases ranging from aqueous solution systems of uranyl fluoride (SCHUSKE and MORFITT, 1949) to uranium metal tamped with water (GWIN and MEE, 1959). The data are tabulated in Table 4 and the correlation is illustrated in Fig. 8.

2.4 *Results—plutonium-graphite assemblies*

Figure 9 is a schematic of the sub-critical assemblies.

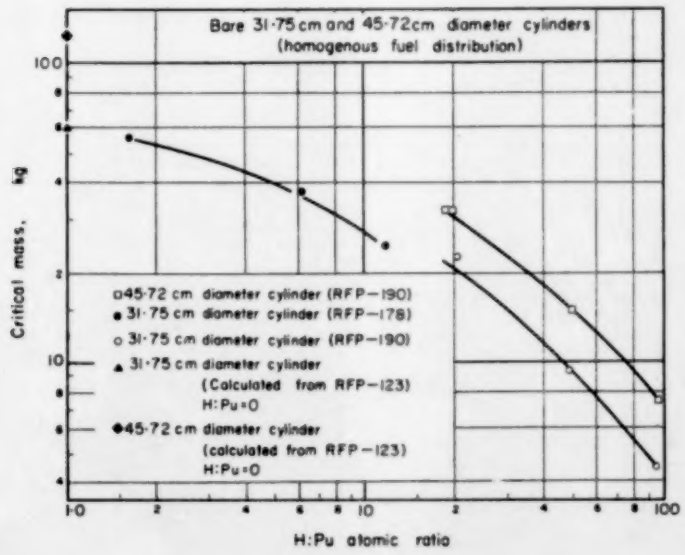

FIG. 4.

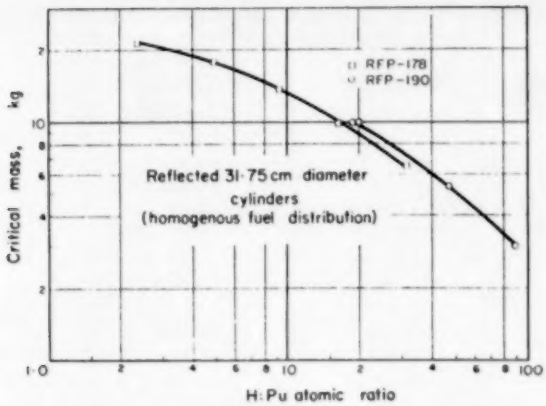

FIG. 5.

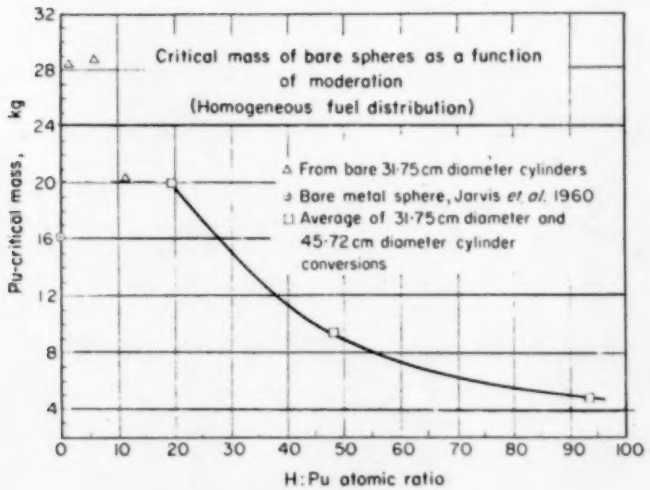
Critical mass of bare spheres as a function
of moderation
(Homogeneous fuel distribution)
From bare 31·75 cm diameter cylinders
Bare metal sphere, Jarvis et al. 1960
Average of 31·75 cm diameter and
45·72 cm diameter cylinder
conversions
Pu-critical mass, kg
H:Pu atomic ratio

FIG. 6.

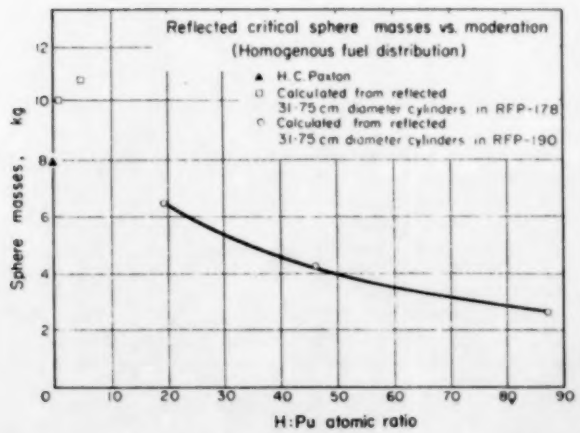
Reflected critical sphere masses vs. moderation
(Homogenous fuel distribution)
H. C. Paxton
Calculated from reflected
31·75 cm diameter cylinders in RFP-178
Calculated from reflected
31·75 cm diameter cylinders in RFP-190
Sphere masses, kg
H:Pu atomic ratio

FIG. 7.

TABLE 4.—EXPERIMENTAL DATA. PLUTONIUM METAL REFLECTED WITH PLEXIGLAS

Array dimensions (cm)	Sq. root of cross-sectional area $\sqrt{A}$ (cm)	Exp. height h (cm)	Emp.* height h (cm)	Lateral tamper (cm)	Radial tamper (cm)	Array density (g/cm³)	Est. exp. error (%)	Source of data
6·35 × 6·985†	6·65	12·7	13·18	10·16	10·16	15·7 –	~10	SCHUSKE, SMITH *et al.*, (1960)
Circle diameter ~9·88	8·74	7·01	7·16	10·01	10·01	15·8	±4	KLOVERSTROM, (1960)
6·985 × 12·7†	9·42	6·35	6·20	10·16	10·16	15·7 –	~10	SCHUSKE, SMITH *et al.*, (1960)
Square	12·7	3·81	3·99	10·16	10·16	15·7 –	~10	SCHUSKE, SMITH *et al.*, (1960)
Approx. square	18·24	2·54	2·64	10·16	10·16	15·7 –	~10	SCHUSKE, SMITH *et al.*, (1960)
Circle diameter ~31·85	28·22	1·71	1·80	10·16	7·62	15·7 –	~10	SCHUSKE *et al.*, (1959)
Square	50·8	1·25	1·23	10·16	5·08	15·8 –	<10	Recent work

* Empirical heights calculated from $(\sqrt{A} - 4{\cdot}45 \text{ cm})(h - 0{\cdot}635 \text{ cm}) = 27{\cdot}74 \text{ cm}^2$.
† Same experimental point.

Figure 10 contains the extrapolated critical mass as a function of the C:Pu atomic ratio (GOODWIN and SCHUSKE, 1958). The C:Pu atomic ratios were calculated on the basis that the core is the smallest cylinder which encloses all of the fuel. The SNG calculations in Fig. 10 are explained in Section 3. In addition to these experiments, studies were made on solid metal slabs 33·65 to 34·29 cm in diameter and end-reflected with varying thicknesses of graphite (GOODWIN and SCHUSKE, 1959). These assemblies contained no lateral reflectors. The results are contained in Table 5 and Fig. 11.

3. CALCULATIONS

3.1 *Computer codes and cross sections*

The calculations were multigroup using the S_n approximation and the diffusion approximation to the transport equation. The S_n method is well documented and will not be further described here (CARLSON, 1955, 1959; CARLSON and BELL, 1958; and CARLSON *et al.*, 1959).

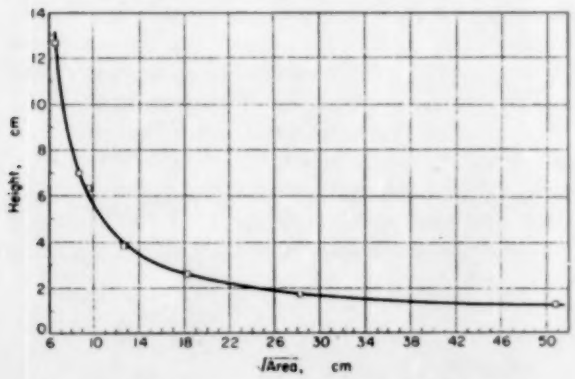

FIG. 8.—Critical arrays of plutonium metal reflected by Plexiglas (approximately 10·16 cm Plexiglas reflector).
□ Rectangular and square cross sections
○ Circular cross sections
— Empirical equation.

The diffusion calculation used here is a fundamental mode solution of the diffusion equation (SAFANOV, 1952). This method assumes the leakage is a function of the buckling and therefore is limited to bare homogeneous reactors. The equations for this method were coded for the Bendix G-15D computer.

The diffusion code yields a critical buckling and an average extrapolation length. The critical dimensions are then obtained from the following formulae:

Spheres $$\frac{Ba \sin Ba}{\sin Ba - Ba \cos Ba} = 2/3\, B\, \overline{\lambda_{tr}}$$

Infinite cylinders $$2/3\, \overline{\lambda_{tr}} = \frac{J_0(Ba)}{J_1(Ba)}$$

Infinite slabs $$2/3\, B\overline{\lambda_{tr}} = \frac{\cos Ba}{\sin Ba}.$$

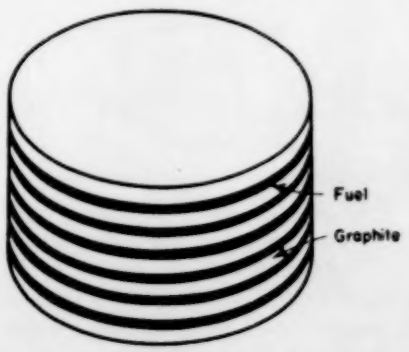

FIG. 9.—Graphite and plutonium metal assemblies.

TABLE 5.—SOLID METAL SLABS WITH GRAPHITE END REFLECTORS

A. End-reflector thickness (cm)	0	0	1·27	2·54	3·81	5·08	7·62
B. Plutonium disk diameter (cm)	33·65	34·29	33·65	33·65	33·65	34·29	34·29
C. Air void in the core %	—	—	5·20	2·97	1·27	—	—
D. Mass plutonium in the experimental core (kg)	—	—	42·7	36·9	33·0	31·5	29·4
E. Experimental extrapolated critical mass (kg)	66	74	54·3	46·2	40·7	42	36·1

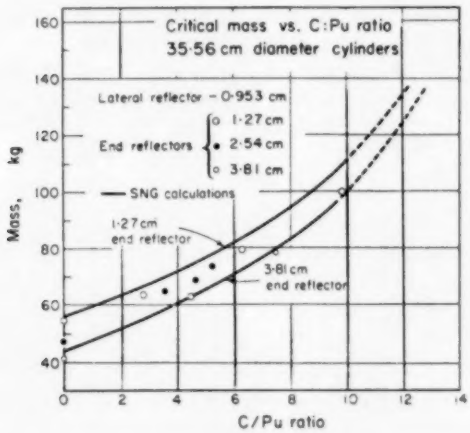

FIG. 10.

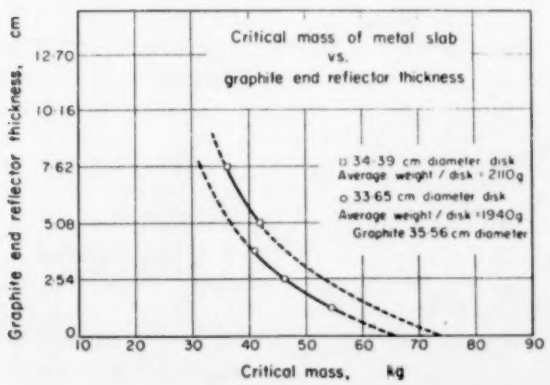
Critical mass of metal slab
vs.
graphite end reflector thickness
□ 34·39 cm diameter disk
Average weight / disk = 2110g
o 33·65 cm diameter disk
Average weight / disk = 1940g
Graphite 35·56 cm diameter
Graphite end reflector thickness, cm
Critical mass, kg

FIG. 11.

In the above formulae:

B^2 = critical buckling

$\overline{\lambda_{tr}}$ = average transport mean free path

a = critical radius of sphere and cylinder or critical half-thickness of slab.

The cross sections used were a sixteen-group set based on specifications given by HANSEN and ROACH (1960). A partial tabulation of these is given by ROACH (1960). Briefly the cross sections are averaged as follows. The first five (high-energy) groups are obtained by fission spectrum weighting (HANSEN, 1958). The next ten groups are obtained essentially by flat collision density weighting except for the heavy element resonance cross sections. The heavy element resonance cross sections are obtained from the resonance integral and therefore account can be taken of resonance self-shielding. The thermal group is a Maxwellian average.

Elements not tabulated by HANSEN and ROACH were treated using their recipes. These included at the time of writing ^{239}Pu and ^{240}Pu. Since diffusion and the SNG code do not allow anisotropic scattering, the transport approximation is used, i.e. the total cross section is replaced by the transport cross section. HANSEN and ROACH have an anisotropic set of hydrogen cross-sections for use with DSN. All DSN calculations with hydrogen moderator used this set.

The diffusion calculations made use of these cross-sections modified to normalize the calculated critical masses to several known experimental values. These modified cross sections were also checked using ^{235}U mixtures since more experimental data are available for uranium. The fit for moderated cases was obtained by arbitrarily increasing the scattering cross sections by 10 per cent. The transport cross sections of the first five groups of ^{239}Pu and ^{235}U were increased by 15 per cent to obtain the metal mass. The metal mass calculated 15 per cent high for plutonium (^{235}U masses were within 2 per cent) but was not reduced further since obtaining a better fit to the metal does not influence the moderated masses above H/Pu atomic ratios of 5.

3.2 *Results of plutonium and hydrogen moderator calculations*

The results of the calculations for mixtures of plutonium and H_2O are given in Fig. 12. The effect of ^{240}Pu reaches a peak when the moderator-to-fuel

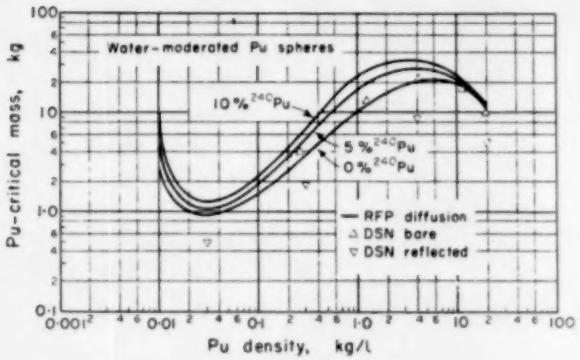

FIG. 12.—Spherical homogeneous masses.
—— Bare—diffusion calculations
△ Bare—DSN calculations 0% ^{240}Pu
▽ Reflected—DSN calculations 0% ^{240}Pu

ratio is approximately 5. This is due to the large resonance at 1·05 eV. At higher H:Pu ratios the resonance escape probability increases and at lower H:Pu ratios most neutrons are captured or escape before being slowed down to 1·05 eV to be captured.

The few DSN points plotted indicate the reliability of the diffusion method. DSN cross sections were not normalized to experimental data. The inverted triangles are DSN calculations of water reflected systems. Experience with ^{235}U indicates that DSN is accurate to within 5 per cent on the critical mass with the cross-sections given by ROACH.

The densities taken for the components of the mixture are:

$$\text{Pu} - 19{\cdot}6\ \text{g/cm}^3$$
$$\text{H}_2\text{O} - 1{\cdot}0\ \text{g/cm}^3.$$

Figure 13 shows a comparison between the experimental results of Section 2 and the diffusion calculations. These calculations were of homogeneous mixtures of Plexiglas and plutonium.

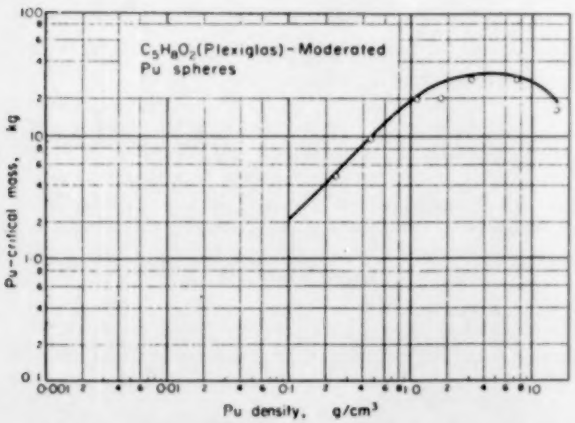

FIG. 13.—Multigroup diffusion calculations on homogeneous mixtures of plutonium and Plexiglas compared with experiment.
—— Bare—diffusion calculations
○ Experimental values (Section 2.3).

The densities taken for the components of these mixtures are:

Plutonium—15·8 g/cm^3
Plexiglas ($C_5H_8O_2$)—1·20 g/cm^3.

3.3 *Results of plutonium plus graphite calculations*

The calculations on graphite systems were both SNG and diffusion calculations. The results of the diffusion calculations are shown in Fig. 14. The effect of ^{240}Pu is also shown. The ^{240}Pu in graphite has a similar effect to that shown for water. However it occurs for a higher moderator-to-fuel ratio for carbon than for water, of course expected since the slowing down length in carbon is longer than in water. The densities taken for the components of the mixture are:

Pu—15·8 g/cm^3
C—1·65 g/cm^3.

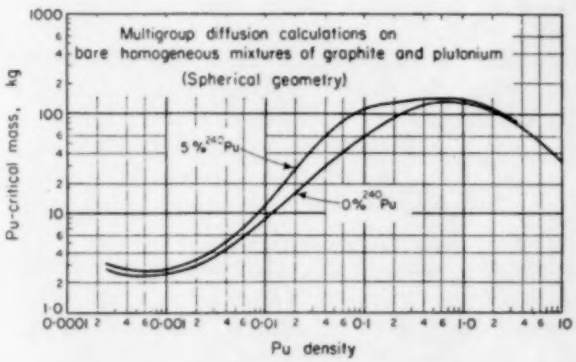

FIG. 14.

The results of the SNG calculations are shown in Fig. 10. The upper curve is for 1·27 cm end reflectors and the lower curve is for 3·81 cm end reflectors. Since the SNG code handles only one-dimensional problems, the method of converting to finite cylinders is explained below.

The bare reactor calculations were converted to finite cylinders by equating bucklings. The bucklings were in general obtained from an infinite cylinder and infinite slab calculation using the following formulae:

$$B_c = \frac{\mu_0}{R_c + \delta} = B_{s1} = \frac{\pi}{T_s + \delta}$$

B_c^2 = cylinder buckling
B_{s1}^2 = slab buckling
R_c = cylinder radius
T_s = slab thickness
δ = extrapolation length
μ_0 = first root of 0th order Bessel function of first kind.

The validity of this method was checked at C: Pu = 0 and C: Pu = 10 by calculating the bare sphere radius by SNG and comparing them with the above. Table 6 shows the results of this comparison.

The above method is therefore seen to be adequate for the range of C: Pu ratios considered here. Table 7 lists the bare buckling and extrapolation lengths obtained from the SNG calculations.

In order to compare these calculations with the experimental results of Section 2.3 it is necessary to determine the effects of the reflector on the ends of the stack. It was determined that the lateral reflector could be assumed to have a reflector savings equal to the reflector thickness. This lateral reflector is just the extension of the graphite disks beyond the plutonium disks, and is small in any case.

The end reflector was full-density graphite and ranged in thickness to 3·81 cm. In order to correct this for reflector savings, several SNG calculations were run at C: Pu = 10. The SNG calculations extended up to a reflector thickness of 5 cm but were extrapolated beyond this by a one-group method (GOODWIN and SCHUSKE, 1959). In the previous reference it was shown that the reflector savings is independent of geometry at this C: Pu ratio. Figure 15 shows this reflector savings as a function of reflector thickness.

Measurements of plutonium metal reflected by carbon have been reported (KLOVERSTROM, 1957). These data permit a determination of the reflector savings versus reflector thickness values. These values are also shown on Fig. 15. An SNG calculation using slab geometry confirms the independence with geometry.

The reflector savings at a C: Pu ratio of 5 was calculated at a reflector thickness of 1·63 cm by SNG.

TABLE 6

C:Pu	Pu density (g/cm³)	Sphere radius SNG (cm)	Sphere radius using buckling from slab and cylinder (cm)
0	15·8	6·15	6·24
10	2·81	20·47	20·83

TABLE 7

C:Pu	Buckling (B^2) (cm^{-2})	Extrapolation length (cm)
0	0·150	1·87
5	0·0323	2·32
10	0·0182	2·46
15	0·0127	2·59
20	0 00986	2·66

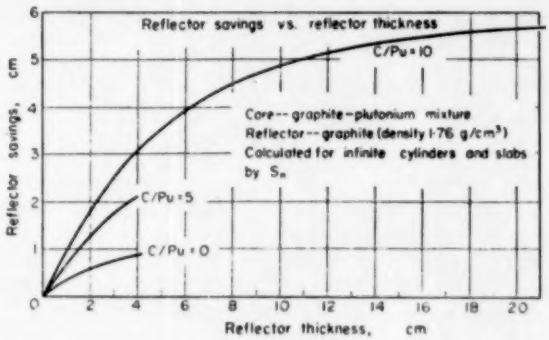

FIG. 15.

This curve is shown on Fig. 15 and was extended to 4 cm by a one-group calculation.

The curves of Fig. 10 were calculated assuming the Pu — C core to be 33·66 cm in diameter and reflected laterally by 0·95 cm of graphite. The reflector savings of this graphite is assumed to be equal to the reflector thickness.

The ends of the core are assumed to be reflected by 1·27 cm graphite or 3·81 cm graphite. The reflector savings for these is then obtained from Fig. 13.

4. CONCLUSIONS

The comparison between theory and experiment indicate that adequate calculations of plutonium mixtures with water and graphite can be made for nuclear safety purposes (see Figs. 10 and 13). Greater experimental accuracy is desirable in order to assess the cross sections and perhaps to obtain better group cross sections. The ^{240}Pu cross sections have not been measured over the entire range of energies needed, and some interpolation is necessary. Since the effect of ^{240}Pu is to increase the critical mass over a range of moderations, a thorough analysis of systems containing gross quantities of ^{240}Pu may in the future have economic merit when power reactor fuels are processed in large quantities.

Acknowledgments—The authors would like to thank DR. G. HANSEN and MR. W. H. ROACH of Los Alamos for the use of their cross sections and for many helpful discussions. We would also like to thank MR. B. CARLSON of Los Alamos for his co-operation in running our S_n problems at Los Alamos.

REFERENCES

BECK C. K., CALLIHAN A. D., MORFITT J. W. and MURRAY R. L. (1949) *Critical Mass Studies, Part III.* USAEC Report, K-343.

BIDINGER G. H., SCHUSKE C. L. and SMITH D. F. (1960) *Plutonium-Plexiglas Assemblies, Part II.* USAEC Report, RFP-190.

CARLSON B. G. (1955) *Solution of the Transport Equation by S_n Approximations.* Los Alamos Report, LA-1891.

CARLSON B. G. (1958) *The S_n Method and the SNG Codes.* Los Alamos Report, LAMS-2201.

CARLSON B. G. (1959) *Numerical Solution of Transient and Steady-State Neutron Transport Problems*. Los Alamos Report, LA-2260.

CARLSON B. G. and BELL G. I. (1958) *Proceedings of the Second International Conference on the Peaceful Uses of Atomic Energy, Geneva*, Paper P/2386. United Nations, N.Y.

CARLSON B. G., LEE C. and WORLTON J. (1959) *The DSN and TDC Neutron Transport Codes*. Los Alamos Report, LAMS-2346.

GOODWIN A. JR. and SCHUSKE C. L. (1958) *Plutonium-Graphite Assemblies*. USAEC Report, RFP-123.

GOODWIN A. JR. and SCHUSKE C. L. (1959) *Plutonium-Graphite Assemblies, Part II*. USAEC Report, RFP-158.

GWIN R. and MEE W. T. (1959) *Critical Assemblies of Uranium Metal*. USAEC Report Y-1248.

HANSEN G. E. (1958) *Proceedings of the Second International Conference on the Peaceful Uses of Atomic Energy, Geneva*, Paper P/592. United Nations, N.Y.

HANSEN G. E. and ROACH W. H. (1960) *Sixteen Group Cross-Sections*. Los Alamos Internal Report N-2-753 Revision 1.

JARVIS G. A., LINENBERGER G. A., ORNDOFF J. D. and PAXTON H. C. (1960) *Nucl. sci. Engng*. **8**, 525.

KLOVERSTROM F. A. (1957) *Spherical and Cylindrical Plutonium Critical Masses*. UCRL-4957.

PAXTON H. C. (1960) *Critical Data for Nuclear Safety Guidance*. Los Alamos Report LAMS-2415.

POND J. A. (1956) *Critical Geometries for Bare Cylinders*. USAEC Report, GAT-189.

ROACH W. H. (1960) *Nucl. sci. Engng*. **8**, 621.

SAFANOV G. (1952) *Notes on Multigroup Techniques for the Investigation of Neutron Diffusion*. TID-2503.

SCHUSKE C. L. and MORFITT J. W. (1949) *An Empirical Study of some Critical Mass Data*. USAEC Report Y-533.

SCHUSKE C. L., BIDINGER G. H., GOODWIN A. JR. and SMITH D. F. (1959) *Interaction of Two Metal Slabs of Plutonium in Plexiglas*. USAEC Report RFP-174.

SCHUSKE C. L., BIDINGER G. H., GOODWIN A. JR. and SMITH D. F. (1960) *Plutonium-Plexiglas Assemblies*. USAEC Report, RFP-178.

SCHUSKE C. L., SMITH D. F. and BELL C. L. (1960) *Plexiglas Reflected Assemblies of Plutonium*. USAEC Report RFP-213.

VOL.
15
1961

Reactor Science and Technology (Journal of Nuclear Energy Parts A/B) 1961, Vol. 15, pp. 130 to 139. Pergamon Press Ltd. Printed in Northern Ireland

LONG-TERM REACTIVITY CHANGES IN IRRADIATED THORIUM

D. C. C. GIBBS, M. GIBSON and W. A. COOPER*
Atomic Energy Establishment, Winfrith, Dorset

(*Received* 13 *December* 1960)

Abstract—An analysis is made of the GLEEP oscillator measurements on thorium cartridges before and after irradiation (1·44 neutrons/kilobarn maximum) in the NRX reactor at the A.E.C.L., Chalk River. A simple theoretical model for neutron behaviour is assumed and basic nuclear data are adjusted to enable this model to predict the GLEEP experimental results. It is found that if the neutron yield from ^{233}U, η_{33}, is lowered by approximately 1 per cent the best agreement between experiment and calculation is obtained, but the discrepancy obtained using 'world' nuclear data is not significant.

1. *Introduction*

THE work described in this paper appears to be the first to be published on the reactivity changes in thorium due to neutron irradiation. It is a part of a joint United Kingdom–Canada programme of experiments. The experiments provide a direct check on the validity of using 'world' nuclear data in conjunction with simple methods of calculation for the prediction of the ^{232}Th–^{233}U fuel cycle.

The reactivity effects of thorium cartridges were measured in the GLEEP reactor at Harwell using perturbation and oscillator techniques. Measurements were carried out before and after irradiation (up to 1·44 neutrons/kilobarn maximum) in the NRX reactor at the A.E.C.L., Chalk River. In the analysis of these measurements a model for neutron behaviour has been adopted similar to that used in an equivalent set of experiments on uranium, reported by ROSE, COOPER and TATTERSALL (1958). Effective cross-section data tabulated by WESTCOTT (1958) for ^{233}U and ^{235}U have been used in the analysis, and basic nuclear data for ^{233}U have been adjusted slightly to obtain agreement between theory and experiment.

The work, though similar to that on natural uranium, differs from it in detail in that no reactivity balance is struck between loss and gain of fissile isotopes and therefore the measured changes in absorption due to irradiation are much larger in the case of thorium.

PART I: EXPERIMENTAL WORK

Cylindrical thorium cartridges, canned in aluminium, were prepared by the A.E.C.L. at Chalk River with the dimensions listed in Table 1; these dimensions being consistent with a thorium density of 11·4 g cm^{-3}. The cartridges were fitted with cobalt monitors for the measurement of neutron irradiation dosage; the monitors were mounted in 1·92 cm long end-pieces and 0·25 cm deep fins of the aluminium canning material.

TABLE 1.—DIMENSIONS OF THE THORIUM CARTRIDGE

	Length (cm)	Diameter (cm)	Mass (g)
Thorium cartridge	15·24	3·45	1635
Canned thorium cartridge	19·08	3·86	1753

For irradiation in the NRX reactor, the canned cartridges were assembled in the demountable rod AGW No. 2, which was irradiated with four different cartridge loadings.

2. *Irradiation in NRX*

The cartridges were irradiated in fuel positions in the NRX lattice. Irradiations received (maximum 1·44 neutrons/kilobarn) were deduced by CRAIG (1959a) from the subsequent activities of cobalt monitors placed at the ends and on the fins of the canning, a correction being applied for initial flux depression in the cartridges. During irradiation, some of the cartridges were several times withdrawn and re-installed in different positions in the reactor so that it was necessary to calculate a 'mean over the irradiation' flux for each cartridge from its total neutron dosage and irradiation time from the NRX daily records. Neutron dosages and fluxes are tabulated in Table 2.

CRAIG (1959b) has quoted a value of 0·025 $\pm$ 0·002 for r in an empty fuel position in NRX, which corresponds to a value for β' of 0·026 $\pm$ 0·002. CRAIG's value has been derived by interpreting experimental reaction rates on the basis of the WESTCOTT (1958) spectrum, which assumes that the neutron density distribution in a well-moderated thermal reactor may be represented by a Maxwellian component and a $1/E$

* Present address: P. S. Group C.E.R.N., Geneva, Switzerland.

TABLE 2.—CARTRIDGE IRRADIATION DATA AND THE MEASURED CHANGES IN APPARENT CROSS SECTION

Cartridge reference number	Neutron dosage in NRX (CRAIG, 1959a) (ϕt) (n/kilobarn)	NRX neutron flux (mean over the irradiation) (n/cm²/sec)	Change in apparent cross section in GLEEP (X) (cm²)
64	0·0137*	$0·384 \times 10^{13}$	$-0·17 \pm 0·05$†
77	0·0178	0·501	$-0·32 \pm 0·05$†
70	0·0283	0·793	$-0·41 \pm 0·05$†
84	0·0359*	0·312	$-0·57 \pm 0·01$
71	0·0516	1·448	$-0·88 \pm 0·05$†
88	0·0651	0·564	$-1·03 \pm 0·05$†
81	0·0665	1·867	$-1·11 \pm 0·05$†
85	0·0846	0·733	$-1·34 \pm 0·05$†
76	0·133	0·884	$-2·07 \pm 0·01$
86	0·164	1·420	$-2·57 \pm 0·05$†
89	0·188*	0·268	$-2·79 \pm 0·01$
80	0·280	1·855	$-4·07 \pm 0·01$
75	0·399	1·224	$-5·40 \pm 0·1$ †
90	0·411	0·585	$-5·55 \pm 0·01$
68	0·609	1·869	$-7·50 \pm 0·13$†
83	0·729	0·861	$-8·51 \pm 0·01$
65	0·788	0·932	$-8·95 \pm 0·01$
92	0·805	1·148	$-9·46 \pm 0·01$
82	0·913	1·079	$-9·99 \pm 0·01$
93	1·076	1·533	$-11·18 \pm 0·01$
66	1·212	1·432	$-11·71 \pm 0·01$
69	1·271	1·503	$-11·93 \pm 0·01$
74	1·384	1·635	$-12·48 \pm 0·01$
87	1·401	1·720	$-12·84 \pm 0·01$
67	1·442	1·705	$-12·62 \pm 0·01$
	±1%		
	* ±5%		

* Larger error because no cobalt monitor was fitted at the base of the bottom cartridge (CRAIG, 1959a) in the demountable rod.
† Train measurements.

component. Since no measurements were available of the ratio of the initial mean flux through a thorium bar in NRX to that in the empty channel, a value of $0·573 \pm 0·006$ was adopted, equal to that measured in GLEEP (Section 4.1). Assuming no fine structure of the epithermal component of the flux this gave a mean β' in thorium of $0·045 \pm 0·003$, equivalent to a mean r value of $0·043 \pm 0·003$. This value was used in the analysis.

The moderator physical temperature, T_p, in NRX was taken as 43°C (CRAIG, 1959b). The neutron temperature, T_n, was deduced from the theoretical expression (COVEYOU, BATE and OSBORN, 1956)

$$T_n = T_p \left[1 + 0·76A\xi\beta' \sqrt{\frac{T_n}{T_p}}\right]$$

which CAMPBELL, FREEMANTLE and POOLE (1958) have shown to be consistent with certain experimental measurements in the D_2O moderated reactor DIMPLE. Using $T_p = 43$°C gave a value for T_n of 55°C; this value was used in the analysis.

3. *Measurements in* GLEEP

The GLEEP oscillator technique has been described by LITTLER (1956). Briefly, the sample is oscillated between the reactor centre and shield thus producing a modulation in pile power; the amplitude of the fundamental mode of this modulation, when compared with a standard boron measurement, is a measure of the apparent absorption cross section of the sample.

The GLEEP 'train' was also used for measurements. This is a danger coefficient system in which the rate of change of pile power caused by the sample remaining for a few minutes at the centre of the reactor and out of the reactor, is used as a measure of its apparent absorption cross section.

Using these facilities the apparent absorption cross-section of each cartridge relative to a standard thorium

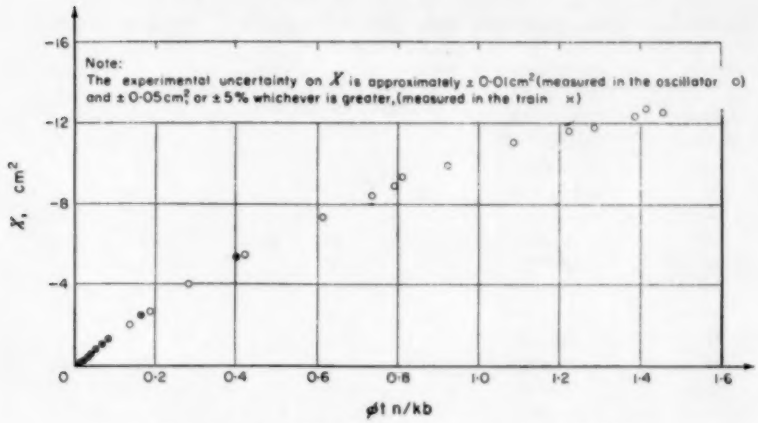

FIG. 1.—Change in cartridge apparent cross section in GLEEP as a function of cartridge irradiation in NRX.

cartridge was measured in GLEEP, before and after irradiation in the NRX reactor. The measurements were made over a number of years, initially in the train but later in the oscillator because the more highly irradiated cartridges required better shielding which was available only on the oscillator facility. The train and oscillator measurements lay on two smooth curves when plotted against irradiation, which were consistent within the accuracy of the calibrations. A few measurements were carried out in both the train and oscillator facilities which enabled normalization of the train measurements to values which would have been measured in the oscillator. The changes in apparent cross section X cm², due to irradiation, are plotted as a function of cartridge irradiation in Fig. 1 (a negative sign conventionally indicating a gain in reactivity in GLEEP). The gain in reactivity due to irradiation arises predominantly from the formation of fissile ^{233}U.

The experimental error in X measured in the oscillator is approximately $\pm 0{\cdot}01$ cm²; this being roughly equivalent to 0·002 barns per initial thorium atom ('bita'). The experimental error in the train measurement of X is approximately $\pm 0{\cdot}05$ cm² (or ± 5 per cent whichever is the greater).

4. *Calibration experiments in* GLEEP

In order to interpret the GLEEP oscillator measurements a number of subsidiary calibration experiments were required. These are described below.

4.1. *Initial flux depression.* The ratio of the mean neutron flux F_e in the unirradiated canned cartridge, to that in the empty GLEEP oscillator channel F_0, was determined by activating copper foils in a sectionalized thorium bar and in a corresponding rod of graphite. The technique adopted was similar to that described by LITTLER (1956).

Since copper is not a '$1/v$ absorber' in the epithermal region it was necessary to correct for the different neutron spectra in thorium and graphite. This was done assuming:

(a) 2200m/sec absorption cross section of copper = 4·0 barns (ROSE, COOPER and TATTERSALL, 1958)

(b) 'above $1/v$' resonance integral of copper = 1·2 barns (ROSE, COOPER and TATTERSALL, 1958)

It should be noted that this flux is total neutron density multiplied by a standard velocity, as defined by WESTCOTT (1958).

Allowing for the flux rise in graphite relative to air, it was found that

$$\frac{F_e}{F_0} = 0{\cdot}573 \pm 0{\cdot}006.$$

4.2. *Flux perturbation.* The flux perturbation in GLEEP $\frac{\Delta F_e}{F_e}$ due to additional thermal absorber growing into a cartridge with irradiation, may be expressed by the relationship:

$$\frac{\Delta F_e}{F_e} = \text{function}\left[\frac{\sum_i \Delta N_i \sigma_{iM} + \sum_p \Delta N_p \sigma_{pM}}{\sum_e}\right]_{\text{GLEEP}} \quad (4.2.1)$$

To determine $\frac{\Delta F_e}{F_e}$ as a function of added absorber, flux depression experiments were carried out on hot-pressed thorium bars, made to the dimensions quoted in Table 1 and containing boron to simulate the effects of added absorber due to irradiation, i.e.

$$\left[\sum_i \Delta N_i \sigma_{iM} + \sum_p \Delta N_p \sigma_{pM}\right]$$

is simulated by

$$[\Delta N_{02} \sigma_{02M} + \Delta N_B \sigma_{BM}].$$

TABLE 3.—DETAILS OF THE BORON-LOADED, HOT-PRESSED THORIUM BARS

Nominal boron loadings (p.p.m. (by weight))	Chemical analysis results (p.p.m. (by weight))	Mass (g)
0	—	1575
80	—*	1600
160	—*	1550
240	220	1435
320	308 ±5 to 10%	1446

* Bar crumbled and was destroyed before analysis. Nominal loading assumed with a probable error of ±10 per cent.

The uniformity of the boron loading was confirmed by comparing absorption cross-section measurements of the individual sections of a bar. Five bars were made, each in four sections to allow the insertions of copper foils; details of the bars are given in Table 3.

Two independent determinations of the flux perturbation were made using the following techniques:

(i) *Activation technique*

The mean flux in each bar was determined relative to that in the unloaded bar, by activation measurements with copper foils (as in Section 4.1). These experiments provide the flux perturbation in each bar, i.e. the difference in flux depression due to added absorber. The results obtained are given in Table 4 and Fig. 2.

(ii) *Reactivity technique*

The difference in apparent absorption cross section (or reaction rate) between each of the loaded bars and a standard bar was measured in the GLEEP oscillator, thus providing the change in reaction rate due to the added boron. It can be shown that this change satisfies the following equation (LITTLER, 1956);

$$X\frac{F_0}{F_e}=\left[1+\frac{\Delta F_e}{F_e}\right][\Delta N_{02}\sigma_{02}+\Delta N_B\sigma_B]+\frac{\Delta F_e}{F_e}\sum_e \quad (4.2.2)$$

From the above equation $\frac{\Delta F_e}{F_e}$ was deduced for each bar, the results being given in Table 4 and Fig. 2. The added thermal absorber (Table 4) was calculated for each bar from the boron content and the difference in the mass of thorium present from that in the unloaded bar.

The experimental values, within their accuracy, may be fitted by a straight line of the form:

$$\frac{\Delta F_e}{F_e}=-\alpha\left[\frac{\Delta N_{02}\sigma_{02M}+\Delta N_B\sigma_{BM}}{\sum_e}\right] \quad (4.2.3)$$

The best straight line through the points is characterized by $\alpha = 0{\cdot}30 \pm 0{\cdot}03$. This value together with equation (4.2.1) enables the flux perturbation in a thorium cartridge in GLEEP to be calculated for any absorber content.

4.3. *Neutron spectrum and temperature.* The epithermal spectrum parameter r has been measured in the empty GLEEP oscillator channel by activation measurements of the cadmium ratio of thin gold foils. It was found that $r = 0{\cdot}042 \pm 0{\cdot}004$ (ROSE, COOPER and TATTERSALL, 1958) which is equivalent to $\beta' = 0{\cdot}045 \pm 0{\cdot}004$. Using the flux depression $F_e/F_0 = 0{\cdot}573 \pm 0{\cdot}006$ of Section 4.1 and assuming no epithermal fine structure gave $\beta' = 0{\cdot}079 \pm 0{\cdot}008$ in the

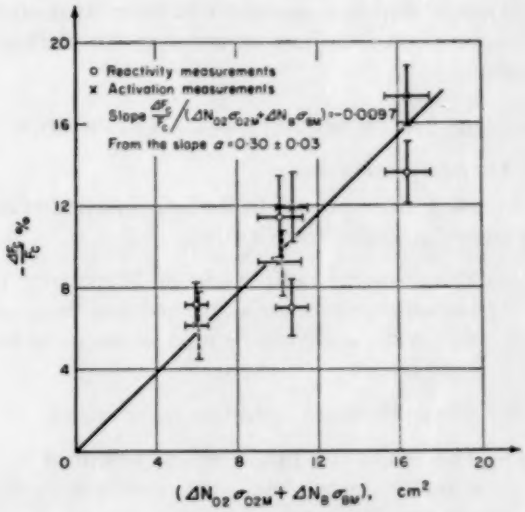

FIG. 2.—Measured flux perturbation in a thorium cartridge in GLEEP as a function of added thermal absorber.

TABLE 4.—THE EXPERIMENTAL FLUX PERTURBATIONS IN GLEEP

Bar (p.p.m.)	X (cm²)	$\Delta N_{02}\sigma_{02M}+\Delta N_B\sigma_{BM}$ (cm²)	$\frac{\Delta F_e}{F_e}$ (activation) (%)	$\frac{\Delta F_e}{F_e}$ (reactivity) (%)
80	2·02 ± ·01	5·96 ± 0·55	−6·1 ± 1·7	−7·2 ± 1·1
160	3·24 ± ·01	10·1 ± 1·1	−9·2 ± 1·6	−11·4 ± 2·0
220	4·62 ± ·02	10·7 ± 0·8	−11·9 ± 1·7	−7·0 ± 1·4
308	5·92 ± ·01	16·4 ± 1·1	−17·3 ± 1·5	−13·6 ± 1·5

TABLE 5.—HEAVY ISOTOPE NUCLEAR DATA

	σ_0(abs) (barns)	σ_0 (fiss) (barns)	$\sigma_{r.i.}$ (barns)	λ (sec^{-1})	η_0
^{233}Th	7·56‡	—	7·6*	—	—
^{233}Pa	80**	—	700**	0·293 × 10^{-6}††	—
^{234}Pa†	—	—	—	28·7 × 10^{-6}††	—
^{233}U	581‡	527‡	—	—	2·28‡
^{234}U	95**	—	700**	—	—
^{235}U	694‡	582‡	—	—	2·07‡

* The effective resonance integral for these cartridges (Table 1) was calculated from the expression

$$\left(\int \sigma \frac{dE}{E}\right)_{eff} = A + B(S/M)^{\frac{1}{2}}$$

where $A = 4{\cdot}1 \pm 0{\cdot}3$, $B = 21{\cdot}1 \pm 1{\cdot}2$ } PETTUS (1959)

† σ_0 and $\sigma_{r.i.}$ for ^{234}Pa have been taken as zero.
‡ HUGHES and SCHWARTZ (1958).
Allowance was made for the $1/v$ contribution which is included in this expression.
** HALPERIN and STOUGHTON (1958).
†† *Chart of the Nuclides* (1956).

thorium cartridge or $r = 0{\cdot}073 \pm 0{\cdot}007$. This value was used in the analysis.

The neutron temperature in the empty oscillator channel, as determined by ROSE, COOPER and TATTERSALL (1958) from oscillator measurements on ^{113}Cd, ^{149}Sm, and Gd is 70 ± 10°C, i.e. 45°C above the physical temperature of the surrounding moderator. This temperature was assumed to be the mean neutron temperature in a thorium cartridge in the oscillator channel.

PART II: INTERPRETATION OF EXPERIMENTS

5. *Assumptions and data*

5.1. *Basic assumptions.* In the interpretation of the experimental results it was assumed that:

(i) There was no radial variation of spectrum or isotopic composition in the rod and the mean flux in the rod could be used to determine the reaction rate.

(ii) The epithermal flux had no fine structure.

(iii) The irradiation flux could be described by a constant mean 'over the irradiation' flux (Section 2).

(iv) The neutron spectrum was not a function of neutron dosage.

5.2. *The thorium chain.* Under neutron bombardment, natural thorium (virtually 100 per cent ^{232}Th) gives rise to the following chain of reactions:

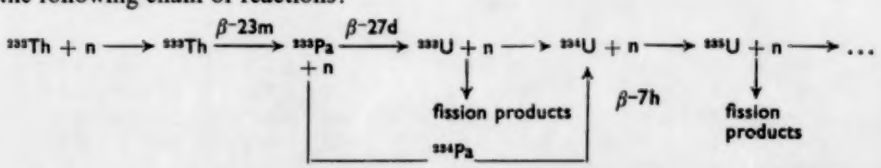

During irradiation therefore, short-lived ^{233}Th and ^{233}Pa produced in a thorium cartridge decay with β^- emission to form uranium isotopes. Some of the ^{233}Pa undergoes radiative capture forming ^{234}Pa, which decays with a short half-life to ^{234}U. Of the uranium isotopes formed, ^{233}U and ^{235}U undergo fission, producing fission product poisons. The uranium isotopes and fission product poisons contribute to the reactivity changes measured in GLEEP. The cross sections of the heavy isotopes and other nuclear data used in the analysis are given in Table 5.

Cross sections and fission yields of the fission product poisons are taken mainly from WALKER (1956) and PATTENDEN (1959).

5.3. *Isotopic composition of irradiated thorium.* The following differential equations were used to describe the changes in isotopic composition of a thorium cartridge during irradiation in NRX:

$$\frac{dN_{02}}{d(\phi t)} = -N_{02}\sigma_{02} \qquad (5.3.1)$$

$$\frac{dN_{13}}{d(\phi t)} = N_{02}\sigma_{02} - N_{13}\sigma_{13} - N_{13}\lambda_{13}/\phi \qquad (5.3.2)$$

$$\frac{dN_{14}}{d(\phi t)} = N_{13}\sigma_{13} - N_{14}\lambda_{14}/\phi - N_{14}\sigma_{14} \qquad (5.3.3)$$

$$\frac{dN_{23}}{d(\phi t)} = N_{13}\lambda_{13}/\phi - N_{23}\sigma_{23} \qquad (5.3.4)$$

$$\frac{dN_{24}}{d(\phi t)} = \alpha'_{23}N_{23}\sigma_{23} - N_{24}\sigma_{24} + N_{14}\lambda_{14}/\phi \qquad (5.3.5)$$

$$\frac{dN_{25}}{d(\phi t)} = N_{24}\sigma_{24} - N_{25}\sigma_{25} \qquad (5.3.6)$$

$$\alpha' = \frac{\sigma - \sigma_f}{\sigma}. \qquad (5.3.7)$$

The ^{233}Th stage is neglected in these equations because of its short half-life (23 minutes); the absorption cross section of ^{234}Pa is taken as zero.

The equations have been programmed for the Ferranti Mercury Computer (Winfrith programme number 656). The programme calculates the number of atoms of the isotopes of the heavy elements per original ^{232}Th atom, together with the macroscopic fission cross sections of ^{233}U and ^{235}U, as functions of irradiation.

6. *Analysis*

6.1. *The* GLEEP *equation.* The build-up of heavy isotopes and fission product poisons in an irradiated thorium cartridge causes a change in the apparent absorption cross section, as measured in GLEEP, and a change in the mean flux through the bar relative to that in the GLEEP oscillator channel. These effects may be described by the following equation, derived from (LITTLER, 1956).

$$X\frac{F_0}{F_c} - \left(1 + \frac{\Delta F_c}{F_c}\right)\sum_p \Delta N_p\sigma_p - \frac{\Delta F_c}{F_c}\Sigma_c = \left(1 + \frac{\Delta F_c}{F_c}\right) \times \sum_i \Delta N_i\sigma_i(1 - W\varepsilon\eta_i) \qquad (6.1.1)$$

The calculated value of ε is 1·005, and LITTLER has quoted a calculated value for W of $0{\cdot}88 \pm 0{\cdot}01$ (LITTLER, 1956).

The left-hand side of (6.1.1) represents the measured change in cartridge apparent cross section allowing for:

(a) the apparent cross section of $\sum_p \Delta N_p$ atoms of fission poisons in the perturbed GLEEP flux $[1 + (\Delta F_c/F_c)]$

and

(b) the change in apparent cross section of the thorium cartridge itself due to the GLEEP flux perturbation $\frac{\Delta F_c}{F_c}$.

Of these two effects the second is much more important; for example, at $\phi t = 1{\cdot}0$ n/kb the value of $\frac{\Delta F_c}{F_c}\Sigma_c$ is $-1{\cdot}16$ bita whilst that of $\left(1 + \frac{\Delta F_c}{F_c}\right)\sum_p \Delta N_p\sigma_p$ is $+0{\cdot}12$ bita. This is in contrast to the natural uranium case, since in thorium there is a much larger increase in thermal absorption with irradiation, causing a larger flux perturbation in GLEEP.

In Fig. 3 the value of $X\frac{F_0}{F_c}$ for each cartridge is plotted as a function of NRX neutron dosage.

The value of $\frac{\Delta F_c}{F_c}$ in GLEEP was calculated for each individual cartridge from the expression of Section 4.2 using isotopic concentrations calculated for the NRX spectrum and flux (Section 2) in which the cartridge was irradiated. The formation of ^{233}U accounts for the majority of the change in thermal absorption due to irradiation.

The build-up of fission product poisons, ΔN_p, were also calculated for each cartridge in detail and multiplied by σ_p, the microscopic cross sections appropriate to the spectrum in a thorium cartridge in GLEEP (Section 4.3). Allowance was made for the decay of ^{147}Pm, ^{149}Pm, ^{151}Sm and ^{155}Eu during the period between cartridge removal from the NRX reactor and measurement in the GLEEP oscillator—the main effect is the build-up of ^{149}Sm from ^{149}Pm.

Allowance was made for the decay of ^{233}Pa to ^{233}U during the period between cartridge removal from the NRX reactor and measurement in the GLEEP oscillator; the correction strictly being dependent on the

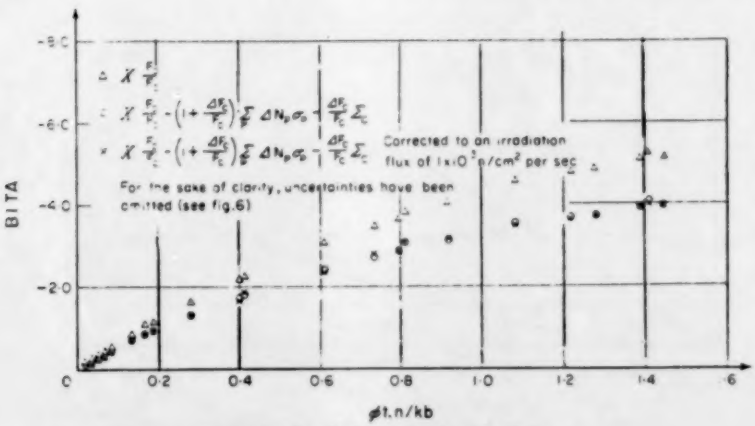

FIG. 3.—The GLEEP unpoisoned values.

NRX flux during the last few months of irradiation. This hold-up of ^{233}U is relatively more important at low irradiation; for example in a flux of $1{\cdot}0 \times 10^{13}$ n/cm²/sec, the hold-up of ^{233}U at $\phi t = 0{\cdot}5$ n/kb is 8·5 per cent of its final concentration and at $\phi t = 1{\cdot}5$ n/kb the percentage is only 3·8.

From these calculations the left-hand side of equation (6.1.1) was evaluated for each individual cartridge; these so called 'GLEEP unpoisoned values' are plotted together with $X\frac{F_0}{F_e}$ in Fig. 3.

The right-hand side of equation (6.1.1) represents the change in cartridge apparent cross section expected in GLEEP due to $\sum_i \Delta N_i$ additional atoms of the heavy isotopes in the perturbed GLEEP flux $\left(1+\frac{\Delta F_e}{F_e}\right)$. Since some of the isotopic concentrations are dependent on irradiation flux, the unpoisoned values (for various cartridges) cannot be expected to fall exactly on a smooth curve. Each cartridge was therefore corrected to a standard irradiation flux of $1{\cdot}0 \times 10^{13}$ n/cm²/sec using the following correction;

$$\left[\left(1+\frac{\Delta F_e}{F_e}\right)_A \sum_i \Delta N_{Ai} - \left(1+\frac{\Delta F_e}{F_e}\right)_B \sum_i \Delta N_{Bi}\right] \times \left[\sigma_i(1 - W\varepsilon\eta_i)\right]$$

where:

suffix A refers to values appropriate to an NRX flux of $1{\cdot}0 \times 10^{13}$ n/cm²/sec,

suffix B refers to values appropriate to actual irradiation fluxes (Table 2).

The effect of different irradiation fluxes is small.

Strictly a correction should also be applied for the fact that the cartridges were irradiated at different neutron temperatures but no NRX moderator temperature distributions were available so it has been assumed that the irradiation moderator physical temperature for each cartridge was 43°C (Section 2). This is a reasonable assumption because the seasonal variation in the NRX inlet and outlet temperatures is approximately ±6°C which roughly corresponds to the temperature variation along a channel. The GLEEP measured change in apparent cross section is appreciably insensitive to an NRX temperature variation of this order.

Figure 3 shows the final unpoisoned values corrected to an irradiation flux of $1{\cdot}0 \times 10^{13}$ n/cm²/sec. There is still some scatter on the points but it is less than the experimental errors (see Section 6.3).

The right-hand side of equation (6.1.1) was then evaluated for the heavy elements, using a flux of $1{\cdot}0 \times 10^{13}$ n/cm²/sec and data from Table 5 and Sections 2, 4 and 5.

The instantaneous isotopic concentrations in the standard NRX flux are plotted against irradiation in Fig. 4 and $\frac{\Delta F_e}{F_e}$ is shown as a function of irradiation in Fig. 5.

6.2. *Uncertainties.* Uncertainties have been assessed on the unpoisoned values allowing:

(a) ±0·01 cm² in oscillator measurements of change in apparent cross section (Table 2), and ±0·05 cm² (or ±5 per cent, whichever is the greater) in train measurements.

(b) ±1 per cent in the initial flux depression (Section 4.1).

(c) ±10 per cent in α (Section 4.2).

(d) ±1 per cent in cartridge irradiation dosage, except for cartridges 64, 84 and 89, which were not fitted with end cobalt monitors, where the uncertainty is ±5 per cent (see Table 2).

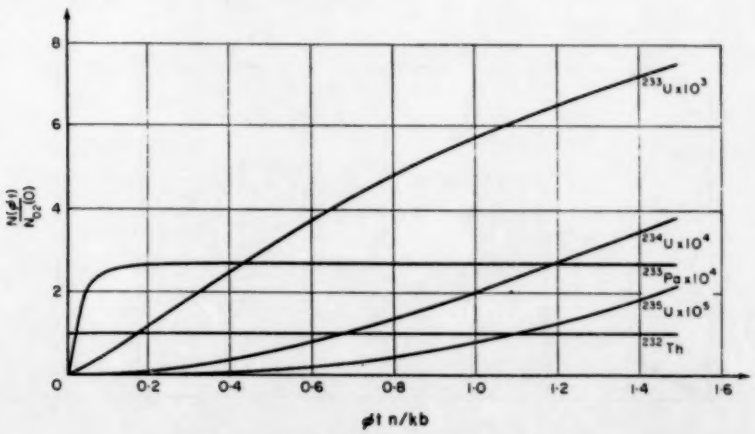

FIG. 4.—Isotopic build-up in a thorium cartridge in the NRX flux of $1{\cdot}0 \times 10^{13}$ n/cm²/sec.

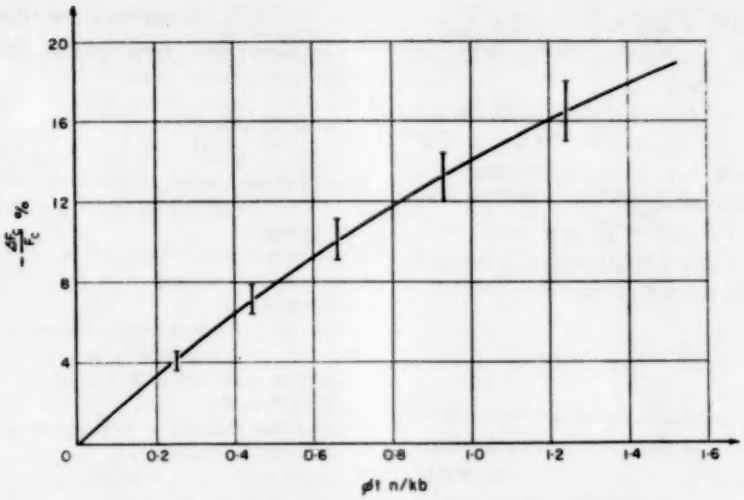

FIG. 5.—Flux perturbation in a thorium cartridge in GLEEP as a function of irradiation (appropriate to the NRX flux of $1{\cdot}0 \times 10^{13}$ n/cm²/sec).

(e) $\pm 10°C$ in the GLEEP neutron temperature (Section 4.3).

On the predicted curve the uncertainties considered were:

(a) ± 10 per cent in α (Section 4.2).
(b) ± 1 per cent in W (Section 6.1).
(c) $\pm 10°C$ in the GLEEP neutron temperature (Section 4.3).

The effect of these uncertainties is shown in Fig. 6.

Uncertainties in nuclear data have been neglected but η_{23} has been treated as a variable parameter so that the prediction could be adjusted to agree with experiment.

6.3. *Comparison of prediction and experiment.* Fig. 6 compares the GLEEP unpoisoned values with predicted curves for two values of η_{23}, including the present HUGHES and SCHWARTZ (1958) value of 2·28. The neutron yield from ^{233}U, η_{23}, has been chosen as the variable parameter because of the sensitivity of this problem to it. The unpoisoned values, while not following exactly the shape of the 2200 m/sec $\eta_{23} = 2{\cdot}28$ (HUGHES and SCHWARTZ, 1958) predicted curve, are in agreement within the experimental errors.

Figure 6, however, shows that agreement between these experimental measurements and prediction based on this neutron model and basic nuclear data, is better if the 2200 m/sec value for η_{23} is reduced by approximately 1 per cent to 2·26. The uncertainty on this

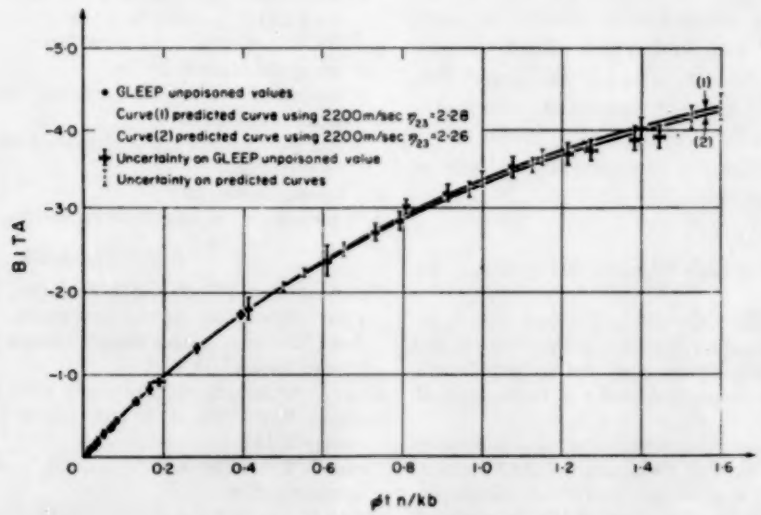

FIG. 6.—The GLEEP unpoisoned values compared with predicted curves.

correlated value is $\pm 0{\cdot}02$, which means that it agrees with the HUGHES and SCHWARTZ (1958) value of $2{\cdot}28 \pm 0{\cdot}02$ within the errors.

It should also be noted that if uncertainties on the basic nuclear data (in particular the ^{232}Th and ^{233}U absorption cross sections) are taken into account, the uncertainties on the calculated curves (Fig. 6) would be increased by approximately 50 per cent while those on the points would not be appreciably altered. This would not alter the overall goodness of fit.

7. *Conclusions*

This analysis of GLEEP oscillator measurements on thorium (irradiated to 1·44 neutrons/kilobarn maximum) shows that these measurements of the reactivity changes due to the destruction of ^{232}Th and formation of the fissile uranium isotopes ^{233}U and ^{235}U and fission products, may be predicted within the errors when using basic nuclear data and a relatively simple model for neutron behaviour.

Although there is overall general agreement between the experimental measurements and calculation when using basic nuclear data and a simple model for neutron behaviour, it would appear from this correlation that the reactivity changes in the ^{232}Th–^{233}U system would be more accurately predicted by this model if the 2200 m/sec value for η_{23} were reduced by approximately 1 per cent to $2{\cdot}26 \pm 0{\cdot}02$ which agrees with the HUGHES and SCHWARTZ (1958) value of $2{\cdot}28 \pm 0{\cdot}02$ within the errors.

8. *Future work*

Chemical and mass spectrometric analyses of some of the irradiated fuel used in this experiment are now being performed at the A.E.C.L., Chalk River. This work will yield the effective cross sections which give the correct isotopic concentrations. When it is completed it is our intention to repeat the analysis of the GLEEP measurements.

Acknowledgments—The authors wish to acknowledge the following:

The A.E.C.L., Chalk River, Canada, in particular MR. A. G. WARD and DR. D. S. CRAIG for their part in the planning and execution of the experimental programme and for their helpful assistance and advice in the interpretation and presentation of the results.

DR. H. ROSE, Harwell, for much helpful advice and discussion.

MESSRS. R. FORDHAM and P. J. ORAM and the GLEEP staff at Harwell, for carrying out some of the GLEEP measurements.

MR. D. H. ROWE, Harwell, for performing the chemical analysis of the boron-loaded thorium bars.

NOMENCLATURE

r parameter defining the proportion of neutron density in the epithermal neutron group

$$\left[r = \frac{(\mu\pi)^{\frac{1}{2}}\beta'}{4(1+\beta')}\right]$$

β' ratio of the epithermal to thermal neutron intensity
μ effective cut-off energy of the epithermal neutron density distribution
T_p moderator physical temperature
T_n neutron temperature
A atomic weight
ξ average logarithmic energy decrement
X change in the apparent absorption cross section of a thorium cartridge with irradiation as measured by the GLEEP oscillator
F_c mean flux through a thorium cartridge in the GLEEP oscillator 'in-position'
ΔF_c change in F_c due to additional thermal absorber
F_0 mean flux at the 'in-position' of the empty GLEEP oscillator channel
N number of atoms of type denoted by suffix
σ microscopic absorption cross section of isotope denoted by suffix
σ_M microscopic Maxwellian absorption cross section of isotope denoted by suffix
σ_f microscopic fission cross section of isotope denoted by suffix
λ radioactive decay constant of isotope denoted by suffix
η neutron yield from fission of the isotope denoted by suffix.
suffix 02 ^{232}Th
13 ^{233}Pa
14 ^{234}Pa
23 ^{233}U
24 ^{234}U
25 ^{235}U
i collectively denotes all the above heavy isotopes
p collectively denotes fission product poisons
B boron
0 2200 m/sec value
Σ_c thermal absorption cross section of a thorium cartridge in the GLEEP oscillator 'in-position' before irradiation
ϕ NRX 'mean over irradiation' flux
ϕt integrated neutron dosage
W importance of a fission neutron relative to a thermal neutron in GLEEP
ε fast fission factor for a thorium cartridge in the GLEEP oscillator channel
σ_{r,i_c} resonance integral
S/M surface area to mass ratio for thorium cartridge.

REFERENCES

CAMPBELL C. G., FREEMANTLE R. G. and POOLE M. J. (1958) *Proceedings of the Second International Conference on the Peaceful Uses of Atomic Energy, Geneva*, Vol. 16, P/10, 233. United Nations, N.Y.

Chart of the Nuclides (1956) General Electric, U.S.A.

COVEYOU R. R., BATE R. R. and OSBORN R. K. (1956) *J. Nucl. Energy* **2**, 153.

CRAIG D. S. (1959a) A.E.C.L., Chalk River, Canada. Private communication.

CRAIG D. S. (1959b) A.E.C.L., Chalk River, Canada. Private communication.

HALPERIN J. and STOUGHTON R. W. (1958) *Proceedings of the Second International Conference on the Peaceful Uses of Atomic Energy, Geneva*, Vol. 16, P/1072, 64. United Nations, N.Y.

HUGHES D. J. and SCHWARTZ R. B. (1958) *Neutron Cross-Sections* (2nd edition) BNL–325.

LITTLER D. J. (1956) *Measurements of the Change in Cross-Section of Irradiated Uranium Made by Modulating the Power of a Nuclear Reactor* A.E.R.E. RS/R. 2092.

PATTENDEN N. J. (1959) *Fission Product Poisoning Data.* O.R.N.L.–2778.

PETTUS W. G. (1959) *Geometric and Temperature Effects in Thorium Resonance Capture.* B.A.W.–T.M.–203.

ROSE H., COOPER W. A. and TATTERSALL R. B. (1958) *Proceedings of the Second International Conference on the Peaceful Uses of Atomic Energy, Geneva*, Vol. 16, P/14, 34. United Nations, N.Y.

WALKER W. H. (1956) *Fission Products Accumulation.* C.R.R.P. –634.

WESTCOTT C. H. (1958 Revision) *Effective Cross-section Values for Well Moderated Thermal Reactor Spectra.* C.R.R.P.–787.

VOL. 15 1961

Reactor Science and Technology (Journal of Nuclear Energy Parts A/B) 1961, Vol. 15, pp. 140 to 159. Pergamon Press Ltd. Printed in Northern Ireland

IRRADIATION OF URANIUM-METAL AND URANIUM-OXIDE FUEL PINS TO HIGH BURN-UP AT HIGH TEMPERATURE

L. R. BLAKE
Dounreay Experimental Reactor Establishment, Caithness, Scotland*

(*Received* 28 *June* 1961)

Abstract—Fuel pins have been tested in Dounreay Materials Testing Reactor under onerous fast-reactor type irradiation conditions and have achieved a high burn-up at higher temperature and rating than heretofore. The fuel pins are representative of a power fast reactor but scaled down proportionally to reduce the diameter to 0·122 in. o.d., which enables a high power density of 550 W/g to be used, so reducing irradiation time to 17 days per 1 per cent burn-up.

Uranium-metal was irradiated to 4·75 per cent burn-up at 700°C centre-temperature, and uranium-oxide to 5·3 per cent burn-up at 1600°C centre-temperature, in 0·011 in. thick cans of Nimonic 80 at 500°C fuel surface-temperature approximately. The pins survived with no measurable distortion. The results appear to confirm the author's theory of burn-up and his proposals to achieve high burn-up (BLAKE, 1961) by introducing about 30 per cent void space in the fuel and containing it in a strong can. Theory suggests that the pins are capable of three times this burn-up, and this is partly confirmed by post-irradiation, high-temperature tests.

Achieving high burn-up at high temperature is the key development problem of the fast reactor: 3 per cent burn-up under similar temperature conditions, should enable economic electrical power to be generated in the U.K.

After one abortive attempt, a rig was developed to test the fuel pins in D.M.T.R. at high power density under controlled temperature conditions. It should now be straightforward to develop this rig further to test four or five 1 ft long fuel pins per rig at up to 1 kW/g rating, with temperatures and specific power indicated to within ±5 per cent error; can failure would also be indicated. A technique has also been established of X-raying the complete rig and returning it to the reactor, so enabling fuel swelling and distortion to be measured and plotted during the irradiation.

1. INTRODUCTION

ECONOMIC power from fast reactors requires a fuel element capable of a high rating, a high centre-temperature and a high burn-up, as indicated in Table 1. Moreover, fuel element swelling must be negligible, with no chance of can failure leading to blockage of a coolant passage. The author previously examined the problems of achieving high burn-up in fast reactors (BLAKE, 1961) and concluded that:

(i) With metal fuel, fission product gas accumulation is chiefly responsible for irradiation swelling. A method was given of predicting irradiation behaviour of metal fuel, both canned and uncanned, which agreed well with test results. It was suggested that high burn-up at high temperature and rating is most likely to be achieved by:

(a) providing appreciable void-space within the can (25–35 per cent of the can internal volume) to accommodate fuel swelling;

(b) introducing the space in a way that mechanically weakens the fuel, so that the space is essentially available for fission-product gas that prevents overstressing the can by fuel thermal-expansion and that ensures a good thermal-bond between fuel and can;

(c) employing a strong can.

(ii) With oxide-fuel, high fuel-density is not necessary and it is again desirable to include substantial void-space, some within but most immediately adjacent to the fuel and at coolant temperature. Again a strong can is essential.

(iii) With cermet fuel, the best approach would appear to be to use 15–20 v/o oxide ($PuO_2 + UO_2$) in a uranium-metal matrix having 25 per cent void, again employing a strong can.

Methods of applying these principles in fuel-pin design are illustrated in Fig. 3. Estimates of likely maximum and safe operational burn-up, assuming about 30 per cent of the can internal volume for void-space and a strong can of thickness-to-diameter ratio of about 10 per cent, are also added to Table 1. It is seen that the burn-up should be raised well above the level for economic power production; this should enable maximum operational burn-up to be limited

* Present address: Brush Electrical Engineering Co., Loughborough, Leics.

TABLE 1.—TYPICAL FUEL IRRADIATION CONDITIONS IN A POWER FAST REACTOR

		Uranium-plutonium metal	Uranium-plutonium oxide	
Power rating	W/g	50–150	80–240	
Centre temperature	°C	650–750	1200	2000
Burn-up				
—minimum for economic power	%	2–4	5–10	4–8
—likely safe maximum with conventional fuel elements	%	½–1	2–5	1½–3
Predicted burn-up with voided-fuel, strong can principle				
—maximum to failure	%	10–20	30–50	20–30
—safe core average	%	5–7	10–15	8–12

to well below the failure point to the advantage of reactor safety. If these results are achievable there is little doubt that electrical power of 0·3–0·4 d/kWh should be achievable from a 250 MW power fast reactor.

Unless testing is to be drawn out over many years, irradiation to 10 per cent burn-up and over demands power densities even greater than fast reactor practice. About 500 W/g was thought best to aim for, giving 1 per cent burn-up in 20 days and about 10 per cent burn-up in a year, allowing for the reactor load-factor. With metal-fuel, the temperatures required are 700 ± 100°C centre and 500 ± 100°C surface, which leads to a small pin diameter of 0·1 in. It is shown in Table 2 that, among the fast reactors, 500 W/g could be achieved only in Enrico Fermi. In Dounreay Fast Reactor it is not possible, even with fuel of maximum enrichment at the core centre, but apart from this D.F.R. is unlikely to be in full-power operation for some years. There was no alternative, therefore, but to test in Dounreay Materials Testing Reactor, despite the difficulty of accurately establishing the appropriate operating temperature conditions, particularly of dropping some 500°C from fuel-surface to heavy-water coolant. Fortunately the high rating and small fuel-pin diameter makes radial flux-depression acceptable (mean-flux/surface-flux ratio is about 0·66).

No prior experience was available of thermal-reactor test-rigs for fuel testing under fast reactor conditions of high rating and high temperature, so it was necessary to develop the rig as well as the fuel-pin.

2. DESCRIPTION OF RIG

The main problem is to design a container for the fuel pin, cooled by the reactor heavy water coolant, which would:

(i) freely suspend the fuel pin, with no external support that would assist it to restrain the fuel pressure;

TABLE 2.—IRRADIATION CONDITIONS IN VARIOUS REACTORS

			D.M.T.R.	D.F.R.	EBR-II	Enrico Fermi
Reactor thermal power		MW	7	60	62·5	300
Reactor coolant temp.	inlet	°C	28	200	360	288
	outlet	°C	32	350	480	427
Reactor-fuel enrichment		%	—	30	49	26
Fuel power density	core average	W / g U5 + U8	—	70	155	172
	core centre		—	126	236	310
	core centre with 93% enriched fuel		1000*	354	430	1040
Time to 10% burn-up at full power and 0·7 load-factor, 93% enr. fuel at core centre		days	140	400	330	130

* In appropriate rig with average flux in fuel approximately 15 per cent of unperturbed flux.

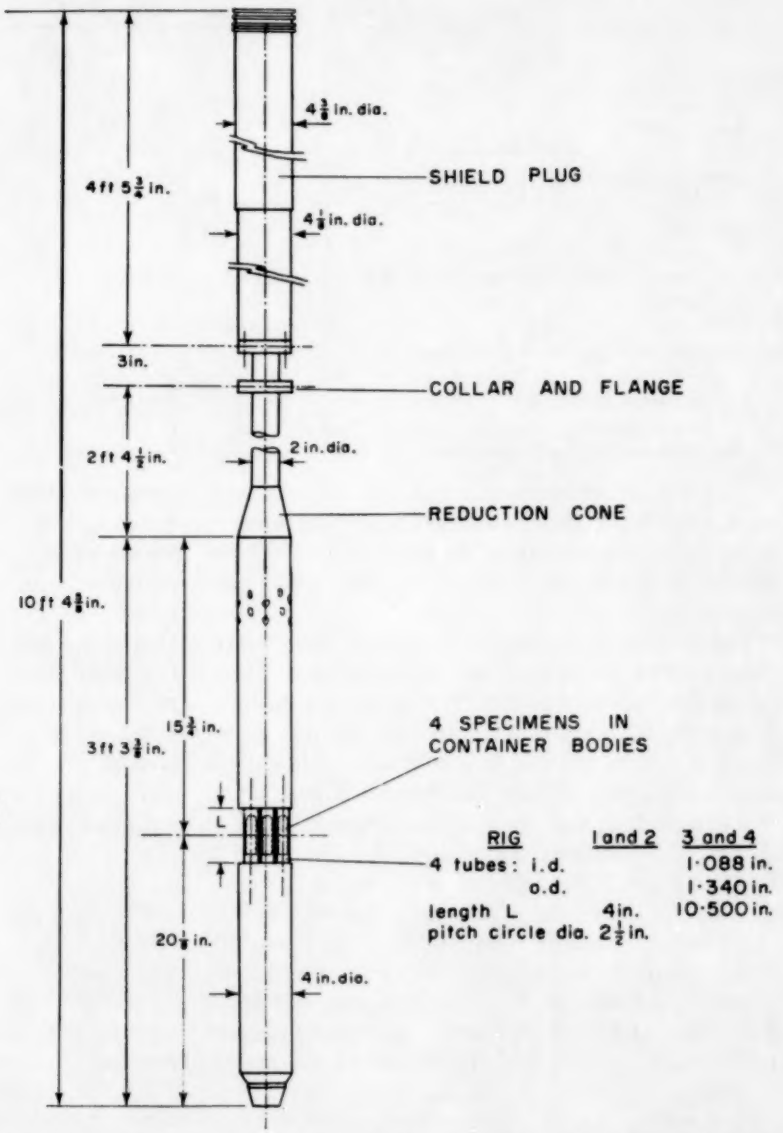

FIG. 1.—Dounreay Materials Testing Reactor fuel-element replacement structure to support fuel capsules and their containers.

(ii) accurately drop the 470–570°C between the fuel-surface and the 30°C reactor-coolant;

(iii) measure fuel-pin power, as flux and power predictions could originally be made only to ±50 per cent;

(iv) continuously indicate fuel-temperature and when fuel-pin failure occurs;

(v) satisfy D.M.T.R. safety requirements, especially since it is required to test the fuel pin to destruction;

(vi) enable good-contrast X-ray photographs of the fuel pin to be taken through the container, even after irradiation when the fuel is highly gamma-active.

The only suitable high-strength canning-materials available were stainless steel or a Nimonic-alloy of Messrs. Henry Wiggin, which are unfortunately incompatible with uranium-metal above 740°C when a U-Ni or U-Fe eutectic alloy forms having a eutectic point at this temperature.* It is important, therefore, to observe the design limit of 600°C on the can/fuel

* This temperature limitation would be acceptable in a power fast reactor (provided that the design limited the can/fuel interface to below this temperature at the maximum power overload condition the reactor is designed to withstand, normally 150 per cent of normal), and indeed EBR-II uses uranium-metal in stainless steel. With plutonium metals, these materials could be incompatible at a temperature as low as 500°C, which would be quite unacceptable. To overcome this, various approaches are possible: for example to use a high-creep strength refractory metal can, several types of which appear to have been successfully developed both in the U.K. and U.S. or to employ the plutonium in an inert oxide-phase dispersed in the uranium.

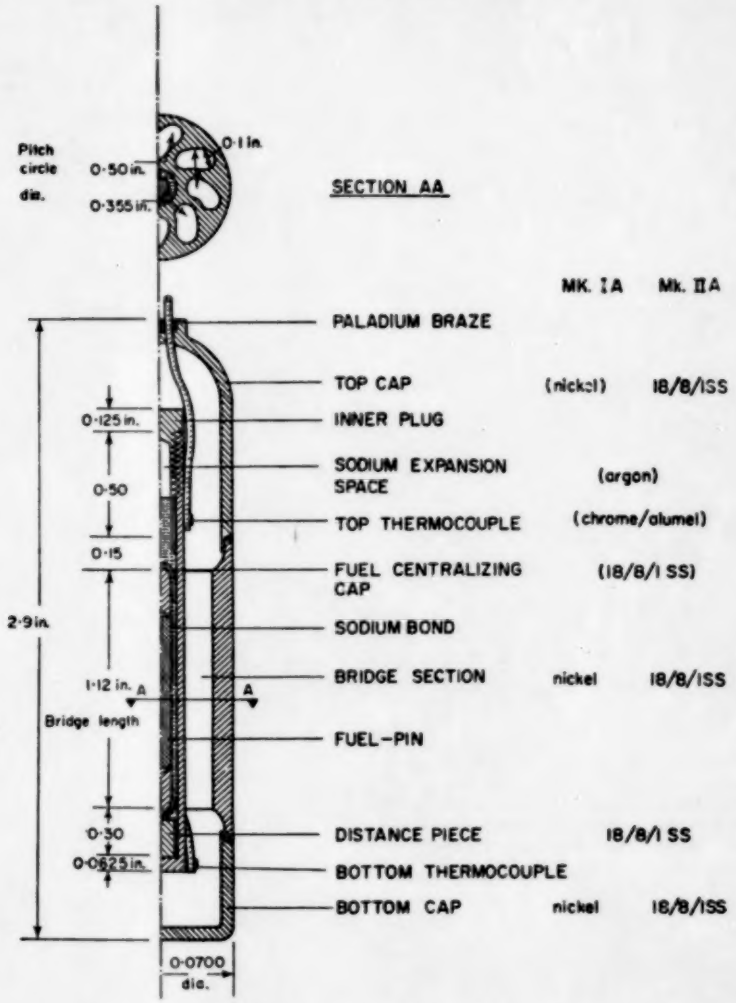

FIG. 2(a).—Container Mk 1 used in Rigs 1 and 2.

interface temperature. Nimonic 80 (about 72 Ni, 19 Cr + additions) was chosen over stainless steel because of its known superior tensile and creep strength properties, particularly on a reactor overload at up to 700°C, though it could not be guaranteed that this would remain true under irradiation conditions. Alloys such as Nimonic 100 (about 54 Ni, 20 Co, 11 Cr, 5 Mo, 5 Al + additions) were not chosen because of their lower ductility which offsets their higher strength.

The rig and container design proposed for achieving these requirements is shown in Figs. 1 and 2. The aluminium support-structure, which supports the fuel specimens in place of the reactor fuel element and restricts the reactor coolant flow, is shown in Fig. 1. This was modified from existing equipment used for another purpose (ROBERTSON and HENDRY, 1958). The author's design of specimen container is shown in Fig. 3. Two types are shown: Mk I used in Rigs 1 and 2 and Mk II in Rig 3; Mk III is a modification of Mk II with narrower bridge-slots and is used in Rig 4.

It is seen from Fig. 2(a) that container Mk I is constructed of three parts: a top cap, a bottom cap and a central bridge-section. This has slots cut in it to increase the effective thermal resistance and in a way so that thermal stresses, despite a drop of about 500°C, are negligible. Although somewhat complicated to make, this continuous metal path from the innermost to outermost surfaces makes the thermal resistance estimate more accurate and reliable, and so reduces uncertainty in the estimated fuel and can temperatures. The thermal resistance of the containers was estimated using a thermal analogue (see Fig. 4) and measured experimentally. Using this value, coupled with thermocouple measurements of temperature immediately above and below the bridge-section, the specimen power and temperatures can be deduced. Change in readings of these thermocouples during irradiation

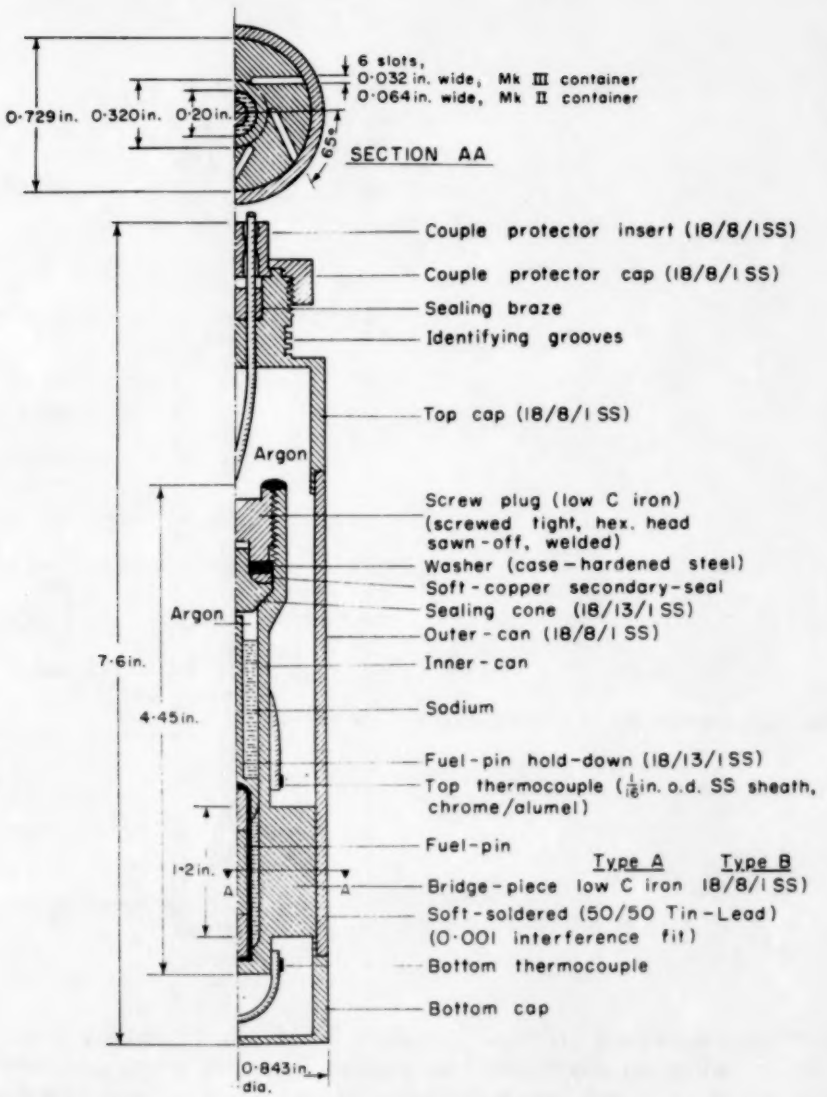

FIG. 2(b).—Fast reactor high burn-up test-rigs 3 and 4, Container Mk II and III.

is taken to indicate a movement of fuel, due either to fuel melting or can bursting. The material of the bridge is chosen to suit the enrichment of the fuel being tested, so that the required fuel temperatures can be obtained.

Mk II containers were introduced for Rigs 3 and 4 for several reasons: manufacture is easier and slots can be milled in the bridge so that the fuel pins could, if desired, be made much longer; the head of sodium above the fuel is substantially increased and the internal can sealing arrangements are much improved; during top and bottom cap welds, the fuel temperature can be kept much lower; 0·064 in. diameter sheathed thermocouples were used in place of 0·040 in., as these were found to be too fragile and as breakage could lead to the rejection of a rig when virtually complete; identification grooves were made in the top cap to positively identify X-ray photographs. A bad feature of the Mk II container is that it is more difficult to X-ray, particularly after irradiation when the fuel specimen is very active, due to the larger and more solid bridge-section. Because of this, further changes are intended for future rigs.

3. EXPLORATORY LABORATORY TESTS

A number of laboratory tests were conducted to predict rig behaviour. Fuel, can and thermocouple temperature estimates were assisted by several tests:

(i) A Teledeltos paper analogue was used to predict the thermal resistance of the containers. (See Fig. 4.)

(ii) Actual containers were tested both electrically

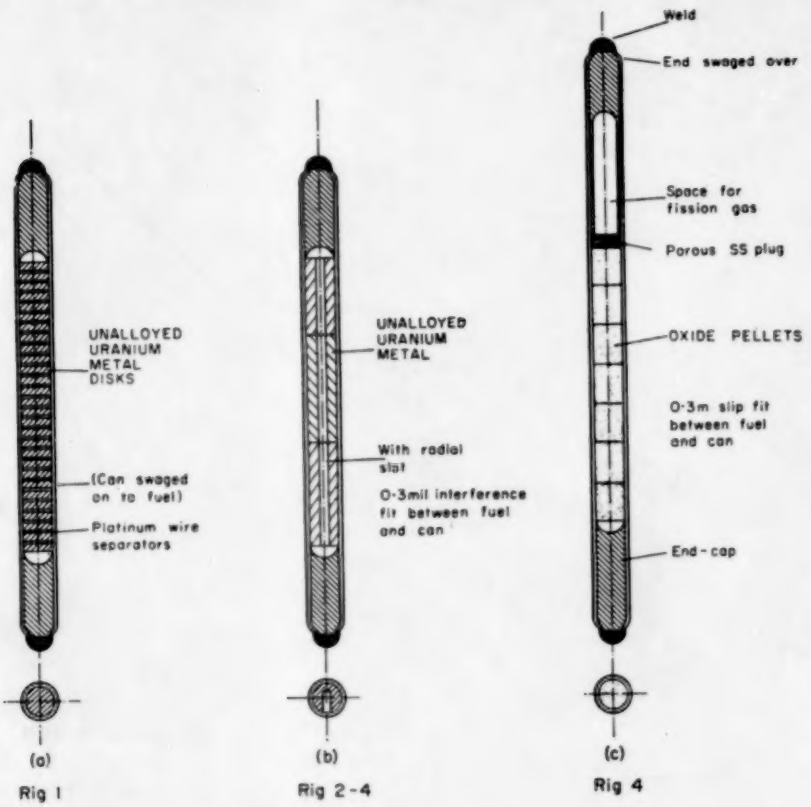

FIG. 3.—Fuel capsules used in Rigs 1–4.

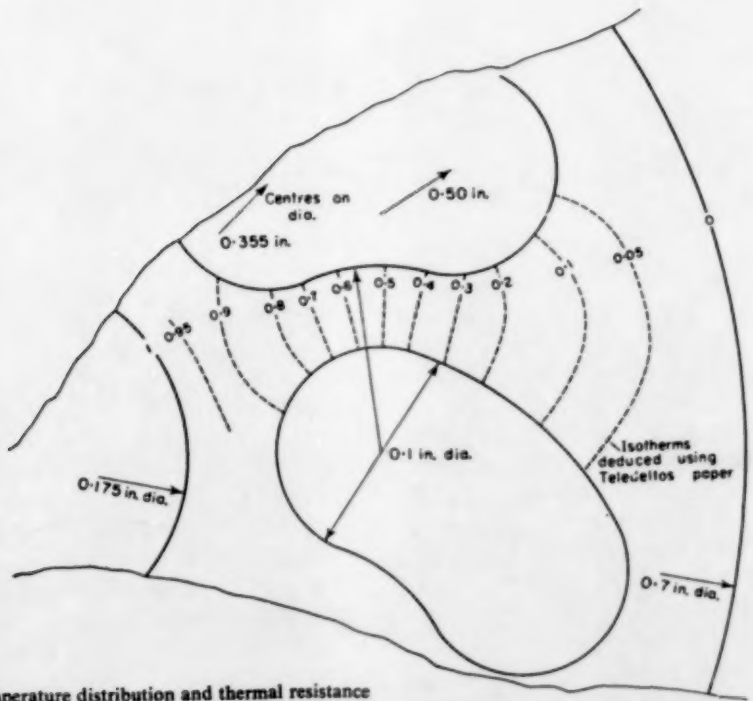

FIG. 4(a–c).—Temperature distribution and thermal resistance estimate of bridge-section of container.
(a) Mk 1 container. [See over.]

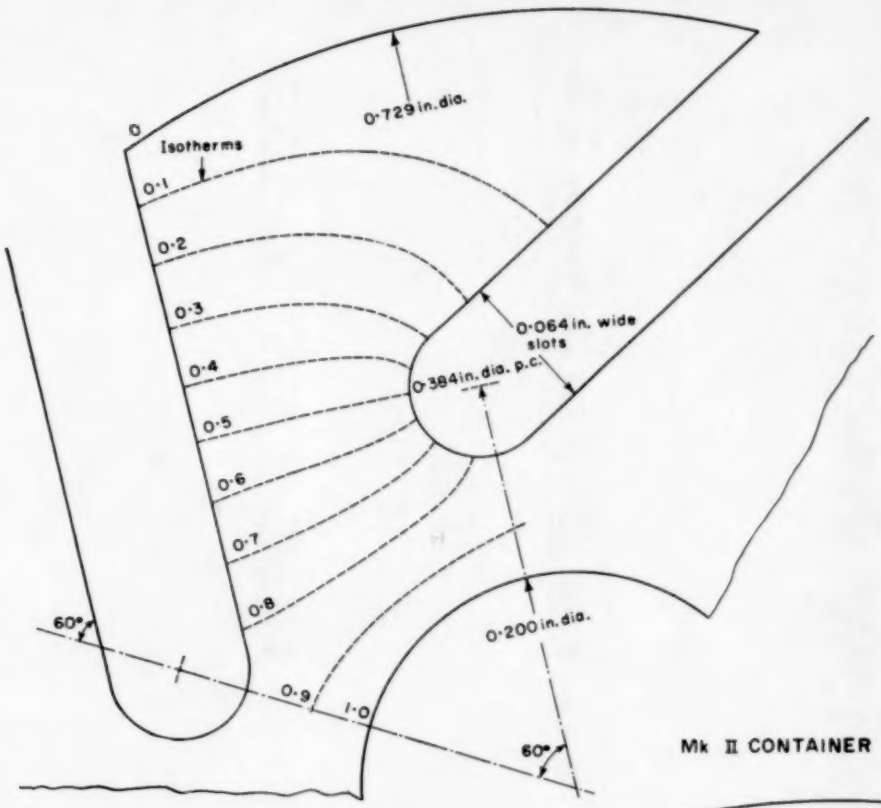

FIG. 4(b).—Mk II container.

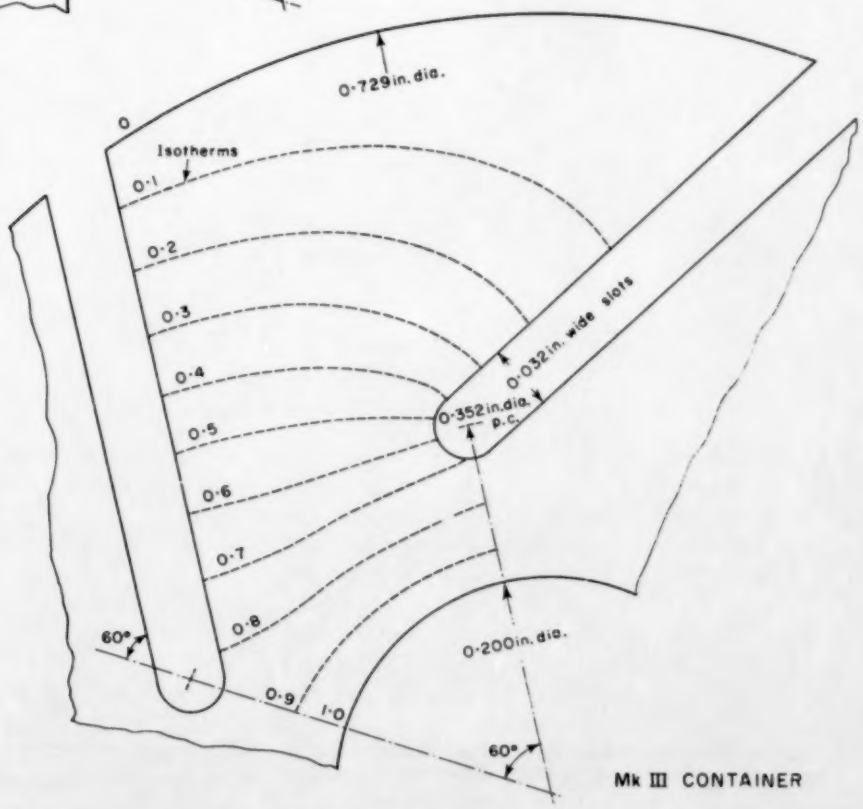

FIG. 4(c).—Mk III container.

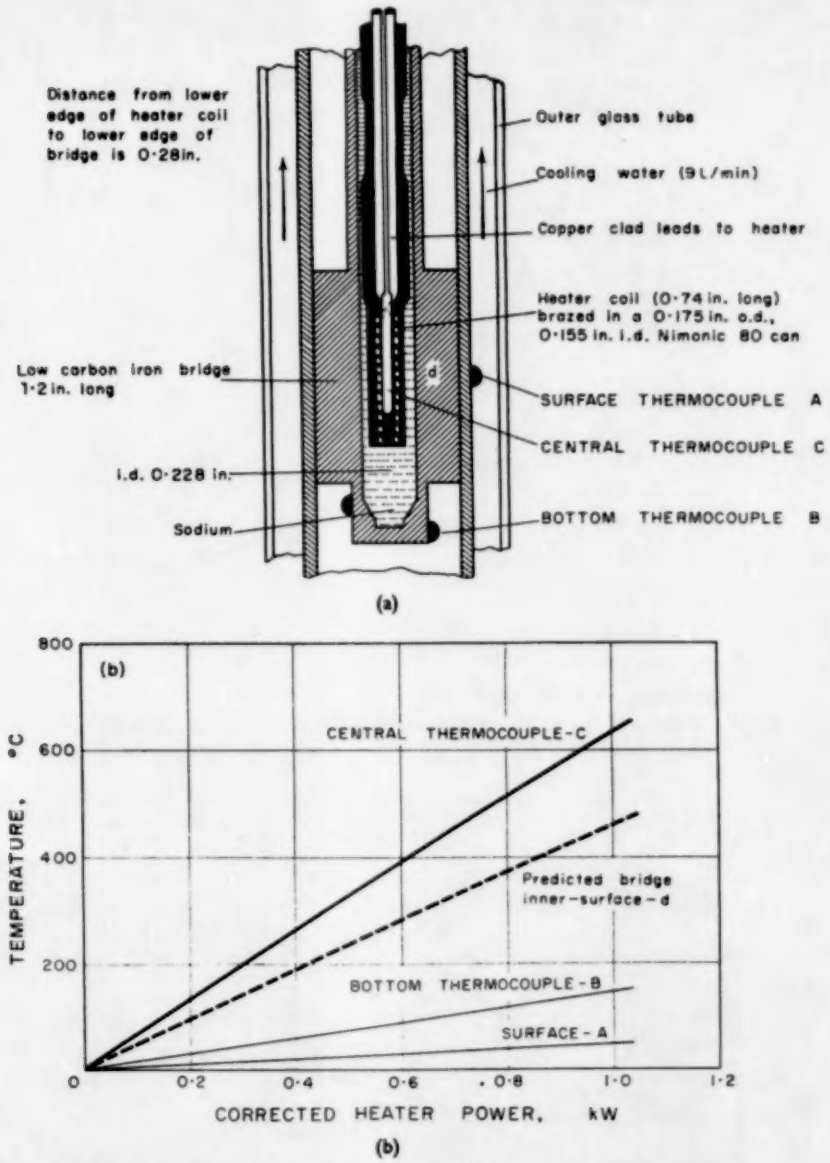

FIG. 5(a,b).—Test results with a Mk II body with an electrical heater in place of the fuel capsule.

and thermally to estimate their thermal resistance. The most conclusive test was with a small high-powered electrical heater (1 kW, 0·175 in. o.d., 0·74 in. long) simulating nuclear heat from the fuel pin. This checked the relation between the thermocouple temperatures, the fuel power and fuel and can temperatures. It also checked the temperature drop across the sodium bond. (See Fig. 5.) It proved that provided the power of the fuel element is known, fuel and can operating temperatures can be predicted very accurately (to within ± 2 per cent).

(iii) The variation of the thermocouple readings with position of the fuel in the bridge-section was estimated using Teledeltos paper, and using a half-section of an actual container body. (See Fig. 6.)

(iv) The wall heat-transfer coefficient between sodium and stainless steel was measured with the steel in a machined and an electrically polished condition (see Fig. 7), as this was suspected and found to be rather low.

Fuel-pin design and irradiation behaviour was assisted by the following tests:

(i) Optimum fuel and can diametric tolerances were estimated, together with the dependence of fuel-element centre-temperature on fuel power and on the diametric clearance between and fuel can. Essential

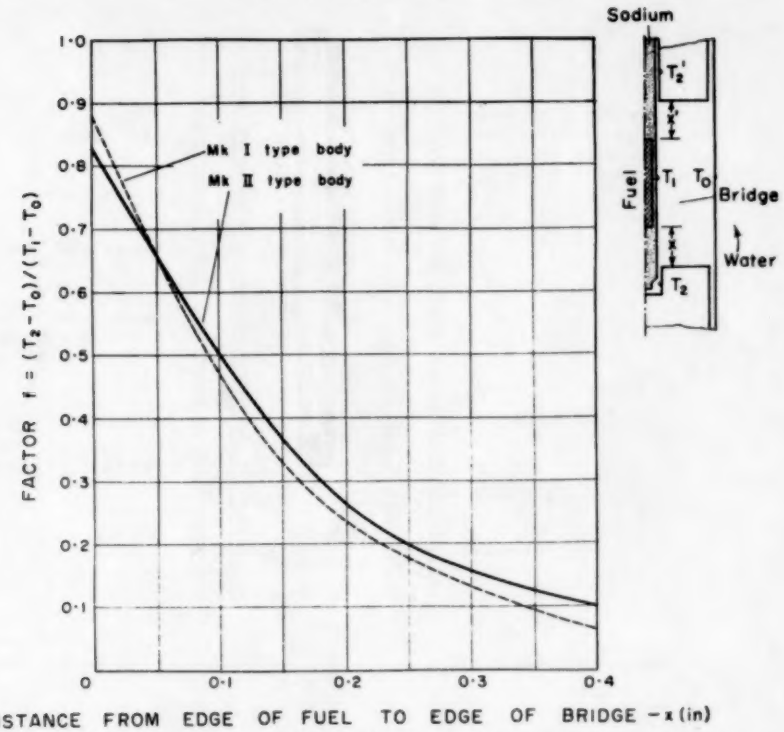

FIG. 6.—Factor used to relate thermocouple temperatures with that at centre plane of inner can.

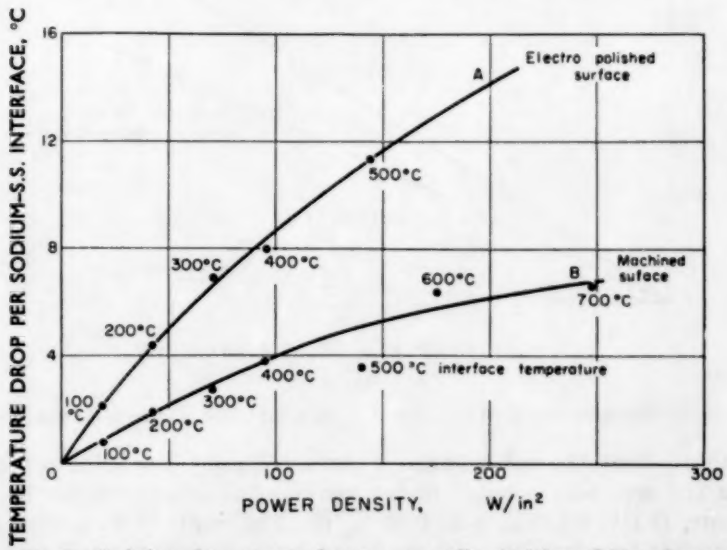

FIG. 7.—Variation of temperature drop across a sodium/stainless-steel interface with power-density for electro-polished and as-machined surfaces.

data in this estimate were determined in special tests. Final predictions are to be confirmed with additional tests. (See Appendix 1 and Fig. 11.)

(ii) Tests were made to confirm that compatibility between uranium metal and Nimonic is satisfactory up to 700°C.

(iii) In conjunction with Chemical Department, D.E.R.E., methods of coating the fuel and can were tried, with the object of raising the permissible fuel/can interface temperature; these were later discontinued.

(iv) The bursting pressure of the can at operating

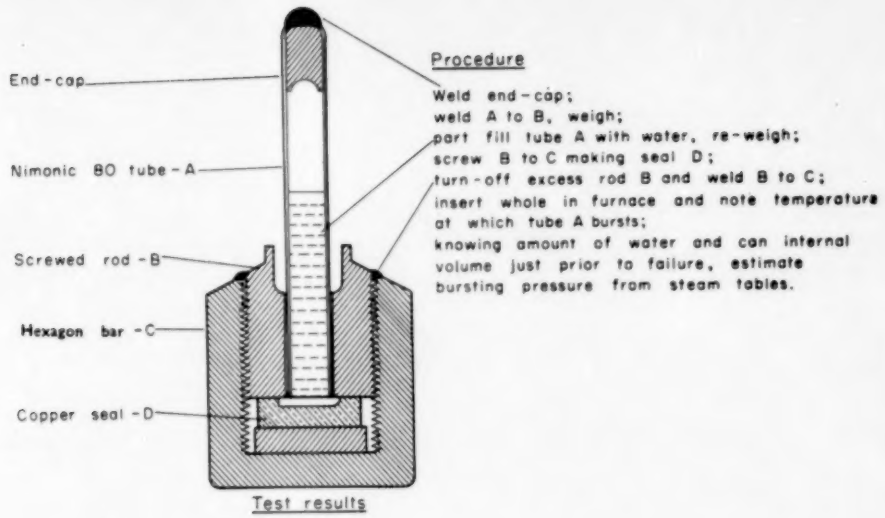
End-cap
Nimonic 80 tube-A
Screwed rod-B
Hexagon bar-C
Copper seal-D
Procedure
Weld end-cap;
weld A to B, weigh;
part fill tube A with water, re-weigh;
screw B to C making seal D;
turn-off excess rod B and weld B to C;
insert whole in furnace and note temperature at which tube A bursts;
knowing amount of water and can internal volume just prior to failure, estimate bursting pressure from steam tables.
Test results

FIG. 8(a).

Pressure (lb/in²)	Bursting temp. (°C)
44,000	645
31,000	625
23,000	600
21,000	600
22,000	600

Bursting temp. (°C)	Pressure (lb/in²)
505	17,000
500	13,200
325	2,500

Nominal can bursting pressure 20,000 lb/in². Accuracy of pressure estimate ~10 per cent.

FIG. 8(b).

FIG. 8(a,b).—Method of determining bursting pressure at operating temperature and end-weld quality.

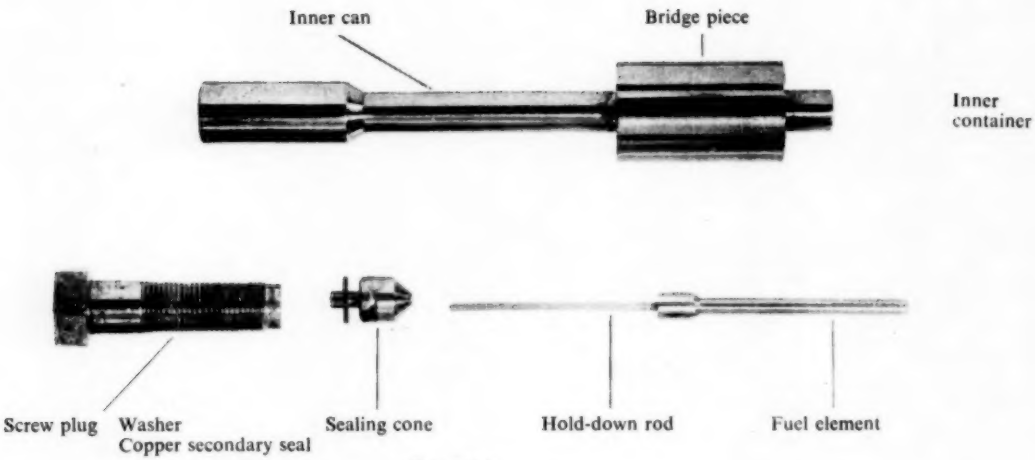

FIG. 10(a).

VOL
15
196

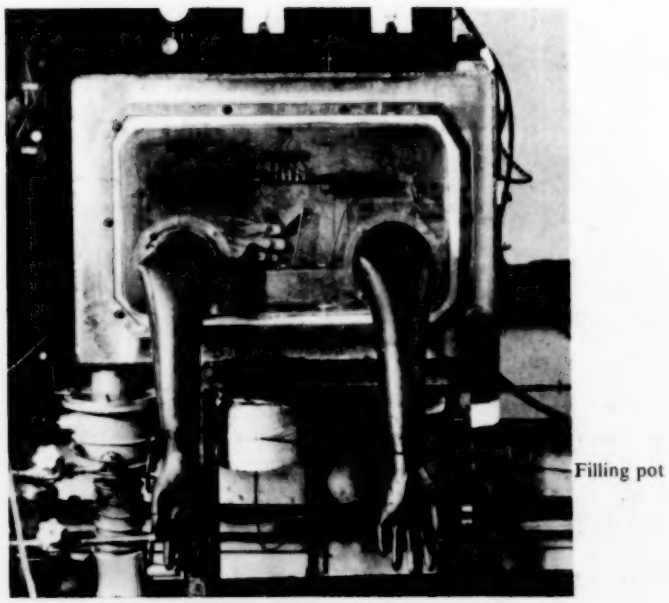

FIG. 10(b).

VOL.
15
1961

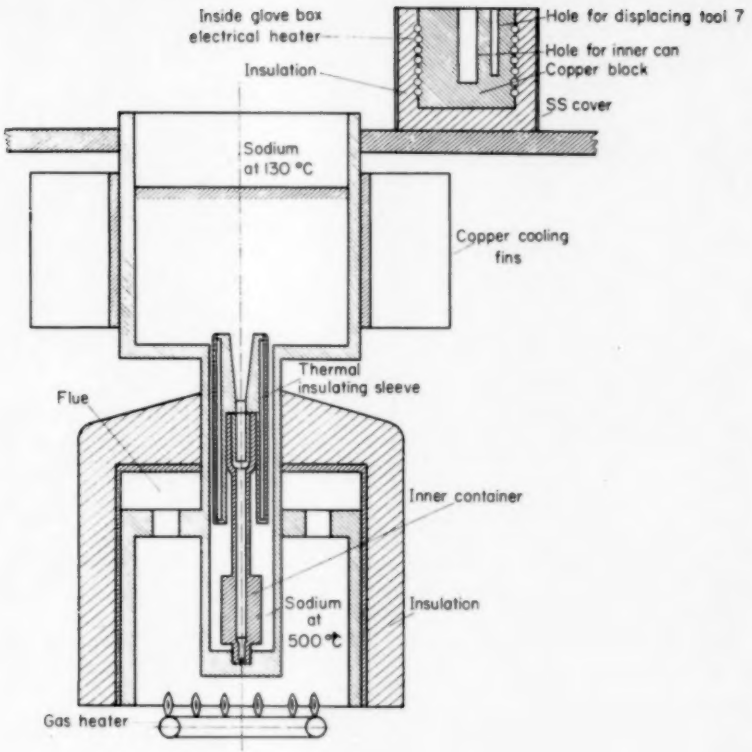

FIG. 10(c).

FIG. 10(d).

FIG. 10(a–d).—Equipment used for sodium-bonding fuel element to container.

[See over

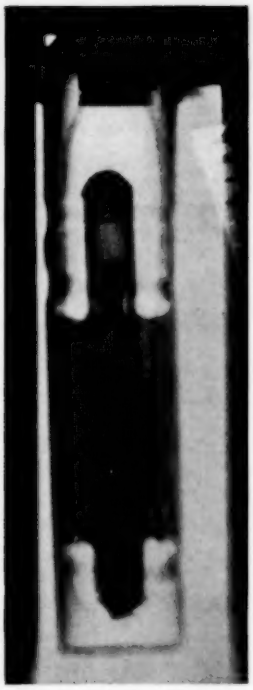

FIG. 13(a).—Typical container before irradiation.

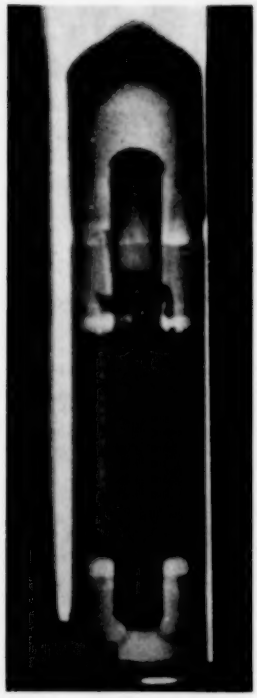

FIG. 13(b).—After irradiation.

FIG. 13(a,b).—Radiographs of specimen containers from the first high burn-up fast-reactor fuel-element rig.

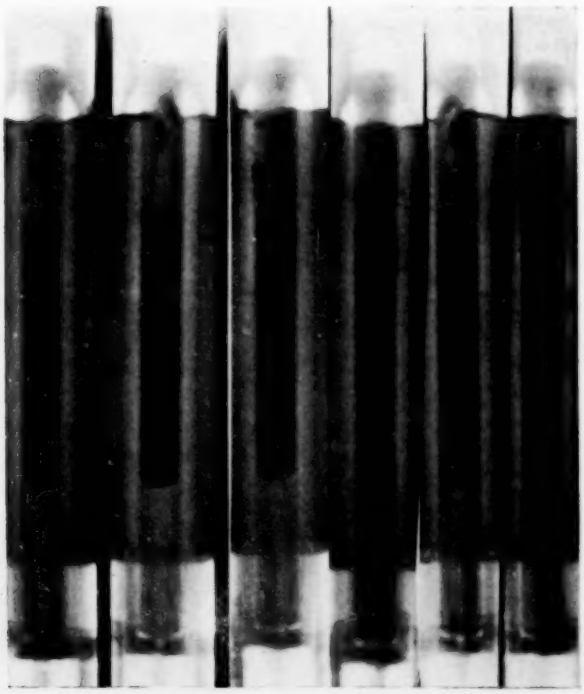

FIG. 14(a).—45% enriched specimen.

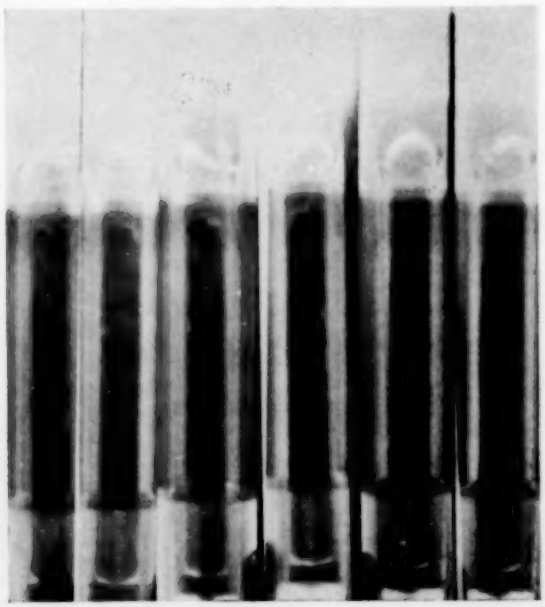

FIG. 14(b).—6·4% enriched specimen.

FIG. 14(a,b).—X-ray photographs of Rig 3 after irradiation, bridge of container is partly machined off. Radiographs are taken at 30° intervals to show up any surface defects.

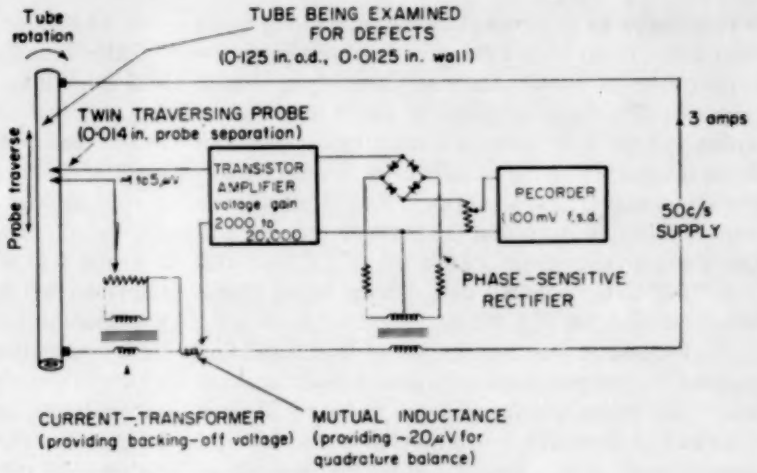

FIG. 9(a).—Electrical method of examining fuel element cans for defects, by recording variations in voltage across a twin probe in contact with the can or tube carrying an electric current.

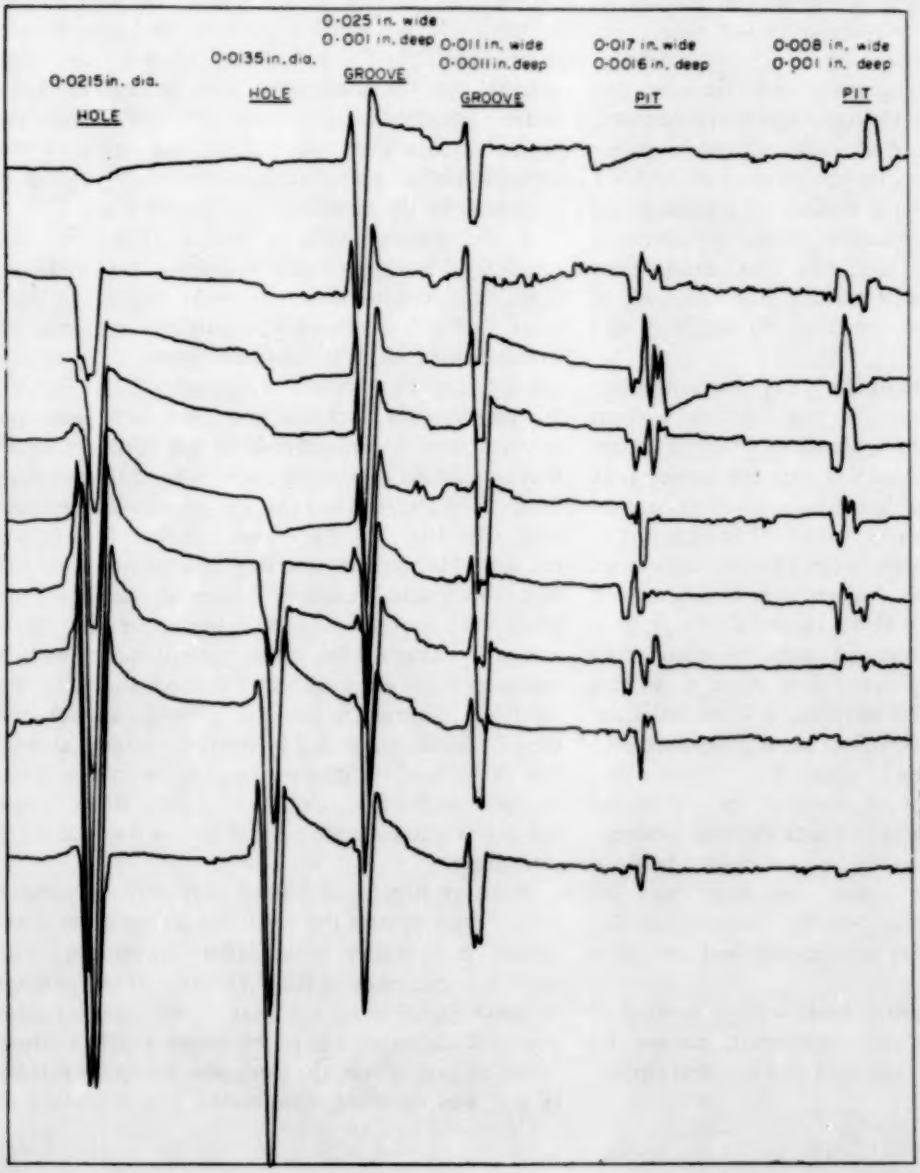

FIG. 9(b).—Recorder traces of linear traverse at 5° rotation of tube, using Nimonic rod specimen with prepared defects.

temperature was determined by partially filling a can with water, inserting in a furnace and determining the temperature at which the can burst from steam pressure. The bursting pressure was determined to within ± 1000 lb/in^2 from a knowledge of the can internal-volume and the amount of water, given high-pressure steam tables (KENNEDY, 1960). Defects were found in the cans such that the bursting pressure and temperature varied from 2500 lb/in^2, 325°C to 40,000 lb/in^2, 645°C, the nominal design figure being 20,000 lb/in^2, 500°C. (See Fig. 8.)

(v) Because of these defects, methods of inspecting cans were developed to ensure rejection of all cans that would fail below the nominal design figure. This is described in Appendix 2. In particular, an electrical probing method was specially developed because of its potential utility for power-reactor fuel cans. (See Fig. 9.)

A number of developments were necessary to facilitate construction of the rig and the fuel specimens, in particular, the fuel capsule end-weld, the container welds and the bridge machining operation of the Mk I containers. In addition, a method of sodium-filling the inner-can of the container needed development to give assurance of negligible gas entrainment in the sodium and good wetting and clean-up of the walls. This is described in Appendix 3 and Fig. 10.

In view of the success of the X-ray photographs of the irradiated specimens in their containers, from Rigs 1 and 2, Radioactive Metallurgy Group undertook an X-ray of a complete rig containing four specimens, without cutting out the containers, so that the rig remained unharmed and could be returned to the reactor for further irradiation. This would permit a fuel-swelling versus burn-up curve to be determined for each specimen; it is also economical in rigs, as it allows irradiation to continue until the destruction of a fuel pin. Arrangements were made to do this with Rig 3 and, for this purpose, a 9 ton radiation shielding flask for the complete rig was designed and built in conjunction with the Engineering Division, D.E.R.E. for transferring the rig to an active examination cave, which was specially modified to accept it. Unfortunately, excess solder between the bridge and the outer can (see Fig. 2b) prevented this from being wholly successful in Rig 3, but the technique is now established and is a valuable step forward.

In addition to the above work, a large number of post-irradiation tests were performed, mainly by Radioactive Metallurgy Group and Analytical Group, D.E.R.E.

4. IRRADIATION RESULTS (RIGS 1 TO 4)

Table 3 and Fig. 12 summarize irradiation results and conditions for Rigs 1 to 4. It will be seen that Rig. 1 failed almost immediately, the rig remaining in the reactor for one day only, whilst checks were made of the thermocouple readings. Figure 13 shows X-ray photographs of specimens before and after irradiation. The reason for failure is now apparent: can and fuel temperatures were some 200°C higher than intended due to a higher temperature drop across the sodium bond than was expected and due to misinterpretation of the thermocouple temperatures, which were expected to be increased due to flux enhancement at the ends of the fuel, sufficient to offset the factor, f (see Fig. 6), depending on the distance of the end of the fuel to the end of the bridge-piece. (In Rig 3 a specimen was divided into three equal parts for burn-up analysis, and this suggests that the effect is not very large.) The high fuel/can interface temperature of 780–880°C obviously promoted attack by the fuel on the can and the formation of a molten uranium-nickel alloy. This is confirmed by the metallographic examination.

In the period available before D.M.T.R. was scheduled for a prolonged shut-down for modifications, time was insufficient to make major modifications, so Rig 2 was tested with only minor changes of lower fuel-enrichment and the improved sodium-filling technique described in Appendix 3 and Fig. 10. In addition the fuel-can and container inner-can surfaces were electropolished in the mistaken belief that this would reduce the sodium-bond temperature drop: later tests showed that this increased it appreciably. (See Fig. 7.) Rig 3 survived four days in the reactor. During the last day, temperatures of the high enrichment specimens began to rise indicating gross fuel movement within the inner-can. Post irradiation examination again showed that a molten uranium-nickel alloy had been formed, indicating an interface temperature exceeding 740°C, though the time to failure suggested lower temperatures around the 740°C level. The two low-enrichment specimens survived undamaged, however. Again, these results are to be expected in the light of the latest temperature estimates.

Although Rigs 1 and 2 failed, they were not without value: they proved the safety of the specimen containers even under gross failure conditions; the surviving specimens of Rig 2 proved that the concept of these highly-rated rigs was sound; also, failure provided the stimulus to probe deeper with laboratory tests. In part excuse, the work was done very rapidly (Rig 1 was designed, constructed and irradiated in

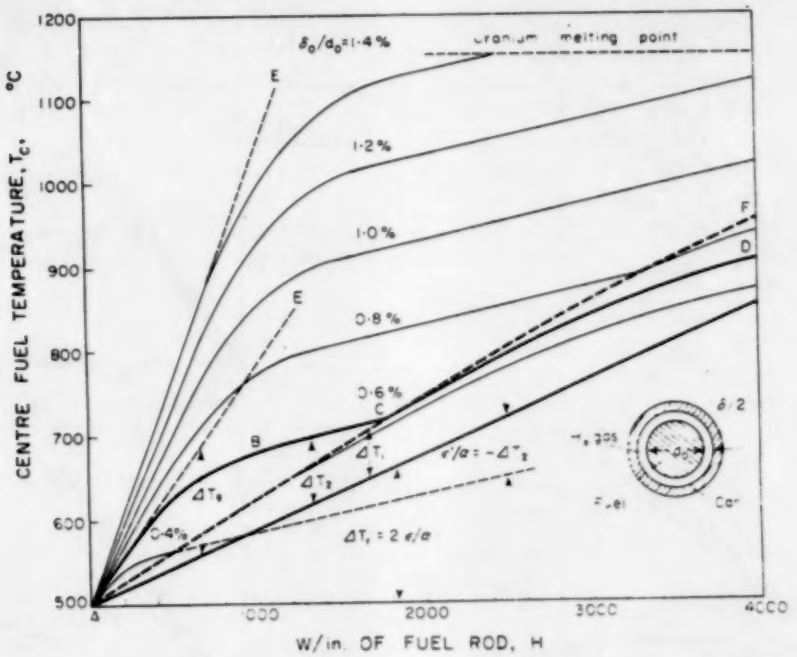

FIG. 11(a).—Estimated centre-fuel temperature as a function of fuel power and cold diametric clearance between fuel and can for solid uranium metal in a Nimonic 80 can.

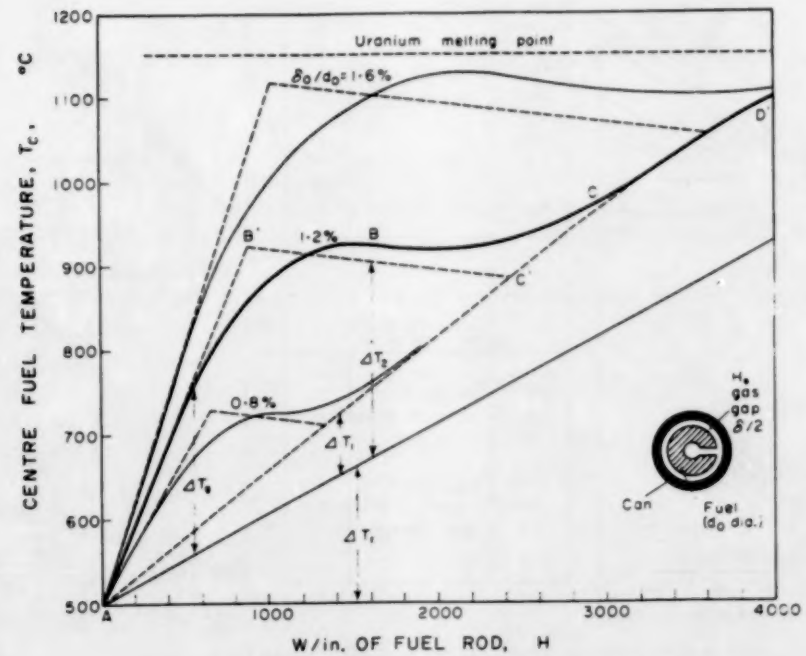

FIG. 11(b).—Estimated centre-fuel temperature for a C-shaped rod of uranium metal in a Nimonic 80 can, as a function of fuel power and cold diametric clearance between fuel and can.

VOL. 15 1961

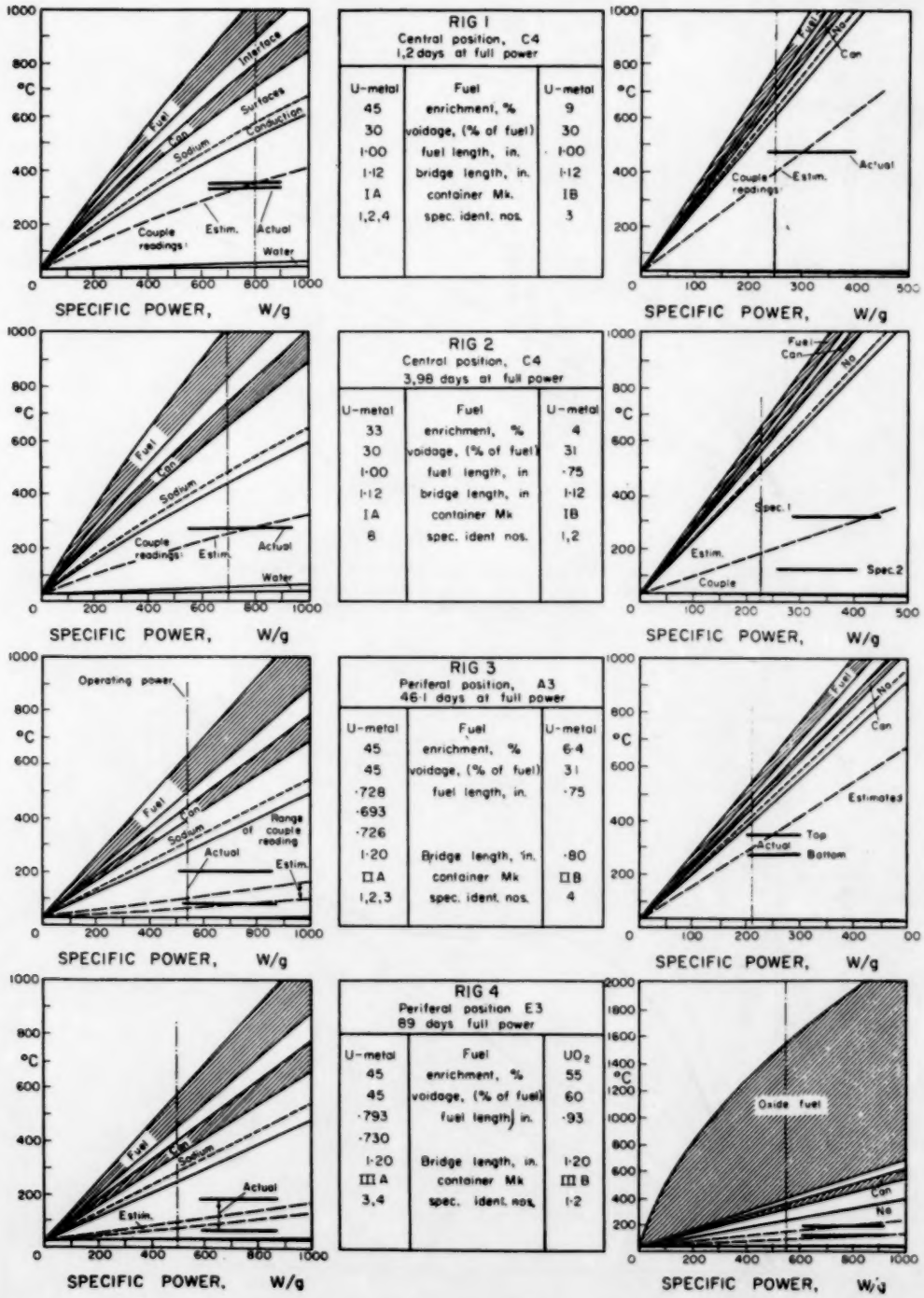
RIG 1
Central position, C4
1,2 days at full power
U-metal | Fuel enrichment, % | U-metal
45 | 9
30 | voidage, (% of fuel) | 30
1·00 | fuel length, in. | 1·00
1·12 | bridge length, in. | 1·12
IA | container Mk. | IB
1,2,4 | spec. ident. nos. | 3
RIG 2
Central position, C4
3,98 days at full power
U-metal | Fuel enrichment, % | U-metal
33 | 4
30 | voidage, (% of fuel) | 31
1·00 | fuel length, in | ·75
1·12 | bridge length, in | 1·12
IA | container Mk | IB
8 | spec. ident nos. | 1,2
RIG 3
Periferal position, A3
46·1 days at full power
U-metal | Fuel enrichment, % | U-metal
45 | 6·4
45 | voidage, (% of fuel) | 31
·728 | fuel length, in. | ·75
·693
·726
1·20 | Bridge length, in. | ·80
IIA | container Mk | IIB
1,2,3 | spec. ident. nos. | 4
RIG 4
Periferal position E3
89 days full power
U-metal | Fuel enrichment, % | UO2
45 | 55
45 | voidage, (% of fuel) | 60
·793 | fuel length, in. | ·93
·730
1·20 | Bridge length, in. | 1·20
III A | container Mk | III B
3,4 | spec. ident. nos. | 1·2
°C
SPECIFIC POWER, W/g
Fuel
Can
Sodium
Surfaces
Conduction
Interface
Couple readings
Estim.
Actual
Water
Na
Operating power
Range of couple reading
Top
Bottom
Estimated
Oxide fuel
Spec.1
Spec.2

FIG. 12.—Estimated operating temperature conditions for Rigs 1–4.

TABLE 3.—SUMMARY OF OPERATING CONDITIONS OF RIGS 1–4

Rig No.	Units	1		2		3		4	
Specimen identification		1,2,4	3	8	1,2	1,2,3	4	3,4	1,2
Container type—Mk		IA	IB	IA	IB	IIA	IIB	IIIA	
Container bridge material		Ni	S.S.	Ni	S.S.	Fe	S.S.	Fe	
Fuel		U-metal		U-metal		U-metal		U-metal	UO_2
enrichment	%	45	9	33	6·4	45	6·4	45	55
Shape		disks		C rods		C rods		C rods	short cyl.
No. of pellets/specimen		27		4	3	2	3	2	7
Can protective coating		platinum		none		none		none	
Wt. of fuel	g	1·96		1·90	1·43	1·27, 1·20,	1·27, 1·38	1·35, 1·25	1·14, 1·10
Void space/can internal volume	%	23		23	24	30	25	30	37
Fuel dia.	in.	0·100		0·100		0·1005 ± 3	0·100	0·1005 ± 3	0·0991;
Overall fuel length	in.	1·00		1·00	0·75	0·728, 0·693, 0·726	0·750	0·793, 0·730	0·93
Can dia. 0·122 in. in each case									
Rig position in D.M.T.R.		C4		C4		A3		E3	
Relative unperturbed flux		1		1		0·72		0·72	
Date first raised to power		28 Nov. 1960		4 Apr. 1960		9 Sept. 1960		14 Oct. 1960	
Days at full power, τ		1·2		3·98		46·1		89	
No. of shutdowns (intermed.)		—		2		8		—	
ESTIMATED OPERATING CONDITIONS									
Fuel specific power, s	W/g	800	300	700	250	550	210	500	560
Fuel-surface power-density	kW/in.²	5·0	1·9	4·2	1·5	3·1	0·9	2·7	2·2
Total specimen power	kW	1·57	0·59	1·33	0·36	0·70	0·30	0·65	0·63
TEMPERATURES (30°C inlet)									
Container o.d.	°C	49	37	46	35	50	44	50	40
i.d.	°C	520	745	440	540	310	390	280	260
Can o.d.	°C	703	815	590	620	423	443	376	340
i.d.	°C	784	845	665	650	484	466	430	380
Fuel o.d.	°C	880	880	750	680	550	490	490	460
centre	°C	1070	950	910	735	700	540	630	1600
BURN-UP ESTIMATES									
From sp. power $b = \tau_s/9350$	%	—		0·30	0·10	2·7	1·0	4·75	5·3
By chem. analysis	%	—		0·35 ± 0·05	—	2·69 ± 0·05	—	—	—
By mass spec.	%	—				2·65 ± 0·05	—	—	—
ACTIVE EXAMINATION									
Description of failure		Excessive can temp. (>740°C) leading to U-Ni eutectic formation		As Rig 1 Undamaged		Fuel pin undistorted with no measurable swelling (diametric increase less than 1 thou.)		Fuel pin undistorted with no measurable swelling (diametric increase less than 1 thou.)	

four months) with only a small staff and at a time when the approach to criticality in D.F.R. was occupying a good deal of time.

Rig 3 and 4 irradiations results were much more satisfactory. Rig 3 was irradiated for two reactor periods and, after failing to obtain sufficiently good X-ray pictures with the complete rig, due to excess solder between the bridge and outer-can of the container confusing the picture, the rig was cut up for detailed examination. The chief results are summarized in Table 3. Every specimen was sound with negligible distortion, as shown by the X-ray photographs before and after irradiation (see Fig. 14). The maximum burn-up achieved of 2·7 per cent is much higher than achieved before with uranium-metal, particularly at 700°C centre temperature. It will be seen that the 45 per cent enriched fuel has swollen to fill-up completely all available space in the fuel capsule; the swelling into the domed cavities of the end-caps is particularly noticeable, whilst the fuel-slots also appear to have completely disappeared. In the 6·4 per cent enriched specimens, this swelling has not progressed so far. Rig 4 results were similar; again no fuel-pin distortion was detectable after an

even higher burn-up of about 5 per cent, with UO_2 specimens as well as unalloyed uranium metal.

As a check of the behaviour of a pin on overload, a uranium metal specimens of 2·7 per cent and 4·7 per cent burn-up were placed in a furnace at 680°C for 1 hour. It was not prudent to go much higher due to the 740°C limitation on fuel/can compatibility. The pins survived this with no more than 1 thou. increase in diameter. At this temperature the can strength could have been weakened and the average fuel temperature was raised by about 90°C above the in-pile condition at the end of irradiation, so the fission-gas pressure would be about 10 per cent higher. It was unfortunate that incompatibility limitation prevented this test being taken to a higher temperature when it would have given an indication of the maximum burn-up capabilities of the pin. With the 5·3 per cent burn-up oxide specimens, since there was no incompatibility limitation, the furnace temperature was taken progressively to 900°C. Again the specimen survived with negligible distortion. Many more post-irradiation checks on these specimens are planned. It is hoped to find out if the large internal voidage leads to interconnexion of fission gas cavities and if much fission gas will escape on drilling a small hole in the can. The same specimen will then be raised to 600°C to see if and how fuel will extrude. This aspect is very pertinent to fast reactor safety. Metallurgical sections of the specimens will be made and as many tests as practical of can and fuel physical and mechanical properties.

CONCLUSIONS

Fuel testing at high power-density in the materials testing reactor

Testing fuel to high burn-up demands much higher fuel ratings than has been used to date. The present test series has demonstrated that 550 watts/gramme at 500°C fuel-element surface temperature can be achieved successfully and safely in a Materials Testing Reactor, with a radial flux depression which is quite acceptable; this accurately represents fast reactor conditions. It has also shown up the important design requirements of the rig. Based on the experience gained and with relatively minor modifications to Rigs 3 and 4, it should now be possible to design future rigs with the following features:

(i) Fuel can be tested up to 1000 watts/gramme (1 per cent burn-up in 10 days) and with a can surface temperature of up to 650°C approximately, in a container immersed in the heavy-water reactor coolant at 30°C.

(ii) The rig is simple in concept and easy to manufacture.

(iii) Specific power and operating temperature of the fuel can be measured to about 5 per cent accuracy, based on four thermocouple readings.

(iv) These thermocouples can be continuously recorded and should indicate can failure and fuel movement.

(v) The rig is sufficiently transparent to X-rays to allow irradiated fuel elements to be X-rayed without being removed from the rig, so permitting the fuel element to be inspected for swelling and distortion at regular intervals during the progress of irradiation.

(vi) Up to four or five elements can be tested per rig, each of up to 1 ft long.

(vii) It should be possible to predict operating flux and temperatures to within about ± 10 per cent and adjusted to a higher accuracy than this by change of position of the rig in the reactor core.

The author agrees with MONAWECK (1960) that radial flux depression is unlikely to make high temperature irradiation results in a thermal flux appreciably different from those in a fast reactor, due to the ready diffusion of fission products. The effect of power rating (rate of burn-up) would appear to be more important. With strong fuels, performance at high-rating is likely to be slightly improved, due to increase in the effective creep stress, but this effect is likely to be small in comparison with the large thermal stresses at high-ratings, which could significantly reduce irradiation performance. With fuel elements of the strong-can, voided-fuel type, performance is likely to be independent of rating up to the level where can thermal stresses are large (when the temperature drop across the can exceeds 100°C approximately, performance depends mostly on the creep-stress/temperature relation of the can).

Fast reactor fuel element development

The irradiation programme described was intended to test the theory (BLAKE, 1961) that high burn-up at high ratings and high centre-temperatures is best achieved by using a strong can with fuel containing void-space for fission product gas. Encouraging results have been obtained: no significant swelling or distortion has occurred in three specimens, taken to 2·7 per cent burn-up at 420°C can surface-temperature and over 700°C centre-temperature. The specimens were unalloyed uranium-metal in Nimonic 80 cans of wall-to-diameter (t/d_0) ratio of 9·3 per cent and with 31 per cent internal void space, mainly in the form of a radial slot in the fuel. After irradiation the fuel had swollen, as expected, to fill up this and all

TABLE 4.—RESULTS OF EBR–II FUEL ELEMENT IRRADIATIONS (MONAWECK and SOWA (1960))

Fuel	Density decrease	Burn-up	W/g	Centre temp.	Remarks
5% Fi cast	12%	0·92 a/o	56	620°C	Surface roughness. No increase in clad dia.
7·5% Fi cast	4%	1·36 a/o	192	427°C	1/16" dia. melt through in clad due to sodium bond defect. Dia. increase only at defect.

other available space within the can. In a less highly rated specimen taken to 1 per cent burn-up at about 540°C centre temperature, fuel swelling within the can was incomplete, not all the available space being filled up. The theory predicts that the fuel pins could have withstood up to about 15 per cent burn-up before the can fractured or was appreciably distorted. Further tests on uranium metal at 640°C centre-temperature and of uranium-oxide at about 1600°C centre-temperature, continued to about 5 per cent burn-up, have also proved equally successful.

The reasons suggested why this form of fuel element is likely to be successful are that the can forms an efficient pressure container (strong fuel or a stainless-steel cermet does not), which operates at the lowest temperature of the fuel element; this overcomes the strong dependence of burn-up on fuel temperature, and enables the fuel centre-temperature to be raised, which leads to a more rugged fuel-element construction and better neutron economy, reflected in lower fuel investment and a better breeding-ratio; the void-space in the can reduces fission-gas pressure appreciably and subjects it to control; defects in fuel and effects of phase-changes can be tolerated and leads to more consistent fuel-element performance; proper introduction of the voidage and control of can and fuel dimensional tolerances enables an intermediate thermal bond to be omitted, which simplifies manufacture and increases fuel-element reliability. Avoidance of a sodium intermediate bond appears to be a step in the right direction in view of troubles this has caused in the Dounreay Fast Reactor and apparently in EBR-II fuel-pins also (see below). Tests of the above uranium-metal fuel-pins (to 2·7 per cent and 4·7 per cent), with a $\frac{1}{16}$ in. dia. hole drilled in the can wall to simulate a bad defect, and held in a furnace to about 600°C has shown no tendency for fuel to extrude and block a coolant passage, so the problem of can defects may not be as difficult as first feared, and double-canning may not be necessary.

A further very significant advantage of the strong-can voided-fuel concept is that the amount of ^{238}U which can be incorporated in a fuel element is acceptably high, particularly in comparison with fuels such as the 30 v/o or 50 v/o stainless-steel cermet. This has a very important effect on the size of the delayed neutron fraction, particularly in plutonium fuels, where the value could drop as low as 0·25 per cent with the stainless-steel cermet; at this low value it becomes a design and safety problem of importance. The core breeding ratio also falls with the low ^{238}U content fuels, causing larger reactivity changes with burn-up. Maximum burn-up, expressed in proportion of uranium and plutonium atoms fissioned, is a poor way of comparing different fuels which is better compared by their maximum fissions or energy released per unit volume; on this basis 1 per cent burn-up in a strong-can 28 per cent void, uranium-metal fuel-element is equivalent to 5·6 per cent burn-up with a 30 v/o cermet, and to 3·4 per cent with 50 v/o cermet. Another important factor in the fast reactor is the reliability with which high burn-up can be achieved: a 50 v/o cermet of uniform properties will be difficult to manufacture; moreover, its performance on reactor overloads will also be poor. Estimates based on the theory of BLAKE (1961) suggest that it is most unlikely that a 50 v/o stainless-steel cermet will achieve much better than 1–2 per cent reliably at a worthwhile centre-temperature; 0·3–0·7 per cent burn-up of 10 w/o molybdenum-uranium alloy fuel would compare with this.

One of the most severe irradiation tests previously reported on uranium metal are the EBR-II fuel element irradiations (MONAWECK and SOWA, 1960) in the thermal test reactors CP-5, MTR and ETR. Uranium–2 per cent zirconium and uranium–5 per cent and 7·5 per cent fission alloy fuels were used, in the form of rods 0·144 in. dia., 14·22 in. long contained in a stainless-steel tube 0·174 in. o.d. 0·005 in. wall. Details are given below of the fuel element irradiated to highest burn-up and the one at highest temperature. Altogether 23 pins were irradiated (0·4 to 1·36 a/o burn-up, at 217°C to 620°C) of which six showed defects due to imperfect sodium bonding;

in one the can swelled to 0·302 in. at the defect. The main conclusions drawn in the report are: all fuel showed surface wrinkling, the 7·5 per cent Fi less than the others; the only increase in clad diameter occurred at sodium-bond defects where the fuel overheated; all irradiated fuel was embrittled, making it difficult to handle; radial flux-depression makes irradiation in a thermal flux slightly more onerous than in a fast flux; the dominant factor controlling fuel expansion is fuel temperature; fuel expands mostly in a radial direction.

Acknowledgments—The author wishes to express his gratitude to members of the Fast Reactor Technology Group, in particular, MR. J. FREW, MR. R. OLIVER, MR. N. LONGSTAFF, MR. J. REFSON and MR. J. RASPIN who constructed the rigs and test equipment under the general direction of MR. L. FISHER and who in conjunction with MR. J. C. W. TELFER performed most of the laboratory tests described.

The work described from conception to completion was done in just over a year, and this was only made possible by the willing help given by Engineering Division D.M.T.R. Project Group, Radioactive Examination Group, Analytical Services, D.E.R.E., and also by MR. H. LLOYD, A.E.R.E. Harwell, who kindly supplied the fuel pellets.

REFERENCES

BLAKE L. R. (1960) *Proc. Instn. elect. Engrs*, **107A**, No. 34.

BLAKE L. R. (1961) *Reactor Sci. Technol. (J. Nucl. Energy* Parts A/B) **14**, 31.

KENNEDY G. C. (1960) *Amer. J. Sci.* **248**, 540.

MONAWECK J. H. and SOWA E. S. (1960) *Summary Report on Irradiation of Prototype EBR-M Fuel Elements*. Argonne National Laboratory Report ANL-6010, (Metallurgy and Ceramics TID-4500, 15th Ed.).

ROBERTSON J. M. and HENDRY K. (1958) UKAEA unpublished document.

APPENDIX 1

Fuel/can thermal bond

The fast reactor employs a high fuel-surface heat-flux of the order of 1000 to 2000 watts/in². Thus a good thermal bond is essential for low fuel temperature. There are two main bonding methods:

A. Using a large gap containing a continuous intermediate metal bond between fuel and can, such as liquid metal, a metallic paste or a low creep strength metal; or

B. Using a small gap with close control of fuel and can diametric tolerances and surface finish, in the belief that the fuel will expand to close the gap and establish a good bond.

The choice of the best method is even more important in the present tests since the fuel heat-flux is up to 5000 watts/in². Introducing void-space in the fuel rules out the use of a sodium-bond, but a soft metallic coating on the fuel is possible. However, calculations indicate that method B is satisfactory provided:

(i) A smooth surface finish is employed both for fuel and can internal surface, preferably of 30 micro-in. r.m.s. or better.

(ii) There is control of the diametric clearance between fuel and can, appropriate to the operating power and the rod size. With 0·2 in. fuel diameter for example, operating at 2000 W/in² and 400°C can i.d. temperature, the cold clearance should be about 1 ± 0·3 thou. If the clearance is made large, say 3 thou. this could lead to uranium melting; if it is made an interference fit, this could lead to excessive can strain of 0·6 per cent and stresses exceeding the yield point.

(iii) All burrs, protrusions or steps on fuel or can are removed and also that the interface is free of any foreign matter.

Relief from excessive can stress due to fuel expansion and relief in the tolerance restrictions of the diametric clearance can be achieved by the simple artifice of making a radial slot in the fuel. The surface finish and cleanliness requirements remain high, however.

In general, manufacture to these tolerances and surface finish requirements is well within current engineering practice. Hence method B is simpler than method A and should also be safer since it lends itself to final pin-inspection by X-raying; moreover, in method A complete sodium-bonding can neither be assured initially or guaranteed thereafter, as sodium can be ejected by differential thermal-expansion mechanism or by displacement by fission gas, which could lead to large gaps locally and high local temperatures.

An attempt will now be made to give the basis for the above conclusions. Consider first the idealized case of a fuel-rod, solid or slotted, located centrally in a can. Let:—

d_0, d = solid fuel-rod dia. at 0°C, during operation (in.)
$\delta_0 + d_0$ = can inside dia. at 0°C (in.)
K_f, K_g = fuel, gas thermal conductivity (W/°C in.)
α', α = can, fuel coeff. of linear expn. (in./in.)
T = temp. of can inside dia. (°C)
ΔT_f = temp. drop from fuel centre to surface (°C)
ΔT_1 = temperature drop across can/fuel interface at pressure p(lb/in²) (°C)
ΔT_2 = rise in temperature of fuel in order that it can just make contact with can (°C)
H = power rating of fuel rod per unit length (W/in.)
h = can/fuel interface heat transfer coefficient at pressure p, for given conditions of fuel surface

The temperature-drop from centre to fuel surface

$$\Delta T_f = k_s H/4\pi K_f \tag{1}$$

where k_s is a constant dependent on the geometry of the fuel-slot, being unity for a solid circular rod.

The temperature-drop across the interface resistance assuming p lb/in. contact pressure is

$$\Delta T_1 = H/\pi dh. \tag{2}$$

It is fortunate that h remains reasonably constant in value for interface pressures up to 1000 lb/in² and increases only by a factor of 2 for pressures up to 1000 lb/in². For the present it will be assumed that h is independent of pressure up to 1000 lb/in² interface pressure (and say a can strain ϵ of 0·025 per cent with Nimonic cans of $t/d = 0{\cdot}1$), and that $h \to \infty$ at pressures $p > 10^4$ lb/in² or $\epsilon > 0{\cdot}2$ per cent.

Assume that a fuel rod with a temperature drop of ΔT_f from centre to surface will have a thermal expansion the same as a rod with a uniform temperature rise of $\beta \Delta T_f$. Then at the operating power when the temperature of the can interval surface is T, and the fuel temperature-drop is ΔT_f, the fuel must rise by an additional temperature ΔT_2 for the fuel surface to contact the can uniformly, such that

$$(d_0 + \delta)(1 + \alpha' T) = d_0[1 + \alpha(T + \beta \Delta T_f + \Delta T_2)].$$

Thus $$\alpha\Delta T_2 = \frac{\delta}{d_0}(1 + \alpha' T) - (\alpha - \alpha')T - \alpha\beta\Delta T_f. \quad (3)$$

As a fuel pin is raised in power, three main operating regimes are evident. Initially the fuel centre-temperature will be

$$T_c = T + \Delta T_g + \Delta T_f$$

where ΔT_g is the temperature-drop across the gas gap between fuel and can and is given by

$$\Delta T_g = \frac{H}{\pi d_0} \cdot \frac{\delta/2}{K_g}$$

assuming conduction across the gas, the controlling heat transfer mechanism and that radiation is negligible. As the power is raised, the gas temperature rises (and hence its thermal conductivity) and the fuel temperature rises (closing the gas gap). In Fig. 14(a), curves such as AB characterizes this regime. The initial slope AE to the curves AB has the expression:

$$T_c - T = \frac{\delta_0}{d_0} \cdot \frac{H}{2\pi (K_g)_{\text{temp } T'}} + \Delta T_f. \quad (4)$$

Beyond the point such as B, over the region BC, the centre fuel temperature is given by

$$T_c - T = \Delta T_2 + \Delta T_f \quad (5)$$

where ΔT_2 is given by equation (3).

At position C the temperature rise ΔT_2 becomes less than ΔT_1, which is not permissible, hence the temperature continues to rise along CF, the heat-transfer coefficient increasing as H increases, due to increasing interfaces temperature and pressure.

Solid fuel rod

Figure 11(a) shows an estimate taking these factors into account, as accurately as the available data permits, for the case of a solid uranium fuel-rod of 0·2 in. dia. at 0°C, in a can of 500°C internal surface temperature, filled with helium at one atmosphere for various values of cold diametric-clearance, δ_0. For simplicity of calculation the following average values are employed:

$\alpha = 20 \cdot 10^{-6}$ (in./in.)
$\alpha' = 13{\cdot}5 \cdot 10^{-6}$ (in./in.)
$K_f = 0{\cdot}9$ (W/°C in.)
$K_g = 0{\cdot}005$ (W/°C in.)
$h = 50$ (W/°C in²)(30 μin., 600°C, He)
$T = 500$°C.

Thus we have

$$\Delta T_f/H = 1/4\pi \cdot 0{\cdot}9 = 0{\cdot}0883 \quad (1')$$

$$\Delta T_1/H = 1/\pi \cdot 0{\cdot}2 \cdot 50 = 0{\cdot}0319 \quad (2')$$

$$\Delta T_2 = \frac{\delta_0}{d_0} \cdot \frac{1{\cdot}00675}{20 \cdot 10^{-6}} - 0{\cdot}325 \cdot 500 - \beta\Delta T_f.$$

$$= 503(\delta_0/d_0\%) - 162 - \beta\Delta T_f \quad (3')$$

(with δ_0/d_0 here in %) and

$$\Delta T_g/H = \frac{(\delta_0/d_0\%)}{100 \cdot 2\pi \cdot 0{\cdot}005} = \frac{(\delta_0/d_0\%)}{\pi}. \quad (4')$$

After the fuel has expanded thermally to make contact with the can, further expansion leads to increased interface pressure and can strain. Assuming the fuel to be incompressible, the can strain under these conditions is

$$\varepsilon' = \frac{d_0[1 + \alpha(\beta\Delta T_f + T)] - (d_0 + \delta_0)(1 + \alpha' T)}{(d_0 + \delta_0)(1 + \alpha' T)}$$

$$= \frac{T(\alpha - \alpha') + \alpha\beta\Delta T_f - \frac{\delta_0}{d_0}(1 + \alpha' T)}{(1 + \delta_0/d_0)(1 + \alpha' T)}$$

$$= \frac{-\alpha\Delta T_2}{(1 + \delta_0/d_0)(1 + \alpha' T)} \simeq -\alpha\Delta T_2. \quad (6)$$

Thus the can strain can be immediately deduced from Fig. 14(a) as indicated. If, say, it is desired to restrict the can strain to less than 0·2 per cent, then the power H must be restricted to a value at which

$$-\Delta T_2 < \frac{0{\cdot}2}{100} \cdot \frac{10^6}{20} = 100°\text{C}.$$

The value of β to employ is given by analysing the thermal stresses and strains. For a long rod with uniform heat generation the well-known expression for the tangential and longitudinal surfaces stresses is

$$\sigma_t = \sigma_z = \frac{\Delta T_f}{2} \frac{E\alpha}{(1 - \mu)}$$

where ΔT is the temperature rise from surface to centre, E is Youngs Modulus, μ is Poissons ratio. The surface strain

$$\varepsilon_t = (\sigma_t - \mu\sigma_z)/E,$$

hence substituting,

$$\varepsilon_t = \alpha\Delta T_f/2.$$

The surface expands by half the amount it would have done had the temperature rise been uniform at ΔT, that is, $\beta = 0{\cdot}5$. In other words, the bar expands appropriate to its average temperature.

C-Shaped fuel rod

Equations (1) to (5) above apply also to the C-shaped bar, provided that K_1 and β are appropriately increased and also provided that the lower interface pressure is allowed for. Under these conditions assume $K_1 = 1{\cdot}2$, $\beta = 1{\cdot}2$ and $h = 30$, when we have:

$$\Delta T_f/H = 0{\cdot}106, \quad (1'')$$

$$\Delta T_1/H = 0{\cdot}0531, \quad (2'')$$

$$\Delta T_2 = 503(\delta_0/d_0\%) - 162 - 1{\cdot}2T_f, \quad (3'')$$

and

$$\Delta T_g/H = (\delta_0/d_0\%). \quad (4'')$$

The results of this calculation are given in Fig. 11(b). The equations plot the curve such as $AB'C'D'$ which has been smoothed off, for reasons as before, to the curve $ABCD$. It will be seen that increased C-rod expansion increases the effect of the ΔT_f term in equation (3''), reducing ΔT_2, at the expense of increasing the contact drop ΔT_1 and the drop across the fuel ΔT_f. Also can-strain due to fuel expansion is reduced, so that interference fits are permissible. For a fuel-pin of 0·2 in.

VOL. 15 1961

diameter, designed for operation at 2000 W/in.² at 500°C can inside-temperature, the fuel diametric clearance permissible can range from −0·5 to +1 thou. Normally a slight interference fit would be called for.

Figure 11(b) shows that the initial slope of the curve ($A'B'$) is controlled by equation (4). Generally, helium at several atmospheres would appear desirable to keep the slope to the minimum. The shape of the portion BC of the curve is controlled by the shape and depth of the slot. It would appear desirable that it should reach the centre-line, but higher interface pressures are possible with a shorter slot than this. The interface drop ΔT_1 is controlled by: the fuel and can surface finish, which should be as smooth as possible and free of contamination; the gas which should be hydrogen or helium for maximum thermal conductivity and at a few atmospheres pressure; the interface pressure which is controlled by depth of slot and fuel/can clearance. As burn-up proceeds the interface pressure builds-up and beyond 1000 lb/in² the interface temperature drop falls to about a tenth of its original value. Attention paid to all these features could lead to appreciably smaller centre temperature than that indicated in Fig. 11(b).

Tests made with an electrically-heated, stainless-steel rod in a stainless-steel tube at up to 3 kW/in. power rating generally confirm the accuracy of the analysis given here, except that partial contact between fuel and can gives rise to somewhat lower centre-temperature with the larger gaps. The value of β of 1·2 was obtained from tests using a $\frac{3}{4}$ in. o.d., 5/32 in. i.d. tube having a 1/32 in. radial slot. Results of Rigs 3 and 4 also appear to confirm that the approach is sound and that no intermediate thermal bond between fuel and can is necessary.

APPENDIX 2

Inspection of fuel can for defects

It is highly desirable to develop a range of can inspection methods of the highest standard, both for the present series of irradiation tests and for can inspection methods generally for a power-reactor fuel-element. The main methods suitable are:

(1) Visual inspection.
(2) Ultrasonic testing.
(3) Eddy-current testing.
(4) Electrical inspection using a twin probe (see Fig. 9).
(5) Pressure testing to nominal value at operating temperature.
(6) Metallurgical testing of samples.

Fuel-can production for a power reactor would employ all these methods each developed to the highest possible level, to ensure that defect-free cans were used for the fuel elements. In the present irradiation series, equipment was unavailable for method (2); method (5) could not be applied in the time available; commercial equipment for method (3) was tried but found too insensitive. Reliance had to be placed therefore on methods (1), (4) and (6).

Method (4) is a special development of a method used by the author for detecting defects in tungsten wire but modified to utilize experience gained in the 'sodium resistivity meter' (BLAKE, 1960) and equipment immediately to hand. It is hoped that the method should lend itself well to production testing and in any case should supplement eddy-current testing due to greater sensitivity to radial cracks (in eddy-current testing the electrical current is radial, in method (4) it is longitudinal). It also probes individually all the tube surface, virtually examining separately each elemental cube of side equal to the wall thickness.

The method is described in Fig. 9(a). An alternating current is passed down the tube via brushes at the ends. A specially constructed twin-probe of constant probe-separation about equal to the wall thickness is placed in contact with the tube and the voltage across it measured. This voltage is compared with a reference voltage derived from a current-transformer, the difference-voltage being amplified and fed to a recorder. Although intended for a different application, the design details given in BLAKE (1960) are applicable here also.

Examples of recorder traces are shown in Figs. 9(b) and (c). Two types of probe-traverse are used; helical—in which the tube rotates and the probe moves axially (like the cutting action in a lathe); and linear—in which the tube is stationary during a traverse of the probe but is rotated a few degrees before another traverse is begun. Figure 9(b) and (c) show examples of the linear traverse on tubes and on a rod with simulated defects so that the sensitivity of the method is demonstrated. Generally, the linear method, with recorder traces lined up adjacent to each other to form a kind of contour map, presents the data on the defects in a way most easy to interpret; however, this method is most tedious to apply in practice unless special equipment is developed. It will be seen that the holes, grooves and pits are readily detected, whilst wall thickness variation can be measured very accurately. So far the method is being used to select the best tubes from a given production batch.

APPENDIX 3

Sodium bonding of fuel can to inner container

Figure 10 shows the equipment used in the sodium filling. Figure 10(a) shows the fuel pin, already attached to its hold-down rod, which is to be inserted into the inner-can and bonded to it by sodium, free of gas inclusion or impurity. The main problem of sodium filling is to eliminate gas-inclusion in the sodium bond, which is encouraged by the high surface-tension of sodium, and to obtain high-purity sodium and a good clean-up of both the fuel pin, outer-surface and of the inner-can, inner-surface. Following this operation, the inner-can has to be sealed to a high standard with a known amount of argon cover-gas above the sodium so that, at reactor operating conditions, sodium pressure is 5 to 10 atmospheres.

For this work a glove box, (Fig. 10(b)), was specially built to high vacuum standard ($< \frac{1}{2}$ micron pressure), which incorporated a special filling-pot (Fig. 10(c)), welded to the glove-box floor. The filling procedure is as follows:

(1) The glove box is evacuated and then filled with 99·995 per cent purity argon at atmospheric pressure.

(2) Sodium is introduced into the glove box through a special pot in the glove-box roof. The sodium is kept at 120°C for several days being introduced to the box via a S.S. fitter. With the sodium molten in the filling-pot (Fig. 10(c)) the thermal insulating sleeve (Fig. 10(d)(1)) is inserted and the sodium heated to establish about 500°C in the lower portion of the pot and 120 to 140°C at the sodium surface. These conditions are maintained while oxide forms on the surface, from contamination on the filling-pot walls, from the insulating sleeve and from oxygen within the sodium itself. This oxide is skimmed-off leaving a mirror-bright sodium-surface. If sodium contamination from the atmosphere is suspected, the sodium is frozen and the box re-evacuated and fresh argon introduced. Conditions are established with the sodium-surface mirror-bright under normal operating temperature conditions of the filling-pot.

(3) The insulating-sleeve is removed, screwed on to the inner-can (Fig. 10(a)), and re-inserted in the sodium in the position shown in (Fig. 10(c)); for about thirty minutes various puddling

tools (Figs. 10(d), (2–4)) are inserted deep into and oscillated in the inner-can to ensure that all the argon gas is removed and that the pot is filled with clean sodium at 500°C. Sodium-filling in this way with the sodium at 500°C ensures that the walls are wetted with sodium, it encourages oxygen clean-up of the walls, and by keeping the surface-tension of the sodium low, it reduces the chance of gas remaining in the sodium. Maintaining a temperature gradient in the sodium filling-pot (500°C at the bottom, 130°C at the top) encourages cold-trap type clean-up so that the oxygen level tends to be appropriate to the 130°C saturation-level, and it makes for acceptable operating temperatures within the glove-box.

(4) With the sodium-surface bright, the fuel-pin hold-down is inserted in tool 5, (Fig. 10(d)), and slowly introduced into the sodium, oscillating it up and down all the while, until in its final lowered position when tool 5 is removed.

(5) Tool 6 is inserted into sleeve 1 which is then removed from the sodium, together with the inner-can, and placed in a special copper-block which is held at 180°C (see Fig. 10(c)). The insulating-sleeve is unscrewed and returned to the filling-pot. The sodium filling the inner-can is now visible and should be clean and bright. When its temperature has fallen to 180°C, tool 7, which has previously been cleaned in the sodium of the filling-pot, is used to displace a known amount of sodium. The sealing-cone and screw-plug, kept at 180°C previously in the copper-block, are then used to seal the inner-can.

(6) Usually 4 to 6 inner-cans are completed in this way, when they can be removed from the glove-box. They are then cleaned-up, the screw-plug turned-off to leave a lip for seal welding. If the cone and the soft-copper seal are not completely effective, this is usually evident by sodium vapour preventing the seal welding; this provides a check of the seal.

VOL.
15
1961

Reactor Science and Technology (Journal of Nuclear Energy Parts A/B) 1961, Vol. 15, pp. 160 to 163. Pergamon Press Ltd. Printed in Northern Ireland

ABSTRACTS AND TITLES OF FUTURE PAPERS

Atomnaya Energiya

Vol. 10, No. 4

Thermionic energy converters: B. A. USHAKOV.

The paper deals with the direct conversion of nuclear energy to electrical form by means of thermionic devices. A study has been made of materials containing fissile isotopes and also possessing good thermionic emission. Results are given from tests made on a converter in the core of a reactor. The converter, which is filled with inert gas, becomes a plasma caesium diode; no caesium need be introduced. It is also possible to pump off the gas while the converter is working, which extends the life and improves the performance.

Effects of neutron bombardment on the internal friction of monocrystalline and polycrystalline zinc: N. F. PRAVDYUK, YU. I. POKROVSKII and V. I. VIKHROV.

The critical stress amplitude, σ_s, has been deduced for zinc (monocrystalline and polycrystalline) before and after neutron bombardment by means of internal-friction measurements. It is found that the radiation increases σ_s, which is to be related to the onset of motion in the dislocations; the rise is caused by the interaction of the dislocations with point defects. A study has been made of the effects on σ_s and on the internal friction of the angle between the (0001) plane and the longitudinal axis of the monocrystal. The results agree well with accepted ideas on slip as derived from static tests on monocrystals stressed in extension on one axis.

Use of ion-exchange membranes in extracting uranium: B. N. LASKORIN and N. M. SMIRNOVA.

Electrodialysis by means of ion-exchange membranes is an important basic operation in chemical technology; it enables us to remove excess acid or alkali, to separate similar elements, and to extract radioactive substances from effluents. The application to the extraction of uranium is discussed. It is found that the excess acid can be removed in this way from solutions in sulphuric, nitric, and hydrochloric acids. It is also possible to remove sodium from carbonate solutions in this way.

Radiations from fission-product preparations: A. G. BYKOV, P. V. ZIMAKOV and V. V. KULICHENKO.

Separated fission-product isotopes are expensive and difficult to prepare, so the use of unseparated mixtures has been considered. Calculations and experimental results are presented for the time variation of the energy and intensity of the β and γ radiations from mixtures of various fission products. It is found that the mean β-ray energy is greatest when the fission products are two years old, the mean γ-ray energy being greatest at two to six months.

Letters to the Editor

Rotating plasma jet in a discharge in a magnetic field: A. V. ZHARINOV.

The method of dimensions in solving particle-transfer problems: SH. A. GUBERMAN.

Mean number of neutrons produced in the fast-neutron fission of ^{237}Np: V. I. LEBEDEV and V. I. KALASHNIKOVA.

Ternary fission in ^{233}U, ^{235}U, ^{239}Pu, and ^{241}Pu: T. A. MOSTOVAYA.

Theory of the ring cyclotron: A. P. FATEEV.

A travelling-wave cascade generator; a new high-voltage supply for accelerators: E. M. BALABANOV and G. A. VASIL'EV.

The *r*-method of measuring the kinetic parameters of a reactor: A. I. MOGIL'NER and V. G. ZOLOTUKHIN.

Distribution of the number of counts recorded by a neutron detector placed in a reactor: V. G. ZOLOTUKHIN and A. I. MOGIL'NER.

Density of a water-stream mixture heated throughout its bulk: V. K. ZAVOISKII.

Use of a monochromator to measure the neutron spectrum of a research reactor: YU. YU. GLAZKOV, B. G. DUBOVSKII, F. M. KUZNETSOV, V. A. SEMENOV and P'ENG FANG.

Heat transfer in a turbulent flow of liquid metal: V. I. SUBBOTIN, M. KH. IBRAGIMOV, M. N. IVANOVSKII, M. N. ARNOL'DOV and E. V. NOMOFILOV.

Power loss and initial shaft torque in seals of frozen sodium: A. V. DROBYSHEV and N. M. TURCHIN.

Calculation of the transmission of fast neutrons through cylindrical channels in a biological shield: B. R. BERGEL'SON.

Spectrum of scattered gamma rays: V. S. ANASTASEVICH.

Monte-Carlo calculations of the transmission of the gamma rays from a two-dimensional ^{137}Cs source through aluminium: A. F. AKKERMAN and D. K. KAIPOV.

Radiometric method of assaying solutions for uranium in the presence of ionium: N. N. SHASHKINA.

The scale factor for use in quantitative interpretations of gamma-gamma logs: A. M. LEBEDEV, S. G. TROITSKII and V. L. SHASHKIN.

Synthesis of uranium dodecaboride: YU. B. PADERNO.

A universal gamma-ray unit for use in radiation chemistry: N. G. ALEKSEEV, K. N. EMEL'YANOV, G. K. KLIMENKO, B. V. RYBAKOV and A. A. ROSTOVTSEV.

Choice of the radioisotope to be used in testing materials by means of gamma-ray back-scattering: A. S. RUDNITSKII.

Time variation of the decay of fission products from ^{235}U and ^{239}Pu: F. K. LEVOCHKIN and YU. YA. SOKOLOV.

News of Science and Technology

Bibliography

Vol. 10, No. 5

A fast-neutron pulsed reactor: G. E. BLOKHIN *et al.*

The pulsed fast neutron reactor at the Joint Nuclear Research Institute went critical in June 1960. The reactor was designed at the Physics Institute of the State Nuclear Energy Committee of the Council of Ministers of the U.S.S.R. A mean power of 1·2 kW was attained in July 1960. The reactor is designed to produce neutrons at a mean power of about 1 kW; the pulses are produced by prompt-neutron multiplication with the reactor in a divergent state. The half-width of the pulses (in power terms) is 36 μsec; the repetition rate can be varied between 8 and 80 pulses per second.

Behaviour of graphite in a nuclear reactor: V. I. KLIMENKOV.

Results are presented of work on radiation damage in graphite and on the effects of such damage on the graphite stacks of a reactor. Some of the effects may make it very difficult to operate the reactor; methods of overcoming these difficulties are presented. A theory is proposed for the physical basis of the damage; it is applicable over a wide range of elevated temperatures. Prevention of oxidation is considered in relation to the high temperatures encountered in new designs of reactor.

An iron canal carrying a current for injecting and extracting charged particles: A. A. ARZUMANOV, N. I. VENIKOV, E. S. MIRONOV, and L. M. NEMENOV.

It is shown that a magnetic canal can be produced without introducing any distortion into the main magnetic field of the accelerator. A method of calculation is given, and the results from calculations are compared with measurements.

Accelerating systems employing analogues of *H*-type waves: P. M. ZEIDLITS and V. A. YAMNITSKII.

During the period 1947 to 1957, little attention was given to linear accelerators employing waves analogous to *H* types because of the lack of exact methods of computation and of the need for lengthy experimental tests. Systematic measurements are presented to show that systems of this type have considerable advantages over the usual E_{010} types. The *H*-type systems can be used to produce speeds almost equal to c without change in their basic structure; this is not possible for the E_{010} type. This may be of considerable advantage for ion accelerators, because long wavelengths can be used in small systems, and because the demand for high-frequency power is reduced, especially in the low speeds range.

The spatial and energy distributions of the neutrons in a stratum containing a borehole: O. A. BARSUKOV and V. S. AVZYANOV.

Theoretical and experimental results are presented for the spatial and energy distributions of the neutron flux in limestone pierced by a borehole. The differential equations are reduced to finite-difference ones; the results are compared with experimental measurements.

An automatic cascade apparatus for producing ^{15}N in highly enriched form: I. G. GVERDTSITELI, YU. V. NIKOLAEV, E. D. OZIASHVILI, K. G. ORDZHONIKIDZE, G. N. MUSKHELISHVILI, N. S. KILADZE, V. R. MIRKIRTUMOV and Z. I. BAKHTADZE.

A description is given of an automatic apparatus for enriching ^{15}N by means of exchange in the NO—HNO_3 system. The apparatus provides about 0·5 g of nitrogen per day (99·8% ^{15}N) from nitrogen of natural isotopic composition (0·365% ^{15}N).

Propagation in air of the γ-rays from a pulsed point source: O. I. LEIPUNSKII, A. S. STRELKOV, A. S. FROLOV and N. N. CHENTSOV.

The Monte Carlo method is used to consider the propagation of γ-rays in an unbounded atmosphere; the rays have an initial energy 1 MeV and are generated by pulsed isotropic point source. The radiation intensity at a point is found as a function of time and of the angle from which the rays arrive; the spectrum of the scattered γ-rays is found as a function of time and distance. The build-up factors and the differential spectra are found by integrating the distributions with respect to time for a steady source; the angular distribution of the intensity and the angular variation in the spectrum are also deduced for three distances from the source.

Letters to the Editor

CsI(Tl) crystals for recording α-particles: L. M. BELYAEV, A. B. GIL'VARG and V. P. PANOVA.

Scintillating glasses of high light yield for detecting neutrons: V. K. VOITOVETSKII and N. S. TOLMACHEVA.

Use of a scintillation counter to detect alpha particles and fission fragments in the presence of a strong β-ray or γ-ray background: V. K. VOITOVETSKII and I. L. KORSUNSKII.

Production and use of polarized resonance neutrons: A. D. GUL'KO and YU. V. TARAN.

Radiative-capture cross sections of ^{55}Mn, ^{65}Cu, ^{138}Ba, and ^{232}Th for neutrons of energies from 0·3 to 2 MeV: YU. YA. STAVISSKII and V. A. TOLSTIKOV.

Transmission through water, pure or with a heavy component, of neutrons with energies of 0·5 and 1·0 MeV: V. I. KUKHTEVICH and B. I. SINITSYN.

Neutron distributions from an off-axis source in media having a cylindrical interface: A. E. GLAUBERMAN, V. B. KOBILYANSKII and I. I. TAL'YANSKII.

The emission from a volume source in the presence of surface activity: E. E. KOVALEVA and D. P. OSANOV.

The spectrum and temperature of the neutron gas in a graphite-water reactor: E. YA. DOIL'NITSYN and A. G. NOVIKOV.

Construction of entropy diagrams from measurements of the speed of sound: I. I. NOVIKOV and YU. S. TRELIN.

Steady-state boiling of a bulk-heated liquid: V. K. ZAVOISKII.

Critical thermal loads for pumped water below its saturation temperature: D. A. LABUNTSOV.

Corrosion of metals in an experimental channel in the IRT reactor: A. V. BYALOBZHESKII and V. D. VAL'KOV.

Activation analysis as a means of determining the isotopic composition of lithium: L. P. BILIBIN, A. A. LBOV and I. I. NAUMOVA.

Electrochemical reduction of U^{VI} to U^{IV} in hydrochloric acid in conjunction with cation-exchange membranes: B. N. LASKORIN and N. M. SMIRNOVA.

Determination of traces of uranium, thorium, and potassium in rocks by means of γ-ray spectra: N. P. KARTASHOV.

News of Science and Technology

Bibliography

Vol. 10, No. 6

Partial fuel reloading modes in nuclear reactors: E. I. GRISHANIN, B. G. IVANOV and V. N. SHARAPOV.

The effects of partial reloading with fuel on the burn-up in the working channels are discussed. The criterion of minimum cost for the electrical output is used to determine the best proportion of fuel to be changed at each reloading, assumed to be performed with the reactor shut down. A formula for this best proportion has been derived for an infinite reactor; allowance has been made for the fuel recovered. Numerical results are given for the reactors at the first nuclear power station and at the Beloyarsk power station.

Theory of the effects of irradiation on some properties of graphite: V. M. AGRANOVICH and L. P. SEMENOV.

The properties of graphite are much affected by the radiations present in a reactor, which damage the lattice structure. Calculations are presented for the changes in the lattice constant and in the internal energy per unit volume for a graphite crystal containing Frenkel defects. The calculations are compared with experimental results.

Neutron yields from ^{6}Li(t, n) and ^{7}Li(t, n) reactions: A. K. VAL'TER, P. I. VATSET, L. YA. KOLESNIKOV, S. G. TONAPETYAN, K. K. CHERNYAVSKII and A. I. SHPETNYI.

The differential cross sections for the production of neutrons at 0° in the reactions ^{6}Li(t, n) and ^{7}Li(t, n) have been measured for triton energies ranging from 0·175 to 2·4 MeV. The first reaction has a resonance at 1·875 MeV, which corresponds to the 18·936 MeV level of ^{9}Be. The second shows two resonances, one at 0·765 MeV and the other at 1·735 MeV; these point to excited levels of ^{10}Be at 17·78 and 18·46 MeV. The cross section at the resonance

$$\frac{d\sigma}{d\Omega}(0°)_{res}$$

is 37·2 mbarn/steradian for the first reaction, 95 mbarn/steradian for the first resonance of the second reaction, and 159 mbarn/steradian for the second resonance. The angular distribution has been measured from 0° to 135° at intervals of 15° for triton energies of 0·358, 0·559, 1·066, 1·218, 1·370, 1·572, and 2·123 MeV. The total cross section at the last energy is 324 ± 32·3 mbarn for the first reaction and 1332 ± 83·3 mbarn for the second.

The effects of certain compounds on the oxidation of uranium in acid media: G. M. NESMEYANOVA and G. M. ALKHAZASHVILI.

Leaching is responsible for most of the uranium lost in wet methods of processing uranium ores. A study has been made of the way in which elements having more than one valency state affect the degree of extraction; vanadium, copper, and iron ensure that the uranium is oxidized completely when the concentration of sulphuric acid is comparatively low. The copper and iron may be added as soluble salts if they are otherwise present only as minerals that are difficult to dissolve.

The 20°C isotherm for the system PuO_2F_2–HF–H_2O: I. F. ALENCHIKOVA, L. V. LIPIS and N. S. NIKOLAEV.

The isothermal-solubility method has been applied to the PuO_2F_2–HF–H_2O system at 20°C. The phases $PuO_2F_2.2H_2O$, $H_2PuO_2F_4.4H_2O$, and PuO_2F_2 have been detected; their compositions have been established by analysis and by means of Schreinemacher's method. The electronic absorption spectra confirm that the phases are distinct chemical compounds. Electromigration and potentiometric titration have been used to demonstrate the existence of the acid, $H_2PuO_2F_4.4H_2O$.

Surface coating of building structures in radioactive locations: A. N. KOMAROVSKII.

The proper surface coatings for walls, floors, and ceilings are discussed. The uses made of various types of coatings in the U.S.S.R. are described, with suggestions as to applications. The costs of the various materials are indicated.

Some thermal strength problems in reactor engineering: YA. B. FRIDMAN, N. D. SOBOLEV, S. V. BORISOV, E. I. EGOROV, V. P. KONOPLENKO, E. M. MOROZOV, L. A. SHAPOVALOV and B. F. SHORR.

A discussion is presented of some aspects of stressed and deformed states, of creep, of thermal fatigue, of thermal shock, of combinations of thermal and mechanical loading, and of stability under conditions of temperatures varying in space or time. The use of small-scale mechanical tests is discussed as a means of determining mechanical properties at various temperatures.

Letters to the Editor

Anisotropy of fission fragments from ^{240}Pu and ^{239}Pu: V. G. Nesterov, G. N. Smirenkin and I. I. Bondarenko.

Half-life of ^{137}Cs: M. P. Glazunov, A. I. Grivkova, B. A. Zaitsev and V. A. Kiselev.

Thermodynamic cycles of nuclear power stations: D. D. Kalafati.

Effects of the composition of uranium ore on the gamma-ray spectrum recorded by a scintillation spectrometer: A. G. Grammakov, V. M. Ovchinnikov and A. M. Sazonov.

Assessment from an aircraft of the Ra, Th, and K content of rock: N. D. Balyasnyi, L. I. Boltneva, A. V. Dmitriev, V. A. Ionov and I. M. Nazarov.

Use of a $CaSO_4$(Sm) phosphor in dosimetry: A. R. Krasnaya, B. M. Nosenko, L. S. Revzin and V. Ya. Yaskolko.

Maximum permissible concentration of fission-product radioactive inert-gas isotopes: Yu. V. Sivintsev.

Separation of the isotopes of neon by means of thermal diffusion: L. S. Kotousov, E. M. Martynov and Yu. P. Stepanov.

News of Science and Technology

Bibliography

VOL.
15
1961

VOL
15
196

Reactor Science and Technology (Journal of Nuclear Energy Parts A/B) 1961, Vol. 15, pp. 165 to 175. Pergamon Press Ltd. Printed in Northern Ireland

THE FISSION CROSS SECTION OF ^{235}U FROM 0·01 eV TO 0·1 eV AND ITS ABSOLUTE VALUE AT 0·0253 eV

A. J. DERUYTTER
Centre d'Etude de l'Energie Nucléaire, Mol, Belgium

(*Received* 11 *January* 1961)

Abstract—The absolute fission cross section of ^{235}U at the reference neutron velocity of 2200 m/sec was measured.

The counting rate of a 4π-fission chamber was compared with that of a ^{10}B ionization chamber by alternate measurements in a neutron beam emergent from the thermal column of BRI. The energy selection was done with a slow chopper previously calibrated with respect to the sharp breaks of σ_t for α Fe, Be, Bi, Al, C (graphite). The efficiency of the ^{10}B chamber was compared to the well-known absorption cross section of ^{197}Au by activation measurements with a $(\beta$–$\gamma)$ coincidence technique. The thickness of the ^{235}U layer was determined by comparison with α-standards of the same isotopic composition, and controlled by a mass-spectrometric method.

Our determination yields:

$$\sigma_f^0 = (587 \pm 6) \text{ barns.}$$

Some information is also obtained about the nearby negative energy levels.

INTRODUCTION

ALTHOUGH the slow neutron properties of ^{235}U were extensively studied for their interest in the theory of the fission process and the study of reactors, large deviations still exist in the experimentally measured values and in the interpretation of results (SAFFORD and HAVENS JR., 1959).

An important parameter is the fission cross section of ^{235}U at the reference neutron speed of 2200 m/sec. It is used for the normalization of relative fission cross sections; in the determination of resonance parameters an error on σ_f produces an error in Γ_f and in Γ_γ, when Γ_γ is deduced from $(\Gamma_t - \Gamma_f)$. One also needs a correctly normalized cross-section curve in the low-energy region, for detecting the negative energy levels necessary to explain the large cross-section in the thermal energy range. A normalized σ_f–curve is also needed to determine correctly the Γ_f distribution and the number of degrees of freedom of the generalized χ^2-distribution. These questions are treated in detail by HAVENS JR. and MELKONIAN (1958).

Existing values of the absolute fission cross section at 2200 m/sec are based on two kinds of measurements:

(a) Indirect measurements combining a value of the absorption cross section σ_a, with an independently measured value of $(1 + \alpha) = \sigma_a/\sigma_f$ fission.

(b) Direct measurements of the fission rate of a ^{235}U layer of known composition and weight in a known neutron flux.

The value quoted in BNL–325 (HUGHES and SCHWARTZ, 1957) is $\sigma_f^0 = 580 \pm 7$ b based on $\sigma_a = 689 \pm 7$ b and $(1 + \alpha) = 1{\cdot}188 \pm 0{\cdot}008$. BOLLINGER (1957) suggested that this value should be changed to 595 ± 12b. SAFFORD and MELKONIAN (1959) determined $(1 + \alpha)$ at 5·3 Å and deduced as value at 2200 m/sec: $(1 + \alpha) = 1{\cdot}171 \pm 0{\cdot}009$. This value yielded $\sigma_f^0 = 580 \pm 7$b. A subsequent careful redetermination of the total cross section of ^{235}U by SAFFORD *et al.* (1959) ($\sigma_t = 695{\cdot}0 \pm 1{\cdot}8$b at 0·0253 eV) and the above value of $(1 + \alpha)$ yield $\sigma_f^0 = 591 \pm 5$ barns.

Recent values obtained by the direct method are: BOLLINGER *et al.* (1957); SAPLAKOGLU (1958):

$$\sigma_f^0 = 605 \pm 6 \text{ barns}$$

BIGHAM *et al.* (1958):

$$\sigma_f^0 = 568 \pm 7 \text{ barns}$$

RAFFLE (1959):

$$\sigma_f^0 = 590 \pm 12 \text{ barns (changed from } 638 \pm 20 \text{ barns (RAFFLE, 1954)).}$$

The situation is not clear. There is however a tendency towards a value higher than the now so-called 'world weighted average value' of 582 ± 4 b.

The aim of this research was to make a careful redetermination of σ_f at 0·0253 eV by a direct method and to get at the same time supplementary information on the behaviour of $\sigma_f\sqrt{E}$ in the energy range from

0·01 eV to 0·1 eV, as below 0·02 eV discrepancies still exist in the $\sigma_f\sqrt{E}$-curves (SAFFORD and HAVENS, 1959).

The most important difficulties generally encountered in a direct method are: the absolute determination of the neutron flux, corrections for the energy spectrum of the neutrons when no energy selection is used, the determination of the efficiencies of the fission counter and the flux detector, and the determination of the quantity, composition and homogeneity of the fission foil.

For our measurements the energy selection was done with the BRI slow chopper after a careful energy-calibration with the sharp breaks in the total cross section for αFe, Be, Bi, C (graphite) and Al (DERUYTTER and CEULEMANS, 1960). As a fission counter a 4π-ionization chamber was studied and the efficiency evaluated (DERUYTTER, 1960). The neutron flux is determined with a 2π-^{10}B ionization chamber, previously calibrated by comparing it to the absolute activation of a gold foil; this avoids among other things using the absorption cross section of ^{10}B which is not as well known as σ_α (^{197}Au). The number of ^{235}U atoms is determined by comparing the fission layer with U-standards of the same isotopic composition, on the same backing material, the same diameter and about the same thickness in a low geometry counter. The method is controlled by a mass-spectrometric determination and the measurement of the α-activity in a 2π-geometry.

1. GENERAL DESCRIPTION OF THE EXPERIMENTAL METHOD

We compare a thin ^{235}U layer with a thin ^{10}B layer in identical ionization chambers and neutron flux. The ^{10}B and ^{235}U chamber are brought alternatively during a preset time at exactly the same place in the neutron beam of the slow chopper. We correct for background by taking the same measurements with Cd filters, and electrical disturbances are checked by an identical empty chamber. The energy selection is done by the BRI slow chopper with a two-meter flight path and a 25 channels time-analyser, and the beam is extracted from a thermal column.

We compare the counting-rates C_f and C_B of the ^{235}U and the ^{10}B chambers in the velocity channel $(v_1 - \Delta v,\ v_1 + \Delta v)$. The assumption is made that $v\sigma_f$ and $v\sigma_B$, the products of the neutron velocity and the corresponding cross section, vary much more slowly than $\rho(v)$ the neutron density, in the channel considered. This comparison yields for $\sigma_f{}^1$:

$$\sigma_f{}^1 = \frac{kC_f}{\varepsilon_f N_U S\, C_B} \cdot \frac{v_0}{v_1} \tag{1}$$

$\sigma_f{}^1$ is the fission cross section of ^{235}U at the neutron velocity v_1; ε_f is the efficiency of the 4π fission chamber; $N_U S$ is the total number of ^{235}U-atoms in the layer; v_0 is the reference velocity of 2200 m/sec;

$$k = \varepsilon_B N_B S \sigma_B{}^0 \tag{2}$$

and ε_B is the efficiency of the ^{10}B chamber, $N_B S$ the total number of ^{10}B atoms in the layer and $\sigma_B{}^0$ the cross section for the ^{10}B (n, α) ^{7}Li reaction at 2200 m/sec neutron velocity.

To determine k we calibrate the ^{10}B chamber against the absorption cross section of ^{197}Au following the method proposed by RAFFLE (1959) by activation measurements. The counting rate of the ^{10}B chamber in the Maxwellian spectrum of the thermal column is given by $C_B{}^M$ in equation (3) after correction for the epi-Cd neutrons:

$$C_B{}^M = \varepsilon_B N_B S \sigma_B{}^0 v_0 \int_0^{Cd} \rho\, dv \tag{3}$$

with $\sigma_B v = \sigma_B{}^0 v_0$ for the whole velocity range of the integration (SCHMITT *et al.*, 1960).

Gold foils of the same dimensions are mounted in an identical ionization chamber, filled at the same pressure with the same gas, and irradiated in the same beam, which is monitored by means of a low-pressure BF_3 counter. The induced radioactivity is determined absolutely by means of a β–γ coincidence circuit first with two plastifluor scintillators and also with an anthracene β-detector and a NaI(Tl) γ-detector.

It can be shown that A_∞ is given by:

$$A_\infty = \frac{A_1}{N_1(1 - e^{-\lambda t_1})} - \frac{A_2}{N_2(1 - e^{-\lambda t_2})}$$
$$= \alpha\beta\, \sigma_{Au}{}^0 v_0 \int_0^{Cd} \rho\, dv. \tag{4}$$

Here A_∞ is the saturated activity due to that part of the neutron spectrum below the Cd cut-off energy, A_1 is the activity due to the irradiation of a gold foil with N_1 atoms during a time t_1 without Cd cover, and A_2 is the induced activity in a foil of N_2 atoms during a time t_2 with a Cd cover. Alpha and β are correction factors for the self-absorption in the gold foils and for the non $1/v$ behaviour of the gold absorption cross section due to the 4·91 eV resonance respectively; $\sigma_{Au}{}^0$ is the $1/v$ part of the absorption cross section at 2200 m/sec; λ is the radioactive decay-constant.

From (2), (3) and (4) we conclude:

$$k = \frac{\sigma_{Au}{}^0\, \alpha\beta}{A_\infty}\, C_B{}^M. \tag{5}$$

The previous method and the error on k are discussed in Section 3.

From the discussion in Section 2, it will be noticed

that ε_f was specially studied and a 4π geometry was used to discriminate more easily for the alpha pile-up pulses. The number of ^{235}U atoms in the fissionable layer $N_U S$, is discussed in Section 4. The calibration of the velocity scale of the slow chopper is studied in detail in Section 5. Other interesting points (accuracy of positioning the chambers and the foils in the beam and energy spectrum of the beam of the thermal column) are discussed in Section 6. In Section 7 the results are summarized.

2. THE FISSION CHAMBER AND ITS EFFICIENCY ε_f

This point was studied in a previous paper. A technique has been developed to prepare fission foils of uniform thickness on thin plastic films (VYNS-3) coated with Al, to be used as a cathode inside a 4π-chamber. The evaluated efficiencies of the counter for typical thicknesses are:

$$1\ \text{mg/cm}^2: \quad \varepsilon_f = (92 \pm 1)\%,$$

$$0{\cdot}1\ \text{mg/cm}^2: \quad \varepsilon_f = (97{\cdot}5 \pm 0{\cdot}3)\%.$$

For the chamber used in the fission measurements, it is attractive to use a 0·1 mg/cm² UO_2 film with its high efficiency. But as we could use only one fission film, in order to reduce the error in the flight path and the velocity determination, such a thin film would give a too low counting rate. Therefore we selected a

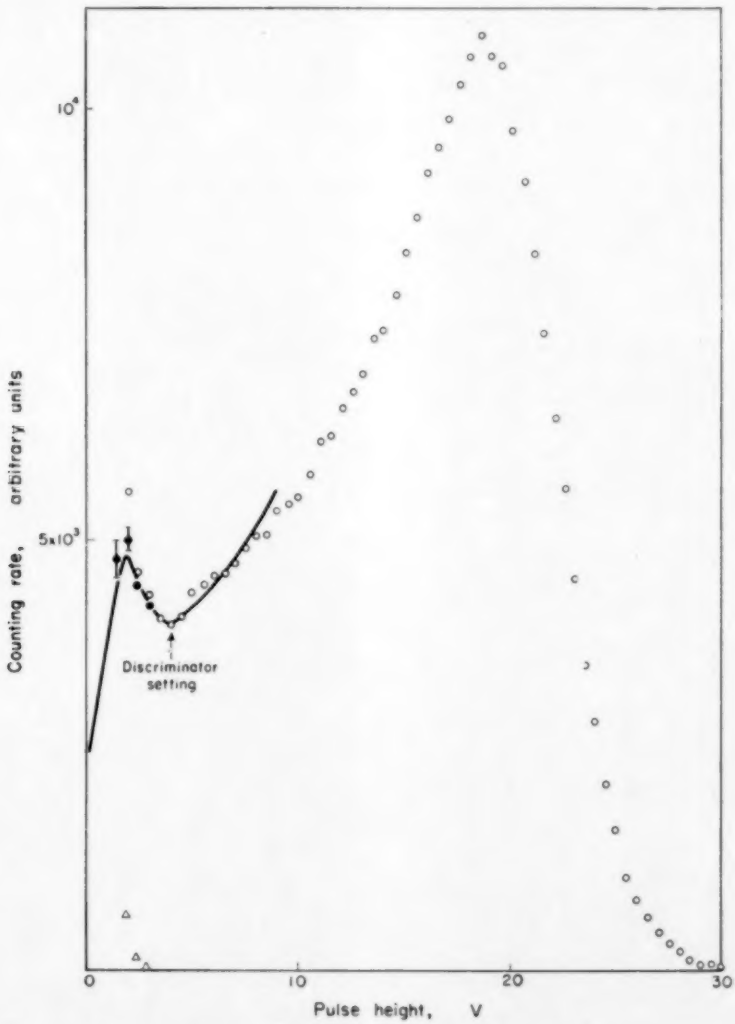

FIG. 1.—Differential curve for the fission chamber.
○: fission counting rate; ●: corrected fission counting rate.
Δ: α-particle background. The solid line is the theoretical self-absorption curve used to extrapolate to zero bias.

VOL. 15 1961

fission film with (0·661 ± 0·003) mg/cm² ^{235}U (discussed in Section 4) and an intermediate value for the efficiency.

The differential pulse-height spectrum was registered with a 100-channel Marshall analyser before and during the measurements with the slow chopper (Fig. 1). For the final measurements a discriminator bias was chosen somewhat higher than the maximum α-pulse height and corresponding to the lowest point of the counting rate valley. The choice of this bias influences the efficiency but not its precision if the whole pulse height distribution is followed continuously. The value found was:

$$\varepsilon_f = (0{\cdot}888 \pm 0{\cdot}005).$$

3. CALIBRATION OF THE ^{10}B IONIZATION CHAMBER

(a) The ^{10}B ionization chamber is identical to the fission chamber except for the anode–cathode distance (1·2 cm). The ^{10}B layer was prepared by vacuum evaporation of metallic boron from tungsten boats. This metallic powder* contains 98·0 per cent boron, of which 96·0 per cent is ^{10}B (isotopical analysis) and 0·07 per cent Fe (spectrographic analysis).

With a ^{10}B layer of approximately 5 μg/cm² (two layers of about 2·5 μg/cm² on both sides of a thin aluminium disk) we obtained a good resolution (Fig. 2) and a sufficient counting rate and stability with the discriminator bias set between the α and the Li-peaks.

The pulses from the chamber are very small and a preamplifier with low noise and a large gain was constructed based on a circuit designed by Chase (Brookhaven) and reported in SAFFORD and MELKONIAN (1959). The signal/shot noise-ratio increases with lower capacities of the chambers. The ^{10}B chamber had a capacity of 10 μμF and the fission chamber of 12 μμF. When we consider the pulse-height distribution of the ^{10}B chamber (Fig. 2) we see that the effect of the noise is negligible.

(b) The calibration of the ^{10}B chamber is done

* Supplied by Oak Ridge National Laboratory, Oak Ridge, Tennessee, U.S.A.

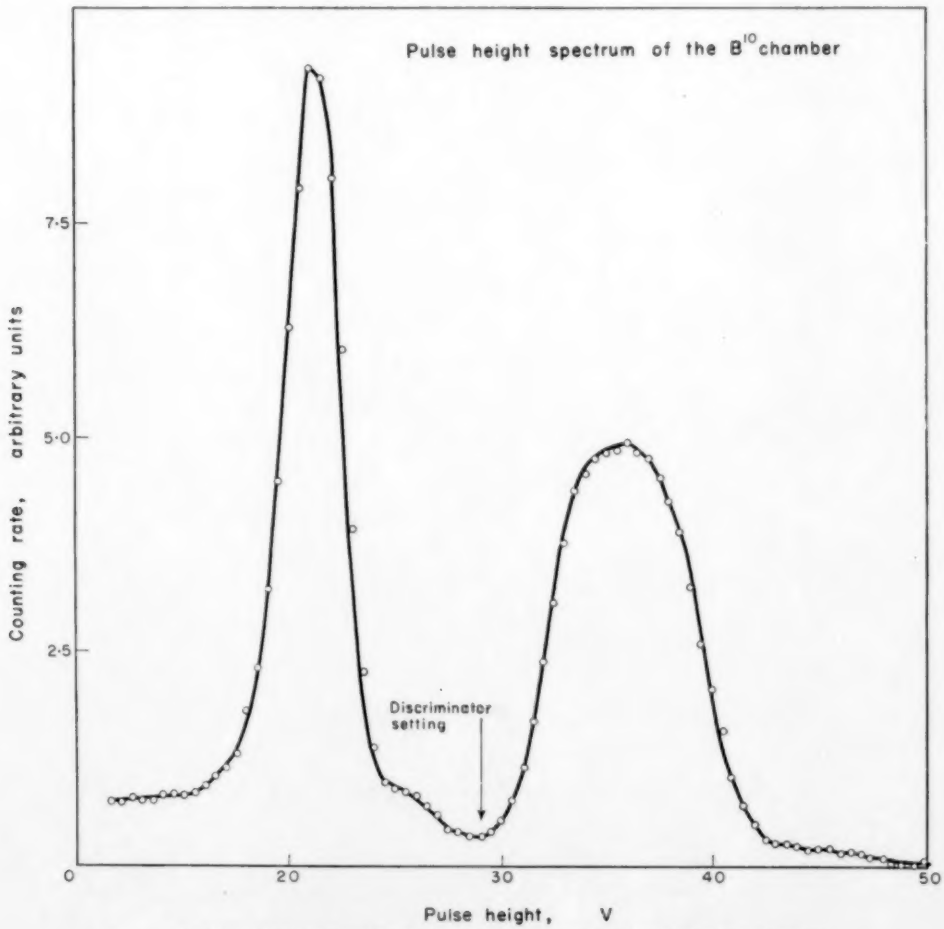

FIG. 2.—The differential pulse-height spectrum of the ^{10}B ionization chamber.

relatively to the absorption cross section of ^{197}Au, because ^{197}Au has a sufficiently large cross section, close to $1/v$ up to 0·02 eV, and ^{198}Au has a simple decay-scheme well suited for a β–γ coincidence measurement. The agreement on the absorption cross section as measured by various laboratories is excellent.

Referring to equation (4), it can be shown (RAFFLE, 1959) that α and β are given by:

$$\alpha = 1 - \frac{N_{Au}}{2} \frac{\int_0^{Cd} \rho_0(v)\sigma_a\sigma_f dv}{\int_0^{Cd} \rho_0(v)\sigma_a v dv} \tag{6}$$

and

$$\beta = 1 + \frac{\int_0^{Cd} \rho_0(v)[(1 - E/E_r)^{-2} - 1]\, dv}{\int_0^{Cd} \rho_0(v) dv} \tag{7}$$

where the integrations are carried out up to the Cd cut-off velocity. For values far below the resonance energy E_r the Breit-Wigner resonance formula is written as:

$$\sigma_a v = \frac{\sigma_{Au}{}^0 v_0}{(1 - E/E_r)^2}.$$

In these formulas $\rho_0(v)$ is the neutron velocity spectrum incident on the foils. This spectrum was determined with the slow chopper, correcting for the rotor transmission probability, the absorption cross section of the air flight path and the losses by dead time of the electronic circuitry. We found a Maxwellian spectrum with a most probable velocity $v_0 = 2336$ m/sec (Fig. 3). For a pure Maxwellian spectrum (7) reduces to

$$\beta = 1 + \frac{3\,E_T}{E_r}.$$

In our case, $E_T = 0{\cdot}0285$ eV and $E_r = 4{\cdot}91$ eV. So $\beta = 1{\cdot}0174$.

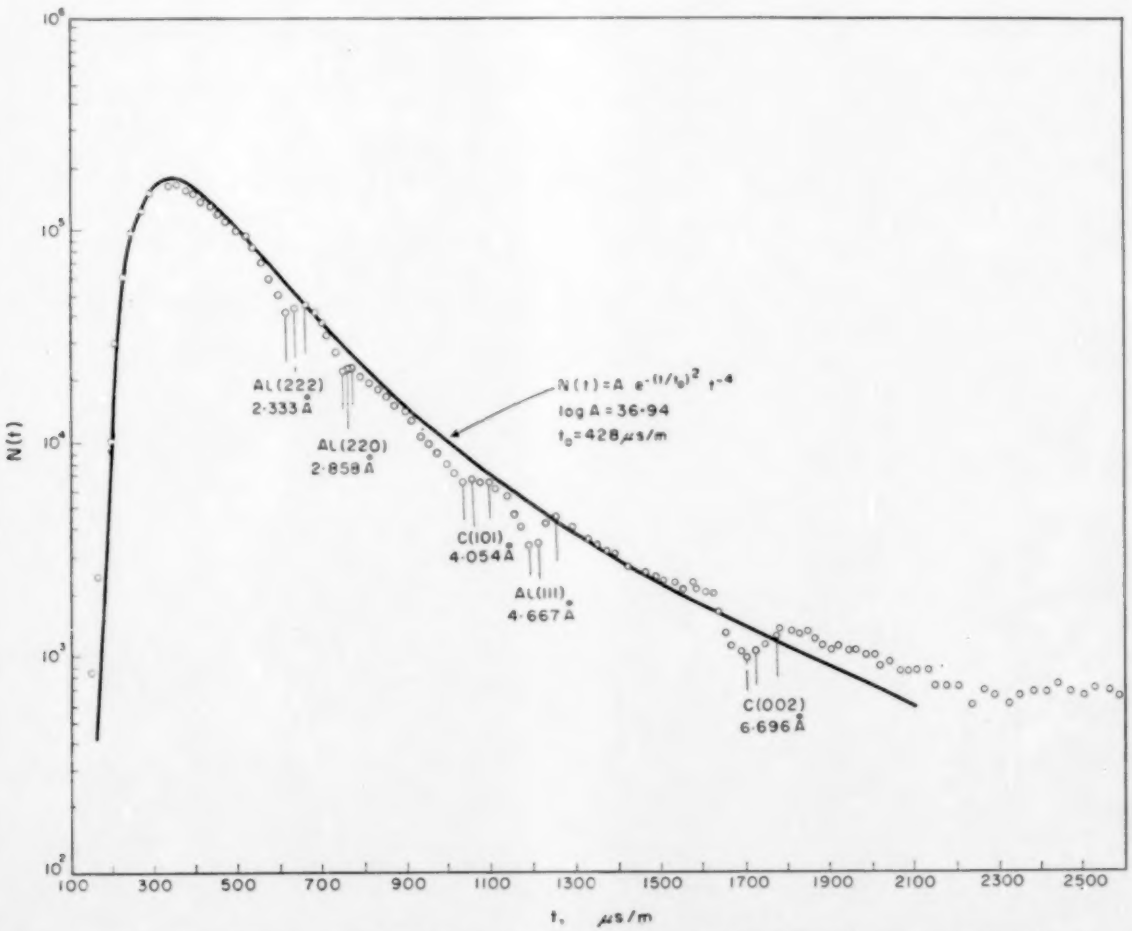

FIG. 3.—The Maxwellian spectrum of the thermal column of BRI, measured with the slow chopper as a function of the flight-time. The open circles are the experimental points; the solid line is the best fit by least squares.

VOL. 15 1961

When we put $\sigma_a = \sigma_t$ in (6) and assume the previous $\rho_0(v)$ one gets $\alpha = 0{\cdot}983$ and $\alpha\beta = 1{\cdot}000$.

Referring to (5), the error on k is composed of the independent errors on the factors present. We assume an error of 5 per cent in the correction terms in α and β due to the inhomogeneity of the gold foils and deviations from the adopted Maxwellian spectrum. This results in a 0·1 per cent error for the product $\alpha\beta$. The error on $C_B{}^M$, the counting rate of the ^{10}B-ionization chamber in the beam of the thermal column, corrected for background and epi-Cd neutrons, can be reduced to 0·1 per cent by taking a sufficiently long measuring time.

The $1/v$ part of the absorption cross section of ^{197}Au quoted in the literature is:

$$\sigma_{Au}{}^0 = 97{\cdot}8 \pm 0{\cdot}5 \text{ barns}$$
(GOULD *et al.*, 1957; CARTER *et al.*, 1953)

$$= 97{\cdot}4 \pm 0{\cdot}9 \text{ barns}$$
(EGELSTAFF, 1954).

We have adopted $97{\cdot}7 \pm 0{\cdot}5$ barns.

The determination of the saturated activity A_∞ of the Au foil was carried out with a β–γ plastifluor coincidence circuit, using a 1 mm thick β-detector and a 5 cm thick γ-detector shielded with a 2 mm thick Al plate.

The elementary equation used for the disintegration rate is:

$$N_0 = \frac{N_\beta N_\gamma}{N_c} \tag{8}$$

N_β and N_γ being the counting rates of the β and the γ-channel and N_c the coincidence-counting rate corrected for background, accidental coincidence rate and dead time when needed.

Corrections were made for efficiency changes over the foil surfaces. The discriminator in the β-channel is set at a level sufficient to eliminate the conversion electrons, and we take into account the complexity of the decay scheme. A correction for the γ-sensitivity of the β-counter and the γ-γ coincidences is made. Bremsstrahlung of these weak β-rays may be neglected. The effect of the recently (STEFFEN, 1960) determined β–γ directional correlation anisotropy was negligible in our counter geometry.

An additional measurement* was made with a coincidence apparatus using an anthracene β-detector and a NaI γ-detector, and the results coincide within the experimental errors. Gold foils irradiated at BRI and measured with our equipments were also controlled independently by A. Detroyer of the UMHK Laboratory in Brussels. The results agreed very well. The value finally adopted for (8) is:

$$\frac{N_\beta N_\gamma}{N_c} = (1{\cdot}035 \pm 0{\cdot}003)N_0.$$

Table 1 lists various values obtained for A_∞, taking $\lambda = 1{\cdot}784 \times 10^{-4}$ min^{-1} (LOCKETT and THOMAS, 1953; STROMINGER *et al.*, 1958) with an error of 0·1 per cent. This shows that A_∞ is determined with an accuracy of 0·6 per cent.

From the measured value of $C_B{}^M$ one obtains for k the values given in Table 2.

The four values agree within the quoted errors and

* This measurement was done by H. DEPUYDT, C.E.N. Mol, Belgium.

TABLE 1

No.	Irradiation time (min)	Activity after irradiation	A_∞	N_{Au} in units 10^{21}	Saturated activity per atom, corrected for epi-Cd neutrons
1	100	60 ± 1	3387 ± 58	$0{\cdot}8649 \pm 0{\cdot}0005$	$(3{\cdot}890 \pm 0{\cdot}066)\ 10^{-18}$
2	902	$505{\cdot}7 \pm 2{\cdot}7$	3402 ± 18	0·8716	$(3{\cdot}876 \pm 0{\cdot}021)\ 10^{-18}$
3	906	$510{\cdot}0 \pm 2{\cdot}7$	3416 ± 18	0·8710	$(3{\cdot}896 \pm 0{\cdot}021)\ 10^{-18}$
4	897 (under Cd)	$3{\cdot}4 \pm 0{\cdot}4$	23 ± 3	0·8655	
5	908	$461{\cdot}7 \pm 2{\cdot}7$	3088 ± 18	0·8933	$(3{\cdot}431 \pm 0{\cdot}020)\ 10^{-18}$
6	918	$485{\cdot}9 \pm 2{\cdot}6$	3216 ± 17	0·8915	$(3{\cdot}582 \pm 0{\cdot}019)\ 10^{-18}$

TABLE 2

No.	Saturation activity per atom and per second	$C_B{}^M$/sec	k in units 10^{-3}
2	$(3{\cdot}876 \pm 0{\cdot}021)10^{-18}$	$(108{\cdot}24 \pm 0{\cdot}16)10^{-18}$	$2{\cdot}729 \pm 0{\cdot}020$
3	$(3{\cdot}896 \pm 0{\cdot}021)10^{-18}$	$(108{\cdot}24 \pm 0{\cdot}18)10^{-18}$	$2{\cdot}715 \pm 0{\cdot}020$
5	$(3{\cdot}431 \pm 0{\cdot}020)10^{-18}$	$(94{\cdot}48 \pm 0{\cdot}29)10^{-18}$	$2{\cdot}691 \pm 0{\cdot}022$
6	$(3{\cdot}582 \pm 0{\cdot}019)10^{-18}$	$(98{\cdot}92 \pm 0{\cdot}23)10^{-18}$	$2{\cdot}698 \pm 0{\cdot}021$

VOL 15 196

yield a mean value of: $k = (2{\cdot}708 \pm 0{\cdot}009)\,10^{-3}$. This standard deviation of 0·3 per cent shows that the reproducibility of results is good. As the error on a single k determination is about 0·8 per cent, we thought it was acceptable to quote 0·6 per cent as a final error on k.

4. DETERMINATION OF THE NUMBER OF ^{235}U ATOMS IN THE FOIL

The most important difficulties encountered in the determination by α-counting of the number of ^{235}U-atoms in a thin layer are:

1. The determination of the efficiency of the detector, influenced by the self-absorption in the layer and the backscattering of the base-plate when using a 2π geometry. With a low geometry counter the above difficulties are avoided but the main difficulty remains namely the exact knowledge of the geometry factor.
2. The knowledge of the disintegration constants of the isotopes present in the layer.

We use a low geometry counter to compare the unknown foil with standards made from the same solution. In this way we do not need an exact knowledge of the geometry factor of the chamber, and as foil and standards have the same isotopic composition and so the same specific activity (disintegrations/min/mg) the disintegration constants of the isotopes are not needed.

As alpha detector, we use a ZnS(Ag) scintillator coupled to a photomultiplier. The plateau of the counter has a slope of $1{\cdot}4 \times 10^{-4}$ per volt between 1320 and 1480 volt PM-H.V.

The standards are prepared on mechanically polished aluminium disks by a TEG-painting technique (JAFFEY, 1954; HUFFORD and SCOTT, 1949; DODSON *et al.*, 1952). The solution used for the preparation was calibrated by conversion of the uranyl-nitrate into U_3O_8 from 10 cm³ of the solution and careful weighing.

TABLE 3

Crystal	Planes (*hkl*)	Measured value (Å)	Calculated value* (Å)
α Fe	(110)	4·048	4·046
Be	(100)	3·921	3·951
	(101)	3·446	3·459
C	(101)	4·040	4·054
(graphite)	(002)	6·693	6·696
Al	(222)	2·337	2·333
	(220)	2·851	2·858
	(111)	4·654	4·667
Bi	(110)	6·535	6·548

* WYCKOFF, 1951; PEARSON, 1958; HENRY and LONSDALE, 1952; HENRY *et al.*, 1953.

The foil and the standards are of about the same thickness and were intercompared for several short periods to eliminate possible positioning errors. No influence of self-absorption was detected.

From this comparison we calculate the total amount of uranium in the layer: $(2{\cdot}075 \pm 0{\cdot}011)$ mg, and by considering the isotopic composition of the foil, we get for the ^{235}U total content:

$$(1{\cdot}833 \pm 0{\cdot}010)\ \text{mg}\ ^{235}U.$$

The isotopic composition of this film† in percentage of weight is:

^{235}U: $(88{\cdot}35 \pm 0{\cdot}02)$
^{234}U: $(1{\cdot}202 \pm 0{\cdot}005)$
^{236}U: $(3{\cdot}756 \pm 0{\cdot}007)$
^{238}U: $(6{\cdot}69 \pm 0{\cdot}02)$

Our method was checked by a mass-spectrometric dilution technique, and the agreement was good. A second check was made with a 2π α-counter; we determined in the foil $(1{\cdot}86 \pm 0{\cdot}07)$ mg ^{235}U in agreement with the previous result.

5. THE ENERGY CALIBRATION OF THE SLOW CHOPPER

The neutron energy selected goes from about 0·01 eV to 0·1 eV. The selection is done by the BRI slow chopper, mounted at the thermal column. The calibration of the time basis was done by using the sharp discontinuous changes in the coherent scattering cross sections of polycrystals as α Fe, Al, graphite, Be, Bi.

Transmission measurements of these elements were carried out with the slow chopper. The data are only accepted after a thorough statistical analysis. We corrected for the shift of the mean detection point of the $^{10}B(n, \alpha)^7Li$ reaction in the 12 EB 70 BF_3 detectors with respect to the central wire. We determined with 0·1 mm accuracy the distance from the rotor axis to the central wire. After these corrections the experimental position of the 'cut-off' was determined and compared to the values calculated from crystallographic data. The comparison is made in Table 3.

The mean deviation is about 0·2 per cent. To calculate this value we did not take the results for Be, because the (002) planes with $\lambda_C = 3{\cdot}577$ Å influence the results. So, we believe the flight time is known to 0·2 per cent.

6. POSITIONING OF THE CHAMBERS IN THE BEAM

The intensity distribution of the neutrons in the beam was measured and it was concluded that an

† The enriched uranium was supplied by the A.E.C. (U.S.A.) The mass-spectrometric measurements were made by Dr. G. H. DEBUS, B.C.M.N. Mol, Belgium.

TABLE 4

Channel number	Flight time (μsec/m)	v (m/sec)	E (eV)	Experimental result (barn)	Best straight line fit (barn)
1	210	4,762	0·11855	246·5 ± 4·5	221·7
2	230	4,348	0·09884	253·1 ± 4·2	251·5
3	250	4,000	0·08365	277·5 ± 4·2	281·3
4	270	3,704	0·07173	308·6 ± 4·5	311·2
5	290	3,448	0·06215	341·5 ± 4·8	341·0
6	310	3,226	0·05441	375·6 ± 5·3	370·9
7	330	3,030	0·04798	406·2 ± 5·8	400·7
8	350	2,857	0·04267	426·7 ± 6·1	430·5
9	370	2,703	0·03820	463·7 ± 6·8	460·4
10	390	2,564	0·03437	483·5 ± 7·2	490·2
11	410	2,439	0·03110	527·6 ± 7·9	520·0
12	430	2,326	0·02829	545·0 ± 8·4	549·9
13	450	2,222	0·02581	579·9 ± 9·3	579·7
14	470	2,128	0·02367	622·9 ± 10·3	609·6
15	490	2,041	0·02178	629·2 ± 10·8	639·4
16	510	1,961	0·02010	659·7 ± 12·0	669·3
17	530	1,887	0·01862	704·2 ± 13·9	699·1
18	550	1,818	0·01728	742·3 ± 15·8	728·9
19	570	1,754	0·01608	778·4 ± 17·6	758·8
20	590	1,695	0·01502	784·8 ± 19·1	788·6
21	610	1,639	0·01404	792·2 ± 19·3	818·5
22	630	1,587	0·01347	855·8 ± 20·4	848·3
23	650	1,538	0·01237	888·9 ± 22·3	878·1
24	670	1,493	0·01165	898·4 ± 24·0	908·0
25	690	1,449	0·01098	903·4 ± 27·5	937·8

error of 1 mm in the horizontal or vertical positioning of the foils causes only a relative change of 5×10^{-4} in the total number of neutrons per second hitting the foil. Such an accuracy is easily achieved by proper design of the sample changer.

7. RESULTS AND DISCUSSION

Scattering corrections for the aluminium of the chambers are estimated and can be neglected as in the expression of σ_f[1] (1) only the ratio of C_f/C_B is present. So the correction may be written as a difference of the corrections on C_f and C_B, which are small and nearly identical.

The correction for backscattering by the plastic support of the ^{235}U layer was difficult to calculate, but a maximum of 10^{-4} was estimated and consequently neglected. Corrections for ternary fission and fission into two fragments and a long range α-particle are also negligible. At these low energies we are far below the fission barrier for ^{238}U, ^{234}U and ^{236}U present in the foil, and their thermal contribution is most probably negligible.

The final fission measurements were done with a rotor speed of 6,000 rev/min (giving a 54 μsec maximum burst time) and 40 μsec wide time channels.

We calculated σ_f[1] for the 25 channels going from 200 μsec/m (0·1307 eV) to 700 μsec/m (0·0107 eV) using (1) with the values of the factors resulting from the previous discussions, and the experimental values of C_f and C_B.

The so-calculated values of σ_f are plotted in Fig. 4 and listed in Table 4. The result for σ_f at 454·5 μsec/m or 2200 m/sec, taking only into account the result obtained in the channel around 450 μsec/m and extrapolating to 2200 m/sec by a $1/v$ law, is (586 ± 9) barns.

The results do not follow a $1/v$ law (Fig. 5), but it is possible to fit a straight line through the experimental points by least squares (Fig. 4).

This weighted best fit is:

$$y_0 = (a + bt) \text{ barns with } a = -91{\cdot}67$$
$$b = 1{\cdot}492$$
$$t \text{ in } \mu\text{sec/m}$$

y_0 is the fission cross section; the individual points are weighted according to $1/\sigma^2$ (where σ is the error on the experimental results). We calculate an average standard deviation for the individual experimental results with respect to the best fit values:

$$S_y^2 = \frac{\sum_i p_i (y_0 - y_i)^2}{\sum_i p_i}$$

p_i are the weights of the individual measurements; y_0 is the best straight line fit and y_i the experimental

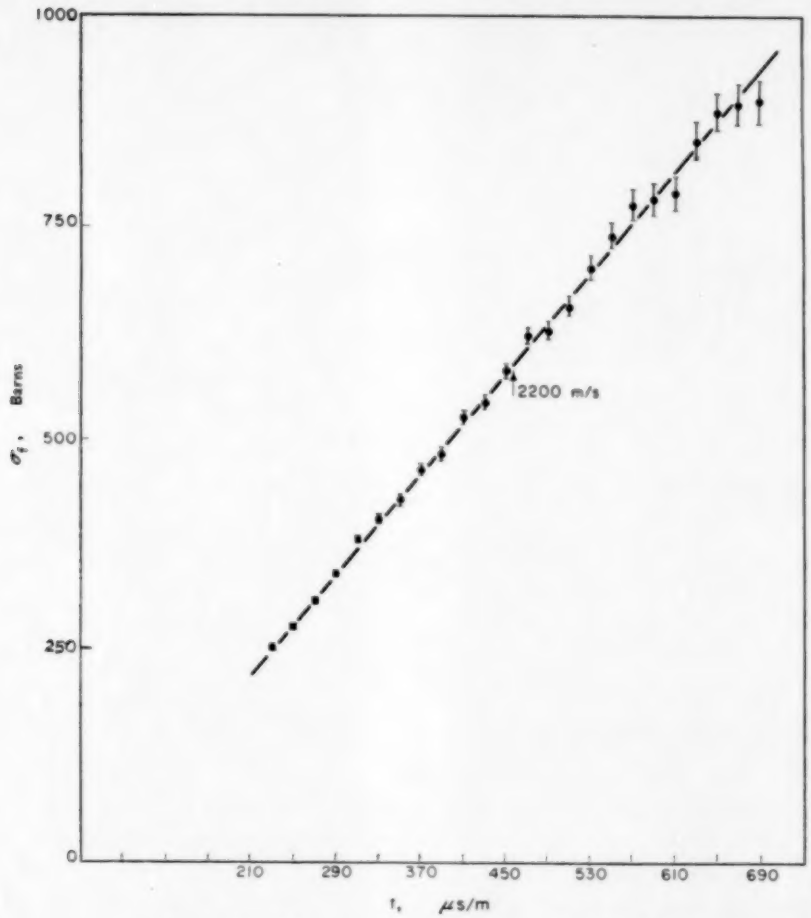

FIG. 4.—The fission cross section of ^{235}U as a function of the neutron flight-time. The solid line is the best straight line fit through the data.

values. S_y is about 6 barns. From this, one deduces as standard error on y_0 at 2200 m/sec a value of 1·2 barn.

It seems however safer to adopt as error on the final result, the average error of individual measurements, as the straight line fit is somewhat arbitrary. But as our results do not contradict this fit, we adopt the result of this fit at 2200 m/sec as representative and quote finally:

$$\sigma_f^0 = 587 \pm 6 \text{ barns.}$$

This value is in good agreement with the last result of SAFFORD *et al.* (1959) (590·8 ± 5·4) barn obtained by an indirect measurement. It shows that the 'world average' value is probably too low as suggested by BOLLINGER (1957).

In Fig. 5 $\sigma_f v$ (barns m/sec) is plotted as a function of the time of flight, together with 2 theoretical fits that have been proposed. The statistical accuracy is not high, but without doubt a Reich-Moore (REICH and MOORE, 1958) formula with the parameters calculated by SHORE and SAILOR (1958) (i.e. two negative resonances at −0·02 eV and −1·45 eV) and normalized to our value of σ_f^0 fits the results better than the fit proposed by VOGT (1958 and 1960) who introduced only one negative level at −0·95 eV.

Acknowledgments—The author wishes to thank DR. M. NEVE DE MEVERGNIES for following the progress of this work with such encouraging interest, and for his many useful suggestions. My thanks are expressed to DR. G. H. DEBUS for the mass-spectrometric measurements, and to MR. H. MORET for the flight-path length measurement, both from BCMN, Euratom, Mol (Belgium).

I should also like to thank MR. H. CEULEMANS for his large contribution in the construction of the slow chopper and the whole staff and technical people of the Neutron Physics especially MME DE CORTE, and MM. DE KEYSER, MARCHAL, MIES, RAVOET and VAN STEELANDT, for their steady and excellent technical assistance during the whole research.

VOL. 15 1961

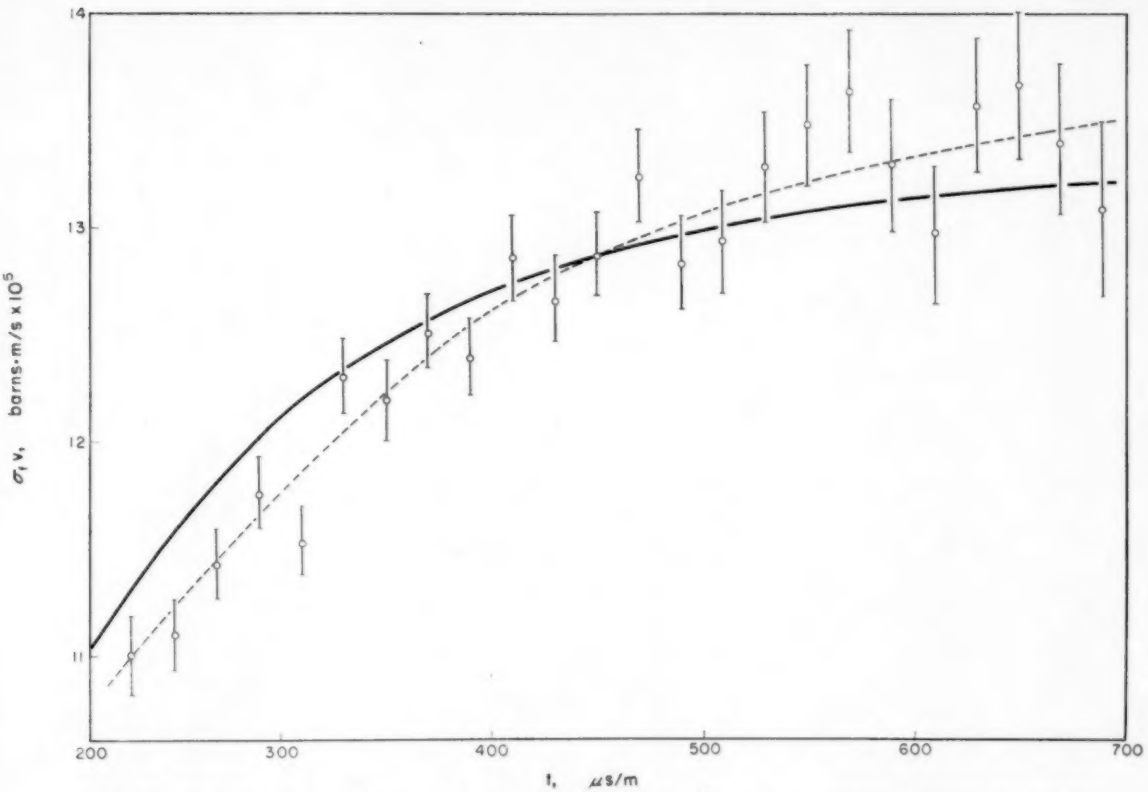

FIG. 5.—$(\sigma_f v)$ plotted as a function of the neutron flight-time. ⊖ are the experimental points; the full line is the VOGT fit and the dotted one is the fit of SHORE and SAILOR with a REICH-MOORE formula, both normalized to our value at 2200 m/sec.

The author also acknowledges useful comments made by DR. J. S. STORY, A.E.R.E., Harwell, about the backscattering of the plastic film supporting the ^{235}U layer and the influence of the β–γ angular correlation anisotropy in the ^{198}Au decay in the present results.

REFERENCES

BIGHAM C. B., HANNA G. C., TUNNICLIFFE P. R., CAMPION P. J., LOUNSBURY M. and MACKENZIE D. R. (1958) *Proceedings of the Second International Conference on the Peaceful Uses of Atomic Energy, Geneva*, Paper A/Conf. 15/P/204. United Nations, N. Y.

BOLLINGER L. M. (1957) Report to the A.E.C. Nuclear Cross Section Advisory Group, Idaho Falls, Idaho, WASH 197.

BOLLINGER L. M., SAPLAKOGLU A., COCEVA C., COTE R. E. and THOMAS G. E. (1957) *Bull. amer. Phys. Soc.*, Ser. II, **2,** 196.

CARTER R. S. *et al.* (1953) *Phys. Rev.* **92,** 716.

DERUYTTER A. J. and CEULEMANS H. (1960) *Mededel. Belg. Nat. Veren* Ser. II, **1,** 62.

DERUYTTER A. J. (1960) *Nucl. Instrum. Meth.* **7,** 145.

DODSON R. W. *et al.* (1952) *National Nuclear Energy Series*, Division V, Vol. 3, pp. 8, 12, McGraw-Hill, New York.

EGELSTAFF P. A. (1954) *J. Nucl. Energy* **1,** 57.

GOULD F. *et al.* (1957) *Bull. amer. Phys. Soc.*, Ser. II, Vol. 2, No. 1, NA 11.

HAVENS W. W. JR. and MELKONIAN E. (1959) *Proceedings of the Second International Conference on the Peaceful Uses of Atomic Energy, Geneva*, Paper 15/P/655. United Nations, N.Y.

HENRY N. F. M. and LONSDALE K. (1952) *International Tables for X-Ray Crystallography*, Kynoch Press, Birmingham.

HENRY N. F. M., LIPSON H. and WOOSTER W. A. (1953) *The Interpretation of X-Ray Diffraction Photographs*, Van Nostrand, New York.

HUFFORD D. L. and SCOTT B. F. (1949) *National Nuclear Energy Series*, Division IV, Vol. 14B, p. 1158, McGraw-Hill, New York.

HUGHES D. J. and SCHWARTZ R. (1957) *Neutron Cross-Sections* BNL-325, Suppl. 1.

JAFFEY A. H. (1954) *National Nuclear Energy Series*, Division IV, 14A, pp. 641, 673, 701, McGraw-Hill, New York.

LOCKETT E. J. and THOMAS R. H. (1953) *Nucleonics* **11,** (3), 14.

PEARSON W. B. (1958) *A Handbook of Lattice Spacings and Structures of Metals and Alloys*, Pergamon Press.

RAFFLE J. F. (1954) AERE Report NRDC-51.

RAFFLE J. F. (1959) *Thermal Neutron Fission Cross-Sections of Several Isotopes.* A.E.R.E. R/2998.

RAFFLE J. F. (1959) *J. Nucl. Energy* **10,** 8.

REICH C. W. and MOORE M. S. (1958) *Phys. Rev.* **111,** 929.

SAFFORD G. J. and HAVENS W. W. JR. (1959) *Nucleonics* **17,** (11), 134.

SAFFORD G. J. and MELKONIAN E. (1959) *A Determination of the Absolute Neutron Fission Cross Section of* 235-U. CU 186.

SAFFORD G. J. and MELKONIAN E. (1959) *Phys. Rev.* **113,** 1285.

SAFFORD G. J., HAVENS W. W. JR. and RUSTADT B. M. (1959) *Nucl. Sci. Engng.* **6,** 433.

SAPLAKOGLU A. (1958) *Proceedings of the Second International Conference on the Peaceful Uses of Atomic Energy, Geneva*, Paper A/Conf. 15, P/1599. United Nations, N. Y.
SCHMITT H. W. *et al.* (1960) *Nucl. Phys.* **17,** 109.
SHORE F. J. and SAILOR V. L. (1958) *Phys. Rev.* **112,** 191.
STEFFEN R. M. (1960) *Phys. Rev.* **118,** 763.
STROMINGER D., HOLLANDER J. M. and SEABORG G. T. (1958) *Rev. mod. Phys.* **30,** No. 2, Part II, 774.
VOGT E. (1958) *Phys. Rev.* **112,** 203.
VOGT E. (1960) *Phys. Rev.* **118,** 724.
WYCKOFF R. W. G. (1951) *Crystal Structures*, Interscience, New York.

VOL.
15
1961

Reactor Science and Technology (Journal of Nuclear Energy Parts A/B) 1961, Vol. 15, pp. 176 to 184. Pergamon Press Ltd. Printed in Northern Ireland

THE OXIDATION AND RELEASE OF IODINE-131 FROM URANIUM SLUGS OXIDIZING IN AIR AND CARBON DIOXIDE

W. J. MEGAW, R. C. CHADWICK, A. C. WELLS and J. E. BRIDGES
Atomic Energy Research Establishment, Harwell, Berks.

(*Received* 20 *January* 1961)

Abstract—Experiments to determine the oxidation rate, particle size distribution of oxide and release of iodine-131 from one kilogram, trace irradiated uranium slugs oxidizing at temperatures up to 1000°C in air and carbon dioxide are described. The release of iodine as a result of rapid melting of uranium is also investigated. It is concluded that extensive release of elemental iodine as vapour is always accompanied by extensive oxidation and that for temperatures below the melting point the release of elemental iodine as vapour is greater for oxidation in air than in carbon dioxide. It is stressed that for the geometrical arrangement and gas velocities used the greater part of the iodine inventory of the uranium remains contained in or adsorbed on particles of uranium oxide.

1. INTRODUCTION

MUCH work has been carried out in the last ten years on the behaviour of reactor fuel materials when exposed to coolant gases at temperatures in excess of normal reactor operating temperatures. The purpose of the work has been to forecast the behaviour of fuel elements under reactor fault conditions and, in particular, ANTILL *et al.* (1958) HILLIARD (1958) and SCHNIZLEIN *et al.* (1959) have determined oxidation rates of portions of fuel elements, HOPKINSON (1957) has investigated the particle size distribution of uranium oxide, and CREEK, MARTIN and PARKER (1959) and HILLIARD (1959) have studied the emission of fission products from molten fragments of fuel elements. Most of the work referred to was performed on quite small specimens of material of volume perhaps a few cubic centimetres and in low gas flows, in some instances amounting to still gas conditions. It is apparent that the physical dimensions of the specimen, particularly its surface-to-mass ratio and the gas flow past it, could have a marked effect on both the oxidation rate and the particle size of the oxide. The experiments described in this paper were, therefore, performed on a specimen of similar surface-to-mass ratio to fuel elements used in conventional gas-cooled natural uranium reactors and in gas velocities of up to several metres per second.

The dimensions of the cylindrical specimens used were 1·15 inches diameter and 3 inches long. The weight of uranium was one kilogram. In addition to determining the effects of sudden melting of irradiated uranium, it was decided also to study the effects on the uranium specimen of being maintained for prolonged periods at temperatures above normal operating temperatures, but below the melting point.

2. EXPERIMENTAL METHOD

2.1 *General description of rig*

The experimental rig which is illustrated in Figs. 1 and 2 consisted of a closed circuit of Pyrex tubing incorporating a fan and various sampling devices, together with an orifice plate for measuring the gas flow rates. The rig could be filled with carbon dioxide from a generator, air from compressed air mains or mixtures of the two. No purification or drying of the gas was carried out. In order to prevent leakage from atmosphere, the rig was run sufficiently above atmospheric pressure to ensure a slight positive pressure at the fan intake and fresh gas was continually pumped into the rig and out through a water lute during runs.

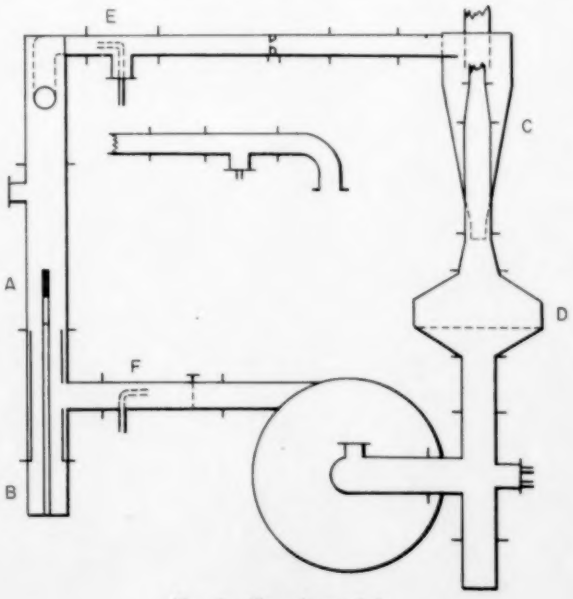

FIG. 1.—Experimental rig.

VOL.
15
1961

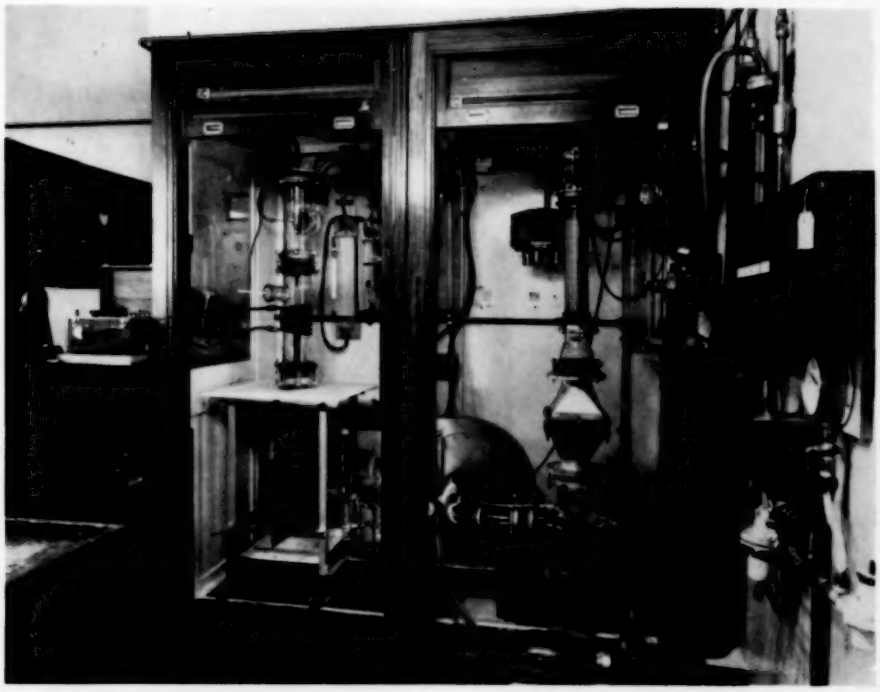

FIG. 2.—Experimental rig.

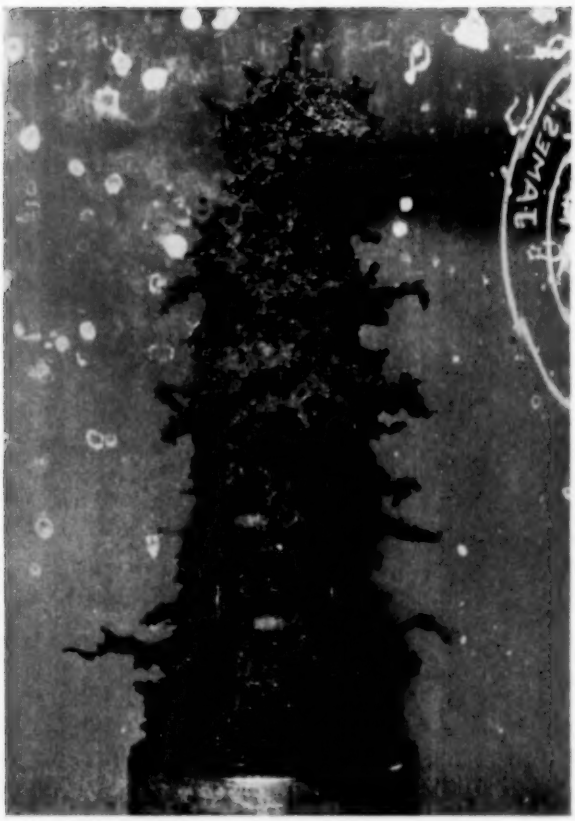

(a)

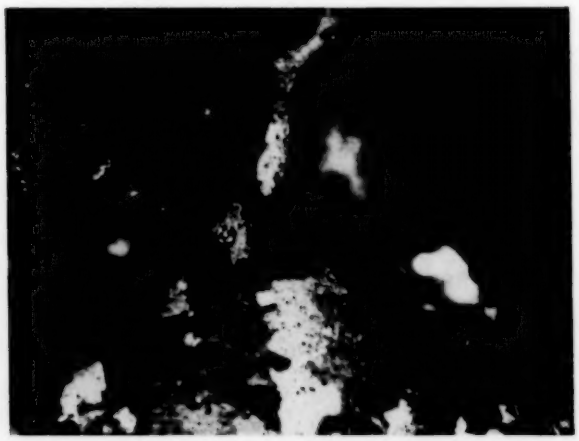

(b)

FIG. 7(a,b).—Uranium cylinder oxidized for 3½ hours at 800°C in carbon dioxide, with microphotograph of 'spine'.

VOL
15
196

The uranium slug was supported in a four-inch diameter section of the rig at *A* (Fig. 1) and could be heated by a radiofrequency heating coil placed round the outside of the Pyrex tube, or in some experiments by an internal electrical resistance heater.

2.2 *Sampling arrangements*

Solid debris from the oxidizing uranium either fell into the waste pot *B* against the gas flow, or was carried around the rig. In a closed circuit rig it is important that material being sampled is not allowed to pass the sampling position more than once. A cyclone was therefore installed at *C* to remove gas-borne solid material and this was followed by a high efficiency filter and a charcoal pack to remove iodine. The gas stream was sampled continuously for iodine at *E* and *F* by passing a fraction of the gas through a filter to remove oxide and then through two bubblers in series each of which contained sodium hydroxide solution with potassium iodide carrier. These samples were usually changed hourly during a run and the iodine was subsequently precipitated as silver iodide and beta-counted as a thick source in an arrangement of known geometry. The purpose of the second iodine sampler at *F* was to check the efficiency of the charcoal pack. Although the thickness of charcoal was eventually reduced to one centimetre, the efficiency of removal of iodine between circuits was consistently greater than 95 per cent. At the end of an experiment oxide samples were taken from both waste pot and cyclone, and particle size analyses were performed by a sieving and sedimentation method.

2.3 *Temperature measurement*

When a metallic specimen is heated by high frequency eddy currents, the heated zone is confined to a shallow surface layer. The central part of the specimen is heated by conduction from the surface and for a given rate of heat generation and coolant flow, a steady state is reached in which there is only a small temperature gradient within the specimen itself. In these experiments, temperature measurements were first made by means of a platinum, platinum-rhodium thermocouple bearing on the top of the specimen. A preliminary check showed that heat generation by eddy currents in the thermocouple itself was negligible. As oxidation proceeded, disks of oxide were formed on top of the uranium and it became progressively more difficult to obtain good thermal contact between the thermocouple and the oxidizing metal surface. The arrangement was then changed and the thermocouples were sunk into holes drilled in the uranium as shown in Fig. 3. The fit of the thermocouple support in the hole was good so that very little oxidation occurred in the hole itself. Figure 3 shows the positions of thermocouple holes for specimens heated by radiofrequency and internal electrical resistance heater respectively. In the latter case the thermocouple was much nearer the oxidizing surface and the question arose as to how closely the temperatures indicated by the thermocouples approached the uranium surface temperature. One check point was provided by the rapid rise in oxidation rate which occurs in carbon dioxide between 750°C and 800°C, which is ascribed in Section 3.1 and by ANTILL (1958) to the beta-gamma phase transition temperature of 771°C. The mean temperatures recorded by the thermocouples for this point were 764°C (standard deviation 11°C) and 772°C (standard deviation 13°C) for the specimens heated by radiofrequency and internal resistance heaters respectively. It is considered that these figures give a reliable measure of the accuracy of determination of uranium surface temperatures.

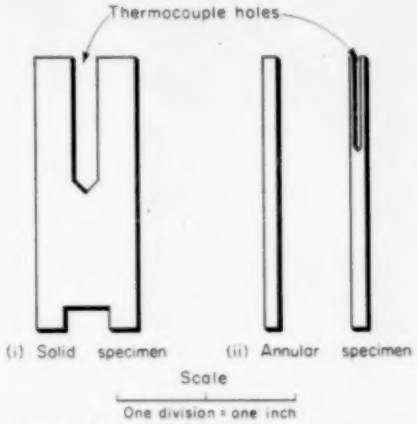

FIG. 3.—Sections of uranium specimens used.

3. OXIDATION RESULTS

3.1 *Measurement of rate of oxidation*

Most experimental work on the oxidation of uranium has been performed in apparatus which enabled the specimen and its oxidation products to be weighed continuously, and it was thus convenient to express the results in terms of weight increase per unit area per hour. Oxidation rates calculated on this basis are open to misinterpretation, since they are usually expressed in terms of the initial surface area of the specimen, whereas in reality the metallic surface area available for oxidation generally decreases continuously during an experiment. In the results reported here, oxidation rates are expressed as milligrams of uranium oxidized per square centimetre per hour and were determined as follows. It was found that most

VOL. 15 1961

of the oxide formed during an experiment of several hours duration was carried away by the gas stream or fell under gravity against the gas flow to the waste pot. At the end of the experiment any oxide adhering to the surface of the uranium was scraped off and the slug pickled for about twenty minutes in five per cent nitric acid. The slug was then weighed and the weight of uranium which had oxidized obtained by subtraction from the original weight of the specimen. It was assumed that the slug had oxidized with a uniform penetration rate and that its final shape was cylindrical. A mean penetration rate was then calculated and from this the oxidation rate was obtained by multiplying by the density of uranium. Such a method is approximate for, in some conditions, as will be seen, the final shape of the specimen is far from cylindrical. Where conditions were similar, however, the agreement between these results and those obtained by WANKLYN (1958), by the more conventional method of measuring the gain in weight of a small specimen, is good.

The results are given as an Arrhenius plot for various Reynolds numbers in Figs. 4 and 5 for oxidation in air and carbon dioxide respectively. In air the oxidation rate rises from 250 mg/cm² hr at 400°C to nearly 2000 mg/cm² hr at 650°C. In the region 660–750°C there is an apparent fall to about 1200 mg/cm² hr but by 800°C the oxidation rate has risen to 3000 mg/cm² hr and falls thereafter to about 1200 mg/cm² hr at 1000°C.

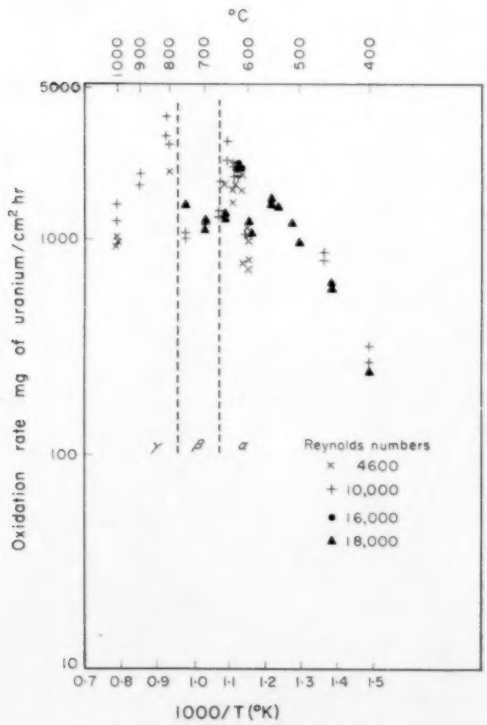

FIG. 4.—Oxidation of uranium in air.

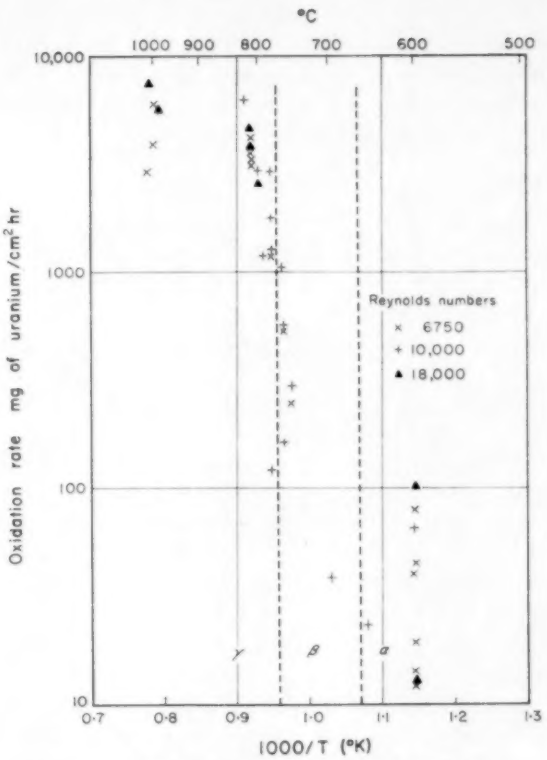

FIG. 5.—Oxidation of uranium in carbon dioxide.

Some experiments were performed to determine the variation of oxidation rate of uranium with increasing oxygen content of the gas circulating in the rig. The results are given in Fig. 6 where oxidation rate is plotted against oxygen content by volume of the circulating gas. The experiments were performed with air/argon and oxygen/argon mixtures and the oxygen content of the gas for each run determined by volumetric analysis of samples taken from the rig. The uranium temperature for these experiments was 600°C. It is seen from Fig. 6 that the oxidation rate rose rapidly from 130 mg/cm² hr when the oxygen content was 0·5 per cent by volume to 900 mg/cm² hr at an oxygen content of 7·5 per cent. Thereafter the curve flattens and an increase of oxygen content from 20 to 30 per cent increases the oxidation rate only from 1400 to 1500 mg/cm² hr. Although these results were obtained using air/argon and oxygen/argon mixtures, it is considered that they would apply also to air/carbon dioxide mixtures at a uranium temperature of 600°C since at this temperature the oxidation rate of uranium in carbon dioxide alone is less than 100 mg/cm² hr.

The whole pattern of oxidation in carbon dioxide is quite different from that in air. At temperatures

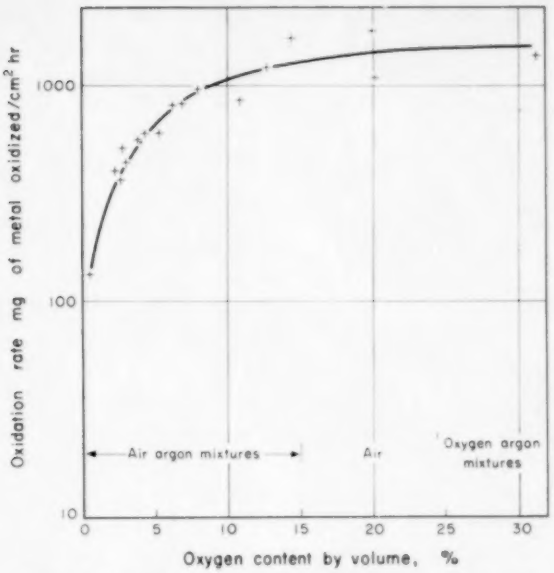

FIG. 6.—Variation of oxidation rate at 600°C with oxygen content of gas stream.

below 750°C the oxidation rate is less than 100 mg/cm² hr which corresponds to a penetration rate of only 55 microns per hour. Above 750°C the increase of oxidation rate to about 4000 mg/cm² hr is very rapid and the rate then increases rather slowly to about 5000 mg/cm² hr at 1000°C.

It is seen from Fig. 5 that the rapid increase in oxidation rate occurs at a temperature very close to the beta-gamma transition temperature of 771°C. This effect has also been reported by ANTILL.

An interesting phenomenon which occurs when a uranium specimen is oxidized at about 800°C in carbon dioxide is illustrated in Fig. 7. Under these conditions the specimen does not maintain the approximately cylindrical shape which is usual, but 'spines' grow out from the body of the uranium giving it an appearance reminiscent of a Christmas tree. The spines grow out even beyond the original dimensions of the uranium and are seen from the microphotograph in Fig. 7 to consist of a uranium metal core surrounded by a coat of oxide. Spine formation was not observed to occur outside the temperature range 770–810°C and it appears reasonable to assume that this phenomenon also is associated with the beta-gamma transition.

The type of oxide formed by oxidation in air was entirely U_3O_8. The oxide formed in carbon dioxide was in the range $UO_{2\cdot2}$ to $UO_{2\cdot4}$.

3.2 *Particle size distribution of oxide*

The results of particle size determinations by sieving and a photoelectric sedimentometer are shown in Figs. 8 and 9 for carbon dioxide and air respectively. The results show mass medians of from 42 to 350 microns, depending on conditions, for oxide particles formed in carbon dioxide, and from 10 to greater than 500 microns for oxide formed in air. It is apparent from the curves that there is a general shift towards a larger particle size distribution as the uranium temperature increases. The results for oxidation in air at a uranium temperature of 1000°C cannot be compared directly with the other results for the following reason. Very few oxide particles were emitted from the uranium while it remained at 1000°C, but a thick layer of oxide built up on the specimen. When the uranium was allowed to cool to about 750°C this oxide coating began to disrupt violently, presumably due to thermal stresses and particles of oxide were projected from the specimen with considerable emission of sparks. Oxidation of uranium at 1000°C in carbon dioxide proceeded quite normally and oxide particles were emitted continually while the uranium remained at temperature.

The analysis of the particle size of gas-borne oxide showed a fairly general reduction in mass median with increasing gas velocity and this is indicative of some breaking-up of oxide particles by increasing turbulence. In general, however, the variation in particle size with

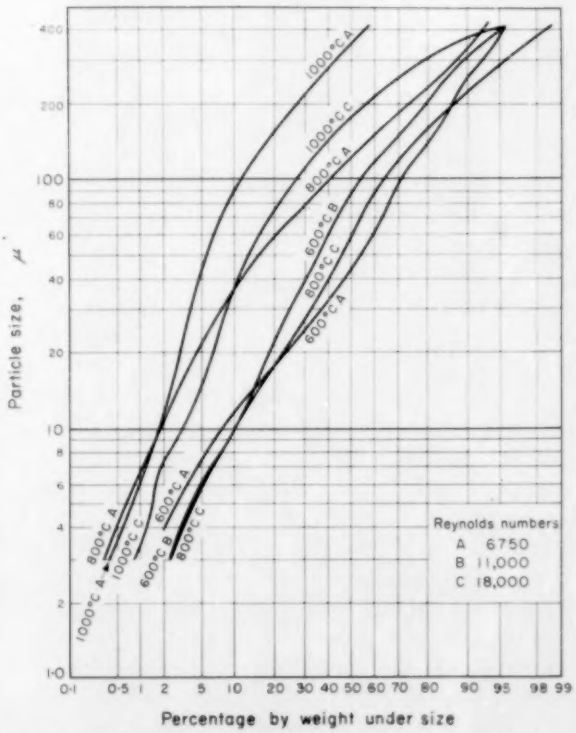

FIG. 8.—Size distribution of oxide from uranium oxidizing in carbon dioxide.

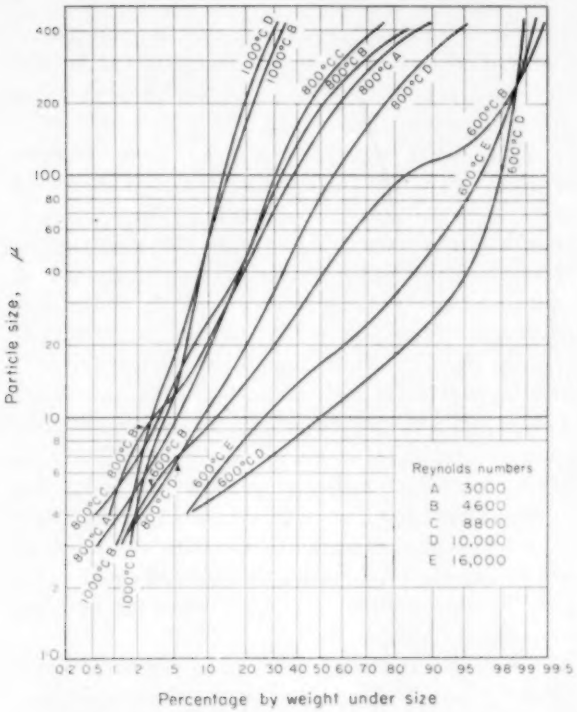

FIG. 9.—Size distribution of oxide from uranium oxidizing in air.

gas velocity is not very great over the range of velocities considered.

4. RELEASE OF IODINE-131

4.1 *General*

The uranium specimens were irradiated for ten minutes in the BEPO reactor and allowed to decay for about ten days. These periods resulted in a beta activity in the one-kilogram specimen of about twenty millicuries of which about 1·5 millicuries were due to iodine-131. The total activity of the specimen was estimated by analysis of uranium wires which had been irradiated in small diameter holes in the specimen and the iodine-131, strontium-89 and barium-140 content of the specimen estimated by radiochemical analyses of these wires. After an experiment similar analyses were performed on the oxide to indicate whether any significant proportion of the isotope concerned was escaping undetected.

The analytical procedures for determination of strontium and barium were relatively straightforward, involving two fuming nitric acid separations, a ferric hydroxide scavenge and precipitation of barium as chromate and strontium as carbonate. Some difficulty was experienced with determination of iodine but eventually a development of a method given by CORYELL and SUGARMAN (1951) was used successfully. It was found necessary to ensure that the fission product and carrier iodine were in the same valency state by passing them through successive oxidation and reduction stages. The iodine was eventually precipitated and counted as palladous iodide.

The results of these determinations are summarized in Table 1 which shows as a mean for each set of conditions the percentage of the isotope originally present which was accounted for after the experiment. The standard deviation is given in parentheses.

It is apparent that the activity balances are within the experimental error with the single exception of the iodine-131 balance for uranium oxidizing in air at 1000°C, and as has been mentioned in Section 3.2, the oxidation pattern for these conditions was peculiar.

4.2 *Release of iodine-131 as elemental iodine in the vapour phase*

The results obtained for the release of iodine-131 from a uranium specimen oxidizing in air and carbon dioxide respectively are given in Tables 2 and 3. The method of sampling described in Section 2.2 was such that only elemental iodine in the vapour phase was sampled.

The releases are given in microcuries and are also expressed as the mean percentage released per hour of the total iodine-131 content of the slug at the commencement of heating. In addition, since it became apparent that the release of iodine was in some way connected with the process of oxidation and the type of oxide formed, the releases have been calculated as a percentage of the iodine-131 content of the oxidized uranium.

It is apparent from Table 2 that when oxidation took place in air in the region of 600°C, between 0·2 and 0·8 per cent of the iodine-131 content of the uranium was released per hour as elemental iodine in the vapour

TABLE 1.—ACTIVITY BALANCES FOR IODINE-131, STRONTIUM-89 AND BARIUM-140

Conditions		Mean percentage of original activity accounted for (with standard deviation)		
		^{131}I	^{89}Sr	^{140}Ba
Air	600°C	97·2 (2·2)	99·1 (4·4)	101·5 (2·9)
	800°C	98·6 (4·9)	100·2 (2·3)	101·0 (2·7)
	1000°C	86·5 (4·6)	96·3 (4·7)	97·1 (3·2)
CO_2	*600°C	100·0 (0)	100·0 (0)	100·1 (0·1)
	800°C	97·9 (2·7)	98·2 (1·2)	98·0 (0·7)
	1000°C	105·4 (4·7)	94·7 (4·9)	95·9 (5·0)

* Very little oxidation occurred in CO_2 at 600°C and these figures are virtually the initial values for the uranium slug.

TABLE 2.—RELEASE OF ^{131}I AS ELEMENTAL IODINE FROM A URANIUM SLUG OXIDIZING IN AIR

Serial	Uranium temp. (°C)	Gas velocity (cm/sec)	Reynolds number	Duration of experiment (hr)	Percentage of uranium oxidized	Release of ^{131}I as elemental iodine		
						Release (μc)	Mean release per hour as percentage of initial ^{131}I content of slug	Release as a percentage of ^{131}I content of oxidized uranium
B23	600	120	4600	6·3	24·8	6·2	0·2	5·2
B25	600	120	4600	6·3	22·8	5·4	0·2	5·2
1/3	610	120	4600	2·3	19·7	4·0	0·8	8·0
B15	640	260	10,000	6·2	56·7	1·1	0·65	7·4
B12	640	260	10,000	5·0	55·4	0·9	0·3	2·8
2C	800	85	3000	3·0	49·8	41	2·1	11·5
28C	810	120	4600	3·1	66·1	93	5·5	25·3
3C	810	260	10,000	1·0	25·0	13	4·9	19·8
4C	810	260	10,000	3·0	57·8	135	4·8	24·9
19C	810	260	10,000	2·1	52·4	8·6	7·4	28·9
5C	1000	120	4600	4·8	35·5	3·1	0·2	2·2
6C	1000	120	4600	4·8	32·4	5·4	0·3	4·4
17C	1000	260	10,000	4·2	37·3	16	1·6	18·5
18C	1000	260	10,000	3·1	31·0	22	1·8	17·3

TABLE 3.—RELEASE OF ^{131}I AS ELEMENTAL IODINE FROM URANIUM SLUG OXIDIZING IN CO_2

Serial	Uranium temp. (°C)	Gas velocity (cm/sec)	Reynolds number	Duration of experiment (hr)	Percentage of uranium oxidized	Release of ^{131}I as elemental iodine		
						Release (μc)	Mean release per hour as percentage of initial ^{131}I content of slug	Release as percentage of ^{131}I content of oxidized uranium
B17	600	100	6750	6·0	3·0	$3·6 \times 10^{-2}$	1×10^{-3}	$1·4 \times 10^{-2}$
20C	600	100	6750	7·2	0·9	$1·2 \times 10^{-2}$	$<1 \times 10^{-3}$	$5·6 \times 10^{-1}$
22C	600	100	6750	7·3	1·2	$2·1 \times 10^{-1}$	2×10^{-3}	1·42
B20	600	160	11,200	5·5	2·6	$1·8 \times 10^{-2}$	$<1 \times 10^{-3}$	$7·2 \times 10^{-2}$
B19	600	260	18,000	6·3	3·5	$2·9 \times 10^{-2}$	4×10^{-3}	$7·0 \times 10^{-1}$
B18	810	100	6750	2·3	77·0	$1·8 \times 10^{-2}$	2×10^{-3}	$1·2 \times 10^{-2}$
7C	810	100	6750	2·8	64·9	$2·2 \times 10^{-2}$	5×10^{-3}	$2·2 \times 10^{-2}$
9C	810	100	6750	3·4	68·7	$5·9 \times 10^{-1}$	$2·6 \times 10^{-2}$	$1·3 \times 10^{-1}$
23C	810	100	6750	1·6	49·7	$4·0 \times 10^{-1}$	$1·9 \times 10^{-2}$	$6·1 \times 10^{-2}$
12C	810	260	18,000	1·0	33·6	$2·1 \times 10^{-2}$	$7·0 \times 10^{-3}$	$2·0 \times 10^{-2}$
14C	810	260	18,000	1·0	29·6	$8·2 \times 10^{-1}$	$8·0 \times 10^{-3}$	$2·8 \times 10^{-2}$
15C	800	260	18,000	1·1	21·0	$2·4 \times 10^{-1}$	$2·8 \times 10^{-2}$	$1·3 \times 10^{-1}$
10C	1000	100	6750	1·3	26·7	3·1	1·67	7·8
11C	1000	100	6750	1·5	60·2	1·9	$3·1 \times 10^{-1}$	$8·1 \times 10^{-1}$
13C	1000	100	6750	3·9	83·5	8·0	$2·4 \times 10^{-1}$	1·1
16C	1000	260	18,000	0·7	31·7	$2·9 \times 10^{-1}$	$6·0 \times 10^{-2}$	$1·3 \times 10^{-1}$
27C	1000	260	18,000	1·0	54·1	$1·7 \times 10^{-1}$	$4·3 \times 10^{-2}$	$8·0 \times 10^{-2}$

phase and the total release corresponded to a maximum of eight per cent of the iodine-131 in the oxidized uranium. At 800°C these values had increased to five per cent per hour and 25 per cent respectively. At 1000°C the results vary rather more widely but the upper limit is a release in the vapour phase of about two per cent per hour of the total iodine-131 content of the specimen, corresponding to 20 per cent of that of the oxidized uranium.

The results for uranium heated in carbon dioxide are quite different. In no case below 1000°C did the release of elemental iodine as vapour approach 0·1 per cent per hour of the iodine-131 content of the slug and in only one instance did the release exceed one per cent

TABLE 4.—RELEASE OF IODINE-131 AS VAPOUR FROM URANIUM ON MELTING

Serial	Gas	Percentage of uranium which oxidized	Iodine-131 content of slug (μc)	Release of iodine-131 (μc)	Percentage of iodine-131 released	Duration of heating (sec)
*29C (1)	Air	12·2	380	31·4	8·25	98
31C	Air	21·0	163	8·3	5·1	73
32C	Air	14·0	19·2	3·0	15·6	80
30C	CO_2	11·5	141	17·2	12·2	90
*29C (2)	Argon	0·13	212	0·37	0·17	57

* Half slug.

of the iodine-131 in the oxidized uranium. At 1000°C the releases were rather higher but were still very much below the corresponding releases from slugs oxidized in air, although the oxidation rate was rather greater than in air.

A few experiments were performed in which uranium slugs were rapidly heated above the melting point and the release of iodine-131 determined. It was not possible to measure accurately the temperature reached by the uranium, the specimen being heated in the r.f. field until the molten uranium broke through the oxide skin and fell out of the field or until the containment of the rig was threatened by the slug slumping and touching the glass rig wall. In no experiment did the heating period exceed 100 seconds. The results are given in Table 4 and show that up to 15 per cent of the iodine-131 may be released as elemental iodine in the vapour phase when a uranium slug is melted rapidly in this manner. This rate of release of 15 per cent in less than 100 seconds is vastly greater than the maximum recorded in Table 2 which was 7·4 per cent per hour at a temperature of 810°C. It is notable that in the single experiment in CO_2 the release of iodine-131 was comparable with the release in air and that where the slug was melted in argon, where relatively little oxidation occurred, the release of iodine was very small. It is remarkable that in Table 4 the percentage of iodine released, whether in air, carbon dioxide or argon, in most cases corresponds fairly closely with the percentage of uranium which oxidized. This should not be taken to mean that the released iodine all came from the uranium which had oxidized. In fact the iodine-131 content of the oxide was as high and sometimes higher than that of the parent metal, and it is probable that additional iodine had adsorbed on the surface of the oxide particles. The oxidation rates in these experiments were extremely high, approximately 80,000 mg/cm² hr, except in the experiment in argon.

4.3 *Desorption of iodine-131 from oxide*

It was considered possible that some proportion of the iodine atoms, after being displaced from the uranium lattice during the process of oxidation, might adsorb on the surface of the oxide particles rather than be emitted as elemental iodine to the gas stream. A series of experiments was therefore performed in which samples of the oxide from both air and carbon dioxide runs were placed on a sintered disk and milligram quantities of iodine-127 passed through. In this manner it was found possible to desorb between 40 and 70 per cent of the iodine-131 content of the oxide.

Other samples of oxide were calcined in air at 600°C and it was found that similar fractions of the iodine-131 content were released. These results indicate that a considerable proportion of the iodine-131 content of the oxide is adsorbed on the surface of the oxide. Further work on this subject is necessary.

5. DISCUSSION OF RESULTS

5.1 *Oxidation results*

Oxidation rates for uranium in carbon dioxide and in air have been reported by several authors, notably ANTILL *et al.* (1958), WANKLYN (1958), HILLIARD (1958) and SCHNIZLEIN *et al.* (1959). Their results were obtained in the main on small specimens of uranium suspended from delicate thermobalances in low gas flows. In the present work the specimens were relatively massive, the gas flows high and the oxide was in most cases removed from the uranium surface very soon after formation. Nevertheless, there is a considerable measure of agreement between the various sets of results. For oxidation in air, WANKLYN quotes results equivalent to 700 and 1820 mg/cm² hr and HILLIARD 950 and 1000 mg/cm² hr at temperatures of 600°C and 800°C. In the present work, the ranges of values are 700–1200 mg/cm² hr at 600°C and 2000–3000 mg/cm² hr at 800°C. In carbon dioxide, the rapid increase in oxidation rate between 700°C and 780°C reported by ANTILL is confirmed by the present results and is seen from Fig. 5 to occur at a temperature very close to the beta-gamma phase transition temperature of 771°C.

The marked reduction in oxidation rate in carbon dioxide found by ANTILL in the temperature range

800°C–1000°C has not been confirmed, and the range of values 3000–8000 mg/cm² hr at 1000°C is very much greater than ANTILL's figure of 1250 mg/cm² hr. It is considered that the differences in the oxidation rates are probably due to different experimental conditions. In previous work there was little or no temperature difference between the specimen and the oxidizing gas. In the present work the specimen was heated directly, the gas temperature rarely rising above 100°C, and there was thus a considerable temperature gradient across any oxide film formed on the surface of the metal. The existence of this temperature gradient would undoubtedly promote the cracking off by thermal stresses of the oxide skin and the exposure of fresh uranium surfaces to the oxidizing gas. It is reported by SCOTT (1958), for example, that cracking and subsequent fracture inevitably occur when sintered uranium oxide pellets are subjected to temperature gradients of the order of 500°C/cm.

5.2 *Particle size distribution of oxide*

Published data on the particle size distribution of oxide from uranium oxidizing in air or carbon dioxide are few. HELLYER (1948) reported a mass median of 300 microns for the oxide from a horizontal uranium rod, one inch in diameter, oxidizing at 250°C in air. The air velocity was 4000 cm/sec. From a number of experiments he concluded that at temperatures up to 300°C, 99 per cent by weight of the oxide particles would be greater than ten microns in diameter. HOPKINSON's (1957) results at furnace temperatures up to 1350°C led to mass medians of the order of 150 microns for oxide particles resulting from the oxidation of thin (0·15 cm) plates of uranium in a slow-moving airstream. These compare with the range (in air) of from 10 to more than 500 microns found in the present work. HOPKINSON's experiments were performed in a small furnace; the air temperature was probably close to the uranium temperature and the oxide was not removed from the uranium surface as it was formed, but was recovered after the apparatus had been allowed to cool. For these reasons it is considered that the present results are more representative of the particle size distribution of oxide which might be formed in reactor accidents. Whether or not they are representative of the oxide size distribution which might be released to atmosphere in the event of such an accident depends on the geometry and gas velocities in the reactor, whether the channels are vertical or horizontal and the degree of filtration which it is possible to provide. In the velocity range used however the dependence of particle size on gas velocity is not great and it is noteworthy that there is fairly good agreement between the present results and the particle size of uranium oxide, probably formed at rather lower temperatures, sampled from time to time in the Windscale stacks (MOORE, 1958).

5.3 *Release of elemental iodine as vapour*

The release of iodine-131 from uranium oxidizing in air has been investigated by HILLIARD (1959) and from molten reactor fuels by CREEK, MARTIN and PARKER (1959).

Using small (11·5 g) cylinders of uranium, HILLIARD found that iodine was emitted only until the oxidation of the uranium was complete and that below the melting point of uranium, release of iodine was less than 25 per cent of the iodine content of the uranium.

It is probable that the smaller releases of elemental iodine in the vapour state found in the present work were due to deposition of iodine on the rapidly cooled oxide, and this is confirmed by the desorption experiments in section 4.3. When conditions were similar, the results of both HILLIARD and CREEK *et al.* for the release of iodine from molten uranium and alloys agree well with the results reported here.

The reason for the very different releases of iodine from uranium oxidizing in air and in carbon dioxide is difficult to understand and no satisfactory explanation has been produced.

6. CONCLUSIONS

The experiments have demonstrated marked differences in the behaviour of uranium oxidizing in air and in carbon dioxide. At temperatures below 771°C the oxidation rate is very much lower in carbon dioxide than in air, but at this temperature there is a rapid increase in the oxidation rate in carbon dioxide and from then onwards the oxidation rate in carbon dioxide is rather higher than in air. Oxide particles formed in carbon dioxide had mass medians of 40 and 300 microns for formation temperatures of 600°C and 1000°C respectively; in air the comparable figures were 10 microns and more than 500 microns.

There were differences also in the quantities of gaseous iodine released from irradiated uranium oxidizing in the two gases, the release in carbon dioxide being very much less than that in air. It has been demonstrated that substantial releases of elemental iodine from heated uranium were always accompanied by substantial oxidation and that the oxide particles retained the greater part of the fission product iodine. These results have some bearing on the consequences of nuclear reactor accidents, and indicate that the

VOL. 15 1961

quantities of iodine emerging from a reactor after an accident will depend to a great extent on whether the oxide formed in the accident cools quickly after formation. Where this is the case, it was found that more than 60 per cent of the iodine involved was adsorbed on or contained in oxide particles. The detailed geometry of the reactor and the prevailing gas flows will determine how far these particles are carried within the reactor. Whether or not they are released to atmosphere will depend on the presence of an efficient particle filter in addition to any iodine removal system which may be provided.

Acknowledgments—The authors are indebted to many of their colleagues for assistance in various parts of the work described in this paper. In particular they are grateful to MR. A. C. CHAMBERLAIN for much helpful advice and criticism, to the Particle Size Group, A.E.R.E., for the performance of analyses and to MESSRS. L. BUNCE, W. CLIFT and G. R. MITCHELL for assistance in experimental work.

REFERENCES

ANTILL J. E., PEAKALL K. A., CRICK N. and GARDNER M. (1958) *Kinetics of the Oxidation of Uranium by Carbon Dioxide*. AERE M/R 2524.

CORYELL C. D. and SUGARMAN N. (1951) *Radiochemical Studies*, Paper 280, McGraw-Hill.

CREEK G. E., MARTIN W. J. and PARKER G. W. (1959) *Experiments on the Release of Fission Products from Molten Reactor Fuels*. ORNL 2616.

HELLYER R. (1948) *Rate of Oxidation of Bare Uranium in a Hot Air Stream with Preliminary Measurement of Particle Size Distribution*. AERE POC/Memo 16.

HILLIARD R. K. (1958) *Oxidation of Uranium in Air at High Temperatures*. HW 58022.

HILLIARD R. K. (1959) *Fission Product Release from Uranium Heated in Air*. HW 60689.

HOPKINSON B. E. (1957) Unpublished information.

MOORE J. (1958) Personal communication.

SCHNIZLEIN J. G. *et al.* (1959) *Ignition Behaviour and Kinetics of Oxidation of Reactor Metals*. ANL 5974.

SCOTT R. (1958) *Thermal Conductivity of* UO_2. AERE M/R 2526.

WANKLYN J. N. (1958) Unpublished information.

VOL
15
196

Reactor Science and Technology (Journal of Nuclear Energy Parts A/B) 1961, Vol. 15, pp. 185 to 191. Pergamon Press Ltd. Printed in Northern Ireland

STORED ENERGY IN THE OAK RIDGE GRAPHITE REACTOR—1960

M. C. WITTELS
Solid State Division, Oak Ridge National Laboratory,* Oak Ridge, Tennessee, U.S.A.

(*Received* 20 *January* 1961)

Abstract—The stored-energy status of the Oak Ridge Graphite Reactor, which went into operation in November, 1943, has been analysed following a low temperature anneal in which fission heat and a reverse air flow system were employed. From more than 100 post-annealing core samples, calorimetric studies revealed that the success of the annealing operation closely conforms to the maximum temperature profiles reached during the anneal.

Between 3·5–4·5 MWh of stored energy in a 15 ft diameter region was released during the pile operation, and the stored energy in that area was reduced to a level where a spontaneous release is now not possible. This was achieved with a maximum fuel element temperature of 275°C and a maximum graphite temperature of 236°C emphasizing the significance of the low temperature method.

The peripheral regions of the fuel zone, including the outer three rows, did not reach sufficiently high temperatures for annealing primarily because of sharply dropping thermal gradients at the edges of the moderator stack. The future stored-energy status of the reactor is discussed.

INTRODUCTION

A CONTROLLED stored-energy release was conducted in September, 1960, in the world's oldest operating reactor, the Oak Ridge Graphite Reactor. As a preliminary to this operation, graphite sample cores were removed from the moderator stack for stored-energy measurements. The purpose of these measurements was threefold: (1) to check on previously determined stored-energy growth rates, (2) to conduct low temperature annealing experiments as an aid in the upcoming annealing operation, and (3) to provide a direct analysis of the success of the annealing operation by means of a later comparison with post-annealing measurements in these same areas.

The thermal characteristics of the reactor (STANFORD, 1961) made it apparent that the reactor could be imagined to consist of two regions: (1) a core region approximately 15 ft in diameter that could be easily annealed by the previously proposed method (STANFORD, 1960) and (2) peripheral region encompassing the outer three fuel channel rows, in which it was recognized that significantly high annealing temperatures might not be easily reached. A typical channel in each of these regions was carefully scanned before and after the annealing operation and will, as shown later, depict the annealing behaviour of the entire reactor fairly accurately. More than 100 cores were taken from the moderator stack, post-anneal, to completely analyse the stored-energy status in the reactor as a whole.

METHOD OF STORED-ENERGY MEASUREMENT

All of the stored-energy measurements described in this report were made by the radiation-calorimetry method (WECHSLER, 1959). A higher oil-bath temperature (240°C) was employed than before, however, since this was a more suitable temperature for producing a quasi-adiabatic rise and, therefore, was more informative. The maximum temperature reached during the measurements ranged between 238°C and 300°C so that in no case did the quasi-adiabatic rise exceed the oil-bath temperature by more than 60°C. The integrated stored-energy release was obtained from calculations on the IBM 704 computer for each of the measurements.

PRE-ANNEALING DATA

Cores that contained the largest amounts of stored energy were subsectioned and annealed at low temperatures slowly and subsequently measured for stored energy. The results confirmed previous observations that a low temperature soak (140°–165°C) greatly reduces the temperature rise in a subsequent spontaneous release of stored energy. In Fig. 1 the temperature-time curves for a typical experiment of this kind are shown. The annealed samples were heated at 0·5°C/minute to the stated annealing temperatures and were then measured for stored energy in the usual manner. It should be pointed out that after the 161°C

* Oak Ridge National Laboratory is operated by Union Carbide Corporation for the United States Atomic Energy Commission.

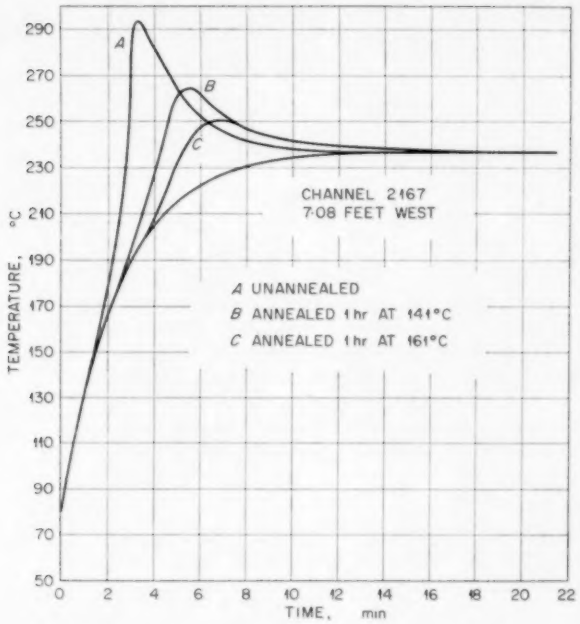

FIG. 1.—Time-temperature curve during stored-energy release.

anneal only 22·4 cal/g remained up to 250°C and, therefore, a spontaneous release in this graphite would no longer be possible.

From the time-temperature data shown in Fig. 1, similar curves can be calculated showing the rate of energy release for the same three cases (Fig. 2). This analysis shows that at a heating rate of 45°C/minute the energy release rate, at peak, is 0·55 watts/g and persists for approximately 30 seconds. Stated in other terms, if the entire mass of damaged graphite in the reactor were heated at 45°C/minute in a quasi-adiabatic environment, a peak power release of approximately 50 MW could be sustained for about 30 seconds. This

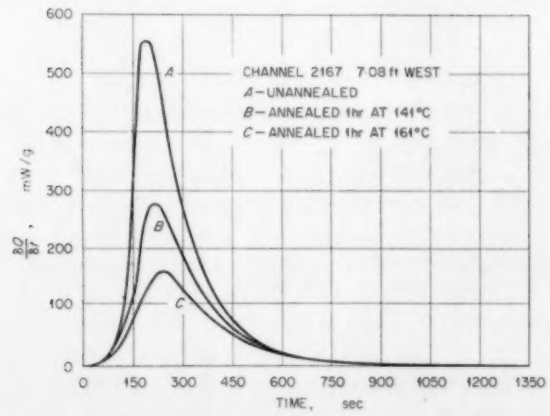

FIG. 2.—Rate of stored-energy release in channel 2167 graphite on immersion in 240°C oil bath.

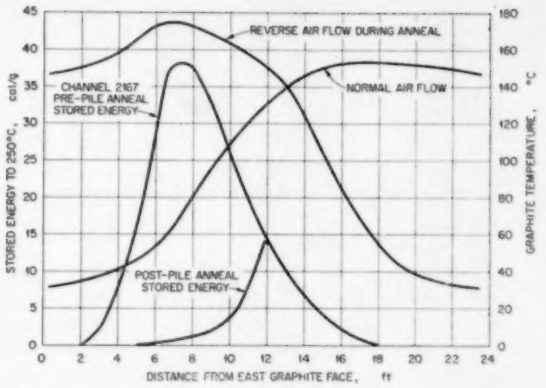
REVERSE AIR FLOW DURING ANNEAL
NORMAL AIR FLOW
CHANNEL 2167 PRE-PILE ANNEAL STORED ENERGY
POST-PILE ANNEAL STORED ENERGY
STORED ENERGY TO 250°C, cal/g
GRAPHITE TEMPERATURE, °C
DISTANCE FROM EAST GRAPHITE FACE, ft

FIG. 3.—Stored-energy distribution before and after pile annealing in channel 2167.

point is entirely academic, however, since these environmental conditions are not possible in this massive graphite structure. The energy-release curves for the low-temperature annealed samples only further emphasize the significance of a slow, low temperature anneal in reducing the dangers of a spontaneous release of stored energy.

A typical profile of the stored-energy distribution before annealing for the core region channel, 2167, is shown in Fig. 3, together with a graphite temperature traverse. In this case the peak damage position and peak reversed-temperature position coincide and therefore present an ideal annealing configuration. A similar profile for the peripheral channel, 3068, is shown in Fig. 4 where it is evident that the damage-temperature profiles are not ideally suited for an annealing operation and, in addition, the peak temperatures are too low for adequate annealing. It should be emphasized that the graphite temperature profiles in these two channels were for conditions of reactor power on: air coolant flowing, and maximum fuel element temperatures, while the graphite temperatures were steady-state.

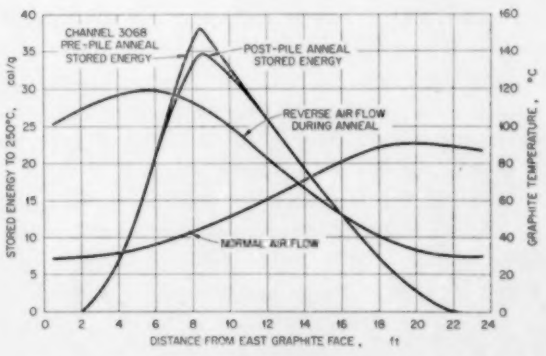
CHANNEL 3068 PRE-PILE ANNEAL STORED ENERGY
POST-PILE ANNEAL STORED ENERGY
REVERSE AIR FLOW DURING ANNEAL
NORMAL AIR FLOW
STORED ENERGY TO 250°C, cal/g
GRAPHITE TEMPERATURE, °C
DISTANCE FROM EAST GRAPHITE FACE, ft

FIG. 4.—Stored-energy distribution before and after pile annealing in channel 3068.

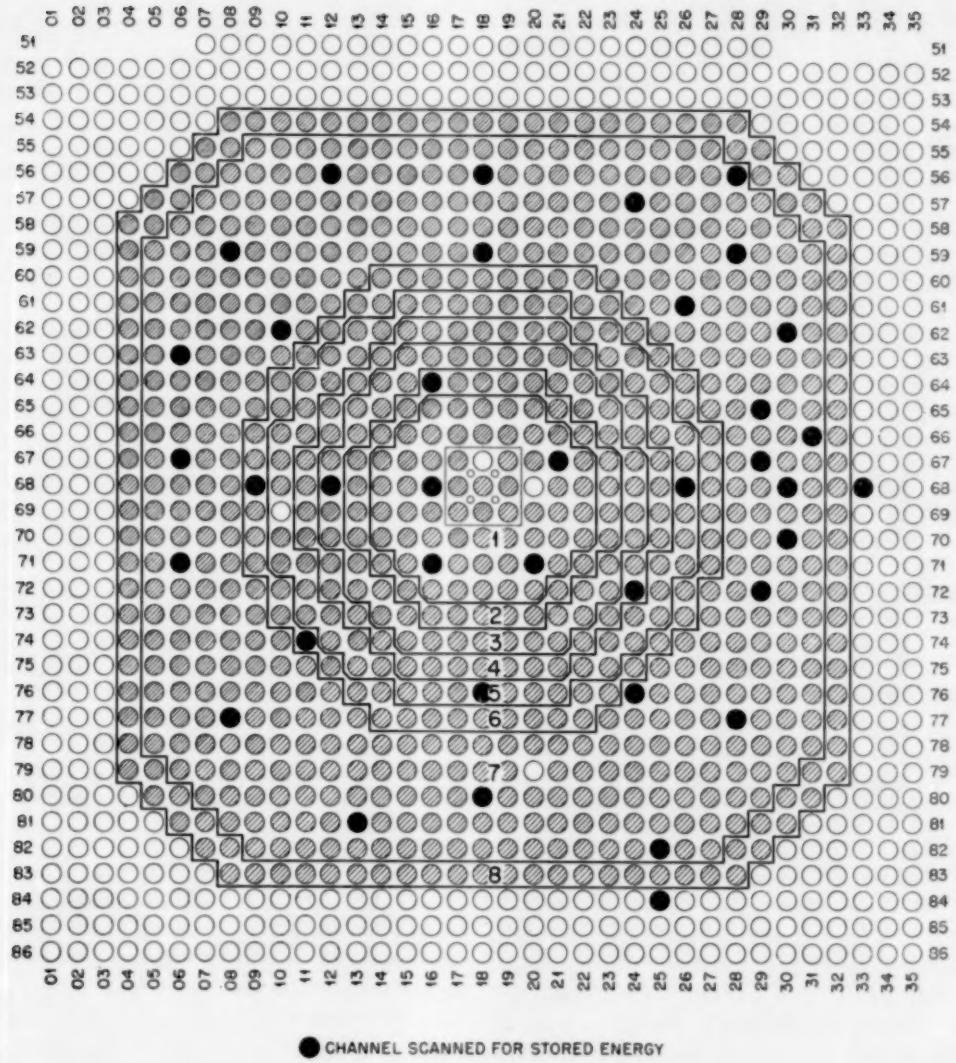

FIG. 5.—Graphite channels scanned for post-annealing stored energy.

POST-ANNEALING DATA

Following the annealing operation the stored-energy distributions in the two above-mentioned channels were again determined and are shown in Figs. 3 and 4. The reversed air-flow temperature profiles were taken during the annealing operation, but after the energy release, when steady-state conditions prevailed. As indicated in the pre-annealing discussion the operation was very successful in channel 2167, and in channel 3068 it was apparent that only a minor degree of annealing had occurred.

From 36 other channels in the stack (Fig. 5) stored energy distributions along the channels were determined and are shown graphically in Figs. 6 and 7 for the two halves of the reactor. The stored energies shown are for the total energy released during the quasi-adiabatic run and are therefore not necessarily related to the identical temperature span. Several facts are evident in this scan: (1) annealing was successful in the 15 ft core region of the graphite moderator (Fig. 8), (2) annealing was unsuccessful in the peripheral region of the moderator, (3) stored energy in the west half of the moderator is nil except for small stringers that extend a few feet west of centre in the peripheral region only, (4) the peak damage position in the south peripheral area is slightly east of that for the north peripheral region and is obviously due to the normal colder temperature distribution in the north half

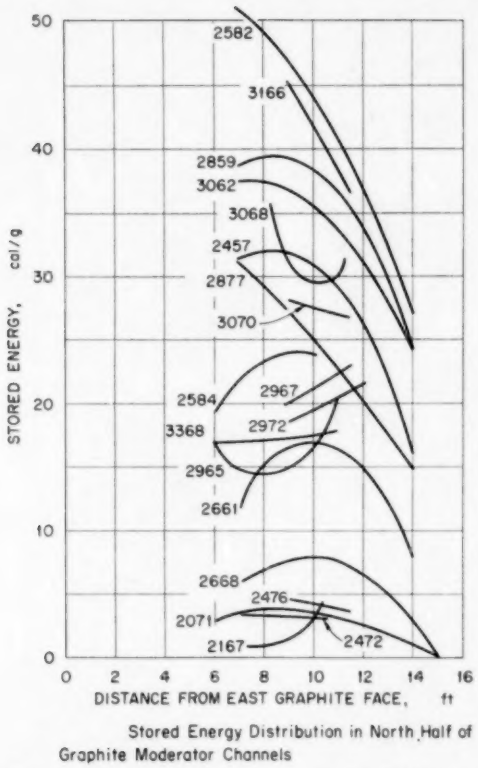

FIG. 6.—Post-annealing stored-energy distribution in south half of graphite moderator measured at temperatures up to 300°C.

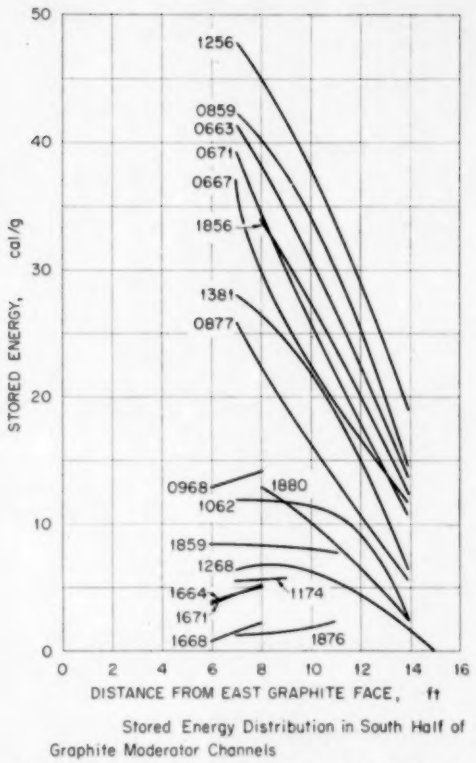

FIG. 7.—Post-annealing stored-energy distribution in north half of graphite moderator measured at temperatures up to 300°C.

of the reactor, and (5) the stored-energy distribution in the north peripheral region is also somewhat broader for the same reason. The unusual curves for channels 2965 and 3068 are due to the proximity of control rod positions. The spatial distribution of stored energy capable of spontaneous release is shown in Fig. 9. This region presently contains approximately 3·5 MWh of releasable energy up to 250°C. Analysis of the annealed core region indicates that 3·5–4·5 MWh were released during the annealing operation.

DISCUSSION

X-ray lattice parameter analysis (WITTELS, 1957) had previously revealed that the stored-energy accumulation had extended into the outermost row of fuel channels on the north edge of the reactor (3268). It is therefore apparent that the other three lateral graphite edges of the fuel region also have suffered similar damage since the fast flux and temperatures in all four of these peripheral areas are comparable.

The discovery of stored-energy accumulations in the corners of the graphite moderator is not so well understood, however, and suggests that the fast flux distribution in the Oak Ridge Graphite Reactor might be somewhat different from the well-known thermal flux (RAMSEY, 1955) distribution (cosine) at the corners of the reactor. This is the case at the core-reflector interface but is of too low intensity to affect the fast flux by more than 15 per cent. It therefore seems more probable that the stored-energy growth rate at temperatures below 30°C may be as much as three times as high as the damage rates at 30°C–100°C (DAVIDSON, 1958; WOODS, 1955). It further suggests that controlled radiation damage experiments with graphite at temperatures between 4°K and 300°K may provide interesting results.

The overall effect of the annealing operation was a complete success from the standpoint of a low temperature procedure confined to narrow operational limits. For example, the maximum permissible fuel element temperature (285°C) was closely adhered to, and in fact only reached a maximum of 275°C. Of even greater significance were the heat transfer properties of the reactor during that period when stored energy was being released. Continuous recording from more than 300 thermocouple positions revealed that at no time during the stored-energy release, with reactor power on, was energy transferred from graphite to uranium; and, therefore, the reactor was under rigid control during the most critical annealing phase. Further, the

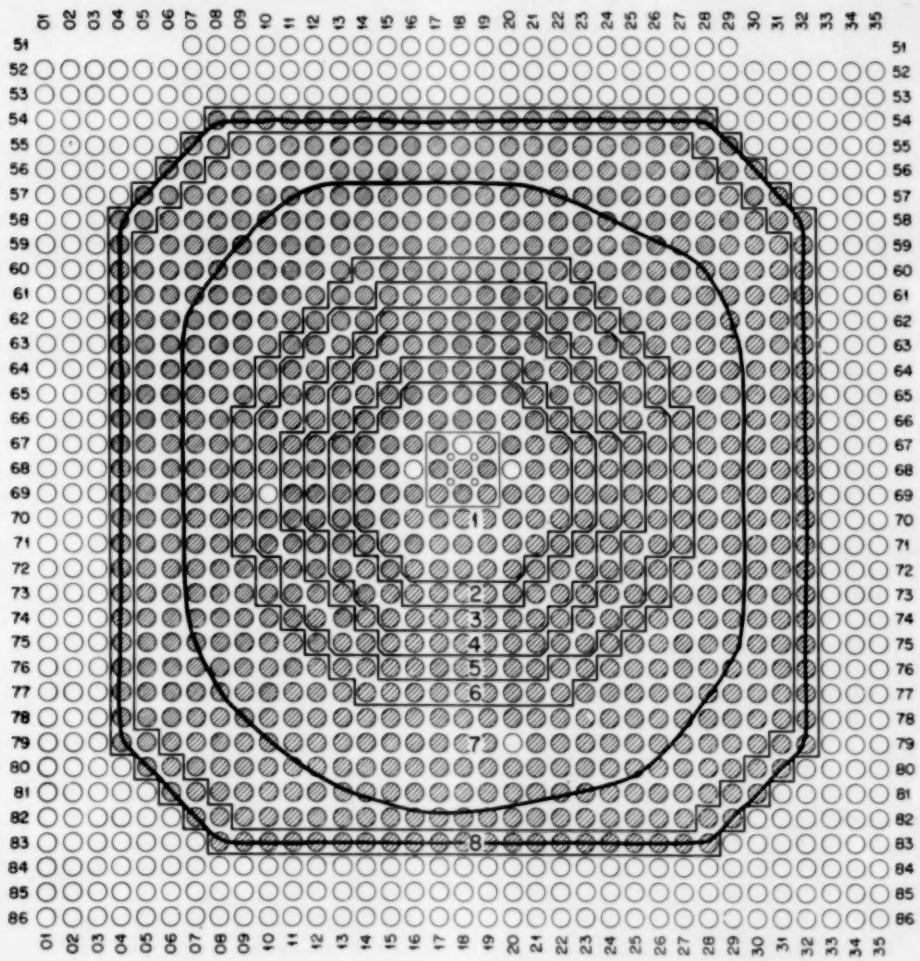

FIG. 8.—Outline of peripheral unannealed region on reactor loading face.

rate of spontaneous release of stored energy was reduced to the extent that the maximum graphite temperature with reactor power on was only 203°C, and with the reactor scrammed at high temperature, and air flow blocked, this maximum recorded graphite temperature only reached 236°C.

The reduction of intensity of a spontaneous release coupled with the subsequent use of fission heat as a power source for higher annealing temperatures is in sharp contrast to other annealing methods (DICKSON, 1958; COTTRELL, 1958; RIMMER, 1959) where the kinetics of the stored-energy release itself are utilized as a major source of power. The final two stages of the annealing operation itself offer conclusive evidence of the continuing safe operation of the reactor with air flow in either direction. In the next-to-last stage, with fuel elements near maximum temperature, the reactor ran for more than twenty hours with a thermally steady-state condition. This means that a large mass of graphite and fuel elements was maintained at temperatures over 100°C higher than was maintained at any time during the reactor's previous seventeen years' history. During the final annealing operation with the reactor scrammed from a maximum temperature condition, and the air flow blocked, there was simulated what might be considered, academically, a maximum credible accident environment. As a result of this operation, as well as of the previous annealing steps, not a single fuel element was ruptured, and the maximum temperatures previously described were not exceeded.

FUTURE STORED-ENERGY STATUS

The evidence for the presently safe stored-energy

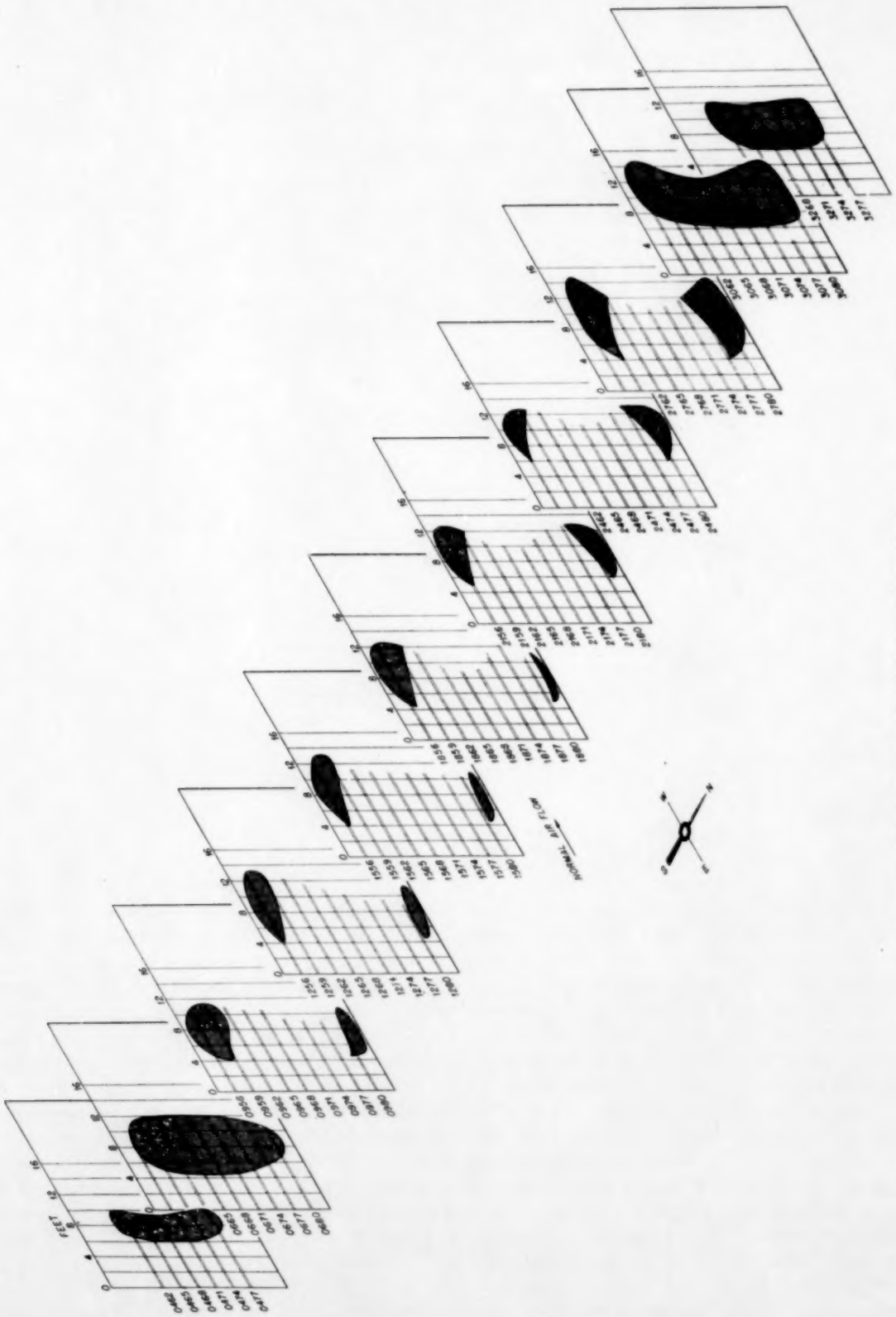

Spatial Distribution of Peripheral Stored Energy Region.

FIG. 9.—Spatial distribution of peripheral stored-energy region containing spontaneously releasable energy.

VOL
15
196

status in the Oak Ridge Graphite Reactor has already been discussed. As for the future stored-energy status, it will be assumed that the reactor is to be operated continuously and indefinitely. It is evident that the 15 ft core region offers no great difficulties because it is within a region of easily attainable annealing temperature (Fig. 3) now that the reactor has a permanently installed reverse air-flow system. The unannealed peripheral regions (Figs. 4, 8 and 9) will continue to accumulate stored energy at the rate of approximately 2 cal/g/yr up to 250°C. That this does not constitute a great hazard can be concluded for several reasons. The already cited evidence for the initiation of annealing (Fig. 4) in a peripheral channel indicates that a longer bake-out period following a scram condition, say 16–20 hours, might produce sufficiently high annealing temperatures in the peripheral area. This probability can be further increased by reducing the thermal losses to air flowing in the reflector channels by restricting the air flow in these channels. Also, the shifting of higher temperatures to the peripheral region could also be accomplished by orificing designated fuel channels. If these efforts do not succeed in annealing the outermost fuel channels, no great hazard presents itself in any event, since release temperatures would therefore be virtually impossible to achieve under any conditions. It might be noted at this point that concern of a 'thermal wave' occurring through an accidental stored-energy release during normal reactor operations is unrealistic if an adequate air coolant flow is available. During the annealing operation it was strongly apparent that with coolant air flowing at 60 per cent of normal capacity and stored energy being released, the thermal resistance at the boundaries of individual graphite blocks was so great as to prevent any large-scale heat transfer from graphite block to graphite block. Instead, the heat transfer due to the stored-energy release was mainly to the coolant air stream and along the unbroken graphite stringers themselves and therefore is narrowly confined in space. In addition, the effectively dispersed nature of the peripheral area is an isolating feature in itself.

This discussion has assumed that the present maximum fuel element temperatures (285°C) would not be exceeded. If the reactor were reloaded with fuel elements capable of safe operation at 350°C, then there seems to be very little doubt that sufficiently high annealing temperatures could be attained rather easily. As a routine operating measure it is believed that the reactor should be placed in a bake-out condition from the reverse flow operation, perhaps annually, to attenuate the accumulation of stored energy throughout the reactor and thereby reduce the higher temperature stored-energy growth as well. This should be a routine experience now that the stored-energy content has been largely eliminated in the central regions of the reactor core.

Acknowledgments—It is a pleasure to thank F. A. SHERRILL for his assistance during the stored-energy measurements and M. T. ROBINSON for programming the data for IBM-704 computation.

Many personnel of the Operations Division contributed to the extensive remote coring programme and the author is especially indebted to L. E. STANFORD, who directed the annealing operation, and to C. B. GAITHER. Their unstinting efforts made this report possible.

REFERENCES

COTTRELL A. H., BELL J. C., GREENOUGH G. B., LOMER W. M. and SIMMONS J. H. W. (1958) *Proceedings of the Second International Conference on the Peaceful Uses of Atomic Energy, Geneva*, P/2485, **7**, p. 315. United Nations, N.Y.

DAVIDSON J. M. (1958) *Stored Energy in Irradiated Graphite*. HW–55736.

DICKSON J. L., KINCHIN G. H., JACKSON R. F., LOMER W. M. and SIMMONS J. H. W. (1958) *Proceedings of the Second International Conference on the Peaceful Uses of Atomic Energy, Geneva*, P/1805, **7**, p. 250. United Nations, N.Y.

RAMSEY M. E. and CAGLE C. D. (1955) *Proceedings of the First International Conference on the Peaceful Uses of Atomic Energy, Geneva*, P/486, **2**, p. 281. United Nations, N.Y.

RIMMER D. E. (1959) *The Validity of the Constant Activation Energy Model for the Release of Stored Energy in Graphite*. AERE-R 3061.

STANFORD L. E. (1960) *Safeguard Report on the Proposed Method of Annealing Graphite in the X-10 Reactor*. ORNL–2725.

STANFORD L. E. (1961) To be published.

WECHSLER M. S., COLTMAN R. R., KERNOHAN R. H. and WITTELS M. C. (1959) *J. appl. Phys.* **30** (1), 42.

WITTELS M. C. (1957) *Evaluation of the ORNL Graphite Reactor*. TID–7565 (Pt. I), 64–81.

WOODS W. K., BUPP L. P. and FLETCHER J. F. (1955) *Proceedings of the First International Conference on the Peaceful Uses of Atomic Energy, Geneva*, P/746. United Nations, N.Y.

VOL. 15 1961

Reactor Science and Technology (Journal of Nuclear Energy Parts A/B) 1961, Vol. 15, pp. 192 to 195. Pergamon Press Ltd. Printed in Northern Ireland

GENERALIZATION OF THE SINGULAR INTEGRAL METHOD FOR AN ANISOTROPIC SCATTERING MEDIUM*

H. TAKAHASHI
Brookhaven National Laboratory, Upton, New York, U.S.A.

(*Received* 9 *February* 1961)

Abstract—The singular integral method suggested by CASE (1960) for solving neutron diffusion problems in an isotropic scattering medium is generalized for a linearly anisotropic medium. The formulation of the anisotropic problem is the same as that of the isotropic scattering problem except for small correction terms. These correction terms are proportional to the absorption probability. In the case of a non-absorbing medium, it is shown that the anisotropic scatterings affect only the asymptotic flux distribution and not the transient flux distribution.†

INTRODUCTION

NEUTRON transport theory for a medium with anisotropic scattering has been studied by various authors, DAVISON and SYKES (1957), DAVISON (1946), TAIT (1948) and TAKAHASHI (1960)‡, using methods such as the Wiener-Hopf method, the Pn method etc. However, the resulting expressions are too complicated to derive physical meaning from them and are limited to special cases. Recently, a general method for solving neutron transport problems in one dimension for a homogeneous medium with isotropic scattering has been suggested by CASE (1960). This method uses the singular integral equation studied by MUSKHELISHVILI (1953) and is systematically applicable to various problems such as the Milne problem or Green functions.

Our present purpose is to generalize this method for an anisotropic scattering medium. For the sake of simplicity, we shall limit ourselves to the case when the scattering law is linear in the cosine of the angle between the directions of the primary and the secondary particle. Where the Wiener-Hopf method treats the factorization of simultaneous equations, the singular integral method reduces to the solution of the Hilbert problem for a single variable. Thus, the resulting expression is simpler in form and has more physical meaning than those found by other methods such as the Wiener-Hopf method etc. It is easily shown that the anisotropic scattering effect in a non-absorbing material appears only in the asymptotic distribution, and that the transient term in the case of an anisotropic scattering medium is exactly the same as that of isotropic scattering.

FORMALISM

Let us consider neutron transport in a medium with linear anisotropic scattering. The neutron transport equation in the one-dimensional system is expressed by equation (1):

$$\mu \frac{\partial \psi}{\partial X}(X, \mu) + \psi(X, \mu) = \frac{C_0}{2}\int_{-1}^{1} \psi(X, \mu)\, d\mu + \frac{3C_1}{2}\mu \int_{-1}^{1} \psi(X, \mu)\, \mu\, d\mu, \quad (1)$$

where distance X is measured by a unit of a mean free path; C_0 is the ratio of scattering cross section to total cross section; C_1 is the ratio of linear term of anisotropic scattering cross section to the total cross section. We define b_1 as C_1/C_0 throughout this paper.

Assuming the solution of $\psi(X, \mu)$ as follows

$$\psi(X, \mu) = e^{-X/\nu}\phi_\nu(\mu) \quad (2)$$

and substituting it to equation (1), we get an equation for $\phi_\nu(\mu)$

$$(1 - \mu/\nu)\,\phi_\nu(\mu) = \frac{C_0}{2}\left[\int_{-1}^{1} \phi_\nu(\mu)\, d\mu + 3b_1\mu \int_{-1}^{1} \phi_\nu(\mu)\mu\, d\mu\right]. \quad (3)$$

In order to get a non-trivial solution for the homogeneous equation (3), the eigenvalue ν is determined as follows; solving equation (3) gives

$$\phi_\nu(\mu) = \frac{C_0}{2(1 - \mu/\nu)} \times \left[\int_{-1}^{1} \phi_\nu(\mu)\, d\mu + 3b_1\mu \int_{-1}^{1} \phi_\nu(\mu)\mu\, d\mu\right]. \quad (4)$$

* Work performed under the auspices of the U.S. Atomic Energy Commission.

† Parallel work on the Wiener-Hopf method has been carried out by TAKAHASHI (1960).

‡ Neutron transport theory for an anisotropic scattering medium has also been studied by AUERBACH, by use of Chandrasekar's methods (private communication).

Integrating equation (4) by μ from -1 to $+1$,

$$\int_{-1}^{1}\phi_\nu(\mu)\,d\mu = C_0\Big[\nu\tanh^{-1}1/\nu \times\int_{-1}^{1}\phi_\nu(\mu)\,d\mu + 3b_1\nu(1-\nu\tanh^{-1}1/\nu)\times\int_{-1}^{1}\phi_\nu(\mu)\mu\,d\mu\Big], \quad (5)$$

and multiplying equation (4) by μ and integrating it over the same interval as equation (5),

$$\int_{-1}^{1}\phi_\nu(\mu)\mu\,d\mu = C_0\Big[\nu(1-\nu\tanh^{-1}1/\nu)\int_{-1}^{1}\phi_\nu(\mu)\,d\mu - 3b_1\nu^2(1-\nu\tanh^{-1}1/\nu)\int_{-1}^{1}\phi_\nu(\mu)\mu\,d\mu\Big]. \quad (6)$$

From equations (5) and (6), ν has to satisfy the following relation

$$C_0\nu\tanh^{-1}1/\nu = \frac{1+3C_1(1-C_0)\nu^2}{1+3b_1(1-C_0)\nu^2}. \quad (7)$$

There are two roots of the equation which will be denoted by $\pm\nu_0$. Following CASE's (1960) discussion, if $\phi_\nu(\mu)$ can be a distribution, the other solution of equation (4) is obtained as follows from equation (3),

$$\phi_\nu(\mu) = \Big[\frac{C_0}{2}P\Big(\frac{\nu}{\nu-\mu}\Big)+\lambda(\mu)\delta(\nu-\mu)\Big]\times\Big[\int_{-1}^{1}\phi_\nu(\mu)\,d\mu + 3b_1\mu\int_{-1}^{1}\phi_\nu(\mu)\mu\,d\mu\Big], \quad (8)$$

where the symbol P indicates that principal values are to be understood when integrating an expression involving $\phi_\nu(\mu)$. In a similar way, the number $\lambda(\mu)$ is determined by the condition

$$\lambda(\nu)\int_{-1}^{1}\delta(\mu-\nu)\,d\mu = \frac{1+3C_1(1-C_0)\nu^2}{1+3b_1(1-C_0)\nu^2} - \frac{C_0}{2}\nu P\int_{-1}^{1}\frac{d\mu}{\nu-\mu}. \quad (9)$$

When ν is not real and is not in between -1 and $+1$, the condition reduces to equation (7). The two roots $\pm\nu_0$ occurs. If we normalize $\phi_\nu(\mu)$ as follows

$$\int_{-1}^{1}\phi_\nu(\mu)\,d\mu = 1, \quad (10)$$

the corresponding functions are expressed by

$$\phi_{0\pm}(\mu) = \frac{C_0}{2}\frac{\nu_0}{\nu_0\pm\mu}[1\pm 3b_1\mu\nu_0(1-C_0)]. \quad (11)$$

When ν is real and lies between -1 and $+1$, $\lambda(\nu)$ is determined by

$$\lambda(\nu) = \frac{1+3C_1(1-C_0)\nu^2}{1+3b_1(1-C_0)\nu^2} - C_0\nu\tanh^{-1}\nu, \quad (12)$$

and the function corresponding to this value of ν is

$$\phi_\nu(\mu) = \Big[\frac{C_0}{2}P\Big(\frac{\nu}{\nu-\mu}\Big)+\lambda(\nu)\,\delta(\mu-\nu)\Big]\times[1+3b_1\,\mu\nu(1-C_0)]. \quad (13)$$

Next, we consider the orthogonality and completeness of these functions. The orthogonality of these functions for an anisotropic scattering medium is expressed from equation (1) as follows

$$\int_{-1}^{1}\phi_{\nu'}(\mu)\phi_\nu(\mu)\mu\,d\mu = 0, \quad \nu\neq\nu'. \quad (14)$$

From the explicit forms of $\phi_\nu(\mu)$ in equations (11) and (13), the orthogonality integrals for $\nu=\nu'$ are

$$\int_{-1}^{1}\mu\phi_{0\pm}{}^2\,d\mu = N_{0\pm} = \pm\frac{C_0^2}{2}\Big[\nu_0{}^2\Big(\frac{\nu_0}{\nu_0{}^2-1}-\frac{k}{C_0\nu_0}\Big) + 6b_1(1-C_0)\nu_0{}^3\Big(\frac{\nu_0{}^2}{\nu_0{}^2-1}-\frac{2k}{C_0}+1\Big) + 9b_1{}^2(1-C_0)^2\nu_0{}^4\times\Big(\frac{\nu_0{}^4}{\nu_0{}^2-1}-\frac{3\nu_0 k}{C_0}+2\nu_0\Big)\Big], \quad (15)$$

where

$$k = \frac{1+3C_1(1-C_0)\nu_0{}^2}{1+3b_1(1-C_0)\nu_0{}^2}.$$

From the formula of Poincare-Bertrand, we get for the function $\phi_\nu(\mu)$

$$\int_{-1}^{1}\mu\phi_\nu{}^2(\mu)d\mu = N_\nu = \nu[1+3b_1\nu^2(1-C_0)]^2\times\Big[\lambda^2(\nu)+\frac{\pi^2C_0{}^2}{4}\nu^2\Big]. \quad (16)$$

Next, let us consider the completeness of these functions over a partial range, (theorem II in CASE's (1960) paper is a special case of theorem III in which the completeness in partial range is proved. We will not describe this special case in this paper). Let α and β be two real numbers such that $-1\leqq\alpha<\beta\leqq 1$, then (a) if $\alpha=-1$ and $\beta=+1$, the functions $\phi_\nu(\mu)$ $(\alpha\leqq\nu\leqq\beta)$ are complete for functions $\psi(\mu)$ defined in the interval $\alpha\leqq\mu\leqq\beta$, (b) is $\alpha=-1$ or $\beta=+1$, the set $\phi_\nu(\alpha\leqq\nu\leqq\beta)$ is complete when supplemented by ϕ_{0-} (ϕ_{0+}). Where $\psi(\mu)$ has to satisfy a Hölder condition. If ψ is an arbitrary function defined in the interval $-1\leqq\alpha\leqq\mu\leqq\beta\leqq 1$, it may be shown that

$$\psi(\mu) = \int_\alpha^\beta A(\nu)\phi_\nu(\mu)\,d\nu \ (\alpha\leqq\mu\leqq\beta), \quad (17)$$

VOL. 15 1961

is a solution of the integral equation

$$\psi(\mu) = \left[\lambda(\mu)A(\mu) + \frac{C_0}{2} \times P\int_\alpha^\beta \frac{\nu A(\nu)}{\nu - \mu}\, d\nu\right] + \left[\lambda(\mu)A(\mu)\mu^2 + \frac{C_0}{2} \times P\int_\alpha^\beta \frac{\nu^2 A(\nu)}{\nu - \mu}\, d\nu\, \mu\right] 3b_1(1 - C_0). \quad (18)$$

If $A(\nu)$ has properties similar to those of $\psi(\mu)$, the function defined

$$N(Z) = \frac{1}{2\pi i}\int_\alpha^\beta \frac{C_0}{2}\frac{\nu A(\nu)}{(\nu - Z)}\,[1 + 3b_1\mu\nu(1 - C_0)]\, d\nu, \quad (19)$$

has the properties

(1) it is analytic in the complex plane with a cut from α to β;
(2) $N(Z) \to 1/Z$ as $Z \to \infty$;
(3) $N(Z)$ is bounded by $C_1/|\alpha - Z|^\gamma$ and $C_2/|\beta - Z|^\gamma$ with $\gamma < 1$ as $Z \to \alpha$ and β, respectively.

Further,

$$N_+ + N_- = \frac{1}{\pi i} P\int_\alpha^\beta \frac{C_0}{2}\frac{\nu A(\nu)}{(\nu - \mu)}\,(1 + 3b_1\nu(1 - C_0)\mu)\, d\nu, \quad (20)$$

$$N_+ - N_- = \frac{C_0}{2}\,[\mu + 3b_1(1 - C_0)\mu^3]\, A(\mu). \quad (21)$$

Substituting equations (20) and (21) to (18), we get

$$\frac{C_0}{2}\mu\psi(\mu) = \left[\lambda(\mu) + \frac{i\pi C_0}{2}\mu\right] N_+(\mu) - \left[\lambda(\mu) - \frac{i\pi C_0}{2}\mu\right] N_-(\mu). \quad (22)$$

Then

$$G(\mu)\, N_+(\mu) - N_-(\mu) = \frac{\dfrac{C_0}{2}\mu\,\psi(\mu)}{\lambda(\mu) - i\pi\mu\dfrac{C_0}{2}} \quad (23)$$

where

$$G(\mu) = \frac{\lambda(\mu) + (i\pi/2)C_0\mu}{\lambda(\mu) - (i\pi/2)C_0\mu} = \frac{X^+(\mu)}{X^-(\mu)}. \quad (24)$$

Similarly to CASE's discussion, we get

$$N(Z) = \frac{1}{X(Z)}\frac{1}{2\pi i} \times \int_\alpha^\beta \frac{C_0}{2}\frac{\mu'\psi(\mu')X^-(\mu')\, d\mu'}{[\lambda(\mu') - (i\pi/2)C_0\mu'](\mu' - Z)} + \frac{F(Z)}{X(Z)}, \quad (25)$$

where $F(Z)$ vanishes in the cases of (a) $X(Z) \to$ constant (now zero) and (b) $X(Z) \to Z^{-n}$ (n integral and positive) when Z is infinity, and $F(Z)$ is equal to $P_{m-1}(Z)$ in the case of (c) $X(Z) \to Z^m$ (m integral and positive) which is an arbitrary polynomial of degree $m - 1$. And in case (b), a unique solution exists only if

$$\int_\alpha^\beta \mu^l \left[\frac{\mu(\mu)X^-(\mu)}{\lambda(\mu) - (i\pi/2)C_0\mu}\right] d\mu = 0, \quad l = 0, 1, 2, \ldots, n - 1. \quad (26)$$

We construct the function $X(Z)$ defined as follows

$$X(Z) = (\alpha - Z)^{l(\alpha)}(\beta - Z)^{k(\beta)}X_0(Z), \quad (27)$$

where

$$X_0(Z) = \exp\frac{1}{2\pi i}\int_\alpha^\beta \frac{\ln G(\mu')}{\mu' - Z}\, d\mu'. \quad (28)$$

It is necessary that $X(Z)$ does not vanish as rapidly as $\alpha - Z$ or $\beta - Z$ as $Z \to \alpha$ or β respectively. That is, the functions $l(\alpha)$ and $k(\beta)$ defined in equation (27) must satisfy the conditions

$$1 > l(\alpha) - \frac{\theta(\alpha)}{\pi} \geq 0, \quad 1 > k(\beta) + \frac{\theta(\beta)}{\pi} \geq 0, \quad (29)$$

where

$$\theta(\mu) = \frac{1}{2i}\ln G(\mu) = \arg\left[\frac{1 + 3C_1(1 - C_0)\mu^2}{1 + 3b_1(1 - C_0)\mu^2} - C_0\mu\tanh^{-1}\mu + \frac{\pi i C_0\mu}{2}\right]. \quad (30)$$

The function $\theta(\mu)$ varies the same interval as in the isotropic case between $-\pi$ and $+\pi$, when μ varies between -1 and $+1$. The classification of functions $X(Z)$ described in Table 1 of CASE's paper is applicable to the anisotropic case.

NON-ABSORBING MEDIUM

We have considered the generalization of singular integral method to anisotropic medium case. We have found that the mathematical formulation is quite similar to the formulation for the isotropic case, so it is quite easy to study the effect of anisotropic scattering by comparison of these formulations. This method is systematically applicable to various problems such as the half-range completeness relation in albedo problem, Milne problem in semi-infinite medium and time-dependent problem, etc. Although we can apply the above described formulation to these problems in the anisotropic scattering medium, the formulation obtained is the same as the formulation considered by CASE except for the expressions $\lambda(\mu)$ and $\theta(\mu)$ in equations (12) and (30). In order to avoid duplication, we do not describe them here.

In all expressions obtained, the terms which express the anisotropic effects are proportional to $(1 - C_0)$ that is the absorption probability. Then, when we consider the non-absorbing medium, $C_0 = 1$, all formulations for an anisotropic medium are exactly the same as that of an isotropic medium except that the ratio of ν_0 in the anisotropic medium to that in the isotropic medium is in the following relation

$$\left.\frac{\nu_{0(\text{anisotropic})}}{\nu_{0(\text{isotropic})}}\right|_{C_0=1} = \frac{1}{(1 - b_1)}. \tag{31}$$

Thus, the transient term of neutron transport in the non-absorbing anisotropic scattering medium which does not involve the ν_0 in their expressions is the same as the transient part for the isotropic scattering case. On the other hand, the asymptotic part is changed such that its distance scale of anisotropic case is expanded by $1/(1 - b_1)$ times that of the isotropic case. The extrapolation length in a Milne problem also becomes a $1/(1 - b_1)$ times of the one of isotropic case, which was shown previously by the author (TAKAHASHI, 1960). The linear anisotropic scattering case has been considered in this paper. From the analysis we expect that the problem with higher anisotropic scattering can also be easily solved by use of the singular integral method.

Acknowledgments—The author would like to express his appreciation to J. CHERNICK and N. CORNGOLD for valuable discussion during this work. He expresses his gratitude to T. AUERBACH for showing his work before publication.

REFERENCES

CASE K. M. (1960) *Ann. Phys.* **9**, 1.

DAVISON B. and SYKES J. B. (1957) *Neutron Transport Theory*, The Clarendon Press, Oxford.

DAVISON B. (1946) *Milne Problem in a Multiplying Medium with a Linearly Anisotropic Scattering*. CRT-358.

MUSKHELISHVILI N. I. (1953) *Singular Integral Equations*, Noordhoff, Groningen.

TAIT J. H. (1948) *The Application of the Wiener-Hopf and of the Spherical Harmonics Method to the Case of Energy Deposition in a Half-Space Consisting of Pure Hydrogen*. AERE T/R 231.

TAKAHASHI H. (1960) *Milne Problem in Non-Absorbing Medium with a Linearly Anisotropic Scattering*. BNL Memorandum.

VOL.
15
1961

Reactor Science and Technology (Journal of Nuclear Energy Parts A/B) 1961, Vol. 15, pp. 196 to 199. Pergamon Press Ltd. Printed in Northern Ireland

THE EVALUATION OF WORTH OF CYLINDRICAL CONTROL RODS IN REFLECTED CYLINDRICAL CORES WITH PARTICULAR REFERENCE TO THE O.M.R.

L. A. TAYLOR
Hawker-Siddeley Nuclear Power Co. Ltd., Langley, Bucks.*

(*First received* 14 *February* 1961 *and in final form* 11 *April* 1961)

Abstract—A calculation is described for predicting control rod worths and radial flux distributions for arrays of cylindrical control rods in reflected cores. The effect on the control rod worths and fluxes of the voids (defined in this article as fuel-free zones containing moderator) that are present in the core as the result of the absence of some of the control rods is also considered. Two-group diffusion theory is used. The computation, which is programmed for 'MERCURY' has been used for O.M.R. core calculations and some results are presented.

1. INTRODUCTION

THE ORGANIC moderated reactor core, which employs a mixture of the polyphenyls as a moderator and maybe coolant, is, by virtue of the hydrogen content of the polyphenyls a very compact design. A satisfactory lattice design from the point of view of reactivity, temperature coefficients and conversion ratio consists of a closely-packed triangular lattice of bundles of cylindrical fuel rods. Such a design means that it is not possible to insert a control rod within the lattice unless it replaces the fuel bundle. This, coupled with the high cost of control rods, motors and related gear, suggests that a control rod layout employing few large rods rather than many small ones is desirable. A control rod displaces a volume of moderator, and when removed causes a local fuel-free moderating zone, which will be referred to in the following text as a void.

The worth of a control rod array suggested by the above type of core cannot be assessed satisfactorily by the most conventional methods. The thermal utilization or cell method is not valid since there are too few rods to approximate an infinite lattice and perturbation theory is inaccurate due to the very considerable shadowing and anti-shadowing effects of the control rods and voids. Moreover when it is required to know the core flux distribution associated with an array of inserted control rods for evaluation of fuel cycles, core temperatures etc., the cell method further requires the use of a two-group, one- or two-dimensional diffusion code in which each control rod or void is represented by modifying the nuclear data of the surrounding cell. When many cases are to be computed use of the two-group numerical diffusion codes is expensive on computer time, particularly as the geometry of a cylindrical core containing cylindrical rods and voids is not easy to represent.

The above considerations suggest then that a heterogeneous method is required during the earlier stages of core design when lattice parameters, control rod layout, fuel cycling schemes and corresponding control rod programming schemes are not fixed and many cases have to be computed.

2. THEORY

The general two-group solution of the diffusion equation in the core is

$$\phi_1(r, \theta) = X_1 + AX_2$$
$$\phi_2(r, \theta) = S_1X_1 + S_2AX_2 \qquad (1)$$

where X_1 and X_2 are solutions of the separated wave equations. Representing each of X_1 and X_2 by the sum of a regular solution and a solution having singularities at all the control rod and void centres (NORDHEIM and SCALETTAR, 1946) the values of X_1 and X_2 at a point having polar co-ordinates (r, θ) may be assumed to be

$$X_1 = \sum_{-\infty}^{\infty} A_n J_n(\mu r)\, e^{in\theta} + \sum_{i=1}^{N} a_i \sum_{j=1}^{M_i} Y_0(\mu \rho_{ij})$$
$$X_2 = \sum_{-\infty}^{\infty} B_n I_n(\nu r)\, e^{in\theta} + \sum_{i=1}^{N} b_1 \sum_{j=1}^{M_i} K_0(\nu \rho_{ij}) \qquad (2)$$

Defining the 'type' of a control rod or void by the image it sees of all the other rods and voids in the core then M_i is the number of rods or voids of type i. If N_R is the number of types of control rod and N_v the number of types of void then $N = N_R + N_v$. Also in the above equations ρ_{ij} is the distance of the point (r,θ) from the j'th rod (or void) of type i. The values of μ, ν in the above equations are determined by the material composition of the core, corresponding to the

* Present address: C.E.I.R. (U.K.) Ltd., London.

required reactivity investment of the chosen array of control rods.

It may be shown that, provided either the control rods or voids are not near the core-reflector interface or, if some are, then there are several of one type, the non-zero order coefficients of powers of $e^{i\theta}$ either vanish or are small. Thus, only the zero-order coefficients, A_0, B_0 will be considered in the expressions for X_1, X_2.

The constants a_i, b_i which are so far arbitrary are determined by the flux and current continuity conditions at all core boundaries including the as yet undetermined boundaries at the control rod surfaces. By suitable approximations described later the boundary conditions at reflector, control rods and voids may be made linear equations in a_i, b_i. The determinant of the coefficients when equated to zero gives an equation for the critical control rod radius which may conveniently be solved. The values of a_i, b_i may then be determined, giving analytic expressions for the fluxes.

3. FORMULATION OF THE BOUNDARY EQUATIONS

(1) *Core-reflector interface*

By using the addition theorems for the Bessel functions and taking $K_0(\nu\rho_{ij})$ small we may, near the reflector, write

$$X_1 \sim J_0(\mu r) + Y_0(\mu r)\sum_{i=1}^{N} M_i a_i J_0(\mu d_i)$$
$$X_2 \sim I_0(\nu r) \qquad (3)$$

where d_i is the distance of the rods (or voids) of type i from the core centre.

The four core-reflector boundary conditions of flux and current continuity give an equation in the a_i's

$$\sum_{i=1}^{N} M_i a_i J_0(\mu d_i) + \frac{\Delta J}{\Delta Y} = 0 \qquad (4)$$

where ΔJ is the usual (4×4) determinant obtained from the core and reflector geometric and nuclear data which would be equated to zero if the reactor was just critical with no control rods or voids present. ΔY is a similar (4×4) determinant with $J_0(\mu R)$, $J_1(\mu R)$ replaced by $Y_0(\mu R)$, $Y_1(\mu R)$. The value of A in equation (1) may also be found directly from the core reflector boundary conditions.

(2) *Core-void interfaces*

The flux components in the core near a void of type i may be approximated by

$$X_1 = a_1 Y_0(\mu\rho_i) + P_i$$
$$X_2 = b_i K_0(\nu\rho_i) \qquad (5)$$

where ρ_i is the distance from the centre of void i and

$$P_i = J_0(\mu d_i) + \sum_{k=1}^{N} a_k \sum_{j=1}^{M_k} Y_0(\mu\rho_{ikj}). \qquad (6)$$

The double summation is taken over all the rods and voids in the core except the void under consideration, and ρ_{ikj} is the distance of the centre of void i from rod (or void) j of type k.

Writing the fluxes in the void as

$$\phi_1 = E_v I_0(\kappa_{1v}\rho_i)$$
$$\phi_2 = F_v I_0(\kappa_{2v}\rho_i) - \frac{D_{1v}}{D_{2v}} \frac{L_v^2 E_i}{L_v^2 - \tau_v} I_0(\kappa_{1v}\rho_i) \qquad (7)$$

in the usual two-group notation, where the suffix v refers to constants within the void, and using the flux and current continuity conditions between equations (5) and (8) N_v equations in the a_i's of the form

$$a_i\Theta + P_i, \quad i = 1 \ldots N_v \qquad (8)$$

may be shown to result, where Θ is a function of the core and void properties. The values of b_i are also found as multiples of a_i.

(3) *Core-control-rod interfaces*

Regarding the control rod as grey to epithermal and black to thermal neutrons, and using a somewhat similar approach to the one used at the core-void interfaces, N_R equations in the a_i's of the form

$$a_i\Psi(a) + P_i = 0, \quad i = N_v + 1 \ldots N \qquad (9)$$

may be shown to result, where $\Psi(a)$ is a function of the as yet undetermined critical control rod radius. Again, the values of b_i are found as multiples of a_i.

4. SOLUTION OF THE ABOVE EQUATIONS

An $(N \times N)$ critical determinant for the critical control rod radius is obtained by homogenizing the $N + 1$ linear equations in a_i labelled (4), (8) and (9). The critical equation may easily be shown to be

$$\det [P_{NN}] = 0 \qquad (10)$$

where, if the element of $[P_{NN}]$ in row i, column k is p_{ik}:

$$p_{ik} = \sum_{j=1}^{M_k} Y_0(\mu\rho_{ikj}) - M_k J_0(\mu d_k) J_0(\mu d_i) \frac{\Delta Y}{\Delta J} + \Phi\,\delta_{ik} \qquad (11)$$

where

$$\Phi = \Theta, \qquad i < N_v$$
$$\Phi = \Psi(a), \quad i > N_v.$$

The matrix $[P_{NN}]$ can be factorized, i.e.

$$[P_{NN}] \equiv [P_{NN}'] \begin{bmatrix} U_{N_v N_v} & P'_{N_R N_v} \\ 0 & P'_{N_R N_R} + \Psi(a) I_{N_R N_R} \end{bmatrix}$$

VOL. 15 1961

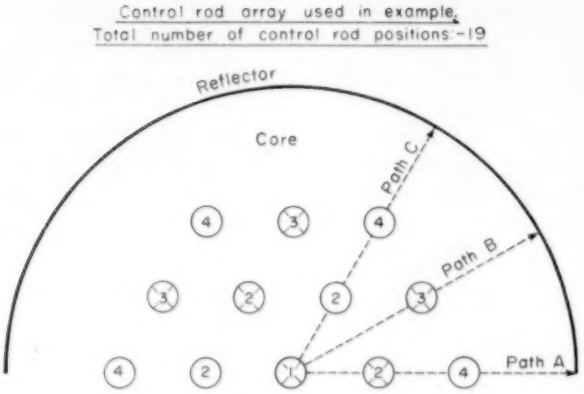

FIG. 1.

where $[U_{N_R N_R}]$ is upper triangular. The orders of the above sub-matrices are denoted by their suffices. Since the matrix of the above identity is singular it must follow that

$$\det [P'_{N_R N_R} + \Psi(a) I_{N_R N_R}] = 0 \qquad (12)$$

TABLE 1.—REACTIVITY WORTH OF GROUPS OF CONTROL RODS AMONG THE 19

Positions containing control rods	Reactivity worth (× 100)	Effective worth of additional groups of rods (× 100)			
		1	2	3	4
0	0	0·8	4·2	2·7	3·1
1	0·8	—	3·7	2·7	2·1
2	4·2	0·3	—	2·9	2·9
3	2·7	0·8	4·4	—	4·7
4	2·4	0·8	5·0	2·3	—
1,2	4·5	—	—	3·0	3·2
1,3	3·5	—	4·0	—	2·3
1,4	2·9	—	4·8	2·9	—
2,3	7·1	0·4	—	—	1·4
2,4	7·1	0·6	—	1·4	—
3,4	4·4	1·4	4·1	—	—
1,2,3	7·5	—	—	—	2·7
1,2,4	7·7	—	—	2·5	—
1,3,4	5·8	—	4·4	—	—
2,3,4	8·5	4·7	—	—	—
1,2,3,4	10·2	—	—	—	—

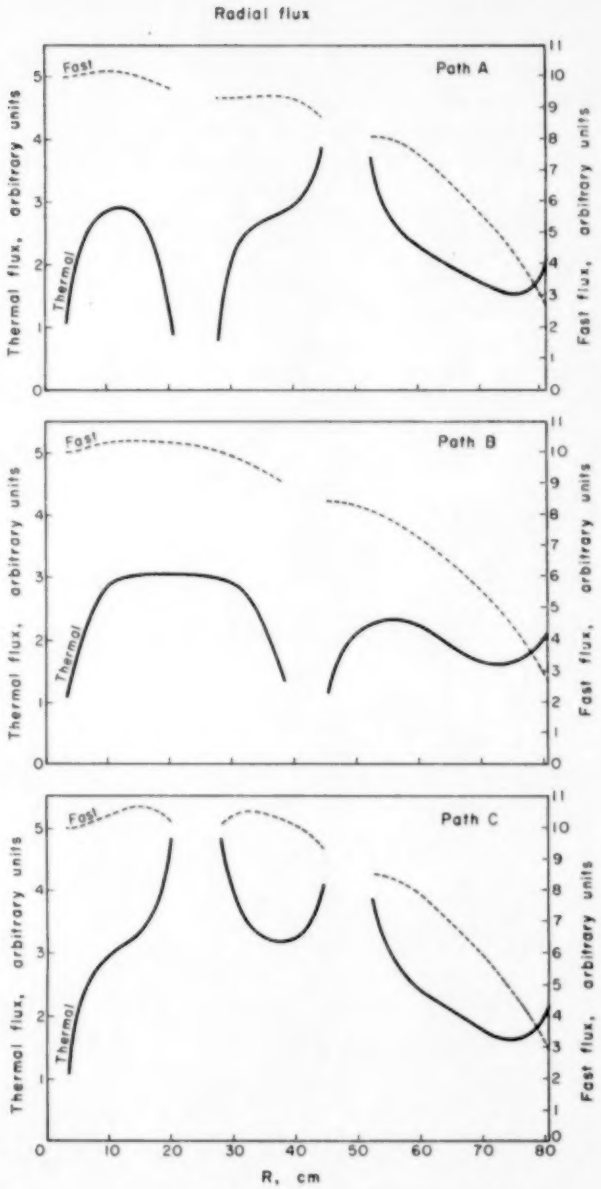

FIG. 2.—Some radial flux distributions obtained from calculation below.

since it is seen to be the only solution of (10) which involves the critical control rod radius.

Equation (12) is the condition for the function $-\Psi(a)$ to be an eigenvalue of the matrix $[P'_{N_R N_R}]$. It may be shown that the eigenvalue of $[P'_{N_R N_R}]$ required is the largest positive one, which may not however be the largest in modulus of all the eigenvalues. It may be shown that the iterative scheme

$$\xi t = [P'_{N_R N_R} + \beta I_{N_R N_R}] \xi t - 1, \qquad (13)$$

where β is an arbitrarily chosen positive scalar,

converges such that if $\tilde{\omega}$ is the largest eigenvalue of the matrix $[P'_{N_R N_R} + \beta I_{N_R N_R}]$ then

$$\tilde{\omega} = \underset{t \to \infty}{Lt} \frac{|\xi t|}{|\xi t - 1|}. \tag{14}$$

If β is chosen sufficiently large then

$$\Psi(a) = -\tilde{\omega} + \beta. \tag{15}$$

This determines the critical control rod radius.

Also, using the value of $\Psi(a)$ obtained from (15) the coefficients a_i and thus b_i $(i = 1 \ldots . N)$ may be determined from the vector equation

$$[T_{NN}]\,\bar{a} = \bar{s} \tag{16}$$

where

$$s_i = -J_0(\mu d_i)$$

$$t_{ik} = \sum_{j=1}^{M_k} Y_0(\mu \rho_{ikj}) + \Phi\,\delta_{ik}. \tag{17}$$

5. PARTICULAR CASE OF AN O.M.R.

As an example of the above, some results of the programme applied to an organic moderated and reflected core are given. Figure 1, which represents a control rod position array of one fuel channel in seven, shows nineteen possible control rod positions. Each position, which can contain a control rod radius 3·6 cm or a void of radius 4·0 cm is numbered according to its type. Table 1 gives the reactivity worths of some combinations of control rods among the nineteen, assuming no epithermal rod absorption. The positions not occupied by control rods are taken to be voids. The rod worth shown in column two of the table is defined as

$$\frac{k_\infty \text{ critical, rods and voids in core}}{k_\infty \text{ critical, nineteen voids in core}} - 1.$$

Each of the other four columns shows the 'effective' reactivity worth of a group of rods when added to those already in the core (as shown in column one). The groups are numbered according to their types when in the core. The wide variations of the 'effective' worths indicate the interaction effects of rods and voids.

Figure 2 is an example of radial flux distributions obtained from the calculation. For the example the core reactivity was chosen to make the reactor just critical with the array of rods inserted indicated in Fig. 1 by crosses. The three fluxes of Fig. 2 are plotted along the dotted lines of Fig. 1. The computer time required for the table and flux plots was about 15 minutes.

6. DISCUSSION

The above method can be used for any cylindrical thermal system in which two-group diffusion theory is applicable, although so far has been applied only to an O.M.R. Although intended for cylindrical control rods, rods of other shapes such as cruciform may be represented by the absorption area method of HURWITZ and ROE (1955) and the control rod replaced by an equivalent cylinder. Control rods of different materials are represented within the limitations of two-group diffusion theory by the inclusion of effective epithermal absorption and removal cross sections. The approximations made by the linearization in a_i, b_i of the boundary conditions have been investigated numerically for several practical cases to determine the magnitude of the resultant errors in predicted rod worth and it has been found that they are small.

REFERENCES

HURWITZ H. and ROE G. M. (1955) *J. Nucl. Energy* **2**, 85.

NORDHEIM L. E. and SCALETTAR R. (1946) *Theory of Pile Control Rods*. MDDC-42.

WATSON G. N. (1958) *A Treatise on the Theory of Bessel Functions*, Cambridge University Press.

VOL. 15 1961

Reactor Science and Technology (Journal of Nuclear Energy Parts A/B) 1961, Vol. 15, pp. 200 to 203. Pergamon Press Ltd. Printed in Northern Ireland

NEUTRON CAPTURE CROSS SECTIONS OF ^{236}U

D. C. STUPEGIA, R. R. HEINRICH and G. H. MCCLOUD
Argonne National Laboratory, Argonne, Illinois, U.S.A.

(*Received* 21 *February* 1961)

Abstract—The neutron capture cross sections of ^{236}U have been measured for monoenergetic neutrons in the energy range 0·30 to 1·7 MeV.

1. INTRODUCTION

ONE OF the products of neutron capture in reactor fuels is ^{236}U. In the prediction of reactor behaviour it is of interest to know the capture cross sections of this species as a function of neutron energy. This paper describes an activation method for the determination of these values. The results show that an anomalous rise in the ^{236}U cross section occurs in the vicinity of 1 MeV, similar to that found in ^{238}U and ^{232}Th (HANNA and ROSE, 1959). This anomaly in the latter two species has been explained by LANE and LYNN (1957), and their explanation presumably accounts also for the shape of the present curve.

2. METHOD

The cross section for the reaction ^{236}U (n, γ) ^{237}U has been determined as a function of neutron energy in the range 0·30 to 1·7 MeV by measuring the absolute ^{237}U activity produced in a known amount of ^{236}U irradiated in a known flux of monoenergetic neutrons. The neutron sources used here were lithium targets bombarded by protons from the Van de Graaff accelerator of Argonne National Laboratory. Neutron flux was measured with a fission chamber which counts fissions in a thin sample of enriched uranium. After irradiation the targets were analysed for the gamma-ray spectrum of ^{237}U by counting with a NaI (thallium activated) crystal and a 256-channel pulse-height analyser. The ^{237}U disintegration rate corresponding to the gamma spectrum was determined by relating this spectrum to that of a known activity of ^{237}U counted under conditions identical to those under which the irradiated targets were counted. The absolute disintegration rate of ^{237}U was determined by 4π beta counting.

The upper limit of neutron energy at which the cross section could be measured was set by the increasing fission rate of ^{236}U, and a simultaneous drop in the capture cross section. The neutron intensity available from the lithium-proton reaction determined the low energy limit.

3. EXPERIMENTAL

Targets

Material for this work was supplied by Oak Ridge National Laboratory in the form of U_3O_8 with the following isotopic composition (weight per cent): ^{236}U, 95·16; ^{234}U, 0·06; ^{235}U, 4·24; ^{238}U, 0·55. The U_3O_8 was reduced to UO_2 and fabricated into target disks 1 cm in diameter, about 0·04 cm thick, and weighing about 0·25 g. Enough material was available to make three targets.

Irradiations and flux monitoring

The flux monitor was a fission chamber which recorded the fission rate in a thin uranium sample, enriched in ^{235}U. The fission chamber was a gas-flow parallel plate ionization chamber, cylindrical in shape, and having thin brass walls. The counting gas was, by volume, 90 per cent argon and 10 per cent methane, flowing at a pressure slightly above atmospheric. The monitors were 1 cm diameter deposits of about 250 micrograms of metallic enriched uranium evaporated upon 0·005 in. thick platinum disks. These deposits were thin enough so that there was no appreciable self-absorption of fission fragments. Their mass was determined by alpha counting in known geometry. Composition of the monitor uranium in atom per cent was as follows: ^{235}U, 93·27; ^{234}U, 1·03; ^{236}U, 0·483; ^{238}U, 5·21.

The target and the monitor were placed in the fission chamber, lying flat against each other, with their 1 cm diameters aligned exactly so that they subtended the same polar angle with respect to the neutron source. With the monitor facing into the counting volume of the chamber, one count was recorded per fission. Pulses from the chamber were amplified and fed into a single-channel analyser. Total fissions were recorded by taking an integral count upwards in energy from a point in the valley between the pulse height of the alpha particles and those of the fission fragments.

Irradiation times were 4 to 6 hr in duration, with proton beam currents 20 to 30 μA, and lithium target

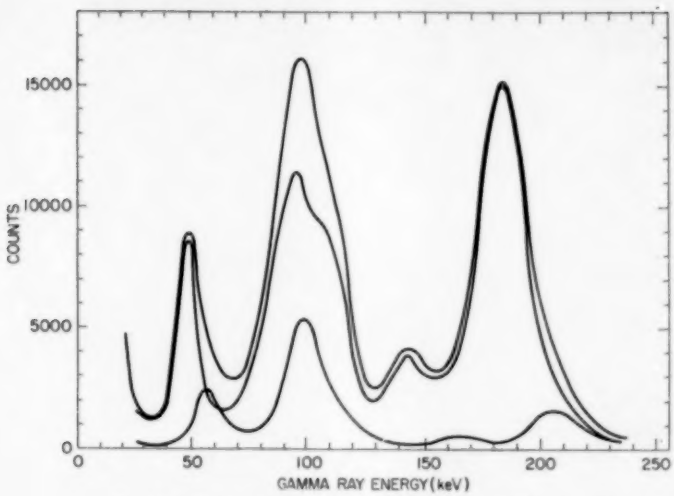

FIG. 1.—Gamma-ray spectrum of ^{236}U target. Upper curve: irradiated target. Middle curve: unirradiated target. Lower curve: net activation. Peak upon which calibration is based is centred at 101 keV (Np K X-rays). Peaks in the unirradiated target are due essentially to X-rays and nuclear gamma rays following the alpha decay ^{235}U and ^{236}U (STROMINGER *et al.*, 1958).

VOL. 15 1961

thicknesses 40 to 50 keV, deposited upon the inside of a tantalum cup. The ^{236}U targets were 1 to 1·5 cm from the neutron source. The targets were irradiated at O° with respect to the proton beam, except in one irradiation, that at the lowest energy, where the angle was 60°. There was no appreciable neutron attenuation in the monitor and its platinum backing. Corrections for attenuation in the target itself were less than 1 per cent.

In computing the effective fission cross section of the monitoring foil, account was taken of all the uranium isotopes present, and of the lower energy neutron group resulting from the excited state of ^{7}Be in the reaction $^{7}Li(p,n)^{7}Be$. Fission cross sections for the species in the monitor were taken from HUGHES and SCHWARTZ (1958). Corrections for the lower energy neutrons were also made in calculating the final ^{236}U cross sections. Values for the ratio of intensity of the lower energy group to the main neutron group for various angles of neutron emission are those of BEVINGTON *et al.* (1961).

Gamma-ray spectral analysis

The gamma spectra of the ^{236}U targets were analysed before and after irradiation, the counting having been done in a reproducible position at approximately 45 per cent geometry on a 4 in. diameter by 4 in. high NaI (thallium activated) crystal. The spectra were analysed with a 256 channel pulse-height analyser equipped with a live-time recorder. The digital readout of the spectrum before irradiation was subtracted from the readout after irradiation to give the net result of the activation. Figure 1 shows a typical spectrum before and after irradiation, and the net activation. The known gamma-ray peaks of ^{237}U (RASMUSSEN *et al.*, 1957) are evident in the spectrum, and the decay could be followed over several half-lives. The gamma-ray peak upon which the calibration was based is located at 101 keV, and consists of K X-rays of neptunium.

It remained therefore to relate the counting rate of the 101 keV gamma peak to the disintegration rate of ^{237}U. To accomplish this, ^{237}U having a known disintegration rate was introduced into a weighed amount of natural uranium in nitric acid solution. The solution was evaporated, and the uranium converted to dioxide and made into several disks of the same size and shape as the target disks. These disks were counted on the gamma analyser under conditions identical to those of the targets, thereby completing the required calibration, that is, the ratio of counts in the gamma-ray peak to the ^{237}U disintegration rate.

Disintegration rate of ^{237}U

The absolute ^{237}U disintegration rate was measured by two separate 4π beta counting methods: (1) proportional counting on a thin mounting in a gas-flow counter (PATE and YAFFE, 1955); (2) integral counting with a liquid scintillation spectrometer. Initially the standard techniques of the proportional counting method were employed. The beta energies of ^{237}U, however, are quite low (0·268 MeV, 96 per cent; 0·068 MeV, per cent) (RASMUSSEN *et al.*, 1957), and

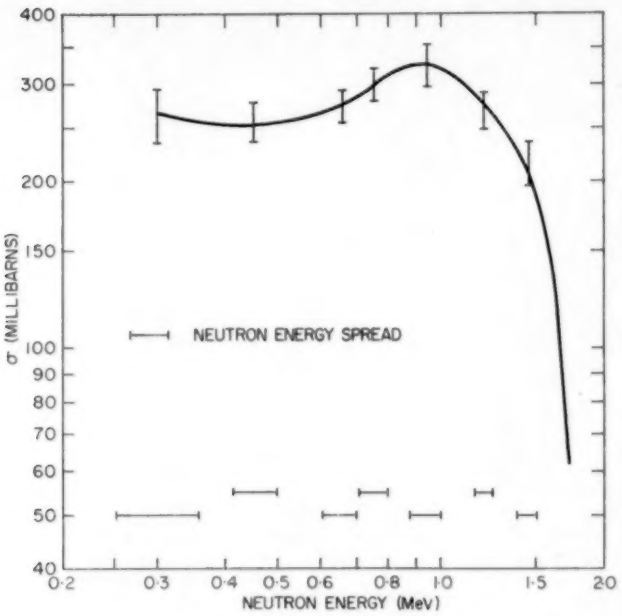

FIG. 2.—Capture cross section of ^{236}U.

appreciable corrections were necessary for self-absorption and source-mount absorption. In order to obtain an independent check on this method, the disintegration rate was also measured by liquid scintillation counting.

To prepare the ^{237}U activity for beta counting, some of the ^{236}U supply (weight per cent: ^{236}U, 95·16; ^{234}U, 0·06; ^{235}U, 4·24; ^{238}U, 0·55) was irradiated in the Argonne reactor, CP-5. The oxide was dissolved, and an ether extraction and peroxide precipitation left a ^{237}U activity free of fission products and ^{239}Np.

The apparatus and techniques of the liquid scintillation method used here are described by HORROCKS and STUDIER (1960). Two separate scintillation media were used. The first of these, compatible with aqueous solutions of the activity, consisted of a mixture, by volume, of 75 per cent dioxane, 12·5 per cent 1,2-dimethoxyethane, and 12·5 per cent anisole, containing the scintillators 7 g/l. 2,5 diphenyloxazole (PPO) and 50 mg/l. [2-(5 phenyloxazolyl)] benzene (POPOP). Introduced directly into the scintillator were samples of aqueous 0·1 N HCl stock solution of ^{237}U. The second scintillation medium used was xylene containing the scintillators 4 g/l. terphenyl and 0·1 g/l. POPOP. An aliquot of stock was evaporated, taken up into 0·2 N HCl, whence the uranium was extracted into a mixture of equal amounts by volume of dioctyl phosphate and toluene, and introduced into the scintillation system. Counting rates determined in the two scintillation media agreed within 1 per cent.

Finally, when corrections for source-mount absorption and self-absorption (PATE and YAFFE, 1955; MERRITT *et al.*, 1959) were made on the proportional counting rate, the results agreed with the scintillation counting rates within 2 per cent.

4. RESULTS

The cross sections of ^{236}U are given in Table 1 and plotted in Fig. 2. Errors attached to the cross sections are standard deviations. Neutron energy spreads given in the table and shown in the figure represent the entire range of neutrons received by the target, the stated neutron energy in both the graph and table being the centre of the energy interval. Our spreads are due to the lithium target thickness (40 to 50 keV), and to the neutron energy variation with angle of emission with respect to the proton beam. The errors in the cross sections are typically made up of 5 to 6 per cent in the flux measurement, 2 to 3 per cent in the 4π beta calibration, 2 to 3 per cent in the gamma-spectral analysis, and 1 to 2 per cent in corrections for the low-energy component of neutrons.

Table 1 also gives results just recently received from BARRY *et al.* (1961) at Aldermaston. These data, obtained by methods similar to those described here, are in substantial agreement with the present data.

The curve shows a rise in the cross section with energy, although a continuous fall might have been anticipated. Similar results were found by HANNA and ROSE (1959) for the capture cross sections of ^{238}U and

TABLE 1.—NEUTRON CAPTURE CROSS SECTION OF ^{236}U

Neutron energy (MeV)	Energy spread (MeV)	Capture cross section (mb)	
		Present work	Aldermaston
0·300	0·115	265 ± 30	
0·360	0·070		311 ± 26
0·457	0·085	257 ± 20	
0·464	0·070		308 ± 30
0·560	0·070		403 ± 32
0·655	0·070		271 ± 25
0·655	0·095	273 ± 21	
0·705	0·070		301 ± 34
0·750	0·095	299 ± 21	
0·850	0·070		297 ± 29
0·940	0·110	324 ± 28	
0·943	0·075		351 ± 41
1·063	0·075		350 ± 43
1·200	0·095	268 ± 19	
1·220	0·075		536 ± 68
1·310	0·080		196 ± 47
1·446	0·125	216 ± 19	
1·585	0·085		147 ± 30
1·732	0·110	<100	
2·020	0·100		88 ± 10
2·790	0·120		68 ± 10
3·970	0·150		28 ± 10

^{232}Th. These authors found an increase in the ^{238}U cross section with increasing energy and a plateau in the ^{232}Th curve. The cross sections in all three cases, as expected, eventually again decrease with still higher neutron energy. The curves for ^{238}U and ^{232}Th were explained theoretically by LANE and LYNN (1957) who attributed the shape of the curves to the small rate of increase with energy of the number of inelastic scattering channels. Although the same treatment might be presumed to apply to the ^{236}U data, the present paper does not give any calculations to prove this.

Acknowledgments—The authors wish to express gratitude to DRS. PETER KAFALAS and CARL E. CROUTHAMEL for advice and discussions concerning this work. We are also grateful for the co-operation of DRS. ALAN B. SMITH of the Reactor Engineering Division Van de Graaff, F. PAUL MOORING of the Physics Division Van de Graaff, DONALD L. HORROCKS, who did the liquid scintillation counting, and RAYMOND J. ACKERMANN, for the preparation of the monitoring foils.

REFERENCES

BARRY J. F., BUNCE J. L. and PERKIN J. L. (1961) *Proc. phys. Soc.* To be published.

BEVINGTON P. R., ROLLAND W. W. and LEWIS H. W. (1961) *Phys. Rev.* **121,** No. 3, 871.

HANNA R. C. and ROSE B. (1959) *J. Nucl. Energy* **8,** 197.

HORROCKS D. L. and STUDIER M. H. (1961) *Analyt. Chem.* To be published.

HUGHES D. J. and SCHWARTZ R. B. (1958) *Neutron Cross-Sections.* BNL–325, 2nd Edn.

LANE A. M. and LYNN J. E. (1957) *Proc. phys. Soc.* **A70,** 557.

MERRITT J. S., TAYLOR J. G. V. and CAMPION P. J. (1959) *Canad. J. Chem.* **37,** 1109.

PATE B. D. and YAFFE L. (1955) *Canad. J. Chem.* **33,** 15; 610; 929; 1656.

RASMUSSEN J. O., CANAVAN F. L. and HOLLANDER J. M. (1957) *Phys. Rev.* **107,** 141.

STROMINGER D., HOLLANDER J. M. and SEABORG G. T. (1958) *Rev. mod. Phys.* **30,** No. 2, Part 2, 585.

VOL. 15 1961

Reactor Science and Technology (Journal of Nuclear Energy Parts A/B) 1961, Vol. 15, pp. 204 to 208. Pergamon Press Ltd. Printed in Northern Ireland

MEASUREMENTS OF THE DIFFUSION LENGTH OF THERMAL NEUTRONS IN WATER FROM 16 TO 89°C AND IN DIPHYL (DOWTHERM A) AT 185°C

J. CSIKAI, A. DARÓCZY and K. DEDE*
Institute of Nuclear Research of the Hungarian Academy of Sciences,
Debrecen, Hungary

(*First received* 3 *January* 1961 *and in final form* 28 *March* 1961)

Abstract—A stationary method was developed to determine the diffusion length of thermal neutrons in moderators containing hydrogen using only a small amount of material. The diffusion length of thermal neutrons was determined in water at temperatures 16·1, 47·8, 69·5 and 88·7°C; the resulting values were: 2·640 ± 0·028, 2·858 ± 0·024, 2·974 ± 0·064 and 3·092 ± 0·062 cm. In linear approximation, for the temperature coefficient of the diffusion length, in the 16–89°C temperature interval, a value of +0·00617 ± 0·00086 cm/°C was obtained. In diphyl (Dowtherm A), the diffusion length of thermal neutrons at 184·4°C was 5·968 ± 0·266 cm.

INTRODUCTION

IN MODERATORS containing hydrogen, a number of measurements have been made in order to determine the diffusion length of thermal neutrons as a basic reactor parameter (FLÜGGE, 1959). Recently, a considerable number of investigations have been made of the temperature coefficient of the diffusion length (WILSON *et al.*, 1944; VON DARDEL *et al.*, 1954; WRIGHT *et al.*, 1956; DEUTSCH, 1956; ANTONOV *et al.*, 1956; DIO *et al.*, 1958; KÜCHLE, 1960; ROCKEY *et al.*, 1960). These measurements have used both stationary and impulse methods. From a technical viewpoint, the impulse method is preferable for determining the temperature coefficient, chiefly because a small amount of moderator is required. It seemed appropriate to develop a method possessing the advantages of stationary methods which would also be suitable for determining accurately the diffusion length even in the case of a small amount (a few litres) of medium. This method is essentially a combination of the exponential experiment and that of the negative source of thermal neutrons.

THEORY OF METHOD

In a stationary case, the diffusion of thermal neutrons is expressed by the so-called diffusion-equation. Its form in a medium without sources is:

$$\Delta\phi(\mathbf{r}) = \frac{1}{L^2}\,\phi(\mathbf{r}), \qquad (1)$$

where $\phi(\mathbf{r})$ is the thermal neutron flux, and L is the so-called diffusion length which, as a function of the absorption cross section Σ_a and the transport mean free path λ_t, may be expressed by

$$L = \sqrt{\frac{\lambda_t}{3\Sigma_a}}\,.$$

The boundary condition to equation (1) is that the flux inside the moderator should be expressed by a function which is zero at $0{\cdot}71\lambda_t$ distance from the boundary. In addition, the integral of neutron current density taken over a closed surface around the concentrated sources satisfies the condition:

$$\int_F \mathrm{j}_n\, df = \frac{\lambda_t}{3}\int_F \mathrm{grad}_n\,\phi\, df = S,$$

where S is the intensity of the thermal source surrounded by the surface F given in neutron/sec.

L can be determined by comparing the solution of equation (1) relating to a given moderator geometry and source distribution with the experimentally determined flux distribution. The thermal source of a given geometry can be effected by means of a cadmium absorbent placed in an arbitrary neutron-space (such as, for example, is produced by a point source emitting fast neutrons).

In the case of a cylindrical medium and a circular symmetric plane source, the solution to equation (1) is:

$$\phi(z,r) = \sum_{n=0}^{\infty} A_n J_0\left(\mu_n \frac{r}{R}\right) \exp\left[-z\sqrt{\frac{1}{L^2} + \left(\frac{\mu_n}{R}\right)^2}\right] \times \left\{1 - \exp\left[-2(Z-z)\sqrt{\frac{1}{L^2} + \left(\frac{\mu_n}{R}\right)^2}\right]\right\}, \qquad (2)$$

where J_0 is the Bessel function of the first kind and

* Present address: Secondary School of Karcag, Hungary.

zero order; while μ_n is its n-th zero point. $Z = Z_0 + 0{\cdot}71\lambda_t$ and $R = R_0 + 0{\cdot}71\lambda_t$: the extrapolated height and radius of the cylinder (Z_0 and R_0 are the real height and radius respectively). For instance, the A_n coefficients can be deduced from the flux distribution in the plane $z = 0$:

$$A_n = \frac{1}{\frac{R^2}{2} J_1(\mu_n)} \cdot \frac{1}{1 - \exp\left[-2Z\sqrt{\frac{1}{L^2} + \left(\frac{\mu_n}{R}\right)^2}\right]} \times \int_0^R \phi(0,r) J_0\left(\mu_n \frac{r}{R}\right) r\, dr. \quad (3)$$

If Z is sufficiently great, the second exponential expression in (2) may be taken as zero and thus expression A_n also will be simplified. On the other hand, as z increases, the upper harmonics will decrease faster, and thus for a certain distance

$$\phi(z,0) = A_0 \exp\left[-z\sqrt{\frac{1}{L^2} + \left(\frac{\mu_0}{R}\right)^2}\right] \times \left\{1 + \frac{A_1}{A_0} \exp\left[-z\left(\sqrt{\frac{1}{L^2} + \left(\frac{\mu_1}{R}\right)^2} - \sqrt{\frac{1}{L^2} + \left(\frac{\mu_0}{R}\right)^2}\right)\right] + \frac{A_2}{A_0} \exp\left[-z\left(\sqrt{\frac{1}{L^2} + \left(\frac{\mu_2}{R}\right)^2} - \sqrt{\frac{1}{L^2} + \left(\frac{\mu_0}{R}\right)^2}\right)\right] + \cdots\right\}. \quad (4)$$

The value of the bracketed { } term is nearly 1, and so it may be regarded as a correction factor and designated by $K(z,0)$. The value of the correction term may still further approach 1, if the axial flux is measured at the first zero point of the first upper-harmonic, i.e. at $r_0 = \frac{\mu_0}{\mu_1} R$, as here,

$$J_0\left(\mu_1 \frac{\frac{\mu_0}{\mu_1} R}{R}\right) = J_0(\mu_0) = 0.$$

Accordingly, the equation (4) can be expressed

$$\phi(z,r_0) = A_0 J_0\left(\frac{\mu_0^2}{\mu_1}\right) \exp\left[-z\sqrt{\frac{1}{L^2} + \left(\frac{\mu_0}{R}\right)^2}\right] \times \left\{1 + \frac{A_2}{A_0} \frac{J_0\left(\frac{\mu_0\mu_2}{\mu_1}\right)}{J_0\left(\frac{\mu_0^2}{\mu_1}\right)} \exp\left[-z\left(\sqrt{\frac{1}{L^2} + \left(\frac{\mu_2}{R}\right)^2} - \sqrt{\frac{1}{L^2} + \left(\frac{\mu_0}{R}\right)^2}\right)\right] + \frac{A_3}{A_0} \frac{J_0\left(\frac{\mu_0\mu_3}{\mu_1}\right)}{J_0\left(\frac{\mu_0^2}{\mu_1}\right)} \times \exp\left[-z\left(\sqrt{\frac{1}{L^2} + \left(\frac{\mu_3}{R}\right)^2} - \sqrt{\frac{1}{L^2} + \left(\frac{\mu_0}{R}\right)^2}\right)\right] + \cdots\right\}. \quad (5)$$

In this case, the correction factor should be designated by $K(z, r_0)$.

L may be determined by iteration. The A_n Fourier-Bessel coefficients can be computed from the radial flux distribution, whilst logarithmic plotting of the axial flux distribution will yield the quantity:

$$\tan\alpha = \sqrt{\frac{1}{L'^2} + \left(\frac{\mu_0}{R}\right)^2}, \quad (6)$$

where L' is the first approximation to L. Thus the correction factor as a function of z can be determined, and L'', the second approximation to L, will be obtained from the directivity factor of

$$\ln\frac{\phi(z,0)}{K(z,0)} = \ln\frac{\phi(z,r_0)}{K(z,r_0)} = -z\sqrt{\frac{1}{L''^2} + \left(\frac{\mu_0}{R}\right)^2}. \quad (7)$$

Taking the last value of L into consideration for calculating the correction, then L is obtained in the third approximation. The process may go on as far as any chosen degree of accuracy.

The smallest geometry to be applied in this method is governed by the fact that, together with the decrease of R, the error of the directly measured

$$\tan\alpha = \sqrt{\frac{1}{L'^2} + \left(\frac{\mu_0}{R}\right)^2}$$

will produce in L a greater and greater error. When $R = 2L$, the error arising from statistics will just about double (the two quantities in the root being of the same magnitude). In this case, the uncertainty in the extrapolated boundary will also cause a relatively greater error in L.

An arrangement corresponding to the above requirements can be realized by placing the finite cylinder containing the liquid to be measured upon the surface of a moderator containing the fast neutron source; the cadmium absorbent placed on the bottom of the finite cylinder will achieve the negative thermal plane source (Fig. 1). The measured flux with and without the cadmium plane is equal to the flux that would be produced by a source of an intensity equivalent to the number of neutrons absorbed in cadmium (according to location, direction and energy).

The distance of the plane $z = 0$ from the negative source of thermal neutrons must be chosen so that the extrapolated boundary experimentally determined by

VOL. 15 1961

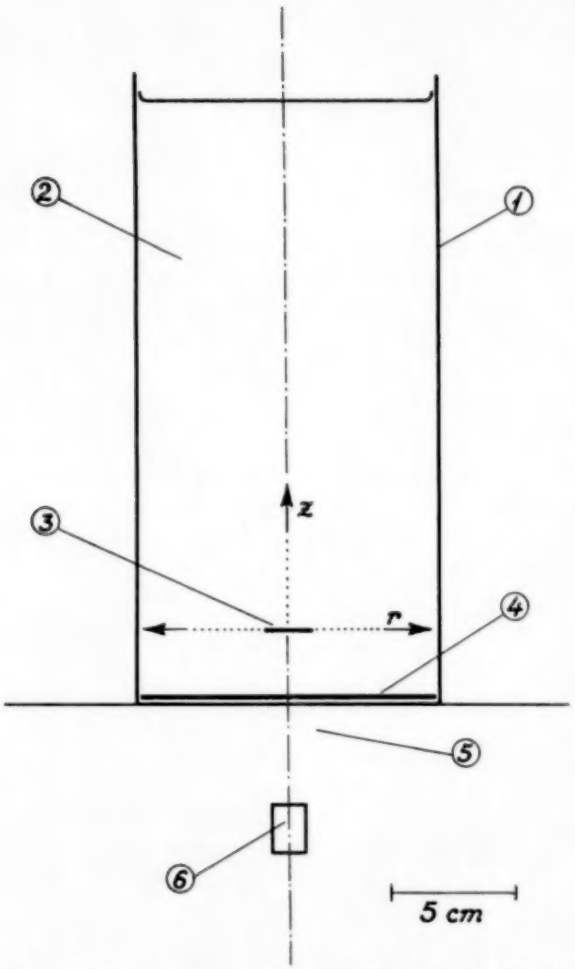

Fig. 1.—Schematic arrangement. 1. Cylindrical vessel; 2. Medium to be measured; 3. Detector foil; 4. Cadmium absorbent (negative source); 5. Moderator; 6. Neutron-source.

the measurement of radial flux should agree, within error, with the extrapolated boundary calculated by the transport mean free path. This distance was taken in our experiments as 2,4 cm.

In order to avoid the disturbing interaction of foils, only one foil was placed in the medium to be measured at each flux measurement.

The applicability of the method was tested by measuring the diffusion length of water. At a temperature of 20°C, the value of the diffusion length was determined in the arrangement shown by Fig. 1, and likewise—for a check-up—in an infinite medium with a circular symmetric plane source and also in an infinite medium with an infinite homogeneous plane source (Csikai *et al.*, 1960).

The results of measurements are contained in Table 1.

The agreement of the three measurements with one another and with data reported by other authors shows that the method is reliable and the diffusion length of thermal neutrons can be determined comparatively quickly, with sufficient accuracy through quite simple means, by using a small amount of material.

Table 1

Geometrical arrangement	L^{∞} (cm)	Detector
Finite cylindrical medium, circular symmetric plane source	2·75 ± 0·08	Ag
∞ medium, circular symmetric plane source	2·73 ± 0·04	Ag
∞ medium, ∞ homogeneous plane source	2·74 ± 0·06	BF_3 counter

EXPERIMENTAL ARRANGEMENT

The arrangement shown in Fig. 2 was used for measuring the temperature dependence of the diffusion length. The measurements were made in a vessel which was placed in a circulating oil-bath to establish the homogeneity of temperature for the medium to be measured. A separate vessel was used for heating the oil, and the temperature was maintained at the required value by a heat-regulator. The circulatory oilpump also was placed in this vessel.

The cadmium absorbent at the bottom of the vessel was the circular symmetric thermal plane-source. The cadmium covering the inside wall of the vessel gave the well-defined radial boundary of the moderator to be measured. The thickness of the cadmium was 0·936 g/cm².

For the measurement, an R.C.C. 178 B-type Po-Be neutron-source of 2×10^6 neutron/sec intensity was used.

The neutrons were detected with Rh-foils 18 mm in diameter and 123·6 mg/cm² thickness, and with a small-size proportional counter filled with BF_3 gas (a cylinder of a sensitive volume 9 mm in diameter and 30 mm length).* The foils were placed in a properly processed part of a steel sword of 1 mm thickness encased in a closed brass sheath of 0·4 mm wall-thickness. The BF_3 counter was encapsulated in a closed brass tube of 0·4 mm wall-thickness. The

* The validity of using detectors extending in direction z is supported by the following consideration. Let $\bar{\phi}$ be the integral flux measured by the detector, $\phi(z)$ the flux at z and d the extension of the detector in direction z, then $\bar{\phi} = A\int_z^{z+d} \phi(z)\,dz$. As $\phi(z) = Be^{-az}$, therefore $\bar{\phi} = C\int_z^{z+d} e^{-az}\,dz = D(e^{-ad} - 1)e^{-az} = Ee^{-az} = F\phi(z)$, where a, A, B, C, D, E, F are constants.

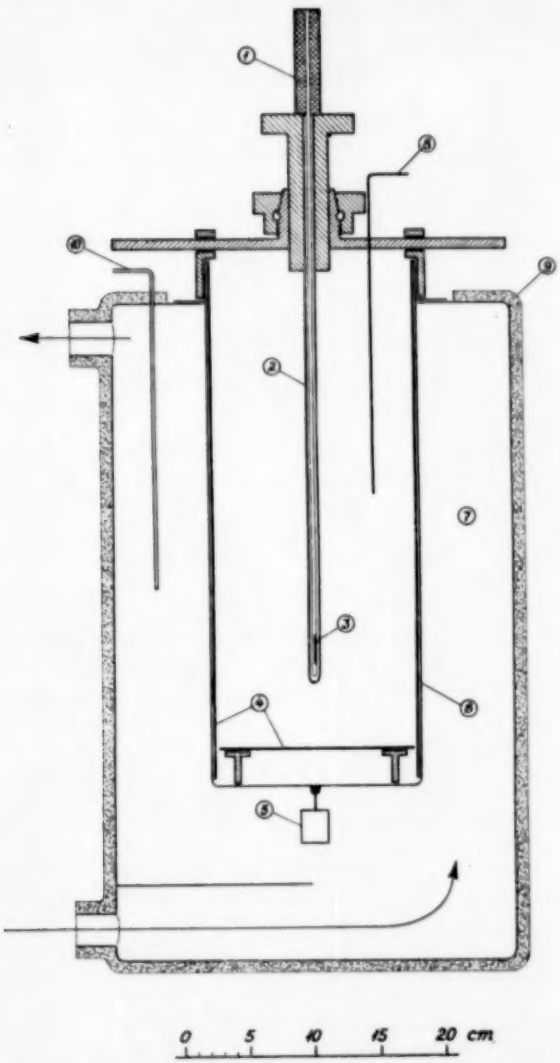

FIG. 2.—Experimental arrangement. 1. Sword; 2. Sheath; 3. Detector foil; 4. Cadmium; 5. Neutron-source; 6. Measuring vessel; 7. Circulating oil-bath; 8. Thermometer; 9. Heat insulation; 10. Heat regulator.

position of the detectors in $r - z$ direction could be determined with an accuracy of 0·1 mm. The β-activity of the detector foils was measured by an end-window GM–counter.

RESULTS OF MEASUREMENT

(*a*) *Measurements in water at different temperatures*

The value of the diffusion length of thermal neutrons was determined at four different temperatures. The results of these measurements are included in Table 2.

Measurements of the axial flux were made in every case at the first zero point of the first upper-harmonic and so the harmonic correction was calculated according to equation (5). The correction gave nearly a 1 per cent alteration in the L' value.

TABLE 2

Temperature (°C)	L'' (cm)	Detector
16·1 ± 0·4	2·640 ± 0·028	BF_3 counter
47·8 ± 0·2	2·858 ± 0·024	BF_3 counter
69·5 ± 0·2	2·974 ± 0·064	Rh
88·7 ± 0·2	3·092 ± 0·062	Rh

Consequently, if determination of the value of the diffusion length with this accuracy is sufficient, a calculation for the harmonic correction may be disregarded. In this manner, the diffusion length of thermal neutrons can be determined directly from the axial flux distribution measured at the first zero point of the first upper-harmonic (see equation (6)).

The results of the measurement as a function of temperature are plotted in Fig. 3. In linear approximation, for the temperature dependence of the diffusion length, the value of

$$\frac{\Delta L}{\Delta T} = +0{\cdot}00617 \pm 0{\cdot}00086 \text{ cm/°C}$$

was obtained in the 16–89°C temperature interval. This value is in good agreement with the results reported by other authors (WILSON *et al.*, 1944; DEUTSCH, 1956; ANTONOV *et al.*, 1956; DIO *et al.*, 1958).

(*b*) *Measurement in diphyl (Dowtherm A) at* 184·4°C

The diphyl (Fluka A. G. Chemische Fabrik Buchs SG, Schweiz) was checked to verify whether it corresponded to the exact eutectic mixture. This check was made by comparing the measured melting and boiling points with data reported in literature. As Table 3 shows, the values obtained are in very good agreement with the data in the literature (KOGAN *et al.*, 1951).

On these grounds, it was assumed that the composition of the diphyl used was 26·5 per cent diphenyl and 73·5 per cent diphenyloxide.

TABLE 3

	Experimental (°C)	Reported (°C)
Melting point	12·2	12·3
Boiling point (760 mm Hg)	257·3	258

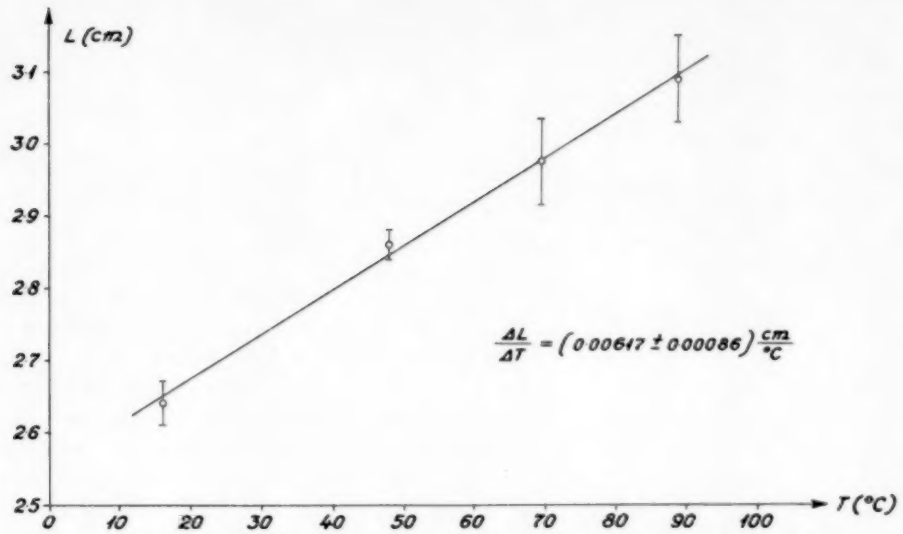

FIG. 3.—Temperature dependence of the diffusion length of thermal neutrons in water.

In the case of diphyl, there is a considerable discrepancy between the two measurements (PÁL *et al.*, 1959; KÜCHLE, 1960) for the temperature dependence of the diffusion length. The disagreement is particularly striking at higher temperatures. For this very reason, the value of the diffusion length was determined at a high temperature (at 184·4 ± 0·8°C) in order to verify the correct result. The value thus obtained was

$$L'' = 5{\cdot}968 \pm 0{\cdot}266 \text{ cm}$$

which, within error, is in good agreement with KÜCHLE's (1960) result.

The measurement for the axial flux was made at the $r = 0$ point and thus the harmonic correction was computed by the equation (4). This time, the correction brought a 2·8 per cent change in the value of L'.

In every case, the calculation for the value of tan α was made by means of the least squares method.

For water, the λ_t values apertaining to different temperatures were calculated by means of the empirical relation reported by DIO and SCHOPPER (1958) regarding the temperature dependence of the diffusion coefficient. In diphyl, the λ_t value was deduced by extrapolating KÜCHLE's (1960) measurements. The error in diffusion length was only slightly influenced by the error of λ_t, compared with the statistical error of the measurements.

The flux depressions arising from the finite thickness of the detector foils as well as from the detector holder sheath and tube were neglected; no correction was made for diffusion cooling either. In the case of both water and diphyl, the media were practically infinite in the z-direction.

Acknowledgments—Thanks are due to PROFESSOR A. SZALAY for his genuine interest in this work, as well as to MR. J. SCHADEK, engineer of this Institute, for the technical design of the experimental apparatus.

REFERENCES

ANTONOV A. V., ISAKOFF A. I., MURIN I. D., NEUPOCOYEV B. A., FRANK I. M., SHAPIRO F. L. and SHTRANICH I. V. (1956) *Proceedings of the First International Conference on the Peaceful Uses of Atomic Energy, Geneva*, P/661. United Nations, New York.

CSIKAI J. and DEDE K. (1960) *Magyar Fiz. Foly.* VIII, 1; (1960) *Atomki Közl.* II, 15.

DEUTSCH R. W. (1956) *Nucl. Sci. Engng.* **1,** 252.

DIO W. H. (1958) *Nukleonik* **1,** 13.

DIO W. H. and SCHOPPER E. (1958) *Nucl. Phys.* **6,** 175.

FLÜGGE S. (1959) *Encyclopaedia of Physics*, Vol. XXXVIII/2, p. 583. Springer-Verlag, Berlin-Göttingen-Heidelberg.

KOGAN S. Z. and CHECHETKIN A. V. (1951) *Visokotemperaturnie Teplonositeli i ikh Primenenie v Promishlennosti*, Moskow, Leningrad.

KÜCHLE M. (1960) *Nukleonik* **2,** 131.

PÁL L., BATA L. and KISS I. (1959) *Acta Phys. Acad. Sci. Hung.* **X,** 173.

ROCKEY K. S. and SKOLNIK W. (1960) *Nucl. Sci. Engng.* **8,** 62.

VON DARDEL G. F. and SJÖSTRAND N. G. (1954) *Phys. Rev.* **96,** 1245.

WILSON V. C., BRAGDON E. W. and KANNER H. (1944) CP-2306. Unpublished.

WRIGHT W. B. and FROST R. T. (1956) KAPL-M-WBW-2.

Reactor Science and Technology (Journal of Nuclear Energy Parts A/B) 1961, Vol. 15, p. 209. Pergamon Press Ltd. Printed in Northern Ireland

BOOK REVIEW

The Mathematics of Radioactive Transfer, I. W. BUSBRIDGE, Cambridge University Press, 143 pp., 30*s*.

THE equation of radiative transfer in stellar atmospheres is very similar to the neutron transport equation: in fact the one-group neutron equation is formally identical to the transfer equation for unpolarized light in a grey atmosphere. However, the aims of the mathematical astrophysicist are very different from those of the neutron transport theorist or reactor physicist. The reactor physicist is concerned to obtain numerical results in systems which may be extremely awkward mathematically, because of difficult geometry and the erratic dependence of cross-sections on energy. The astrophysicist (or perhaps one should say astrophysical mathematician) is more concerned to push his mathematical techniques to the limit: he therefore restricts drastically the class of problems which he is prepared to study. Furthermore, the methods and notations of the astrophysicist will be very unfamiliar to the reactor physicist.

This book gives a clear and attractive account of its subject. It deals only with plane geometry. The Milne problem is completely solved by the H-function method of Chandrasekhar, which seems clearer than the usual Wiener-Hopf technique: no definite results are obtained for finite slabs. It is much preoccupied with existence theorems. It can be recommended to those who wish to study this subject, but the ordinary reactor physicist will find little in it to interest him.

D. C. LESLIE

VOL.
15
1961

Reactor Science and Technology (Journal of Nuclear Energy Parts A/B) 1961, Vol. 15, pp. 210 to 213. Pergamon Press Ltd. Printed in Northern Ireland

MODELS FOR FINDING THE CONTROL RESPONSE AND TEMPERATURE COEFFICIENT OF URANIUM-WATER REACTORS OPERATING WITH INTERMEDIATE ENERGY NEUTRONS*

V. B. KLIMENTOV and V. M. GRIAZEV

(*Received* 12 *March* 1959)

Abstract—Experiments using physical models to represent the control response and reactivity changes caused by changes in the density of the water in water-moderated intermediate energy uranium reactors are described. The efficiencies of various kinds of control rod have been determined and a relation between the critical size of the reactor and the density of the water in the core has been derived.

1. INTRODUCTION

PHYSICAL models of the various processes which take place in nuclear reactors may be constructed by simulating these processes in a critical assembly. The information required to design and build nuclear reactors can be obtained far more cheaply by making experiments with models than by conducting critical experiments during the start-up period of the reactor. Furthermore, the optimum full power loading of a nuclear reactor can be estimated more accurately from the results of model experiments than from theoretical calculations.

Two problems of particular interest are the temperature effect due to density changes in the water and the control response of uranium-water reactors operating with intermediate energy neutrons. We have studied these problems by conducting experiments on a critical assembly of a uranium-water multiplying system. The construction of this assembly and details of the experiments carried out on it have been described elsewhere[1]. In constructing this assembly, provision was made for changing the layout and composition of the reflector core and for altering the position of the control rods.

The active components of the critical assembly were a number of $250 \times 70 \times 2{\cdot}7$ mm plates made of compressed mixed oxides of uranium (90 per cent ^{235}U) mixed with polyethylene. These were assembled $5 \rightarrow 8$ at a time in stainless steel boxes or stacks which could be clamped in a framework to form a core of the required size and shape. The volume of each stack was 0·62 l. and the ratio of the number of hydrogen nuclei to the number of ^{235}U nuclei (ρ_H/ρ_{235}) was varied from 17 to 50. Two hollow cadmium rods which formed part of the automatic control system and two safety rods were installed near the core. The critical assembly was placed in an aluminium tank, diameter 3 m and height 1·6 m, equipped with a device which enabled the tank to be filled with water under controllable conditions or to be rapidly emptied. The level of the water in the tank was registered by a water gauge. In addition, all the equipment necessary to ensure reliable monitoring and control of the critical assembly throughout the working range was provided. Special attention was given to ensure the maintenance of nuclear safety during the actual experiments.

2. CONTROL ROD EFFICIENCY

The efficiency of the control rods can be readily determined on a critical assembly of the type we are considering at power levels below 1 watt. We made measurements on a 60 mm diameter solid boron rod (B_4C) and on a hollow cadmium rod having the same diameter and a wall thickness of 1 mm. The length of the rods was 400 mm and the height of the core of the multiplying system was 250 mm. The measurements were made on systems having a water reflector and a graphite side reflector (thickness 210 mm and height 400 mm). In all the systems the upper and lower reflectors were of water. The rods under study were placed at distances of 35, 70 and 140 mm from the core. A plan of the multiplying system for a graphite side reflector is shown in Fig. 1. The system was ring-shaped and the dimensions of the internal water cavity were 140×140 mm. The safety rods were capable of shutting down the system irrespective of the position of the control rods or of the rods under study. The neutron energy spectrum was deduced from the ratio $\rho_H/\rho_{235} = 31$. According to FEINBERG *et al.*,[1] the fraction of ^{235}U fissions induced by neutrons having energies above 0·4 eV is about 30 per cent in this type of system.

* Translated by D. L. ALLAN from *Atomnaya Energiya* **7**, 519 (1959).

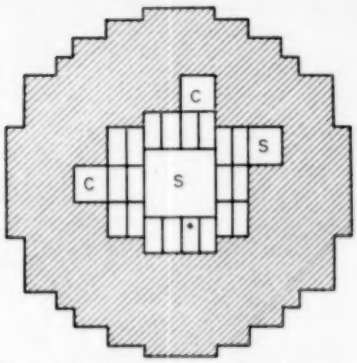

FIG. 1.—Plan of the ring-shaped uranium-water system with graphite side reflector ($\rho_H/\rho_{235} = 31$). Unshaded region—active stacks; shaded region—graphite; *C*—control rods; *S*—safety rods; *x*—moveable stack.

In some preliminary experiments the control rods *C* were calibrated using a stack which could be moved to and fro by a lead screw device. In addition, the efficiency of the cadmium and boron rods and the efficiency of the stacks were determined by inserting the automatic control rods and partially withdrawing the moveable stack from the core. At the same time the control rods *C* were automatically raised, the efficiency of the withdrawn portions of the control rods having been determined beforehand by observing the doubling time of the reactor power. This procedure was continued until the stack had been withdrawn completely from the core. During these tests the position of the rods was indicated by a Selsyn position indicator.

The efficiency $\Delta\rho$ of one stack in the 25 stack multiplying system with the water reflector was 0·015, while in the 20 stack system with the graphite side reflector it was 0·021. The calibration curve for the two coupled rods in the graphite side reflector near the core is shown in Fig. 2. The efficiencies of the boron and of the hollow cadmium rods were found to be almost the same. The efficiency of these rods depends upon their position in the core, which is determined by the thermal neutron distribution in the reflector. This dependence is shown in Fig. 3.

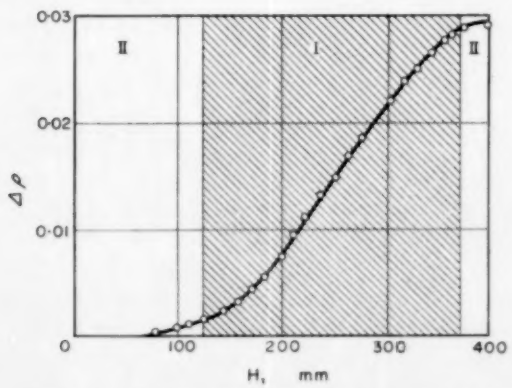

FIG. 2.—Control rod calibration curve. I—core; II—upper and lower water reflectors.

For the control of pressurized uranium-water reactors it may be advantageous to employ liquid absorbers. Liquid absorber regulators have the advantage that they have no moving parts to complicate the reactor construction. We have made an experimental determination of the efficiency of a mercury absorber

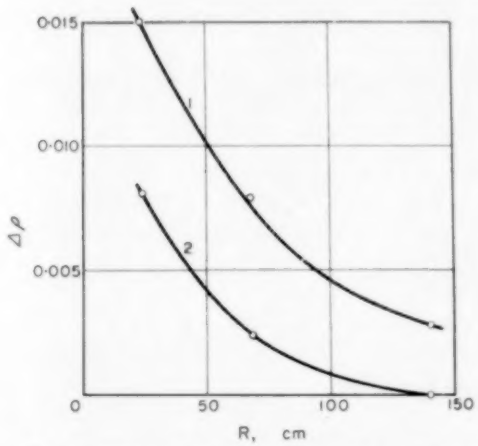

FIG. 3.—Efficiency of the absorbing rods as a function of their position in relation to the core. 1—reflector (210 mm graphite); 2—reflector (water).

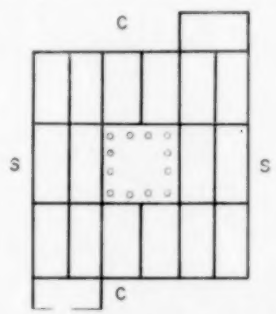

FIG. 4.—Plan of uranium-water system containing a mercury absorber ($\rho_H/\rho_{235} = 25$). *C*—control rods; *S*—safety rods. The mercury absorber is in the centre of the system.

placed at the centre of a uranium-water system with a water reflector, a plan of which is shown in Fig. 4. The neutron energy spectrum in the multiplying system was determined from the ratio $\rho_H/\rho_{235} = 25$. The number of fissions induced by neutrons having energies above 0·4 eV was not less than 50 per cent[1]. The mercury absorber consisted of 12 copper pipes filled with mercury (2·7 kg Hg). To make room for this absorber two stacks were removed from the assembly. The external and internal diameters of the pipes were 10 and 8 mm, respectively, their heights were 400 mm,

and they were arranged around the perimeter of a square on a side of 53 mm. The corrosive action of the mercury on the copper caused no trouble, because these rods were in use for less than 24 hours. With the reactor working under automatic control, the mercury absorber was gradually withdrawn and the reactivity change was compensated by inserting the control rods and removing the peripheral stacks. With the pipes filled with mercury $\Delta\rho' = 0{\cdot}088$ while for the empty pipes $\Delta\rho'' = 0{\cdot}023$. Thus, the efficiency of 2·7 Kg of mercury in the form of rods with the above dimensions was $\Delta\rho' - \Delta\rho'' = 0{\cdot}065$.

3. A PHYSICAL MODEL OF THE TEMPERATURE EFFECT RESULTING FROM CHANGES IN THE WATER DENSITY

The change in the density of water due to temperature variations causes the neutron migration length to increase and this can substantially change the physical characteristics of uranium-water reactors. Such changes in the density of the water in the core of a nuclear reactor were simulated by inserting special intermediate layers in the spaces between the uranium oxide plates of the critical assembly. These layers were made of thin air-impregnated rubber films attached to a copper frame. The volumes occupied by air and material in these layers were measured by measuring the volume of water which they displaced. The distance between the plates was small compared with the neutron diffusion length in water: it was less than 3→4 mm and the thickness of the layers containing air was about 2 mm. Calculations made by FEINBERG *et al.*[1] on the degree of heterogeneity of uranium-water systems with laminated fuel elements show that a system may be considered homogeneous if the density ratio $\rho_H/\rho_{235} < 40$. For the case $\rho_H/\rho_{235} = 50$, the effect on critical size of the system of the gaps between the plates inside the stacks was less than 4 per cent. The uranium-water systems used in the experiments described here were quasi-homogeneous, i.e. the addition of the special air-impregnated layers was assumed to have the same effect as reducing the density of the water in the core. The average density of the water was calculated from the known amount of air in the layers and from the amount of polyethylene in the uranium oxide plates. Polyethylene, which has a density of 0·9 g cm^{-3}, has moderating and diffusion properties which are similar to those of ordinary water. The density of the water in the stack was 1 g cm^{-3} at the operating temperature of about 5°C. The density of the water in the reflector was not altered.

The effect of changing the mean density of the water in the core on the critical size of the multiplying system was studied for various moderator-fuel ratios ρ_H/ρ_{235}. The effect of the solid component of the air-impregnated layers on the critical size was found from a number of control experiments.

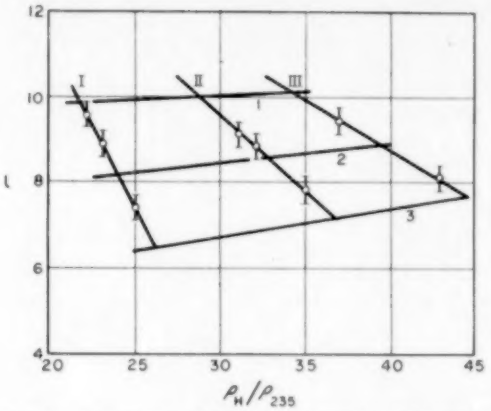

FIG. 5.—Dependence of the critical dimensions of a uranium-water system on the ratio ρ_H/ρ_{235} for various water densities. 1, 2, 3—water density γ equal to 0·8, 0·9 and 1·0 g cm^{-3} respectively; I, II, III—^{235}U concentration, 836, 627 and 523 gl.$^{-1}$

In these experiments the usual procedure was to gradually fill the already assembled core with water. The core shape was arranged to be as nearly cylindrical as possible. The degree of sub-criticality of the system was determined by using the $1/n$ relationship between the level of the water in the tank and the number of counts n recorded by the start-up equipment, which measures the neutron flux density in the vicinity of the core. During these experiments a Po-Be neutron source was continuously present near the core. We determined the number of stacks N such that the system was critical when N stacks were present in the assembly and sub-critical when N-1 stacks were present.

Using this method the error ΔV in the critical size determination was $\pm 0{\cdot}31$ l. and the mean water density was estimated to within an accuracy $\gamma = \pm 0{\cdot}005$ g cm^{-3}. The results of these experiments, which include a correction for the presence of the solid material in the air layers, are shown in Fig. 5. This figure gives the dependence of the critical volume of uranium-water systems on the ratio ρ_H/ρ_{235}.

This dependence is represented in Fig. 5 by lines of equal density for average water densities $\gamma = 1$ g cm^{-3}, $\gamma = 0{\cdot}9$ g cm^{-3} and $\gamma = 0{\cdot}8$ g cm^{-3}. Figure 5 also shows three straight lines representing constant ^{235}U concentrations, one for each of the three cycles of measurements. In any one cycle the number of active plates in a stack remained fixed (8, 6 or 5 per stack) and the number of air layers was varied to represent

moderator-fuel density ratios in the interval $\rho_H/\rho_{235} = 45 - 20$. An almost linear dependence between the critical volumes of the uranium-water system and the moderator-fuel density ratio was found. From these experiments it is possible to make a quantitative estimate of the changes in the critical dimensions of intermediate energy uranium-water systems caused by changes in the density of the water in the core. It was found that for ^{235}U concentrations of 836, 627 and 523 gl.$^{-1}$, a decrease in the water density of 0·1 g cm^{-3} caused an increase in the critical volume $\Delta V = (1{\cdot}6 \pm 0{\cdot}4)$l, $\Delta V = (1{\cdot}4 \pm 0{\cdot}4)$l, and $\Delta V = (1{\cdot}2 \pm 0{\cdot}4)$l, respectively. An estimate of the corresponding change in reactivity $\Delta\rho/\Delta\gamma$ was made, based upon the experience obtained on the control of this type of multiplying system. For the three cases we are considering and for a water density change of 0·1 g cm^{-3}, the reactivity changes turned out to be 0·039, 0·034 and 0·029.

Since the active plates contained polyethylene, which has a density different from that of water, the values for the critical dimensions of intermediate energy uranium-water systems obtained by FEINBERG *et al.*[1] were somewhat too large. The correction to allow for this difference in density can be obtained from Fig. 5 for the density interval $\rho_H/\rho_{235} = 45 - 20$. The results obtained agree closely with those obtained by CALLIHAN[2]. The effect of polyethylene on the critical dimensions of the systems we studied is particularly important for small values of ρ_H/ρ_{235} and it is unfortunate that it was not possible for us to make direct experimental measurements of this effect. FEINBERG *et al.*[1] estimated the effects of various constructional materials on the critical dimensions of uranium-water systems. They found that for ρ_H/ρ_{235} values in the range 30–17 inserting aluminium into the core led to a sharp increase in the critical size of the system. In our experiments, the effects of aluminium and layers containing air on the critical size of systems with $\rho_H/\rho_{235} < 30$ turned out to be the same as those found by FEINBERG *et al.*[1] When 190 g of aluminium (volume 70 cm^3) was inserted into a core where the ^{235}U concentration was 836 gl.$^{-1}$, the critical volume of the system increased by $(3{\cdot}2 \pm 0{\cdot}3)$l. In the experiments with air-impregnated layers it was found that reducing the average density by an amount corresponding to the displacement of 70 cm^3 of water caused the same change in the critical dimensions as was caused by the addition of 190 g of aluminium.

Acknowledgments—In conclusion, the authors thank S. M. FEINBERG who was responsible for the overall scientific direction of this work, V. A. TIKANOV for discussion and A. D. MERKULOV, N. N. KOLPAKOV and B. A. PRIADEKHIN and others who assisted with the experimental work.

REFERENCES

1. FEINBERG S. M., BOROB'EV E. D., GRIAZEV V. M., KLIMENTOV V. B., TSIKANOV V. A. and LIASHCHENKO N. YA., *Proceedings of the Second International Conference on the Peaceful Uses of Atomic Energy, Geneva*, Vol. 10, p. 296. United Nations, New York (1958).
2. CALLIHAN D., *Nucleonics*, **14**, No. 7 (1956).

VOL. 15 1961

Reactor Science and Technology (Journal of Nuclear Energy Parts A/B) 1961, Vol. 15, pp. 214 to 219. Pergamon Press Ltd. Printed in Northern Ireland

THE BURN-UP OF NATURAL URANIUM IN A HOMOGENEOUS REACTOR*

V. BARTOŠEK

(*Received* 4 *June* 1959)

Abstract—Homogeneous reactors have the advantage that fuel-element stability problems are absent; the degree of burn-up may therefore be made greater than in the corresponding heterogeneous system, with consequent economic advantage. The burn-up in a reactor operating with recycled uranium is given as a function of the initial parameters of the system, and the condition on the probability of neutron capture in ^{238}U ensuring maximum burn-up is determined.

1. INTRODUCTION

A HOMOGENEOUS natural uranium-heavy-water reactor, burning enriched plutonium bred in the same reactor, operates during most of the run in the so-called stationary regime where the quantity of fissile isotopes (^{235}U, ^{239}Pu and ^{241}Pu) built up in the reactor remains constant[1]. The economics of such a reactor depend substantially upon the degree of burn-up of the natural uranium which can be achieved in this regime of operation. Since the reactivity of the system is the principal factor determining the degree of burn-up in a homogeneous reactor, it is from this point of view that we will try to find the conditions for maximum burn-up.

2. THE NEUTRON BALANCE EQUATION

In order to describe how the isotopic concentration changes with time during the period the reactor is operating, we will choose as independent variable the integral flux s which is related to the average neutron flux Φ and the time the reactor is operating t by the expression

$$s = 10^{-21}\int_0^t \Phi\,(t')\,dt'.$$

Thus an integral flux $s = 1$ corresponds to an irradiation for one year in a flux $\Phi = 3{\cdot}17 \times 10^{13}$ neutrons $cm^{-2}\,sec^{-1}$. We will also use the following notation: N_n is the number of nuclei per cm^3 of the nth isotope: N_n^0 is the number of nuclei per cm^3 of the nth isotope at the time of start-up of the reactor;

$$\rho_n = N_n/N_5^0; \qquad \rho_n^0 = N_n^0/N_5^0; \qquad \beta = N_M/N_5^0; \qquad \vartheta^0 = N_8^0/N_5^0;$$

σ_n is the absorption cross section of the nth isotope; I_n is the resonance absorption integral of the nth isotope; φ_n is the probability that a neutron escapes resonance absorption in the nth isotope; ν_i is the number of fast neutrons produced in the fission of the ith isotope; $\nu_i' = \nu_i \dfrac{\sigma_i^f}{\sigma_i}$; D is the diffusion coefficient; B^2 is the Laplacian of the system; ξ is the logarithmic neutron energy loss per collision and τ is the age of the neutrons. The indices have the following significance; c denotes radiative capture, f denotes fission; s denotes scattering; st refers to slagging and poisoning and M refers to the moderator. The indices 5, 6, 8, 9, 0, 1, 2, refer to the isotopes ^{235}U, ^{236}U, ^{238}U, ^{239}Pu, ^{240}Pu, ^{241}Pu and ^{242}Pu.

The fuel balance in a reactor with uranium exchange can be expressed by the equations

$$\frac{d\rho_5}{ds} \equiv \rho_5' = -\rho_5\left(\sigma_5 + \frac{1}{S}\right) + \frac{\rho_5^d}{S}; \qquad (1a)$$

$$\rho_6' = \rho_5\sigma_5^c - \rho_6\left(\sigma_6 + \frac{1}{S}\right); \qquad (1b)$$

$$\rho_8' = -\rho_8\left(\sigma_8 + \frac{1}{S}\right) - (1-\varphi_8)\,e^{-B^2\tau}f + \frac{\rho_8^d}{S}; \qquad (1c)$$

$$\rho_9' = \rho_8\sigma_8 + (1-\varphi_8)\,e^{-B^2\tau}f - \rho_9\sigma_9; \qquad (1d)$$

$$\rho_0' = \rho_9\sigma_9^c - \rho_0\left(\sigma_0 + \frac{I_0}{\xi\sigma_{M^s}}\frac{\varphi_8 e^{-B^2\tau}}{\beta}f\right); \qquad (1e)$$

$$\rho_1' = \rho_0\left(\sigma_0 + \frac{I_0}{\xi\sigma_{M^s}}\frac{\varphi_8 e^{-B^2\tau}}{\beta}f\right) - \rho_1\sigma_1; \qquad (1f)$$

$$\rho_2' = \rho_1\sigma_1^c - \rho_2\left(\sigma_2 + \frac{I_2}{\xi\sigma_{M^s}}\frac{\varphi_8 e^{-B^2\tau}}{\beta}f\right), \qquad 1(g)$$

where the relative number of fast neutrons is denoted by

$$f = \nu_5'\rho_5\sigma_5 + \nu_9'\rho_9\sigma_9 + \nu_1'\rho_1\sigma_1 \qquad (2)$$

and the terms containing S express the effect of renewing the uranium: ρ_5^d/S determines the relative number of ^{235}U nuclei introduced into the system during unit irradiation and ρ_5/S determines the relative number of ^{235}U nuclei extracted from the

* Translated by D. L. ALLAN from *Atomnaya Energiya* **7**, 524 (1959).

system during the same period. In equations (1b) and (1c) the terms containing S have a similar significance. Equations (1a)–(1g) take no account of the effect of the neptunium, which is assumed to be very small, and resonance absorption in ^{240}Pu is treated in a rather simplified way.

Equations (1a)–(1g) form a set of non-linear differential equations which, for the general case, can be solved numerically. In the stationary state (index ∞) $\rho_n' = 0$ and $f = f^\infty = \text{const.}$ for the isotopes ^{235}U—^{241}Pu. Using the notation

$$\gamma_8 = \sigma_8 + \frac{(1-\varphi_8)e^{-B^2\tau}}{\rho_8} f \tag{3a}$$

and

$$\gamma_k = \sigma_k + \frac{I_k}{\xi\sigma_M{}^8}\frac{\varphi_8 e^{-B^2\tau}}{\beta} f \quad (k = 0,2) \tag{3b}$$

one can write down the solution of the set of equations for the stationary state in the following way

$$\rho_5{}^\infty = \frac{\rho_5{}^d}{1+\sigma_5 S} \tag{4a}$$

$$\rho_6{}^\infty = \frac{\sigma^c S}{1+\sigma_6 S}\rho_5{}^8 \tag{4b}$$

$$\rho_8{}^\infty = \frac{\rho_8{}^d}{1+\gamma_8{}^\infty S} \tag{4c}$$

$$\rho_9{}^\infty = \frac{\gamma_8{}^\infty \rho_8{}^\infty}{\sigma_9} \tag{4d}$$

$$\rho_0{}^\infty = \frac{\gamma_8{}^\infty \rho_8{}^\infty}{\gamma_0{}^\infty}\frac{\sigma_9{}^c}{\sigma_9} \tag{4e}$$

$$\rho_1{}^\infty = \frac{\gamma_8{}^\infty \rho_8{}^\infty}{\sigma_1}\frac{\sigma_9{}^c}{\sigma_9}. \tag{4f}$$

It follows from the numerical solution of equations (1a)–(1g) that, as a result of the relatively small value of σ_2, the ^{242}Pu concentration approaches the equilibrium value very slowly and may be considered insignificant at the beginning of the stationary state. Consequently, the behaviour of $\rho_2(s)$ can be found quite satisfactorily by solving the set of equations (1a)–(1g) with the coefficients $\gamma_8{}^\infty$, $\gamma_0{}^\infty$ and $\gamma_2{}^\infty$. From the solution so obtained it follows that the ^{242}Pu concentration for an irradiation $s \simeq 50$ has the equilibrium value

$$\rho_2{}^\infty = \frac{\gamma_8{}^\infty \rho_8{}^\infty}{\gamma_2{}^\infty}\frac{\sigma_9{}^c}{\sigma_9}\frac{\sigma_1{}^c}{\sigma_1} \tag{5a}$$

and in the interval $s = 10 \to 50$,

$$\rho_2(s) \simeq \rho_2{}^\infty\, 0{\cdot}02s. \tag{5b}$$

From equations (4a)–(4f) and from (5a)–(5b) it follows that the equilibrium values of the plutonium isotopic concentrations depend on the amount of ^{239}Pu converted from ^{238}U. This can be expressed by the relation

$$\rho_8{}^\infty\gamma_8{}^\infty = \rho_8{}^\infty\sigma_8 + (1-\varphi_8)e^{-B^2\tau}\nu_5'\rho_5{}^\infty\sigma_5 + \rho_8{}^\infty \times \gamma_8{}^\infty(1-\varphi_8) \times e^{-B^2\tau}\left(\nu_9' + \nu_1'\frac{\sigma_9{}^c}{\sigma_9}\right);$$

from which the ^{239}Pu conversion coefficient in the steady state is seen to be

$$R_9{}^\infty = \frac{\rho_8{}^\infty\gamma_8{}^\infty}{\rho_5{}^\infty\sigma_5} = \frac{\theta^\infty\frac{\sigma_8}{\sigma_5} + (1-\varphi_8)e^{-B^2\tau}\nu_5'}{1-(1-\varphi_8)e^{-B^2\tau}\nu_{\mathrm{Pu}}} \tag{6}$$

where we have used the notation

$$\nu_{\mathrm{Pu}} = \nu_9' + \frac{\sigma_9{}^c}{\sigma_9}\nu_1' \;;\; \theta^\infty = \frac{\rho_8{}^\infty}{\rho_5{}^\infty}. \tag{7}$$

3. NEUTRON RESERVE

To enable us to make use of the solution of the fuel balance equation, we will write the criticality equation in the form

$$\frac{e^{-B^2\tau}\varphi_8\varphi_0\varphi_2 f}{(1+L^2B^2)\left(\sum_i\rho_i\sigma_i + \sum_j\rho_j\sigma_j + \sum_l\rho_l\sigma_l\right)} = 1 + \Delta k \tag{8}$$

where we have split up the thermal neutron absorption into:
(i) absorption by the fissile isotopes (index i), (ii) absorption by isotopes which can be converted into fissile isotopes ($j = 8,0$) and (iii) absorption by poisons (index l), as follows:-

$$\Delta k\left(\sum_n\rho_n\sigma_n + \frac{DB^2}{N_5{}^0}\right) = e^{-B^2\tau}f - \sum_i\rho_i\sigma_i - \rho_8\sigma_8 - (1-\varphi_8)e^{-B^2\tau}f - \rho_0\sigma_0 - (1-\varphi_0)\varphi_8\varphi_2\, e^{-B^2\tau}f - \rho_2\sigma_2 - (1-\varphi_2)\varphi_8\, e^{-B^2\tau}f - \rho_6\sigma_6 - \beta\sigma_M - \frac{DB^2}{N_5{}^0}.$$

We will define the neutron reserve δ as the number of excess thermal neutrons (above the number required to maintain the chain reaction) per neutron absorbed in the fissile isotopes. Using the same approximation as we used for equations (1a)–(1g), i.e. with

$$(1-\varphi_0) \simeq \rho_0\frac{I_0}{\beta\xi\sigma_M{}^8} \;;\; (1-\varphi_2) \simeq \rho_2\frac{I_2}{\beta\xi\sigma_M{}^8}$$

neglecting quantities of the second order of smallness

$(1-\varphi_0)(1-\varphi_2)\simeq 0$, we obtain an expression for the neutron reserve:

$$\delta = \frac{\Delta k\left(\sum_n \rho_n\sigma_n + \frac{DB^2}{N_5^0}\right)}{\sum_i \rho_i\sigma_i}$$

$$= \frac{e^{-B^2\tau}f}{\sum_i \rho_i\sigma_i} - 1 - \frac{\sum_j \rho_j\gamma_j}{\sum_i \rho_i\sigma_i}$$

$$- \frac{\rho_2\gamma_2 + \rho_6\sigma_6 + \beta\sigma_M + \frac{DB^2}{N_5^0}}{\sum_i \rho_i\sigma_i}. \quad (9)$$

The neutron reserve is a measure of the reactivity of the system: the reactor is critical when $\delta = 0$ and the reactivity is positive for values of $\delta > 0$.

The first term on the right of equation (9) (which we shall designate η) determines the number of epithermal neutrons remaining in the system per neutron absorbed in the fissile isotopes. The term

$$R = \frac{\sum_j \rho_i\gamma_i}{\sum_i \rho_i\sigma_i} = \frac{\rho_8\gamma_8 + \rho_0\gamma_0}{\sum_i \rho_i\sigma_i} \quad (10)$$

is the conversion coefficient of the fissile isotopes in the system (i.e. it determines the number of fissile nuclei produced per fissile nucleus destroyed). The final term (which we will designate Z) determines the relative poisonous capture in the non-fissile plutonium and uranium isotopes, the relative loss in the moderator and the thermal neutron leakage.

For the initial state of a homogeneous uranium system (index 0), we obtain

$$\eta^0 = e^{-B^2\tau}\nu_5'; \quad (11a)$$

$$R^0 \equiv \frac{\theta^0\gamma_8^0}{\sigma_5} = \theta^0\frac{\sigma_8}{\sigma_5} + (1-\varphi_8)e^{-B^2\tau}\nu_5';$$

$$Z^0 \equiv \frac{\beta\sigma_M + \frac{DB^2}{N_5^0}}{\sigma_5} = (1 + L_M{}^2B^2)\theta^0\frac{\sigma_8}{\sigma_5}\frac{N_M}{N_8}\frac{\sigma_M}{\sigma_8} \quad (11b)$$

(where it has been assumed that $D = D_M$).

4. NEUTRON RESERVE IN THE STEADY STATE

The solution of the fuel balance equation which we have obtained above enables us to give an expression for the neutron reserve in the steady state. The relative number of epithermal neutrons which remain in the system is

$$\eta^\infty = \nu_5' e^{-B^2\tau} + \frac{a_{Pu}R_9{}^\infty}{1 + a_{Pu}R_9{}^\infty} e^{-B^2\tau}(\nu_{Pu}' - \nu_5') \quad (12)$$

where

$$a_{Pu} = 1 + \frac{\sigma_9{}^c}{\sigma_9}\ ;\ \nu_{Pu}' = \frac{\nu_{Pu}}{a_{Pu}}$$

and $R_9{}^\infty$ is the ^{239}Pu conversion coefficient obtained from equation (6).

The conversion coefficient expressed by (10) is

$$R^\infty = \frac{a_{Pu}R_9{}^\infty}{1 + a_{Pu}R_9{}^\infty}. \quad (13)$$

From expression (12) and (13) it follows that the difference between the number of fast neutrons produced per neutron absorbed in the plutonium fissile isotopes and the number produced per neutron absorbed in ^{235}U affects the neutron reserve with a weight equal to that of the conversion coefficient of the system.

The thermal neutron losses which occur in an equilibrium system are mainly due to capture by the non-fissile uranium and plutonium isotopes, i.e. by ^{236}U and ^{242}Pu. The losses in ^{236}U are

$$Z_6 = \frac{\sigma_6 S}{1 + \sigma_6 S}\frac{\sigma_5{}^c}{\sigma_5}\frac{1}{1 + a_{Pu}R_9{}^\infty} \quad (14)$$

and the losses in ^{242}Pu in the interval $s = 10 - 50$ are dependent upon s:

$$Z_2 = \frac{R_9{}^\infty}{1 + a_{Pu}R_9{}^\infty}\cdot\frac{\sigma_9{}^c}{\sigma_9}\frac{\sigma_1{}^c}{\sigma_1}0{\cdot}02s \quad (15)$$

while with $s = 50$ the losses assume an equilibrium (i.e. a maximum) value. The losses arising from capture in the moderator and those due to leakage are

$$Z^\infty = \frac{\beta\sigma_M + \frac{DB^2}{N_5^0}}{\rho_5{}^\infty\sigma_5(1 + a_{Pu}R_9{}^\infty)}. \quad (16)$$

In the steady state regime losses also occur as a result of neutron capture by the slag. If the relative capture by the slag arising from the fission of ^{235}U, ^{239}Pu and ^{241}Pu is denoted by $\sum_k \rho_k\sigma_k$, then the losses in the slag are

$$Z_{st} = \frac{\sum_k \rho_k\sigma_k}{\rho_5{}^\infty\sigma_5(1 + a_{Pu}R_9{}^\infty)}. \quad (17a)$$

With the removal of the major fission products which make up the overwhelming majority of those present in the slag, the following equation is valid

$$\frac{d\rho_k}{ds} = w_{5k}\rho_5\sigma_5{}^f + w_{9k}\rho_9\sigma_9{}^f + w_{1k}\rho_1\sigma_1{}^f$$

$$- \rho_k\sigma_k\left(1 + \frac{\lambda_k}{\Phi\sigma_k} + \frac{1}{S_k\sigma_k}\right),$$

VOL 15 196

where w_{ik} is the yield of the kth fission product formed by the fission of the ith isotope, λ_k is the decay constant of the kth fission product and S_k (as in the case of uranium renewal) denotes an irradiation during the course of which the whole equilibrium quantity of the kth fission product is removed from the reactor. In the steady state the losses in the separate fission products are

$$Z_{st} = \frac{W_5 + R_9^{\infty} W_9}{1 + a_{\mathrm{Pu}} R_9^{\infty}} \tag{17b}$$

where

$$W_5 = \sum_k \frac{w_{5k} \dfrac{\sigma_5^f}{\sigma_5}}{1 + \dfrac{\lambda_k}{\Phi\sigma_k} + \dfrac{1}{S_k\sigma_k}} \tag{18}$$

and

$$W_9 = \sum_k \frac{w_{9k} \dfrac{\sigma_9^f}{\sigma_9} + w_{1k} \dfrac{\sigma_1^f}{\sigma_1} \dfrac{\sigma_9^c}{\sigma_9}}{1 + \dfrac{\lambda_k}{\Phi\sigma_k} + \dfrac{1}{S_k\sigma_k}}. \tag{19}$$

5. BURN-UP OF URANIUM

In the steady state, the reserve of neutrons in the system is expressed by equations (9), (11a) and (11b). If fresh uranium is added to the reactor in such a way that the number of ^{238}U nuclei per cm^3 remains unchanged ($N_8^{\infty} = N_8^0$), then one can show that the relative change in the volume of the moderator will be

$$\frac{\Delta V_M}{V_M} < 0{\cdot}1 \text{ per cent.}$$

This means that the moderating and diffusion characteristics of the system remain almost unchanged and that it is possible to write

$$(N_M\sigma_M + DB^2)^0 = (N_M\sigma_M + DB^2)^{\infty} \tag{20}$$

$$\varphi_8{}^0 = \varphi_8{}^{\infty} = \varphi_8 ;$$

$$(B^2\tau)^0 = (B^2\tau)^{\infty}. \tag{21}$$

The neutron reserve in such an equilibrium system is given by the expression

$$\delta^{\infty} = \nu_5' e^{-B^2\tau} - 1 - R^{\infty}\left[1 + e^{-B^2\tau}(\nu_5' - \nu_{\mathrm{Pu}}') + \frac{\sigma_9^c}{\sigma_9}\frac{\sigma_1^c}{\sigma_1}\frac{0{\cdot}02s}{a_{\mathrm{Pu}}} + \frac{W_9}{a_{\mathrm{Pu}}}\right] - \frac{1}{1 + a_{\mathrm{Pu}}R_9^{\infty}}\left(\frac{Z^0}{\rho_5^{\infty}} + W_5 + \frac{\sigma_5^c}{\sigma_5}\frac{\sigma_6 S}{1 + \sigma_6 S}\right). \tag{22}$$

If the initial neutron reserve of the system was δ^0, then we can transform expression (22) into the expression

$$\bar{\delta}^{\infty} \equiv \delta^{\infty}(1 + a_{\mathrm{Pu}}R_9^{\infty}) = \eta^0 - 1 - \bar{W}_5 - K \times \frac{\psi_8\eta^0}{1 - \psi_8 e^{-B^2\tau}\nu_{\mathrm{Pu}}} - \frac{1}{\rho_5^{\infty}}\left(\eta^0 - 1 - \delta^0 - \theta^0\frac{\sigma_8}{\sigma_5} - \theta_0\frac{\sigma_8}{\sigma_5} - \psi_8\eta^0 + K\frac{\theta^0\dfrac{\sigma_8}{\sigma_5}}{1 - \psi_8 e^{-B^2\tau}\nu_{\mathrm{Pu}}}\right), \tag{23}$$

where we have used the notation

$$\bar{W}_5 = W_5 + \frac{\sigma_6 S}{1 + \sigma_6 S}\frac{\sigma_5^c}{\sigma_5} \tag{24a}$$

$$K(s) = a_{\mathrm{Pu}}(2 - e^{-B^2\tau}\nu_{\mathrm{Pu}}') + 0{\cdot}02s\frac{\sigma_9^c}{\sigma_9}\frac{\sigma_1^c}{\sigma_1} + W_9 \tag{24b}$$

$$\psi_8 = 1 - \varphi_8 \tag{24c}$$

and have made use of equations (6), (7) and (11b).

If the reactor is initially critical ($\delta^0 = 0$) and if it remains critical ($\bar{\delta}^{\infty} = 0$) throughout a given irradiation s in the stationary state, then equation (23) will be satisfied and will give the attainable burn-up of the added uranium ρ_5^{∞}. In the calculations we will make use of the fact that, because of the small value of $\bar{W}_5$, σ_6 may be considered independent of s.

The duration of the run S (which we shall define as that irradiation during which the uranium in the reactor is completely renewed) is related to the concentration of the added uranium, $\rho_5^d = N_5^d/N_5^0$, and that of the burnt-up uranium (equation 4a), by the expression

$$S = \frac{1}{\sigma_5}\left(\frac{\rho_5^d}{\rho_5^{\infty}} - 1\right). \tag{25}$$

During a run in the equilibrium state, for each tonne of added natural uranium the amount of energy generated is

$$E = \left(1 - \frac{\rho_5^{\infty}}{\rho_5^d}\right)\left[\frac{\sigma_5^f}{\sigma_5} + R_9^{\infty}\left(\frac{\sigma_9^f}{\sigma_9} + \frac{\sigma_1^f}{\sigma_1}\frac{\sigma_9^c}{\sigma_9}\right)\right] 6450 \text{ MW. day. tonne}^{-1}. \tag{26}$$

If we substitute ρ_5^{∞} and R_9^{∞} into equation (26) we obtain the corresponding power yield. It can be seen from this equation that, in general, E increases as ρ_5^{∞} is reduced and as R_9^{∞} is increased, but both these interrelated quantities are restricted by the criticality condition which, according to (22), requires that $\bar{\delta}^{\infty} = 0$.

Table 1 presents some values of the equilibrium concentration of ^{235}U (ρ_5^{∞}) and the corresponding energy generation (E) per tonne of added natural uranium as a function of the total irradiation s measured from the time the reactor commences

TABLE 1.—BURN-UP IN A NATURAL URANIUM HOMOGENEOUS REACTOR

s	$\varphi_8 = 0{\cdot}766$, $R_{crit} = 182$ cm		$\varphi_8 = 0{\cdot}788$, $R_{crit} = 172$ cm		$\varphi_8 = 0{\cdot}813$, $R_{crit} = 166$ cm		$\varphi_8 = 0{\cdot}827$, $R_{crit} = 166$ cm		$\varphi_8 = 0{\cdot}855$, $R_{crit} = 173$ cm		$\varphi_8 = 0{\cdot}869$, $R_{crit} = 181$ cm	
	ρ_5^{∞}	E, MW. day. tonne^{-1}	ρ_5^{∞}	E, MW. day. tonne^{-1}	ρ_5^{∞}	E, MW. day. tonne^{-1}	ρ_5^{∞}	E, MW. day. tonne^{-1}	ρ_5^{∞}	E, MW. day. tonne^{-1}	ρ_5^{∞}	E, MW. day. tonne^{-1}
10	0·453	9671	0·464	8026	0·476	6660	0·468	6320	0·495	5060	0·503	4603
20	0·499	7557	0·501	6546	0·506	5625	0·493	5520	0·517	4457	0·523	4092
30	0·548	5534	0·540	5122	0·537	4624	0·518	4750	0·539	3868	0·543	3594
40	0·602	3571	0·582	3740	0·570	3649	0·545	4003	0·561	3292	0·563	3107
50	0·659	1641	0·627	2385	0·604	2696	0·572	3278	0·585	2728	0·584	2628

operation. The data applies to the critical assemblies considered by ROČEK[2] and to the following values of the parameters:

$$\theta^0 = 97{\cdot}8, \quad \rho_5^{d} = 0{\cdot}712, \quad \theta^0 \frac{\sigma_8}{\sigma_5} = 0{\cdot}4086,$$

$$T = 500^{\circ}\mathrm{K}, \quad \nu_5' = 2{\cdot}08, \quad \nu_{Pu} = 2{\cdot}64, \quad \nu_{Pu} = 1{\cdot}97,$$

$$a_{Pu} = 1{\cdot}34, \quad \frac{\sigma_9^{c}}{\sigma_9}\frac{\sigma_1^{c}}{\sigma_1} = 0{\cdot}106, \quad \frac{\sigma_9^{f}}{\sigma_9} + \frac{\sigma_1^{f}}{\sigma_1}\frac{\sigma_9^{c}}{\sigma_9} = 0{\cdot}994,$$

$$W_{Pu} = 0{\cdot}0210, \quad \bar{W}_5 = 0{\cdot}216, \quad \nu_9' = 1{\cdot}91, \quad \nu_1' = 2{\cdot}14.$$

Figure 1 shows the attainable burn-up per tonne of added natural uranium (E) as a function of s. This figure shows that for reactors having identical dimensions a greater degree of burn-up is achieved in short duration runs if the uranium concentration is large whereas for large s the burn-up is greater if the uranium concentration is low. Thus for a given size of reactor there exists an optimum uranium concentration (optimum φ_8) for each irradiation and consequently it is possible to minimize ρ_5^{∞} and so achieve maximum burn-up.

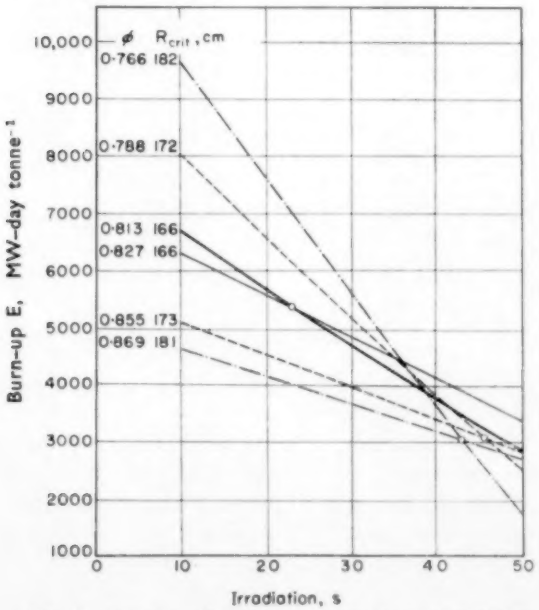

FIG. 1.—Burn-up of natural uranium in a homogeneous reactor.

6. OPTIMUM REGIME IN THE EQUILIBRIUM STATE

For a reactor of given dimensions, the condition

$$\delta^0 \equiv \eta^0(1 - \psi_8) - 1 - \theta^0\frac{\sigma_8}{\sigma_5} \times \left[1 + \frac{N_M\sigma_M}{N_8\sigma_8}(1 + L_M{}^2B^2)\right] = 0$$

determines the mutual relation between θ^0 and ψ_8. The requirement $\bar{\delta}^{\infty} = 0$ (23), means that an equilibrium concentration ρ_5^{∞} with respect to θ^0 and ψ_8 is attained. Equation (23) implies that for $\bar{\delta}^{\infty} = 0$, ρ_5^{∞} falls off monotonically with θ^0. On the other hand, as a function of ψ_8 it can rise as well as fall and takes on a local extreme value when $\frac{\partial\rho_5^{\infty}}{\partial\psi_8} = 0$. From this it follows that

$$(1 - \psi_8 e^{-B^2\tau}\nu_{Pu})^2 = K\left(\rho_5^{\infty} + \frac{\nu_{Pu}}{\nu_5'}\frac{\sigma_8}{\sigma_5}\theta^0\right) \quad (27a)$$

or

$$\psi_8 = \frac{1}{e^{-B^2\tau}\nu_{Pu}}\left[1 \pm \sqrt{K\left(\rho_5^{\infty} + \frac{\nu_{Pu}}{\nu_5'}\frac{\sigma_8}{\sigma_5}\theta^0\right)}\right]. \quad (27b)$$

A more detailed analysis shows that the negative sign in equation (27b) corresponds to a local minimum of ρ_5^{∞}. The negative sign in this equation corresponds to physically real conditions ; the positive sign does not.

ρ_5^{∞} can be eliminated from equations (27) and (23) and one can derive the relation between ψ_8 and θ^0 which gives a maximum value of ρ_5^{∞}:

$$\theta^0\frac{\sigma_8}{\sigma_5} = \frac{1 - K - (\eta^0 - 1 - \bar{W}_5)\frac{\nu_{Pu}}{\nu_5'}}{\eta^0 - 1 - \frac{\eta_0 - 1 - \bar{W}_5}{K}(1 - \psi_8 e^{-B^2\tau}\nu_{Pu})^2 - \psi_8{}^2\eta^0 e^{-B^2\tau}\nu_{Pu}} \quad (28)$$

The following condition must be satisfied if the reactor is to be critical at the commencement of the run

$$\theta^0 \frac{\sigma_8}{\sigma_5} = \frac{\eta^0(1 - \psi_8)}{1 + \frac{N_M}{N_8}\frac{\sigma_M}{\sigma_8}(1 + L_M{}^2B^2)}. \qquad (29)$$

Thus equations (28) and (29) determine the values of the parameters which will ensure that the reactor is initially critical and that the optimum uranium concentration ψ_8 is such that the minimum concentration $\rho_5{}^\infty$ reached during the run s is given by equation (27). By calculating the values of $\psi_{8\,\mathrm{opt}}$ corresponding to various values of s in the range $s = 10$–50, we obtain $\psi_{8\,\mathrm{opt}}$ as a function of s and the corresponding concentration of uranium in heavy water which will guarantee maximum uranium burn-up.

One expects to find that $\varphi_{8\,\mathrm{opt}}$ will be small for small values of s (i.e. the uranium concentration in the moderator will be large) and that as s increases $\varphi_{8\,\mathrm{opt}}$ also will increase (i.e. the uranium concentration is reduced). This means that in the equilibrium state the optimum regime does not correspond to a fixed uranium concentration but to one which is progressively being reduced; i.e. it recalls the dilution regime mentioned by BIAKOV and JOFFE[1]. These authors suggested that this regime might be used to prolong the operating period of a reactor which becomes subcritical in the equilibrium state.

We must emphasize that this analysis of the optimum regime rests upon the assumption that W_5 and W_9 are constants and are independent of the burn-up. That is, we have assumed that the fission products are being continuously removed at a constant rate independent of the duration of the run. It has been assumed also that the absorption in ^{236}U is small. However, even when the removal of fission products is carried out simultaneously with the uranium replenishment ($S_k = S$), the analysis we have given remains qualitatively correct.

REFERENCES

1. BIAKOV V. M. and JOFFE B. L., *Proceedings of the Second International Conference on the Peaceful Uses of Atomic Energy, Geneva*, Vol. 13, p. 462. United Nations, New York (1958).
2. ROČEK J., *Calculations of the Critical Dimensions of Homogeneous Reactors*. Report No. 325 of the Institute of Nuclear Physics, Prague (1958).

VOL. 15 1961

Reactor Science and Technology (Journal of Nuclear Energy Parts A/B) 1961, Vol. 15, pp. 220 to 228. Pergamon Press Ltd. Printed in Northern Ireland

THE EFFECT OF THE TEMPERATURE CHARACTERISTICS OF A REACTOR ON THE CHOICE OF THE OPTIMUM THERMODYNAMIC CYCLE FOR AN ATOMIC POWER STATION*

D. D. KALAFATI

Abstract—Permissible changes in the temperatures within a nuclear power plant are considered in relation to the thermal output of the reactor for two limiting temperatures: the cladding temperature and the central temperature of the fuel elements. In addition, possible changes in the thermal and electrical power output are given as a function of the thermodynamic cycle parameters and the concepts of the limiting thermal power of the reactor and the power efficiency of the steam generator are introduced. Formulae suitable for making the preliminary calculations of the optimum parameters of the thermodynamic cycle are presented and the conditions under which they are applicable are indicated. The analysis deals with the prospects of increasing the parameters and efficiency of atomic power stations by making a suitable choice of the cladding material and type of fuel element.

1. INTRODUCTION

IN AN atomic power station a change in the initial parameters of the thermodynamic cycle and the consequent change of coolant temperature will affect both the cycle efficiency and the thermal output of the reactor. For this reason the optimum parameters for the thermodynamic cycle and coolant can be found only by considering the operating conditions of the cycle and reactor jointly. However, before one can begin to make calculations on the thermal aspects of the system, one must know the optimum initial parameters of the cycle and coolant. These can be found only by rather tedious calculations involving variational methods.

The following formula[1], which was obtained by minimizing the cost of the electricity generated, can be used in preliminary calculations of the optimum mean temperature of the heat supplied to the steam turbine cycle of an atomic power station

$$T_{1\,\text{cycl.}}^{\text{opt. }m} = \sqrt{\frac{T_r^l\, T_{1\,\text{cycl.}}^2}{1-z}}\ ^\circ\text{K} \qquad (1)$$

where T_r^l is either the limiting temperature of the cladding (T_s^l) or of the centre of the reactor fuel elements (T_c^l), $T_{2\,\text{cycl.}}$ is the temperature in the condenser and $z = \eta_t c_f$ (η_t is the thermal cycle efficiency and c_f is the fuel component of the electricity costs).

If the fuel costs are low we can put $c_f = 0$ and formula (1) then gives the condition for maximum electrical power output from the station[2]:

$$T_{1\,\text{cycl.}}^{\text{opt. }m} = \sqrt{T_r^l T_{2\,\text{cycl.}}}\ ^\circ\text{K} \qquad (2)$$

It should be noted that formula (2) gives the optimum mean temperature of the thermodynamic cycle and not that of the coolant, as in the derivation given by Melets.[3,4] The results obtained with the limiting temperature at the centre and in the cladding are identical[1,2] and consequently the temperature T_r^l in formulae (1) and (2) should be taken to be whichever temperature is the limiting temperature in the reactor. Since the optimum temperatures of the thermodynamic cycle will be different for these two cases it is necessary to decide whether it is better to have the limiting temperature set by the cladding or the centre of the fuel elements. Often the limiting temperature is taken to be that of both the cladding and the centre of the fuel elements simultaneously and a problem arises as to how one finds the optimum cycle parameters for such a case.

2. PERMISSIBLE TEMPERATURE CHARACTERISTICS OF A NUCLEAR POWER STATION

We will now consider the temperature changes which may take place in a given nuclear power station as a result of changes in the thermal output of the reactor which are themselves induced by changes to the initial parameters of the thermodynamic cycle of the plant. We will suppose that the number, shape and surface area of the fuel elements have been specified and that we have chosen the velocity and mass flow rate of the coolant. The thermal output from the reactor is then proportional to the difference between the limiting temperature of the cladding (or of the centre) of the fuel elements and the mean temperature of the heat supplied to the cycle[1]:

$$Q_r = k_r n\, k_t F_r \omega (T_r^l - T_{1\,\text{cycl.}}^m) \qquad (3)$$

* Translated by D. L. ALLAN from *Atomnaya Energiya* **8**, 5 (1960).

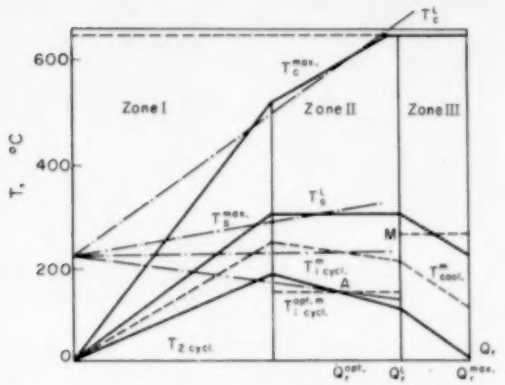

FIG. 1.—Allowable temperature variations in a power station for which $T_{1\,cycl.}^{opt.\,m}$ occurs in zone II.

where k_r is a coefficient characterizing the non-uniform generation of heat along a radius of the reactor, n is the number of fuel elements, k_t is the heat transfer coefficient, F_r is the surface area of the fuel element and ω is a coefficient which determines the possible power utilization of the reactor.

The electrical power generated by the station is

$$N_{el} = Q_r \eta_{st.}^{ch.} - \Delta N_{int.} = k_r n k_t F_r \omega (T_r^l - T_{1\,cycl.}^m) \times \left(1 - \frac{T_{2\,cycl.}}{T_{1\,cycl.}^m}\right) \eta_{oi} \eta_M \eta_{st.\,gen.} \quad (4)$$

where $\eta_{oi}\eta_M\eta_{st.\,gen.}$ is the product of three efficiencies: the internal relative efficiency, the mechanical efficiency and the generator efficiency. $\Delta N_{int.}$ represents the power requirements of the station itself. If the heat transfer resistance of the fuel elements and transfer resistance to the coolant and steam generator can be regarded as fixed and we change the thermal output Q_r, the temperature drops in all these components will change in direct proportion to the thermal output of the reactor. However, the temperatures of these components will not change uniformly but will depend upon the conditions under which the thermal output of the reactor has been changed (Fig. 1).

For low thermal outputs (zone I) an increase in the heat flux raises the temperatures throughout the plant, except that of the condenser, which remains fixed ($T_{2\,cycl.}$ = const.). In zone I an increase in the thermal output from the reactor raises the mean cycle temperature; that is, the electrical power output does not reach a maximum value in zone I. Although it is quite practicable to operate research reactors in this zone, for power reactors it has always been more advantageous to increase the thermal output up to the point where the maximum cladding temperature $T_g^{max.}$ is just below the limiting temperature. Any further increase in reactor power must then be made with

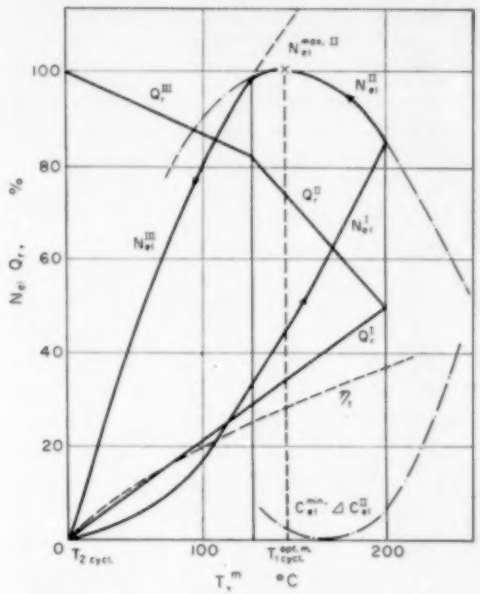

FIG. 2.—Dependence of the thermal and electrical power on $T_{1\,cycl.}^m$ for the case in which $T_{1\,cycl.}^{opt.\,m}$ occurs in zone II.

T_g^l = const., which can only be achieved by reducing the mean cycle and coolant temperatures while at the same time increasing the maximum central temperature $T_c^{max.}$ of the fuel elements. Since this implies an increase in the thermal output and a drop in the cycle efficiency then, according to equation (4), we can obtain maximum electrical power output from the station in zone II which will correspond to the optimum mean cycle temperature obtained from formula (2) with T_g^l substituted for T_r^l. The corresponding optimum in the thermal power of the reactor is given by the point of intersection A (Fig. 1) of the lines representing the optimum and possible cycle temperatures.

KALAFATI[1,2] has given the relationship between the thermal and electrical power outputs of a station and the mean cycle temperature for the case of a single limiting temperature, which can be either that of the cladding or of the centres of the fuel elements. The possible changes in the thermal and electrical power, calculated using equations (3) and (4) for the case where there are two limiting temperatures, are plotted in Fig. 2 as a function of the temperature $T_{1\,cycl.}^m$ of the heat supplied to the cycle upon the assumption that an optimum occurs in the intermediate power zone II. From Figs. 1 and 2, it can be seen that in zone II it is possible for the thermal output to increase with T_g^l = const. so long as the limiting temperature at the centre of the fuel elements is not exceeded. Beyond that point any further change in the thermal and

electrical output must take place with $T_c^l = \text{const.}$; that is, in the high thermal output zone III where we must substitute T_c^l for T_r^l in equation (3).

Limiting cladding temperatures are determined by the material used for the cladding and by the properties of the coolant; they do not normally exceed 300–400°C. If the condenser pressure $p_2 = 0{\cdot}04$ atmospheres ($t_s = 28{\cdot}6$°C) and $T_s^l = 300$°C, then from equation (2) we have:

$$T_{1\,\text{cycl.}}^{\text{opt. }m} = \sqrt{573 \times 302} = 416\text{°K} = 143\text{°C}.$$

For the range of cladding temperatures given above, this corresponds to a saturated steam cycle with an initial pressure of 5 to 10 atmospheres. The adoption of such steam parameters would lead to a low efficiency (20 per cent or less) and consequently it would be uneconomic to operate a power station in zone II. With the thermal output of the reactor unchanged, an increase in the efficiency of the station (the factor $\eta_{\text{st.}}^{\text{ch.}}$ in equation (4)) results in a proportional increase in N_{el} or a reduction in the specific capital outlay. For a given electrical output, the fuel consumption is reduced, i.e. for the same degree of burn-up the duration of the reactor run is directly proportional to the efficiency of the station. Thus, even where the fuel component of the electricity cost is low, it is profitable to raise the efficiency of the station.

Limiting temperatures are appreciably greater at the centre of fuel elements than at the surface of the cladding: they range from $T_c^l = 660$°C for metallic uranium to $T_c^l = 2800$° for uranium dioxide. As a result, when the limiting temperature at the centre of the fuel elements is substituted into equation (2) the optimum mean temperature of the heat supplied to the cycle jumps to a much higher level. For example, with $T_c^l = 1000$°C it is $T_{1\,\text{cycl.}}^{\text{opt. }m} = 1273{\cdot}302 = 623$°K $= 350$°C. Such a mean temperature corresponds to

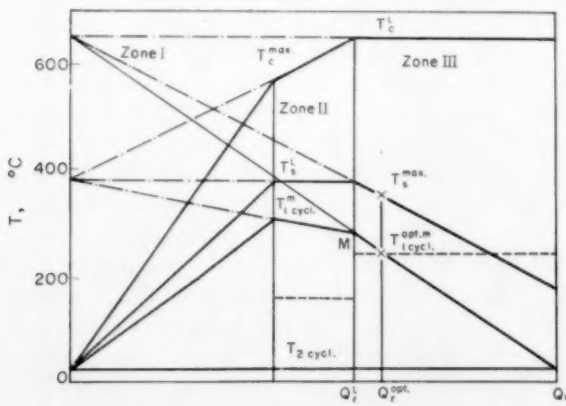

FIG. 3.—Allowable temperature variations in a nuclear power station in which $T_{1\,\text{cycl.}}^{\text{opt. }m}$ occurs in zone III.

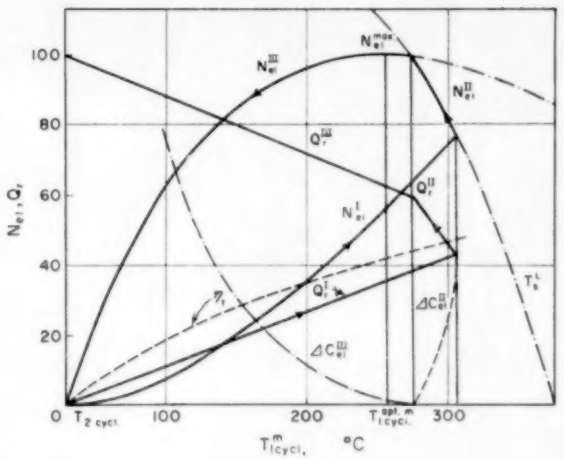

FIG. 4.—Dependence of the thermal and electrical power on $T_{1\,\text{cycl.}}^m$ for the case in which $T_{1\,\text{cycl.}}^{\text{opt. }m}$ occurs in zone III.

very high steam parameters and leads to a power station efficiency of the order of 40 per cent—i.e. double the efficiency of a station operating under zone II conditions. It is therefore desirable to arrange that the permissible temperature characteristics of the nuclear power plant are such that the lines representing the optimum and limiting cycle temperatures intersect in zone III rather than in zone II, for in zone III we can obtain not only a larger output of heat from the reactor but also optimum cycle efficiency.

When the limiting temperatures are reached at the cladding and at the centre of the fuel elements simultaneously, the thermal power, which hereafter we shall call the limiting thermal reactor power Q_r^l, is still not at its maximum possible value, though this has sometimes been implied in the literature, but merely corresponds to a point lying near the beginning of zone III. It is possible to increase the thermal power of the reactor in zone III with $T_c^l = \text{const.}$ by lowering both the mean coolant temperature and the maximum cladding temperature.

The possible changes in the thermal and electrical output of a nuclear power station are given in Fig. 4 as a function of the mean cycle temperature for the case where there is an optimum in zone III. It can be seen from this figure that as the mean cycle temperature increases within this zone the electrical output from the station at first increases, reaches a maximum at $T_{1\,\text{cycl.}}^{\text{opt. }m}$ (determined from equation (2) by substituting T_c^l for T_r^l) and then begins to decline. Once the limiting thermal reactor power has been reached any further increase in the thermal or electrical power can occur only under the conditions of zone II.

Thus operation of an atomic power station in zone III, where we have at the same time a higher thermal

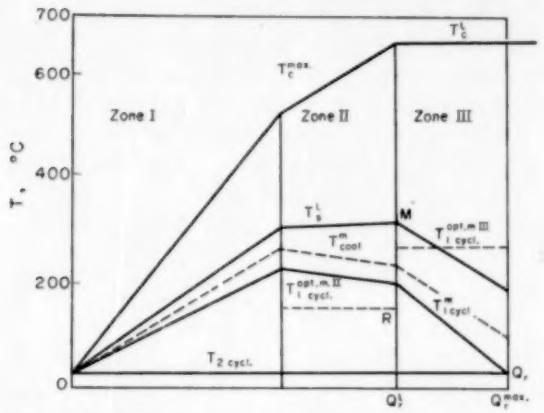

FIG. 5.—Allowable temperature variations in a nuclear power station with the reactor operating at its limiting thermal power (Q_r^l).

output and a greater cycle efficiency, is significantly more economic than zone II operation, where the optimum cycle parameters are set by the limiting cladding temperature. The best possible conditions for atomic power station operation are those of zone III where the optimum cycle parameters are determined by equation (2) with the limiting temperature taken as the central temperature of the fuel elements. In zone III the cladding and cycle temperatures fall off rather rapidly so that the best operating point in this zone is near point *M* (Fig. 5).

If the coefficient of heat generation and heat transfer are independent of the mean temperature the allowable temperature characteristics will be represented in Fig. 3 by segments of straight lines. If, however, these coefficients are slightly temperature dependent these lines will have a slight curvature, but the general character of the diagram and its partition into three zones will be unaffected. It should be stressed that this diagram does not represent a number of alternative reactor operating modes by means of which the reactor power can be varied while it is running (e.g. with a mean coolant temperature $T^m_{\text{cool.}} = \text{const.}$, see broken line in Fig. 1). It is a characteristic diagram showing how the temperatures in the plant vary as the chosen level of reactor heat output is varied.

Limiting thermal reactor power and the electrical power output peak

The line representing the permissible variations in the mean cycle temperature does not always intersect the optimum mean cycle temperature line in zone III. Whether an intersection occurs or not depends on a number of factors: on the relation between the limiting temperatures of the cladding and of the centre of the fuel elements, on the ratios of the heat transfer resistances of the fuel elements, on the mechanisms of heat transfer to the coolant and on the transfer resistance of the steam generator. In particular, these lines cannot intersect when the limiting temperature of the cladding of a reactor operating in zone III is lower than the optimum mean cycle temperature determined by equation (2) with the limiting temperature taken as that of the central temperature of the fuel elements, that is, if

$$\sqrt{T_c^l T_{2\,\text{cycl.}}} > T_s^l. \qquad (5)$$

For example, such a temperature relationship occurs in water–water reactors using uranium oxide fuel. Thus, for the VVER reactor, $T_c^l = 2200°\text{C}$ and with the pressure $p_{\text{cool.}} = 100$ atmospheres the condition that the coolant shall not boil requires that $T_s^l = 309°\text{C}$[5]. Then according to equation (5):

$$\sqrt{2473 \times 302} = 860°\text{K} > 582°\text{K}.$$

That is, because of the low limiting temperature of the fuel element cladding it is not possible to attain the optimum mean cycle temperature in the zone III operation of this type of reactor. For this particular case the mean cycle temperature should be as close as possible to the limiting cladding temperature, since we want to raise the permissible temperature characteristics and the only limitation is that which arises from the necessity of providing for an optimum temperature drop $\Delta t^m_{\text{gen.}}$ in the steam generator. The temperature characteristics for such a station are given in Fig. 5, and in Fig. 6 we give the permissible variations of the

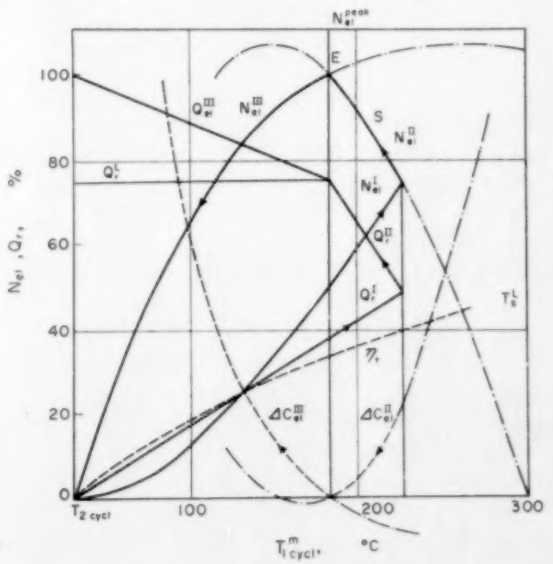

FIG. 6.—Dependence of the thermal and electrical output on $T^m_{1\,\text{cycl.}}$ with the reactor operating at its limiting thermal power (Q_r^l).

thermal and electrical output as a function of the mean cycle or coolant temperature. For this case there is no maximum in the electrical power output either in zone II or in zone III because in both these zones the limiting temperatures are reached at the cladding and at the centre of the fuel elements simultaneously before maximum electrical output is reached. However, with the reactor operating at its limiting thermal output power, the electrical power output reaches a peak at the boundary between zones II and III, where the electrical power curves of these two zones intersect. (Fig. 6).

The optimum mean cycle temperature corresponding to the peak electrical power output is always somewhere in-between the two values given by equation (2), corresponding to the substitution of first the limiting cladding temperature and then the limiting temperature at the centre of the fuel elements. It is not possible to find the value of the mean cycle temperature corresponding to the electrical power output peak using equation (2) and an attempt[6] which has been made to find $N_{\text{el.}}^{\text{max.}}$ by inserting the limiting cladding temperature into this equation and applying a correction factor was inevitably unsuccessful. However, with the reactor operating at its limiting power, the condition that the limiting temperatures of the cladding and the centre of the fuel elements shall be reached simultaneously leads to a uniquely determined value for the mean coolant temperature and provides a solution to the problem. In this case the optimum mean cycle temperature is

$$T_{1\text{ cycl.}}^{\text{opt. }m} = T_{\text{cool.}}^{m.\text{ lim}} - \Delta t_{\text{st. gen.}}^{\text{opt. }m} \qquad (6)$$

If the power curve has a finite slope over the portion corresponding to maximum electrical power output such that the mean cycle temperature and coolant temperature can deviate slightly from the optimum values without substantially reducing the electrical power, the derivative $dN_{\text{el.}}/dT_{1\text{ cycl.}}^{m}$ passes through a discontinuity at the point where the maximum electrical power output is attained. A sharp peak (E) occurs on the electrical output curve (see Fig. 6) and, as a result, even a small deviation of the mean coolant temperature from the optimum value may lead to a considerable reduction in the electrical output of the plant. For example, for the Shippingport power station, SIMPSON *et al.*[7] give the maximum temperature at the centre of the fuel elements as 1200°C so that at present it does not reach the limiting temperature of the uranium dioxide fuel elements; in other words the steam pressure $p_1 = 39{\cdot}2$ atmospheres is too high for this plant and corresponds to point S in Fig. 6. Thus this power station is not giving its maximum possible electrical power output.

We see therefore that provided the limiting temperature is reached at the centre of the fuel elements it is profitable to raise the mean cycle temperature. If, on the other hand, we have a power station for which $T_c^{\text{max.}} < T_c^{l}$ then it is desirable to reduce the mean cycle temperature until the central temperature becomes limiting.

Steam generator efficiency

The maximum electrical power output from the station fixes the limiting thermal output power from the reactor. If the mass flow of the coolant is constant then the mean temperature and heat uptake of the coolant are also specified. Under these conditions the plant parameters and cycle efficiency can only be altered by changing the temperature drop in the steam generator. This can be done by changing either the area of the heating surface or the heat transfer coefficient $K_{\text{st. gen.}}$

If, with a variable thermal output from the reactor, a change of the temperature drop in the steam generator affects the coefficients of thermal utilization of the reactor[1,2] then when the reactor operates at its limiting thermal power a change of the mean temperature drop in the steam generator brought about by changing its heating surface will affect only the change in the thermal efficiency of the cycle.

There are instances in the literature where the concept of a steam generator efficiency has been introduced into the boiler design calculations. This takes heat losses into account but it is more usual to neglect these.

With the thermal power of the reactor $Q_r^{l} = \text{const.}$ specified we should regard the power efficiency rather than the thermal efficiency as the indicator of steam generator efficiency because of the non-reversible nature of the heat exchange process in the generator. The power efficiency is equal to the ratio of the maximum heat efficiency before and after heat exchange in the steam generator:

$$\eta_{\text{st. gen}}^{\text{power}} = \frac{AL_t^{\text{cycl.}}}{AL_t^{\text{rev.}}} = \frac{\eta_t^{\text{cycl.}}}{\eta_t^{\text{rev.}}} = \frac{(T_{1\text{ cycl.}}^{m} - T_{2\text{ cycl.}})\,T_{\text{cool.}}^{m}}{(T_{\text{cool.}}^{m} - T_{2\text{ cycl.}})\,T_{1\text{ cycl.}}^{m}}$$

where $AL_t^{\text{cycl.}}$ is the work done in the ideal steam cycle (Fig. 7); $AL_t^{\text{rev.}}$ is the maximum possible heat efficiency of the coolant equivalent to the work done in the reverse cycle *abcda* with a variable temperature of heat intake to the coolant. The work ratio given in equation (7) is equal to the ratio of the thermal efficiencies of the steam and reverse cycles expressed

in terms of the temperatures, since the heat supplied is exactly the same.

To give some idea of the thermodynamic efficiency of the steam generators in atomic power stations we will give two examples: for the VVER power station the steam generator efficiency calculated from equation (7) is $\eta_{\text{st. gen.}}^{\text{power}} = 0{\cdot}92$ and for the power plant in the atomic ice-breaker *Lenin*, $\eta_{\text{st. gen.}}^{\text{power}} = 0{\cdot}835$. That is, the power efficiencies of the steam generators are close to the thermal efficiencies of the boiler units. The optimum temperature drop in the steam generator can be determined uniquely by comparing the heating area in the steam generator and the energy losses which occur during the heat exchange process. However this would require a separate exposition.

The effect of the fuel component of electricity costs on the optimum cycle parameters

Up to now we have for the sake of simplicity been considering installations in which the fuel component of the electricity costs is so small that it can be neglected, i.e. the optimum parameters of the plant are determined from the condition for maximum electrical power output.

When the fuel component of the electricity costs reaches values of 0·1–0·2 and above, the optimum mean cycle temperature should be determined from the condition for minimum electricity costs. Changes in the electricity costs can be expressed as a function of the electrical power output and efficiency of the station[1].

$$C_{\text{el.}} = C_{\text{cap.}} + C_f = \frac{K}{N_{\text{el.}}} + \frac{B}{\eta_{\text{station}}} \text{ Kopecks kW}^{-1}.\text{hr}^{-1}$$

where K accounts for the capital outlay*, amortization, wages and other running expenses which are proportional to time and are reckoned on the basis of 1 hour's operation of the power station: B is the cost of the nuclear fuel consumed per KWh of heat delivered.

The optimum mean cycle temperature allowing for the cost of the nuclear fuel with $K = \text{const.}$ is determined by equation (1) and all the conclusions we have reached concerning the effect of the permissible temperature characteristics of the plant on the optimum mean cycle temperature remain valid.

For each of the zones II and III (corresponding to limiting temperatures at the surface and centre of the fuel elements, respectively) the optimum mean cycle temperature and cycle efficiency corresponding to minimum electricity costs[1] will be rather greater than

* The pay-off period for the power station is taken as 8 years.

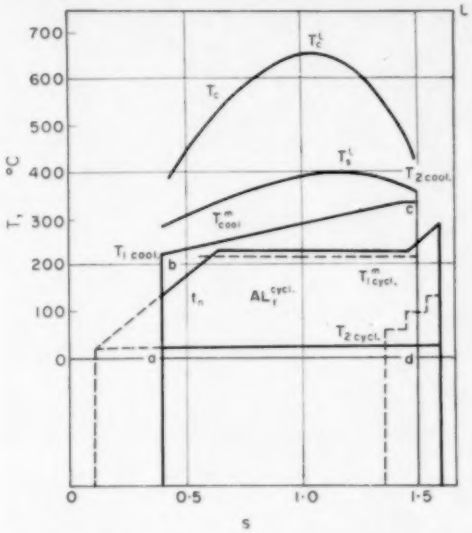

FIG. 7.—Loss of heat efficiency during irreversible exchange in the steam generator.

where these quantities correspond to maximum electricity output[2]. However when the reactor is operating at its limiting power the discontinuity in the power derivative $dN_{\text{el.}}/dT_{1\,\text{cycl.}}^m$ at point E (see Fig. 6) will be accompanied by a discontinuity in the cost derivative $dC_{\text{el.}}/dT_{1\,\text{cycl.}}^m$. Thus, instead of a minimum cost at limiting thermal power we obtain a least value for the electricity costs (apart from the boundary regions near the points M and R in Fig. 5). Thus, with the reactor operating at its limiting thermal power, the condition corresponding to peak electricity output usually coincides with the condition for the least electricity cost.

For uranium, with $T_e^l = 650°\text{C}$, $c_f = 0{\cdot}40$ and $\eta_l = 0{\cdot}45$, we have $z = 0{\cdot}18$. Under these conditions, the optimum mean temperature of the heat supplied to the cycle is, from equation (1):

$$T_{1\,\text{cycl.}}^{\text{opt. m}} = \sqrt{\frac{923 \times 302}{1 - 0{\cdot}18}} = 585°\text{K} = 312°\text{C}.$$

In this cycle we have taken $p_1 = 90$ atmospheres, $t_1 = 500°\text{C}$ and a superheated water temperature t_p 215°C, so that the mean temperature of heat intake is

$$T_{1\,\text{cycl.}}^m = \frac{i_1 - i_p}{s_1 - s_p} = \frac{810{\cdot}1 - 220{\cdot}4}{1{\cdot}5934 - 0{\cdot}5866} = 585°\text{K} = 312°\text{C}.$$

From this example it follows that the optimum initial cycle parameters for an atomic power station using metallic uranium at a temperature $T_e^l = 650°\text{C}$ calculated from the condition for minimizing the electricity costs are roughly 90 atmospheres and

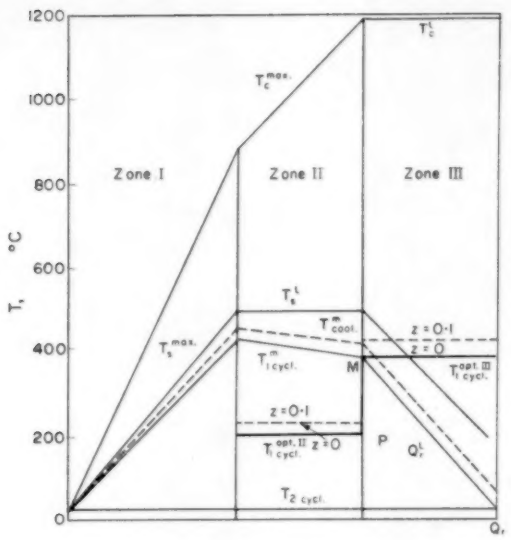

FIG. 8.—The line of optimum heat intake temperature ($T_{1\,cycl.}^{opt.\,m}$) for an atomic power station.

500°C. For this type of fuel any further increase in the initial steam parameters is undesirable. Exactly this conclusion was reported by STARR[8] in connexion with an attempt to improve the steam cycle of an atomic power station incorporating a sodium graphite uranium reactor (SGR). The effect of increasing the initial steam parameters from 56 atmospheres (440°C) to 885 atmospheres (510°C) was studied and it was found that these changes did not increase the electricity output, they only reduced the cost of the electricity. There is no point in increasing the cycle parameters any further unless at the same time the central temperature of the fuel elements is also increased. This could be done by using other nuclear fuels or alloys able to withstand higher limiting central temperatures.

The line of optimum heat intake temperature for atomic power station cycles

All the lines representing optimum mean cycle temperatures in the different zones can be combined so that the optimum mean cycle temperature is represented by the single thick line in the TQ_r diagram given in Fig. 8.

The point of intersection of the permissible cycle temperature line (which can be plotted during the initial planning stage of the station) with the optimum mean cycle temperature line will give the optimum conditions for the operation of the power station. In the case of a reactor operating at its limiting thermal power, the point of intersection of the permissible mean coolant temperature line with that part of the line representing optimum conditions which is parallel to the ordinate gives the optimum mean coolant temperature.

When the fuel component of the electricity costs is taken into account the optimum cycle temperature line in zones II and III will be raised by the factor $z = c_f \eta_t$ in equation (1) to give the broken line in Fig. 8. It should be noted that the points on the optimum cycle temperature line are not all on a par with each other. The best conditions, ensuring the highest heat output and plant efficiency simultaneously, correspond to the region of zone III near point *M*.

Up to now we have been considering the optimum mean cycle and coolant temperatures for a nuclear power plant in which the number, shape and surface area of the fuel elements could be regarded as specified. In addition we have been assuming that the velocity and mass flow rate of the coolant and the heating surface of the steam generator were fixed.

If the permissible temperature variations in the nuclear power plant are such that no optimum mean cycle temperature can be obtained in zone III (defined by equation (2) with a central limiting temperature) then one should raise the permissible coolant and cycle temperature lines so as to be able to select the highest permissible optimum parameters. This can be done by changing the relationship between the heat transfer resistances of the fuel elements, the heat transfer of the coolant and the boiler transfer resistance. The temperature characteristics of both the coolant and the cycle can be raised by changing their diameter and heat conductivity. The surface area of the steam generator and the heat transfer coefficients, which depend on the flow rate and other parameters of the coolant and working substance, can also be changed. It is generally possible to move away from zone II operation altogether and operate in zone III or its left-hand boundary only.

Although raising the allowable temperature characteristics of the plant provides a method of realizing the optimum thermodynamic operating conditions for a nuclear power station, one should first make the necessary reactor calculations to make sure that these changes are desirable.

We can check the validity of the conclusions and of the formulae we have given by looking at Fig. 9. This figure presents curves representing the optimum mean temperatures of the heat intake to the cycle as functions of the central or surface temperatures of the fuel elements for different values of C_f (the fuel component of the electricity costs). The mean temperatures of the thermodynamic cycles of existing or projected atomic power stations, or of stations under

TABLE 1.—MEAN HEAT INTAKE TEMPERATURE FOR THE CYCLES OF VARIOUS POWER PLANTS

Conditions of comparison	No. of point in Fig. 9	Description of plant	T_r^1°C	$T_{1\,cycl.}^{m}$, °C
Limiting temperatures at surface of the fuel elements	1	Uranium–graphite reactor (approximate calculation in Reference [9])	230	118
	2	Uranium–graphite reactor (approximate calculation Reference [4])	300	137
	3	Marcoule dual-purpose reactor (France)	400	157
	4	Calder Hall reactor (U.K.)	408	165
Limiting temperatures at centre of the fuel elements	5	First Atomic Power Station (USSR)	370	185*
	6	Hunterston station (U.K.)	569	227
	7	Heavy-water reactor with organic coolant (Switzerland)	600	224
	8	Uranium–graphite reactor with superheated steam (USSR)	550	312
	9	Sodium–graphite reactor, Santa Susana (USA)	642	245
	10	SGR reactor (USA), version 1[8]	650	269
	10′	SGR reactor (USA), version 3[9]	650	297
	11	Enrico Fermi reactor (USA) version 1	713	262
	11′	Enrico Fermi reactor (USA) version 2	713	287
Limiting thermal reactor power	12	Shippingport station (USA)[7]†	1200	241
	13	Kahle boiling-water reactor (Federal German Republic)	1760	247
	14	VVER reactor (USSR)[5]	2200	235
	15	Dresden reactor (USA)	2520	258
	16	Yankee Atomic Electric Plant (USA)	2600	243
	17	SGR reactor (USA)	2760	297

* $T_{1\,cycl.}^{m}$, is given incorrectly in Reference [8] in the case of points 5, 8, 10, 12 and 14: this temperature is 40–60°C lower when no allowance is made for regeneration.

† In Fig. 3 of Reference [1] point 6 for the Shillingport station is incorrectly plotted.

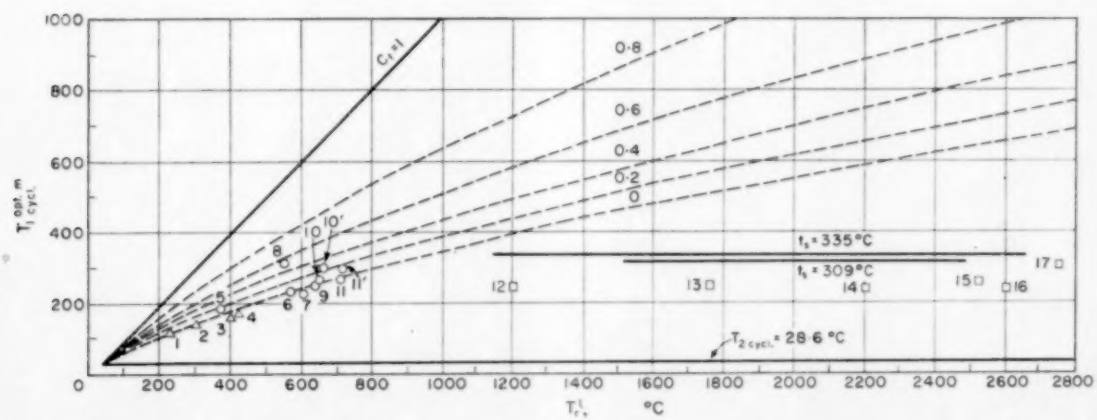

FIG. 9.—Comparison of actual values of $T_{1\,cycl.}^{m}$ for both projected and completed power stations with the theoretical $T_{1\,cycl.}^{opt.\ m}$ curves for different fuel cost components.

construction, are represented in Fig. 9 by the points 1–17.

The results of the rough calculations for the dual-purpose stations, represented in Fig. 9 by points 1–4, agree very well with the theoretical curves calculated for the case where the limiting temperature is that of the cladding. Points 5–11, representing power stations operating with uranium fuel, agree well with the curves for which the optimum cycle temperature is calculated on the basis of the limiting temperature

at the centre of the fuel elements and for which the fuel component of the electricity cost lies between 0 and 30 per cent.

With uranium dioxide nuclear fuel the limiting temperature at the centre of the fuel elements can be taken to be 2200–2760°C. The optimum mean cycle temperature for atomic power stations (points 12–17 in Fig. 9) are then greater than the limiting cladding temperature and such stations operate at the limiting thermal output of the reactor.

With a limiting central temperature of the order of 1000–1200°C the optimum parameters will be so high that they cannot be reached even when the steam parameters are extremely high. In such a case one should choose parameters which are realizable for the turbine cycle and it will be necessary to determine optimum parameters only when it is intended to use gas turbine plant.

In this paper we have been considering temperature limits imposed by the fuel elements only. However, there are other limiting factors: for example, critical heat loading, the limiting temperature of the moderator, radiation instability etc. All these factors set limits to the temperature characteristics of the TQ_r diagram and each of these require individual treatment.

From the data presented above and from the results of the approximate calculations carried out by the author[1,2] we can conclude that formulae (1) and (2) are good enough for making preliminary choice of the optimum parameters for the thermodynamic cycle of the steam turbine plant in an atomic electricity generating station. Using these formulae one can find which are the principle factors affecting the optimum cycle parameters and discover the lines along which future work on the thermodynamic cycles of atomic power stations should proceed.

REFERENCES

1. KALAFATI D. D., *Physics and Heat Technology of Reactors*, Moscow, Atomizdat, p. 164 (1958).
2. KALAFATI D. D., *Trans. Moscow Inst. Power* **30**, 186 (1958).
3. YVON J., *Proceedings of the First International Conference on the Peaceful Uses of Atomic Energy, Geneva*, Vol. 2, p. 337. United Nations, New York (1956).
4. PETROV P. A., *Nuclear Power Stations*, Moscow, Gosenergoizdat 1958.
5. SKVORTSOV S. A., *Atomnaya Energiya* **5**, 245 (1958).
6. ARSEN'EV IU. D. and AVERIN K. E., *Teploenergetika* No. 5, 29 (1959).
7. SIMPSON J. *et al.*, *Proceedings of the First International Conference on the Peaceful Uses of Atomic Energy, Geneva*, Vol. 3, p. 211. United Nations, New York (1956).
8. STARR C., *Proceedings of the First International Conference on the Peaceful Uses of Atomic Energy, Geneva*, Vol. 3, p. 98. United Nations, New York (1956).
9. ALIKHANOV A. I., VLADIMIRSKII V. V., PETROV P. A. and KHRISTENKO P. I., *J. Nucl. Energy* **3**, 77 (1956).

Reactor Science and Technology (Journal of Nuclear Energy Parts A/B) 1961, Vol. 15, pp. 229 to 233. Pergamon Press Ltd. Printed in Northern Ireland

LETTERS TO THE EDITORS

New isotopes of erbium and holmium*

THE CONVERSION electron spectrum of the erbium isotopes formed in the bombardment of tantalum by 660 MeV protons from the synchrocyclotron at the Joint Institute of Nuclear Studies has been studied.

A type BPP-1 $\sqrt{2}\pi$-spectrometer was used in this work. The source had dimensions 1×30 mm and the solid angle of acceptance was 4 per cent of 4π. From measurements on the ^{137}Ba K661·6 line the resolution of the instrument was 0·2–0·25 per cent. A special magnetometer was used to measure the magnetic field which ensured reliable working and permitted us to study conversion lines having half-lives of 15 min or greater. The accuracy of the conversion line energy determinations was 0·1–0·3 per cent.

Amongst the large number of conversion lines (more than 100) belonging to the neutron-deficient isotopes of erbium and holmium,[1] a group of lines was observed with a half-life $T_{1/2} = 2{\cdot}4$ hr. From a study of these lines transitions to an isotope of holmium ($Z = 67$) and also to an isotope of dysprosium ($Z = 66$) were identified (see Table 1).

The holmium daughter product was separated from the erbium fraction within 2 hr of separating the erbium from the tantalum and it was found that the intensity of the lines corresponding to transitions in dysprosium fell to half-value in (28 ± 2) min.

These facts are consistent with the following decay chain

$$\mathrm{Er} \xrightarrow{2{\cdot}4\ \mathrm{hr}} \mathrm{Ho} \xrightarrow{27\ \mathrm{min}} \mathrm{Dy}$$

while the relationship between the energies (98·6 and 218·2 keV) and intensities of the transitions implies that these transitions take place between levels with energies $E_1 = 98{\cdot}6$ keV (2^+) and $E_2 = 316{\cdot}8$ keV (4^+), which correspond to the first rotational band of an even-even dysprosium nucleus. From the position of the first excited level in relation to the number of neutrons[2] it can be assumed that the mass number of the nuclei in this chain is $A = 158$.

The values of the constants A and B in the expression $E = AI(I-1) - BI^2(I+1)^2$ giving the energies of these levels were determined from the position of the first two levels; they are respectively 16·7 ± 0·35 and 0·042 ± 0·008.

TABLE 1.—GAMMA TRANSITIONS IN ERBIUM AND DYSPROSIUM

$h\nu$, keV	$T_{1/2}$ hr	Charge of nucleus in which transition occurs	Multipolarity
98·6	2·4 ± 0·1	66	$E2$
218·2	2·5 ± 0·1	66	—
320·5	2·4 ± 0·1	66	$E2$ or $M3$
357·1	2·4 ± 0·1	66	—
387·3	2·4 ± 0·1	67	—
945·9	2·5 ± 0·1	—	—
848·5	2·5 ± 0·1	—	—

Acknowledgments—The author takes pleasure in thanking B. S. DZHELEPOV and K. IA. GROMOV for advice and discussion and I. A. YUTLANDOV and Y. V. NARSEEV for undertaking the chemical separation of the samples.

I. S. DNEPROVSKII

REFERENCES

1. BEKKERMAN I. M., GUMENIUK B. A. and DNEPROVSKII I. S., *The Beta-Spectrometer Type BPP*. All Union Institute of Scientific and Technological Information, Moscow (1959).
2. DNEPROVSKII I. S. and KOLESOV G. M., *Izv. Akad. Nauk. SSSR* (*Ser. fiz.*) **22**, 935 (1958).
3. DZHELEPOV B. S. and PEKER L. F., *Deformed Nuclei in the Region Nd-Os*. Dubna (1958).

Effect of boron-containing layers on the yield of secondary gamma rays†

(*Received* 3 *August* 1959)

THE WEIGHT and dimensions of the biological shield of a reactor are usually determined by the hard γ-radiation arising from neutron capture in the reactor shell and in the first few layers of the shield. It is therefore extremely important to find ways of reducing this γ-ray flux.

The most intense secondary γ-radiation arises from the radiative capture of the thermal and comparatively low energy neutrons which have been slowed down in the light materials of the shield. If these neutrons are absorbed in a layer containing boron, fewer of them are captured in the constructional materials, particularly steel, which would otherwise have the effect of hardening the γ-radiation.[1,2] Neutron capture in the boron gives rise to soft, weakly-penetrating γ-quanta with an energy ~0·5 MeV and the provision of shielding against these is very much easier.

We have studied the effect of boron carbide, inserted between steel and Plexiglas (which was used to simulate water) on the intensity of production of γ-rays in steel. The geometry of the experiment is illustrated in Fig. 1. Two kinds of steel were investigated: ST-3 and IX18N9T, which is a stainless steel. The steel and Plexiglas were fitted together to form a prism having cross-sectional dimensions 710 × 710 mm.

A (Po–α)Be neutron source with an intensity of 2×10^7 neutrons sec^{-1} was placed inside a water shield in front of the steel prism. There were channels in the steel prism and Plexiglas into which plugs containing detectors could be inserted and between the steel and Plexiglas were filters containing boron, which absorbed the thermal and epi-thermal neutrons passing from the water (Plexiglas) into the steel. Three types of filter were used and these are designated II, III and IV in Fig. 1.

* Translated by D. L. ALLAN from *Atomnaya Energiya* **8**, 46 (1960).

† Translated by D. L. ALLAN from *Atomnaya Energiya* **8**, 49 (1960).

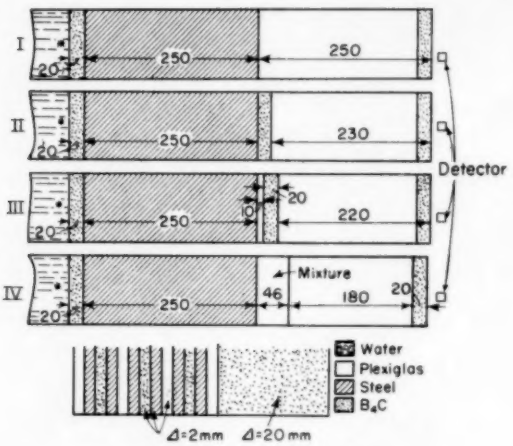

FIG. 1.—Geometry of the experiment.

The spatial distributions of thermal and resonance neutrons were measured and also the spectra of γ-rays produced in the steel and Plexiglas as a result of neutron capture in these materials. The neutron distributions were determined using circular indium foils with a diameter of 20 mm, either enclosed in a cadmium filter or exposed bare. The γ-ray measurements

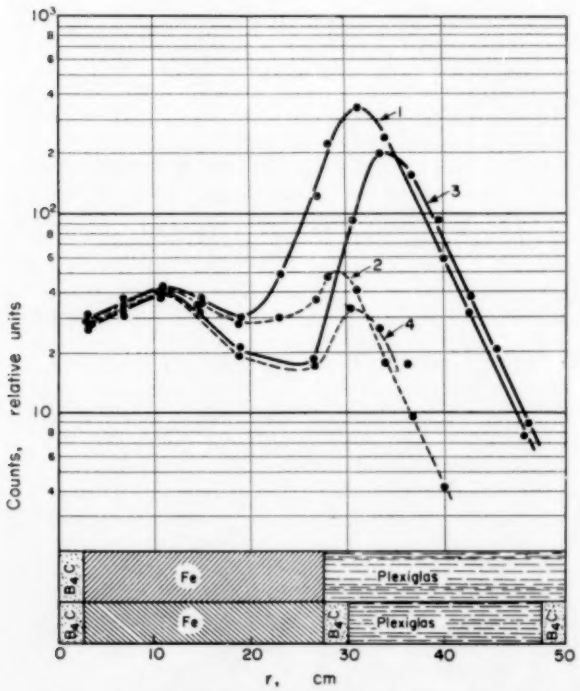

FIG. 2.—Spatial distribution of neutrons in the ST-3 steel and Plexiglas prism:
(1) measurements with indium detectors (no B_4C layer);
(2) measurements with indium under cadmium (no B_4C layer);
(3) measurements with indium (with a layer of B_4C, thickness 20 mm and density 1·1 g cm^{-3}, placed between the steel and Plexiglas);
(4) measurements with indium under cadmium (with a layer of B_4C, thickness 20 mm and density 1·1 g cm^{-3}, placed between the steel and Plexiglas).

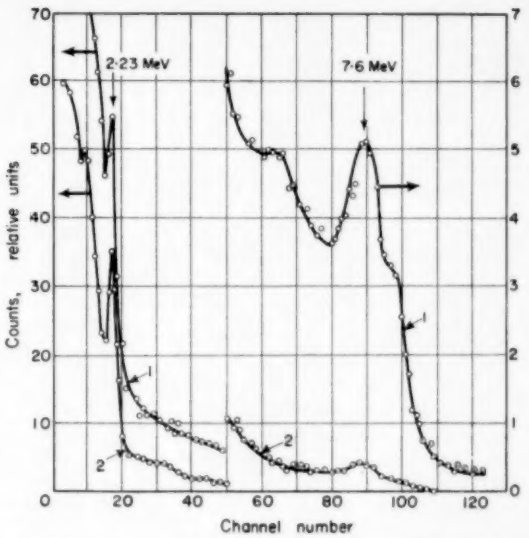

FIG. 3.—Spectrum of γ-rays produced in the ST-3 steel prism.
(1) no B_4C layer;
(2) with a layer of B_4C, thickness 20 mm and density 1·1 g cm^{-3}, placed between the steel and Plexiglas.

were made with a single crystal scintillation spectrometer incorporating a NaI(Tl) crystal with diameter and height both 40 mm. The resolution for the ^{65}Zn line was 11 per cent. The pulses were analysed by a 128-channel kicksorter with a ferrite core memory circuit. The location of the scintillation crystal during the measurements is shown in Fig. 1.

Figure 2 shows the spatial distribution of the neutrons measured in the ST-3 steel and Plexiglas prism with and without an intervening boron carbide layer. Figures 3 and 4 give the

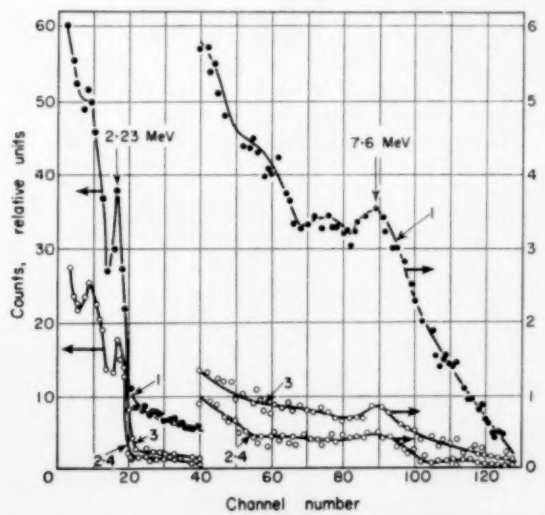

FIG. 4.—Spectrum of γ-rays produced in the IX18N9T stainless steel prism.
(1) no B_4C layer;
(2), (4) with a B_4C layer between the steel and Plexiglas (Fig. 1, arrangement II) or with a layer containing a mixture of Plexiglas, ST-3 and B_4C (Fig. 1, arrangement IV);
(3) with a layer of Plexiglas and a layer of B_4C between the steel and Plexiglas (Fig. 1, arrangement III).

VOL 15 196

results of our γ-ray measurements, which were also taken with and without the boron carbide layer.

The capture γ-radiation spectrum illustrated in Fig. 3 contains γ-ray lines at 2·2 and 7·6 MeV, corresponding to neutron absorption in boron and iron.

The insertion of boron carbide between the steel and Plexiglas reduces the intensity of the 7·6 MeV γ-radiation by a factor of 13·4. The spectrum of γ-rays from the IX18N9T steel contains, as well as the lines already mentioned, some extra lines arising from neutron capture in chromium and nickel, which enter into the composition of this type of steel. Absorption of the thermal and epi-thermal neutrons in a 20 mm boron carbide layer reduces the flux of 7·6 MeV γ-rays from the IX18N9T steel by a factor of 7·8.

We have calculated the reduction in the capture γ-radiation from ST-3 steel when a boron carbide layer is interposed between the steel and Plexiglas. For the purpose of this calculation the measured neutron distribution given in Fig. 2 was used. For the spectrum of the neutrons undergoing moderation in the steel we used the age approximation for neutrons in a semi-infinite steel block bounded by a completely 'black' medium. Corrections were applied for the self-screening of the detectors due to the 1·44 eV resonance. The calculated value of the reduction in intensity of the secondary γ-ray yield from steel was 9·5 and this agrees quite well with the results of the direct measurement of the spectrum.

Acknowledgments—The authors are deeply grateful to N. A. Aleshin, V. S. Borisov, G. V. Rikov and E. V. Shestonalov for their assistance in this work.

D. L. Broder
A. P. Kondrashov
A. A. Kutuzov
A. I. Lashuk

VOL. 15 1961

REFERENCES

1. *Reactor Physics Constants*. ANL-5800 (1958).
2. Rockwell T., *Reactor Shielding Design Manual*, McGraw-Hill, New York (1956).

An investigation of the e.m.f. developed when a system of semiconductors containing uranium is irradiated in a reactor*

(*Received* 3 *August* 1959)

It is well known that an e.m.f. is developed in a system of electron and hole semiconductors when subjected to ionizing radiation in the presence of a contact field. Most of the information about this phenomenon which has appeared in the literature relates to irradiation by light, X-rays, γ-rays, β-particles and α-particles.[1] We have studied a system of such hole and electron semiconductors while they were undergoing irradiation by uranium fission products. Certain compounds of uranium (e.g. U_3O_8) are known[2] to be semiconductors. If a semiconducting system containing uranium is irradiated in a flux of thermal neutrons fission fragments will arise from the fissions induced in the uranium. In addition to the ionization they produce, fission fragments also cause considerable radiation damage, thereby substantially changing the electrical properties of the irradiated materials.[3,4] For this reason, systems of semiconductors containing uranium should consist of materials whose electrical properties undergo only slight change during irradiation: for example, semiconducting materials containing many lattice defects, such as polycrystalline semiconductors, or monocrystals containing large amounts of impurities.

In our investigations we used polycrystalline oxide semiconductors. In all the experiments the *p*-type semiconductor consisted of the lower oxide of uranium, U_3O_8, which has a large work-function. For *n*-type semi-conductors with low work-functions we used the oxides: BaO, TiO_2, MgO and Al_2O_3.[5] We used gold or copper for the electrodes which made contact with the *p*-type semiconductors and magnesium or titanium for the *n*-type. The samples of U_3O_8–BaO and U_3O_8–TiO_2 were prepared by successive vacuum deposition on to a support to form layers of semiconductor and electrode as described by Gus'kov *et al.*[6] The Al_2O_3 layer in the U_3O_8–Al_2O_3 sample was deposited by the Schoope process on to a titanium support. The U_3O_8 was then evaporated on to the Al_2O_3 layer and finally the gold or copper electrode was evaporated on to the U_3O_8. In the case of the U_3O_8-MgO sample neither evaporation nor Schoope's process would give an MgO layer and we were obliged to use a 0·5 mm thick ceramic plate of MgO upon one side of which we deposited a magnesium electrode and upon the other side a U_3O_8 layer and a gold or copper electrode. The effective areas of these samples were 6 and 2·8 cm^2; the thickness of the U_3O_8, BaO and TiO_2 layers was 5–20 μ and that of the Al_2O_3 was 100–200 μ.

The samples were mounted on holders and fixed in position by bronze clamping electrodes. The surface temperatures of the samples were monitored by copper-constantan thermocouples soldered to one of the electrodes. The holders with the samples were inserted in cylindrical aluminium containers and irradiated in the experimental cooling channel of an atomic power station reactor in a region where the flux density of neutrons and γ-rays varied between 10^{10} and 10^{13} cm^{-2} sec^{-1}, according to the reactor power. The temperature of the samples during the irradiations was ~120°C.

The following characteristics were observed for each sample during the irradiation: the open-circuit voltage V_∞, the short circuit current $I_{s.c.}$, the load characteristic, the surface temperature of the sample and the electrical resistance R of the sample with an applied voltage of 1·4 V in both the forward and reverse directions. The volt-amp characteristics of the samples were recorded before and after irradiation in the reactor.

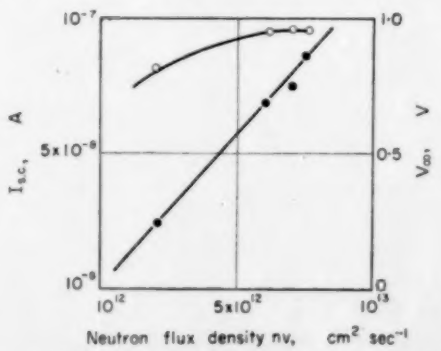

Fig. 1.—Dependence of the voltage V_∞ (○) and current $I_{s.c.}$ (●) of the U_3O_8–MgO sample on the neutron flux density nv.

---

* Translated by D. L. Allan from *Atomnaya Energiya* **8**, 72 (1960).

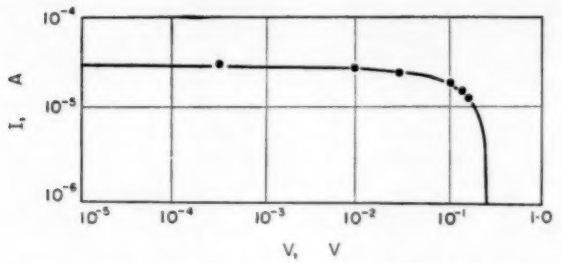

FIG. 2.—Load characteristic of the U_3O_8–MgO sample.

For each of the samples an e.m.f. was observed during the irradiation and as the neutron flux density nv was increased the voltage V_∞ and current $I_{s.c.}$ also increased. The dependence of V_∞ and $I_{s.c.}$ on the flux density is shown in Fig. 1 for a U_3O_8–MgO sample. It is evident that V_∞ reaches a saturation value when $nv \simeq 6.10^{12}$ cm^{-2} sec^{-1} and that $I_{s.c.}$ rises linearly with increasing neutron flux density. Figure 2 gives the load characteristics of the U_3O_8–MgO sample; it is similar to the load characteristic of a rectifier photocell. The neutron flux density in this case was 8.10^{12} cm^{-2} sec.$^{-1}$

In Fig. 3 we give typical current-voltage characteristics for a U_3O_8–Al_2O_3 sample taken before and after irradiation in an integrated neutron flux of $5 . 10^{17}$ cm^{-2}. It can be seen that the irradiation has reduced the resistance of the sample by an order of magnitude and that the sample has also acquired rectifying properties at low voltages which were not present before the irradiation. A particularly large degree of rectification was

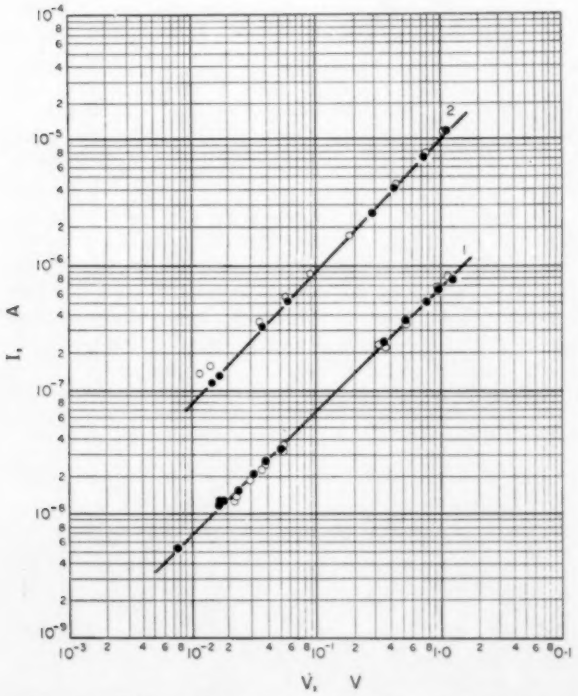

FIG. 3.—Current-voltage characteristic of a U_3O_8–Al_2O_3 sample. (1) before irradiation in a reactor and (2) after irradiation.
●—Negative voltage applied to the titanium electrode.
○—Positive voltage applied to the titanium electrode.

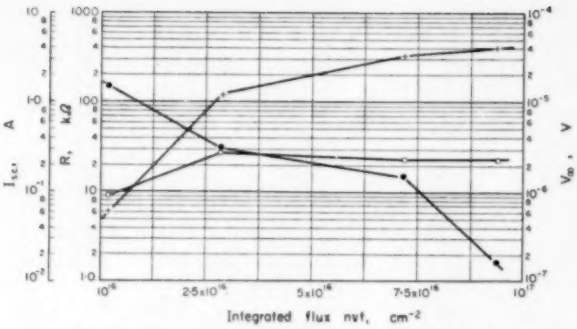

FIG. 4.—Dependence of $I_{s.c.}$ (×), V_∞ (○) and R (●) for a sample of U_3O_8–MgO on the integrated flux of radiation nvt. The flux density was constant and equal to $8 . 10^{12}$ cm^{-2} sec^{-1}.

observed at the time of irradiation, the coefficient of rectification reaching values between 2 and 10 at 1·4 V.

The behaviour of the U_3O_8–MgO samples as a function of the integrated flux of radiation is shown in Fig. 4. All the characteristics underwent a considerable change during the irradiation. The resistance of the sample was 10 MΩ before the irradiation but during the irradiation it fell to 2 kΩ causing a sharp rise in the current $I_{s.c.}$. V_∞ was observed to increase with increasing flux. With an integrated flux of radiation $\sim 10^{17}$ cm^{-2} a tendency towards stabilization was observed. At the end of the reactor irradiation the resistance of the sample rose to 1 MΩ.

Additional experiments were carried out in order to discover the part played by the uranium fission fragments in the generation of the e.m.f. Some of the samples were given a preliminary γ-irradiation before the reactor irradiation. The effect produced in the samples by γ-rays was three orders of magnitude less than that produced by the same flux of neutrons, a result which is in accord with the difference in the magnitudes of the specific ionization produced by γ-rays and fission fragments. We also prepared a double sample of U_3O_8–Al_2O_3: on one half of the sample a layer of uranium containing a 10 per cent enrichment of ^{235}U was deposited and on the other half we deposited natural uranium. The enriched sample gave an effect 15 times greater than the natural uranium sample. We can conclude from these results that the e.m.f. observed in the samples is due to the action of the fission fragments.

In addition to the semiconductors mentioned above we also carried out a qualitative examination of the oxides and sulphides of beryllium, nickel, molybdenum, tungsten, zinc and copper. An e.m.f. was generated in all these samples but the best combination of semiconducting materials was the combination U_3O_8–MgO.

We have calculated that in the U_3O_8–MgO samples 0·01 per cent of the energy of the fission fragments is converted to electrical energy. This low efficiency appears to be due to the short life-time of the current carriers and to the adverse ratio between the diffusion length of the current carriers and the thickness of the semiconducting layers in the samples. An analysis of our results leads us to conclude that the e.m.f. generated in the samples arises mainly from the rectifying properties of the samples although here the thermal and volume e.m.f.s also play a part.

Acknowledgments—In conclusion, the authors thank PROFESSOR A. K. KRASIN for his interest in this work. They thank also

G. N. USHAKOV for his co-operation and R. G. BULICHEVA, V. A. SHALIN and G. V. RIKOV for assisting with the experiments.

IU. K. GUS'KOV
A. V. ZVONAREV
V. P. KLICHKOVA

REFERENCES

1. LINDER E. G., RAPPAPORT P. and LOFERSKII J. J., *Proceedings of the First International Conference on the Peaceful Uses of Atomic Energy, Geneva*, Vol. 15 p. 283. United Nations, New York (1956).
2. IOFFE A. V., *Zh. tekh. fiz.* **18**, 1488 (1948).
3. KINCHIN G. and PEASE R., *Reports on Progress in Physics* **18**, 1 (1955).
4. GLEN J., *Advances in Physics* **4**, No. 16, 381 (1955).
5. TSAREV B. M., *Contact Potentials* Gostekhizdat, Moscow (1955).
6. GUS'KOV IU. K. *et al.*, *Prib. tekh. eksp.* No. 1, 143 (1960).

Measurement of fast neutron flux distribution in the core of VVR-C reactor using electrical conductivity changes in germanium*

(*Received* 28 *December* 1959)

IN CONNEXION with the studies of semiconductors behaviour under neutron irradiation currently conducted at the Institute for Nuclear Studies in Warsaw it became necessary to investigate the fast neutron flux distribution in the reactor core.

It is known[1–7] that the electrical conductivity of *n*-type single crystals of germanium decreases under fast neutron irradiation and eventually the crystal is converted into *p*-type. Figure 1 shows a typical curve of electrical conductivity of germanium as a function of fast neutron irradiation time. For neutrons of energies greater than approximately 300 eV the initial part of the curve is linear.

Measurements were conducted using nine selected samples of highest conductivity and size 0·15 × 0·15 × 1·0 cm cut from a germanium single crystal. Each sample was wrapped in 0·25 mm thick cadmium foil to shield it from thermal neutrons and all samples were placed evenly spaced in a special aluminium probe. The probe was inserted into the core of VVR-C reactor between fuel elements and when the probe was in position seven germanium samples were located within the core and two were outside viz. one above and one below the core.

The electrical conductivity was determined as a function of irradiation time from measurements of current passing through each sample from a constant voltage supply. There was no appreciable heating of the samples due to the electric current. During the experiment the reactor power was kept constant at 1·5 kW. Figure 2 shows electrical conductivity changes in all samples as a function of irradiation time. The discontinuities in the slope $d\sigma/dt$ at $t = 1$ hr and $t = 2$ hr were caused by altering the position of the probe in the reactor. The slope of the $\sigma(t)$ curve gives a measure of the fast neutron flux at each position of the germanium samples and Fig. 3 shows the observed distribution of the flux along the reactor axis. This figure was constructed using the measurements shown in Fig. 2 between $t = 1$ and $t = 2$ hr.

* Translated by J. ADAM from *Atomnaya Energiya* **8**, 451 (1960).

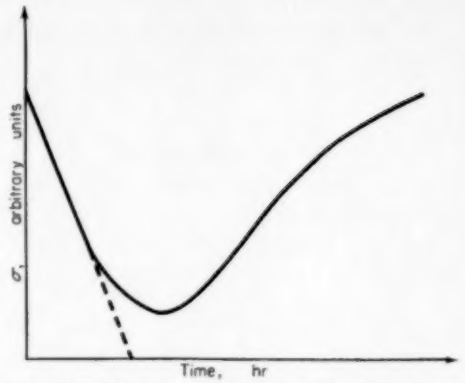

FIG. 1.—Variation in electrical conductivity (σ) of a germanium single crystal as a function of fast neutron irradiation time.

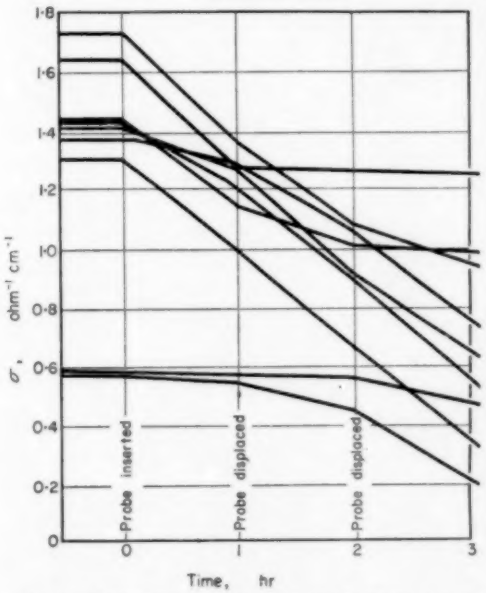

FIG. 2.—Variations in electrical conductivity (σ) of germanium samples positioned at various depths in VVR-S reactor core and irradiated with fast neutrons.

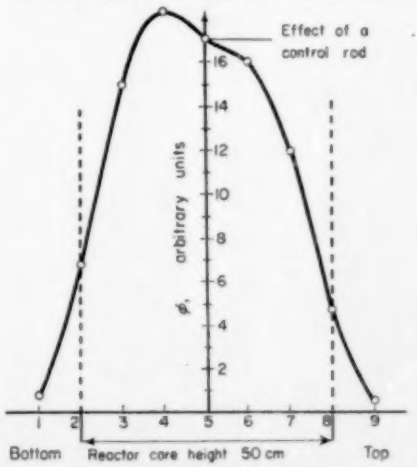

FIG. 3.—Fast neutron flux distribution along the axis of VVR-S reactor core.

The method described here could be used for absolute flux measurements.

E. Aleksandrovich
M. Bartenbakh

REFERENCES

1. Davis R., Johnson W., Lark-Horovitz K. and Siegel S., *Phys. Rev.* **74,** 1255 (1948).
2. Johnson W. and Lark-Horovitz K., *Phys. Rev.* **76,** 442 (1949).
3. Crawford J. Jr. and Lark-Horovitz K., *Phys. Rev.* **78,** 815, (1950); *Phys. Rev.* **79,** 889 (1950).
4. Cleland J. *et al.*, *Phys. Rev.* **83,** 312, (1951); *Phys. Rev.* **84,** 861, (1951).
5. James H. and Lark-Horovitz K., *Z. phys. Chem.* **198,** 107, (1951).
6. Cleland J., Crawford J. and Pigg J., *Phys. Rev.* **98,** 1742 (1955).
7. Buras B. *et al.*, Report No. 101/I-B, Institute of Nuclear Research, Warsaw (1959).

VOL
15
196

Reactor Science and Technology (Journal of Nuclear Energy Parts A/B) 1961, Vol. 15, p. 235. Pergamon Press Ltd. Printed in Northern Ireland

PAPERS TO BE PUBLISHED IN FUTURE ISSUES

D. C. LESLIE: **The weighting of diffusion coefficients in cell calculations.**

J. A. H. KERSTEN: **An aqueous homogeneous zero energy suspension reactor—I. Experiments with a subcritical reactor in which an aqueous suspension of UO_2-particles is circulating.**

R. CENERINI: **An aqueous homogeneous zero energy suspension reactor—II. Analysis of the neutron flux fluctuations in an aqueous homogeneous subcritical reactor with circulating UO_2-particles.**

T. MARKESTEIN and TH. VAN DER PLAS: **An aqueous homogeneous zero energy suspension reactor—III. Measurement of the fission recoil separation effect in an aqueous fuel suspension using a homogeneous subcritical reactor assembly.**

J. KALSHOVEN: **An aqueous homogeneous zero energy suspension reactor—IV. The measurement of the colloid chemical stability of suspensions.**

C. BEETS, J. L. CAMPAN, H. DECKERS et C. P. ZALESKI: **Analyse spectrale des neutrons rapides dans un massif d'uranium naturel.**

K. E. LARSSON and U. DAHLBORG: **Some vibrational properties of solid and liquid H_2O and D_2O derived from differential cross-section measurements.**

P. N. COOPER, K. FIRTH, M. KERRIDGE, R. F. MATHAMS, A. J. SALMON and K. G. STEPHENS: **Some measurements of reactivity in a light-water moderated highly enriched uranium assembly.**

VOL.
15
1961